ISSN 0021-9673

VOL. 470 NO. 1 MAY 24, 1989

including

6th Int. Symp. on Isotachophoresis and Capillary Zone Electrophoresis Vienna, September 21–23, 1988

JOURNAL OF CHROMATOGRAPHY

INTERNATIONAL JOURNAL ON CHROMATOGRAPHY, ELECTROPHORESIS AND RELATED METHODS

ELSEVIER

JOURNAL OF CHROMATOGRAPHY

Scope. The *Journal of Chromatography* publishes papers on all aspects of chromatography, electrophoresis and related methods. Contributions consist mainly of research papers dealing with chromatographic theory, instrumental development and their applications. The section *Biomedical Applications*, which is under separate editorship, deals with the following aspects: developments in and applications of chromatographic and electrophoretic techniques related to clinical diagnosis or alterations during medical treatment; screening and profiling of body fluids or tissues with special reference to metabolic disorders; results from basic medical research with direct consequences in clinical practice; drug level monitoring and pharmacokinetic studies; clinical toxicology; analytical studies in occupational medicine.

Submission of Papers. Papers in English, French and German may be submitted, in three copies. Manuscripts should be submitted to: The Editor of *Journal of Chromatography*, P.O. Box 681, 1000 AR Amsterdam, The Netherlands, or to: The Editor of *Journal of Chromatography, Biomedical Applications*, P.O. Box 681, 1000 AR Amsterdam, The Netherlands. Review articles are invited or proposed by letter to the Editors. An outline of the proposed review should first be forwarded to the Editors for preliminary discussion prior to preparation. Submission of an article is understood to imply that the article is original and unpublished and is not being considered for publication elsewhere. For copyright regulations, see below.

Subscription Orders. Subscription orders should be sent to: Elsevier Science Publishers B.V., P.O. Box 211, 1000 AE Amsterdam, The Netherlands, Tel. 5803 911, Telex 18582 ESPA NL. The *Journal of Chromatography* and the *Biomedical Applications* section can be subscribed to separately.

Publication. The *Journal of Chromatography* (incl. *Biomedical Applications*) has 37 volumes in 1989. The subscription prices for 1989 are:

J. Chromatogr. + *Biomed. Appl.* (Vols. 461–497):
Dfl. 6475.00 plus Dfl. 999.00 (p.p.h.) (total *ca.* US$ 3737.00)

J. Chromatogr. only (Vols. 461–486):
Dfl. 5200.00 plus Dfl. 702.00 (p.p.h.) (total *ca.* US$ 2951.00)

Biomed. Appl. only (Vols. 487–497):
Dfl. 2200.00 plus Dfl. 297.00 (p.p.h.) (total *ca.* US$ 1248.50).

Our p.p.h. (postage, package and handling) charge includes surface delivery of all issues, except to subscribers in Argentina, Australia, Brasil, Canada, China, Hong Kong, India, Israel, Malaysia, Mexico, New Zealand, Pakistan, Singapore, South Africa, South Korea, Taiwan, Thailand and the U.S.A. who receive all issues by air delivery (S.A.L. — Surface Air Lifted) at no extra cost. For Japan, air delivery requires 50% additional charge; for all other countries airmail and S.A.L. charges are available upon request. Back volumes of the *Journal of Chromatography* (Vols. 1–460) are available at Dfl. 195.00 (plus postage). Claims for missing issues will be honoured, free of charge, within three months after publication of the issue. Customers in the U.S.A. and Canada wishing information on this and other Elsevier journals, please contact Journal Information Center, Elsevier Science Publishing Co. Inc., 655 Avenue of the Americas, New York, NY 10010. Tel. (212) 633-3750.

Abstracts/Contents Lists published in Analytical Abstracts, ASCA, Biochemical Abstracts, Biological Abstracts, Chemical Abstracts, Chemical Titles, Chromatography Abstracts, Current Contents/Physical, Chemical & Earth Sciences, Current Contents/Life Sciences, Deep-Sea Research/Part B: Oceanographic Literature Review, Excerpta Medica, Index Medicus, Mass Spectrometry Bulletin, PASCAL-CNRS, Referativnyi Zhurnal and Science Citation Index.

See inside back cover for Publication Schedule, Information for Authors and information on Advertisements.

0021-9673/89/$03.50

CONTENTS

(Abstracts/Contents Lists published in Analytical Abstracts, ASCA, Biochemical Abstracts, Biological Abstracts, Chemical Abstracts, Chemical Titles, Chromatography Abstracts, Current Contents/Physical, Chemical & Earth Sciences, Current Contents/Life Sciences, Deep Sea Research/Part B: Oceanographic Literature Review, Excerpta Medica, Index Medicus, Mass Spectrometry Bulletin, PASCAL-CNRS, Referativnyi Zhurnal and Science Citation Index)

6TH INTERNATIONAL SYMPOSIUM ON ISOTACHOPHORESIS AND CAPILLARY ZONE ELECTROPHORESIS, VIENNA, SEPTEMBER 21–23, 1988

(end of symposium papers)

AQUEOUS SIZE-EXCLUSION CHROMATOGRAPHY

edited by **P.L. DUBIN,** *Indiana-Purdue University*

(Journal of Chromatography Library, 40)

The rapid development of new packings for aqueous size-exclusion chromatography has revolutionized this field. High resolution non-adsorptive columns now make possible the efficient separation of proteins and the rapid and precise determination of the molecular weight distribution of synthetic polymers. This technology is also being applied to the separation of small ions, the characterization of associating systems, and the measurement of branching. At the same time, fundamental studies are elucidating the mechanisms of the various chromatographic processes.

These developments in principles and applications are assembled for the first time in this book.

- Fundamental issues are dealt with: the roles of pore structure and macromolecular dimensions, hydrophobic and electrostatic effects, and the determination and control of column efficiency.
- High-performance packings based on derivatized silica are reviewed in detail.
- Special techniques are thoroughly described, including SEC/LALLS, inverse exclusion chromatography, and frontal zone chromatography.
- Attention is focussed on special applications of size-exclusion methods, such as the characterization of micelles, separations of inorganic ions, and Hummel-Dreyer and related methods for equilibrium systems.
- Protein chromatography is dealt with in both dedicated sections and throughout the book as a whole.

This is a particularly comprehensive and authoritative work - all the contributions review broad topics of general significance and the authors are of high repute.

The material will be of special value for the characterization of synthetic water-soluble polymers, especially polyelectrolytes. Biochemists will find fundamental and practical guidance on protein separations. Researchers confronted with solutes that exhibit complex chromatographic behavior, such as humic acids, aggregating proteins, and micelles should find the contents of this volume illuminating.

1988 xviii + 454 pages
US$ 144.75 / Dfl. 275.00
ISBN 0-444-42957-3

ELSEVIER SCIENCE PUBLISHERS

P.O. Box 211, 1000 AE Amsterdam, The Netherlands
P.O. Box 882, Madison Square Station, New York, NY 10159, USA

An authoritative review... highly recommended...

Optimization of Chromatographic Selectivity

A Guide to Method Development

by **P. Schoenmakers,** *Philips Research Laboratories, Eindhoven, The Netherlands*

(Journal of Chromatography Library, 35)

"The contents of this book have been put together with great expertise and care, and represent an authoritative review of this very timely topic... highly recommended to practising analytical chemists and to advanced students." (Jnl. of Chromatography)

"...an important contribution by a worker who has been in the field almost from its inception and who understands that field as well as anyone. If one is serious about method development, particularly for HPLC, this book will well reward a careful reading and will continue to be useful for reference purposes." (Mag. of Liquid & Gas Chromatography)

This is the first detailed description of method development in chromatography - the overall process of which may be summarized as: method selection, phase selection, selectivity optimization, and system optimization. All four aspects receive attention in this eminently readable book.

The first chapter describes chromatographic theory and nomenclature and outlines the method development process. Guidelines are then given for method selection and quantitative concepts for characterizing and classifying chromatographic phases. Selective separation methods (from both GC and LC) are given - the main parameters of each method are identified and simple, quantitative relations are sought to describe their effects. Criteria by which to judge the quality of separation are discussed with clear recommendations for different situations. The specific problems involved in the optimization of chromatographic selectivity are explained. Optimization procedures, illustrated by examples, are described and compared on the basis of a number of criteria. Suggestions are made both for the application of different procedures and for further research. The optimization of programmed analysis receives special attention, and the last chapter summarizes the optimization of the chromatographic system, including the optimization of the efficiency, sensitivity and instrumentation.

Those developing chromatographic methods or wishing to improve existing methods will value the detailed, structured way in which the subject is presented. Because optimization procedures and criteria are described as elements of a complete optimization package, the book will help the reader to understand, evaluate and select current and future commercial systems.

Contents: 1. Introduction. 2. Selection of Methods. 3. Parameters Affecting Selectivity. 4. Optimization Criteria. 5. Optimization Procedures. 6. Programmed Analysis. 7. System Optimization. Indexes.

1986 1st repr. 1987 xvi + 346 pages
US$ 110.50 / Dfl. 210.00
ISBN 0-444-42681-7

ELSEVIER SCIENCE PUBLISHERS

P.O. Box 211, 1000 AE Amsterdam, The Netherlands
P.O. Box 882, Madison Square Station, New York, NY 10159, USA

JOURNAL OF CHROMATOGRAPHY

VOL. 470 (1989)

JOURNAL *of* CHROMATOGRAPHY

INTERNATIONAL JOURNAL ON CHROMATOGRAPHY,
ELECTROPHORESIS AND RELATED METHODS

ELSEVIER
AMSTERDAM — OXFORD — NEW YORK — TOKYO

J. Chromatogr., Vol. 470 (1989)

0021-9673/89/$03.50

This issue is printed on acid-free paper

Printed in The Netherlands

SPECIAL ISSUE

6TH INTERNATIONAL SYMPOSIUM ON ISOTACHOPHORESIS AND CAPILLARY ZONE ELECTROPHORESIS

Vienna (Austria), September 21–23, 1988

Guest Editors

P. BOČEK
(Brno)

E. KENNDLER
(Vienna)

CONTENTS

6TH INTERNATIONAL SYMPOSIUM ON ISOTACHOPHORESIS AND CAPILLARY ZONE ELECTROPHORESIS, VIENNA, SEPTEMBER 21–23, 1989

Journal of Chromatography, 470 (1989) 1
Elsevier Science Publishers B.V., Amsterdam — Printed in The Netherlands

CHROM. 21 380

PREFACE

The *6th International Symposium on Isotachophoresis and Capillary Zone Electrophoresis* was the most recent one in the series. After the symposia held in Baconfoy in Belgium (1979), in Eindhoven in The Netherlands (1980), in Goslar in the Federal Republic of Germany (1982), in Hradec Králové in Czechoslovakia (1984) and in Maastricht in The Netherlands (1986), the sixth symposium was held in Vienna from September 21st to 23rd, 1988, and was organized by Dr. Ernst Kenndler under the auspices of Honorary President Professor Dr. H. Tuppy, Federal Minister of Science and Research, and Honorary Chairman Professor Dr. J. F. K. Huber, University of Vienna. The organization of the symposium was facilitated by the Österreichische Gesellschaft für Mikrochemie und Analytische Chemie and by the Institute of Analytical Chemistry, University of Vienna. Dr. Kenndler chaired the Scientific Committee, involving Drs. F. M. Everaerts, J. W. Jorgenson and D. Kaniansky, and also the Organizing Committee, involving Drs. P. Jenner and P. J. Oefner.

Eight lecture sessions were devoted to Fundamentals of electrophoresis in capillaries, Selectivity in electrophoresis, Recent developments in isotachophoresis, Capillary zone electrophoresis —Separation of biomolecules, Isotachophoresis —Separation of biomolecules, Electrochromatography and related techniques, Separation of enantiomers and Application of electrophoresis.

Two poster sessions that provided substantial space and time for direct discussions of the results and ideas in small groups were followed by panel discussions of these sessions.

There were over 120 participants from 15 European countries, the U.S.A., Japan and China, who presented 35 lectures and 42 posters, and submitted 28 manuscripts that have led to this special issue.

The Vienna symposium introduced a new step in these symposia by bringing together experts in capillary isotachophoresis and capillary zone electrophoresis, including those having a broad theoretical knowledge and experimental experienced in gas and liquid chromatography. This broad participation has already led to new interdisciplinary aspects, and forms the basis for the future promotion of electrophoresis as a powerful analytical tool.

It is my pleasure to express congratulations and thanks to everyone concerned who made the Vienna symposium a most successful event in electrophoresis. I also thank Dr. Karel Macek for the care devoted to this special issue.

Brno (Czechoslovakia)
January 1989

PETR BOČEK

Journal of Chromatography, 470 (1989) 3–20
Elsevier Science Publishers B.V., Amsterdam — Printed in The Netherlands

CHROM. 21 211

INVERSE ELECTROLYTE SYSTEMS IN ISOTACHOPHORESIS

IMPACT OF THE TERMINATING ELECTROLYTE ON THE MIGRATING ZONES IN CATIONIC ANALYSIS

PETR GEBAUER, LUDMILA KŘIVÁNKOVÁ and PETR BOČEK*

Institute of Analytical Chemistry, Czechoslovak Academy of Sciences, Leninova 82, CS-611 42 Brno (Czechoslovakia)

SUMMARY

An insight is given into the nature of cationic isotachophoretic systems with H^+ as the leading constituent. It is shown both theoretically and experimentally that the parameters of all zones in such a system depend not only on the composition of the leading electrolyte, but also on the composition (pH) of the terminator. The theory presented enables one to predict the parameters of all zones involved, including the effective mobility of the leading hydrogen constituent, thus allowing the correct construction of such systems. Moreover, the theory predicts the impact of the terminating electrolyte on the quantitative analysis. The practical importance of the systems in question is exemplified showing the possibility of determining either very mobile ions (K^+, NH_4^+) or very weak organic bases (with $pK_{XH} = 2–3$ or even lower).

INTRODUCTION

The fundamental role of a discontinuous electrolyte system consists in the creation of conditions under which the sample components show different effective mobilities and good separation. The leading electrolyte plays the key role here as it determines, according to the principle of zone adjustement, what qualitative and quantitative composition any arbitrary sample zone has and what the effective mobility of the corresponding substance is[1,2]. In accordance with the importance of this role, one must pay great attention to the choice of a suitable leading electrolyte, which is usually selected in such a way that the resulting system is correct (*i.e.*, it provides sharp boundaries between all zones which are stable)[2]. Simultaneously, the pH of the electrolytes is usually selected so that it lies in the so-called safe region[3] where the disturbing effect of the migration of H^+ and OH^- ions can be neglected. We can say more exactly that the leading electrolyte is selected in such a way that the disturbing ion (H^+ or OH^-) forms the real or potential rear (terminating) zone of the system[4,5].

The actual terminator has first a practical role, fulfilling the following requirements: the effective mobility of the terminator in its adjusted zone should be lower than that of any sample substance so that a quantitative termination of all sample zones is ensured; and the effective mobility of the terminator and hence the

0021-9673/89/$03.50

conductivity of the terminating zone should not be too low in order not to make the analysis time too long. Because in correct systems the composition of all adjusted zones is a function of the composition of the leading electrolyte, it is not necessary to pay excessive attention to the composition of the terminating electrolyte as the composition of the terminating zone is automatically adjusted to the parameters of the given leading electrolyte. We can say that in correct isotachophoretic systems which have been used and recommended so far, the composition of the terminator does not show any influence on the composition (properties) of the sample zones.

In isotachophoretic practice, however, there sometimes electrolyte systems are used that do not possess the above-mentioned properties; non-buffered electrolyte systems may serve as an example. Here the counter ion does not have any buffering properties, such as an alkali metal cation in anionic isotachophoresis or an anion of a strong acid (chloride, sulphate) in cationic isotachophoresis. As the leading ions H^+ and K^+ and/or OH^- and Cl^- are usually used. Even in the early days of isotachophoresis, the use of such systems was not recommended as a result of qualitative considerations on possible disturbing effects caused by uncontrolled migration of H^+ or OH^- ions from the terminating electrode chamber[1,6,7]. A detailed analysis of the behaviour of H^+ and OH^- ions in isotachophoresis[4,5,8] has also shown that for a correct isotachophoretic migration it is necessary to control the migration of one of these two ions by the counter ionic system in such a way that the respective ion (H^+ or OH^-) serves as the natural terminator of the system. Nevertheless, the practical use of non-buffered systems has grown as these systems allow one to analyse, *e.g.*, K^+ when using H^+ as the leader[6,9] or Cl^- with OH^- as the leader[9]. Analytical practice, however, shows that for a reproducible analysis it is necessary to find empirically a suitable pH of the terminating solution and to perform each analysis with a fresh terminator in the terminating electrode chamber[10,11].

It is evident that a quantitative knowledge of the role of the terminator has not yet been established, especially the problem of the influence of the composition (pH) of the terminator on the zones of migrating substances. Further, the use of non-buffered systems has so far not overcome the stage of empirical searching and a theoretical idea of the conditions under which H^+ may be used as the leading ion in correct isotachophoresis is still lacking. This paper considers the above problems, establishes an adequate theory and gives answers to the related practical questions.

THEORETICAL

Description of the system

Let us consider a system (Fig. 1) in which the zone of a weak (or strong) acid HA (zone H) serves as the leading zone of cationic migration. The solution of this acid, HA, and of its salt with a weak (or strong) base, BH^+A^-, serves as the terminator (zone T). Let us assume that the composition of the terminator does not change with time. After switching on the electric current, the terminating zone B is created, its concentration being adjusted to the parameters of zone H.

The physico-chemical description of such a system starts from its understanding as a moving-boundary system, where not only the counter constituent but also the constituent "H^+" are present in all zones. To describe such a type of system, the

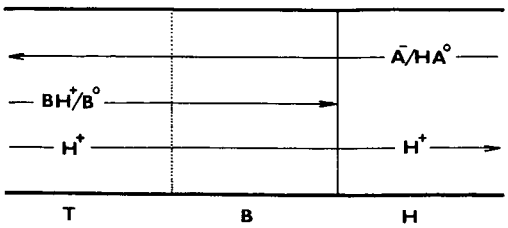

Fig. 1. Scheme of the formation of the adjusted terminating zone B between the leading zone H and the original terminating electrolyte T.

moving-boundary equations[1,2] may be advantageously adopted[2]. In our case, the following equations may be written for the boundary B → H:

$$\frac{\bar{u}_{B,B}}{\kappa_B} = W_{B-H} \tag{1}$$

$$\frac{u_H c_{H,B} + u_{BH} c_{BH,B}}{\kappa_B} - \frac{u_H c_{H,H}}{\kappa_H} = W_{B-H}\,(\bar{c}_{H,B} - \bar{c}_{H,H}) \tag{2}$$

where u_i is the electrophoretic mobility of ion i, $\bar{u}_{i,j}$ and $\bar{c}_{i,j}$ are the effective mobility and the total (analytical) concentration, respectively, of constituent i in zone j, $c_{i,j}$ is the concentration of ion i in zone j, κ_j is the conductivity of zone j, and W_{B-H} is the volume swept by the boundary B–H per coulomb passed. Note that, *e.g.*,

$$\bar{c}_{H,B} = c_{H,B} + c_{BH,B} + c_{HA,B} \tag{3}$$

is the constituent concentration of H^+ in zone B. For the immobile concentration boundary T::B the following balances can be written:

$$\frac{u_{BH} c_{BH,T}}{\kappa_T} = \frac{u_{BH} c_{BH,B}}{\kappa_B} \tag{4}$$

$$\frac{u_H c_{H,T} + u_{BH} c_{BH,T}}{\kappa_T} = \frac{u_H c_{H,B} + u_{BH} c_{BH,B}}{\kappa_B} \tag{5}$$

from which

$$\frac{c_{H,T}}{\kappa_T} = \frac{c_{H,B}}{\kappa_B} \quad \text{and} \quad \frac{c_{BH,T}}{c_{BH,B}} = \frac{c_{H,T}}{c_{H,B}} \tag{6}$$

By combination of eqns. 1, 2 and 5, we obtain

$$\frac{u_H c_{H,T} + u_{BH} c_{BH,T}}{\kappa_T} - \frac{u_H c_{H,H}}{\kappa_H} = a = \frac{\bar{u}_{B,B}}{\kappa_B}\,(\bar{c}_{H,B} - \bar{c}_{H,H}) \tag{7}$$

When expressing the last term of eqn. 7 by using eqns. 3 and 6, the definition of effective mobility

$$\bar{u}_{B,B} = u_{BH}c_{H,B}/(c_{H,B} + K_{BH}) \tag{8}$$

and electroneutrality

$$c_{A,B} = c_{H,B} + c_{BH,B} \tag{9}$$

we obtain, after rearrangement an equation that is a function of only one unknown, $c_{H,B}$:

$$\frac{a\ \kappa_T}{c_{H,T}} = \frac{u_{BH}}{c_{H,B} + K_{BH}}\left[c_{H,B}\left(1 + \frac{c_{H,B}}{K_{HA}}\right)\left(1 + \frac{c_{BH,T}}{c_{H,T}}\right) - \bar{c}_{H,H}\right] \tag{10}$$

where K_{HA} and K_{BH} are the dissociation constants of HA and BH^+, respectively. The solution of eqn. 10 (and the use of eqns. 6 and 9) provides the complete description of the composition of zone B. From eqn. 10, one important conclusion can be drawn: the composition of the adjusted terminator (zone B) depends not only on the parameters of the leading zone (as is usual in normal isotachophoretic systems), but also on the composition of the terminating solution (zone T), especially on the ratio $c_{BH,T}/c_{H,T}$. Obviously, the above ratio can be expressed as a function of the total concentration $\bar{c}_{B,T}$: $c_{BH,T}/c_{H,T} = \bar{c}_{B,T}/(K_{BH} + c_{H,T})$.

In the treatment of systems as shown in Fig. 1, the question arises of whether the phenomenological description of isotachophoretic systems may be applied here. The understanding of the boundary B → H as an isotachophoretic boundary allows the application of the general isotachophoretic condition

$$W_{B-H} = \frac{\bar{u}_{B,B}}{\kappa_B} = \frac{\bar{u}_{H,H}}{\kappa_H} \tag{11}$$

where the concept of the effective mobility of hydrogen ion[5], $\bar{u}_{H,H}$ (originally introduced for H^+ as the terminator), is generalized to any isotachophoretic zone containing H^+ as the only constituent (apart from the counter constituent). The combination of eqns. 7 and 11 gives, after rearrangement,

$$\bar{u}_{H,H} = \frac{c_{H,H}u_H}{\bar{c}_{H,H} - \bar{c}_{H,B} + c_{H,B}\left(\frac{u_H}{\bar{u}_{B,B}}\right) + c_{BH,B}\left(\frac{u_{BH}}{\bar{u}_{B,B}}\right)} \tag{12}$$

Comparison of this equation with eqn. 4 in ref. 5 shows additional terms expressing the contribution of B being a weak base; for $K_{BH} \to 0$ both of the compared equations become the same. It is cleary seen from eqn. 12 that $\bar{u}_{H,H}$ is a function of the parameters of both zones H and B (and thus T). The value of $\bar{u}_{H,H}$ is in direct proportion to W_{B-H} (*i.e.*, to the velocity of the isotachophoretic boundary) since κ_H is constant for a given leading electrolyte (*cf.*, eqn. 11).

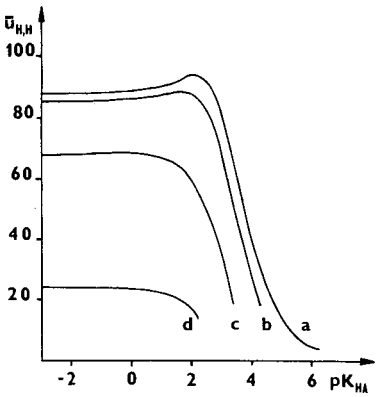

Fig. 2. Calculated dependence of the effective mobility of H^+, $\bar{u}_{H,H}$ (in 10^{-9} m^2 V^{-1} s^{-1}) on pK_{HA} of the counter constituent, for various pK_{BH} of the terminating substance: (a) 20; (b) 5; (c) 4; and (d) 3. $u_A = -60 \cdot 10^{-9}$ m^2 V^{-1} s^{-1}; $u_{BH} = 30 \cdot 10^{-9}$ m^2 V^{-1} s^{-1}; $\bar{c}_{B,T}/\bar{c}_{H,T} = 0.5$.

Figs. 2–4 illustrate how the value of $\bar{u}_{H,H}$ depends on the parameters of the system. Fig. 2 shows the dependence of $\bar{u}_{H,H}$ on the value of pK_{HA} of the counter constituent, for four selected values of pK_{BH} of the terminating substance and for a constant ratio $\bar{c}_{B,T}/\bar{c}_{H,T} = 0.5$. It can be seen from Fig. 2 how the value of $\bar{u}_{H,H}$ depends on pK_{BH} and that it decreases rapidly with increasing $pK_{HA} \geq 2$.

Fig. 3 shows the dependence of $\bar{u}_{H,H}$ on the content of free acid in the terminator expressed as $\bar{c}_{A,T} - \bar{c}_{B,T}$, for B being a strong base. For a strong acid (curve a , pK_{HA}

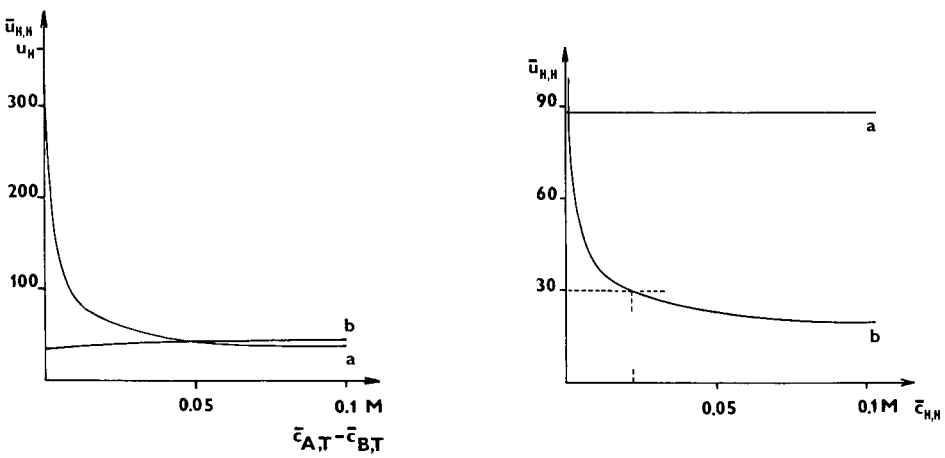

Fig. 3. Calculated dependence of $\bar{u}_{H,H}$ (in 10^{-9} m^2 V^{-1} s^{-1}) on the content of free acid in the terminator, $\bar{c}_{A,T} - \bar{c}_{B,T}$, for a strong (curve a, $pK_{HA} = -3$) and a weak (curve b, $pK_{HA} = 4$) acid as the counter constituent. $u_A = -60 \cdot 10^{-9}$ m^2 V^{-1} s^{-1}; $u_{BH} = 30 \cdot 10^{-9}$ m^2 V^{-1} s^{-1}; $pK_{BH} = 20$; $\bar{c}_{B,T} = 0.01$ *M*.

Fig. 4. Calculated dependence of $\bar{u}_{H,H}$ (in 10^{-9} m^2 V^{-1} s^{-1}) on the total concentration of H^+ in the leading zone, $\bar{c}_{H,H}$, for a strong (curve a, $pK_{HA} = -3$) and a weak (curve b, $pK_{HA} = 4$) acid as the counter constituent. The dashed line shows the $\bar{c}_{H,H}$ value corresponding to $\bar{u}_{H,H} = 30 \cdot 10^{-9}$ m^2 V^{-1} s^{-1}; $u_A = -60 \cdot 10^{-9}$ m^2 V^{-1} s^{-1}; $u_{BH} = 30 \cdot 10^{-9}$ m^2 V^{-1} s^{-1}; $pK_{BH} = 20$; $\bar{c}_{B,T} = 0.01$ *M*; $\bar{c}_{H,T} = 0.02$ *M*.

$= -3$), the value of $\bar{u}_{H,H}$ increases with decreasing concentration of the free acid in zone T, reaching the limiting value $\bar{u}_{H,H} = u_H$ for values of $\bar{c}_{A,T} - \bar{c}_{B,T}$ near zero. Another type of dependence occurs for the case of a weak acid (curve b, $pK_{HA} = 4$), where the relatively low value of $\bar{u}_{H,H}$ increases only slightly with increasing $\bar{c}_{A,T} - \bar{c}_{B,T}$.

As follows from Fig. 4, the concentration in zone H, $\bar{c}_{H,H}$, has the opposite influence. For a strong acid ($pK_{HA} = -3$, curve a), $\bar{u}_{H,H}$ is almost independent of $\bar{c}_{H,H}$; in contrast, for a weak acid as the counter constituent ($pK_{HA} = 4$, curve b), the value of $\bar{u}_{H,H}$ increases rapidly with decreasing $\bar{c}_{H,H}$.

All the conclusions drawn from Figs. 2–4 are in accordance with eqn. 12 and illustrate some simple rules on how the value of $\bar{u}_{H,H}$ depends on the parameters of the electrolyte system in some special situations. For a strong acid HA and a strong base B, for example, it holds that $\bar{c}_{H,H} = c_{H,H}$ and $\bar{u}_{B,B} = u_{BH}$; eqn. 12 therefore becomes

$$\bar{u}_{H,H} = u_H \cdot \frac{1}{1 - \frac{c_{H,B}}{c_{H,H}} \left(1 + \frac{u_H}{u_{BH}}\right)} \tag{13}$$

This equation corresponds to curve a in Fig. 3 and explains both its course and the limiting value $\bar{u}_{H,H} = u_H$ (for $c_{H,B} = 0$).

As was shown above, the value of $\bar{u}_{H,H}$ depends on the parameters of the zones H and B in a defined way which is the same irrespective of whether B is the leader and H^+ the terminator or *vice versa*. The condition of correct migration[8] of zones B and H can be formulated as follows:

(a) The system H → B is correct (the moving boundary H → B is sharp) if

$$\bar{u}_{B,H} > \bar{u}_{H,H} \tag{14}$$

(b) The system B → H is correct (the moving boundary B → H is sharp) if

$$\bar{u}_{B,H} < \bar{u}_{H,H} \tag{15}$$

In case (a), the electrolyte system in question is a normal cationic system with H^+ as the terminator. In case (b), the electrolyte system is that from Fig. 1 and condition 15 determines the region of correct migration. The only difference between the two situations is that in case (b) the behaviour of the system depends not only on the parameters of the leading zone but also on the parameters of the terminating zone, *viz*, the ratio $c_{BH,T}/c_{H,T}$ (*cf.*, eqn. 10).

It is obvious that, when taking a series of systems with increasing $\bar{u}_{H,H}$, the transition between systems of type (a) and (b) can be documented. Let us, as an example, consider curve b in Fig. 4, depicting the dependence of $\bar{u}_{H,H}$ on the concentration in the zone H, $\bar{c}_{H,H}$, for a weak acid as the counter ion ($u_A = -60 \cdot 10^{-9}$ $m^2\ V^{-1}\ s^{-1}$, $pK_{HA} = 4$). A strong base B ($u_{BH} = 30 \cdot 10^{-9}$ $m^2\ V^{-1}\ s^{-1}$) serves as the constituent of the zone B and the dashed line shows the transition corresponding to a concentration of $\bar{c}_{H,H} = 0.019\ M$ where $\bar{u}_{H,H} = u_B$. For concentrations higher than this (critical[4]) value, condition 14 holds true and the system shows a correct migration for the migration order H → B. For concentrations lower than the transition value, a correct system is obtained if the inverse migration order is selected, *i.e.*, B → H.

Correct migration of sample zones

Let us now describe the migration of the zone of a weak (or strong) base X in the type of systems under consideration (see Fig 5). The mass balance for the counter ion can be written in the usual way (note that u is a signed quantity):

$$\bar{c}_{A,H}\left(1 + \frac{|\bar{u}_{A,H}|}{\bar{u}_{H,H}}\right) = f_H = \bar{c}_{A,X}\left(1 + \frac{|\bar{u}_{A,X}|}{\bar{u}_{X,X}}\right) \tag{16}$$

The use of the electroneutrality condition, $c_{H,X} + c_{XH,X} = c_{A,X}$, and rearrangement lead to

$$(c_{H,X} + c_{XH,X})\left(\frac{K_{HA} + c_{H,X}}{K_{HA}} + \frac{|u_A|}{u_{XH}} \cdot \frac{K_{XH} + c_{H,X}}{c_{H,X}}\right) = f_H \tag{17}$$

Simultaneously, the isotachophoretic condition

$$\frac{\bar{u}_{H,H}}{\kappa_H} = \frac{\bar{u}_{X,X}}{\kappa_X} \tag{18}$$

holds. The set of the two equations 17 and 18 can be solved for the two unknowns, $c_{H,X}$ and $c_{XH,X}$, by, *e.g.*, the usual RFQ method[6].

Obviously, $\bar{u}_{H,H}$ in eqn. 18 is dependent on the composition of the terminating electrolyte, and hence the composition of zone X and the value of $\bar{u}_{X,X}$ are also dependent on the terminator.

Of greatest practical importance in any electrolyte system is the question of the correct migration of sample zones. In order to explain some new aspects which accompany the type of electrolyte systems described in this paper, we take advantage of the zone existence diagrams[13].

Let us first consider the following model system with formate ($pK_{HA} = 3.75$) as the weak counter constituent. When taking 0.0053 *M* KCOOH + 0.002 *M* HCOOH as the leading electrolyte for cationic isotachophoresis, we have a normal system with H^+ as the terminator. Its effective mobility is $\bar{u}_{H,H} = 54.4 \cdot 10^{-9}$ m^2 V^{-1} s^{-1} and its adjusted concentration is $\bar{c}_{H,H} = 0.01$ *M*. The zone existence diagram of such a system is shown in Fig. 6 (the existence region of this system is K–A–H–D–K). The contours have the usual meaning[13]; point K corresponds to the leading zone of K^+ and point H corresponds to the terminating zone of H^+.

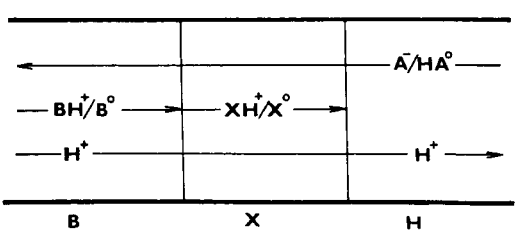

Fig. 5. Scheme of the migrating system of zones H, X and B.

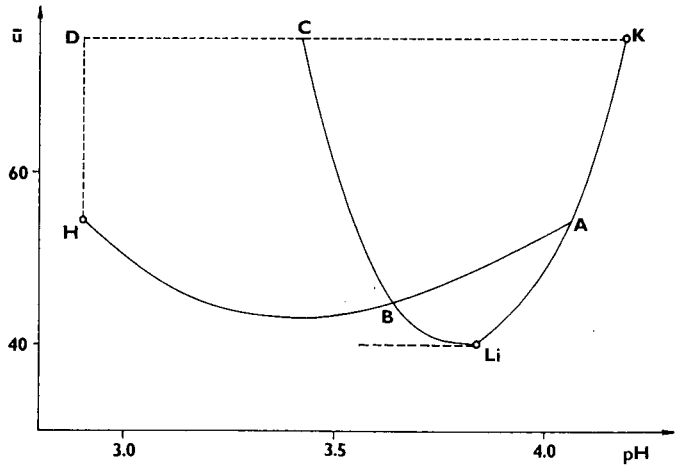

Fig. 6. Zone existence diagram, pH *vs.* $\bar{u}$ (in 10^{-9} $m^2V^{-1}s^{-1}$), for the cationic system with 0.0053 *M* potassium formate + 0.002 *M* formic acid as the leading electrolyte and H^+ as the terminator; for explanation, see text. $u_K = 76.2 \cdot 10^{-9}$ m^2 V^{-1} s^{-1}; $u_{For} = -57.1 \cdot 10^{-9}$ m^2 V^{-1} s^{-1}; $u_H = 362.5 \cdot 10^{-9}$ m^2 V^{-1} s^{-1}; $pK_{HFor} = 3.75$.

Let us now take an inverse system where 0.01 *M* HCOOH serves as the leading zone and the terminator is 0.00334 *M* LiCOOH + 0.0029 *M* HCOOH. The terminator is selected so that its concentrations are adjusted to the leading H zone and, moreover, for the leading zone it holds again that $\bar{u}_{H,H} = 54.4 \cdot 10^{-9}$ m^2 V^{-1} s^{-1}. When returning to Fig. 6, we can depict the leading zone H by the same point which depicts the terminating zone of the former system. The terminating zone of the present system is depicted by point Li which lies on the continuation of the curve KA. The existence region of the system involves points corresponding to bases X for which it simultaneously holds that $\bar{u}_{X,H} < \bar{u}_{H,H}$ and $\bar{u}_{X,Li} > \bar{u}_{Li,Li}$. The first condition holds true for points below curve AH in Fig. 6 (*i.e.*, below the lower existence contour of the former system). The second condition holds true for points above curve LiC (*i.e.*, above the upper sequence contour of zone Li). The resulting zone existence diagram of the present system has an unusual appearance; it is formed by the region Li–A–B–Li and by point H lying separately. All points lying on the diagram below curve LiC and above the lower sequence contour of zone Li (dashed line) do not give correct zones in the system as they are in the region of formation of steady-state mixed zones with the Li zone. Point H (zone H) represents here an apparent exception to this rule although, in fact, H^+ is present in all zones. We can say that point H represents the individual pure zone of the H^+ constituent, which is in steady-state coexistence with the terminating zone consisting of $Li^+ + H^+$.

Fig. 7 presents a schematic treatment of the various possibilities of constructing correct cationic electrolyte systems where 0.01 *M* HCOOH is involved as a separate zone. Fig. 7A shows the normal cationic system (A) where H^+ is the terminator; its concentration in the column adapts automatically to the value adjusted to the parameters of the leading electrolyte. In this system, substances from regions a and b (*cf.*, the diagram in Fig. 6) provide correct zones. Fig. 7B shows the novel inverse system (B) with the H^+ zone as the leader; here the terminating Li zone must have the

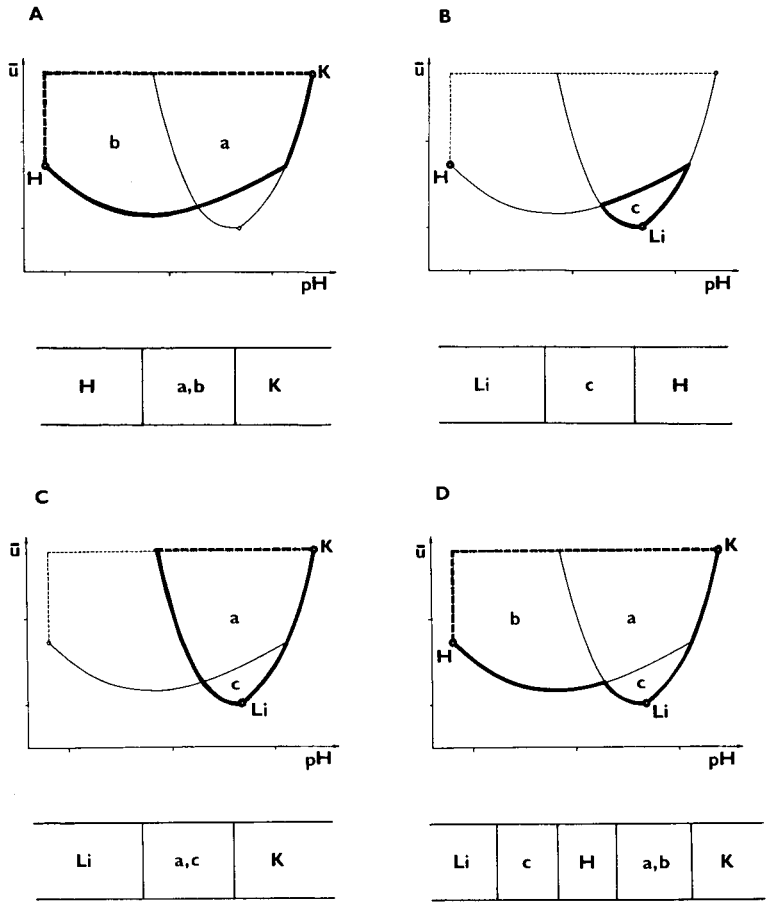

Fig. 7. Scheme of possible cationic isotachophoretic systems where 0.01 *M* formic acid is involved as an individual zone (the contours of the zone existence diagram are those from Fig. 6): (A) normal system; (B) inverse system; (C) combined system; (D) extended combined system. For explanation, see text.

concentrations of both LiCOOH and HCOOH selected so that $\bar{u}_{H,H}$ has the required value. In this system, substances from region c provide correct zones.

When taking the leading zone K from system A and the terminating zone Li from system B, a composed system (C) as depicted in Fig. 7C is the result. In this system, substances from region a and c provide correct zones. An interesting possibility of how to extend the system C should be mentioned here. By introducing the zone H^+ as a sample, a system (D) arises representing the coupled systems A and B (Fig. 7D). When comparing systems C and D, we can see that in system D also the substances from region b provide correct zones, their correct migration being enforced by the H^+ zone migrating behind them. It should be stressed here that both systems C and D are very sensitive to any change in the composition of either the leading or terminating electrolyte. A change in the composition of the terminator (Li zone) leading to a decrease in the corresponding $\bar{u}_{H,H}$ value, for example, results in the virtual existence

of two different $\bar{u}_{H,H}$ values in the system; one of them is defined with respect to the terminating zone of Li^+, $\bar{u}_{H,H}(Li)$, and the other with respect to the leading zone of K^+, $\bar{u}_{H,H}(K)$. In our example $\bar{u}_{H,H}(Li) < \bar{u}_{H,H}(K)$, the boundaries Li → H and H → K migrate with different velocities (here $v_{Li-H} < v_{H-K}$) and consequently, a growing H^+ zone will appear between the leading (K) and terminating (Li) zones. The (originally) single isotachophoretic system splits in this way into two isotachophoretic systems moving with two different velocities, bound by the common zone of the H constituent which had a double role, being simultaneously terminator for one system and leader for the other.

For systems with a strong acid as the counter constituent, the zone existence diagram shows a very narrow existence region which can be approximated by only a single line. Fig. 8, for example, shows the diagram for the system with 0.05 *M* HCl as the leading zone and 0.02 *M* hydroxyproline + 0.06 *M* HCl as the terminating solution. In this instance the pH of zones of strong bases decreases with increasing u_{XH} (in contrast to the former formate system). It is obvious that the above-mentioned operational electrolyte system offers the possibility of analysing even very weak bases in a correct way (see Results and Discusion, Fig. 15).

Quantitative aspects

As mentioned above, the composition of the terminating electrolyte strongly influences the qualitative parameters of the sample zones in the systems studied here. This fact has a strong impact on quantitative analysis.

The basic principle of quantitation in isotachophoresis is expressed by the known equation[2]

$$N_i = k_i Q_i \tag{19}$$

which expresses the proportionality between the amount N_i of a substance i and its

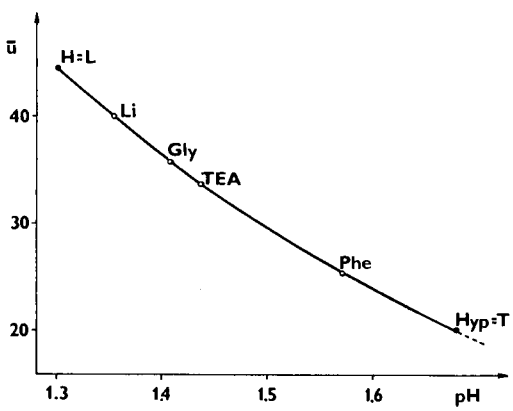

Fig. 8. Zone existence diagram, pH *vs.* $\bar{u}$ (in 10^{-9} m^2 V^{-1} s^{-1}), for the cationic system with 0.05 *M* HCl as the leading electrolyte and 0.02 *M* hydroxyproline + 0.06 *M* HCl as the terminator. Gly = glycine; TEA = tetraethylammonium; Phe = phenylalanine; Hyp = hydroxyproline. $u_{HypH} = 32 \cdot 10^{-9}$ m^2 V^{-1} s^{-1}; $u_{PheH} = 28 \cdot 10^{-9}$ m^2 V^{-1} s^{-1}; $u_{TEA} = 32.9 \cdot 10^{-9}$ m^2 V^{-1} s^{-1}; $u_{GlyH} = 40 \cdot 10^{-9}$ m^2 V^{-1} s^{-1}; $u_{Cl} = -79.1 \cdot 10^{-9}$ m^2 V^{-1} s^{-1}; $pK_{HypH} = 1.92$; $pK_{PheH} = 2.58$; $pK_{GlyH} = 2.35$.

zone-passage charge Q_i. The proportionality (calibration) constant for the given electrolyte system may be expressed by

$$k_i = \bar{c}_{i,i} \frac{|\bar{u}_{i,i}|}{\kappa_i} \tag{20}$$

When considering an acidic cationic system where a constant flow of H^+ passes through the sample zones, it is obvious from eqn. 19 that the higher the flow of H^+, the lower is k_i. An explicit description of the effect of H^+ may be given here by considering the simple example of the system in Fig. 5 with the assumption that all of the constituents involved are strong acids and bases. Then we may write the counter ion balance for zones B and X as

$$c_{A,B} \left(1 + \frac{|u_A|}{u_{BH}}\right) = c_{A,X} \left(1 + \frac{|u_A|}{u_{XH}}\right) \tag{21}$$

and the isotachophoretic condition for these zones is

$$\frac{u_{BH}}{\kappa_B} = \frac{u_{XH}}{\kappa_X} \tag{22}$$

By using the condition of electroneutrality and after rearrangement, eqns. 21 and 22 provide the following expression:

$$k_X = \frac{u_{XH} c_{X,X}}{\kappa_X} = \frac{1}{F} \cdot \frac{u_{XH}}{u_{XH} + |u_A|} \left(1 - \frac{u_H - u_{BH}}{u_H - u_{XH}} \cdot \frac{1}{1 + \frac{c_{BH,B}}{c_{H,B}} \cdot \frac{u_{BH} + |u_A|}{u_H + |u_A|}}\right) \tag{23}$$

showing that k_X is a function of $c_{H,B}/c_{BH,B} = c_{H,T}/c_{BH,T}$ (*cf.*, eqn. 6), *i.e.*, of the ratio of H^+ and BH^+ in the terminating zone. For $c_{H,T} = 0$ we obtain the constant $k_X = u_{XH}/F(u_{XH} + |u_A|)$. With increasing $c_{H,T}/c_{BH,T}$ the value of k_X decreases and becomes zero at $c_{H,T}/c_{BH,T} = (u_{BH} + |u_A|)(u_H - u_{XH})/(u_{XH} - u_{BH})(u_H + |u_A|)$.

Fig. 9 shows the calculated dependence of $1/k_X F$ on the pH of zone B for the system 0.01 *M* HCl (leading electrolyte), 0.01 *M* Tris + HCl (terminator). Curve a shows the dependence for a strong base ($u_{XH} = 55 \cdot 10^{-9}$ m^2 V^{-1} s^{-1}) and curve b an analogous dependence for a weak base ($u_{XH} = 35 \cdot 10^{-9}$ m^2 V^{-1} s^{-1}, p$K_{XH} = 6$); the end of the latter curve towards the alkaline region indicates the end of correct migration owing to insufficient protonation of base X.

EXPERIMENTAL

For all calculations, a PMD 85-2 microcomputer (Tesla, Piešťany, Czechoslovakia) was used.

Experiments were carried out using a CS isotachophoretic analyser (URVJT, Spišská Nová Ves, Czechoslovakia) equipped with one capillary (170 mm × 0.3 mm I.D.) and conductivity detection. Some experiments were carried out on a Shimadzu

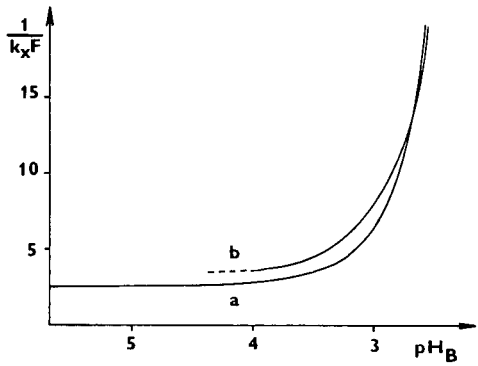

Fig. 9. Calculated dependence of $1/k_X F$ (reciprocal calibration constant) on pH_B of the adjusted terminating zone for a strong (curve a, $u_{XH} = 55 \cdot 10^{-9}$ m^2 V^{-1} s^{-1}, $pK_{XH} = 20$) and a weak (curve b, $u_{XH} = 35 \cdot 10^{-9}$ m^2 V^{-1} s^{-1}, $pK_{XH} = 6$) base in the system with 0.01 *M* HCl as the leading electrolyte and 0.01 *M* Tris [tris(hydroxymethyl)aminomethane] + HCl as the terminator. $u_{TrisH} = 30 \cdot 10^{-9}$ m^2 V^{-1} s^{-1}; $u_{Cl} = -79.1 \cdot 10^{-9}$ m^2 V^{-1} s^{-1}; $pK_{TrisH} = 8$.

IP-3A isotachophoretic analyser (Shimadzu, Kyoto, Japan) equipped with a separation (0.7 mm I.D.) and a detection (0.2 mm I.D.) tube, with potential gradient and UV-absorption (254 nm) detection. When performing experiments only in the detection capillary, the sample was pumped into the separation capillary and electric current was applied for some time. After stopping this electromigration sampling, the sample solution in the separation capillary was replaced with the terminating solution and the analysis was carried out.

An OP-208 Precision Digital pH meter (Radelkis, Budapest, Hungary) with glass and calomel electrodes served for pH measurements.

All chemicals were of analytical-reagent grade (Lachema, Brno, Czechoslovakia) and were dissolved in distilled water deionized with a mixed-bed ion exchanger.

RESULTS AND DISCUSSION

As stated under Theoretical, in systems with H^+ as the leading constituent, the composition of the terminating solution shows a strong influence on the migration behaviour and on all substantial parameters of zones migrating in front of it. For practical users of these systems, the impact of this fact on quantitative analysis is very important. Related to the *Quantitative aspects* section, Fig. 10A illustrates the influence of the pH of the terminator on the step lengths of Na^+ and K^+. The system used was 0.01 *M* HCl as the leading electrolyte and 0.01 *M* (0.1 *M*) Tris + HCl as the terminator. The results show good coincidence with the theory: with decreasing the pH of the terminator, the step lengths increase (*cf.*, Fig. 9, curve a). Fig. 10B shows a similar experimental dependence for a weak base (ε-aminocaproic acid) in the system with 0.005 *M* formic acid as the leading electrolyte and 0.005 *M* tetrabutylammonium hydroxide + formic acid as the terminator. Also here we can make a good comparison with Fig. 9 (curve b); it is seen that weak bases can be analysed only under conditions of sufficient protonation (at a sufficiently low pH value of the terminator). The point marked with an arrow in Fig. 10B indicates incorrect migration of the sample zone.

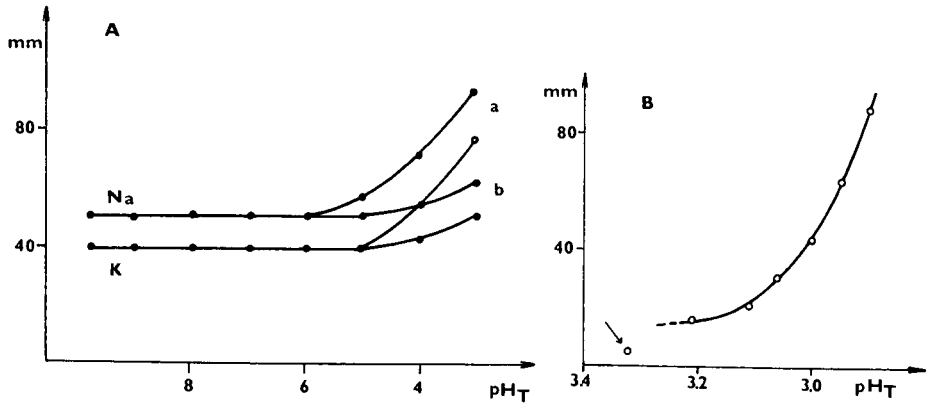

Fig. 10. (A) Experimental dependence of the step lengths of the zones of K^+ and Na^+ (25 μl of 0.0019 *M* KCl + 0.0017 *M* NaCl) on the pH_T of the terminator in the system with 0.01 *M* HCl as the leading electrolyte and (a) 0.01 *M* and (b) 0.1 *M* Tris + HCl as the terminator. (B) The same dependence for ε-aminocaproic acid (25 μl of 30 μM solution) in the system with 0.005 *M* formic acid as the leading electrolyte and 0.005 *M* tetrabutylammonium hydroxide + formic acid as the terminator. Both experiments were performed in the CS isotachophoretic analyser with a detection current *I* of (a) 250 μA and (b) 25 μA and a chart speed of 1 mm/s.

The prolongation of the zones at low pH of the terminator may apparently offer a means of increasing the sensitivity of the analysis; however, this is accompanied by an increase in the analysis time. Another important feature for practical applications is the impact of the terminating electrolyte on the reproducibility of the analysis. This can be ensured only if a constant composition of the terminator is provided during all analyses. If Cl^- is used as the counter ion, the reproducibility of analyses can be considerably decreased owing to the change in the composition of the terminator by the production of H^+ at the anode. Fig. 11 shows the variation of the zone lengths of Na^+ and K^+ in five consecutive analyses when the content of the terminating electrode chamber was not replaced with fresh electrolyte after each analysis. The prolongation of the zones caused by the increasing concentration of H^+ in the terminator is clearly

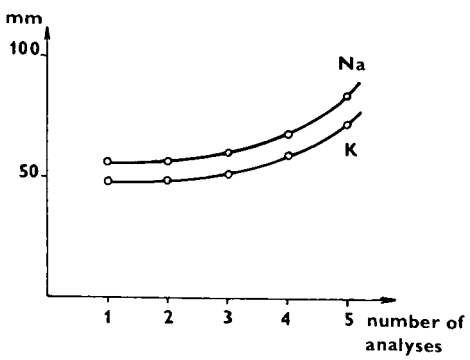

Fig. 11. Experimental dependence of the step lengths of the zones of K^+ and Na^+ (25 μl of 0.0019 *M* KCl and 0.0017 *M* NaCl) on the number of analyses (without refreshing the content of the terminating electrode chamber) in the system with 0.01 *M* HCl as the leading electrolyte and 0.01 *M* Tris + HCl (pH_T = 7) as the terminator. CS isotachophoretic analyser, *I* = 250 μA, chart speed 1 mm/s.

seen, indicating that the refilling of the terminating electrode chamber after each analysis is necessary. The original pH of the terminator, $pH_T = 7$, decreased to 3.8 after the fifth analysis, which caused a prolongation of the Na^+ zone by 46% (see Fig. 11). In a similar experiment an original value of $pH_T = 3.2$ decreased to 3.05 after the third analysis, resulting in a prolongation of the Na^+ zone by 35%.

A possible means of eliminating the negative effects of H^+ production at the anode is the use of a carboxylic acid instead of HCl in the terminating solution. Fig. 12 shows the record of an analysis of a relatively complex mixture of cations with 0.01 *M* HCl as the leading electrolyte and 0.01 *M* tetrabutylammonium hydroxide + acetic acid as the terminator at $pH_T = 4.9$. The system showed excellent reproducibility (repeatibility) without the need to refill the terminating electrode chamber after each analysis as acetate did not produce any H^+ at the anode.

Under *Description of the system*, the effects of the concentration of the leading zone on the migration behaviour were described and discussed (*cf.*, Fig. 4). The experimental evidence is given in Fig. 13, where the possibility of how we can change the role of the H^+ constituent from the leader to the terminator by only a change in concentration is exemplified. Fig. 13a shows the record of an analysis in a system with 0.015 *M* sodium formate as the leading electrolyte and 0.01 *M* formic acid as the terminator. In this system, the calculated value of the effective mobility of H^+ is $\bar{u}_{H,H} = 28.1 \cdot 10^{-9}\ m^2\ V^{-1}\ s^{-1}$ and H^+ thus acts as the terminator, also for Li^+ migrating as a sample zone. Fig. 13b shows the case where the concentrations were decreased by an order of magnitude. Here 0.0018 *M* formic acid serves as the leading zone as the calculated effective mobility of H^+ is $\bar{u}_{H,H} = 97.1 \cdot 10^{-9}\ m^2\ V^{-1}\ s^{-1}$. In this system sodium is the terminator and K^+ can be determined here without problems.

Under *Correct migration of sample zones*, the coexistence of normal and inverse systems of zones was predicted, resulting in a combined system with the potential to

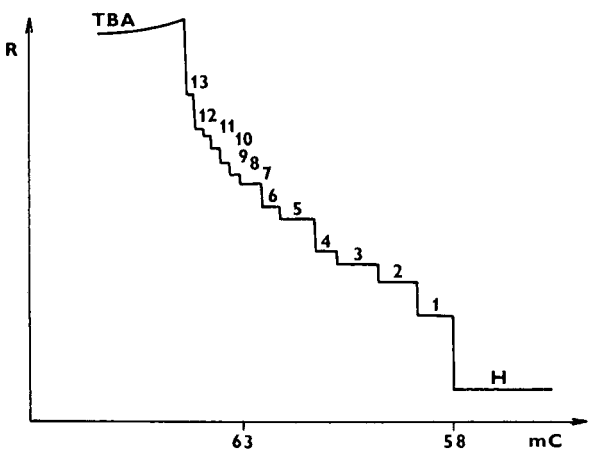

Fig. 12. Experimental record of an analysis in the system with 0.01 *M* HCl as the leading electrolyte and 0.01 *M* TBAOH + acetic acid ($pH_T = 4.9$) as the terminator. The sample was 1 μl of a solution containing *ca.* 0.5 m*M* of the following bases: (1) K^+, (2) Ca^{2+}, (3) Na^+, (4) pyridine, (5) piperidine, (6) lutidine, (7) ammediol, (7) collidine, (8) Tris, (9) ornitine, (9) histidine, (10) lysine, (10) citrulline, (11) ephedrine, (12) arginine and (13) procaine; steps 7, 9 and 10 on the record correspond to mixed zones. TBA = tetrabutylammonium; CS isotachophoretic analyser, $I = 50\ \mu A$, R = conductivity detection signal.

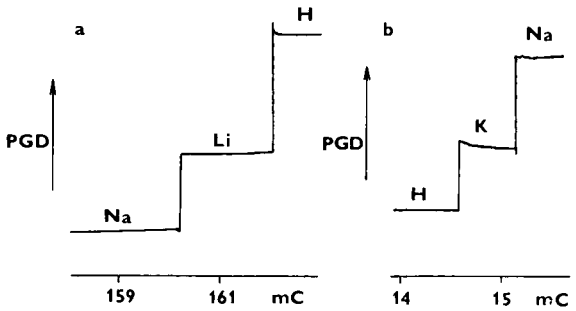

Fig. 13. (a) Isotachopherogram of 1 μl of 0.01 *M* $LiNO_3$ in the system with 0.015 *M* sodium formate as the leading electrolyte and 0.01 *M* formic acid as the terminator. Shimadzu IP-3A instrument, I = 300 μA (separation), 40 μA (detection). (b) Isotachophoregram of 0.1 μl of 0.015 *M* KCl in the system with 0.0018 *M* formic acid as the leading electrolyte and 0.0015 *M* sodium formate as the terminator. Shimadzu IP-3A instrument, I = 50 μA (separation), 5 μA (detection), PGD = potential gradient detection signal.

show the correct isotachophoretic migration and analysis of the zone of the H^+ constituent. Fig. 14 confirms this theoretical assumption by experiment; the leading electrolyte was 0.005 *M* ammonium formate + 0.0024 *M* formic acid and the terminating electrolyte was 0.0036 *M* lithium formate + 0.0024 *M* formic acid. Fig.14a shows a blank run; the small zone of H^+ on the record indicates that the

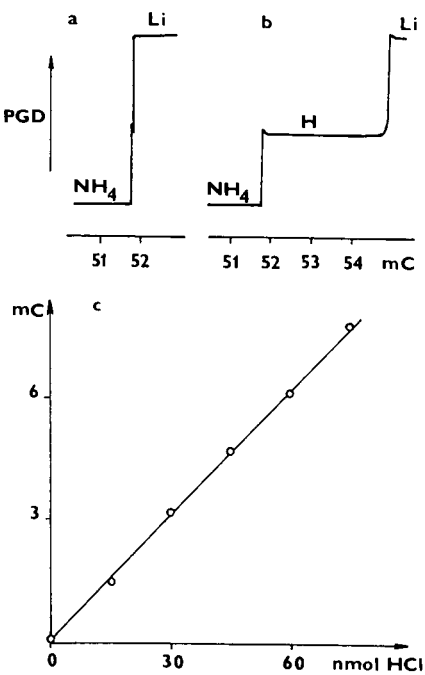

Fig. 14. (a, b) Isotachopherograms in the system with 0.005 *M* ammonium formate + 0.0024 *M* formic acid as the leading electrolyte and 0.0036 *M* lithium formate + 0.0024 *M* formic acid as the terminator. (a) Blank run; (b) 2 μl of 0.015 *M* HCl sampled (zone H). Shimadzu IP-3A instrument, I = 100 μA (separation), 25 μA (detection). (c) Calibration line for the above system and 0.015 *M* HCl as the sample in the range 0–5 μl.

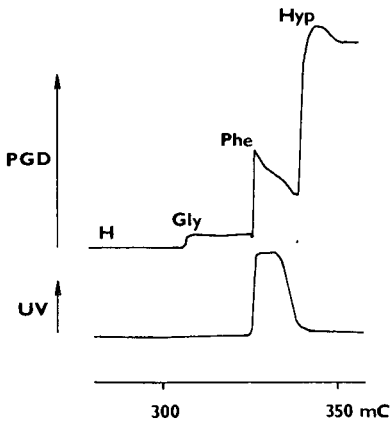

Fig. 15. Isotachopherogram of phenylalanine (Phe) and glycine (Gly) in the system with 0.05 *M* HCl as the leading electrolyte and 0.02 *M* hydroxyproline (Hyp) + 0.06 *M* HCl as the terminator. Shimadzu IP-3A instrument; the sample (0.01 *M* glycine, 0.02 *M* phenyalanine, 0.04 *M* HCl) was introduced electrically (20 μA for 1 min) into the detection capillary; $I = 100$ μA.

balance of the velocities of the $H^+ \rightarrow NH_4^+$ and $Li^+ \rightarrow H^+$ boundaries is nearly perfect. Fig. 14b shows the record of the analysis of 2 μl of 0.015 *M* HCl; the calibration line in Fig. 14c confirms the possibility of isotachophoretic determination of H^+.

An important practical aspect of the theory presented here is the possibility of constructing correct isotachophoretic systems working at very low pH (see last part of the section *Correct migration of sample zones* and Fig. 8). This opens the way to the protonation and analysis of even very weak bases. Fig. 15 shows the results for glycine ($pK_{XH} = 2.35$) and phenylalanine ($pK_{XH} = 2.58$) in the system with 0.05 *M* HCl as the leading electrolyte and 0.02 *M* hydroxyproline + 0.06 *M* HCl as the terminating solution. In accordance with theory (*cf.*, Fig. 8), correct migration of both sample zones is seen.

CONCLUSIONS

The fundamental feature of a correct isotachophoretic system is that the migration of H^+ (in cationic isotachophoresis) and/or OH^- (in anionic isotachophoresis) is fully controlled. This is achieved, from the classical point of view, by the selection of a suitable leading electrolyte with a suitable buffering counter ionic system which controls fully the effective mobility of H^+ and/or OH^- so that it forms the real or potential terminator of the whole system. In such a system the parameters of the terminating zone are also unambiguously controlled by the leading zone and the parameters of the terminating electrolyte itself (especially it pH) do not show any influence on the behaviour (parameters) of the sample zones.

It has been shown in this paper both theoretically and experimentally that inverse systems where H^+ (in cationic isotachophoresis) and OH^- (in anionic isotachophoresis) serve as the leading ions may show, under certain conditions, correct behaviour. In cationic isotachophoresis, *e.g.*, H^+ serves as the leading cation and the terminator is formed by a suitable cation (*e.g.*, organic base, B) the zone of which

contains also some amount of H^+. Thus, the velocity of the T → L boundary is a function of the composition of both the leading and terminating zones. As H^+ forms here its individual zone, the concepts of the H^+ constituent and of its effective mobility may be introduced; the actual value of the latter depends on the parameters of both the leading and terminating zones (*cf.*, eqn. 12).

By calculation of the effective mobility of the leading H^+ constituent and of the terminating constituent B, and also the pH values of their zones, one may decide for a given substance X whether it provides a correct isotachophoretic zone in the B → H system.

From a more detailed treatment of the theory of cationic systems with a weak acid as the counter ionic substance, it follows that from each combination of two arbitrary zones of "acid" (constituent H^+) and "base + acid" (constituent B), one can construct a correct isotachophoretic system. There remains only the question of which is the correct order of these two zones (*i.e.*, B as the terminator and H^+ as the leader or *vice versa*). This order can be established by the calculation of the parameters of both zones (as indicated under Theoretical), especially of the effective mobilities $\bar{u}_{H,H}$ and $\bar{u}_{B,H}$, and by their comparison according to conditions 14 and 15. The concentration level of the electrolyte system here plays an important role. The detailed study of both classical and inverse systems has revealed that a combined system may exist where H^+ can migrate and be determined as an individual zone constituent, *e.g.*, between the acidic zones of ammonium formate (leader) and lithium formate (terminator).

From the quantitative point of view, the systems in question show prolongation of the sample zones. This prolongation is the more pronounced the more acidic the terminator is. To achieve a good reproducibility of the analyses, the composition (pH) of the terminating solution should remain constant. This could be ensured by using fresh terminating electrolyte in the terminating electrode chamber after each analysis. To avoid the disturbing electrode reactions producing H^+ at the anode it is advisable to use acetate or formate instead of chloride for the preparation of the terminating solution.

The practical aspects of acidic systems with H^+ as the leading constituent consist not only in the possibility of determining very mobile ions (such as K^+ or NH_4^+) but, especially, in the potential to determine also very weak bases with pK_{XH} even lower than 2.

SYMBOLS

$c_{i,j}$	concentration of ion i in zone j;
$\bar{c}_{i,j}$	concentration of constituent i in zone j;
F	Faraday constant;
k_i	calibration constant of constituent i;
K_{HA}	dissociation constant of acid HA;
K_{BH}	dissociation constant of protonated base B;
L	leading zone, leading constituent;
N_i	amount of constituent i;
Q_i	zone passage charge of constituent i;
T	terminating zone, terminating constituent;
u_i	electrophoretic mobility of ion i;

$\bar{u}_{i,j}$ effective electrophoretic mobility of constituent i in zone j;
W_{B-H} rate of movement of boundary B → H (volume per charge);
κ_j conductivity of zone j;
:: stationary boundary;
→ moving boundary with indicated direction of movement.

REFERENCES

1 F. M. Everaerts, J. L. Beckers and Th. P. E. M. Verheggen, *Isotachophoresis—Theory, Instrumentation and Applications*, Elsevier, Amsterdam, Oxford, New York, 1976.
2 P. Boček, M. Deml, P. Gebauer and V. Dolník, *Analytical Isotachophoresis*, VCH, Weinheim, 1988.
3 R. J. Routs, *Thesis*, Technological University of Eindhoven, Eindhoven, 1971.
4 P. Boček, P. Gebauer and M. Deml, *J. Chromatogr.*, 217 (1981) 209.
5 P. Boček, P. Gebauer and M. Deml, *J. Chromatogr.*, 219 (1981) 21.
6 J. L. Beckers and F. M. Everaerts, *J. Chromatogr.*, 68 (1972) 207.
7 J. L. Beckers, *Thesis*, Technological University of Eindhoven, Eindhoven, 1973.
8 P. Boček and P. Gebauer, *Electrophoresis*, 5 (1984) 338.
9 J. Vacík and I. Muselasová, *J. Chromatogr.*, 320 (1985) 199.
10 S. Fanali, F. Foret and P. Boček, *Pharmazie*, 40 (1985) 653.
11 Z. Chmela, J. Čižmárik and Z. Stránský, *Collect. Czech. Chem. Commun.*, 51 (1986) 993.
12 L. G. Longsworth, J. Am. Chem. Soc., 67 (1945) 1109.
13 P. Gebauer and P. Boček, *J. Chromatogr.*, 267 (1983) 49.

Journal of Chromatography, 4700 (1989) 21–41
Elsevier Science Publishers B.V., Amsterdam — Printed in The Netherlands

CHROM. 21 212

SEPARATION PROCESS IN ISOTACHOPHORESIS

III. TRANSIENT STATE MODELS FOR A THREE-COMPONENT SYSTEM

TAKESHI HIROKAWA*, KIYOSHI NAKAHARA and YOSHIYUKI KISO
Applied Physics and Chemistry, Faculty of Engineering, Hiroshima University, Shitami, Saijo, Higashi-hiroshima 724 (Japan)

SUMMARY

The separation of a three-component mixture (4,5-dihydroxy-3-(*p*-sulphophenylazo)-2,7-naphthalenedisulphonic acid, monochloroacetic acid and picric acid) was measured by the use of a multichannel ultraviolet-photometric zone detector. Two theoretical models which previously applied to binary systems were extended to treat the transient state of a three-component system. The formulation and the computational procedure are described in detail. Good agreement was obtained between the observed and simulated boundary velocities and resolution time, confirming the validity of the models used. Especially, the slight sample pH dependence of the resolution time was successfully simulated by one of the models (modified sample property reflecting model). The decrease in the separation capacity in the three-component system in comparison with that in the binary system was explained by the difference in the boundary velocities caused by the different potential gradients of the mixed zones.

INTRODUCTION

In isotachophoresis it is known that the resolution times for two adjacent samples in the separation of a multi-component system are always larger than those when the equivalent two samples are separated independently. As far as we know, the transient state for a three component system has not yet been simulated and the cause of the above decrease in the separation efficiency with increasing number of components in a sample has not been elucidated theoretically.

In the previous paper[1], two transient state models were proposed for the analysis of binary systems. One is based on the transient state model proposed by Mikkers *et al.*[2,3]. In this model the resolution time depends on the pH of the sample solution (pH_S) besides the pH of the leading electrolyte, the mobility of the buffer used, the mobilities and pK_a of the sample components, the migration current, etc. Since this model is sample property reflecting, we will abbreviate it as the SPR model.

According to the SPR model, the agreement between the observed and simulated

0021-9673/89/$03.50

resolution time was very good in the case of a weak acid–weak acid system, however in the case of a strong acid–weak acid system the pH_S dependence was overestimated. It was concluded that the above overestimation of the pH_S dependence was caused by the pH of the injected sample solution being perturbed by the buffer ions from the leading electrolyte at the initial stage of migration[1]. Then the SPR model was modified by considering the pH perturbation (the modified SPR model, MSPR). According to the MSPR model, the pH of the injected solution interfacing with the transient mixed zone was not kept constant after the start of the electrophoretic process. The pH shifted to higher values in anionic analysis. The shift was large enough to decrease the pH_S dependence on the separation capacity of a strong acid–weak acid system. The discrepancy between the observed and the simulated resolution time was less than 10% when the MSPR model was used[1].

The other model proposed was based on the separation diagram suggested by Brouwer and Postema[4]. In this model the separation efficiency was not affected by pH_S (non-SPR model). It was concluded that the estimation by the non-SPR model was not valid exactly, however from the practical viewpoint it cannot be denied absolutely because the simulated and the observed t_{res} agreed within *ca.* 20% not only for a weak acid–strong acid system but also a strong acid–strong acid system.

In this paper the MSPR and non-SPR models developed for binary systems were extended to treat three-component systems. To examine the validity of these models, the transient state of the system 4,5-dihydroxy-3-(*p*-sulphophenylazo)-2,7-naphthalenedisulphonic acid (SPADNS)–monochloroacetic acid (MCA)–picric acid (PIC) was observed by the use of a multi-channel UV-photometric detector[5], and the observed resolution time and the boundary velocities were compared with the theoretical estimates. The cause of the decrease in the separation efficiency of the three-component system in comparison with that of the equivalent two-component system is discussed in detail.

THEORETICAL

Fig. 1 shows the separation diagram for a three-component mixture (I) of A, B and C. Three mixed zones ABC, AB and BC are formed in the separation process. The diagram is in accord with the separation diagram for a multi-component mixture reported by Brouwer and Postema[4]. The solid lines in Fig. 1 shows the separation process in the particular case that the zone length of the injected sample solution is equal to the whole zone length at the steady state. When the concentration is high for the equivalent sample, the separation process may follow, for example, the broken lines. It was assumed that the separation diagram when the distance of the boundaries from the position of sample injection, $D>=0$ does not depend on the sample concentration. It was revealed in the preceding paper[1] that this assumption is not strictly valid, but as already discussed it was useful as a first approximation. As revealed later, one of the practical utilities of the non-SPR model is that three mixed zones (ABC, AB and BC in Fig. 1) can be analyzed independently and therefore the time required for the iterative calculations to reach a self-consistent state is very short.

The distance, D, from the position of sample injection (the initial interface of the injected sample solution and the leading zone) was expressed as a linear function of

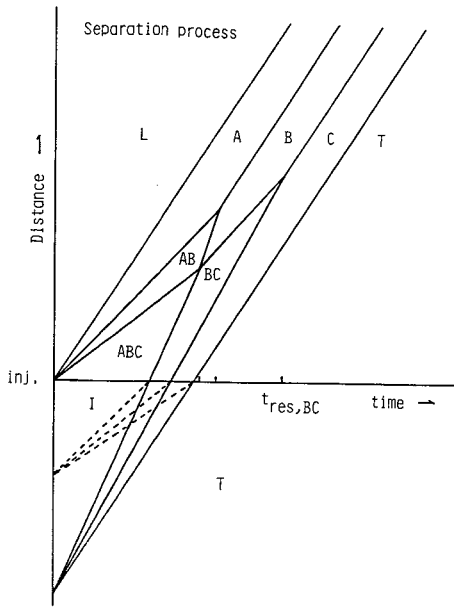

Fig. 1. Separation diagram for a three-component mixture in a separation tube. Distance = distance from injection port(inj.); time = migration time, I = zone of injected sample solution; L = leading zone; A, B and C = steady state zones; ABC, AB and BC = mixed zones; T = terminating zone and $t_{res,BC}$ = resolution time of zone BC.

time, t. We will call these linear functions the boundary functions. The separation diagram in Fig. 1 can be described by the following boundary functions

$$D_{L/A} = V_{IP}t \quad (1)$$
$$D_{A/B} = V_{IP}t - l_A \quad (2)$$
$$D_{B/C} = V_{IP}t - (l_A + l_B) \quad (3)$$
$$D_{C/T} = V_{IP}t - (l_A + l_B + l_C) \quad (4)$$
$$D_{A/AB} = V_{A/AB}t \quad (5)$$
$$D_{AB/B} = V_{AB/B}t - D_{0,AB/B} \quad (6)$$
$$D_{B/BC} = V_{B/BC}t - D_{0,B/BC} \quad (7)$$
$$D_{BC/C} = V_{BC/C}t - D_{0,BC/C} \quad (8)$$
$$D_{AB/ABC} = V_{AB/ABC}t \quad (9)$$
$$D_{ABC/BC} = V_{ABC/BC}t - (l_A + l_B + l_C) \quad (10)$$

where AB, BC and ABC denote the mixed zones, V_{IP} the isotachophoretic velocity, V the velocity of the boundary, D_0 the intercepts of the boundary function and l_A, l_B and l_C are the zone lengths of the components at the steady state, which vary in proportion to the sample amounts.

The velocities of the mixed zone boundaries can be derived from the moving boundary equation[6] as

$$V_{A/AB} = E_{AB}\bar{m}_{B,AB} \quad (11)$$
$$V_{AB/B} = E_{AB}\bar{m}_{A,AB} \quad (12)$$
$$V_{B/BC} = E_{BC}\bar{m}_{C,BC} \quad (13)$$
$$V_{BC/C} = E_{BC}\bar{m}_{B,BC} \quad (14)$$
$$V_{AB/ABC} = E_{ABC}\bar{m}_{C,ABC} \quad (15)$$
$$V_{ABC/BC} = E_{ABC}\bar{m}_{A,ABC} \quad (16)$$

where E denotes the potential gradient of the mixed zone and $\bar{m}$ the effective mobility of the sample components in the mixed zone, for example, $\bar{m}_{A,ABC}$ is the effective mobility of A in the mixed zone ABC.

Non-SPR model for three-component system

This model directly depends on the separation diagram shown in Fig. 1: the total amount of samples in the zone interposed by the boundaries L/A and C/T equals the injected amount, and is constant regardless of whether the separation process is at the transient state or at the steady state. It should be noted that both the non-SPR and the MSPR models utilize the effective mobilities of samples and the buffer, the concentration and the zone length at the steady state. These can be simulated exactly as reported previously[7,8].

Mixed zone ABC. Relationships between the sample concentrations of the steady state zones, $C^t_{A,S}$, $C^t_{B,S}$ and $C^t_{C,S}$, and those of the mixed zone ABC can be derived, which are closely related with t_{res}:

$$C^t_{A,ABC} = l_A/(l_A + l_B + l_C)C^t_{A,S} \quad (17)$$
$$C^t_{B,ABC} = l_B/(l_A + l_B + l_C)C^t_{B,S} \quad (18)$$
$$C^t_{C,ABC} = l_C/(l_A + l_B + l_C)C^t_{C,S} \quad (19)$$

The concentration of the buffer ion in the mixed zone ABC can be expressed as

$$C^t_{Q,ABC} = (l_A C^t_{Q,A} + l_B C^t_{Q,B} + l_C C^t_{Q,C})/(l_A + l_B + l_C) \quad (20)$$

where $C^t_{Q,A}$, $C^t_{Q,B}$ and $C^t_{Q,C}$ denote the buffer concentrations in the steady state zones, A, B and C.

On the other hand, resolution time of the mixed zone ABC is obtained by solving the simultaneous eqns. 9, 10, 15 and 16:

$$t_{res,ABC} = (l_A + l_B + l_C)/[E_{ABC}(m_{A,ABC} - m_{C,ABC})] \quad (21)$$

The iterative calculations to fulfil the electrophoretic conditions were as follows.

(1) l_A, l_B, l_C, $C^t_{A,S}$, $C^t_{B,S}$, $C^t_{C,S}$, $C^t_{Q,A}$, $C^t_{Q,B}$ and $C^t_{Q,C}$ were evaluated from the steady state analysis[7,8].

(2) The mobilities of the sample components A, B and C and the buffer ion Q were calculated on the basis of the dissociation constants and the pH of the mixed zone. In the first stage of iteration, the pH of the zone ABC(pH_{ABC}) was assumed equal to the pH of the leading electrolyte (pH_L). The correction for ionic strength was considered for the mobilities and acid dissociation constants throughout the present simulation.

(3) $C^t_{A,ABC}$, $C^t_{B,ABC}$ and $C^t_{C,ABC}$ were evaluated by use of eqns. 17–19. The partial concentrations of the component ions at pH_{ABC} were also calculated.

(4) $C^t_{Q,ABC}$ was calculated on the basis of the electroneutrality principle ($C^t_{Q,ABC} \equiv$ CTQ1).

(5) $C^t_{Q,ABC}$ was calculated by use of eqn. 20 ($\equiv$ CTQ2). The partial concentration of the buffer ion at pH_{ABC} was calculated from CTQ2.

(6) The specific conductivity of the mixed zone, κ_{ABC}, was calculated considering all ionic constituents.

(7) The potential gradient of the zone ABC(E_{ABC}) was calculated by the use of κ_{ABC} and the migration current.

(8) CTQ1 should be equal to CTQ2. The consistency was checked by use of the following RFC function:

$$RFC = (CTQ1/CTQ2) - 1 \tag{22}$$

Until RFC was considered as zero (actually we used a threshold value of 10^{-5}), steps 1–8 were repeated, varying the pH of the mixed zone. The right direction of the pH change was judged by the change of |RFC|.

Mixed zone AB. Instead of eqn. 20 for the mixed zone ABC, the total concentration of the buffer ion in the mixed zone, $C^t_{Q,AB}$, was calculated from the following equation derived from the moving boundary equation[6] for the boundary A/AB:

$$C^t_{Q,AB} = \frac{\bar{m}_{Q,A}E_A + \bar{m}_{B,AB}E_{AB}}{(\bar{m}_{Q,AB} + \bar{m}_{B,AB})E_{AB}} \cdot C^t_{Q,A} \tag{23}$$

The potential gradient, E_{AB}, was also derived from the moving boundary equation:

$$E_{AB} = \frac{\bar{m}_A C^t_A}{\bar{m}_{A,AB}C^t_{A,AB} + \bar{m}_{B,AB}(C^t_A - C^t_{A,AB})} \cdot E_A \tag{24}$$

The total concentrations of the components A and B can be expressed as follows by applying the moving boundary equation to the boundary AB/ABC:

$$C^t_{A,AB} = \frac{(\bar{m}_{A,ABC} - \bar{m}_{C,ABC})E_{ABC}}{\bar{m}_{A,AB}E_{AB} - \bar{m}_{C,ABC}E_{ABC}} \cdot C^t_{A,ABC} \tag{25}$$

$$C^t_{B,AB} = \frac{(\bar{m}_{B,ABC} - \bar{m}_{C,ABC})E_{ABC}}{\bar{m}_{B,AB}E_{AB} - \bar{m}_{C,ABC}E_{ABC}} \cdot C^t_{B,ABC} \tag{26}$$

The resolution time, $t_{res,AB}$, can be expressed as in the binary system using eqns. 2 and 5:

$$t_{res,AB} = l_A/(V_{IP} - V_{A/AB}) \tag{27}$$

The iterative calculations for the mixed zone AB were performed as follows.

(1) The mobilities of the sample components A, B and C and the buffer ion

Q were calculated on the basis of the dissociation constants and the pH of the mixed zone. In the first stage of iteration, the pH of the zone AB(pH_{AB}) was assumed equal to pH_{ABC}.

(2) $C^{t}_{Q,AB}$ was calculated by use of eqn. 23 ($\equiv$ CTQ3). The partial concentration of the buffer ion at pH_{AB} was calculated from CTQ3.

(3) The potential gradient of the zone AB(E_{AB}) was calculated by the use of eqn. 24.

(4) $C^{t}_{A,AB}$ and $C^{t}_{B,AB}$ were evaluated by use of eqns. 25 and 26. The partial concentrations of the component ions at pH_{AB} were also calculated.

(5) $C^{t}_{Q,AB}$ was calculated on the basis of the electroneutrality principle ($C^{t}_{Q,AB} \equiv$ CTQ4).

(6) CTQ3 should be equal to CTQ4. The consistency was checked by use of the following RFC function:

$$\mathrm{RFC} = (\mathrm{CTQ3}/\mathrm{CTQ4}) - 1 \tag{28}$$

Until RFC was considered as zero (actually we used a threshold value of 10^{-5}), steps 1–6 were repeated, varying the pH of the mixed zone.

Mixed zone BC. The moving boundary equation[6] was adopted for the boundary BC/C, the following expression for the total concentration of buffer being derived:

$$C^{t}_{Q,BC} = \frac{\bar{m}_{Q,C}E_C + \bar{m}_{B,BC}E_{BC}}{(\bar{m}_{Q,BC} + \bar{m}_{B,BC})E_{BC}} \cdot C^{t}_{Q,C} \tag{29}$$

The potential gradient, E_{BC}, is given by:

$$E_{BC} = \frac{\bar{m}_C E_C C^{t}_C}{\bar{m}_{C,BC}C^{t}_{C,BC} + \bar{m}_{B,BC}(C^{t}_C - C^{t}_{C,BC})} \tag{30}$$

The total concentration of the components B and C can be expressed as follows by applying the moving boundary equation to the boundary ABC/AB:

$$C^{t}_{B,BC} = \frac{(\bar{m}_{A,ABC} - \bar{m}_{B,ABC})E_{ABC}}{\bar{m}_{A,ABC}E_{ABC} - \bar{m}_{B,BC}E_{BC}} \cdot C^{t}_{B,ABC} \tag{31}$$

$$C^{t}_{C,BC} = \frac{(\bar{m}_{A,ABC} - \bar{m}_{C,ABC})E_{ABC}}{\bar{m}_{A,ABC}E_{ABC} - \bar{m}_{C,BC}E_{BC}} \cdot C^{t}_{C,ABC} \tag{32}$$

The resolution time, $t_{res,BC}$, may be expressed as follows:

$$t_{res,BC} = l_C/(V_{BC/C} - V_{IP}) \tag{33}$$

The iteration was carried as described for the mixed zone AB.

MSPR model for three-component system

This model does not utilize eqns. 17–20 to express the concentration of the zone constituents. Instead, the moving boundary equation[6] was adopted for the boundary between the injected sample solution and the mixed zone ABC on the assumption that the boundary is solvent-fixed. The formulation and the iterative calculation were somewhat complex, a more exact simulation was expected in comparison with the non-SPR model.

In the MSPR model, a zone (I*) of which the pH is different from the pH_S is considered between the injection position and the boundary moving with velocity $E_I m_{Q,I}$(E_I = the potential gradient of the injected solution and $m_{Q,I}$ the effective mobility of the buffer ion)[1]. The pH perturbation was caused by the counter ion from the leading electrolyte. On the assumption that the velocity of the boundary I*/ABC is zero, the concentration of the counter ions in the zone I*, $C^t_{Q,I}$*, can be written as follows from the continuity principle

$$C^t_{Q,I}{}^* = E_L \bar{m}_{Q,L} C^t_{Q,L} / E_I \bar{m}_{Q,I} + C^t_{Q,I} \tag{34}$$

where E_L denotes the potential gradient of the leading zone, $\bar{m}_{Q,L}$ the effective mobility of buffer ions in the leading zone and $C^t_{Q,L}$ and $C^t_{Q,I}$ the total concentration of buffer in the leading zone and in the initial sample solution respectively. Although the sample concentrations in the zone I* are equal to those of the injected sample solution, the potential gradient and effective mobilities are different from those in the injected solution.

Mixed zone ABC. On the assumption that the boundary I*/ABC is an ideal concentration boundary, namely the boundary velocity is zero, one can obtain the following equations to correlate the concentrations of the sample solution and those of the mixed zone

$$E_I{}^* \bar{m}_{A,I}{}^* C^t_{A,I}{}^* = E_{ABC} \bar{m}_{A,ABC} C^t_{A,ABC} \tag{35}$$

$$E_I{}^* \bar{m}_{B,I}{}^* C^t_{B,I}{}^* = E_{ABC} \bar{m}_{B,ABC} C^t_{B,ABC} \tag{36}$$

$$E_I{}^* \bar{m}_{C,I}{}^* C^t_{C,I}{}^* = E_{ABC} \bar{m}_{C,ABC} C^t_{C,ABC} \tag{37}$$

where E_I* is the potential gradient of the zone (I*) actually interfacing the mixed zone ABC, $\bar{m}_{A,I}$*,$\bar{m}_{B,I}$* and $\bar{m}_{C,I}$* the effective mobilities in the zone and $C^t_{A,I}$*, $C^t_{B,I}$* and $C^t_{C,I}$* the total concentrations in the zone. Hereafter I* is abbreviated as I for convenience. From these equations the ratios of the sample concentrations in the zone ABC can be expressed as:

$$\frac{C^t_{B,ABC}}{C^t_{A,ABC}} = \frac{\bar{m}_{A,ABC} \bar{m}_{B,I} C^t_{B,I}}{\bar{m}_{B,ABC} \bar{m}_{A,I} C^t_{A,I}} \equiv F_5 \tag{38}$$

$$\frac{C^t_{C,ABC}}{C^t_{A,ABC}} = \frac{\bar{m}_{A,ABC} \bar{m}_{C,I} C^t_{C,I}}{\bar{m}_{C,ABC} \bar{m}_{A,I} C^t_{A,I}} \equiv F_6 \tag{39}$$

From the electroneutrality relationship in the mixed zone, the concentrations of components A, B and C can be calculated

$$C^{t}_{A,ABC} = F_1/(F_2 + F_3F_5 + F_4F_6) \tag{40}$$

$$C^{t}_{B,ABC} = C^{t}_{A,ABC}F_5 \tag{41}$$

$$C^{t}_{C,ABC} = C^{t}_{A,ABC}F_6 \tag{42}$$

$$F_1 = -[C_H - C_{OH} + C^{t}_{Q,ABC}/(1 + k_Q/C_H)] \tag{43}$$

$$F_2 = \frac{\sum_{i=1}^{n_A}\left[z_{A,i}\left(\prod_i k_{A,i}\right)\Big/ C_H^i\right]}{1 + \sum_{i=1}^{n_A}\left(\prod_i k_{A,i}\right)\Big/ C_H^i} \tag{44}$$

$$F_3 = \frac{\sum_{i=1}^{n_B}\left[z_{B,i}\left(\prod_i k_{B,i}\right)\Big/ C_H^i\right]}{1 + \sum_{i=1}^{n_B}\left(\prod_i k_{B,i}\right)\Big/ C_H^i} \tag{45}$$

$$F_4 = \frac{\sum_{i=1}^{n_C}\left[z_{C,i}\left(\prod_i k_{C,i}\right)\Big/ C_H^i\right]}{1 + \sum_{i=1}^{n_C}\left(\prod_i k_{C,i}\right)\Big/ C_H^i} \tag{46}$$

where C_H and C_{OH} denote the concentration of H^+ and OH^-, $C^{t}_{Q,ABC}$ the total concentration of buffer in the zone ABC, k_Q, k_A, k_B and k_C the acid dissociation constants, $z_{A,i}$, $z_{B,i}$ and $z_{C,i}$ the ionic charge of the ith dissociated ion of the components A, B and C and n_A, n_B and n_C the numbers of the constituent ionic species. The monovalent cationic buffer was assumed in eqn. 43.

On the other hand, the following relationship is obtained between the buffer concentration of the mixed zone AB and that of the mixed zone ABC by applying the moving boundary equation to the boundary AB/ABC:

$$C^{t}_{Q,AB} = \frac{(\bar{m}_{C,ABC} + \bar{m}_{Q,ABC})E_{ABC}}{\bar{m}_{C,ABC}E_{ABC} + \bar{m}_{Q,AB}E_{AB}} \cdot C^{t}_{Q,ABC} \tag{47}$$

By combining eqns. 23 and 47, one obtains a relationship between the buffer concentration of the mixed zone ABC and that of the zone A at the steady state:

$$C^{t}_{Q,ABC} = \frac{(\bar{m}_{C,ABC}E_{ABC} + \bar{m}_{Q,AB}E_{AB})(\bar{m}_{Q,A}E_A + \bar{m}_{B,AB}E_{AB})}{(\bar{m}_{C,ABC} + \bar{m}_{Q,ABC})E_{ABC}(\bar{m}_{Q,AB} + \bar{m}_{B,AB})E_{AB}} \cdot C^{t}_{Q,A} \tag{48}$$

The potential gradient of the zone ABC(E_{ABC}) in eqn. 48 can be estimated by the following equations which correlate E_{ABC} and E_A:

$$E_{ABC} = \bar{m}_A C_A^t \bar{m}_{A,AB} C_{A,AB}^t E_A/(F_7 F_8) \tag{49}$$

$$F_7 = \bar{m}_{B,AB} C_A^t + (\bar{m}_{A,AB} - \bar{m}_{B,AB}) C_{A,AB}^t \tag{50}$$

$$F_8 = \bar{m}_{C,ABC} C_{A,AB}^t + (\bar{m}_{A,ABC} - \bar{m}_{C,ABC}) C_{A,ABC}^t \tag{51}$$

Eqns. 48 and 49 contain E_{AB}, $\bar{m}_{A,AB}$ and $\bar{m}_{B,AB}$ suggesting that the mixed zone ABC cannot be analyzed independently, in contrast to the non-SPR model.

Mixed zone AB. From eqns. 25 and 35, the concentration of component A of the mixed zone AB can be correlated with that of the injected solution. The concentration of component B can be correlated in a similar manner. Accordingly the ratio of the sample concentrations can be expressed as follows:

$$\frac{C_{B,AB}^t}{C_{A,AB}^t} = \frac{F_9 \bar{m}_{A,AB} \bar{m}_{B,I} C_{B,I}^t}{F_{10} \bar{m}_{B,AB} \bar{m}_{A,I} C_{A,I}^t} \tag{52}$$

$$F_9 = \frac{(\bar{m}_{C,ABC} - \bar{m}_{B,ABC})}{\bar{m}_{C,ABC} E_{ABC} - \bar{m}_{B,AB} E_{AB}} \tag{53}$$

$$F_{10} = \frac{(\bar{m}_{C,ABC} - \bar{m}_{A,ABC})}{\bar{m}_{C,ABC} E_{ABC} - \bar{m}_{A,AB} E_{AB}} \tag{54}$$

In case of the binary system, F_9 and F_{10} in eqn. 52 are unity. Eqn. 52 contains the effective mobilities of the components A, B and C in the zone ABC and the potential gradient. Thus the zones ABC and AB should be analyzed simultaneously. The buffer concentration and the potential gradient of the zone AB can be correlated with those of the zone A as shown in eqns. 23 and 24.

Mixed zone BC. From the moving boundary equations for boundary ABC/BC, the concentration ratio of the components B and C can be expressed as follows:

$$\frac{C_{C,BC}^t}{C_{B,BC}^t} = \frac{F_{11} C_{C,ABC}^t}{F_{12} C_{B,ABC}^t} \tag{55}$$

$$F_{11} = \frac{(\bar{m}_{C,ABC} - \bar{m}_{A,ABC}) E_{ABC}}{\bar{m}_{C,BC} E_{BC} - \bar{m}_{A,ABC} E_{ABC}} \tag{56}$$

$$F_{12} = \frac{(\bar{m}_{B,ABC} - \bar{m}_{A,ABC}) E_{ABC}}{\bar{m}_{B,BC} E_{BC} - \bar{m}_{A,ABC} E_{ABC}} \tag{57}$$

The concentration of buffer can be expressed as:

$$C_{Q,BC}^t = \frac{(\bar{m}_{Q,ABC} + \bar{m}_{A,ABC}) E_{ABC}}{\bar{m}_{Q,BC} E_{BC} + \bar{m}_{A,ABC} E_{ABC}} \cdot C_{Q,ABC}^t \tag{58}$$

The potential gradient, E_{BC}, is correlated with E_{ABC} as:

$$E_{BC} = \frac{(\bar{m}_{B,ABC} - \bar{m}_{A,ABC})C^{t}_{B,ABC} + \bar{m}_{A,ABC}C^{t}_{B,BC}}{C^{t}_{B,BC}\bar{m}_{B,BC}} \cdot E_{ABC} \tag{59}$$

Thus in the MSPR model, even if the sample amount is constant, the properties of the mixed zone (the pH, the total concentration of the constituents, the effective mobilities, the potential gradient) depend on the pH_S, therefore the resolution time depends on pH_S. This dependence is remarkable in that weak electrolytes are contained in the sample system.

As mentioned before, the properties of the mixed zones ABC, AB and BC are correlated with each other; they cannot be analyzed independently in contrast to the case of the non-SPR model. By the use of the present formulation, at least the zones ABC and AB can be treated at once. The iterative calculations to reach the self-consistent state using the above equations are as follows.

(1) l_A, l_B, l_C, $C^{t}_{A,S}$, $C^{t}_{B,S}$, $C^{t}_{C,S}$, $C^{t}_{Q,A}$, $C^{t}_{Q,B}$ and $C^{t}_{Q,C}$ were evaluated from the steady state analysis[7,8]. The pH, potential gradient, the effective mobilities in the zone I* were evaluated by iterative calculation so as to fulfil eqn. 34.

(2) The zone AB was analyzed using the MSPR model for a binary system to give appropriate initial values in the subsequent iterative calculation. This process is decisive for the smooth convergence of the iteration.

(3) The zone ABC was first treated. The effective mobilities of the sample components A, B and C and the buffer ion Q were calculated on the basis of the dissociation constants and the pH of the mixed zone. In the first stage of iteration, the pH of the zone ABC(pH_{ABC}) was assumed being equal to the averaged pH of the steady state zones.

(4) The potential gradient of the zone ABC(E_{ABC}) was calculated by the use of eqn. 49. In the first stage of the iteration, E_{AB} and the effective mobilities in the zone AB were those estimated in the above step (2).

(5) $C^{t}_{Q,ABC}$ was calculated by use of eqn. 48. The partial concentration of the buffer ion at pH_{ABC} was also calculated.

(6) $C^{t}_{A,ABC}$, $C^{t}_{B,ABC}$ and $C^{t}_{C,ABC}$ were evaluated from the electro neutrality relationship using eqns. 40–46. The partial concentrations of the component ions at pH_{ABC} were also calculated.

(7) The specific conductivity of the mixed zone, κ_{ABC}, was calculated considering all ionic constituents.

(8) The consistency of the current density was checked by use of the following RFQ function

$$RFQ_{ABC} = (E_{ABC}\kappa_{ABC}/E_L\kappa_L) - 1 \tag{60}$$

where E_L and κ_L denote the potential gradient and the specific conductivity of the leading zone. In the first stage of iteration RFQ_{ABC} was never zero, since E_{AB} and the effective mobilities in the zone AB were the assumed values. To decrease $|RFQ_{ABC}|$, more appropriate values were necessary.

(9) Then the zone AB was treated. The effective mobilities of the samples and the

buffer were calculated at the pH of the mixed zone (pH_{AB}). In the first stage of iteration, pH_{AB} was assumed equal to that estimated in step (2).

(10) The potential gradient, E_{AB}, was calculated by eqn. 24.

(11) $C^{t}_{Q,AB}$ was calculated by use of eqn. 23.

(12) $C^{t}_{A,AB}$ and $C^{t}_{B,AB}$ were evaluated from the electroneutrality relationship on the basis of the concentration ratio (eqn. 52).

(13) The specific conductivity of the mixed zone, κ_{AB}, was calculated considering all ionic constituents.

(14) The iterative calculation, steps (9)–(13), was carried until the following RFQ function was zero on varying pH_{AB}:

$$RFQ_{AB} = (E_{AB}\kappa_{AB}/E_{L}\kappa_{L}) - 1 \tag{61}$$

Unless the estimated properties of the zone ABC were extremely wrong, the iterative calculation converged within 30 cycles.

(15) After the convergence of RFQ_{AB}, the new values of E_{AB} and the effective mobilities were obtained. Using these values, steps (3)–(14) were repeated varying pH_{ABC} until $|RFQ_{ABC}|$ was less than 10^{-5}. When pH_{ABC} and pH_{AB} were determined, all properties of the zones ABC and AB were obtained simultaneously.

(16) Last, the zone BC was treated. The effective mobilities of the samples and the buffer were calculated at the pH of the mixed zone (pH_{BC}). In the first stage of iteration, pH_{BC} was assumed equal to pH_{AB}.

(17) The potential gradient, E_{BC}, was obtained by use of eqn. 59.

(18) $C^{t}_{Q,BC}$ was calculated by use of eqn. 58.

(19) $C^{t}_{B,BC}$ and $C^{t}_{C,BC}$ were evaluated from the electroneutrality relationship on the basis of the concentration ratio (eqn. 55).

(20) The specific conductivity of the mixed zone, κ_{BC}, was calculated considering all ionic constituents.

(21) The iterative calculation, steps (16)–(21), was carried out until the following RFQ function was regarded as zero upon varying pH_{BC}:

$$RFQ_{BC} = (E_{BC}\kappa_{BC}/E_{L}\kappa_{L}) - 1 \tag{62}$$

Thus all mixed zones were analyzed successfully. It should be noted that RFQ_{ABC} and RFQ_{AB} have to be zero simultaneously.

The resolution time of the mixed zone AB($t_{res,AB}$) can be expressed by eqn. 27. However, in the MSPR model, t_{res} of the mixed zones ABC and BC were not expressed by eqns. 21 and 33, because the equations were derived from the separation diagram in Fig. 1 on the assumptions that the intercepts of the boundary functions of ABC/BC, BC/C and C/T coincide with each other. Once $t_{res,AB}$ was evaluated, the boundary function of AB/B (eqn. 6) can be expressed as follows:

$$D_{AB/B} = \bar{m}_{A,AB}E_{AB}t - (\bar{m}_{A,AB} - \bar{m}_{B,AB})E_{AB}t_{res,AB} \tag{6'}$$

Using eqns. 6′ and 9, one can obtain $t_{res,ABC}$ without use of the above assumption as follows:

$$t_{res,ABC} = \frac{(\bar{m}_{B,AB} - \bar{m}_{A,AB})E_{AB}t_{res,AB}}{\bar{m}_{C,ABC}E_{ABC} - \bar{m}_{A,AB}E_{AB}} \tag{63}$$

Similarly, the boundary function of B/BC (eqn. 7) can be expressed using $t_{res,ABC}$ as follows:

$$D_{B/BC} = \bar{m}_{C,BC}E_{BC}t - (\bar{m}_{C,BC}E_{BC} - \bar{m}_{C,ABC}E_{ABC})t_{res,ABC} \tag{7'}$$

Then $t_{res,BC}$ can be defined as the time when the difference of the distances between eqn. 7' and eqn. 2 for the boundary A/B equals the steady state zone length, l_B:

$$t_{res,BC} = \frac{l_A + l_B + (\bar{m}_{C,ABC}E_{ABC} - \bar{m}_{C,BC}E_{BC})t_{res,ABC}}{V_{IP} - \bar{m}_{C,BC}E_{BC}} \tag{64}$$

The boundary functions of BC/C and ABC/BC can be expressed as follows:

$$D_{BC/C} = \bar{m}_{B,BC}E_{BC}t - [(\bar{m}_{B,BC} - \bar{m}_{C,BC})E_{BC}t_{res,BC} + \\ + (\bar{m}_{C,BC}E_{BC} - \bar{m}_{C,ABC}E_{ABC})t_{res,ABC}] \tag{8'}$$

$$D_{ABC/BC} = \bar{m}_{A,ABC}E_{ABC}t - (\bar{m}_{A,ABC} - \bar{m}_{C,ABC})E_{ABC}t_{res,ABC} \tag{10'}$$

Using the above formulation, a computer program SIPSR for the analysis of the transient state of the binary system[1] was modified to deal with the three-component system. The difference in the estimates between the non-SPR and the MSPR models is discussed in a later section.

EXPERIMENTAL

A 32-channel UV-photometric detector was used to observe the transient isotachopherogram[5]. The 32 photometric cells with photodiode detectors were arrayed along the separation tube at intervals of *ca.* 5 mm (16.6 cm/32 channels). Quartz optical fibres were used to pass UV light from a deuterium lamp to the tube. The UV light from each lamp was passed through an UV-glass filter (Toshiba Glass, Tokyo, Japan; Model D33S, λ_{max} = 330 nm). A single cycle to scan the 32 detectors required *ca.* 0.25 s, and the speed was sufficiently high to trace the variation of the zone lengths accurately. For the data acquisition, an NEC PC9801E microcomputer was used (Tokyo, Japan). The separating tube (polychlorofluoroethylene) was 0.51 mm I.D. and 1 mm O.D. All experiments were carried at 25°C.

The samples were SPADNS, MCA and PIC. Except for MCA, these samples absorb visible and UV light. The sodium salt of SPADNS was obtained from Dojin in the most pure form. The others were obtained from Tokyo Kasei (extra pure grade).

The concentration of the leading electrolyte (HCl) was 5 m*M*. The pH was adjusted to 3.6 by adding β-alanine. The terminator was 10 m*M* caproic acid. Hydroxypropylcellulose (HPC, 0.2%) was added to the leading and terminating electrolytes to suppress electroendosmosis. The viscosity of the 2% aqueous solution is 1000–4000 cps at 20°C according to the specification. The sample solution was injected

into the terminating electrolyte near the boundary between the leading and the terminating electrolytes. The pH of the terminating electrolyte was also adjusted by β-alanine to ensure the pH of the sample solution at the initial stage of migration was equal to the prepared value. The pH measurements were carried using a Model F7ss expanded pH meter (Horiba, Tokyo, Japan).

The data processing and the simulation were performed by the use of an NEC PC9801VX microcomputer.

RESULTS AND DISCUSSION

Under the electrolyte conditions used, the samples were detected in the order of SPADNS, MCA and PIC. The simulated effective mobilities, m, at the steady state were $47.7 \cdot 10^{-5}$, $35.1 \cdot 10^{-5}$, and $29.3 \cdot 10^{-5}$ cm^2 V^{-1} s^{-1}, and the R_E values ($R_E = \bar{m}_L/\bar{m}_S = E_S/E_L$, where E = the potential gradient and L and S are the leading and sample ions) were 1.59, 2.16 and 2.59 respectively. Table I shows the m_0 and pK_a values of the samples and electrolyte constituents used in the simulations.

The mobility and pK_a values of SPADNS were obtained by the isotachophoretic method. The pK_a value of the trivalent anion was rather high considering the chemical structure, suggesting that ion pairs might be formed between the β-alanine monocation and the SPADNS trianion. However, we treated them as free ions, because the simulated zone lengths and the R_E values agreed well with those observed.

Validity of the transient state models

At first the validity of the models was examined by comparing the observed resolution time with that observed. The sample was an equimolar (1.39 mM) mixture of SPADNS (S), MCA (M) and PIC (P). The pH values of the sample solution (pH$_S$) were 3 and 4.

Fig. 2 shows the evolution of the observed transient isotachopherograms of the SPADNS–MCA–PIC system. The number of data used for the evolution was 2600 (650 s). The pH$_S$ was 3 and the sample amounts were 11.1 (A), 16.7 (B) and 22.2 nmol (C) respectively. In Fig. 2, the boundaries between the leading and SPADNS zones

TABLE I

PHYSICO-CHEMICAL CONSTANTS USED IN SIMULATION (25°C)

m_0 = Absolute mobility (cm^2 V^{-1} s^{-1}) $\cdot 10^5$; pK_a = thermodynamic acid dissociation constant; assumed values being used for Cl$^-$, SPADNS$^-$ and SPADNS^{2-}.

Ions	m_0	pK_a
Cl$^-$	79.08	−2
β-Alanine$^+$	36.7[a]	3.552
SPADNS$^-$	21.0	−3
SPADNS^{2-}	42.0	−2
SPADNS^{3-}	63.0	3.55
Monochloroacetate$^-$	41.1[a]	2.865
Picrate$^-$	31.5	0.708

[a] The mobilities were obtained by our isotachophoretic method or conductivity measurement. The other mobilities and pK_a values are taken from ref. 9.

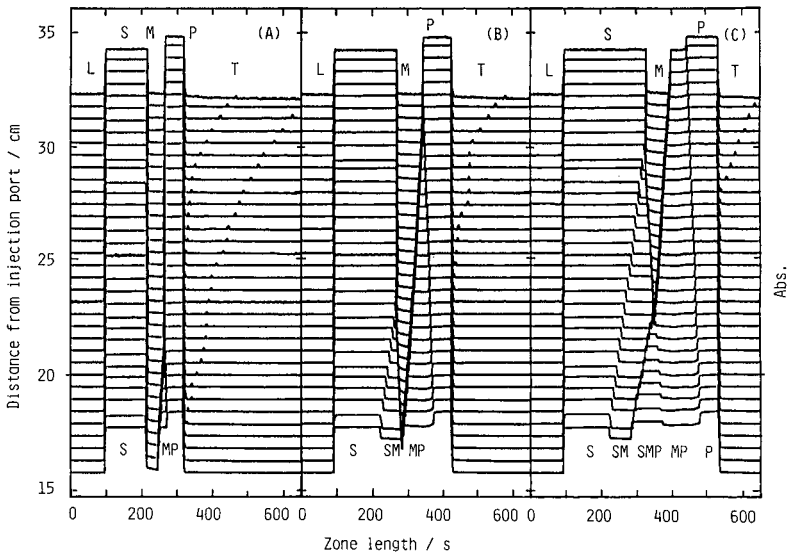

Fig. 2. Transient isotachopherogram of SPADNS(S), monochloroacetic acid (M) and picric acid (P) observed by the use of a 32-channel UV-photometric detector. The sample concentration was 1.39 m*M* and the pH was 3. The sample amounts were 11.1 (A), 16.7 (B) and 22.2 nmol (C), The positions of the baselines of the UV absorption show the distance of the photocell from the sample injection port. The migration current was 49.2 μA. The leading electrolyte was 5 m*M* HCl and the pH was adjusted to 3.6 (buffer: β-alanine). The terminator was 10 m*M* caproic acid.

have been rearranged at the same abscissa position to demonstrate clearly the change in the individual zone lengths at the transient state. The observed overall time-based zone lengths were 222.8, 332.4 and 439.8 s respectively. In Fig. 2A, the mixed zone observed was only that of MCA and PIC (MP). In Fig. 2B the SPADNS–MCA mixed zone (SM) was observed too, and in Fig. 2C the SPADNS–MCA–PIC mixed zone (SMP) was observed in addition to them. The cause of the small peaks in the terminating zone was not apparent.

In order to determine the boundary detection time and subsequently the boundary velocity, the observed UV signals in Fig. 2 were differentiated with respect to time. From the data number at the resultant positive and negative peaks and the sampling rate, the boundary detection time was obtained. The boundary functions were determined by the linear least-squares method on the basis of the boundary detection time and the exact position of each detector. The resolution time was obtained by solving simultaneous boundary equations. For example, the boundary functions of S/SM and SM/S were used to obtain $t_{res,SM}$. For the evaluation of $t_{res,SMP}$, the boundary functions for SM/M and M/MP were used together with those of SM/SMP and SMP/MP. They coincided within 10 s and the average was used for $t_{res,ABC}$. The probable error of the evaluated t_{res} was *ca.* 10 s.

Fig. 3 shows t_{res} *vs.* the time-based whole zone length at $pH_S = 3$ and 4 for the mixed zones SM, MP and SMP. Apparently $t_{res,MP}$ depended on pH_S. On the other hand, the pH_S dependence of $t_{res,SM}$ and $t_{res,SMP}$ was slight. The best-fitted linear functions were as follows:

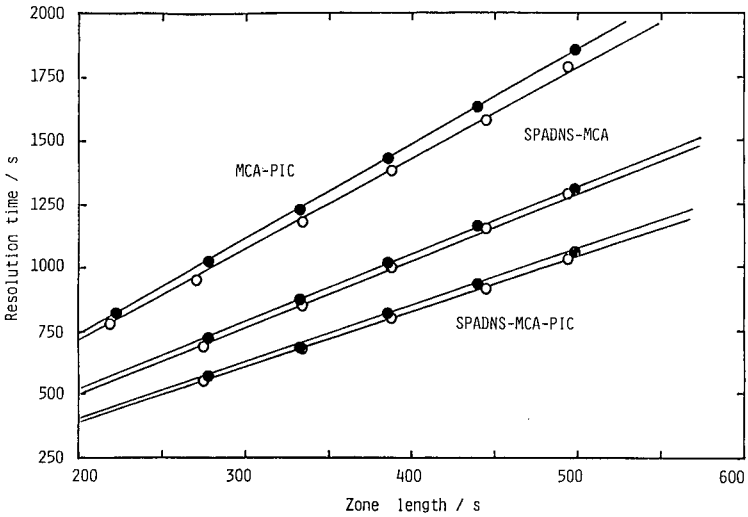

Fig. 3. The observed resolution time *vs.* the whole zone length in the SPADNS–monochloroacetic acid–picric acid system. pH_S 3 (⅛) and 4 (@). For the operating system, see Fig. 1. The sample amounts were 11.1, 13.9, 16.7, 19.5, 22.2 and 25.0 nmol, respectively.

$$\begin{array}{lll} \text{SMP} & t_{res} = 2.13\ t_{zone} - 8.7 & pH_S = 3.0 \\ & t_{res} = 2.08\ t_{zone} - 8.0 & pH_S = 4.0 \\ \text{SM} & t_{res} = 2.63\ t_{zone} - 2.7 & pH_S = 3.0 \\ & t_{res} = 2.60\ t_{zone} - 10.8 & pH_S = 4.0 \\ \text{MP} & t_{res} = 3.72\ t_{zone} - 4.7 & pH_S = 3.0 \\ & t_{res} = 3.59\ t_{zone} - 9.0 & pH_S = 4.0 \end{array} \tag{65}$$

where t_{zone} is the time-based zone length of the whole sample. The pH_S dependence of $t_{res,MP}$ was *ca.* 4% over the pH range studied.

Table II shows the observed and simulated resolution times and the separation numbers. For simulation, both the non-SPR and the MSPR models were used. The separation number, which correlates with the amount of sample separable per unit time, was defined as follows[2]:

$$S = \frac{F}{i} \cdot \frac{\partial n_A}{\partial t} = \frac{F}{i} \cdot \frac{n_A}{t_{res}} \tag{66}$$

where F is the Faraday constant, i the migration current and n_A the sample amount of constituent A. The slight pH dependence of $t_{res,MP}$ was simulated by the MSPR model. Good agreement between the observed and the simulated t_{res} was obtained, confirming the validity of this model. Although the observed small pH dependence was not simulated by the non-SPR model, the approximation used in this model is rather good because the discrepancy between the observed and the simulated t_{res} was small. Table III summarizes the pH_S dependence of the observed and simulated boundary velocities. The agreement was satisfactory.

In our previous work on the binary system MCA–PIC (1:1)[1], the separation

TABLE II

SIMULATED AND OBSERVED SEPARATION NUMBERS AND RESOLUTION TIMES FOR THE SPADNS–MONOCHLOROACETATE–PICRATE SYSTEM (1:1:1)

Operational system: leading electrolyte 5 m*M* HCl–β-alanine (pH 3.60); current 49.2 μA; diameter of the separation tube 0.51 mm; sample amount 25 nmol. *S* = Separation number, see text; t_{res} = resolution time; sim = simulated; obs = observed.

pH_S	*SMP*			*SM*			*MP*		
	sim		*obs.*[a]	*sim*		*obs.*	*sim*		*obs.*
	Non-SPR	*MSPR*		*Non-SPR*	*MSPR*		*Non-SPR*	*MSPR*	
Resolution time (s)									
3	1037	1040	1049	1258	1286 (1186)[b]	1304	1788	1808 (1367)	1843
4	–	1037	1025	–	1293 (1214)	1281	–	1765 (1279)	1774
Separation number									
3				0.0390	0.0381 (0.0413)	0.0377 ±0.0001	0.0274	0.0271 (0.0359)	0.0266 ±0.0001
4				–	0.0379 (0.0404)	0.0383 ±0.0003	–	0.0278 (0.0383)	0.0279 ±0.0004

[a] The probable error for t_{res} was *ca.* 10 s.

[b] The values in parentheses are the estimates when the simulation was carried out for the binary systems.

TABLE III

SIMULATED AND OBSERVED RELATIVE BOUNDARY VELOCITY AT pH_S = 3 AND 4

For the electrolyte systems, see Table II. V_R = relative boundary velocity, $V_{boundary}/V_{IP}$.

	V_R		
	Non-SPR	*MSPR*	*obs*
pH_S = 3			
SM/SMP	0.713	0.710	0.724 ± 0.002
SMP/MP	1.210	1.204	1.154 ± 0.004
S/SM	0.784	0.788	0.799 ± 0.003
SM/M	1.117	1.121	1.102 ± 0.012
M/MP	0.886	0.894	0.891 ± 0.002
MP/P	1.074	1.073	1.068 ± 0.005
pH_S = 4			
SM/SMP	0.713	0.708	0.720 ± 0.005
SMP/MP	1.210	1.201	1.150 ± 0.007
S/SM	0.784	0.790	0.795 ± 0.001
SM/M	1.117	1.122	1.101 ± 0.004
M/MP	0.886	0.890	0.881 ± 0.006
MP/P	1.074	1.068	1.053 ± 0.006

number decreased with decreasing pH_S. A similar tendency was found in the SPADNS–MCA–PIC system (1:1:1).

Table IV shows the simulated R_E values, effective mobilities and concentrations of the zone constituents of the SPADNS–MCA–PIC system at both the steady state and the transient state. The difference in these estimates between the models used was significant for the sample concentrations in the mixed zone.

Difference in separation capacity between the two- and three-component systems

The resolution time of adjacent samples in multi-component systems is larger than that of the binary system even if the amount of each component is the same. In this section the cause of this difference is discussed.

TABLE IV

SIMULATED R_E VALUES, EFFECTIVE MOBILITIES AND CONCENTRATIONS IN THE STEADY AND TRANSIENT ZONES OF THE SPADNS–MONOCHLOROACETATE–PICRATE SYSTEM AT pH_L = 3.6 (25°C)

R_E = Ratio of potential gradients, $E_{zone}/E_{leading}$; $\bar{m}_S$, $\bar{m}_M$ and $\bar{m}_P$ = effective mobilities of SPADNS(S), monochloroacetate (M) and picrate ions (P) ($cm^2\ V^{-1}\ s^{-1}$) · 10^5; pH = pH of zones at the steady and transient states; C_S^t, C_M^t and C_P^t = total concentrations of samples (m*M*); C_Q^t = total concentration (m*M*) of buffer (β-Ala); $\bar{m}_Q$ = effective mobility of buffer ($cm^2\ V^{-1}\ s^{-1}$) · 10^5; I = ionic strength · 10^3.

Zone	R_E	*pH*	$\bar{m}_S$	$\bar{m}_M$	$\bar{m}_P$	C_S^t	C_M^t	C_P^t	$\bar{m}_Q$	C_Q^t	I
Steady state zone											
S	1.597	3.721	47.5	–	–	1.500	–	–	14.3	9.07	7.66
M	2.153	3.820	–	35.2	–	–	3.669	–	12.6	8.69	3.32
P	2.574	3.840	–	–	29.5	–	–	3.096	12.3	8.33	3.09
Transient zones, three-component system Non-SPR model[a]											
SMP	1.875	3.771	48.9	34.4	28.9	0.791	0.791	0.791	13.4	8.79	5.57
SM	1.760	3.717	48.1	33.8	–	0.974	1.521	–	14.4	8.86	6.29
MP	2.282	3.877	–	35.7	29.5	–	2.095	1.215	11.6	8.96	3.13
MSPR model[a] pH_S = *3*											
SMP	1.868	3.769	48.9	34.4	28.8	0.793	0.785	0.813	13.5	8.81	5.59
SM	1.752	3.756	48.5	34.2	–	0.954	1.353	–	13.7	8.94	6.10
MP	2.305	3.827	–	35.3	29.4	–	2.140	1.295	12.5	8.55	3.24
MSPR model[a] pH_S = *4*											
SMP	1.862	3.768	48.9	34.4	28.8	0.797	0.828	0.767	13.5	8.82	5.60
SM	1.754	3.756	48.6	34.2	–	0.948	1.368	–	13.7	8.94	6.08
MP	2.295	3.826	–	35.3	29.4	–	2.232	1.218	12.5	8.56	3.24
Transient zones, two-component system Non-SPR model[a]											
SM	1.716	3.748	48.3	34.0	–	1.070	1.070	–	13.8	8.97	6.43
MP	2.360	3.830	–	35.3	29.4	–	1.679	1.679	12.4	8.50	3.20
MSPR model[a] pH_S = *3*											
SM	1.718	3.749	48.3	34.1	–	1.063	1.087	–	13.8	8.97	6.41
MP	2.368	3.830	–	35.3	29.4	–	1.617	1.731	12.4	8.49	3.20
MSPR model[a] pH_S = *4*											
SM	1.728	3.751	48.4	34.1	–	1.030	1.167	–	13.8	8.96	6.32
MP	2.353	3.830	–	35.3	29.4	–	1.741	1.626	12.4	8.50	3.21

[a] For the definitions of the transient state models, see text.

The equimolar SPADNS–MCA–PIC, SPADNS–MCA and MCA–PIC systems were analyzed by the MSPR model. The sample amount was 25 nmol, the leading electrolyte was 5 m*M* HCl buffered by β-alanine (pH 3.6), the capillary diameter was 0.5 mm and the migration current was 50 μA. Fig. 4 shows the pH_S dependence of the sample concentration in the mixed zones simulated by the MSPR model (A = SPADNS–MCA–PIC, B = SPADNS–MCA and C = MCA–PIC). Mixed zones with the same constituents are formed in the two- and three-component systems. To distinguish, for example, the SPADNS–MCA mixed zone formed in the three-component system from that formed in the two-component system, the former was abbreviated as SM(3) and the latter as SM(2). From Fig. 4B and C, the concentrations of the sample constituents in the mixed zones SM(2) and MP(2) were similar to each other when the samples were equimolar. In the SMP zone, the concentrations of the sample constituents were also very similar. On the other hand, a remarkable difference was found between the concentrations of SPADNS and MCA in the SM(3) zone. A similar situation was found for the concentrations of MCA and PIC in the MP(3) zone. The concentrations of the individual samples in the SM(2) and MP(2) zones were split into lower and higher values in the SM(3) and MP(3) zones. It should be noted that the abundance of the more mobile component SPADNS in the SM(3) zone is smaller than that in the SM(2) zone, and the abundance of the more mobile component MCA in the MP(3) zone is larger than that in the SM(2) zone. This phenomena was decisive in elucidating the decrease in the separation capacity in the three-component system. We call this the concentration splitting hereafter.

Fig. 5A shows the pH_S dependence of the R_E values ($E_{\text{mixed zones}}/E_{\text{leading zone}}$) of the mixed zones simulated by the MSPR model. From Fig. 5A the following relationship among the potential gradients, E, of the mixed zones is valid:

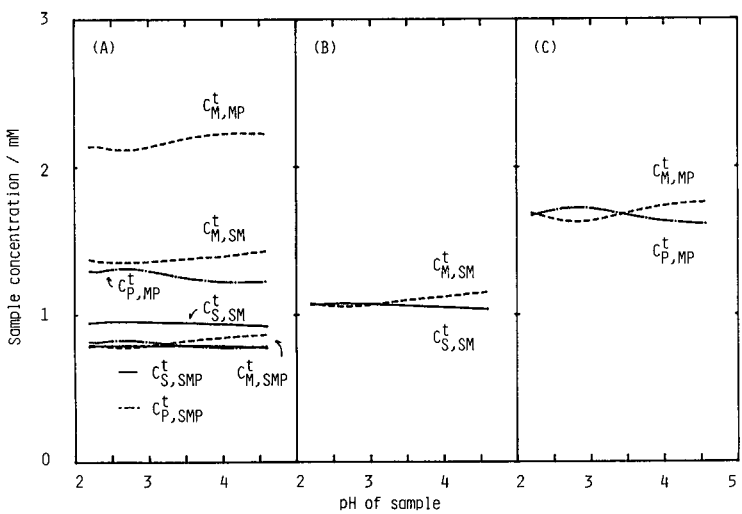

Fig. 4. The pH_S dependence of the sample concentration in the mixed zones simulated by the MSPR model. (A) SPADNS–MCA–PIC equimolar system, (B) SPADNS–MCA equimolar system, (C) MCA–PIC equimolar system. C^t = Total concentration of the sample. The subscripts SMP, SM and MP represent the mixed zones of SPADNS–MCA–PIC, SPADNS–MCA and MCA–PIC. For the operating system, see Fig. 1. The migration current was 50 μA and the I.D. of the separating tube was 0.5 mm.

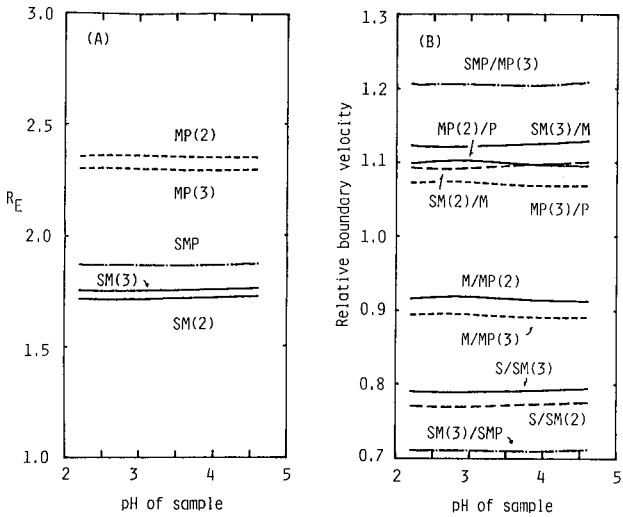

Fig. 5. (A) The pH_S dependence of the R_E values of the mixed zones formed in the SPADNS–MCA–PIC, SPADNS–MCA and MCA–PIC equimolar systems. (B) The pH_S dependence of the relative boundary velocities (boundary velocity/isotachophoretic velocity). Figures in parentheses show the number of components in the sample solution. For the operating system, see Fig. 1. The migration current was 50 μA and the I.D. of the separating tube was 0.5 mm.

$$E_{SM(2)} < E_{SM(3)} \tag{67}$$

$$E_{MP(3)} < E_{MP(2)}$$

Since the pH values of the mixed zones of SM(2) and SM(3) as well as of the MP(2) and MP(3) zones were very similar, the main cause of the above relationship was attributed to the concentration splitting.

Fig. 5B shows the pH_S dependence of the relative boundary velocities, $V_{boundary}/V_{IP}$. The boundary velocities were expressed by eqns. 11–16. From Fig. 5B, the following relationship is valid:

$$V_{R,S/SM(2)} < V_{R,S/SM(3)} < 1 < V_{R,SM(2)/M} < V_{R,SM(3)/M}$$
$$V_{R,M/MP(3)} < V_{R,M/MP(2)} < 1 < V_{R,MP(3)/P} < V_{R,MP(2)/P} \tag{68}$$

From the above relationship and eqns. 27 and 33 for $t_{res,SM}$ and $t_{res,MP}$, one can easily estimate the following result:

$$t_{res,SM(2)} < t_{res,SM(3)} \tag{69}$$

$$t_{res,MP(2)} < t_{res,MP(3)}$$

The $t_{res,MP(3)}$ should be evaluated by the use of eqn. 64, however, the use of the approximation of eqn. 33 is more straightforward for the present situation.

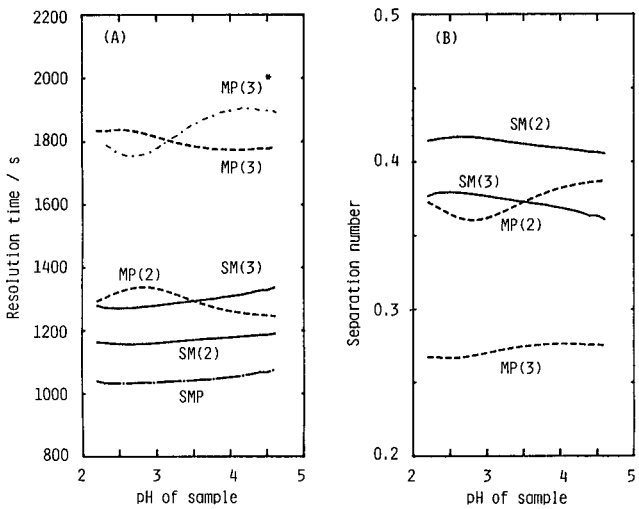

Fig. 6. The pH_S dependence of t_{res} (A) and the separation number (B) in the SPADNS–MCA–PIC, SPADNS–MCA and MCA–PIC equimolar systems. For the operating system, see Fig. 1. The migration current was 50 μA and the I.D. of the separating tube was 0.5 mm.

Fig. 6A and B show the pH_S dependence of t_{res} and the separation number (eqn. 66) simulated by the MSPR model. The relationships 69 were valid. In Fig. 6A, $t_{res,MP(3)}{}^*$ was evaluated by use of eqn. 33. Apparently, the pH_S dependence of $t_{res,MP(3)}{}^*$ was in conflict with observation, suggesting that the approximation of the non-SPR approach is not accurate.

Thus the separation process of the three-component system and the decrease in the separation capacity in comparison with the binary system was elucidated exactly by the MSPR model. Although the pH_S dependence was simulated only by the MSPR model, at least for the present samples, the non-SPR model was useful for the approximate evaluation of t_{res}.

As described, the iteration calculations in the MSPR approach to the self-consistent state were rather complex, and time-consuming. The time needed for the non-SPR approach for the analysis of the present three-component system was 11 s by the use of microcomputers equipped with a CPU i80286 (clock 8 MHz; part of the calculation was performed with a coprocessor i80287). However, it took 80 s when the MSPR model was used. Beside the transient state simulation, it took 15 s for the steady state analysis. The selective use of these models may be adequate for the purpose of the simulation.

ACKNOWLEDGEMENTS

One of the authors (T.H.) thank the Ministry of Education, Science, and Culture of Japan for support of part of this work under a Grant-in-Aid for Scientific Research (No. 61540423).

REFERENCES

1 T. Hirokawa, K. Nakahara and Y. Kiso, *J. Chromatogr.*, 463 (1989) 51.
2 F. E. P. Mikkers, F. M. Everaerts and J. A. F. Peek, *J. Chromatogr.*, 168 (1979) 293.
3 F. E. P. Mikkers, F. M. Everaerts and J. A. F. Peek, *J. Chromatogr.*, 168 (1979) 317.
4 G. Brouwer and G. A. Postema, *J. Electrochem. Soc.*, 117 (1970) 874.
5 T. Hirokawa, K. Nakahara and Y. Kiso, *J. Chromatogr.*, 463 (1989) 39.
6 R. A. Alberty, *J. Am. Chem. Soc.*, 72 (1950) 2361.
7 F. M. Everaerts, J. L. Beckers and Th. P. E. M. Verheggen, *Isotachophoresis*, Elsevier, Amsterdam, 1976.
8 T. Hirokawa, M. Nishino, N. Aoki, Y. Kiso, Y. Sawamoto, T. Yagi and J.-I. Akiyama, *J. Chromatogr.*, 271 (1983) D1.
9 R. A. Robinson and R. H. Stokes, *Electrolyte Solutions*, Butterworths, London, 1959.

Journal of Chromatography, 470 (1989) 43–55
Elsevier Science Publishers B.V., Amsterdam — Printed in The Netherlands

CHROM. 21 264

GENERATION OF OPERATIONAL ELECTROLYTES FOR ISOTACHOPHORESIS AND CAPILLARY ZONE ELECTROPHORESIS IN A THREE-POLE COLUMN

J. POSPÍCHAL, M. DEML, P. GEBAUER and P. BOČEK*
Institute of Analytical Chemistry, Czechoslovak Academy of Sciences, CS-611 42 Brno (Czechoslovakia)

SUMMARY

A new method has been developed for controlling the composition of the operational electrolytes directly in the separation capillary in isotachophoresis or capillary zone electrophoresis. The method is based on feeding the capillary with two different suitable ionic species from two separate electrode chambers by simultaneous electromigration. The composition and pH of the electrolyte in the separation capillary is thus controlled by setting the ratio of two electric currents. The theory has been developed and verified experimentally to predict both the electrolyte composition in the separation capillary and the time necessary to change this composition in the required way. Some of the possible ionic matrices realizable in the three-pole arrangement have been studied experimentally and used in isotachophoretic experiments. The technique described does not require moving parts in the instrumentation and provides the possibility to make very fine changes of pH in the capillary in a reproducible and easy way. The procedure itself is feasible for automation.

INTRODUCTION

In the analysis of real samples in capillary isotachophoresis (ITP) or zone electrophoresis (CZE) it is necessary to choose a convenient electrolyte[1]. There are two ways of doing this.

If the ionic mobilities and pK values of the substances to be separated are known, we can use a computing procedure[2]; if not, experiments must be done to create an ionic matrix in the separation column which ensures sufficient differences in the effective mobilities of the substances to be separated. All ions in the electrophoretic column move, and therefore the ionic matrix consists of coions and counter ions flowing between the electrode chambers through the separation column; the composition of this matrix depends on the composition of the electrolytes in these chambers. Commonly, only two electrode chambers are used and the ionic matrix can be changed only by altering the composition of the electrolyte in these chambers. In practice, when looking for a suitable electrolyte system, laborious and material-consuming wet chemistry procedures are performed, *e.g.*, preparation of new electrolytes, rinsing, filling until a successful separation is obtained or optimized.

0021-9673/89/$03.50

The essence of this paper is to describe a new procedure for the above mentioned purposes, where the required ionic matrix is created directly in the separation column by electrophoretic means. Here, each ionic species creating the ionic matrix is fed into the separation column by electromigration from its individual electrode (pole) chamber and the flow of each ionic species can be regulated electrically by controlling the magnitude of the current passing through each electrode chamber (each pole). This paper develops the necessary theory for calculation of the operational electrolyte composition, the description of suitable equipment for this procedure[3] and some model examples of its utilization.

THEORETICAL

The effective mobility of an ion is affected by all ions in its surroundings which may be called the ionic matrix. An important role in this ionic matrix is played by the solvolytic ions H^+ and OH^- which dramatically change the effective mobilities of weak acids and bases. In an electrophoretic column, when an electric field is applied, each ionic species migrates in the direction determined by its net charge and creates a flow of ions. These flows then create an ionic matrix around an individual ion, see Fig. 1. It is evident that the ionic matrix can be altered by changing these flows.

An electrode chamber filled with a working electrolyte represents a source of such a flow of ions. If an electrode of given polarity, *e.g.*, + is immersed in a working electrolyte containing a mixture of a common (G) and a solvolytic (S) ion of the same polarity, *e.g.*, Na^+ and H^+ the concentrations of which are c_G and c_S (see Fig. 2), then the respective electrode chamber produces flows of both ions, J_G and J_S. Their magnitude is proportional to the magnitude of the input electric current, I, passing through the electrode

$$J_i = Iu_i c_i/\kappa \qquad (\text{mol s}^{-1}) \tag{1}$$

where i = G or S, u_i is the electrophoretic mobility of ion i and κ is the conductivity of the electrolyte. For the ratio of both flows we may write:

$$\frac{J_S}{J_G} = \frac{c_S u_S}{c_G u_G} = \frac{c_S}{c_G} \cdot \text{constant} \tag{2}$$

It is obvious that in the commonly used two-pole arrangement (one cathode and one anode), the ratio of the flows of ions S and G in the ionic matrix can be changed only by an exchange of the working electrolyte in the respective electrode chamber, *i.e.*, by change of the ratio c_S/c_G.

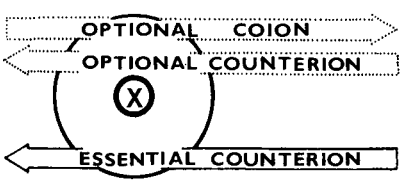

Fig. 1. Scheme of flows of ions forming the ionic matrix surrounding the analyzed ion X.

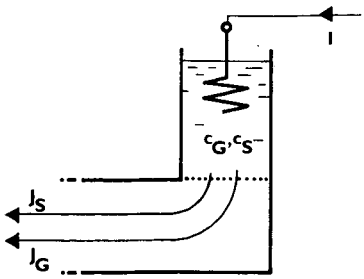

Fig. 2. Electrode chamber containing ions S and G of concentrations c_S and c_G, respectively, as a source of flow (J_S, J_G) of these ions.

The method suggested here allows the flows of ions of the same sign to be changed continuously and independently of those of the others. The electrode chamber serves again as the source of the flow of the ions. In this case, however, each electrode chamber contains only one cation and one anion, *i.e.*, there must be more than one electrode chamber for poles of the same sign. Each such chamber generates a flow of one kind of ions which is directly proportional to the magnitude of the electric current through the corresponding immersed electrode.

Assuming that the electrode chamber contains only one binary strong electrolyte, we may introduce the transference number, t_i, into eqn. 1 and write

$$J_i = I_i t_i / z_i F \tag{3}$$

where I_i is the electric current passing through the electrode in the chamber with ion i, z_i is the charge number of ion i and F is the Faraday constant. When neglecting the influence of ionic strength on t_i (within a limited concentration range), we may conclude from eqn. 3 that the flow of ions i is independent of their concentration in the electrode chamber.

A pair of electrode chambers of the same polarity which contain ions S and G and through which pass electric currents I_S and I_G produces ionic flows J_S and J_G (see Fig. 3) for which its holds that:

$$\frac{J_S}{J_G} = \frac{I_S \kappa_G c_S u_S}{I_G \kappa_S c_G u_G} = \frac{I_S}{I_G} \cdot k_1 \tag{4}$$

where k_1 in a proportionality constant. From this it follows that the ratio of the flows of the two ionic species S and G is directly proportional to the ratio of the respective electric currents.

In the case of the common ion G belonging to a uni-univalent weak electrolyte we must take into account that its solution contains also the solvolytic ion S of the same sign. The flow of this ion from electrode chamber G must be introduced into eqn. 4

$$\frac{J_S}{J_G} = \frac{I_S \kappa_G c_S u_S}{I_G \kappa_S c_G u_G} + \frac{c_{S,G} u_S}{c_G u_G} = \frac{I_S}{I_G} \cdot k_1 + k_2 \tag{5}$$

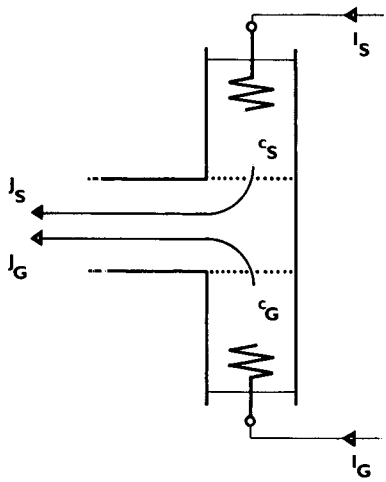

Fig. 3. Simultaneous control of the flow of two ions S and G by using two separate electrode chambers, each containing only one of these ions, by means of input electric currents I_S and I_G of the electrodes.

where $c_{S,G}$ is the concentration of ion S in chamber G and k_2 is an additive constant. The resulting ratio of flows depends on the ratio of the electric currents through both electrodes and its constant part depends also on the composition of the electrolyte in chamber G.

If a pair of electrode chambers of the described type (of the same polarity) are connected to a separation column filled with an electrolyte containing, *e.g.*, ion S, then we may call the electrode chamber which contains ion G the modifying electrode chamber. In comparison with the normal two-pole arrangement, the modifying chamber represents an addition which allows modification of the original electrolyte in the column. In the above example, *e.g.*, the original electrolyte containing ion S is modified to another one which contains a mixture of ions S and G. If, in the given analytical arrangement, the ions S and G are counter ions, then naturally the modifying electrode must be connected to the detection side of the separation column (see also Fig. 4). If the modification is performed by means of a coion, then the modifying electrode chamber is connected to the sampling side of the column. After switching on the electric current, a new zone of the modified electrolyte starts to be formed at the point of connection of the two electrode chambers to the column. This zone is displaced into the separation column and thus the modification of the original electrolyte proceeds. Let us call the original and modified electrolytes the primary and secondary ones, respectively.

In order to use the above arrangement for electrolyte modification successfully in practice, two things must be known, *viz.*, the composition of the resulting secondary electrolyte and the migration velocity of the boundary between the primary and the secondary electrolytes through the separation column.

Obviously the ratio of the ionic flows from the two electrode chambers equals the ratio of the flows in the zone, Z formed. In analogy with eqn. 2 we may write:

$$\frac{J_S}{J_G} = \frac{J_{S,Z}}{J_{G,Z}} = \frac{c_{S,Z}u_S}{c_{G,Z}u_G} \tag{6}$$

By combination of eqns. 5 and 6 we obtain

$$\frac{J_{S,Z}}{J_{G,Z}} = \frac{c_{S,Z}}{c_{G,Z}} \cdot \frac{u_S}{u_G} = \frac{I_S}{I_G} \cdot k_1 + k_2 \tag{7}$$

which shows how the ratio of concentrations of both ions in the secondary electrolyte, $c_{S,Z}/c_{G,Z}$, depends on the ratio of the electric currents passing through both electrodes, I_S/I_G.

The velocity of generation of the secondary electrolyte in the separation column is an important parameter describing the velocity of displacement of the zone formed. For the calculation of this quantity, W_Z (expressed in $m^3\ C^{-1}$), the moving boundary equation[4] may be used, *e.g.*, for substance S (ion constituent S) in the form

$$W_Z = \left(\frac{c_{S,A} u_S}{\kappa_A} - \frac{c_{S,Z} u_S}{\kappa_Z} \right) \Big/ (\bar{c}_{S,A} - \bar{c}_{S,Z}) \tag{8}$$

where A and Z indicate the primary and secondary zones, respectively, and $\bar{c}_S$ is the total concentration of constituent S including, *e.g.*, for H^+ also the protonated base BH^+ and/or the neutral acid HA. In the case when the constituent S involves also such a charged form, *e.g.*, BH^+, an additional term must appear in the numerator in eqn. 8, $c_i u_i/\kappa$ with the corresponding subscript and sign depending on whether it is present in zone A and/or Z. In analogy, the corresponding balance for the counter constituent may be written:

$$W_R = \left(\frac{c_{R,Z} u_R}{\kappa_Z} - \frac{c_{R,A} u_R}{\kappa_A} \right) \Big/ (\bar{c}_{R,A} - \bar{c}_{R,Z}) \tag{9}$$

The unknown value of $c_{S,Z}$ may be obtained as follows. By combination of eqns. 5–9 with the electroneutrality condition and with the equation describing the present chemical (acid–base) equilibria, we may iterate for $c_{S,Z}$ as the parameter until:

$$W_Z = W_R \tag{10}$$

Then the value of $c_{S,Z}$ represents the solution of the system of equations and the corresponding W_Z is the true migration velocity. From these parameters, a complete description of the secondary zone Z may be obtained. For experimental purposes we may define the relative velocity as

$$v_r = \frac{W_Z}{W} = \frac{W_Z \kappa_A}{u_S} \tag{11}$$

where W is the reference frame selected so that it corresponds to the migration of a boundary between the primary and secondary zone where the secondary zone contains only G and no S. The value of v_r may easily be obtained by experiment from the time of passing of the boundary between the primary and secondary zones through the column (through the detector). From two experiments (one without S in zone Z), two passage times are obtained, their ratio being equal to v_r.

Usually it is convenient to select such experimental conditions that the boundary between the primary and secondary electrolytes (zones) is sharp. This is true as long as the modifying constituent has a lower effective mobility than that of the constituent in the primary zone (for a detailed treatment see ref. 5).

EXPERIMENTAL

The apparatus for the described method of regulation of the ionic matrix by either a modifying coion or a modifying counter ion must have at least three electrode chambers. An apparatus allowing simultaneous regulation of coions and counter ions must have four electrode chambers. Such four electrode equipment is suitable even in cases when the electrolyte generation is performed by the three-pole method since it facilitates the operation and manipulation of electrolytes.

Apparatus

The instrumentation for performing experiments with the three-pole arrangement is shown in Fig. 4. The apparatus consists of an electrolyte unit, a high-voltage power supply[6] and a device for controlling the electric current ratio.

The electrolyte unit consists of a PTFE separation capillary both ends of which are equipped with a potential-gradient detection cell. Both cells are connected to electrode blocks (Perspex), each equipped with a sampling device, input and output of electrolytes and two electrode chambers equipped with platinum electrodes and separated from the capillary by semipermeable membranes. The two electrode blocks are identical; however, they differ in the manner of connection to the power supply. The two electrode chambers of one block (M, see Fig. 4) are connected to the power supply and the ratio of the two input currents is controlled; one of these two electrode chambers contains the modifying electrolyte. From the second electrode block (S),

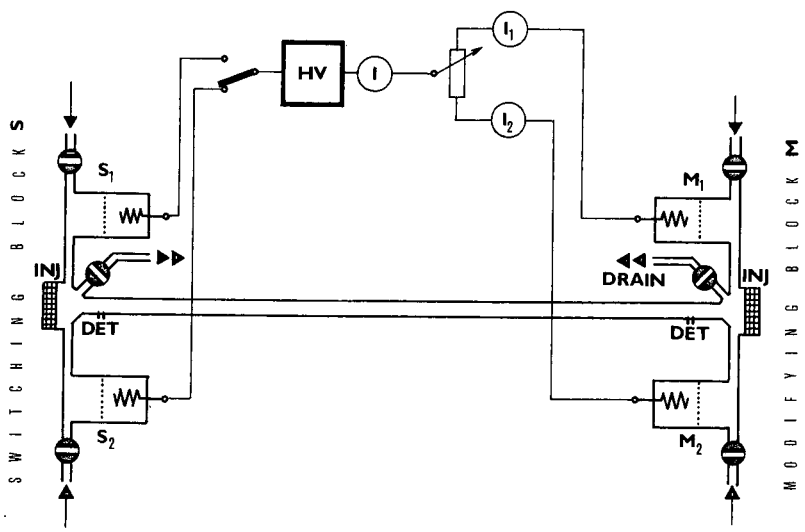

Fig. 4. Apparatus for the experiments with a three-pole column: INJ = injection port; DET = potential gradient detector; HV = high-voltage power supply; for explanation, see text.

only one electrode chamber is connected to the power supply and we may switch over from one chamber to the other.

Chemicals

All chemicals used were of analytical reagent grade (Lachema, Brno, Czechoslovakia).

Measurement of pH and v_r

For the verification of the theory, a simple apparatus was made equipped with a horizontal glass capillary (260 × 1.5 mm I.D.), three electrode chambers, sampling device and measuring scale. This apparatus was used for the determination of the two times necessary for the calculation of v_r (see Theoretical). The movement of the boundary was visualized by the sampling of a small amount of a suitable coloured indicator, *e.g.*, ferroin for cationic analyses. After the measurement of the migration velocity, the zone of the secondary electrolyte (volume approx. 150 μl) was purged from the capillary by a stream of air; its pH was measured by a capillary microelectrode (Radelkis, Budapest, Hungary).

Generation of ionic flows creating ionic matrices in a three-pole column

With a modifying counter ion. For zone electrophoresis the separation column and chambers M1 and S1 (see Fig. 4) were filled with the primary electrolyte, and chamber M2 was filled with the modifying electrolyte (differing from the primary one by containing another counter ion). After switching on the electric current, the zone of the secondary background electrolyte was formed in the separation column. After this zone had reached the detector in block S, the electric current was switched off, the sample introduced via the septum in block S and the analysis was performed.

For isotachophoresis the separation column and chambers M1 and S1 were filled with the primary electrolyte, chamber M2 was filled with the modifying electrolyte and chamber S2 with the terminating electrolyte. After switching on the electric current (so that it passes through chamber S1), the zone of the secondary (leading) electrolyte was formed in the separation column. After this zone had reached the detector in block S, the electric current was switched off, the sample introduced via the septum in block S and the electric current was again switched on (but now so that it passes through chamber S2) and the analysis was performed.

With a modifying coion. For zone electrophoresis the separation column and chambers M1 and S1 were filled with the primary electrolyte, chamber M2 with the modifying electrolyte, the sample was introduced via the septum in block M and the electric current was switched on for analysis.

For isotachophoresis the separation column and chamber S1 were filled with the primary electrolyte, chamber M1 with the modifying electrolyte, chamber M2 with the terminating electrolyte, the sample was introduced via the septum in block M and the electric current was switched on for analysis.

Note that the arrangement with the modifying coion is very advantageous since the analysis is performed simultaneously with the modification and there is no need to wait for the modification of the content of the whole separation column. The modifying constituent, however, must obviously have an higher effective mobility than those of the sample components the separation of which is to be controlled by the performed modification.

RESULTS AND DISCUSSION

For the verification of the theory and of the accuracy of setting of the pH, we compared the measured and calculated relative migration velocities, v_r, and the pH values in a buffered and a non-buffered electrolyte system.

In the case of the non-buffered system, 0.01 *M* HCl served as the primary electrolyte and 0.01 *M* tetrabutylammonium hydroxide (TBAOH) as the modifying electrolyte (modifying ion TBA^+). Table I shows the values of v_r and pH for various ratios I_H/I_{TBA}. The average relative difference between the measured and calculated values of v_r is 3.1% and that between the measured and calculated pH values is 0.03 units.

In the case of the buffered system, 0.01 *M* ammonium formate served as the primary electrolyte and 0.01 *M* formic acid as the modifying electrolyte (modifying ion H^+). The results for this system are given in Table II; here the average relative difference between the measured and calculated values of v_r is 1.4% and that between the measured and calculated pH values is 0.01 units.

From both Tables I and II it is seen that the experimental values are in good agreement with the theoretical ones and that the accuracy of the setting of pH is comparable with the accuracy of a common pH measurement.

For the change of pH in a real electrophoretic system, an example is the preparation of an extended buffer-free system[7] with a solution of HCl and KCl as the secondary electrolyte. For this, the separation column and the electrode chambers M1 and S1 were filled with 0.01 *M* HCl and the chamber M2 was filled with 0.01 *M* KCl. At $I_H/I_K = 1$, the secondary zone formed has the following composition: $c_{Cl} = 0.0067$ *M*, $c_H/c_K = 0.35$, pH 2.76. The calculated dependences of the pH, c_{Cl} and v_r of the secondary zone on I_H/I_K for this system are shown in Fig. 5. By varying the ratio I_H/I_K within the range 0–1 we may thus control the pH of the resulting secondary electrolyte within the range 7–2.7. In this way it is easy to prepare zones which would be otherwise

TABLE I

COMPARISON OF EXPERIMENTAL AND CALCULATED VALUES OF pH AND v_r FOR THE NON-BUFFERED SYSTEM HCl–TBA

Exptl. = experimental value; S.D. = standard deviation; diff. = difference between calculated and experimental values; calc. = calculated values; R.S.D. = relative standard deviation; r.d. = relative difference between calculated and experimental values; the relative values (R.S.D. and r.d.) are given in %.

I_H/I_{TBA}	pH_Z				v_r			
	Exptl.	*S.D.*	*Calc.*	*Diff.*	*Exptl.*	*R.S.D.*	*Calc.*	*r.d.*
0.000	6.19	0.245	–	–	1.000	1.92	1.000	–
0.111	4.28	0.079	4.22	0.06	0.925	2.31	0.906	2.1
0.250	3.85	0.022	3.87	0.02	0.835	1.39	0.811	3.0
0.493	3.56	0.013	3.58	0.02	0.710	1.33	0.688	3.2
0.695	3.41	0.013	3.44	0.03	0.628	0.73	0.612	2.6
1.000	3.28	0.010	3.29	0.01	0.550	1.11	0.527	4.4
average difference				0.03	average difference			3.1%

TABLE II

COMPARISON OF EXPERIMENTAL AND CALCULATED VALUES OF pH AND v_r FOR THE BUFFERED SYSTEM $HCOONH_4$–HCOOH

For abbreviations, see Table I.

I_{NH_4}/I_H	pH_Z				v_r			
	Exptl.	*S.D.*	*Calc.*	*Diff.*	*Exptl.*	*R.S.D.*	*Calc.*	*r.d.*
0.000	2.82	0.006	2.81	0.01	1.000	0.70	1.000	–
0.111	2.87	0.003	2.88	0.01	0.944	0.63	0.951	0.7
0.250	2.95	0.007	2.96	0.01	0.877	0.55	0.889	1.3
0.666	3.07	0.006	3.09	0.02	0.719	0.68	0.729	1.4
1.000	3.15	0.001	3.17	0.02	0.631	0.86	0.644	2.0
average difference				0.014	average difference			1.4%

difficult to obtain by classical means. As follows from the results, the time necessary for the formation of the secondary zone is approximately equal to the analysis time (when preparing the secondary electrolyte, we may use a higher electric current than for the analysis).

Analogously, we may prepare secondary electrolytes with a buffering modifier. The preparation time, however, increases to 2–4 times that of the analysis time, depending on the required pH. In this case the amount of the modifying ion in the secondary electrolyte depends also on the pH of the modifying electrolyte and it is convenient to select its pH so that it equals the pK_a of the buffering ion. An example of such a system is represented by 0.01 *M* HCl as the primary electrolyte and 0.01 *M* β-alanine + HCl (pH 3.6) as the modifying electrolyte. The calculated dependences

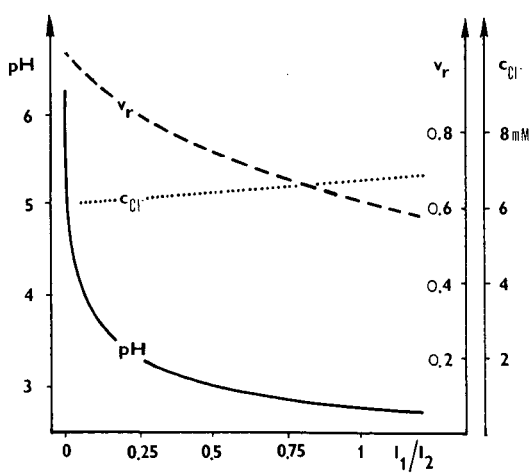

Fig. 5. Calculated dependences of pH, chloride concentration, c_{Cl}, and v_r of the secondary zone on the electric current ratio, $I_H/I_K = I_1/I_2$. The primary electrolyte was 0.01 *M* HCl and the modifying electrolyte was 0.01 *M* KCl.

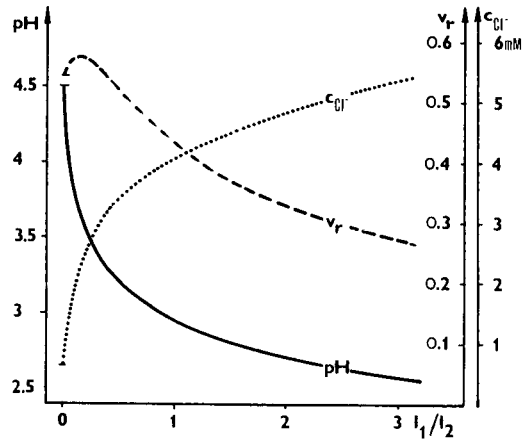

Fig. 6. Calculated dependences of pH, c_{Cl} and v_r of the secondary zone on the electric current ratio, I_1/I_2. The primary electrolyte was 0.01 *M* HCl and the modifying electrolyte was 0.01 *M* β-alanine + HCl (pH 3.6).

of pH, c_{Cl} and v_r on I_1/I_2 are shown in Fig. 6. It is seen that, by changing the electric current ratio, the whole buffering range of β-alanine can be covered.

The possibility to use the method described for an easy change of the ionic matrix in ITP is illustrated by the following example of anionic separation of citrate, lactate and succinate. The primary electrolyte was 0.01 *M* HCl, the modifying electrolyte was 0.01 *M* KCl (modifying ion K^+) and the terminator was 0.01 *M* caproic acid. At the ratio $I_1/I_2 = 0$ (the secondary electrolyte contains only K^+), the migration order of the three acids is citrate, succinate, lactate (see Fig. 7a). A current ratio, $I_1/I_2 = 0.5$ results in the order citrate, lactate, succinate (Fig. 7b).

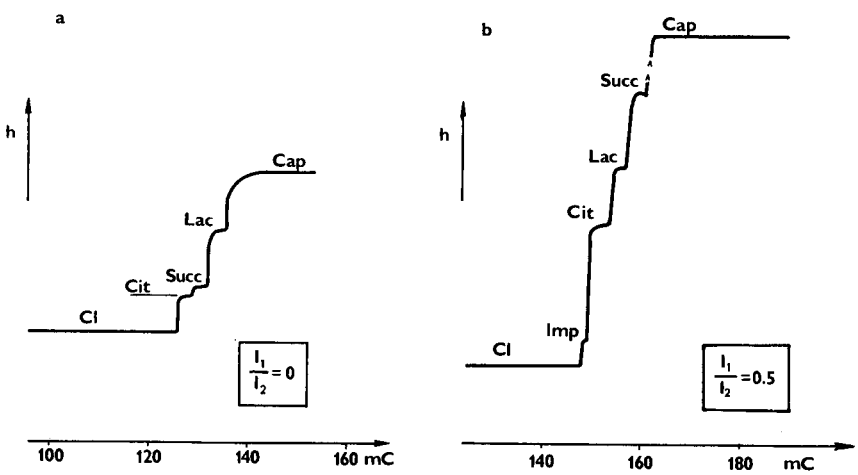

Fig. 7. Potential gradient records of the analysis of citrate (Cit), succinate (Succ) and lactate (Lac) in the system with 0.01 *M* HCl (primary electrolyte), 0.01 *M* KCl (modifying electrolyte), Cl^- (leading ion), 0.01 *M* caproic acid (Cap, terminator) for $I_1/I_2 = 0$ (a) or 0.5 (b). (a) $I = 150$ μA (modification and separation), 100 μA (detection); (b) $I = 150$ μA (modification and separation), 60 μA (detection). Sample amounts (nmol): (a) 3.75, Cit; 7.5, Succ and 18.8, Lac; (b) 7.15, Cit; 14.3, Lac and 28.6, Succ; Imp = impurity.

Another example shows the cationic ITP separation of methylamine and tetrabutylammonium (TBA), where 0.01 *M* $Ca(OH)_2$ served as the primary electrolyte and 0.01 *M* KCl was the modifier. At the ratio $I_{OH}/I_{Cl} = 0.05$, methylamine migrates in front of TBA (TBA is the terminator), see Fig. 8a. At $I_{OH}/I_{Cl} = 1.7$ methylamine migrates behind TBA (Fig. 8b) and NH_4^+ serves as the terminator; at $I_{Cl} = 0$, the effective mobility of methylamine was further changed (Fig. 8c).

The use of a modifying coion is illustrated by the cationic isotachophoretic analysis of a mixture of K^+, Na^+, tetrapropylammonium (TPA) and aniline. The primary electrolyte was 0.01 *M* HCl, as was the modifying electrolyte (modifying coion H^+) and the terminating electrolyte was 0.01 *M* TBACl. At $I_2 = 0$ ($I_H = 0$), aniline did

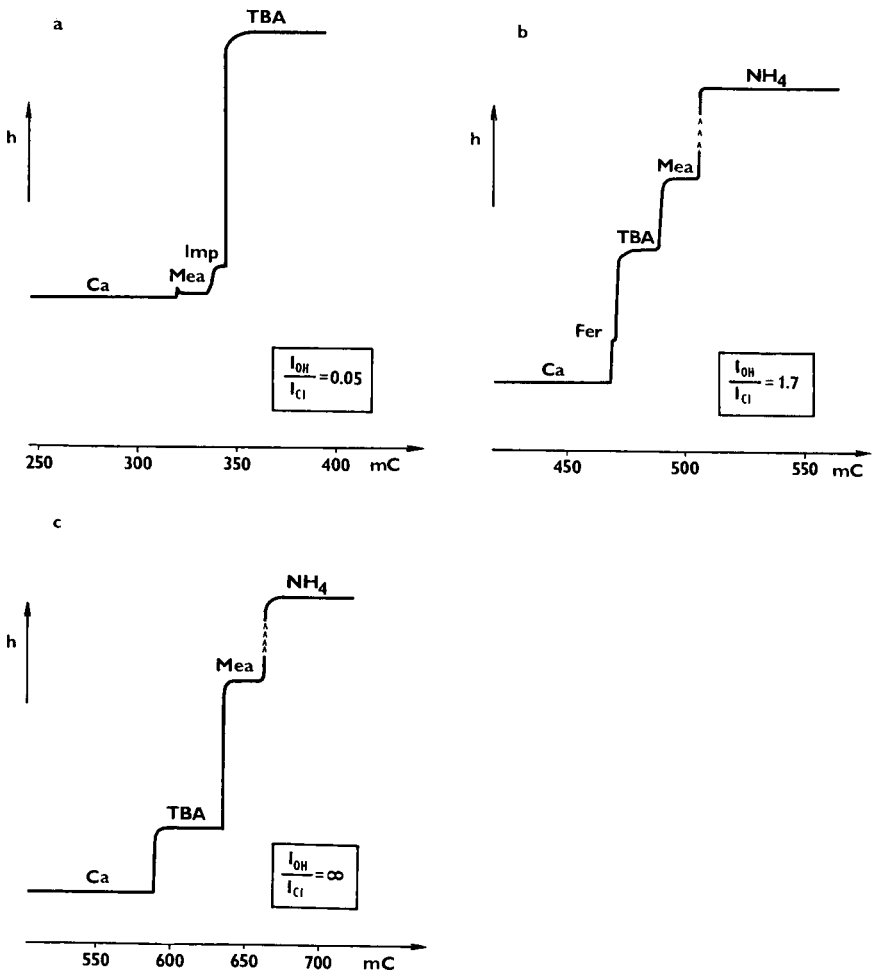

Fig. 8. Potential gradient records of the analysis of methylamine (Mea) and tetrabutylammonium (TBA) in the system with 0.01 *M* $Ca(OH)_2$ (primary electrolyte), 0.01 *M* KCl (modifying electrolyte), Ca^{2+} (leading ion), 0.01 *M* TBAOH (a) or 0.01 *M* NH_4OH (b, c) (terminator), for (*a*) $I_{OH}/I_{Cl} = 0.05$, (b) $I_{OH}/I_{Cl} = 1.7$ and (c) $I_{Cl} = 0$; $I = 140$ μA (modification and separation), 70 μA (detection). Sample amounts: (nmol) (a) 50, MeaCl; (b) 26, MeaCl and 13, TBACl; (c) 67, MeaCl and 33, TBACl; Imp = impurity, Fer = ferroin.

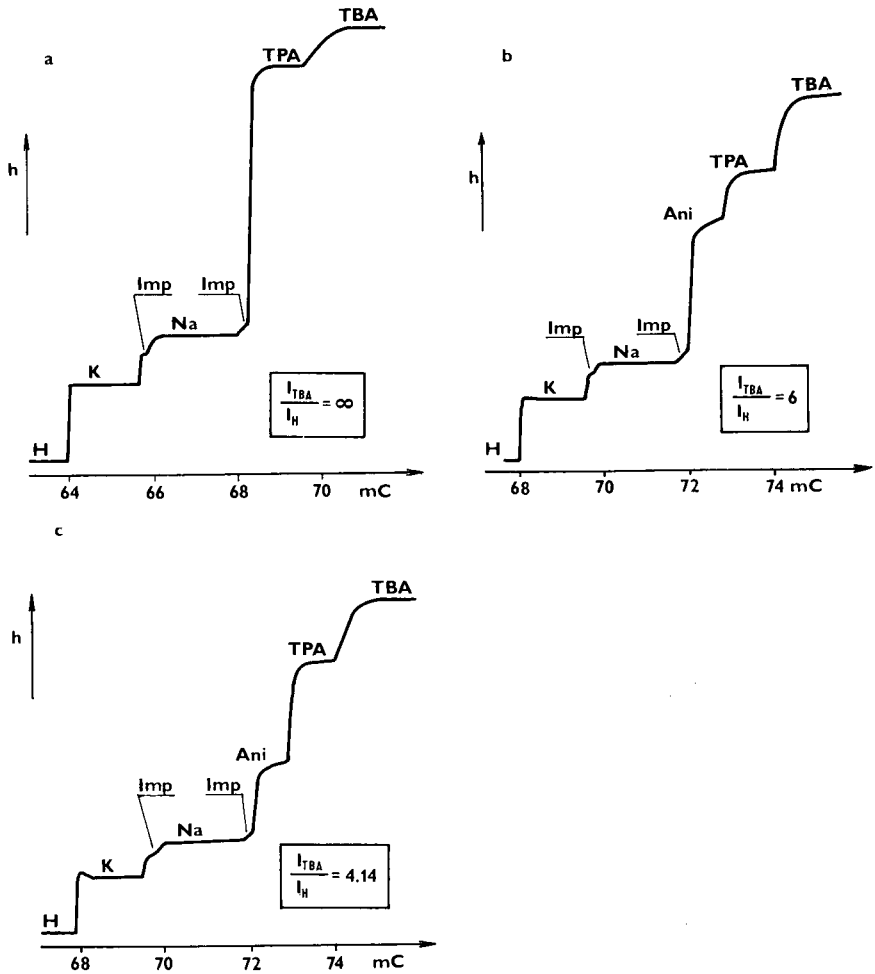

Fig. 9. Potential gradient records of the analysis of KCl, NaCl, tetrapropylammonium (TPA) iodide and aniline (Ani) (each 2.5 nmol) in the system with 0.01 *M* HCl (primary electrolyte and modifying electrolyte), H^+ (leading ion), 0.01 *M* TBACl (terminator) for (a) $I_2 = I_H = 0$, (b) $I_{TBA}/I_H = 6$ and (c) $I_{TBA}/I_H = 4.14$. (a) $I = 315\ \mu A$ (separation), 105 μA (detection); (b) $I = 200\ \mu A$ (separation), 100 μA (detection); (c) $I = 270\ \mu A$ (separation), 50 μA (detection); Imp = impurity.

not migrate (see Fig. 9a); at the ratios $I_{TBA}/I_H = 6$ and 4.14, aniline migrated and changed its effective mobility (Fig. 9b and c).

CONCLUSIONS

The composition of the ionic matrices in isotachophoresis and zone electrophoresis can be changed directly in the separation capillary by electromigration with two different ions of the same charge from two separate electrode chambers. The flows of these ions from the electrode chambers can be regulated electrically by the

magnitude of the input current to each electrode, and thus the ionic matrix can effectively be changed.

The composition of the ionic matrix and the time necessary for its change can be calculated from the ratio of the input currents on the basis of moving boundary equations, which was verified experimentally. The calculated and experimental values of pH and v_r for a non-buffered system (primary electrolyte HCl, modifying electrolyte TBACl) and a buffered system (primary electrolyte $HCOONH_4$, modifying electrolyte HCOOH) were compared. The values of pH agreed very well and did not differ on average by more than 0.03 units for the non-buffered and 0.013 units for the buffered system. The values of v_r for the non-buffered and buffered systems differed by about 3 and 1.4%, respectively.

The procedure described enables one to make very fine changes in the composition of the ionic matrix directly in the separation column in an easy and reproducible way, which is useful especially for experimental determination of suitable separation conditions in electrophoretic techniques.

REFERENCES

1 P. Boček, M. Deml, P. Gebauer and V. Dolník, *Analytical Isotachophoresis*, VCH Verlagsgesellschaft, Weinheim, 1988.
2 V. Dolník, *Thesis*, Institute of Analytical Chemistry, Czechoslovak Academy of Sciences, Brno, 1987.
3 M. Deml, J. Pospíchal, P. Gebauer and P. Boček, *Czech. Pat.*, Pending, PV 6036-88.
4 L. G. Longsworth, *J. Am. Chem. Soc.*, 67 (1945) 1109.
5 P. Gebauer, L. Křivánková and P. Boček, *J. Chromatogr.*, 470 (1989) 3.
6 M. Deml, P. Boček and J. Janák, *J. Chromatogr.*, 109 (1975) 49.
7 L. Křivánková, F. Foret, P. Gebauer and P. Boček, *J. Chromatogr.*, 390 (1987) 3.

Journal of Chromatography, 470 (1989) 57–68
Elsevier Science Publishers B.V., Amsterdam — Printed in The Netherlands

CHROM. 21 213

ISOTACHOPHORESIS IN MIXED SOLVENTS CONSISTING OF WATER, METHANOL AND DIMETHYL SULPHOXIDE

III. INFLUENCE OF THE SOLVENT COMPOSITION ON THE DISSOCIATION CONSTANTS AND MOBILITIES OF NON- AND HYDROXY-SUBSTITUTED ALIPHATIC CARBOXYLIC ACIDS

ERNST KENNDLER*, CHRISTINE SCHWER and PATRICIA JENNER
Institute for Analytical Chemistry, University of Vienna, Währingerstrasse 38, A 1090 Vienna (Austria)

SUMMARY

The electrophoretic properties of uncharged acids of the type HA were investigated in operational systems consisting of mixed aqueous–organic solvents. The mixed solvents applied consisted of water, methanol and dimethyl sulphoxide in which the molar fraction of water was held constant at 0.3 and those of the organic co-solvents were varied. The analytes were C_1–C_5 non- and monohydroxy-substituted *n*-alkanoic acids.

The changes in the pK values were found to be linearly correlated with the molar fraction of dimethyl sulphoxide within the mixing range considered. The changes in the pK values can be qualitatively described by the transfer activity coefficients, which are related to the solvation abilities of the solvents involved.

The mobilities and the corresponding normalized values, where the different viscosities of the particular solvents are taken into account, were determined in operational systems with apparent pH values of 8.7. No changes in the selectivities occurred within the two groups of acids. The normalized mobilities of the non-substituted acids, on the other hand, increased with increasing concentration of dimethyl sulphoxide to a smaller extent than those of the hydroxy-substituted acids. The grouping of these two classes is demonstrated by cluster analysis.

INTRODUCTION

The electrophoretic mobility of an analyte can be influenced by a variety of factors. Properties of the bulk solvent such as viscosity on the one hand affect the mobilities of all analytes in the same way, and therefore do not change the selectivity of the electrophoretic system. On the other hand, solute–solute and solute–solvent interactions can lead to pronounced specific changes in the electrophoretic properties. These interactions either determine the size of the ion, and therefore the absolute mobility m_i^0 (at infinite dilution), or the actual mobility m_i (of the totally dissociated or protonated molecule at finite concentration), or they determine the acid–base

0021-9673/89/$03.50

properties of the analytes. This can lead to different changes in the pK values due to different solvation of the particles considered and can be used to adjust the effective mobility, $m_i^{eff} = \alpha m_i$, via the degree of dissociation, α.

One possibility of increasing the range of solute–solvent interactions lies in the application of non-aqueous or mixed solvents for the electrolyte systems. In previous studies[1,2] we investigated the effects of two different mixed aqueous–organic solvents, the first consisting of water (with a molar fraction $x = 0.3$) and methanol ($x = 0.7$) and the second of water ($x = 0.3$), methanol ($x = 0.4$) and dimethyl sulphoxide (DMSO) ($x = 0.3$). In these systems, the electrophoretic properties of aromatic uncharged (or molecular) acids of type HA, and of aliphatic positively charged acids, HB^+ (of the ammonium ion type), were investigated. In some cases strong changes in the migration sequence of the cations were found, which were attributed to changes in the size of the ions. The increased applicability to the separation of substituted benzenecarboxylic acids due to selective changes in their apparent pK values (pK' values) was demonstrated.

In this study, the changes in the properties of uncharged acids by variation of the composition of the mixed solvents within the mixing range mentioned above were investigated in greater detail. As solutes, homologues series of aliphatic carboxylic acids were selected. One series consisted of non-substituted acids and the other of monohydroxy-substituted acids, where interaction of the hydroxy group with polar solvents via hydrogen bonding is possible.

Four solvent mixtures were applied, in which the molar fraction of water was kept constant ($x = 0.30$) and those fractions of methanol and DMSO were varied (Table I). In contrast to previous work[1], here the mobilities of the analytes were determined at such high apparent pH (pH') values that the properties of these analytes can be considered to be influenced to only a minor extent by the degree of dissociation.

EXPERIMENTAL

Chemicals and solvents

Unless stated otherwise, the chemicals and solvents used for the electrolyte systems were of analytical-reagent grade, obtained from E. Merck (Darmstadt, F.R.G.), Fluka (Buchs, Switzerland) or Serva (Heidelberg, F.R.G.). The non-substituted, the 2-hydroxy-substituted n-alkanoic acids and 3-hydroxybutyric acid (3C4) were purchased from E. Merck, Serva or Fluka, either as free acids or as their

TABLE I

COMPOSITION OF MIXTURES OF WATER, METHANOL AND DMSO USED AS SOLVENTS FOR THE ELECTROLYTE SYSTEMS

Solvent code	*Molar fraction (x)*		
	Water	*Methanol*	*DMSO*
1	0.300	0.700	0.000
2	0.300	0.600	0.100
3	0.300	0.500	0.200
4	0.300	0.400	0.300

salts. 3-Hydroxypropionic acid (3C3), 4-hydroxybutyric acid (4C4) and 5-hydroxyvaleric acid (5C5) were synthesized from the corresponding lactones (Fluka, Serva). 3-Hydroxyvaleric acid (3C5) was synthesized from 2-pentenoic acid by addition of HBr and subsequent hydrolysis of the 3-bromovaleric acid to the hydroxy derivative.

Buffer substances were recrystallized three times before use. Water, methanol and DMSO were distilled twice before use.

Apparatus

The apparent pK values were determined by potentiometric titration of the free acids or their salts, using an all-aqueous combined glass–calomel electrode as described previously[1]. The initial analyte concentration was 0.01 mol/l.

The measurements of the relative step heights were carried out using an isotachophoresis instrument with a capillary (25 cm × 0.3 mm I.D.) made from polytetrafluoroethene and equipped with an electrical conductivity detector. The constant driving current was 40 μA. This instrument was also used for the determination of the mobilities of the leading and the reference ions in the mixed aqueous–organic solvents, applying a modified moving boundary method as described[1,2].

The viscosity coefficients were determined with an Ubbelohde viscosimeter and a pyknometer, thermostated to within 0.1°C.

The dielectric constants were determined with a Type DK 03 instrument (WTW, Weilheim, F.R.G.), thermostated to within 0.1°C.

Cluster analysis was carried out by a computer program[3] using the Euclidian distances of the points representing the compounds in a multi-dimensional pattern space, as discussed previously[2]. These distances were calculated from the scaled values of the differences in the normalized mobilities, given by the product of the mobility and the viscosity coefficient.

RESULTS AND DISCUSSION

pK values in mixed solvents

The apparent pK values of non- and hydroxy-substituted carboxylic acids are given in Table II, together with thermodynamic pK values in pure water, taken from the literature[4,5]. The problems of the experimentally determined apparent pK values, which include effects arising from liquid junction potentials, were discussed previously[1,2].

It can be seen from Table II that, in accordance with some literature data[6], the pK values increase by about 1.5–2 pK units when methanol is added to aqueous solutions at a molar fraction of 0.7. In this special case, the increase in pK is roughly linearly dependent on the methanol content, at least in the concentration range up to a molar fraction of 0.7. At higher concentrations, the corresponding curve becomes steeper and reaches values that are approximately 5 pK units higher in pure methanol than in water[6,7].

The increase in the pK (or pK' values) in system 1 given in Table II is in accordance with the fact that methanol and water–methanol mixtures have lower dielectric constants than water, as shown in Table III. This leads to positive values for the electrostatic part of the "medium effect", log ${}_m\Gamma_{HA}$, and the corresponding

TABLE II

APPARENT pK VALUES (pK') OF NON- AND HYDROXY-SUBSTITUTED ALIPHATIC CARBOXYLIC ACIDS IN MIXTURES OF WATER, METHANOL AND DMSO

The solvent codes correspond to Table I. The number after the C in the acid codes indicates the number of carbon atoms of the acid molecule and the number before the C indicates the position of the hydroxy group (*e.g.*, 2C4 = 2-hydroxybutyric acid; C2 = acetic acid). Temperature, 25°C.

Acid	*pK in water*[a] *(20°C)*	*pK' in solvent system*			
		1	*2*	*3*	*4*
C1	3.75	5.25	5.75	6.12	6.70
C2	4.76	6.62	7.09	7.62	8.20
C3	4.87	6.78	7.26	7.84	8.44
C4	4.81	6.84	7.27	7.86	8.43
C5	4.79	6.79	7.26	7.85	8.42
2C2	3.82	5.55	6.02	6.41	7.05
2C3	3.86	5.73	6.33	6.60	7.09
2C4	–	5.55	5.79	6.40	6.92
2C5	–	5.45	5.87	6.45	6.71
4C5	4.69[b]	6.56	6.99	7.42	8.19
5C5	–	6.81	7.07	7.52	8.27

[a] From refs. 4 and 5.
[b] Value at 18°C.

standard free energy of transfer, $\Delta G^0_{t,HA}$, of the dissociation reaction of uncharged acids, HA, as given by Born's treatment:

$$\Delta pK = p_sK - p_wK = \frac{N_L e_0^2}{2RT(\ln 10)}\left(\frac{1}{r_{H^+}} + \frac{1}{r_{A^-}}\right)\left(\frac{1}{\varepsilon_s} - \frac{1}{\varepsilon_w}\right) \quad (1)$$

where the subscripts w and s indicate water and organic or mixed solvent, respectively, e_0 = elementary charge, N_L = Loschmidt's number, T = absolute temperature, R = gas constant, r = crystallographic radius of the ion and ε = dielectric constant. ${}_m\Gamma_{HA} = ({}_m\gamma_{H^+} \cdot {}_m\gamma_{A^-})/{}_m\gamma_{HA}$ is related to the transfer activity coefficients, ${}_m\gamma_i$, of the single species, i[8–13].

TABLE III

DIELECTRIC CONSTANTS OF THE MIXED SOLVENTS AT DIFFERENT TEMPERATURES

The solvent codes correspond to Table I.

Temperature (°C)	*Dielectric constants of mixed solvents*			
	1[a]	*2*	*3*	*4*[a]
20	43.78	47.80	51.40	54.29
25	42.52	46.74	50.48	53.04
30	40.99	45.15	48.96	51.57

[a] From ref. 1.

The restriction to pure electrostatic work, according to Born's treatment, neglects the effects on the pK values originating from the different basicities and from the different solvation abilities of the solvents. Therefore, this simple approach does not explain the variation of the pK values in most instances. However, for some water–alcohol mixtures, this rough approach leads to results that are at least qualitatively in accordance with the observed effects. In fact, the transfer of a uncharged acid and its dissociation products from water (with a dielectric constant of 78.30 at 25°C) to, *e.g.*, system 1 would lead to a calculated increase in the pK value of 1.1 units when values of 2 and 3 Å are assumed for the crystallographic radii of the proton (or the H_3O^+ ion) and the anion, respectively. The observed values are of about the same magnitude as the predicted values, which can be seen from Table II.

If methanol is replaced with DMSO, as is carried out in the sequence of the solvents 1–2–3–4, an aprotic dipolar solvent is introduced which (a) has a higher dielectric constant than methanol, (b) is a stronger base than both water and methanol and (c) has the lowest ability to solvate anions of all solvent constituents under consideration.

The resulting change in the pK' values with solvent composition is shown in Fig. 1, where the differences in the means of the pK' values, $\overline{\Delta pK'}$, of the carboxylic acids in the particular solvent systems, relative to system 1, are plotted against the concentration of DMSO and methanol. There is a linear increase in $\overline{\Delta pK'}$ with increasing molar fraction of DMSO (the linear correlation coefficient, r, is 0.999). This is in clear

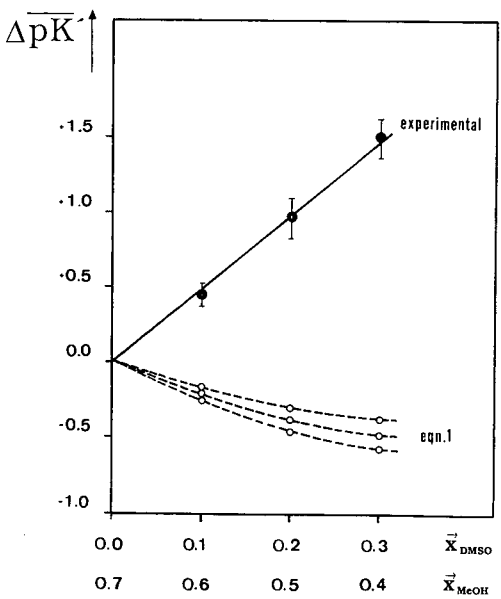

Fig. 1. Variation of the apparent pK values with the composition of the mixed solvents. $\overline{\Delta pK'}$ = differences in the means of the apparent pK values of the acids given in Table II, relative to the values in the binary mixed aqueous–methanolic solvent 1. The molar fraction of water was held constant at 0.3. ⅛, Experimental values (standard deviations indicated); @, values calculated from eqn. 1, assuming different crystallographic radii of the ions. MeOH = Methanol.

contrast to the results of the calculation according to eqn. 1, which would give negative values for $\Delta pK'$ with increasing DMSO concentration, as indicated in Fig. 1 by the broken lines. The curves shown there were calculated from eqn. 1 using the values of the dielectric constants at 25°C given in Table III. They were obtained for different crystallographic radii for the ions: upper curve, $r_{H^+} = 3$ Å, $r_{A^-} = 3$ Å; middle curve, $r_{H^+} = 2$ Å, $r_{A^-} = 3$ Å; lower curve, for both ions $r = 2$ Å.

Replacing the crystallographic radii in eqn. 1 by the Stokes' radii as proposed in the literature (*cf. e.g.* ref. 10) is also unable to explain the effects actually observed; only if negative values for the Stokes' radii are applied in eqn. 1, which is of no physical meaning, would the calculated values be in accordance with the experimental data.

It should be mentioned that the observed result also conflicts with an explanation based solely on the acid–base properties of DMSO. This solvent, being a stronger base than methanol, should also decrease the pK values with increasing concentration.

The effects found experimentally seem to result from the very low ability of DMSO to solvate anions, which leads to highly positive values for the medium effect on the anion. This effect overcompensates the contributions of the electrostatic work to the change in the standard free energy of transfer, and also the contribution of the medium effect on the proton, $\log {}_m\gamma_{H^+}$.

The resulting effects of the composition of the mixed solvents on the pK' values of the uncharged acids can be summarized as follows: for the analytes under consideration, the partial replacement of water as a solvent with methanol up to a molar fraction of 0.7 leads to an almost linear increase in the pK values of about 1.5–2 units, compared with pure aqueous solutions; and the replacement of methanol by DMSO in ternary mixtures of water, methanol and DMSO leads to a further linear increase in the pK' values of about 0.5 unit per 10 mol% DMSO.

Migration properties of the anions of non- and hydroxy-substituted carboxylic acids in mixed solvents

Obviously the migration properties of the analytes are highly dependent on their acid–base properties, as the degree of dissociation in a given electrolyte system, which determines the effective mobilities, is related to the pK values. Therefore, in this work the conditions were chosen such as to suppress the effects originating from different degrees of dissociation by applying electrolyte systems with sufficiently high pH (or pH′) values. The migration properties in the solvent systems at pH′ 8.7 [with tris(hydroxymethyl)aminomethane as buffering counter ion] were, in a first step, determined with the aid of the step heights of the isotachophoretic analyte zones, measured with an electrical conductivity detector. They were determined at an ambient temperature of 28°C, for which the problem of the actual temperature of the analyte zones has already been mentioned[1]. This temperature can be assumed to be slightly higher than ambient. At pH′ values of the leading electrolytes of 8.7, and at the higher pH′ values within the analyte zones, the acids are dissociated to more than 95%, at least in the electrolyte systems consisting of solvents 1, 2 and 3. In the electrolyte with solvent 4, formic acid and the 2-hydroxy-substituted acids are dissociated to more than 99% and the other acids to a smaller extent.

The relative step heights are given in Table IV. From these values, the mobilities in the respective buffered solvent systems can be calculated. For this calculation the

TABLE IV

RELATIVE STEP HEIGHTS OF NON- AND HYDROXY-SUBSTITUTED CARBOXYLIC ACIDS AT APPARENT pH VALUES OF 8.7 IN ELECTROLYTE SYSTEMS WITH MIXED SOLVENTS CONSISTING OF WATER, METHANOL AND DMSO

The step heights are related to trichloroacetate as the reference ion. The leading ion was chloride (c = 0.01 mol/l). The acid and solvent codes correspond to Tables I and II, respectively.

Acid	*Relative step height (× 100) in solvent*			
	1	*2*	*3*	*4*
C1	53.7	46.2	36.8	47.3
C2	120	121	156	192
C3	143	142	199	258
C4	159	161	224	287
C5	170	178	260	326
2C2	104	100	95.5	92.1
2C3	128	124	129	127
2C4	147	145	159	159
2C5	162	159	190	190
3C3	162	167	210	221
3C4	170	178	220	237
3C5	189	196	245	255
4C5	218	239	316	376
5C5	237	256	346	393

values of the mobilities of the leading and a reference ion are required, as discussed in a previous paper[2]. However, no data for the mobilities of chloride (used as the leading ion) and trichloroacetate (used as the reference ion) in the mixed solvents were found in the literature. Therefore, these data were measured by a moving boundary method described previously[2], using an electrical conductivity detector to determine the position of the moving boundary. The results are presented in Table V. With these mobility data and with the values of the relative step heights, the mobilities of the analytes were calculated (Table VI). It can be seen that they range between approximately 18 and 32 units, and are therefore much lower than the comparable data in water, where they range between approximately 30 and 57 units. The highest values for the aqueous–organic solvents are observed in the electrolyte system with

TABLE V

MOBILITIES OF LEADING AND REFERENCE IONS IN THE ELECTROLYTE SYSTEMS CONTAINING MIXED SOLVENTS

Temperature, 30°C. The solvent codes correspond to Table I. c = 0.01 mol/l.

Ion	*Mobility (10^{-5} cm^2 V^{-1} s^{-1}) in solvent*			
	1	*2*	*3*	*4*
Chloride	38.1	32.4	27.4	26.3
Trichloroacetate	28.2	25.1	23.7	24.1

TABLE VI

MOBILITIES OF NON- AND HYDROXY-SUBSTITUTED CARBOXYLIC ACIDS IN ELECTROLYTE SYSTEMS CONSISTING OF SOLVENT MIXTURES OF WATER, METHANOL AND DMSO AT AN APPARENT pH VALUE OF 8.7

The mobilities were derived from the relative step heights given in Table IV. The acid and solvent codes correspond to Tables I and II, respectively. Temperature, 30°C.

Acid	*Mobility (10^{-5} cm^2 V^{-1} s^{-1}) in solvent*			
	1	*2*	*3*	*4*
C1	31.8	28.6	25.9	25.2
C2	26.6	24.0	22.0	22.4
C3	25.0	22.9	20.9	21.3
C4	24.2	22.1	20.3	20.8
C5	23.4	21.3	19.5	20.3
2C2	27.9	25.1	23.8	24.3
2C3	26.1	23.8	22.8	23.6
2C4	24.9	22.8	22.0	23.0
2C5	24.1	22.2	21.1	22.4
3C3	24.1	21.8	20.6	21.9
3C4	23.3	21.4	20.4	21.6
3C5	22.7	20.6	19.6	21.3
4C5	21.2	19.1	18.4	19.6
5C5	20.5	18.6	17.8	19.4

solvent 1; in the electrolyte systems consisting of solvents 2, 3 and 4, the mobilities of a particular analyte differ by only 10%.

One can compare the effects of the electrolyte systems on the migration properties of the analytes better when the different viscosities of the bulk liquids are compensated, according to Stokes' law. The viscosity coefficients, η, of the mixed solvents at different temperatures are given in Fig. 2. A linear increase in the viscosity coefficients with increasing molar fraction of DMSO (and decreasing molar fraction of methanol) is found. The linear correlation coefficient, r, is >0.999 for all three curves.

The values at 30°C were used to calculate the products $m_i\eta$, which are plotted in Fig. 3 against the solvent composition. There is a non-linear but continuous increase of $m_i\eta$ with increasing concentration of DMSO for all analytes. Both the non-substituted carboxylic acids (Fig. 3a) and the hydroxy-substituted acids (Fig. 3b) show roughly parallel curves, which means that the selectivity of the systems has not changed within either class of analyte. This result is in accordance with predictions which can be made based on the solvation properties of the solvents involved, especially of DMSO. The behaviour of the uncharged acids differs from that of positively charged acids of the ammonium type[2], where changes in the migration sequence were observed for small ions with relatively high charge densities.

For the particular anions, the changes of in $m_i\eta$ from system 1 to system 4 are in the range of about 50% for the hydroxy derivatives and about 25–30% for the non-substituted acids. This means that much larger effects are found for the carboxylic acids compared with cations with low charge densities such as tetrapropylammonium

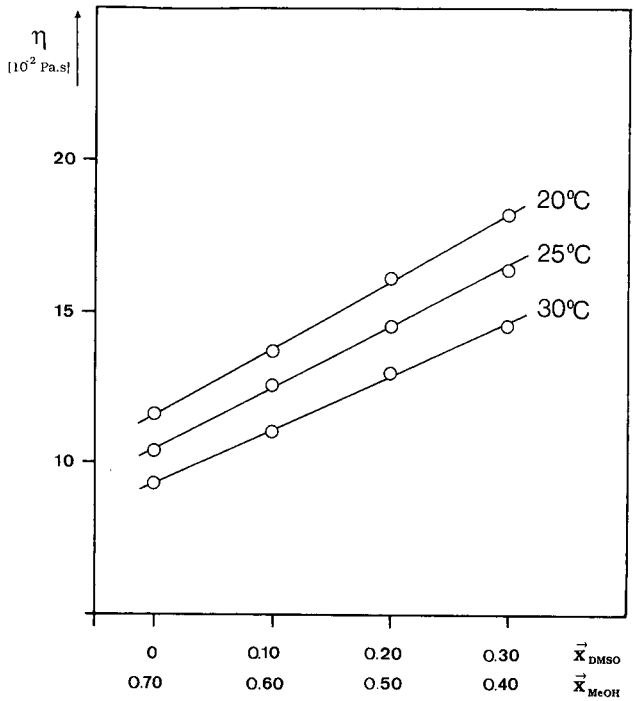

Fig. 2. Viscosity coefficients, η, of the mixed solvents at different temperatures.

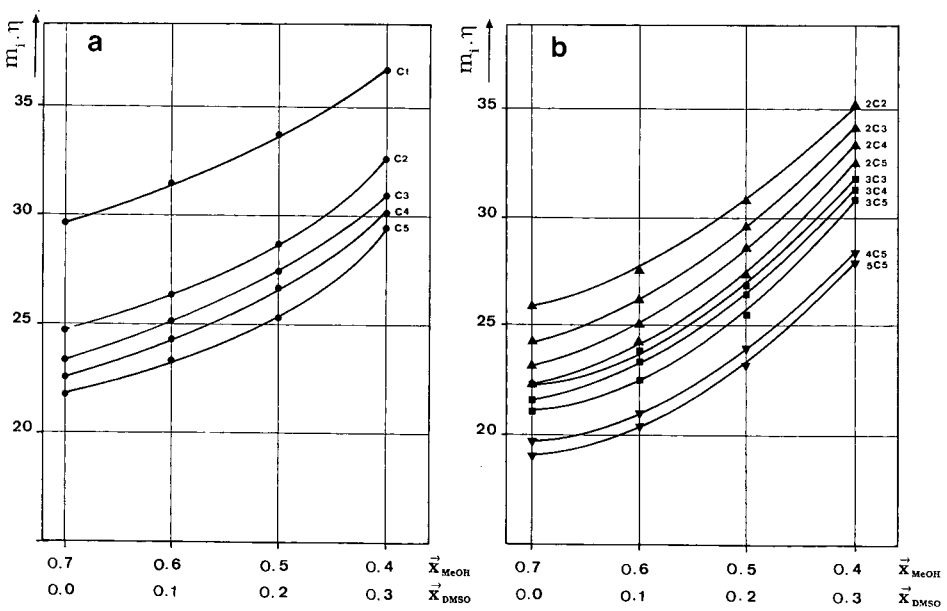

Fig. 3. Products $m_i\eta$ (10^{-12} N V^{-1}) of the mobilities, m_i, of the analyte anions and the viscosity coefficients, η, of the mixed solvents *versus* the composition of the operational system. (a) Non-substituted carboxylic acids; (b) hydroxy-substituted carboxylic acids. The codes for the acids correspond to Table II.

or tetrabutylammonium ions[2], for which we can assume that they are not solvated, and where only small changes (< 10%) were found for the particular cation.

It can be concluded from the parallel shape of the curves for 4C5 and 5C5, which have relatively high pK' values compared with those of the 2-hydroxycarboxylic acids (with lower pK' values), as shown in Fig. 3a and b, that the effect of the degree of dissociation has only a minor effect on the mobilities under the conditions given. This means that the mobilities calculated were in fact the actual mobilities of the solutes. This assumption is confirmed when the curves for the higher non-substituted acids in Fig. 3a are compared with that of formic acid, which also has lower pK' values but shows the same trend.

Although for both classes of compounds the sequence of the mobilities does not change within a given class, changes can be observed when compounds from different classes are compared. It can be seen from Fig. 3 that the curves for the hydroxy-substituted acids show a steeper increase with increasing molar fraction of DMSO than the corresponding curves for the non-substituted acids. This steeper increase leads, *e.g.*, to the effect that C3, C4 and C5, which have about the same mobilities as 2C4, 2C5

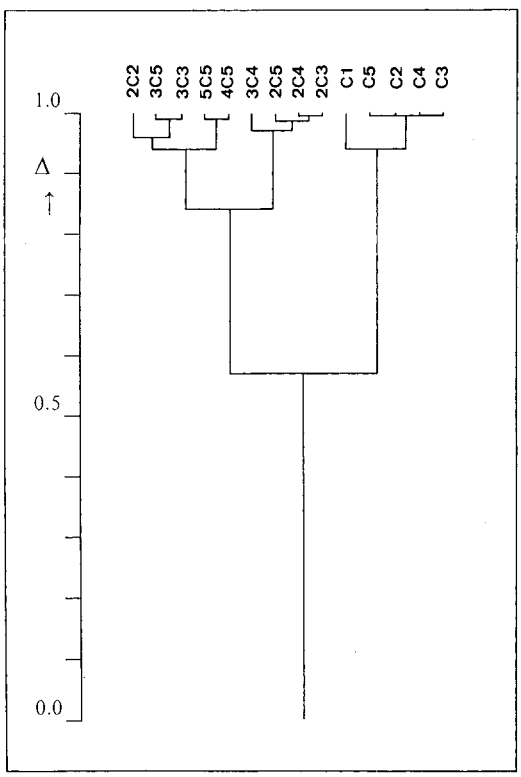

Fig. 4. Dendrogram resulting from the hierarchical clustering procedure for characterizing the electrophoretic properties of the solutes. The differences in the products $m_i\eta$ in operational systems 2, 3 and 4, relative to the values in system 1, were used as features. Δ = relative Euclidian distance. The codes for the acids correspond to Table II.

and 3C4 in system 1, and have higher mobilities than 3C5 and 4C5 in this particular system, show mobilities between 3C5 and 4C5 in system 4.

In general, similarities of species such as ions in different solvents (or electrolyte systems with different pH or solvent composition), can be characterized and evaluated by chemometric methods such as cluster analysis, as shown in previous papers[1,2,14]. The same method can be used to show the different migration properties of the compounds investigated in this study. For this procedure, the differences in the normalized mobilities, $m_i\eta$, in the particular electrolyte systems relative to system 1 were used as features. The Euclidian distances were used as a measure of resemblance. The dendrograms were constructed by an average linkage method.

The results of the clustering procedure are shown in Fig. 4. One can see the differentiation of the analytes into two main subclusters, which is clearly in accordance with the discussion given above; two groups of compounds are differentiated, based on their different migration properties. These groups formed are not dependent on the chain lengths or the pK' values, but are characterized only by their chemical structure; one group is formed by the non-substituted acids and the other group consists of all the hydroxy-substituted acids.

The electrophoretic behaviour of the hydroxy derivatives of the carboxylic acids is found to be similar to that of some of these compounds in the presence of methanol, where they also show higher mobilities, when compared with the corresponding non-substituted compounds; *e.g.*, 2C3 and C3 have the same mobilities in water, but 2C3 has a higher mobility than C3 in 99.5% methanol[15].

These changes cannot be related to a single or predominant effect such as ion solvation by DMSO, as was shown for cations[2], and seem to have more complex sources. Considering the behaviour of the anions investigated, not only are structural changes in the mixed solvents of importance compared with the pure solvents, but also various competing solvation and desolvation reactions seem to play an important role. This leads finally to effects that cannot be explained by a simple model.

REFERENCES

1 E. Kenndler and P. Jenner, *J. Chromatogr.*, 390 (1987) 169.
2 E. Kenndler and P. Jenner, *J. Chromatogr.*, 390 (1987) 185.
3 D. L. Duewer, A. M. Harper, A. M. Koskinen, J. L. Fasching and B. R. Kowalski, *ARTHUR*, University of Washington, Seattle, WA, 1978.
4 A. Albert and E. P. Serjeant, *The Determination of Ionization Constants*, Chapman and Hall, London, 3rd ed., 1984.
5 G. Kortüm, W. Vogel and K. Andrussow, *Dissociation Constants of Organic Acids in Aqueous Solution*, Butterworth, London, 1961.
6 R. G. Bates and R. A. Robinson, in B. E. Conway and R. G. Barradas (Editors), *Chemical Physics of Ionic Solutions*, Wiley, New York, 1966, p. 211.
7 B. G. Cox, *Annu. Rep. Chem. Soc.*, 70 (1973) 249.
8 C. D. Ritchie, in J. F. Coetzee and C. D. Ritchie (Editors), *Solute–Solvent Interactions*, Marcel Dekker, New York, 1969, p. 219.
9 R. G. Bates, in J. F. Coetzee and C. D. Ritchie (Editors), *Solute–Solvent Interactions*, Marcel Dekker, New York, 1969, p. 45.
10 E. J. King, in A. K. Covington and T. Dickinson (Editors), *Physical Chemistry of Organic Solvent Systems*, Plenum, London, 1973, p. 331.
11 O. Popovych, in M. K. Chantooni, Jr. and P. J. Elving (Editors), *Treatise on Analytical Chemistry, Part I*, Vol. I, Wiley, New York, 2nd ed., 1978, p. 711.

12 I. M. Kolthoff and M. K. Chantooni, Jr., in I. M. Kolthoff and P. J. Elving (Editors), *Treatise in Analytical Chemistry, Part I*, Vol. 2, Wiley, New York, 2nd ed., 1979, p. 239.
13 B. E. Conway, J. O'M. Bockries and E. Yeager (Editors), *Comprehensive Treatise of Electrochemistry*, Vol. 5, Plenum, London, 1983.
14 E. Kenndler and G. Reich, *Anal. Chem.*, 60 (1988) 120.
15 T. Hirokawa, T. Tsuyoshi and Y. Kiso, *J. Chromatogr.*, 408 (1987) 27.

Journal of Chromatography, 470 (1989) 69–78
Elsevier Science Publishers B.V., Amsterdam — Printed in The Netherlands

CHROM. 21 265

MEASUREMENT OF LIMITING MOBILITIES BY CAPILLARY ISOTACHOPHORESIS WITH A CONSTANT TEMPERATURE AT THE SITE OF DETECTION

BOHUSLAV GAŠ, JIŘÍ ZUSKA and JIŘÍ VACÍK*
Department of Physical Chemistry, Faculty of Sciences, Charles University, Albertov 2030, 128 40 Prague 2 (Czechoslovakia)

SUMMARY

A method is described for the determination of limiting mobilities from isotachophoretic experiments. The data from an universal detector in the isotachophoretic apparatus were fed to an on-line computer and recalculated to the actual resistance. The computer simultaneously regulates (on the basis of the calculated actual resistance in the detected zone) the driving current passing through the capillary tube, so that the thermal power at the detection site is constant and the temperature of the test solution has a required (preferably standard) value. An advantage of an isotachophoretic experiment controlled in this way is the fact that the dependence of the physical and physico-chemical quantities used on the temperature need not be considered in the recalculation of the experimental data to the limiting ionic mobilities. The limiting mobility calculation considers all the substances as ampholytes. The method was verified using an apparatus with an high-frequency contactless detector.

INTRODUCTION

Production of Joule heat in the separation chamber or the separation medium is inherent to all electromigration methods. In isotachophoresis the situation is further complicated by the fact that the separation occurs in a free solution system without excess of the background electrolyte, so that the zones of the species separated have different conductivities. Therefore, different amounts of heat are produced in different zones and the zones generally have different temperatures. This offers the possibility of a simple detection of zones, and therefore several thermometric detectors have been constructed, especially at the beginning of development of instrumentation for isotachophoresis, *e.g.*, refs. 1 and 2.

The heat production has however an unfavourable effect upon the sharpness of the zone boundary. Capillary tubes of most commercial instruments are therefore thermostatted, but thermostatting of the capillary tube does not preclude different zone temperatures. It is necessary to take account of this if isotachophoresis is to be used for determination of physico-chemical constants.

The temperature influences many quantities that play a role during isotacho-

0021-9673/89/$03.50

phoretic separation, *e.g.*, the relative permitivity and viscosity of a solvent and, of course, acid dissociation constants, pK_A, and limiting ionic mobilities, u^0. For example, the temperature coefficient of the ratio of limiting mobilities, $u^0(T)/u^0(298)$ is for the majority of ions *ca.* 0.023 K^{-1}. This means that if we want to determine mobilities with an accuracy better than 1%, we must assure the temperature control better than 0.4 K.

Some isotachophoretic experiments were performed[3,4] by manual control of the driving current in order to maintain a constant potential gradient in all zones. The zones were characterized qualitatively from changes in the driving current. The temperature differences at the site of detection were slight in the constant potential gradient regime in comparison with the constant driving current regime. The same authors[3,4] tried a manually controlled constant thermal power regime, but the results did not convincing.

In our laboratory, we have carried out isotachophoretic experiments with a constant temperature at the site of detection[5]. The signal from the thermometric detector —thermocouple— was treated by a computer which controlled the driving current in such a manner as to maintain a constant signal from the detector. The changes in driving current were processed by the computer to determine the qualitative parameters of the zones.

In this contribution, a method is described for maintaining a constant temperature at the site where the universal detector senses the property of zones which is a continuous and monotonous function of the specific resistance.

THEORETICAL

During isotachophoretic experiments, radial differences in temperature exist in the zones and axial differences in temperature between the different zones. Many studies has been concerned with these problems, *e.g.*, refs. 6–9. Owing to a temperature dependence of the electrolyte conductivity, the radial temperature profile is somewhat steeper than parabolic. For our purposes, we can cope with the mean radial temperature, T_r, at the detection site of the universal detector. We intend to keep T_r constant for all zones passing through the detector.

A thermal power, p, related to the unit length, arising in the solution in all parts of the capillary tube can be expressed as

$$p = \mathrm{d}P/\mathrm{d}l = IE = I^2\rho/S \tag{1}$$

where P is the input thermal power in the capillary tube, l is the length axis of the capillary tube, I is the electric current, E is the electric field strength, S is the cross-section of the capillary tube and ρ is the specific resistance of the electrolyte. The thermostatting of the capillary tube is generally performed by keeping a constant temperature, T_0, outerside of the tube. A thermal power arising in the solution owing to a driving current entails an increase of the electrolyte temperature above the thermostatting temperature, T_0. The mean radial temperature, T_r, in any length coordinate of the capillary tube can be approximated as

$$T_r = T_0 + qp = T_0 + qI^2\rho/S \tag{2}$$

where q is the thermal transfer coefficient describing the efficiency of the thermal transfer from an electrolyte inside the capillary tube to the thermostat. The value of q depends greatly on constructional details[10] and is sometimes cited by suppliers of commercial equipment.

For our purposes, we need to know q at the site of the sensing detector. It was determined by filling the capillary tube with a calibrating solution of KCl and measuring the dependence of the solution resistance on the current flowing through the capillary tube. The detector used was an high-frequency contactless conductivity detector whose construction allows easy thermostatting of both the measuring cell and the surrounding capillary tube. The rest of the capillary tube was not thermostatted. The determination of the physico-chemical constants is convenient at a temperature of 25°C (298.15 K) at the detection site since the values of these constants are tabulated mostly for 25°C.

We need therefore to maintain the mean radial temperature, T_r, at 25°C. The thermostatting temperature, T_0, has to be

$$T_0 = T_r - qI^2\rho/S \tag{3}$$

where for ρ we take the specific resistance of the leading electrolyte and for I the starting current of the experiment. We assume a negligibly small temperature dependence of the cross-section of the capillary tube. Maintaining a constant temperature at the detection site is based on the computer control of the driving current in order to hold the thermal power term, $qI^2\rho/S$, constant, at the same value as in the leading electrolyte.

EXPERIMENTAL

Equipment

Our device is shown in Fig. 1. A reconstructed high-frequency contactless conductivity detector was used[11–16]. We have sought simplicity of the electric circuits and temperature and time stability. An autocalibrating principle was used for signal treatment. Into the signal processing circuits (SPC), both the signal from the measuring cell (MC) and the part of the alternating voltage from the exciting signal generator (ESG) are fed. The measurements were continuously calibrated for zero drift and gain. In this way, the temperature and time fluctuations of all parts of the measuring chain are efficiently suppressed, with the exception of the preamplifier (PA). However, the latter was thermostatted together with the measuring cell and the surrounding of the capillary tube.

By calculating the transfer function of the equivalent circuits of the measuring cell, we have shown a proportionality between the optimum electrolyte concentration interval and the frequency of the exciting signal[15]. Therefore, we constructed two versions of the detector, one for a frequency of 1 MHz, and the second for a frequency of 10 MHz. It was demonstrated that the former was most suitable for a leading electrolyte concentration of 0.001 M and the latter for one of 0.01 M.

The 1-MHz version was used in the equipment described. A signal from the processing circuits SPC was read by an analog-to-digital converter (ADC) and recalculated in a computer by means of a calibrating function, because the response of

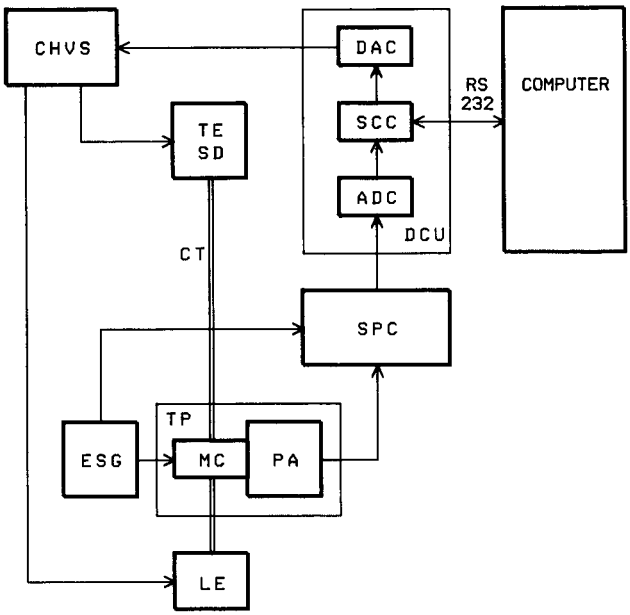

Fig. 1. Block diagram of the equipment. CHVS = Controlled high voltage supply; TE = terminating electrolyte reservoir; SD = sampling device; CT = capillary tube; MC = measuring cell; ESG = exciting signal generator; PA = preamplifier; LE = leading electrolyte reservoir; TP = thermostatted part of the equipment; SPC = signal processing circuit; ADC = 12 bit analog-to-digital converter; SCC = serial communication circuits; DAC = 12 bit digital-to-analog converter; DCU = data conversion unit.

the detector is not linearly dependent on the specific resistance of the electrolyte. A digital-to-analog converter (DAC) controls the driving current supplied to the capillary tube by a controlled high-voltage supply (CHVS). Communication between the computer and the isotachophoretic equipment was realized by means of an optically isolated RS 232 serial line. Before measurement, the thermostat was set at the temperature, T_0 calculated according to eqn. 3. After sample introduction, the control of the experiment was passed to the computer. The control program operates in a conversational manner. The flow chart of that part of the computer program that carries out the temperature control is shown in Fig. 2. A requested starting current together with other data are entered via the keyboard and the computer switches on the current to capillary tube. Subsequently, the computer calculates the thermal power generated in the leading electrolyte. The computer then drives the current in the capillary tube so as to attain the same thermal power in the course of the whole experiment. A programmable timer in a program loop permits variation of the clock frequency of the measurement from 10 Hz to an arbitrarily low value. At the same time, the specific resistance measured is stored in a memory and displayed on a CRT screen in the form of an isotachopherogram.

After the termination of the measurement, any part of the experiment can be graphically presented in any way. Values of the specific resistance or the time can be read with a 12-bit accuracy by means of a cursor. In addition, it is possible to store any

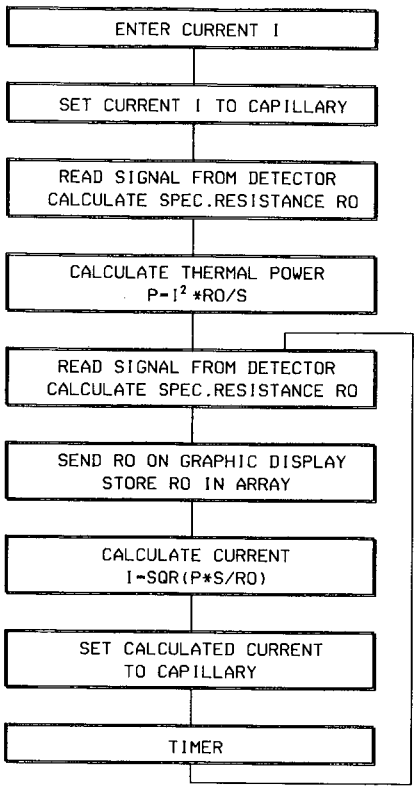

Fig. 2. Flow chart of the control program.

part of or the whole experiment on a floppy disc. An illustration of the isotachopherograms is shown in Fig. 3.

The above described control of the driving current is rapid and without any overshoots. This is due to the small time constant and small open loop gain of the feedback loop. In our earlier work[5], temperature was measured by means of a thermometric detector and the computer controlled the current so as to achieve a constant signal from the detector. To attain a small control error, the open loop gain was higher and, in addition, the time constants in a loop were higher due to thermometric detection. Therefore, the transfer function of the control had to be properly chosen in order to maintain rapid and stable control. We used a so-called self-adaptive control algorithm.

Measurements and calculations

In order to confirm the general applicability of the method and equipment proposed, the limiting mobilities of some anions were determined. Our model[17,18] of the isotachophoretic steady state has been reported previously. In this study, the computational method[18] was modified for evaluation of limiting mobilities from constant temperature isotachophoretic experiments. The model is based on the same

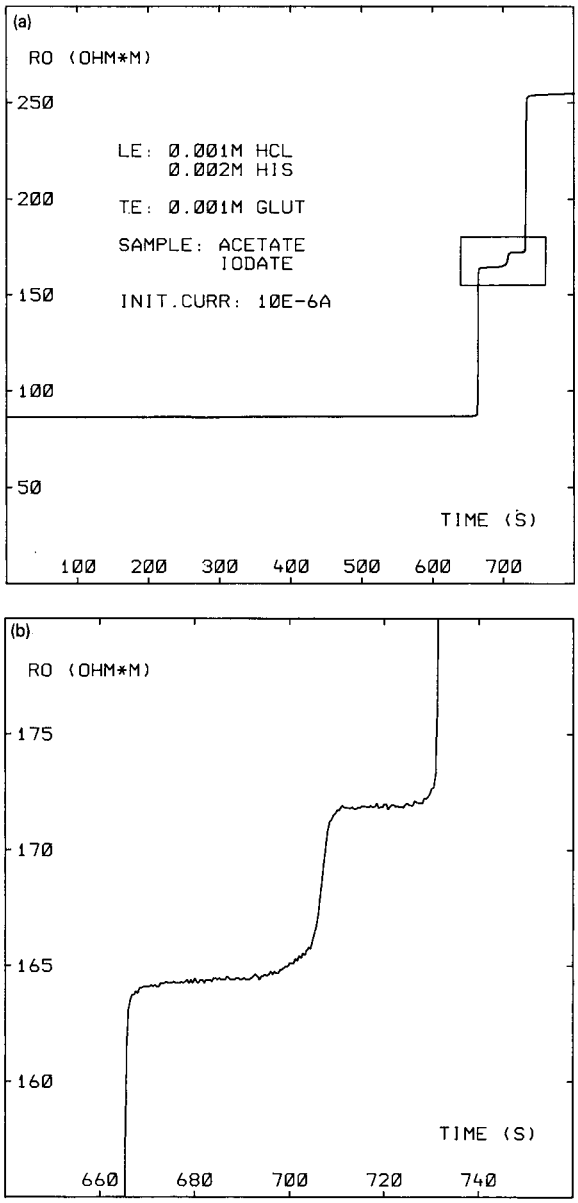

Fig. 3. Illustration of an isotachopherogram and of its computer treatment. (a) Separation of acetate and iodate obtained with the operational system His/His · HCl. The terminating electrolyte was glutamic acid. The initial current was 10 μA. (b) Amplified part of the isotachopherogram.

presumptions as those used for a model described by Everaerts[2], Hirokawa and Kiso[19,20] and other authors and has the following aspects:

(a) All substances can be considered as ampholytes.

(b) The Onsager–Fuoss theory[21] (taking into account the so-called "mixture effect") is used for the relationship between actual and limiting mobilities.

(c) The limiting mobilities, dissociation constants, relative permittivity and viscosity of the solvent can be considered as temperature dependent. In the method proposed, it is not necessary however, because the experiments are carried out at constant temperature.

(d) Acid dissociation constants are not corrected for the ionic strength. (This will be improved on in the near future by using Debye–Hückel equations[22,23].)

The leading electrolyte was 0.002 *M* hydrochloric acid with 0.003 (pH 5.82) and 0.004 *M* (pH 6.12) histidine as a counter ion. The terminating electrolyte was 0.002 *M* glutamic acid. The separation tube had 0.45 mm I.D. The starting driving current was 15 μA. All chemicals used were of analytical reagent grade. The water used was twice distilled. The limiting mobilities of the following acids were determined: strong acids, nitric, iodic, chloric and perchloric; weak monovalent acids, acetic and propionic; weak divalent acids, oxalic, succinic, adipic and maleic; amphiprotic glutamic acid. For oxalic, succinic and adipic acids, the limiting mobilities of the mono- and divalent components could not be obtained simultaneously, because they are almost completely dissociated to the divalent forms. Therefore, the limiting mobilities of the monovalent components were entered into the computer as input data. Similarly, for glutamic acid, the mobility of the ion $glut^+$ is considered to be the same as that of the ion $glut^-$ and the mobility of the ion $glut^{2-}$ is entered as an input datum. For maleic acid, the mobilities of both forms were obtained.

In Table I are listed both the input data for calculation and the data evaluated

TABLE I

LIMITING MOBILITIES EVALUATED (25°C)

pK_a = Thermodynamic acid dissociation constant from refs. 30 and 33. U^0 = evaluated limiting mobility ($m^2\ V^{-1}\ s^{-1}$) · 10^9. σ = Standard deviation of a single measurement of mobility ($m^2\ V^{-1}\ s^{-1}$) · 10^9. U^0(lit) = Limiting mobility from ref. 30.

Anion of acid	pK_a	U^0	σ	U^0(lit)
Hydrochloric (1−)	−6.1[a]	79.1[a]	–	79.1
Nitric (1−)	−1.34[a]	74.5	0.1	74.1
Iodic (1−)	0.77[a]	42.1	0.2	42.0
Chloric (1−)	−2.70[a]	66.9	0.1	67.0
Perchloric (1−)	−7.3[a]	70.0	0.1	69.8
Acetic (1−)	4.76[a]	41.9	0.1	42.4
Propionic (1−)	4.87[a]	36.5	0.1	37.1
Oxalic (1−)	1.27[a]	42.4[a]	–	42.4
Oxalic (2−)	4.27[a]	77.8	0.1	77.0
Succinic (1−)	4.21[a]	33.0[a]	–	33.0
Succinic (2−)	5.64[a]	60.2	0.1	60.9
Adipic (1−)	4.43[a]	24.6[a]	–	24.6
Adipic (2−)	5.41[a]	52.7	0.5	52.4
Maleic (1−)	1.92[a]	40.7	0.4	41.3
Maleic (2−)	6.22[a]	62.0	0.4	62.4
Glutamic (1−)	4.38[a]	29.1	0.2	28.9
Glutamic (2−)	9.96[a]	49.6[a]	–	49.6
Glutamic (1+)	2.16[a]	29.1[b]	–	28.9

[a] Input data for evaluation.

[b] Value set the same as for glutamic acid (1−).

TABLE II

CALCULATED AND EXPERIMENTAL MOBILITIES OF K^+ AND Cl^- (25°C)

U_i = Mobility of ion i calculated by means of Onsager–Fuoss theory[21]. U_i^0 = Limiting mobility of ion i. $U_{K^+} + U_{Cl^-}$(exptl.) = Experimental value of mobility[31,32]. All mobilities in $(m^2\ V^{-1}\ s^{-1}) \cdot 10^9$.

Concentration	U_{K^+}	$U^0_{K^+} - U_{K^+}$	U_{Cl^-}	$U^0_{Cl^-} - U_{Cl^-}$	$U_{K^+} + U_{Cl^-}$	$U_{K^+} + U_{Cl^-}$*(exptl.)*
0	76.2		79.1		155.3	155.3
0.0001 *M* K^+, 0.0001 *M* Cl^-	75.7	0.5	78.6	0.5	154.3	154.6
0.001 *M* K^+, 0.001 *M* Cl^-	74.6	1.6	77.5	1.6	152.1	152.5
0.01 *M* K^+, 0.01 *M* Cl^-	71.3	4.9	74.1	5.0	145.4	146.9

TABLE III

CALCULATED MOBILITIES OF K^+ AND SO_4^{2-} (25°C)

Symbols as in Table II.

Concentration	U_{K^+}	$U^0_{K^+} - U_{K^+}$	$U_{SO_4^{2-}}$	$U^0_{SO_4^{2-}} - U_{SO_4^{2-}}$
0	76.2		82.9	
0.0001 *M* K^+, 0.00005 *M* SO_4^{2-}	75.4	0.8	81.7	1.2
0.001 *M* K^+, 0.0005 *M* SO_4^{2-}	73.7	2.5	79.1	3.8
0.01 *M* K^+, 0.005 *M* SO_4^{2-}	68.4	7.8	71.0	11.9

according to our model. The data reported by Hirokawa *et al.*[24–30] are also given for comparison. A very good agreement with published limiting ionic mobilities is apparent from the table, especially for the anions of strong acids.

In earlier versions of our models[17,18] we calculated the temperatures of the zones by means of eqn. 2 and recalculated temperature-dependent quantities to 25°C. In the method described, the temperature of 25°C is maintained automatically, so that no temperature corrections are necessary. This results in a better accuracy of the physico-chemical quantities evaluated.

An autocalibrating contactless detector having a long-term thermal stability has been used. It follows that the sensing electrodes do not sustain any chemical and physical changes and thus the measurement is not disturbed.

Furthermore, the 1-MHz version of the detector facilitates the use of the electrolyte systems in millimolar range. The lower the concentration of the electrolyte, the lower is the correction of ionic mobilities to infinite dilution carried out by the Onsager–Fuoss theory. The electrolyte system is roughly speaking closer to infinite dilution. For comparison, the calculated mobilities of Cl^- and SO_4^{2-} with a common counter ion K^+ are given in Table II. The difference between the limiting mobility and the mobility at a given concentration together with the values of $u_{K^+} + u_{Cl^-}$ obtained from the experimentally measured dependence of the conductivity on the concentration[31,32] for KCl are also shown. The decrease in the mobility with increasing concentration of di- and polyvalent ions is higher than for monovalent ions (see Table III), so that, for example, SO_4^{2-} cannot be isotachophoretically determined with a 0.001 *M* Cl^- leading electrolyte system, due to the fact that SO_4^{2-} is more mobile than Cl^- at this concentration. It is seen also that the correction required by the theory at 0.01 *M* is more than three times higher than for that of 0.001 *M* as follows from the square root dependence of the mobility on the ionic strength. Even for the most simple case of an uni-univalent electrolyte, the calculated mobility deviates by 1% from the experimentally obtained value at 0.01 *M* (compare the values 145.4 and 146.9).

REFERENCES

1 J. Vacík, J. Zuska, F. M. Everaerts and Th. P. E. M. Verheggen, *Chem. Listy*, 66 (1972) 545.
2 F. M. Everaerts, J. L. Beckers and Th. P. E. M. Verheggen, *Isotachophoresis*, Elsevier, Amsterdam, Oxford, New York, 1976.
3 J. Pospíchal, M. Deml, Z. Žemlová and P. Boček, *J. Chromatogr.*, 320 (1985) 139.
4 J. Pospíchal, M. Deml and P. Boček, *J. Chromatogr.*, 390 (1987) 17.

5 C. Szitás, J. Vacík and J. Zuska, *Fifth International Symposium on Isotachophoresis, Maastricht, Sept. 3–5, 1986.*
6 M. Coxon and M. J. Binder, *J. Chromatogr.*, 95 (1974) 133.
7 M. Coxon and M. J. Binder, *J. Chromatogr.*, 101 (1974) 1.
8 M. Coxon and M. J. Binder, *J. Chromatogr.*, 107 (1975) 43.
9 V. Kašička, *Diploma Thesis*, Charles University, Prague, 1977.
10 Z. Ryšlavý, P. Boček, M. Deml and J. Janák, *J. Chromatogr.*, 144 (1977) 17.
11 M. Demjaněnko, *CS Pat. Certification*, A0 169,577 (1974).
12 B. Gaš, *CS Pat. Certification*, A0 204,104 (1979).
13 B. Gaš, *CS Pat. Certification*, A0 206,186 (1979).
14 B. Gaš, M. Demjaněnko and J. Vacík, *J. Chromatogr.*, 192 (1980) 253.
15 B. Gaš and J. Vacík, *Chem. Listy*, 74 (1980) 652.
16 J. Vacík, J. Zuska and I. Muselasová, *J. Chromatogr.*, 320 (1985) 233.
17 V. Kašička, J. Vacík and Z. Prusík, *J. Chromatogr.*, 320 (1985) 33.
18 V. Zadražil and J. Vacík, in P. Boček (Editor), *Isotachophoresis, Basic Course, Advanced Course, ITP-84, Hradec Králové*, Ústav radioekológie a využitia jadrovej techniky, Spišská Nová Ves, 1984.
19 T. Hirokawa and Y. Kiso, *J. Chromatogr.*, 242 (1982) 227.
20 T. Hirokawa and Y. Kiso, *J. Chromatogr.*, 248 (1982) 341.
21 L. Onsager and R. M. Fuoss, *J. Phys. Chem.*, 36 (1932) 2689.
22 P. Debye and E. Hückel, *Phys. Z.*, 24 (1923) 185.
23 P. Debye and E. Hückel, *Phys. Z.*, 24 (1923) 305.
24 T. Hirokawa and Y. Kiso, *J. Chromatogr.*, 252 (1982) 33.
25 T. Hirokawa, M. Nishino and Y. Kiso, *J. Chromatogr.*, 252 (1982) 49.
26 T. Hirokawa, S. Kobayashi and Y. Kiso, *J. Chromatogr.*, 318 (1985) 195.
27 T. Hirokawa, T. Gojo and Y. Kiso, *J. Chromatogr.*, 369 (1986) 59.
28 T. Hirokawa, T. Gojo and Y. Kiso, *J. Chromatogr.*, 390 (1987) 201.
29 T. Hirokawa, T. Tsuyoshi and Y. Kiso, *J. Chromatogr.*, 408 (1987) 27.
30 T. Hirokawa, M. Nishino, N. Aoki, Y. Kiso, Y. Sawamoto, T. Yagi and J. Akiyama, *J. Chromatogr.*, 271 (1983) D1.
31 R. Brdička and J. Dvořák, *Základy fysikální chemie*, Academia, Praha, 1977.
32 R. Brdička and J. Dvořák, *Grundlagen der physikalischen Chemie*, VEB Deutscher Verlag der Wissenschaften, Berlin, 1988.
33 J. A. Dean (Editor), *Lange's Handbook of Chemistry*, McGraw-Hill, New York, 1973.

Journal of Chromatography, 470 (1989) 79–88
Elsevier Science Publishers B.V., Amsterdam — Printed in The Netherlands

CHROM. 21 214

DATA ACQUISITION IN CAPILLARY ISOTACHOPHORESIS

B. J. WANDERS, A. A. G. LEMMENS, F. M. EVERAERTS and M. M. GLADDINES*
Laboratory of Instrumental Analysis, Eindhoven University of Technology, P.O. Box 513, 5600 MB Eindhoven (The Netherlands)

SUMMARY

A computer program was developed for data acquisition in capillary isotachophoresis. The program consists of two modules, one for data acquisition and the other for data analysis. The data analysis module calculates zone lengths and step heights automatically. This can also be done by the operator on a graphics screen. The program was tested on the analysis of both a thirteen-component standard mixture and a more complex sample.

INTRODUCTION

During the last decade, capillary isotachophoresis (ITP) has been increasingly used for complex samples, but an important drawback is that the zone lengths and step heights still have to be measured manually. The few computer programs[1–3] that have been developed are sufficiently accurate for standard mixtures, but for complex mixtures they still have major limitations.

The program developed by Reijenga *et al.*[1] is based on conversion of the conductometer signal to a signal with chromatographic properties. This was done for two reasons: the smaller amount of memory in the computer needed for data storage, and the fact that a commercial chromatographic signal-processing system can process the converted data and calculate the zone lengths (surface of the peak) and the step heights (time of the peak). Disadvantages of this method of measurement are the loss of time information: a zone with a smaller step height than that for the previous zone, *i.e.*, an enforced zone[4,5] cannot be recognized as such, and the fact that a slightly increasing or decreasing zone can be subdivided by the computer program into more zones[6].

Stover *et al.*[2] developed a program based on a Hewlett-Packard HP-85 microcomputer. In this program, the differentiated conductivity signal is acquired via a 12-bit analogue-to-digital converter (ADC) and the original isotachopherogram can be reconstructed from these differentiated data. A disadvantage of this system is that slightly increasing or decreasing zones will be reconstructed as straight zones. As a consequence, an error may occur in the step-height measurement. In a later version of the program[3] both the analogue and the differentiated signal were acquired. The analogue signal was used for terminator recognition and step-height measurement,

0021-9673/89/$03.50

and zone lengths were determined from the differentiated signal. This program belongs to a system for complete automation of capillary isotachophoresis and will be sufficient for simple isotachophoretic experiments.

A computer program, however, should provide more possibilities for the user, *e.g.*, to manipulate some thresholds, if the automatic data processing fails. This may happen, for example, with complex mixtures. A new program has therefore been developed that possesses, in addition to possibilities for automatic data handling, several routines for manual data analysis, data smoothing and zone-type determination (straight zone, increasing or decreasing zone).

EXPERIMENTAL

The program, written in Turbo Pascal 4.0 (Borland International, Scotts Valley, Ca, U.S.A.), runs on an IBM MS-DOS computer (IBM, Boca Raton, FL, U.S.A.) with a LabMaster ADC (Scientific Solutions, Solon, OH, U.S.A.). The program supports several graphics cards (Hercules, CGA, EGA and VGA).

The program was tested by analysing: a standard sample consisting of thirteen components and a more complex sample, beer ("Bavaria", Lieshout, The Netherlands). This beer sample was taken because the isotachopherogram consisted of both large and small zones.

The zone lengths and step heights were measured both manually on a recorder and by the computer. The analyses were carried out on the laboratory-made equipment described by Everaerts *et al.*[4]. The diameter of the capillary was 0.2 mm and the length was 20 cm. The driving current, delivered by a high-voltage supply (LKB, Bromma, Sweden), was 25 μA. The electrolyte system used for both samples is listed in Table I. The analogue signal of the conductivity detector was digitized by the ADC, which was connected with the IBM computer. The analogue signal was also plotted on a BD41 line-feed recorder (Kipp & Zonen, Delft, The Netherlands) for the manual determination of the step heights. The electronic differentiated conductivity signal, plotted on the recorder, was used for the manual determination of the zone lengths.

TABLE I

ELECTROLYTE SYSTEM FOR THE ITP ANALYSIS OF THE TEST MIXTURE (FIG. 4) AND BEER (FIG. 5)

Leading ion	Chloride
Concentration	0.01 *M*
pH	6.0
Counter ion	Histidine (Merck, Darmstadt, F.R.G.)
Additive	0.2% Hydroxyethylcellulose (Polysciences, Warrington, PA, U.S.A.)
Terminating ion	Morpholinoethanesulphonic acid (MES) (Sigma, St. Louis, MO, U.S.A.)
Concentration	0.005 *M*

RESULTS

Description of the program

Fig. 1 shows the structure of the program. It consists of two modules, a data acquisition and a data analysis module.

Data acquisition module (Fig. 1A)

This is for the regulation of the data collection of the analogue signal of the conductivity detector by the ADC and for writing the data to floppy disk. This module consists of three parts:

"Measure". This starts the data acquisition. The sampling frequency can be varied from 1 to 30 000 Hz. For most routine analyses a sampling frequency of 40 Hz will be satisfactory. During the measurement a real-time plot is displayed on the

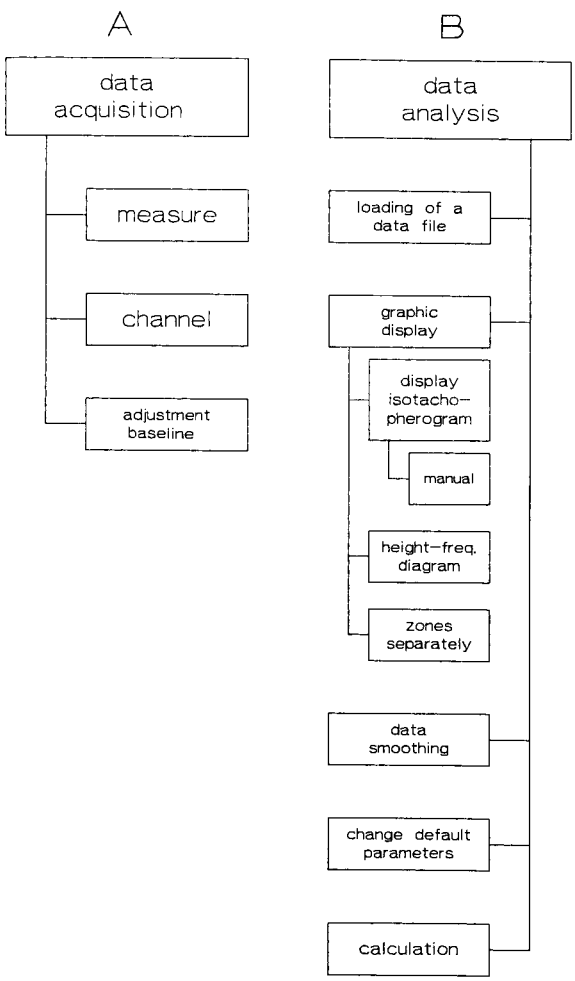

Fig. 1. Outline of the computer program.

screen. After the measurement the user is asked for a name under which the datafile has to be saved.

"Channel". This changes the channel number.

"Adjustment baseline". This adjusts the base line above zero.

Data analysis module (Fig. 1B)

This is for the automatic or manual calculation of the step heights and zone lengths. This module consists of six parts:

Loading of a datafile. This part serves for the loading of an earlier saved datafile from the floppy disk into the RAM of the computer and a first rough definition of the zone borders and a zone-type determination. For the determination of the zone borders the isotachopherogram is transformed into a height-frequency diagram as described[1]. The values which exceed the noise level are indicated as zones, provided that the distance between two zones is larger than the value of the parameter "minimal zone distance". In Fig. 2 zones 1, 2 and 5 are recognized by the program as separate zones, whereas zones 3 and 4 are linked. The peak between 1 and 2 is not identified as a zone at this noise level. Finally, a routine "zone-type determination" attributes to each zone a zone-type number: 1 for a straight zone, 2 for a decreasing zone, 3 for an increasing zone and 4 for a small zone.

Graphics display of the results. With three graphics screen plot functions, the determination of the zone borders can be examined. The first function can display the whole isotachopherogram, the inflection points and estimated zone borders. The

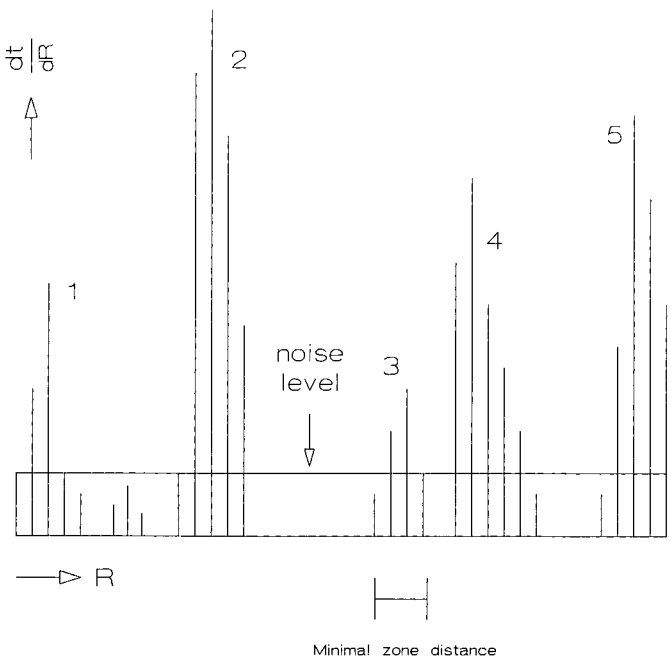

Fig. 2. A converted diagram of a isotachopherogram according to Reijenga *et al.*[1]. t = time; R = electric resistance.

second function plots the height–frequency diagram (Fig. 2). The third function plots the zones separately.

Data smoothing. This part smooths the data when the noise is too high. This routine works with a digital noise filter; the value of a certain point is recalculated from the mean of the surrounding points, where the contribution of each point to the mean value depends on the distance to the original point. In this routine a 25-point filter is used according to the theory of Savitsky and Golay[7,8].

Change default parameters. This part gives the possibility of changing the (default) parameters "noise level" and "minimal zone distance".

Calculation. In this part the step heights and zone lengths are calculated automatically. First, the inflection points are determined. The inflection points are the maxima of the first derivative of the signal. The first derivative is calculated with a Savitsky and Golay filter as described under *Data smoothing*. The parameter "differentiation limit" determines the minimal value that the first derivative must fulfil in order to be recognized as an inflection point. The parameter "differentiation limit" can be entered by the user before the automatic calculation. In flat zone borders, where the first derivative is below this value, no inflection point will be found. The inflection point is estimated from the middle between the temporary zone borders. The zone length is now determined from the distance between two inflection points.

The step height is determined separately for each zone type:

Zone type 1 (straight zone): the mean of all points between the left and right border for which the first derivative is zero.

Zone type 2 (decreasing zone): the highest point between the left border and right zone border.

Zone type 3 (increasing zone): the mean of the step height of the first part (40 points) of the zone to obtain reproducible step heights for zones of different lengths.

Zone type 4 (small zone): the step height of very small zones (fewer than 40 points) is determined from the mean step height of all points between the left and right zone border.

Finally, the results of this part are printed. An example of this is shown in Table II, where a computer output is shown of the analyses of the beer sample (Fig. 5).

"Manual" determination of the zone characteristics. If the zones are not correctly determined in the previous part, then with this part zone lengths and step heights can be determined "manually". This means that the zone lengths and step heights can be determined on the screen.

Starting with the plot procedure "graphic display of results", the whole isotachopherogram is displayed on the screen (Fig. 3). If necessary it is possible to enlarge a certain part of the isotachopherogram. For the determination of the zone lengths two vertical lines can be displayed on the screen. With the cursor keys the lines can be moved. Under the isotachopherogram the distance between the two lines is displayed. For determining the length of a certain zone the lines have to be moved to the inflection points of the zone. The zone length is then displayed under the isotachopherogram. The minimal error of the "manual" zone length determination is 0.025 s (at 40 Hz) with full enlargement of the isotachopherogram.

Analogously the step height can be determined with horizontal lines.

TABLE II

EXAMPLE OF OUTPUT FROM THE COMPUTER AFTER AN AUTOMATIC CALCULATION

Sample, 1 μl of beer (see Fig. 5). Ba6 = sample name; Diff. Limit = differentation limit; Min. Zone Dis. = minimal zone distance; Type = see text; I/Z = method of zone length calculation (I = between inflection points; Z = between zone borders if one or two inflection points are not found); SH = step height; RSH = relative step height; ZL = zone length.

Ba6	Noise Level= 3			Diff. Limit= 25	Min.Zone Dis.= 5	
	Zone	Type	I/Z	SH	RSH	ZL
Leading		3	-	224	0.0000	-
	1	1	I	327	0.0295	3.40
	2	1	I	382	0.0453	2.38
	3	4	I	619	0.1132	1.22
	4	3	I	692	0.1342	16.27
	5	1	I	770	0.1565	6.95
	6	3	I	880	0.1881	2.25
	7	3	I	1044	0.2351	4.52
	8	3	Z	1141	0.2629	12.30
	9	1	Z	1350	0.3228	70.70
	10	3	I	1363	0.4134	14.00
Terminator		2	-	3712	1.0000	-

Testing of the program

Fig. 4 shows the isotachopherogram of a standard mixture. In Table III the results are shown of the zone length measurements for five analysis of the sample with an injection amount of 4 μl, which corresponds to an absolute injection amount of 1 nmol for each component. To test the program for small zones, we also analysed 1 μl. These results are also shown in Table III. In Table IV the results are shown for the relative step-height measurements for the same injection amounts.

It can be seen that the automatic measurements for both the zone lengths and step heights agree with the manual measurements. The coefficients of variation of the zone-length measurements vary from 0.5 to 3% for both methods. With the manual measurement, however, a recorder speed of 30 cm/min was used, whereas the normal speed is 6 cm/min. If the latter speed had been used a larger error (30 cm/min ± 0.1 s,

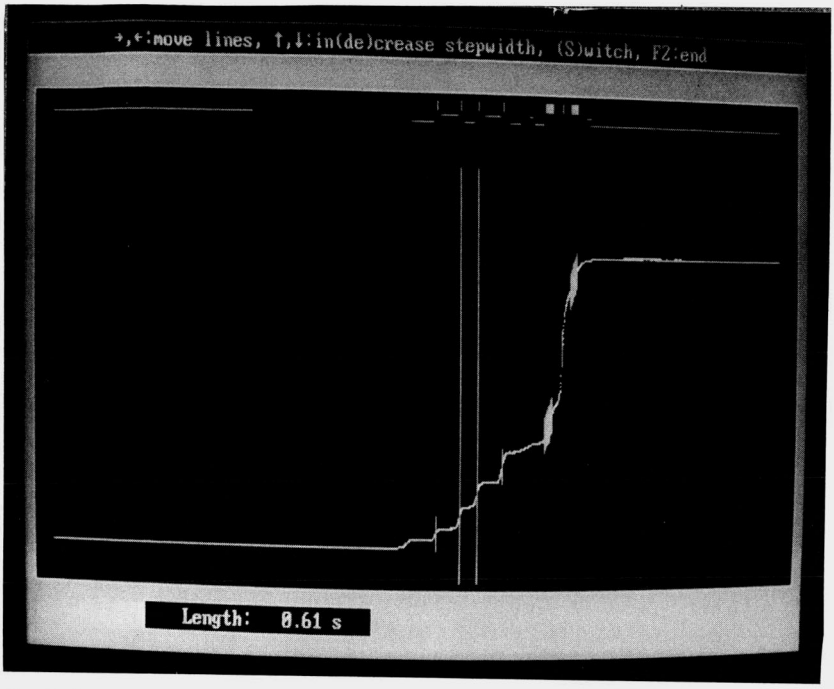

Fig. 3. Screen display of an isotachopherogram.

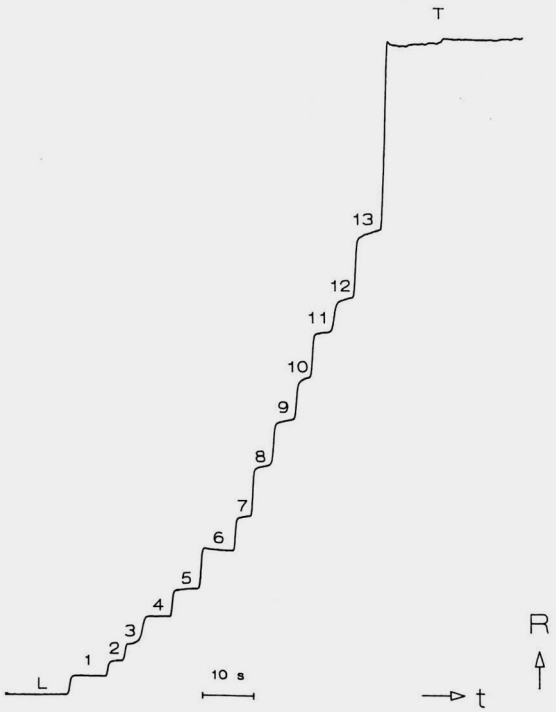

Fig. 4. Isotachopherogram of a test mixture analysed using the electrolyte system in Table I. L = Leading; 1 = sulphate; 2 = chlorate; 3 = chromate; 4 = malonate; 5 = pyrazole-3,5-dicarboxylate; 6 = adipate; 7 = acetate; 8 = β-chloropropionate; 9 = benzoate; 10 = naphthalene-2-monosulphonate; 11 = glutamate; 12 = enanthate; 13 = benzylaspartate; T = terminator. t = time; R = resistance.

TABLE III

MEAN AND STANDARD DEVIATION (S.D.) FOR THE MANUAL (USING A LINE FEED RECORDER) AND AUTOMATIC (USING THE COMPUTER) ZONE-LENGTH MEASUREMENTS ON THE TEST MIXTURE (n = 5)

The numbers correspond to the zones indicated in Fig. 4.

Zone No.	*Injection amount*							
	1 nmol				*0.25 nmol*			
	Manual		*Computer*		*Manual*		*Computer*	
	Mean (s)	*S.D.*	*Mean (s)*	*S.D.*	*Mean (s)*	*S.D.*	*Mean (s)*	*S.D.*
1	7.39	0.42	7.32	0.48	2.16	0.10	2.16	0.08
2	3.25	0.00	3.24	0.04	1.21	0.02	1.20	0.05
3	3.35	0.06	3.38	0.06	0.79	0.02	0.79	0.03
4	5.42	0.06	5.43	0.08	1.56	0.02	1.54	0.02
5	5.31	0.02	5.32	0.04	1.50	0.03	1.50	0.02
6	6.09	0.04	6.09	0.07	2.38	0.07	2.37	0.06
7	3.15	0.06	3.12	0.07	1.03	0.03	1.03	0.03
8	3.78	0.06	3.76	0.05	1.18	0.02	1.19	0.04
9	4.02	0.04	4.03	0.05	1.23	0.01	1.24	0.01
10	2.83	0.06	2.84	0.06	0.86	0.02	0.86	0.01
11	3.77	0.07	3.81	0.07	1.06	0.01	1.07	0.01
12	3.71	0.08	3.73	0.09	1.02	0.02	1.02	0.03
13	4.99	0.16	5.02	0.18	1.43	0.03	1.41	0.02

TABLE IV

MEAN AND STANDARD DEVIATION (S.D.) FOR THE MANUAL (USING A LINE FEED RECORDER) AND AUTOMATIC (USING THE COMPUTER) RELATIVE STEP-HEIGHT MEASUREMENTS ON THE TEST MIXTURE (n = 5)

The numbers correspond to the zones indicated in Fig. 4.

Zone No.	*Injection amount*							
	1 nmol				*0.25 nmol*			
	Manual		*Computer*		*Manual*		*Computer*	
	Mean	*S.D.*	*Mean*	*S.D.*	*Mean*	*S.D.*	*Mean*	*S.D.*
1	0.029	0.0007	0.029	0.0005	0.029	0.0009	0.030	0.0006
2	0.051	0.0000	0.051	0.0007	0.051	0.0006	0.053	0.0006
3	0.078	0.0005	0.079	0.0012	0.081	0.0009	0.084	0.0010
4	0.119	0.0005	0.119	0.0008	0.116	0.0009	0.116	0.0007
5	0.161	0.0005	0.161	0.0007	0.160	0.0020	0.160	0.0008
6	0.219	0.0005	0.223	0.0011	0.222	0.0027	0.221	0.0011
7	0.269	0.0007	0.269	0.0007	0.275	0.0010	0.273	0.0011
8	0.348	0.0018	0.347	0.0008	0.353	0.0040	0.350	0.0017
9	0.419	0.0019	0.418	0.0015	0.424	0.0026	0.419	0.0018
10	0.483	0.0009	0.483	0.0015	0.487	0.0044	0.480	0.0022
11	0.552	0.0018	0.552	0.0018	0.555	0.0032	0.550	0.0017
12	0.605	0.0019	0.604	0.0021	0.603	0.0041	0.598	0.0023
13	0.709	0.002	0.705	0.0006	0.704	0.0047	0.699	0.0030

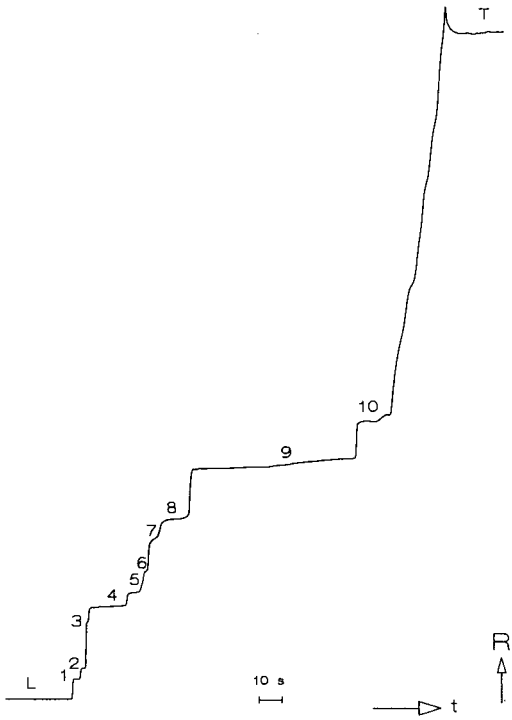

Fig. 5. Isotachopherogram of a beer sample analysed using the electrolyte system in Table I. L = Leading; 1 = sulphate; 3 = formate; 4 = malate; 5 = citrate; 10 = phosphate; 2,6,7,8,9 = not identified; T = terminator. t = time; R = resistance.

TABLE V

MEAN AND STANDARD DEVIATION (S.D.) FOR THE MANUAL (USING A LINE FEED RECORDER) AND AUTOMATIC (USING THE COMPUTER) ZONE-LENGTH AND RELATIVE STEP-HEIGHT MEASUREMENTS ON THE BEER SAMPLE (n = 10)

The numbers corresponds with the zones indicated in Fig. 5. The numbers in parenthesis denote the number of zones which are measured "manually" using the graphics screen plot.

Zone No.	*Zone length*				*Step height*			
	Manual		*Computer*		*Manual*		*Computer*	
	Mean	*S.D.*	*Mean*	*S.D.*	*Mean*	*S.D.*	*Mean*	*S.D.*
1	3.27	0.17	3.30	0.19	0.029	0.0003	0.030	0.0004
2	2.31	0.09	2.34	0.07	0.044	0.0004	0.045	0.0003
3	1.21	0.01	1.22	0.02	0.111	0.0010	0.113	0.0010
4	16.20	0.10	16.18	0.12	0.136	0.0015	0.134	0.0013
5	6.93	0.05	6.96	0.07(1)	0.158	0.0012	0.157	0.0010
6	2.19	0.02	2.22	0.04	0.185	0.0020	0.188	0.0015
7	4.57	0.07	4.55	0.09(1)	0.236	0.0015	0.234	0.0019
8	12.60	0.35	12.55	0.58(3)	0.264	0.0025	0.262	0.0023
9	69.45	1.20	69.53	1.30	0.325	0.0039	0.327	0.0042
10	14.40	0.37	14.37	0.41(1)	0.410	0.0018	0.412	0.0024

60 cm/min ± 0.5 s), due to the thickness of the recorder pen, could be expected for the manual measurements, especially for small zones.

Finally, the program was tested with a complex sample. A 1-μl volume of beer was injected ten times and Fig. 5 shows the isotachopherogram obtained. The zone lengths and relative step heights of the ten zones were measured by the computer and manually, using the analogue differentiated signal on the recorder. The results are given in Table V. The automatic measurements correspond well with the manual measurements. In Table V those zones which were measured "manually", using the graphics screen plot, when the automatic data processing failed are indicated.

CONCLUSIONS

The use of this computer program for data acquisition in capillary isotachophoresis will expand its applications in routine analysis. The program can measure zone lengths and step heights automatically or "manually" using a graphics screen plot. For most applications the automatic data processing will be sufficiently accurate. For complex samples a manual correction may be necessary for some zones. Tests with the program have shown that the automatic measurements agree with the manual measurements.

REFERENCES

1 J. C. Reijenga, W. van Iersel, G. V. A. Aben, Th. P. E. M. Verheggen and F. M. Everaerts, *J. Chromatogr.*, 292 (1984) 217.
2 F. S. Stover, K. L. Depperman and W. A. Grote, *J. Chromatogr.*, 269 (1983) 198.
3 F. S. Stover, K. L. Depperman, W. A. Grote and D. V. Vinjamoori, *J. Chromatogr.*, 390 (1987) 61.
4 F. M. Everaerts, J. L. Beckers, Th. P. E. M. Verheggen, *Isotachophoresis—Theory, Instrumentation and Applications* (*Journal of Chromatography Library*, Vol. 6), Elsevier, Amsterdam, 1976.
5 P. Gebauer and P. Boček, *J. Chromatogr.*, 267 (1983) 49.
6 M. Gladdines, *Training Report*, Eindhoven University of Technology, 1983.
7 A. Savitzky, M. J. E. Golay, *Anal. Chem.*, 36 (1964) 1627.
8 J. Steiner, Y. Termonia, J. Deltour, *Anal. Chem.*, 44 (1972) 1906.

Journal of Chromatography, 470 (1989) 89–93
Elsevier Science Publishers B.V., Amsterdam — Printed in The Netherlands

CHROM 21 215

METHODS FOR ON-LINE DETERMINATION AND CONTROL OF ELECTROENDOSMOSIS IN CAPILLARY ELECTROCHROMATOGRAPHY AND ELECTROPHORESIS[a]

B. J. WANDERS,* A. A. A. M. VAN DE GOOR and F. M. EVERAERTS
Laboratory of Instrumental Analysis, Eindhoven University of Technology, P. O. Box 513, 5600 MB Eindhoven (The Netherlands)

SUMMARY

Systems are described for the on-line determination and control of electroendosmosis that offer several advantages for both electrochromatographic and electrophoretic separations. For electrochromatographic separations the control system can be used to stabilize the electroendosmosis and obtain a better reproducibility of the results. For electrophoretic separations this control system offers the possibility of a so-called "upstream" separation, which results in a decrease in the plate height and thus a better resolution. Further, the controlable electroendosmosis can be used to determine with high reproducibility, in one run, both ionic (anions and cations) and non-ionic components, using only one detector.

INTRODUCTION

Electroendosmotic flow (EOF) is a liquid flow that occurs if an electric field is applied over the length of a capillary that has an active surface and is filled with an electrolyte. This flow originates from the existence of an electric double layer between the charged capillary wall and the liquid. The theoretical background has been discussed more extensively elsewhere[1–7].

In capillary zone-electrophoresis (CZE), in which ionic components are separated on basis of the difference in their effective mobilities in an electric field, and in capillary electro-chromatography (CEC, also called electroendosmotically driven liquid chromatography[8–10]), in which non-ionic components are separated, EOF can be used as a liquid pump. Instead of open capillaries, capillaries packed with small particles or tubes can also be applied[11].

In all these instances it is of the greatest importance that the EOF is constant, or at least is known during the experiment (for the identification of the components). A solution to this problem is an on-line measurement and control system for EOF, as described here.

[a] Patent pending, application No. 8802273 (The Netherlands).

0021-9673/89/$03.50

THE CONTROL SYSTEM

The control system for electroendosmosis consists of two main parts. The first part is a unit which measures the EOF on-line and the value is registered by a computer. The second part is the control unit, which can execute control both directly and indirectly.

The measurement unit

On-line determination of EOF using an analytical balance. With the use of an analytical micro-balance, the weight of one electrode vessel is monitored in a specified time interval (1–10 s) and this value is sent to a computer through an interface (IEEE or RS232) (Fig. 1). With this value the EOF can be calculated using the equation.

$$v_{eo} = \Delta W/\Delta t \cdot 1/(\pi r^2 \rho) \quad (1)$$

where v_{eo} is the EOF (m/s), $\Delta W/\Delta t$ the change in weight during the specified time interval (kg/s), r the radius (m) of the capillary and ρ the density of the electrolyte (kg/m^3).

On-line determination of EOF using a post-column detector. In this method a constant reference flow is used in which a strong UV-absorbing marker is dissolved. This flow is mixed with the main flow (= EOF). By measuring the UV absorption in this mixed flow, information can be obtained about the ratio between the reference flow and the main flow. Because the reference flow is constant and known, the flow-rate of the main flow can also be calculated.

As a liquid pump for the reference flow, both a mechanical (Fig. 2) and an electroendosmotic (Fig. 3) pump can be used. Gas bubbles formed when using an "EOF" pump can be trapped, if they interfere with the main flow and stop the EOF (current switch-off), in different ways [*e.g.*, bubble trap (Fig. 3, III)]. The result of the

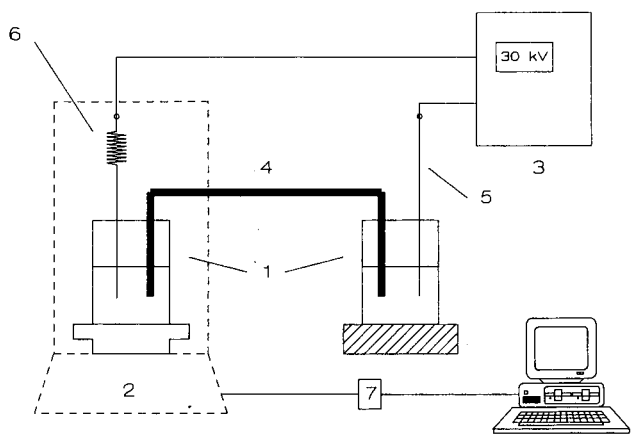

Fig. 1. Schematic representation of the on-line determination of the EOF by weighing. 1 = Electrolyte vessels; 2 = balance; 3 = high-voltage power supply; 4 = capillary; 5 = platinum electrode; 6 = balanced electrode; 7 = interface.

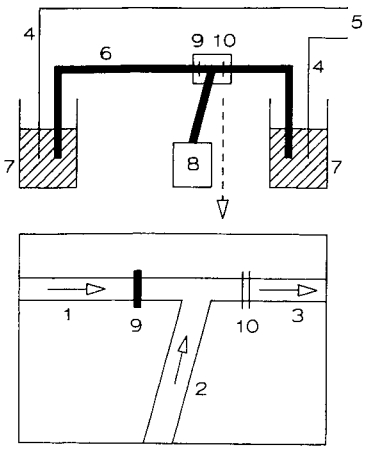

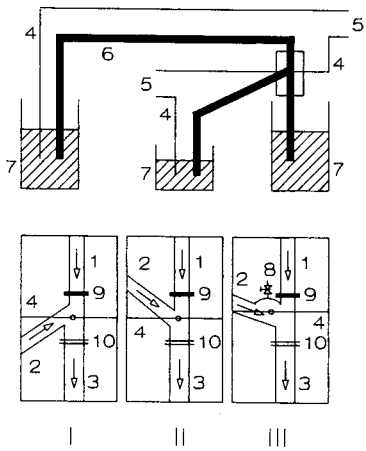

Fig. 2. Schematic representation of the on-line determination of the EOF using a post-column detector and a mechanical pump. 1 = Main flow; 2 = reference flow; 3 = mixed flow; 4 = electrodes; 5 = high-voltage power supply; 6 = capillary; 7 = electrolyte vessels; 8 = mechanical pump; 9 = analytical detector; 10 = post-column detector.

Fig. 3. Schematic representation of the on-line determination of the EOF using a post-column detector and an EOF pump. 1 = Main flow; 2 = reference flow; 3 = mixed flow; 4 = electrodes; 5 = high-voltage power supply; 6 = capillary; 7 = electrolyte vessels; 8 = bubble trap; 9 = analytical detector; 10 = post-column detector.

on-line measurement of the EOF is registered by a computer, to be used in the control unit.

The control unit

Direct control of the EOF can be achieved by coupling the computer to the high-voltage power supply (*e.g.*, Gamma HV50000/1.25; Gamma High Voltage Research, Mt. Vernon, NY, U.S.A.). A change in the EOF can then be corrected by decreasing or increasing the voltage applied. Indirect control can be achieved by adjusting the speed of the recorder or by correcting the results, after the experiment, for the values of the EOF (Fig. 4).

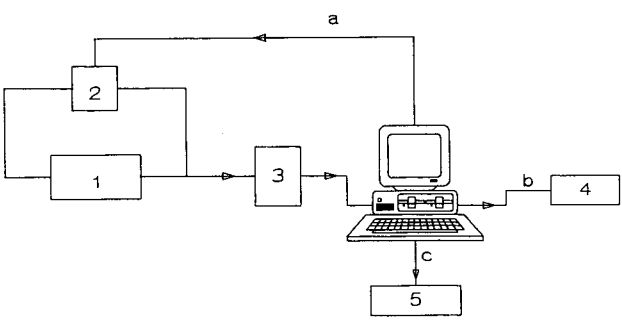

Fig. 4. Schematic representation of the control system. 1 = Separation compartment; 2 = high-voltage power supply; 3 = on-line measurement of the EOF; 4 = recorder; 5 = printer/screen. a = Direct control; b = indirect control by adjusting the speed of the recorder; c = indirect control by recalculation of the results after the experiment.

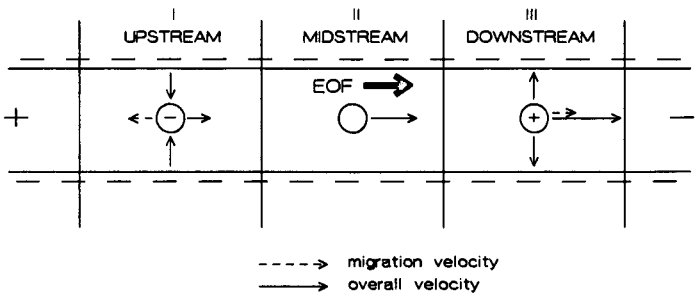

Fig. 5. Representation of the simultaneous separation of anions, cations and non-ionic components. The wall carries a negative charge. Repulsion of the anions in the upstream section and attraction of the cations in the downstream section is obtained.

Advantages of the control system

Without an on-line measurement and control system, the EOF may vary under the influence of, *e.g.*, temperature or surface-active components, between two experiments, or even during one experiment. This leads to poor reproducibility of the results. The first advantage of the control system is an improvement in reproducibility for both electrophoretic and electro-chromatographic separations. In addition on-line control of the EOF also offers other possibilities for both CEC and CZE.

In CEC, the EOF can now be used as a reproducible pump, which can compete with, or even is better than, a mechanical pump. The advantage of using an "EOF" pump is its almost flat velocity profile. Consequently, the peak broadening is reduced and the separation is of better quality. In CZE, this control system for the EOF offers the possibility of a so-called "upstream" separation (Fig. 5, I). In this instance the separation of, *e.g.*, anions is performed while the EOF is flowing in the opposite direction. The combination of the increase in separation time and the repulsion between the ions and the capillary wall results in smaller plate heights and hence better resolution.

A final advantage of the control system is the possibility of combining both CZE and CEC techniques for the simultanous separation of ionic and non-ionic components using only one detector. In Fig. 5 a difference is made between the "upstream" separation (discussed in the previous example), the "downstream" separation and "midstream" separation. In a "downstream" separation, non-ideal separation conditions can arise because of interactions between the wall and sample components and the decrease in separation time. The term "midstream" separation is used for the chromatographic separation of the non-ionic components; moreover, stationary phases can be used.

In this study the EOF has been measured[12]. The regulation of EOF and its contribution to the separation is under investigation.

CONCLUSIONS

The vital condition of using EOF in both CEC and CZE is the possibility of an on-line measurement and control system. Such a control system not only improves the quality of CZE and CEC, but also adds some new possibilities to both techniques

such as the simultaneous separation of anions, cations and non-ionic components, using only one detector.

REFERENCES

1. A. J. Rutgers, M. de Smet and W. Rigole, in H. van Olphen and K. J. Mysels, *Physical Chemistry: Enriching Topics from Colloid and Surface Sciences*, Theorex, La Jolla, CA, 1975.
2. R. J. Hunter, *Zeta Potential in Colloid Science*, Academic Press, London, 1981.
3. J. T. Davies and E. K. Rideal, *Interfacial Phenomena*, Academic Press, New York, 2nd ed., 1963.
4. A. W. Adamson, *Physical Chemistry*, Interscience, New York, 2nd ed., 1967.
5. F. E. P. Mikkers, F. M. Everaerts and Th. P. E. M. Verheggen, *J. Chromatogr.*, 169 (1979) 11.
6. J. E. Jorgenson and K. D. Lukacs, *Anal. Chem.*, 53 (1981) 1298.
7. H. H. Lauer and D. McManigill, *Anal. Chem.*, 58 (1986) 166.
8. J. H. Knox and I. H. Grant, *Chromatographia*, 24 (1987) 135.
9. V. Pretorius, B. J. Hopkins and J. D. Schieke, *J. Chromatogr.*, 99 (1974) 23.
10. T. Tsuda, K. Nomura and G. Nakagawa, *J. Chromatogr.*, 248 (1982) 241.
11. A. S. Cohen and B. L. Karger, *J. Chromatogr.*, 397 (1987) 409.
12 A. A. A. M. van de Goor, B. J. Wanders and F. M. Everaerts, *J. Chromatogr.*, 470 (1989) 95.

Journal of Chromatography, 470 (1989) 95–104
Elsevier Science Publishers B.V., Amsterdam — Printed in The Netherlands

CHROM. 21 216

MODIFIED METHODS FOR OFF- AND ON-LINE DETERMINATION OF ELECTROOSMOSIS IN CAPILLARY ELECTROPHORETIC SEPARATIONS

A. A. A. M. VAN DE GOOR*, B. J. WANDERS and F. M. EVERAERTS
Laboratory of Instrumental Analysis, Eindhoven University of Technology, P.O. Box 513, 5600 MB Eindhoven (The Netherlands)

SUMMARY

Two modified methods for measuring the ζ-potential and electroosmotic flow in capillaries for electrophoretic or electrochromatographic separations are discussed. Streaming potential measurements with computer control and data acquisition can be used off-line for rapid screening of the behaviour of capillaries. To test the equipment, the variation of the ζ-potential with pH was performed and the characteristics of the system are discussed. Weighing measurements were performed on-line. The variation of the measurements with increased electric field strength are shown. For both methods the reproducibility and the accuracy are discussed.

INTRODUCTION

In the last 15 years electroosmosis has been introduced as a way of transporting the mobile phase in capillary chromatography[1] and the electrolyte solution in capillary electrophoresis[2]. The benefit for chromatography is the flat velocity profile of electroosmotic flow (EOF) compared with the parabolic flow profile arising from mechanical pumping. This often leads to a decrease in band broadening and, therefore, to higher plate numbers[3,4]. The advantage for electrophoresis is the streaming electrolyte, which can be used to sweep all ions towards the detector irrespective of the sign of their charge. In this instance the absolute value of the electroosmotic velocity must be higher than the absolute value of the electrophoretic velocities of each of the sample components. If the electroosmosis is oriented opposite to the electrophoretic direction of the ion and has a lower absolute value, then a counter flow of electrolyte occurs[5,6]. This always leads to an increase in separation time to obtain full resolution.

EOF in capillaries originates from an electric double layer between the capillary wall and the liquid present in the capillary. If an electric field is applied over the length of the capillary, the liquid starts to flow. However, other electrokinetic phenomena, such as electrophoresis and surface conductance, appear simultaneously. These phenomena influence the electroosmosis. Therefore, many parameters characterize the separation. Understanding, predicting and controlling the EOF, therefore, demands a measuring technique that resembles closely the experimental separation conditions.

0021-9673/89/$03.50

Several methods have already been applied. A neutral marker molecule can be used to estimate the EOF[7–9]. This molecule is transported by the liquid flow and should not be influenced by the electric field gradient or any adsorption effect. This method, however, meets the same problems as finding a good zero retention time (t_{R0}) marker, in liquid chromatography.

Colloidal particles, of the same material as the capillary, can be used[10]. Their electrophoretic migration gives information about the electrokinetic behaviour of the material, although a large difference exists between this method and the separation conditions.

Streaming potentials can be used to characterize the EOF[11–14]. Reijenga *et al.*[15] applied this method to predict the effect of the EOF on the boundary conditions in isotachophoresis.

Altria and Simpson[16,17] introduced the idea of weighing the electrolyte which leaves the capillary, giving direct information about the EOF. This technique, however, gives only time-averaged results. On the other hand, no additives are needed to determine the flow. Therefore, it resembles most closely the experimental conditions.

We have adapted the method of Reijenga *et al.*[15] and modified it to a computer-controlled measuring system, which allows the changes in the capillary with time to be monitored. We also modified the technique of Altria and Simpson[16,17] to an on-line measuring system. Both techniques are discussed after a brief theoretical explanation.

THEORY

The theory of electrokinetic phenomena such as electroosmosis, electrophoresis, surface conductance and streaming potential has been discussed extensively elsewhere[11,12,18,19]. Some necessary aspects will be pointed out in order to understand the techniques described. When an insulator is immersed in a liquid, an electric double layer results at the interface. This is caused by the charged surface arising from ionic substances, which can be adsorbed, or from charged groups that are introduced by dehydration. Because of this charged surface, ionic species with similar charge sign

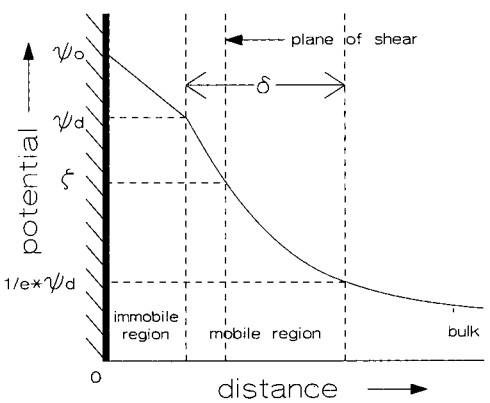

Fig. 1. Representation of the double layer.

(co-ions) are repelled from the surface while species with opposite charge sign (counter ions) are attracted. This results in the so-called electric double layer. Part of these counter ions are immobilized by a strong interaction with the surface. Others, which reach further into the liquid, form the mobile, diffuse part. Because no electroneutrality exists within the electric double layer, a potential gradient arises as described in the Gouy–Chapman theory.

Fig. 1 shows schematically the potential gradient at the solid–liquid interface. ψ_0 is the electric potential at the surface. From this surface the potential decreases, while entering the liquid, because the space charge diminishes. The potentials at certain planes are defined to characterize the double layer. ψ_d is the potential at the interface between the immobile and mobile parts of the double layer. The thickness of the double layer, δ, is defined as the length between the two planes where the potential is $(1/e)\,\psi_d$ and ψ_d, respectively[11]. A third characteristic potential is the ζ-potential, which is the potential at the plane of shear, occurring when the liquid is forced to move.

The described interface is found in capillary electrochromatography and capillary electrophoresis between the capillary wall and the liquid present in the capillary. When an external electric field is applied tangentially to the surface, several electrokinetic phenomena arise. Bulk electrolyte conductance and surface conductance are a direct consequence of the electric field. Under operational conditions the surface conductance can usually be ignored. Electroosmosis arises from the movement of the ions in the diffuse part of the double layer. The electrolyte is dragged along by these ions, which causes a liquid flow in the direction of the counter ions.

The Smoluchowski equation (eqn. 1) can be used to describe the velocity of the liquid flow. It should be stated that this equation is valid only for capillary systems in which the diameter is considerably larger than the double layer thickness. Also, a uniform electrolyte in the system and a constant ζ-potential over the whole capillary surface is expected[20].

$$v_{eo} = \frac{\varepsilon\ \zeta\ E}{\eta} \tag{1}$$

where v_{eo} is the electroosmotic velocity (m/s), ε the dielectric constant (F/m), η the viscosity of the electrolyte (kg/m · s), ζ represents the ζ-potential (V) of the capillary wall and E is the electric field strength (V/m) over the capillary. When, instead of an electric field, a pressure gradient is applied tangential to the solid–liquid interface, a potential difference, the streaming potential, is the result. The streaming potential, E_{st}, can also be correlated with the ζ-potential of the surface and thus to the EOF by the equation

$$E_{st} = \frac{\Delta P\ \varepsilon\ \zeta}{\eta\ \kappa} \tag{2}$$

were ΔP is the pressure drop (N/m^2) over the system and κ is the specific conductance ($1/\Omega m$) of the electrolyte. Eqn. 2 can only be used when surface conductance can be neglected with respect to the specific conductance of the electrolyte. A laminar flow within the capillary is also required.

EXPERIMENTAL

Streaming potentials

The experimental setup used was similar to that in the method of Reijenga *et al.*[15]. The situation is depicted in Fig. 2.

A capillary was fitted between two electrolyte vessels through plastic plugs. Ag/AgCl electrodes (40 × 1 mm), made according to the method of Thomson[21], were placed in the vessels. The vessels contained connections allowing nitrogen to enter for pumping the electrolyte.

From eqn. 2, it is clear that high streaming potentials and, therefore, high resolution can be obtained by using high pressure drops. Therefore, care should be taken with chosing proper capillary dimensions. Using PTFE capillaries the pressure applied is limited to 1 atm because of the porosity of the capillary wall. This pressure drop, on the other hand, limits the maximum length of the capillary because of the minimum liquid flow required. However, to obtain a laminar flow during at least 90% of the capillary, a minimum length of 20 cm (I.D. 300 μm) was necessary[13]. The nitrogen pressure was switched using two magnetic valves, controlled by a computer, through an analytical interface (Perkin-Elmer, Norwalk, CT, U.S.A.).

Streaming potentials were measured by connecting the electrodes directly to a high-input impedance (10^{12} Ω) mV meter (PW9414; Philips, Eindhoven, The Netherlands). The signal was then both recorded on a BD41 strip-chart recorder (Kipp & Zonen, Delft, The Netherlands) and sent to an Apple IIe computer (Apple Computer, Cupertino, CA, U.S.A.) through the same interface.

The following cycles were performed. First, pressure was applied to one of the vessels during a period of 20 s. In this time interval the potential difference across the capillary had time to stabilize and the streaming potential was read and stored. In the following 20 s the flow was forced in the opposite direction by applying the pressure to

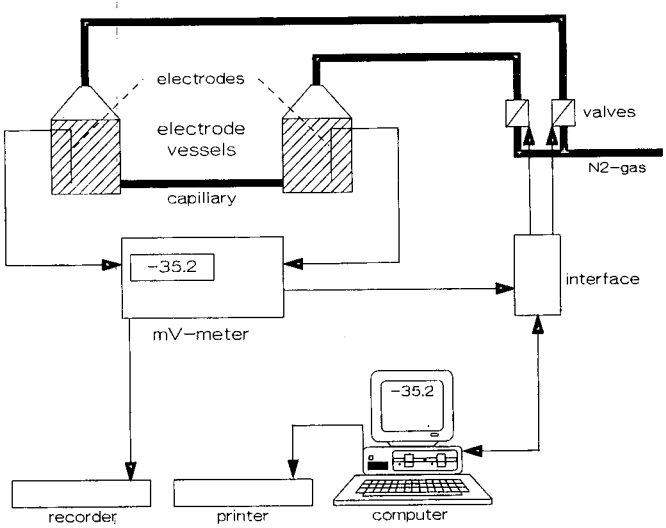

Fig. 2. Experimental setup used for streaming potential measurements.

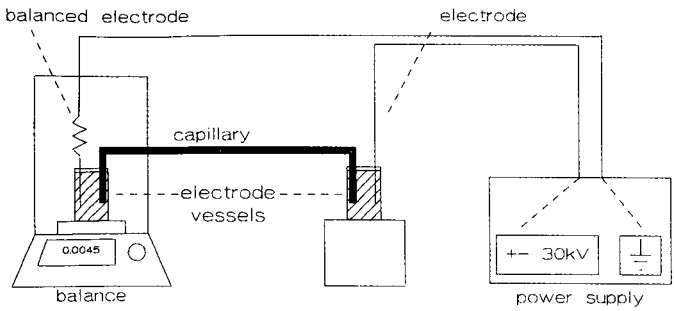

Fig. 3. Experimental setup used for weighing measurements of electroosmotic flow.

the other vessel. Again the streaming potential was measured. Finally, no pressure was applied for another 20 s. The potential difference between the electrodes was measured and used as a reference. By this procedure an acceptable constant liquid level in the vessels and, therefore, a constant liquid–electrode contact surface area was obtained. This procedure also minimizes disturbances by gravity flow and corrects for asymmetry between the electrolyte vessels. The streaming potential was calculated by averaging the absolute value of both potential differences, corrected for the reference value.

ζ-Potentials were calculated (eqn. 2) using the specific conductivity of the solution, measured off-line with a digital conductivity meter (CDM83; Radiometer, Copenhagen, Denmark).

Weighing

The weighing setup is shown schematically in Fig 3. Again the capillary was fitted in a similar way between the electrode vessels. The electrodes in those measurements were made of platinum wire (0.2 mm diameter). The grounded electrolyte vessel was placed directly on a Model MP8-1 microbalance (Sartorius, Göttingen, F.R.G.). A high voltage was applied over the capillary using a Model HN 30000-1 high-voltage power supply (Heinzinger, Rosenheim, F.R.G.) in the constant-voltage mode.

The electrodes had no contact with the vessel and even a spring was used to avoid any disturbances, *e.g.*, contraction of the capillary when an electric field is applied. Also, the capillary was isolated from the balance to prevent current leakage. The change in weight could be read directly from a display, from which the EOF could be calculated.

First, the levels of the electrolyte in both vessels were brought to the same height using gravity flow. This position was used as the starting position for all experiments. Next, voltage was applied to the system, causing an EOF. The change in weight in the vessel on the balance was registered every 5 min. This was sufficient to suppress errors occurring from instability in the read-out. Next the flow was forced in the opposite direction until the starting point was reached again. The same procedure was repeated but, to compensate for any asymmetry in the system, the polarity was changed. Finally, a run was performed without applying any voltage to correct for the gravity

TABLE I
0.01 *M* HYDROCHLORIC ACID ELECTROLYTE SOLUTIONS USED

pH	*Buffer ion*	κ *(1/Ωm)*
3.0	β-Alanine	0.1219
3.5	β-Alanine	0.1000
4.8	Creatine	0.0908
6.0	Histidine	0.0893
8.2	Tris	0.0853
9.0	Ammediol	0.0863

flow. The EOF was calculated by averaging the values of the two flows obtained, corrected for gravity flow, using the equation

$$v_{eo} = \frac{\Delta W}{\Delta t \ \rho \ A} \tag{3}$$

where $\Delta W/\Delta t$ is the weight difference measured in a given time interval, ρ the density of the electrolyte used and A the cross-sectional area of the capillary.

Water used for preparing electrolytes was taken from a Milli-Q purification system (Millipore, Bedford, MA, U.S.A.). All reagents were of analytical-reagent grade and purchased from Merck (Darmstadt, F.R.G.). PTFE capillaries were purchased from HABIA (Breda, The Netherlands) (I.D. 300 μm). The lengths of the capillaries were 15 and 20 cm for measuring streaming potentials and 48 cm for measuring the electroosmotic flow by weight. The electrolyte solutions used consisted of 0.01 *M* chloride buffers of several pH values (Table I). The viscosity of these buffers was 0.001 kg/m · s, the dielectric constant $695 \cdot 10^{-12}$ F/m and the density 1000 kg/m^3. The specific conductances, κ, of the buffers are also listed in Table I.

RESULTS AND DISCUSSION

Streaming potential

For the measurement of the streaming potential, Fig. 4 shows the dependence of the potential difference accross the capillary on the pressure drop. The electrolyte had a pH of 6.0 (Table I). A linear relationship was found for the streaming potential, as predicted by theory, with a regression coefficient of 0.99996. The corresponding ζ-potential was calculated from these experiments. As can be seen, it is independent of the ΔP introduced. From these values it was concluded that further experiments could be performed with a ΔP of 10^5 Pa to achieve the maximal response.

In Fig. 5 the variation of the ζ-potential with the pH of the electrolyte solution is shown. The data are the averages of three experiments, performed with the electrolytes given in Table I. The general deviation of the data is indicated. As can be seen from Fig. 5, there is a strong dependence of ζ-potential on pH, resulting in a corresponding change in electroosmotic velocity (eqn. 1). The direction of EOF changes at a pH of *ca.* 3.5. The values given correspond to those reported in the literature[2,15].

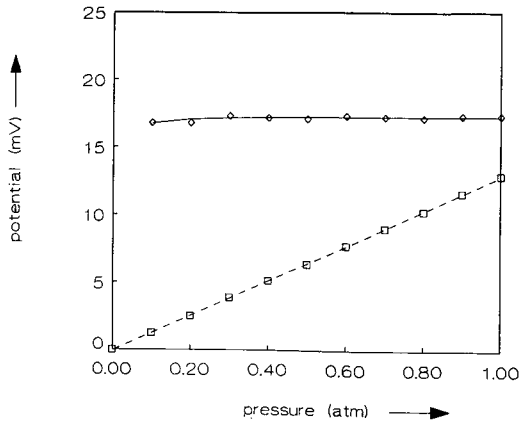

Fig. 4. Streaming potential (measured values) (□) and ζ-potential (calculated values) (◇) *versus* applied pressure drop. PTFE capillary, 15 cm × 300 μm I.D. Electrolyte, pH 6.0 (Table I).

During the experiments it was found that for new capillaries exposed to electrolyte solutions, time is needed to obtain equilibrium. An example of such an adaptation period is presented in Fig. 6, which shows the time dependence of the ζ-potential measured with a 1-min time interval. After exposure of a new PTFE capillary to an electrolyte solution of pH 6.0 (Fig. 6, situation 1) a period of 20 min was required to reach a stable value. The change from a solution of pH 3.0 to pH 4.8 (Fig. 6, situation 2) required a period of nearly 120 min. Therefore, care should be taken when changing the operational conditions.

Weighing

The weighing experiments were performed in the electrolyte system (pH 8.2) listed in Table I.

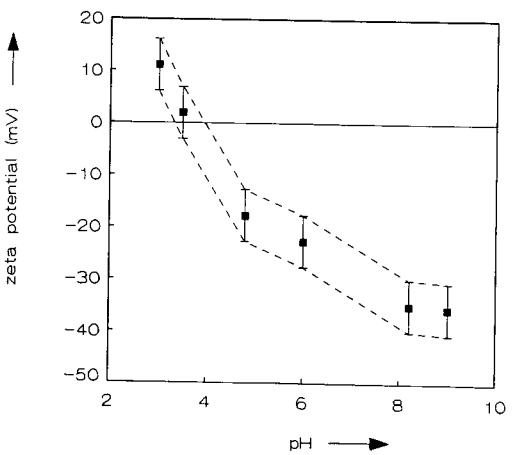

Fig. 5. ζ-Potential (calculated value) obtained from streaming potential measurements *versus* pH of the electrolyte solution. PTFE capillary, 20 cm × 300 μm I.D. Electrolytes are listed in Table I.

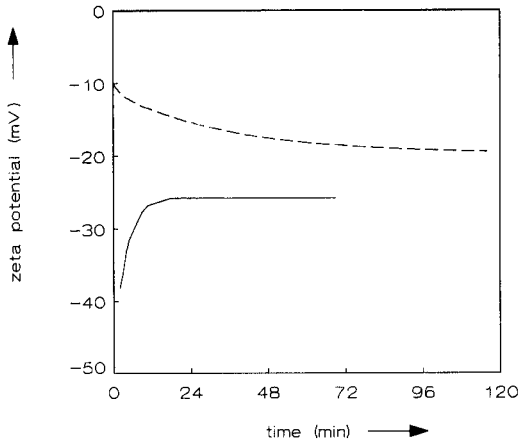

Fig. 6. Change of ζ-potential with time after change in electrolyte conditions. Situation 1 (solid line), pH 6.0 buffer and new capillary: situation 2 (broken line), change from pH 3.0 to pH 4.8 buffer. Buffers are listed in Table I. PTFE capillary, 20 cm × 300 μm I.D.

Fig. 7A shows the dependence of the electroosmotic velocity on the voltage applied over the capillary. Theory predicts an increase in flow with voltage. This is certainly visible, although at high voltages a deviation arises towards higher velocities. This can be explained by temperature effects. At high electric field strength an increase in electrolyte temperature causes a decrease in viscosity, resulting in a higher electroosmotic velocity (eqn. 1). In Fig. 7A it can be seen that at 6 kV the linear

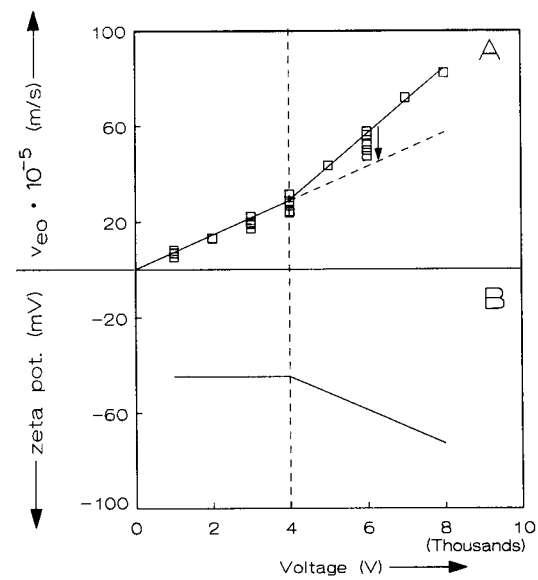

Fig. 7. (A) Electroosmotic velocity *versus* voltage applied, calculated from weighing experiments; (B) ζ-potential, calculated from electroosmotic velocity *versus* voltage applied. PTFE capillary, 48 cm × 300 μm I.D. Electrolyte, pH 8.2 (Table I).

relationship can be approached when sufficient time is used to allow the electrolyte to cool (indicated by the arrow). The ζ-potentials calculated from the average electroosmotic velocities are shown in Fig. 7B. At voltages up to 4 kV the ζ-potential is constant and approximates the values in the literature[2,15]. At higher potential differences the observed ζ-potential is higher.

The deviation in the experiments performed at a given field strength is also a result of temperature differences in the experiments. When an experiment is performed at a high electric field strength, the current density increases (up to 30%) with time because of heating effects. After such an experiment it took several hours to regain the starting current density.

There is a difference between the value of -35 mV obtained with the streaming potential method at pH 8.2 and the value of -45 mV resulting from the weighing measurements. From Figs. 5 and 7 it can be seen, however, that an inaccuracy of *ca.* 5 mV in the data has to be accounted for. Also, it is difficult to compare these two values because data on temperature inside the capillary and therefore its influence on viscosity and mobilities are not known.

CONCLUSIONS

Data obtained with streaming potential measurements give better information on the behaviour of the materials because temperature effects are hardly present. However, more stable electrodes need to be made in order to measure the streaming potential better than the present inaccuracy of 5 mV. The method of determination of the EOF by weighing approaches the experimental conditions of electrophoresis and electrochromatography. It opens up the possibility for a complete characterization of the separation conditions, *e.g.*, the capillary wall, solvent, surface-active components, viscosity and temperature.

For the weighing experiments the calculated ζ-potentials are of minor interest, because the EOF is directly accessible. This on-line measurement of EOF opens up possibilities for regulation through a feedback to the power supply[22]. An increase in electroosmotic velocity is compensated for by means of a decrease in electric field strength. On-line computer data acquisition is, of course, necessary in this instance. The regulation of the electroosmotic flow is discussed elsewhere[23].

ACKNOWLEDGEMENTS

The investigations were supported by the Netherlands Foundation for Chemical Research (SON) with financial aid from the Netherlands Organization for Scientific Research (NWO).

REFERENCES

1 V. Pretorius, B. J. Hopkins and J. D. Schieke, *J. Chromatogr.*, 99 (1974) 23.
2 J. W. Jorgenson, K. D. Lukacs, *Anal. Chem.*, 53 (1981) 1298.
3 M. M. Martin and G. Guiochon, *Anal. Chem.*, 56 (1984) 614.
4 M. Martin, G. Guiochon, Y. Walbroehl and J. W. Jorgenson, *Anal. Chem.*, 57 (1985) 559.
5 F. M. Everaerts, Th. P. E. M. Verheggen and J. L. M. van de Venne, *J. Chromatogr.*, 123 (1976) 139.
6 J. Vacik and J. Zuska, *J. Chromatogr.*, 91 (1974) 795.

7 T. S. Stevens and H. J. Cortes, *Anal. Chem.*, 55 (1983) 1365.
8 K. D. Lukacs and J. W. Jorgenson, *J. High Resolut. Chromatogr. Chromatogr. Commun.*, 8 (1985) 407.
9 H. H. Lauer and D. McManigill, *Anal. Chem.*, 58 (1986) 166.
10 B. J. Herren, S. G. Shafer, J. van Alstine, J. M. Harris and R. S. Snyder, *J. Colloid Interface Sci.*, 115 (1987) 46.
11 A. J. Rutgers, M. de Smet and W. Rigole, in H. van Olphen and K. J. Mysels (Editors), *Physical Chemistry: Enriching Topics from Colloid and Surface Science*, Theorex, La Jolla, CA, 1975.
12 R. J. Hunter, *Zeta Potential in Colloid Science*, Academic Press, London, 1981.
13 R. A. van Wagenen, J. D. Andrade and J. B. Hibbs, Jr., *J. Electrochem. Soc.*, 123 (1976) 1438.
14 R. A. van Wagenen and J. D. Andrade, *J. Coloid Interface Sci.*, 76 (1980) 305.
15 J. C. Reijenga, G. V. A. Aben, Th. P. E. M. Verheggen and F. M. Everaerts, *J. Chromatogr.*, 260(1983) 241.
16 K. D. Altria and C. F. Simpson, *Anal. Proc.*, 23 (1986) 453.
17 K. D. Altria and C. F. Simpson, *Chromatographia*, 24 (1987) 527.
18 J. T. Davies and E. K. Rideal, *Interfacial Phenomena*, Academic Press, New York, 2nd ed., 1963.
19 A. W. Adamson, *Physical Chemistry*, Interscience, New York, 2nd ed., 1967.
20 C. L. Rice and R. Whitehead, *J. Phys. Chem.*, 69 (1965) 4017.
21 P. T. Thomson, *Ph.D. Thesis*, Pittsburgh, PA, 1956.
22 B. J. Wanders, A. A. A. M. van de Goor, F. M. Everaerts and C. A. Cramers, The Netherlands Patent Application No. 8802273.
23 B. J. Wanders, A. A. A. M. van de Goor and F. M. Everaerts, *J. Chromatogr.*, 470 (1989) 89.

Journal of Chromatography, 470 (1989) 105–112
Elsevier Science Publishers B.V., Amsterdam — Printed in The Netherlands

CHROM. 21 266

CONCEPT OF RESPONSE FACTOR IN CAPILLARY ISOTACHOPHORESIS

DETERMINATION OF DRUGS IN SOLUTION FOR INTRAVENOUS INJECTION

M. M. GLADDINES*, J. C. REIJENGA and R. G. TRIELING

Laboratory of Instrumental Analysis, Eindhoven University of Technology, P.O. Box 513, 5600 MB Eindhoven (The Netherlands)

M. J. S. VAN THIEL

Department of Clinical Pharmacy and Toxicology, Eindhoven, Diaconessenhuis, P.O. Box 90052, 5600 PD Eindhoven (The Netherlands)

and

F. M. EVERAERTS

Laboratory of Instrumental Analysis, Eindhoven University of Technology, P.O. Box 513, 5600 MB Eindhoven (The Netherlands)

SUMMARY

Twenty-six drugs in solutions for intravenous injection were determined by capillary isotachophoresis with only one calibration point for each component. The maximum deviation of the labelled concentration was 2%. A new calibration constant is introduced, *viz.*, the response factor (RF, dimensionless), which is independent of the diameter of the capillary, the construction of the universal detector and the driving current used during detection. It is shown that the RF can be used on different equipment, using different currents during detection. It appears that the RF is usable for routine analysis when a deviation of 5% is acceptable. Daily one-point recalibration, however, improves this value to 1%.

INTRODUCTION

During the past 5 years, capillary isotachophoresis has been recognized as a promising technique for the determination of biochemical substances in pharmaceutical preparations and biological matrices, with studies on ephedrine alkaloids[1–6], isoquinoline alkaloids[7,8,9], sympathomimetics[10], amantadine and rimantactine[11], codeine[1,2], local anaesthetics including procaine[3,12–15], papaverine, morphine and aminophenazone[2], oral anaesthetics[16], nicotinic acid[17], minoxidil[18], amoxycillin and carboxymethylcysteine[19], aminoglycoside and lincomycin[20], cephalosporin, berberin and glycyrrhizin[21] acetylsalicylate[22], chincona alkaloids[23,24] and obidoxime[25].

Capillary isotachophoresis (ITP) is considered to be a precise and accurate method for the determination of these substances. In our view, however, capillary

0021-9673/89/$03.50

isotachophoresis offers more advantages. Usually, when a calibation graph is constructed, the zone length is plotted against the amount injected. This calibration graph depends on the equipment and the current used. If, however, the zone length is divided by the amount injected and multiplied by the driving current, a new variable is created. This variable is independent of the diameter of the capillary, the construction of the detector and the driving current used during detection. This variable, which is called the response factor (RF), is dimensionless:

$$\mathrm{RF} = \frac{ZL \cdot I}{|z| \cdot F \cdot Q}$$

where $|z|$ is the charge of the ion [equiv./mol], ZL the zone length (s), I the driving current (A), F the number of Faradays (coulombs/equiv.] and Q the amount injected (mol). For each component the RF depends only on the concentration of the leading electrolyte, which can be prepared very precisely[26]. This implies that the RF is a universal calibration constant, independent of the ITP instrument used for its measurement. The RF is the reciprocal transference number and denotes the sensitivity. The transference number equals the fraction of the driving current carried by the ions migrating in the steady state.

To demonstrate the use of the RF, 26 drugs (23 cations and 3 anions) in solution for intravenous injection were determined by capillary isotachophoresis. These solutions often contain additives, such as sodium pyrosulphite, for preservation. For each component the RF was determined by one injection of the pure component. Further, the concentration of the drug in the solution was determined by injection of the solution for intravenous injection. Qualitative parameters such as relative step height and UV absorption were also measured for identification of the drugs.

To test the reproducibility of the RF, four components (acetate, phosphate, benzoate and citrate) were determined on instruments with different capillary diameters and different driving currents on the same equipment. Also, the day-to-day variation and the variation when different analysts carried out the analyses were determined. The four components were chosen because they are more stable than the drugs.

EXPERIMENTAL

The isotachophoretic analyses were performed on equipment built by Everaerts *et al.*[27]. The separation compartment consisted of a PTFE capillary of I.D. 0.2 or 0.4 mm and a length of *ca.* 25 cm. The direct, constant driving current was taken from a modified high-voltage supply (Brandenburg, Thornton Heath, U.K.). The zones were detected by measuring the electrical conductivity and the UV absorption at 254 nm.

The zone lengths and step heights on the electropherograms were measured with an IBM-XT computer (IBM, Boca Raton, FL, U.S.A.), which was connected via an ADC (Labmaster, Scientific Solutions, OH, U.S.A.) with the conductivity detector. The program used was written in Turbo Pascal (Borland International, Scotts Valley, CA, U.S.A.)[28].

The reproducibility of the RF was tested by injection of four components (acetate, phosphate, benzoate, and citrate) on equipment with different capillary diameters and using different currents. These analyses were carried out on three different days with leading electrolyte systems prepared freshly each day. On the third day the analyses were also carried out by a second analyst. The electrolyte system used is listed in Table I (system 1).

The currents used were 20 and 30 μA for the 0.2 mm I.D. capillary and 70 and 85 μA for the 0.4 mm I.D. capillary. Fig. 1 shows an isotachopherogram of the four-component mixture.

For the analyses of drugs anionic and cationic electrolyte systems were used, as listed in Table I. The driving current was 30 μA for anions. For the cations it was 40 μA during the first 6 min of the analysis and 30 μA during detection. Both analyses took *ca.* 10 min.

The RF was calculated by injection of one standard solution containing 100 mg per 100 ml of the pure component. For the quantitative measurement no internal standard was used. The samples were injected with a 10-μl syringe (Hamilton, Bonaduz, Switzerland) equipped with a fixed-volume accessory. The determinations of both the pure component and the component in the solution were made in duplicate. A difference in the two measurements of less than 1% was considered sufficiently precise. If this difference was greater than 1% a third injection was made.

The relative step height (RSH) was calculated using the equation

$$\mathrm{RSH} = \frac{h_X - h_L}{h_{IS} - h_L}$$

where h_X is the height of the step of the component, h_L is the height of the step of the leading ion and h_{IS} is the height of the step of the internal standard. The internal standards used were chlorate (sodium chlorate, Merck, Darmstadt, F.R.G.) for anions

TABLE I

OPERATIONAL SYSTEMS USED FOR THE ISOTACHOPHORETIC EXPERIMENTS

MES = 2-(N-Morpholino)ethanesulphonic acid (Sigma, St. Louis, MO, U.S.A.); HEC = hydroxyethylcellulose (Polysciences, Warrington, PA, U.S.A.); PVA = poly(vinyl alcohol) (Hoechst, Frankfurt, F.R.G.); HIBA = hydroxyisobutyric acid (Fluka, Buchs, Switzerland). All other chemicals from Merck (Darmstadt, F.R.G.). For system 3, see also ref. 29.

Parameter	*System*		
	1	*2*	*3*
Leading ion	Chloride	Potassium	Potassium
Concentration (*M*)	0.01	0.01	0.01
pH	6.0	5.0	4.2
Complex ion	–	–	HIBA to pH 5.2
Counter ion	Histidine	Acetate	Acetate to pH 4.2
Additive	0.2% HEC	0.05% Mowiol	0.05% Mowiol
Terminating ion	MES	H^+	H^+
Concentration (*M*)	0.005	0.005	0.005

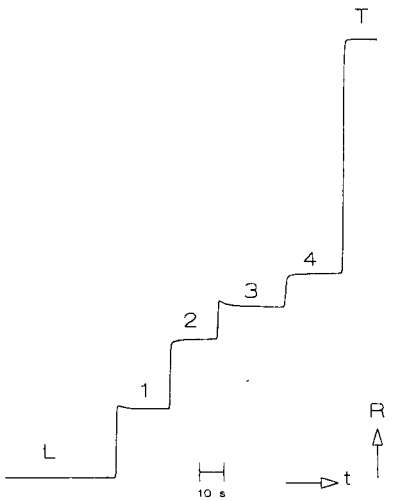

Fig. 1. Isotachopherogram of the four-component mixture analysed in system 2 (Table I). L = Leading ion; 1 = citrate; 2 = acetate; 3 = phosphate; 4 = benzoate. T = Terminator; t = time; R = Resistance.

and sodium for cations. The linearity of the conductivity detector electronics was tested by applying ten resistances in the range from 100 kΩ to 1 MΩ. The response of the conductivity detector was plotted against the resistance. The correlation coefficient of the regression line was 0.9999.

The UV absorption was expressed as a percentage of full absorption:

$$\text{UV absorption} = \frac{H_x}{H_{100\%}} \cdot 100\%$$

where H_x is the height of the UV signal of the component and $H_{100\%}$ is the height of the UV signal at 100% absorption.

RESULTS AND DISCUSSION

The reproducibility of the RF

Table II gives the results for the determination of acetate. The mean value and standard deviation of five measurements are indicated by a line (mean value) and a hatched box (standard deviation). The difference between the highest and the lowest mean value is 0.053 or 3.0%. For the other components these values are in the same range: 3.8% for phosphate, 3.5% for benzoate and 4.8% for citrate. It appears that the RF is usable for routine analysis when a deviation of 5% is acceptable. Daily one-point recalibration, however, improves this value to 1%.

Analysis of drugs for intravenous injection

Fig. 2 shows an isotachopherogram of codeine sulphate. Table III gives the results for the determination of drugs in solution for intravenous injection. For each component the following parameters are given: RF, the electrolyte system used, the

TABLE II

MEAN VALUE (LINE) AND STANDARD DEVIATION (HATCHED BOX) (n = 5) OF THE RF OF ACETATE ON DIFFERENT DAYS, BY TWO ANALYSTS, USING DIFFERENT CURRENTS AND CAPILLARY DIAMETERS

Electrolyte system 1 (Table I) was used. I = Current; I.D. = inner diameter.

Analyst	Day	I (μA)	I.D. (mm)
A	1	20	0.2
A	1	30	0.2
A	1	70	0.4
A	1	85	0.4
A	2	20	0.2
A	2	30	0.2
A	2	70	0.4
A	2	85	0.4
A	3	20	0.2
A	3	30	0.2
A	3	70	0.4
A	3	85	0.4
B	3	20	0.2
B	3	30	0.2
B	3	70	0.4
B	3	85	0.4

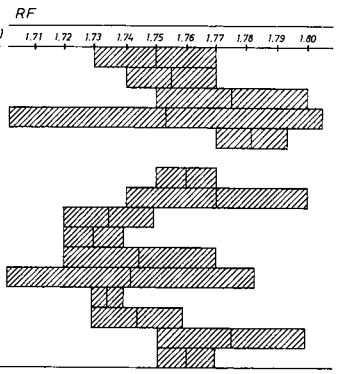

concentration determined (C_{DE}), the labelled concentration (C_{LA}), the deviation, calculated using the equation

$$\text{Deviation} = \frac{C_{DE} - C_{LA}}{C_{LA}} \cdot 100\%$$

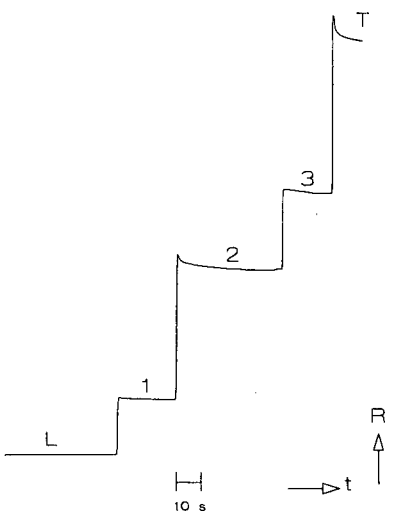

Fig. 2. Isotachopherogram of codeine sulphate analysed in system 1 (Table 1). L = Leading ion; 1 = sodium (internal standard for qualitative analysis); 2 = Tris (not used); 3 = codeine. T = Terminator; t = time; R = Resistance.

TABLE III

RESULTS OF DETERMINATION OF DRUGS IN SOLUTION FOR INTRAVENOUS INJECTION

System numbers according to Table I. For definitions of deviation, RSH and UV absorption, see text.

Component	*RF*	*System*	C_{DE} *(mg/ml)*	C_{LA} *(mg/ml)*	*Deviation (%)*	*RSH*	*UV absorption (%)*
Isoniazide	3.8	2	100.1	100.0	0.1	10.7	44
Neostigmine methylsulphate	2.6	2	0.49	0.50	−2.0	4	8
Suxamethonium chloride	4.0	2	50.4	50.0	0.8	1.5	0
Isoprenaline sulphate	5.9	2	0.98	1.0	−2.0	5.2	7
Lidocaine hydrochloride	2.8	2	10.0	10.0	0.0	4.9	8
Codeine sulphate	2.8	2	29.9	30.0	−0.3	5	25
Gallamine triethiodide	5.4	2	20.4	20.0	2.0	1.7	0
Levarterenol tartrate	2.4	2	2.0	2.0	0.0	3.4	8
Atropine sulphate	5.7	2	0.25	0.25	0.0	5.2	3
Apomorphine hydrochloride	2.4	2	4.9	5.0	−2.0	4.7	79
Quinine gluconate	2.8	2	80.4	80.0	0.5	4.3	7
Adrenaline tartrate	2.6	2	1.9	1.8	5.5	4.5	8
Scopolamine hydrobromide	3.1	2	0.25	0.25	0.0	4.8	4
Chlorpromazine hydrochloride	2.4	2	5.7	5.6	1.8	4.5	93
Promethazine hydrochloride	2.9	2	24.5	25.0	−2.0	4.9	92
Imipramine hydrochloride	2.9	2	12.5	12.5	0.0	5.2	80
Procaine hydrochloride	2.8	2	19.6	20.0	−2.0	5.2	55
Thiamine hydrochloride	3.5	2	24.8	25.0	−0.8	3.4	86
Tetracaine hydrochloride	3.0	2	9.9	10.0	−1.0	6.1	25
Fysostigmine salicylate	2.8	2	0.98	1.0	−2.0	5.1	79
Promazine hydrochloride	2.8	2	24.6	25.0	−1.6	4.7	92
Fluorescein	2.5	1	199.8	200.0	−0.1	11.8	91
Ascorbate	2.0	1	101.1	100.0	1.1	–	86
Citrate	2.2	1	32.5	32.3	0.6	2.7	0
Magnesium sulphate	5.0	3	149.0	150.0	−0.7	–	0
Calcium chloride	5.8	3	37.1	36.8	1.0	1.2	0

the RSH and the UV absorption. It can be seen that the quantitative deviation is 2% or less, with one exception (adrenaline tartrate, 5.5%). In view of the accuracy and precision of the RF, only the adrenaline tartrate concentration differs significantly from the labelled concentration.

It must be stressed that one-point calibration can only be used when the zones are sufficiently large. To determine the minimum zone length for which the RF may be used, several amounts of the four-component test mixture were analysed. Fig. 3 shows the calibration graph for acetate. On the ordinate the factor $(ZL \cdot \mathrm{I})/F$ is plotted, so that the slope of the calibration line represents the RF. This slope amounts to 1.72 (regression coefficient 0.9999).

In Table IV the RFs are given for each amount injected (one-point calibration). A systematic deviation of the RF from the true value is encountered only with a 2.3-s zone length, an effect associated with differences in the front and rear zone boundary profiles[30]. The other components show similar deviations with zone lengths of 2.1 s for phosphate and 2.9 s for benzoic acid and citrate. The minimum zone length for which

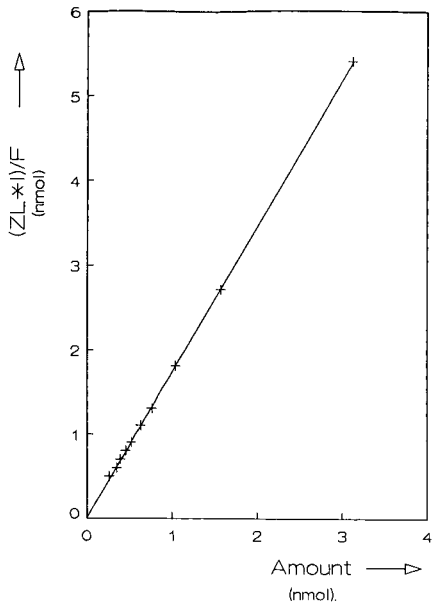

Fig. 3. Calibration graph for acetate. The slope represents RF. Slope = 1.72; intercept on ordinate = 0.0095 (nmol); $r = 0.9999$.

TABLE IV

RF OF ACETATE, MEASURED IN SYSTEM 1 (TABLE I), FOR DIFFERENT AMOUNTS INJECTED

Amount (nmol)	*Zone length (s)*	*RF*
3.12	26	1.73
1.57	13.1	1.73
1.04	8.5	1.70
0.78	6.5	1.73
0.63	5.3	1.75
0.52	4.4	1.74
0.45	3.7	1.71
0.39	3.3	1.74
0.35	2.9	1.71
0.26	2.3	1.84

the RF can be used, in a one-point calibration, is approximately 3 s if a 20-μA driving current is applied (*ca.* 1 mm in a 0.2-mm I.D. capillary).

CONCLUSIONS

It has been shown that capillary ITP is suitable for the determination of drugs in solution for intravenous injection. For the quantitative quality control of these

components the use of only one calibration point yields a maximum deviation of 2%. For each component a new calibration constant, the response factor (RF), is determined, which is independent of the diameter of the capillary, the construction of the universal detector and the current used during detection. The RF is an universal calibration constant, which is sufficiently accurate for routine analysis.

REFERENCES

1 J. Pospichalova and V. Jokl, *Pharmazie*, 42 (1987) 55.
2 I. Valka, J. Minarcik, J. Pumpria and D. Walterova, *Cesk. Farm.*, 35 (1986) 81.
3 S. Fanali, F. Foret and P. Boček, *J. Chromatogr.*, 330 (1985) 436.
4 H. Klein and R. Teichman, *Pharm. Ztg.*, 8 (1982) 447.
5 Y. Kasahara, H. Hikino and T. Hine, *J. Chromatogr.*, 324 (1985) 503.
6 A. Barcuchova and V. Jokl, *Cesk. Farm.*, 1 (1983) 12.
7 D. Walterova, Z. Stransky, V. Preininger and V. Simanek, *Acta Univ. Palacki. Olomuc., Fac. Med.*, (1985) 23.
8 D. Walterova, Z. Stransky, V. Preininger and V. Simanek, *Electrophoresis*, 6 (1985) 128.
9 D. Walterova, V. Preininger and V. Simanek, *Planta Med.*, 50 (1984) 149.
10 W. Schollack, M. Tkaczyk and J. Koerbl, *Zentralbl. Pharm. Pharmakother. Laboratoriumsdiagn.*, 126 (1987) 1.
11 R. Jannasch, *Pharmazie*, 41 (1986) 478.
12 J. Kostelecka and A. Haller, *Cesk. Farm.*, 36 (1987) 198.
13 H. Klein and R. Teichman, *Ernährung*, 10 (1986) 608.
14 P. Boček, in *Topics in Current Chemistry*, Springer, Berlin, Heidelberg, New York, 1981, p. 131.
15 H. Klein, *Arzneim.-Forsch/Drug. Res.*, 11 (1982) 795.
16 J. Cizmarik and Z. Stransky, *Collect. Czech. Chem. Commun.*, 51 (1986) 993.
17 E. Kenndler and R. Katzenberger, *Mikrochim. Acta*, I (1986) 415.
18 S. Fanali, M. Cristalli and P. Catellani, *J. Chromatogr.*, 405 (1987) 385.
19 S. Fanali, M. Sinibaldi and M. G. Quaglia, *J. Chromatogr.*, 408 (1987) 441.
20 H. Klein and R. Teichmann, *J. Chromatogr.*, 250 (1982) 152.
21 H. Miyazaki and K. Katoh, in K. Nobusawa (Editor), *Electrofocusing and Isotachophoresis*, Yoritsu Shuppan, Tokyo, 1978, p. 173.
22 F. M. Everaerts, M. Geurts, F. E. P. Mikkers and Th. P. E. M. Verheggen, *J. Chromatogr.*, 119 (1976) 129.
23 J. C. Reijenga, G. V. A. Aben, A. A. G. Lemmens, Th. P. E. M. Verheggen, C. H. M. M. De Bruin and F. M. Everaerts, *J. Chromatogr.*, 320 (1985) 245.
24 H. Klein and R. Teichmann, *Pharm. Ztg.*, 132 (1987) 1131.
25 R. Jannasch, *Pharmazie*, 41 (1986) 511.
26 N. Groot, *Graduation Report*, Eindhoven University of Technology, Eindhoven, 1980.
27 F. M. Everaerts, J. L. Beckers and Th. P. E. M. Verheggen, *Isotachophoresis—Theory, Instrumentation and Applications* (*Journal of Chromatography Library*, Vol. 6), Elsevier, Amsterdam, 1976.
28 B. J. Wanders, A. A. G. Lemmens, F. M. Everaerts and M. M. Gladdines, *J. Chromatogr.*, 470 (1989) 79.
29 F. M. Everaerts, Th. P. E. M. Verheggen, J. C. Reijenga, G. V. A. Aben, P. Gebauer and P. Boček, *J. Chromatogr.*, 320 (1985) 263.
30 J. C. Reijenga, A. A. G. Lemmens, Th. P. E. M. Verheggen and F. M. Everaerts, *J. Chromatogr.*, 320 (1985) 67.

Journal of Chromatography, 470 (1989) 113–121
Elsevier Science Publishers B.V., Amsterdam — Printed in The Netherlands

CHROM. 21 217

CONCEPT OF EFFECTIVE AND NON-EFFECTIVE INCLUSION COMPLEX FORMATION IN ISOTACHOPHORESIS

IVAN JELÍNEK*
Research Institute for Pharmacy and Biochemistry, Kouřimská 17, 130 60 Prague 3 (Czechoslovakia)
JIŘÍ SNOPEK
Laboratory of Bioseparation and Bioanalytical Methods, Institute of Biotechnology, Charles University, Albertov 2030, 128 43 Prague 2 (Czechoslovakia)
JURAJ DIAN
Department of Chemical Physics, Charles University, Ke Karlovu 3, 121 16 Prague 2 (Czechoslovakia)
and
EVA SMOLKOVÁ-KEULEMANSOVÁ
Department of Analytical Chemistry, Charles University, Albertov 2030, 128 43 Prague 2 (Czechosovakia)

SUMMARY

On the basis of experimental experiences, a simple mathematical model of 1:1 cyclodextrin–solute complex formation is proposed. A possible role of two limiting cyclodextrin–solute interactions, introduced as effective and non-effective complex formation, on the quality of isotachophoretic resolution has been studied and is discussed. Additional parameters, *e.g.*, the solute molecular weight, its effective charge and the molecular weight of the cyclodextrin used, are involved in the proposed model. Their influence on the isotachophoretic separation was estimated by comparing the computer simulated mobility ratio curves of cyclodextrin-complexed solutes obtained at various values of the corresponding parameters.

INTRODUCTION

The optimization of the electrolyte system for the resolution of given solutes involves in general the influence of many physical-chemical and operational parameters[1]. As follows from the theory of isotachophoresis (ITP), a maximum resolution for a given solute pair is obtained in the electrolyte system ensuring the maximum (minimum) solute effective mobility ratio in the mixed zone. According to definition, the effective mobility, U, of a migrating ion is determined predominantly by its molecular weight, M, and effective charge, Z. Using relevant correlative equations[2–4] expressing the direct proportionality between U and $Z/(M)^R$ where $0 < R \leq 1$, an effective mobility ratio can be expressed as a function of M and Z. This is useful especially for the description of the resolution changes in electrolyte systems containing a complex-forming discriminator where the solute molecular weights and effective charges are selectively altered by complexation.

0021-9673/89/$03.50

Several theoretical studies dealing with inclusion complex formation in ITP have been published[5–7]. Proposed theories of complex formation and derived mathematical equations were successfuly utilized for the evaluation of important physical-chemical constants of complexed solutes such as effective mobilities and stability constants. The aim of this paper is to present a relatively simple mathematical model of the cyclodextrin (CD) supported separation of structurally related solute pairs and isomers under ITP conditions. The whole concept originates in the description of the changes in solute molecular weights and the effective charges caused by the complex formation with CD. Using the mentioned correlative equations, corresponding changes in the mixed zone solute mobilities were derived. Final considerations about the resolution are based on a computer simulation of the mobility ratio of CD-complexed solutes in the mixed zone.

THEORETICAL

The ITP separation of model solutes is outlined schematically in Fig. 1. The compounds I, III (II, III) represent pairs of structurally related solutes with identical fundamental molecular skeletons differing only in the variable substituents A, B. The charge of the groups G is supposed to be identical. Compounds I and II form pairs of structural isomers (positional isomers or enantiomers) with equal molecular weights and identical G-group charge. Each solute is proposed to have two binding sites available for the complexation with CD. The binding site N is relatively distant and isolated from the central framework C, which represents the area of structural differentiation of the solutes. The CD molecule bonded at N is not able to interact effectively with substituents G, A (B) and alter the effective charge of the solute. The stability of the CD complexes formed is the same for all three solutes, irrespective of the structural and geometrical changes in the central framework C. Such a type of complex formation can be considered as non-effective. The second CD binding site E is closely connected with the central framework C. The CD bonded at E is able to interact with substituents A (B) and alter the effective charge of group G. The stability of the CD complexes formed depend on the type and/or geometrical orientation of the

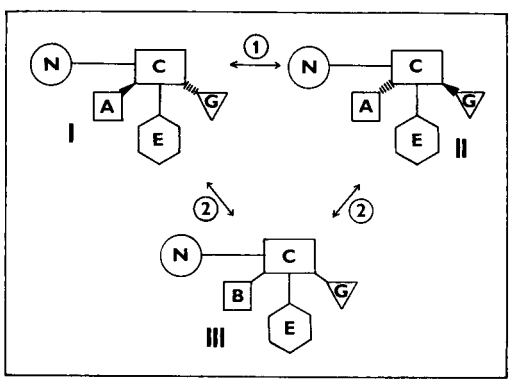

Fig. 1. Schematical outline of the model solutes studied. 1 = Enantiomers (positional isomers); 2 = structurally related compounds differing in substituents A and B; G = charged group; E = effective CD-binding site; N = non-effective CD-binding site; C = central framework of the molecule.

substituents; the differences in the stability constants may result in G-group effective charge differentiation. This type of structurally dependent complex formation may be considered as effective.

A possible role of the effective and non-effective CD-complex formation in ITP separation has been studied theoretically, using eqn. 1 as an initial correlation introduced according to Fujishita *et al.*[4]

$$U = a + b \cdot \frac{|Z|}{M} \tag{1}$$

where Z is the effective charge, M the solute molecular weight, U the effective mobility in the mixed zone and a, b are empirical coefficients.

Certain simplifications and limitations resulting from the proposed scheme of CD-complex formation and eqn. 1 must be taken into account. Sufficient linearity of eqn. 1 is expected in the range of solute $M/|Z|$ values from about 50 to 150 daltons. The extension of the validity of eqn. 1, as well as all considerations and conclusions based on its utilization, to higher and lower $M/|Z|$ values is rather unsafe. Assumed invariability of coefficients a, b for both complexed and uncomplexed solutes, as a necessary condition for further calculations, leads to ignoring all ionic interactions and hydration envelope changes influencing the quality of ITP separation. The proposed simplified scheme of complexation supposes attachment of only a single CD molecule either to the site N or E of the solute. Polymolecular inclusion complex formation is not considered.

Non-effective complex formation

Assumptions: $M_X \leqslant M_Y$[a] (X = I and Y = III for the pair of structurally related solutes, X = I and Y = II for the pair of positional isomers or enantiomers), $|Z_X| = |Z_Y| = Z$. The degree of CD-complex association, α, in the mixed zone is the same for all solutes ($0 < \alpha < 1$). Using eqn. 1, the mixed zone mobilities of uncomplexed ions can be expressed as:

$$\begin{aligned} U_X &= a + bZ/M_X \\ U_Y &= a + bZ/M_Y \end{aligned} \tag{2}$$

Likewise the effective mobilities of non-effectively complexed solutes can be expressed as

$$\begin{aligned} (U_X)_C &= a + bZ/\bar{M}_X \\ (U_Y)_C &= a + bZ/\bar{M}_Y \end{aligned} \tag{3}$$

where $\bar{M}_X = M_X + \alpha M_{CD}$ and $\bar{M}_Y = M_Y + \alpha M_{CD}$ (M_{CD} = relative molecular weight of CD used). Combining eqns. 2 and 3 we obtain:

---

[a] There is no need to process $M_X \geqslant M_Y$ separately because it leads to the same conclusions.

$$(U_X)_C = U_X + bZ \Big/ \left(1 + \alpha \cdot \frac{M_{CD}}{M_X}\right) M_X - \frac{bZ}{M_X}$$
$$(U_Y)_C = U_Y + bZ \Big/ \left(1 + \alpha \cdot \frac{M_{CD}}{M_Y}\right) M_Y - \frac{bZ}{M_Y} \quad (4)$$

From eqn. 4 it follows directly that $(U)_C < U$ for each α from the interval [0;1]. This means that non-effective complex formation may result in solute retardation only.

Eqn. 4 can be utilized for the estimation of the interval for which expression 5 is valid.

$$\left(\frac{U_X}{U_Y}\right)_C > \frac{U_X}{U_Y} \quad (5)$$

Combining eqns. 4 and 5 we obtain:

$$\frac{U_X + bZ \Big/ \left(1 + \alpha \cdot \frac{M_{CD}}{M_X}\right) M_X - \frac{bZ}{M_X}}{U_Y + bZ \Big/ \left(1 + \alpha \cdot \frac{M_{CD}}{M_Y}\right) M_Y - \frac{bZ}{M_Y}} > \frac{U_X}{U_Y} \quad (6)$$

It can be proved mathematically that inequality 6 is regular only for negative, physically unreal α values. This means in practice that non-effective complex formation of structurally related solutes leads to a decrease in mobility ratio of separated solutes which is reflected in the deterioration of the separation quality.

The influence of changing α and M_{CD} values is illustrated in Fig. 2. The initial rapid decrease in the function $(U_X/U_Y)_C = f(\alpha)$ at lower α changes to a plateau for α values converging to one. Comparing curves 1, 2, it should be noted that the influence of the CD molecular weight on the decrease in the mobility ratio is only marginal, owing to the limiting range of M values for available CD types.

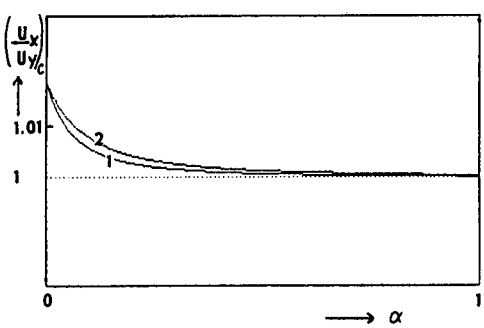

Fig. 2. Effect of the CD relative molecular weight, M_{CD}, on the decrease in the mobility ratio of non-effectively complexed solutes. $M_X = 150$, $M_Y = 200$, $Z = 0.5$, $a = 69.85$, $b = 1588$; $M_{CD} = 1430$ [corresponds to heptakis (2,3,6-tri-O-methyl)-β-cyclodextrin] (1) or 972.9 [corresponds to α-cyclodextrin] (2) Estimates for coefficients a, b were obtained according to ref. 4.

For a pair of geometrical isomers with equal molecular weights and effective charges, we obtain from eqn. 6:

$$\frac{U_X}{U_Y} = \left(\frac{U_X}{U_Y}\right)_C = 1 \tag{7}$$

It is obvious that a non-effective complex formation cannot contribute to the resolution of geometrical isomers in any way.

Effective complex formation

For the mixed zone mobilities of effectively complexed solutes, where the average effective charge and relative molecular weight of separated solutes depend on the selective complex formation ($\alpha_X \neq \alpha_Y$), it follows that

$$\begin{aligned}(U_X)_C &= a + b\,|\bar{Z}_X|/\bar{M}_X \\ (U_Y)_C &= a + b\,|\bar{Z}_Y|/\bar{M}_Y\end{aligned} \tag{8}$$

where $\bar{M}_X = M_X + \alpha_X M_{CD}$, $\bar{M}_Y = M_Y + \alpha_Y M_{CD}$, $\bar{Z}_X = Z + \alpha_X \Delta Z$ and $\bar{Z}_Y = Z + \alpha_Y \Delta Z$. The ΔZ value, defined as the difference between the effective charge of an uncomplexed and fully complexed solute, may be positive or negative and is supposed to be equal for all solutes studied. Combining eqns. 2 and 8 we obtain:

$$\begin{aligned}(U_X)_C &= U_X + b\,|Z|\left(1 + \alpha_X\left|\frac{\Delta Z}{Z}\right|\right) \Big/ M_X\left(1 + \alpha_X \cdot \frac{M_{CD}}{M_X}\right) - \frac{b\,|Z|}{M_X} \\ (U_Y)_C &= U_Y + b\,|Z|\left(1 + \alpha_Y\left|\frac{\Delta Z}{Z}\right|\right) \Big/ M_Y\left(1 + \alpha_Y \cdot \frac{M_{CD}}{M_Y}\right) - \frac{b\,|Z|}{M_Y}\end{aligned} \tag{9}$$

Using eqn. 9 it can be mathematically proved that $(U)_C > U$ only for $M_{CD} < M_{X(Y)}\left|\frac{\Delta Z}{Z}\right|$. This condition cannot be satisfied for experimentally possible M_{CD}, $M_{X(Y)}$, ΔZ and Z values. Therefore it may be concluded that the effective complex formation leads to a solute retardation only.

Two different cases must be distinguished when the role of effective CD-complex formation is discussed. For $U_X > U_Y$ and $\alpha_Y > \alpha_X$ the condition for improvement in the CD-based separation can be obtained by substituting eqn. 9 into eqn. 5:

$$\frac{\alpha_Y}{\alpha_X} > \underbrace{\frac{M_Y + \dfrac{b\,|Z|}{a}}{M_X + \dfrac{b\,|Z|}{a}}}_{A} \cdot \underbrace{\frac{1 - \dfrac{M_{CD}}{M_X}\left|\dfrac{Z}{\Delta Z}\right|}{1 - \dfrac{M_{CD}}{M_Y}\left|\dfrac{Z}{\Delta Z}\right|}}_{B} \cdot \underbrace{\frac{1 + \alpha_Y \cdot \dfrac{M_{CD}}{M_Y}}{1 + \alpha_X \cdot \dfrac{M_{CD}}{M_X}}}_{C} \tag{10}$$

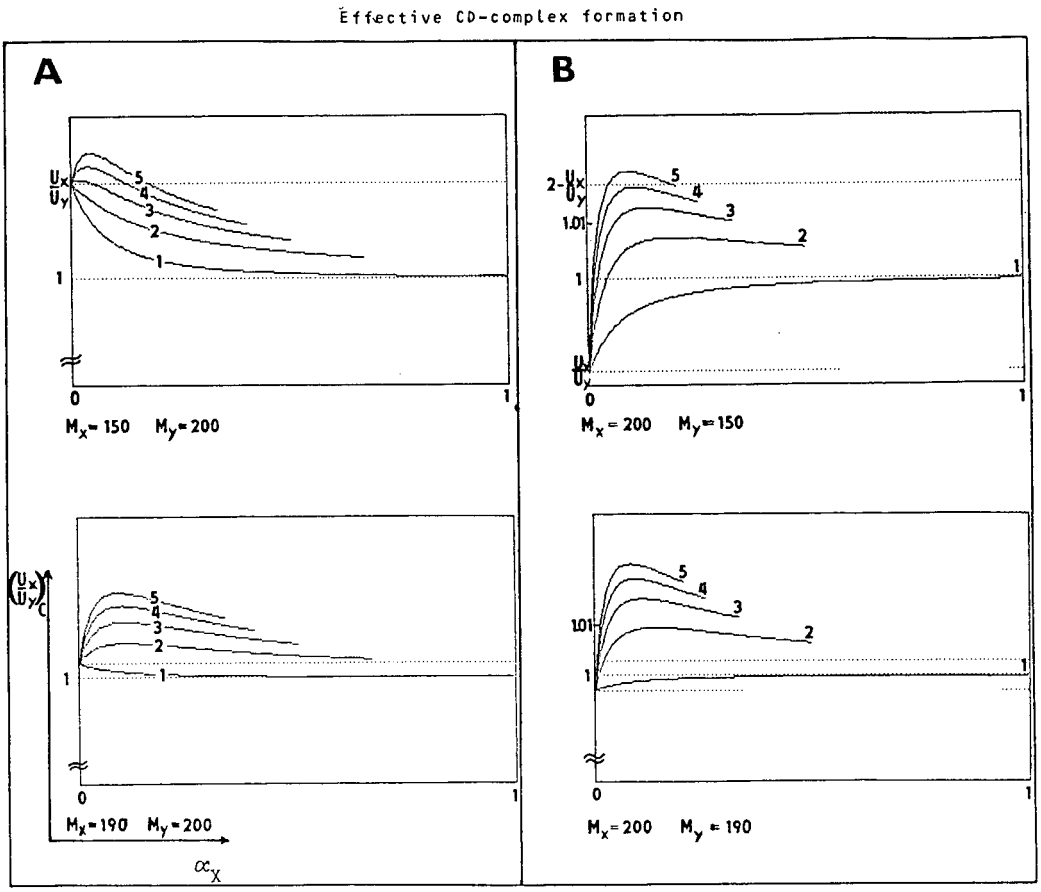

Fig. 3. Effect an increase in the solute molecular weight differences on the possibility of CD-based separation improvement. (A) $U_X > U_Y$, $\alpha_Y > \alpha_X$; $\alpha_Y = K\alpha_X$ where K = 1.0 (1), 1.5 (2), 2.0 (3), 2.5 (4) and 3.0 (5). (B) $U_X < U_Y$, $\alpha_Y > \alpha_X$; $\alpha_Y = K\alpha_X$ where K = 1.0 (1), 2.0 (2), 3.0 (3), 4.0 (4) and 5.0 (5). In all cases: Z = 0.5, M_{CD} = 1135, a = 69.85 and b = 1588.

It follows from eqn. 10 that a resolution improvement is expected for $\alpha_Y/\alpha_X > AB$. The additional requirement on the increase in α_Y/α_X results from the existence of the α-dependent term C. From the computer simulated mobility ratio curves illustrated in Fig. 3A, it should be noted that the effect of an increase in solute molecular weight, caused by CD-complex formation, results in a lowering of the ratio $(U_X/U_Y)_C$ at higher α_X, α_Y values and leads to a re-deterioration of the resolution. This effect must be compensated by an increase in the ratio α_Y/α_X in order to preserve the separation improvement.

Comparing eqn. 10 with Fig. 3A it is possible to estimate the influence of the parameters involved. The most significant is undoubtedly the effect of the solute molecular weight and the effective charge. The requirement of α_X, α_Y having different behaviours, necessary for the achievement of a separation improvement, grows rapidly

with increasing ratio M_Y/M_X and decreasing $|Z|$ value. The influence of M_{CD} and ΔZ is not so significant.

For $U_X < U_Y$ and $\alpha_Y > \alpha_X$ a general condition for a separation improvement is:

$$\left(\frac{U_X}{U_Y}\right)_C > 2 - \frac{U_X}{U_Y} \tag{11}$$

This criterion is, of course, much more demanding than the previous one mentioned for $U_X > U_Y$ and $\alpha_Y > \alpha_X$. Comparing the computer simulated dependences of $(U_X/U_Y)_C$ on α_X values for given solute characteristics (Fig 3B), it can be estimated that the ratio α_Y/α_X increases very quickly with increasing ratio M_X/M_Y. Therefore it is almost impossible to achieve an improved CD-based resolution for higher solute molecular weight differences.

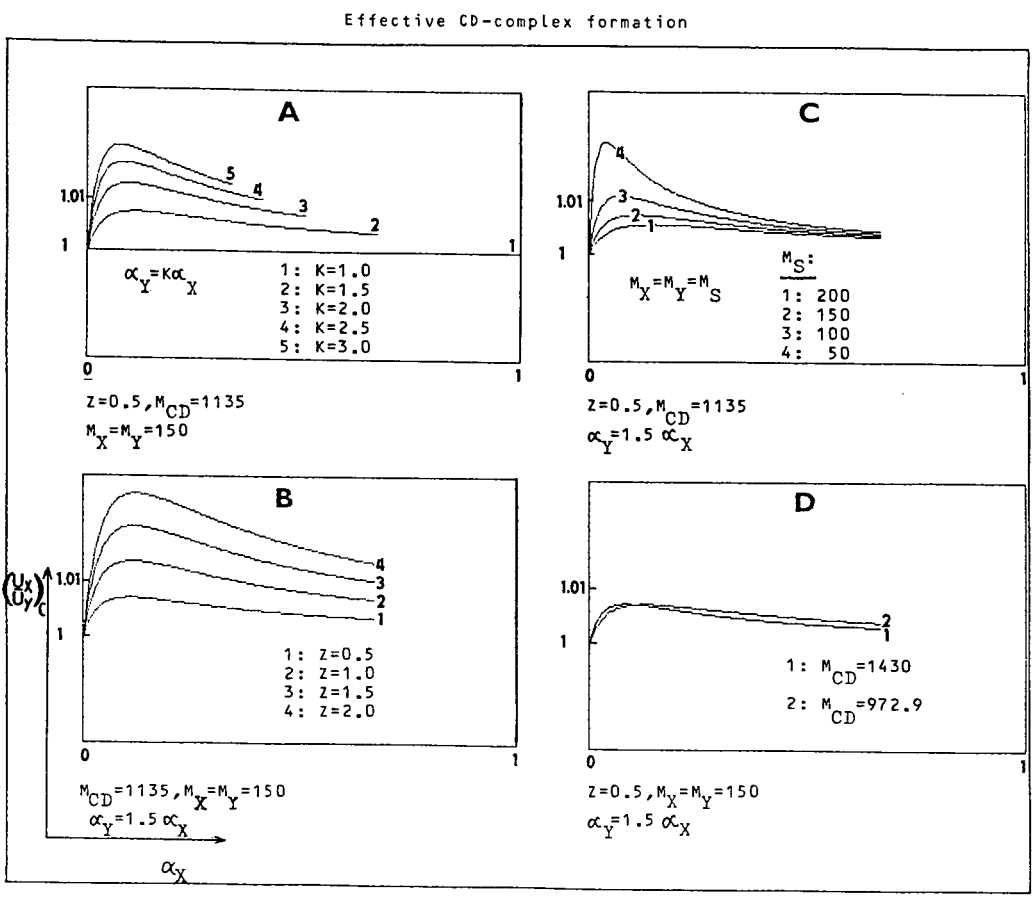

Fig. 4. Effect of changing ratio α_Y/α_X (A), effective charge, Z (B), solute molecular weight, M_S (C), and CD molecular weight, M_{CD} (D), on the quality of CD-based separation improvement.

The criterion for the CD-based separation improvement of structural isomers ($M_X = M_Y = M_S$), which is most important from the analytical point of view, is:

$$\left(\frac{U_X}{U_Y}\right)_C \neq 1 \tag{12}$$

Combining eqns. 9 and 12 it follows that:

$$\alpha_Y/\alpha_X \neq 1 \tag{13}$$

It is obvious that there is no additional requirement on the ratio α_Y/α_X resulting from the existence of an area of deteriorated resolution.

The influence of changing parameters characterizing separated solutes, complex-forming CD and the selectivity of complex formation can be simply estimated by a computer simulation of $(U_X/U_Y)_C = f(\alpha_X)$ for various α_Y, M_S, Z, ΔZ and M_{CD} values. From Fig. 4A it follows directly that higher selectivity of complex formation, characterized by increasing ratio α_Y/α_X, leads to an apparent increase in the maximum $(U_X/U_Y)_C$ value and to a separation improvement. It should be noted that the $(U_X/U_Y)_C$ maximum shifts towards lower α_X values. The same separation improvement can be observed by increasing the absolute value of the solute effective charge, but the position of the maximum shifts slightly towards higher α_X values (Fig. 4B). An increase in the solute molecular weights results on the contrary in a lowering of the CD-separation supporting effect and a decrease in the maximum mobility ratio value (Fig. 4C). A significant shift of the maximum towards higher α_X was observed. The influence of changing M_{CD} (Fig. 4D) and especially ΔZ is only marginal, owing to their limited numerical range.

CONCLUSIONS

The experiences with CD-modified electrolyte systems in ITP confirmed that the concept of effective and non-effective complex formation has meaning in the strategy of optimization of experimental conditions. In practice, unfortunately, the case of non-effective complex formation, connected with a loss in resolution, is not so rare[8,9]. Therefore it is highly important to compare the analytical results obtained in non-modified and CD-modified electrolyte systems, in order to exclude a possible disappearence of the resolution caused by non-effective complex formation.

The most important way of altering insufficient complex formation for a given solute pair is the replacement of one CD type which does not provide sufficient resolution by another one, the parameters of which are more suitable for a structural differentiation[8–13]. The set of CDs and their derivatives commercially available is sufficient for this purpose and makes it possible to achieve effectivity of CD-complex formation for a wide range of solutes.

Another factor altering significantly the effectivity of the CD-complex formation is the choice of suitable counter ion. As was suggested experimentally, competitive CD-complex formation with a "structurally suitable" counter ion decreases the degree of solute–CD complexation, distorts the resolution or even makes it impossible[8]. Therefore the use of weakly complexing counter ions is recommended.

The proposed model of effective complex formation indicates that the function $(U_X/U_Y)_C = f(\alpha_X)$ passes through a maximum. The character of this maximum depends on the parameters characterizing the solutes, the CD and the selectivity of the complexation. From computer simulated dependences, the maximum became flat and non-significant for similar α values, high solute molecular weights and low effective charges. This conclusion is in harmony with the generally known fact that the separation efficiency improves with increasing solute–pseudophase velocity differences and increasing structure-differentiating ability of the pseudophase[14]. As was shown for structurally related solutes with different molecular weights, the maximum completely disappears even for considerable α_X, α_Y differences and an improvement in separation was not achieved.

Due to a dependence of the α value on the concentration of CD in the mixed zone for a given CD stability constant, there must be an optimum CD concentration, where the separation improvement is maximal. This conclusion, which indicates that the concentration of CD in the leading electrolyte is an important optimization parameter, was confirmed experimentally and shown to be decisive especially for the resolution of enantiomers[8,12,13].

The possibility of predicting the optimum CD concentration for a given solute pair is interesting both from the theoretical point of view and for practical analytical purposes. The main problem of such a calculation results from the lack of data characterizing the stability of the CD complexes formed, necessary for the transformation of the values obtained into the mixed-zone CD concentrations. The mixed-zone CD concentration is equal to the initial analytical concentration of CD in the leading electrolyte because of the typical non-electrolyte behaviour of CD, the concentration of which is the same throughout the separation compartment and does not depend on the electrophoretic mass-distribution process.

REFERENCES

1 F. E. P. Mikkers, F. M. Everaerts and J. A. F. Peek, *J. Chromatogr.*, 168 (1979) 293.
2 V. Jokl, *J. Chromatogr.*, 13 (1964) 451.
3 E. Offord, *Nature (London)*, 211 (1966) 591.
4 O. Fujishita, S. Higuchi, M. Yoshikawa, T. Aoyama and M. Horioka, *Chem. Parm. Bull.*, 31 (1983) 2134.
5 F. S. Stover, *J. Chromatogr.*, 298 (1984) 203.
6 F. S. Stover, *J. Chromatogr.*, 368 (1986) 476.
7 M. Tazaki, T. Hayashita, Y. Fujino and M. Takagi, *Bull. Chem. Soc. Jpn.*, 59 (1986) 3459.
8 J. Snopek, E. Smolková-Keulemansová, I. Jelínek, J. Dohnal, J. Klinot and E. Klinotová, *J. Chromatogr.*, 450 (1988) 373.
9 I. Jelínek, J. Dohnal, J. Snopek and E. Smolková-Keulemansová, *J. Chromatogr.*, 464 (1989) 139.
10 J. Snopek, I. Jelínek and E. Smolková-Keulemansová, *J. Chromatogr.*, 411 (1987) 153.
11 S. Fanali and M. Sinibaldi, *J. Chromatogr.*, 442 (1988) 371.
12 J. Snopek, I. Jelínek and E. Smolková-Keulemansová, *J. Chromatogr.*, 438 (1988) 211.
13 I. Jelínek, J. Snopek and E. Smolková-Keulemansová, *J. Chromatogr.*, 439 (1988) 386.
14 S. Terabe, K. Otsuka and T. Ando, *Anal. Chem.*, 57 (1985) 834.

Journal of Chromatography, 470 (1989) 123–129
Elsevier Science Publishers B.V., Amsterdam — Printed in The Netherlands

CHROM. 21 218

HOST–GUEST COMPLEXATION IN CAPILLARY ISOTACHOPHORESIS

II[a]. DETERMINATION OF AMINOPHENOL AND DIAMINOBENZENE ISOMERS IN PERMANENT HAIR COLORANTS BY USING CAPILLARY ISOTACHOPHORESIS

SALVATORE FANALI
Istituto di Cromatografia del CNR, Area della Ricerca di Roma, C.P. 10, 00016 Monterotondo Stazione, Rome (Italy)

SUMMARY

The separation of 2-, 3- and 4-aminophenol and 1,2-, 1,3- and 1,4-diaminobenzene is studied by using capillary isotachophoresis. In order to obtain complete resolution of the six cations β-cyclodextrin was used. The analytical method was used for the determination of aminophenol and diaminobenzene isomers in permanent hair colorant creams.

INTRODUCTION

Oxidative hair colorants are permanent hair colourings usually used by mixing the dye precursor and hydrogen peroxide in an alkaline medium (ammonia and/or monoethanolamine). Hydrogen peroxide reacts with a primary intermediate (*e.g.*, 1,4-diaminobenzene, 4-aminophenol) to produce an imine, which in its turn reacts rapidly with a coupler (*e.g.*, 3-aminophenol, resorcinol) to produce the dye.

Allergic dermatitis due to 1,4-diaminobenzene and nefrotoxic effects due to 2-, 3-, 4-aminophenol have been reported[1,2]. The content and the tolerated concentrations of the chemical compounds in permanent hair colorants are listed in the Italian normative law No. 713, October 11th, 1986, in accord with European Economic Community (EEC) instruction No. 87/137.

Methods used so far for the determination of aminophenols and/or diaminobenzenes in hair colorants and other matrices are[3–8] gas–liquid, thin-layer (TLC) and high-performance liquid chromatography, titrimetry and spctrophotometry. The technique recommended by the Italian Gazette is TLC[9].

As capillary isotachophoresis is a promising method in pharmaceutical analysis[10–12], we decided to apply it to the analysis of cosmetics.

1,2-, 1,3- and 1,4-diaminobenzene and 2-, 3- and 4-aminophenol were complete-

[a] For Part I, see ref. 13.

0021-9673/89/$03.50

ly resolved by adding β-Cyclodextrin to the leading electrolyte. Samples were injected directly after dissolution and analysed with good results.

EXPERIMENTAL

Chemicals

Ethanol (95°), potassium hydroxide, acetic acid and 1,3-diaminobenzene dihydrochloride (*m*-BDA) were obtained from Carlo Erba (Milan, Italy), 2-pyridinecarboxylic acid (picolinic acid), 1,4-diaminobenzene (*p*-BDA), 2- (*o*-AP), 3- (*m*-AP) and 4-aminophenol (*p*-AP), α-cyclodextrin (α-CD) and vitamin C from Fluka (Buchs, Switzerland), poly(vinyl alcohol) 28/20 (PVA) from Serva (Heidelberg, F.R.G.), tetrahydrofuran and 1,2-diaminobenzene (*o*-BDA) from Merck (Darmstadt, F.R.G.) and β-cyclodextrin (β-CD) from Sigma (St. Louis, MO, U.S.A.). Samples of permanent hair colorants (designated A, B, C and D) were purchased from retail stores. Doubly distilled water was used to prepare the solutions.

All chemicals were of analytical-reagent grade and used as received, except for PVA, which was purified with a mixed-bed ion exchanger.

Apparatus

Experiments were performed by using a Tachophor 2127 apparatus (LKB, Bromma, Sweden) equipped with a conductivity detector. A polytetrafluoroethylene (PTFE) capillary tube (24 cm × 0.5 mm I.D.) was used. The detector cell was laboratory made as described previously[13]; the distance between the platinum sensing electrodes was 0.5 mm. The resistance and its derivative were recorded with an LKB 2210 line recorder at a chart speed of 50 mm/min.

The driving current used was 200 μA, reduced during the isotachophoresis. The zones were detected at 25 μA, unless specified otherwise. Samples and standards were injected with a 10-μl Hamilton (Bonaduz, Switzerland) microsyringe.

Electrolytes

Potassium hydroxide (10 m*M* adjusted to pH 5.4 with picolinic acid and acetic acid (5 m*M*) were used as the leading and terminating electrolytes, respectively. The leading electrolyte contained 0.4% (w/v) of PVA and the appropriate amount of α- and β-CD.

Preparation of standard solutions and samples

Standard solutions were prepared by dissolving the appropriate amount of aminophenol and diaminobenzene isomers in water containing 1 mg/ml of vitamin C. Calibration graphs were obtained with a mixture of *p*-BDA, *p*-AP and *o*-AP and 1 mg/ml of vitamin C. The final concentration of each standard was $1 \cdot 10^{-3}$ *M*. The solutions were stored in a refrigerator until their use.

Hair dyes were dissolved in water–ethanol–tetrahydrofuran (10:80:10, v/v/v) containing 1 mg/ml of vitamin C.

RESULTS AND DISCUSSION

In order to find the optimum conditions for the separation of aminophenol and diaminobenzene isomers, several electrolyte systems were tested. The cationic

electrolyte system recommended by Jokl *et al.*[14] with H^+ as terminator with a very low mobility allowed the analysis of *m*-AP, which otherwise is difficult. Under these conditions, *o*-BDA and *o*-AP were not separated from each other and it was therefore necessary to modify their effective mobilities. The use of uncharged complexing agents, *e.g.*, cyclodextrins is well known in capillary isotachophoresis for the separation of structural isomers, *e.g.*, benzoic acid derivatives[13,15] and aromatic quaternary ammonium ions[16]. In order to find the optimum separation conditions, different amounts of α- and β-cyclodextrins were added to the leading electrolyte and their effect was observed.

Fig. 1a and b show the relationship between the amount of α- and β-CD, respectively, added to the leading electrolyte and the RSH values of six aminophenol and diaminobenzene isomers, where RSH is the relative step height calculated using the equation

$$\mathrm{RSH} = \frac{h_x - h_L}{h_s - h_L} \tag{1}$$

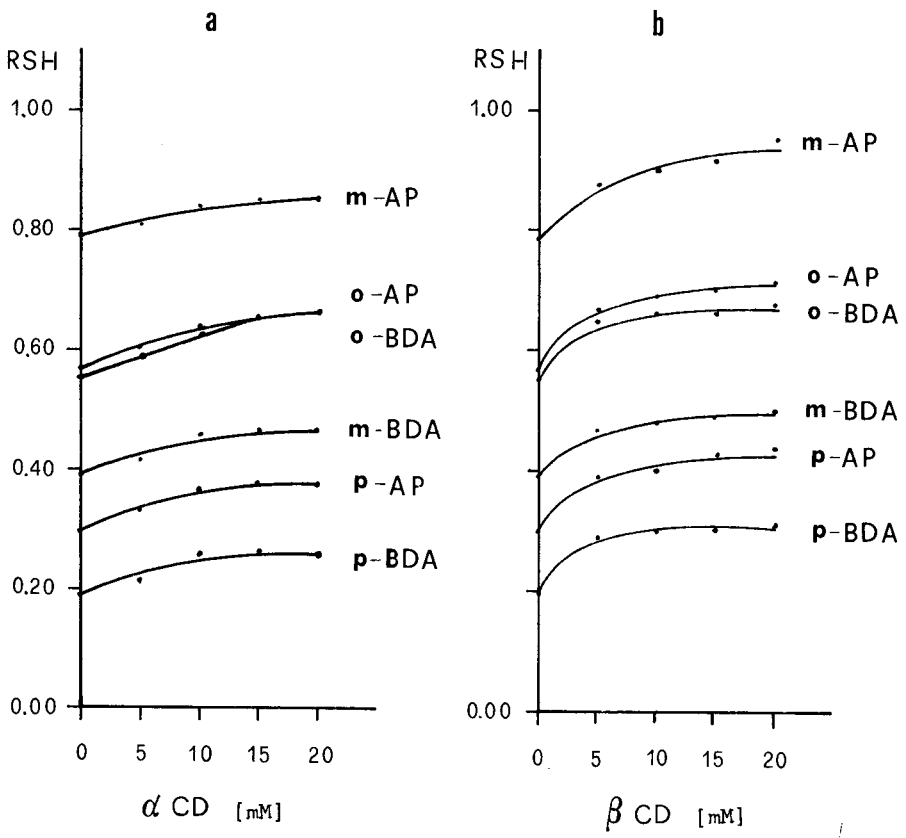

Fig. 1. Effect of the amount of cyclodextrins added to the leading electrolyte on the RSH values of 2-, 3- and 4-aminophenol (*o*-, *m*- and *p*-AP) and 1,2-, 1,3- and 1,4-diaminobenzene (*o*-, *m*- and *p*-BDA). (a) α-Cyclodextrin; (b) β-cyclodextrin.

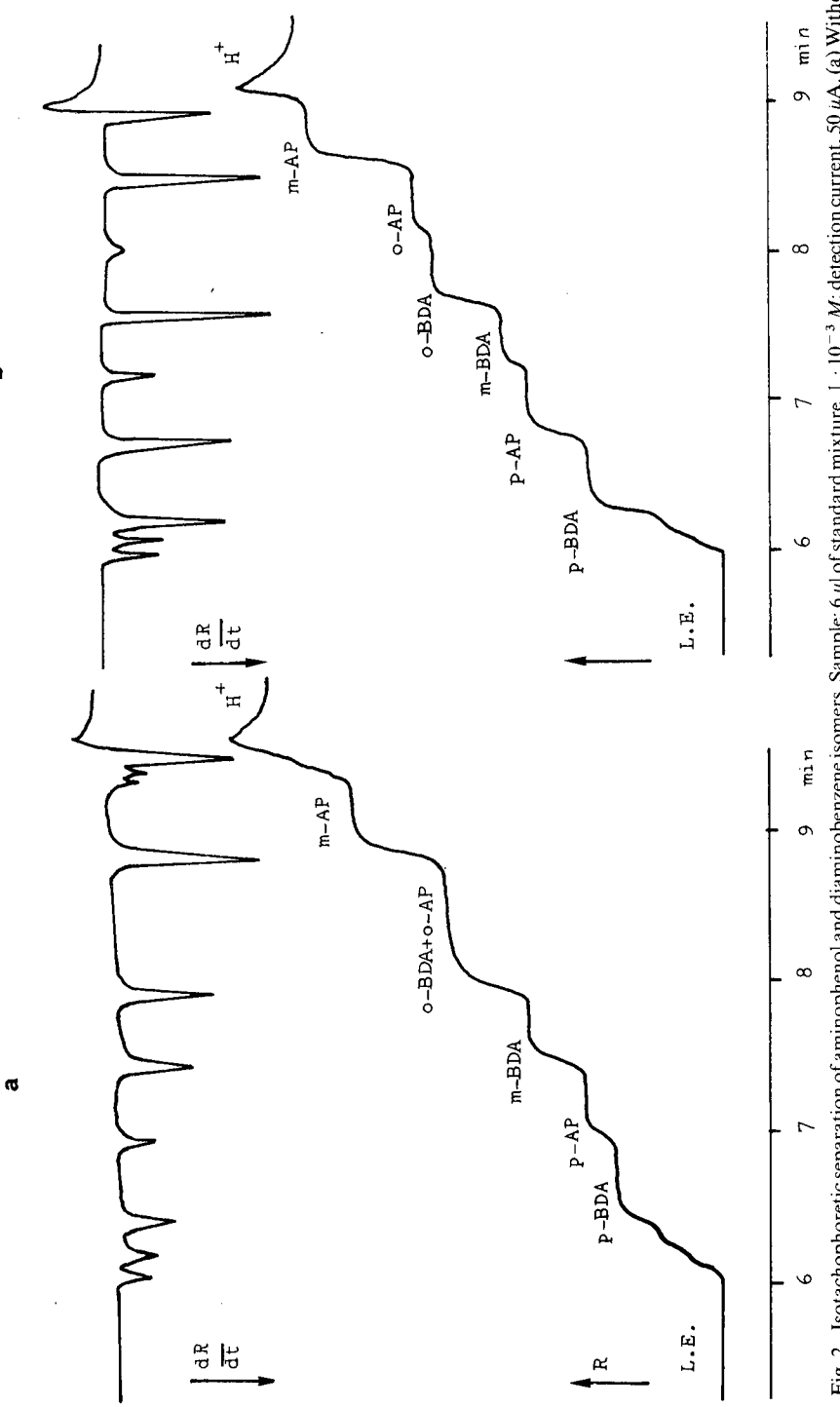

Fig. 2. Isotachophoretic separation of aminophenol and diaminobenzene isomers. Sample: 6 μl of standard mixture, $1 \cdot 10^{-3}$ *M*; detection current, 50 μA. (*a*) Without cyclodextrin; (b) with 15 m*M* β-cyclodextrin.

where h_x, h_L and h_s are the step heights of the examined, leading and reference (H^+) cations, respectively.

By adding α-CD to the leading electrolyte, a reduction in effective mobility was achieved for all compounds, but an increase in the amount of α-CD did not result in resolution. The effective mobilities of the six examined compounds were reduced more effectively by using β-CD than α-CD. In fact, by increasing the amount of β-CD in the leading electrolyte all the RSHs increased and complete resolution was achieved with 15 m*M* β-CD.

Fig. 2a and b show the separation of *o*-, *m*- and *p*-aminophenols and *o*-, *m*- and *p*-diaminobenzenes without and with cyclodextrin, respectively. To verify the validity of the method, four hair colorant creams were examined. Qualitative analysis was performed by measuring the RSH and by injecting samples and standards together. Calibration graphs were drawn for *p*-BDA, *o*-AP and *p*-AP present in the samples. The lengths of the steps were plotted against concentration and the linearity was observed from $1 \cdot 10^{-9}$ to $15 \cdot 10^{-9}$ mol. The correlation coefficients were 0.9999, 0.9999 and 0.9997 for *p*-BDA, *p*-AP and *o*-AP, respectively. Relative standard deviations were obtained by injecting 7 μl of the standard solution (six measurements) and good results were achieved (0.6, 0.2 and 0.4%, respectively).

The recovery was determined by adding more of the analytes present in the samples and the results are presented in Table I. Fig. 3 shows the isotachopherogram of

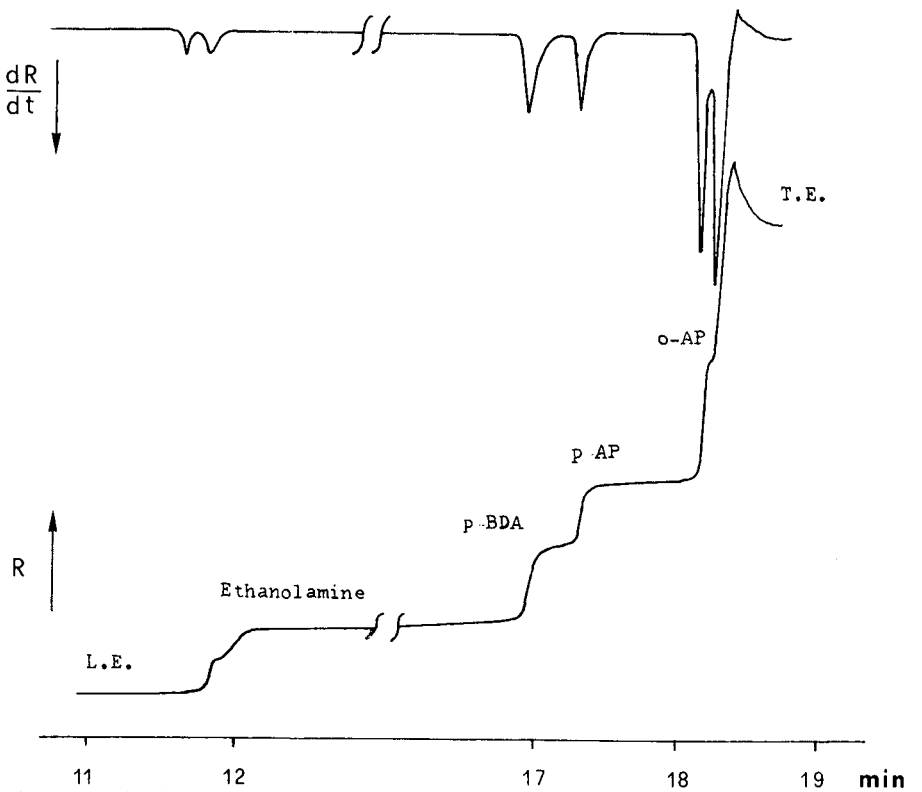

Fig. 3. Isorachopherogram of the analysis of a commercial hair colorant (D, Table I). Amount injected, 8 μl; detection current, 25 μA.

TABLE I

DETERMINATION OF 1,4-DIAMINOBENZENE, 2-AMINOPHENOL AND 4-AMINOPHENOL IN COMMERCIAL HAIR COLORANT CREAMS

Sample	*Compounds declared*[a]	*Prepared solution (g per 100 ml)*	*Amount found (%)*			*Recovery*					
			p-BDA	*p-AP*	*o-AP*	*p-BDA*		*p-AP*		*o-AP*	
						Added (mg)	*Recovered (%)*	*Added (mg)*	*Recovered (%)*	*Added (mg)*	*Recovered (%)*
A	*p*-BDA, RES, NH_3	0.403	1.92	–	–	11.6	98	–	–	–	–
B	*p*-BDA, *p*-AP, RES, NH_3	0.622	1.20	0.38	–	11.1	97	11.3	97	–	–
C	*p*-BDA, *o*-, *m*-, *p*-AP, RES, NH_3	1.549	0.24	0.36	–	10.0	92	13.1	100	–	–
D	*p*-BDA, RES, NH_3, *o*-, *m*-, *pp*-AP	2.840[b]	0.06	0.13	0.04	3.5	98	4.7	92	4.9	96

[a] RES = resorcinol.

[b] g per 50 ml.

one sample. The presence of ammonia and/or ethanolamine under these conditions does not interfere with the determinations.

From the results it can be concluded that capillary isotachophoresis is a rapid method for the qualitative analysis of aminophenol and diaminobenzene isomers present in cosmetics. The method can be used for routine control in order to reveal compounds that should not be included in the composition of the cosmetics, *e.g.*, 1,2-BDA[9], and to check if the allowed chemicals are or not in accord with the statutory requirements. Analysis can be performed without pre-treatment in spite of the complexity of the matrix.

Further studies will be made in order to determine other components, *e.g.*, derivatives such as aminotoluene, that could be present in hair colorants.

ACKNOWLEDGEMENTS

The author thanks Prof. P. Catellani for some suggestions which led to the start of this research. Thanks are due to Mr. M. Cristalli for skillful technical assistance.

REFERENCES

1 J. F. Corbett, in F. Frost and S. N. Horwitz (Editors), *Principles of Cosmetics for the Dermatologist*, C. V. Mosby, St. Louis, Toronto, London, 1982, p. 160.
2 I. Ito, *Tokyo Joshi Ika Daigaku Zasshi*, 57 (1987) 1655; *C.A.*, 108 (1988) 181763t.
3 G. Choudhary, *J. Chromatogr.*, 193 (1980) 277.
4 H. Tokuda, Y. Kimura and S. Takano, *J. Chromatogr.*, 367 (1986) 345.
5 K. Kijima, E. Saito, N. Teshirogi and M. Honda, *Eisei Shikensho Hokoku*, 101 (1983) 32; *C.A.*, 101 (1984) 11988h.
6 B. Schultz, *J. Chromatogr.*, 299 (1984) 484.
7 D. Amin, *Analyst (London)*, 110 (1985) 211.
8 T. T. Ngo and C. F. Yam, *Anal. Lett.*, 17 (1984) 1771.
9 *Gazz. Uff.*, Suppl. No. 7, Jan. 23rd (1987) 32.
10 S. Fanali, F. Foret and P. Boček, *J. Chromatogr.*, 330 (1985) 436.
11 E. Kenndler and R. Katzenberger, *Mikrochim. Acta*, 1 (1986) 415.
12 S. Fanali, M. Sinibaldi and M. G. Quaglia, *J. Chromatogr.*, 408 (1987) 441.
13 S. Fanali and M. Sinibaldi, *J. Chromatogr.*, 442 (1988) 371.
14 V. Jokl, J. Pospichalova and M. Polasek, *Electrophoresis*, 7 (1986) 433.
15 J. Snopek, I. Jelínek and E. Smolková-Keulemansová, *J. Chromatogr.*, 411 (1987) 153.
16 M. Tazaki, T. Hayashita, Y. Fujino and M. Takagi, *Bull. Chem. Soc. Jpn.*, 59 (1986) 3459.

Journal of Chromatography, 470 (1989) 131–137
Elsevier Science Publishers B.V., Amsterdam — Printed in The Netherlands

CHROM. 21 267

UTILITY OF COPPER-CONTAINING ELECTROLYTES FOR ISOTACHOPHORESIS OF AMINO ACIDS

FREDERICK S. STOVER
Central Research Laboratories, Monsanto Co., 800 N. Lindbergh Blvd., St. Louis, MO 63167 (U.S.A.)

SUMMARY

Isotachophoretic separation of free amino acids using Cu^{2+}–diethylene triamine (Den) in high-pH leading electrolytes is investigated. Large changes in relative step heights of free amino acids are seen. Mobility order depends on both Cu^{2+} concentration and Cu^{2+}/Den ratios. Mobility differences seen with CuDen addition can be ascribed to both polyvalent counterion effects and specific interactions forming tertiary complexes. These electrolytes offer a new dimension for mobility variation of complexing amino acids and peptides.

INTRODUCTION

A major drawback to the isotachophoresis (ITP) of free amino acids is that the separations are essentially one dimensional. Leading electrolytes with pH values from 8.6 to 9.6 generally are employed to impart anionic mobilities to neutral amino acids sufficient for isotachophoretic migration[1]. The useable pH range is restricted by decreased ionization at lower pH values and by OH^--migration at higher pH values. Thus, the usual practice of altering effective mobilities by changing leading electrolyte pH is limited for mixtures of amino acids. Also, using pH 8.6–9.6 electrolytes, several pairs of amino acids often form mixed zones (*e.g.* Asp–Glu, Ser–Thr, Tyr–Met and Val–Trp). Hirokawa *et al.*[2] recently evaluated the separability of 26 amino acids under typical electrolyte conditions, and noted the frequent occurrence of mixed zones.

A second, widely used method of obtaining improved ionic mobility differences is addition of complexing agents to samples or leading electrolytes[3–5]. Everaerts *et al.*[1] added Cu^{2+} to amino acid samples in an effort to obtain separation of the cationic complexes. Except for histidine, copper–amino acid complexes were not sufficiently stable to be detected as cationic species in a pH 5.4 electrolyte. A more successful approach involved addition of propionaldehyde to an anionic pH 7.5 electrolyte[6]. Schiff base formation between amino acid and aldehyde resulted in lower amino group pK_a values. While some improved separations were obtained, many amino acid pairs remained unresolved.

Recently, "pre-capillary" derivatization of free amino acids with dinitrophenol[7] and citraconic anhydride[8] has been reported. Advantages of these approaches include the ability to operate at lower pH values and use of specific detectors.

0021-9673/89/$03.50

We report here investigations of anionic amino acid ITP utilizing labile equilibria between copper complexes in the leading electrolyte and free amino acids. Such systems offer totally aqueous electrolytes, no derivatization step and the possibility of tailoring separations by altering the distribution of counterions in the leading electrolyte.

EXPERIMENTAL

ITP was performed using an LKB (Bromma, Sweden) 2127 Tachophor with a 200 mm × 0.8 mm PTFE capillary and an LKB 2127-140 conductivity detector. Separation currents were 250 μA and detection currents were 100 μA. Leading and terminating reservoirs were refilled with electrolytes after every two to three runs. HCl (Ultrex® grade) was obtained from J.T. Baker (Phillipsburg, NJ, U.S.A.); $CuCl_2$ (Gold Label® grade), 95% diethylene triamine (Den), and hydroxypropyl methylcellulose (HPMC) were obtained from Aldrich (Milwaukee, WI, U.S.A.); L-histidine (His), L-alanine (Ala), glycine (Gly), L-glutamic acid (Glu), L-aspartic acid (Asp), L-phenylalanine (Phe), L-valine (Val), β-alanine (Bala) and 2-amino-2-methyl-1,3-propanediol (ammediol) were obtained from Sigma (St. Louis, MO, U.S.A.); 2.5 *M* NaOH and $Ba(OH)_2$ were obtained from Fisher Scientific (Pittsburgh, PA, U.S.A.). All chemicals were reagent grade unless otherwise specified and used as received.

RESULTS AND DISCUSSION

The use of Cu^{2+} complexation in high-pH electrolytes to alter amino acid mobilities is complicated by the hydrolysis of $Cu(aquo)^{2+}$. We recently measured formation constants for tertiary complexes of Cu^{2+} with N-methyliminodiacetic acid (MIDA) and various amino acid analogues[9]. It was found that the formation constant for the reaction

$$Cu(MIDA) + AA \rightarrow Cu(MIDA)AA \quad (1)$$

generally is within an order of magnitude of the constant for complexation with the bare metal ion

$$Cu + AA \rightarrow CuAA \quad (2)$$

where AA is an amino acid or derivative and charges have been omitted for clarity. These results indicated that the use of copper complexes in leading electrolytes could maintain solubility while providing a site for amino acid complexation. This is often the case when using complexing metal counterions. For example, the HCl–$ZnCl_2$–His leading electolyte used in phosphonate analysis[5] probably contains $Zn(His)_2$ as the complexing counterion. Similar tertiary equilibria have been used successfully for the separation of amino acid enantiomers by liquid chromatography[10] and capillary zone electrophoresis[11].

There are several criteria to consider when selecting a secondary ligand, X, for use in an ITP electrolyte where the equilibrium

$$CuX + AA \rightleftarrows Cu(AA)X \quad (3)$$

TABLE I
OPERATING SYSTEMS
Additive to leading electrolytes: 0.2% HPMC.

Leader (all pH 9.0)		*Terminator*	
No.	*Composition*	*No.*	*Composition*
L1	10 m*M* HCl + ammediol	T1	10 m*M* β-alanine adjusted to pH 9.0 with $Ba(OH)_2$
L2	10 m*M* HCl + Den	T2	10 m*M* L-histidine adjusted to pH 9.0 with $Ba(OH)_2$
L3	5 m*M* $Cu(Cl)_2$ + 5 m*M* Den + NaOH		
L4	5 m*M* $Cu(Cl)_2$ + Den		
L5	3 m*M* $Cu(Cl)_2$ + 4 m*M* HCl + Den		
L6	1 m*M* $Cu(Cl)_2$ + 8 m*M* HCl + Den		

governs the effective mobility. (1) The complex CuX must have a high enough stability to prevent hydroxide formation at pH 9. (2) Since copper must act as a counterion in the anionic electrolyte, the complex CuX should have a net positive or zero charge. (3) Since the strongest coordinating sites on copper occupy square-planar positions[12], X should be no more than tridentate to allow strong amino acid interaction with CuX. (4) To maximize the amount of CuX available for AA binding, X should preferentially form 1:1 over 1:2 complexes. This also will minimize $Cu(OH)_2$ precipitation if equimolar Cu–X concentrations are employed. (5) Formation of an acidic or basic complex, CuHX or Cu(OH)X, with a pK_a of 8.5–9.5 would eliminate the need for a buffering counterion B, which may form a mixed complex Cu(B)X. A candidate ligand that fulfills these requirements is Den.

Table I lists the electrolytes employed in this study. Electrolyte system L1–T1 is commonly used in amino acid ITP. Use of polyvalent Den as a counterion could cause changes in AA mobilities due to electrophoretic and relaxation effects[13]. Electrolyte L2 was tested to determine the extent of these retardations. Electrolyte L3 was designed based on the above criteria for Cu(AA)X formation to give maximum Cu–AA interactions. Finally, electrolyte L4, using Den instead of NaOH to adjust pH, was tested as an intermediate strength system.

Separation of mixtures with electrolyte systems L1–T1, L2–T1,L3–T2 and L4–T2 are given in Figs. 1 and 2. Inspection of these results shows that use of Cu + Den in the leading electrolyte has a profound effect on AA mobilities. For electrolytes containing Cu, the decrease in His mobility is so great that it can be used as a terminating ion for the other seven AAs. A plot of AA relative step heights, on a log scale, for electrolytes L1–L4 is shown in Fig. 3. Large decreases in mobilities for His, Gly and Asp are observed with Cu-containing electrolytes. Benefits of using L3 or L4 include improved Glu and Asp separations and better resolution of Gly from Phe and His. Ala, Val and Phe remain mixed with other AAs in all four electrolytes. Disadvantages to using the Cu-containing systems include higher impurity levels which interfere with some AAs, longer analysis times and, for certain pairs, poorer resolution.

Use of Den alone (L2) shows modest changes in the separation patterns obtained

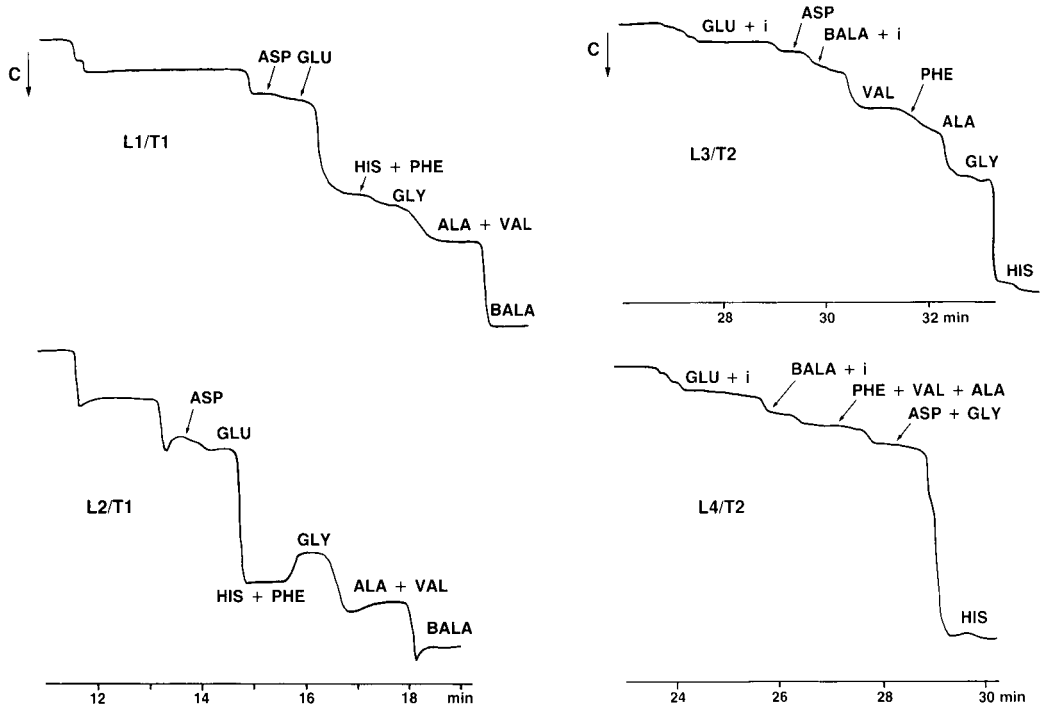

Fig. 1. Conductivity traces for injections of a mixture containing 0.14 mg/ml each of Asp, Glu, His, Phe, Gly, Ala and Val. Top: 10 μl mixture in L1–T1 electrolytes; bottom: 5 μl mixture in L2–T1 electrolytes. C axis is decreasing conductivity.

Fig. 2. Conductivity traces for injections of (top) 5 μl amino acid mixture in L3–T2 electrolytes and (bottom) 3 μl in L4–T2 electrolytes. Same mixture as in Fig. 1 but with His replaced by Bala. i = Electrolyte impurities. C axis is decreasing conductivity.

due to electrophoretic and relaxation effects of the polyvalent counterion. All amino acids are retarded with reference to Bala. The most interesting feature of the L2 electrolyte is the enforced migration of His and Phe ahead of Gly.

Mobility effects resulting from variation in Cu^{2+} content of the leading electrolyte were investigated using electrolyte systems L5–T2 and L6–T2. These electrolytes, along with L2 and L4 form a consistent set with Cu^{2+} concentrations of 0, 1, 3 and 5 m*M*. Separation of AA mixtures in 1 and 3 m*M* Cu^{2+} electrolytes with Den adjustment of pH is shown in Fig. 4. Fairly large changes in AA mobilities and migration orders are obtained with the 3 m*M* system, but electrolyte L6 with 1 m*M* Cu^{2+} gives identical separations as a Den-only electrolyte (L2).

To gain insights into the active counterion compositions of the leading electrolytes, calculations were performed to determine copper speciation in electrolytes L2–L6. Motekaitis and Martell's computer program BEST[14] and literature values for stability constants [15] were used for the calculations and the results are given in Table II. Equilibrium calculations show that leading electrolyte compositions depend on the method of pH adjustment. Use of excess Den (L4) instead of NaOH results in formation of $Cu(Den)_2$ at the expense of CuDen and Cu(OH)Den.

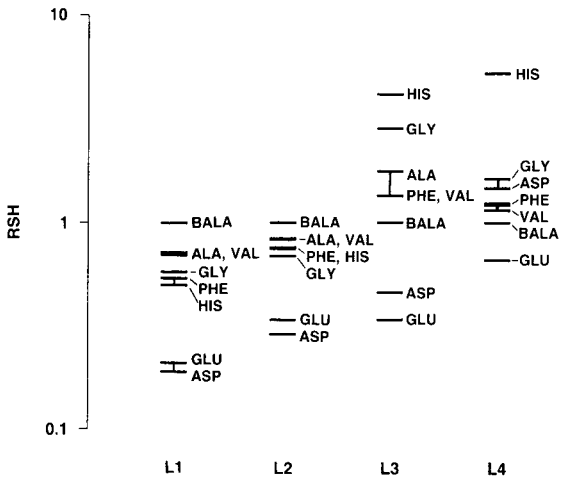

Fig. 3. Plot of relative step heights, on a log scale, referenced to Bala for individual amino acids in leading electrolytes L1–L4. Vertical bars represent mixed or non-resolved zones.

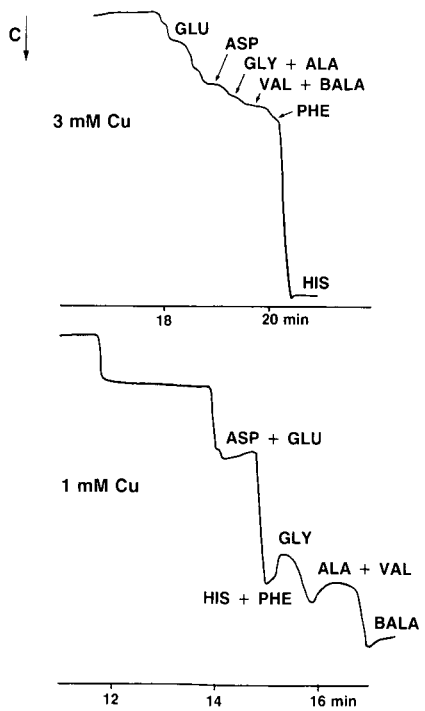

Fig. 4. Conductivity traces for injections of (top) 1 μl mixture with Bala in L5–T2 electrolytes and (bottom) 5 μl mixture with His in L6–T1 electrolytes. C axis is decreasing conductivity.

TABLE II
CALCULATED LEADING ELECTROLYTE COMPOSITIONS

Leader	*Total [Cu] (mM)*	*Total [Den] (mM)*	*[CuDen] (mM)*	*[Cu(Den)$_2$] (mM)*	*[Cu(OH)Den] (mM)*	*[HDen+H$_2$ Den] (mM)*
L3	5.0	5.0	3.0	–	2.0	–
L4	5.0	8.8	1.0	3.4	0.6	0.4
L5	3.0	8.8	0.1	2.8	0.1	2.8
L6	1.0	7.8	–	1.0	–	5.4
L2	–	7.2	–	–	–	6.6

The counterion with the strongest presumed AA binding is the binary CuDen complex. Electrolyte L3, with the highest CuDen content, gave the lowest absolute His mobility as measured from adjusted terminator resistances. However, the relative step height of His was higher in L4, due to significant Cu(Bala)Den formation in L3.

Reducing the total Cu concentration to 3 m*M* (L5) also causes considerable change in counterion distributions. Although this electrolyte contains Cu(Den)$_2$ as the primary counterion, enough complexation power is retained so that His can be used as a terminator. Apparently, 0.1 m*M* CuDen is sufficient to cause changes in AA mobilities. Further reduction in total Cu to 1 m*M* (L6) yields an electrolyte with performance similar to the non-Cu-containing L2 electrolyte. Thus, a Cu(Den)$_2$ level of 1 m*M* causes no mobility change and this species is inactive.

Unique mobility profiles are seen with all electrolytes except the L2–L6 pair. Changes in effective mobilities are a combination of electrophoretic and relaxation effects from changing +1/+2 counterion distributions and specific binding effects with $CuDen^{2+}$. The power of this approach to tailoring separations is demonstrated by the fact that only Ala and Val fail to separate from other amino acids using the electrolytes tested here.

Discontinuities in leader conductivity signals were observed with Cu-containing electrolytes L3–L5. Shown in Fig. 5 are anomolous conductivity changes seen at 12–16

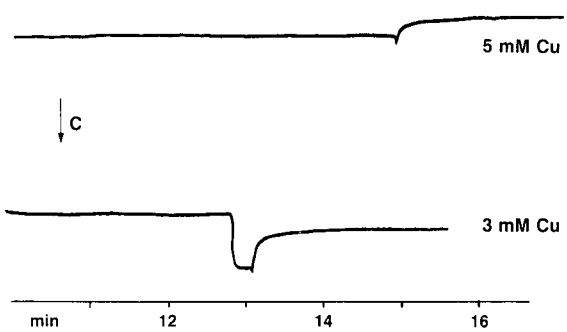

Fig. 5. Conductivity record of Cu-containing leading electrolyte signals prior to leader/terminator boundary. Top trace: L4; bottom trace: L5. Signals recorded at 100 μA and same decreasing conductivity scale (C axis) as previous figures.

min in the L4 and L5 electrolytes. Discontinuities occur near the expected time of the Cl^- leading boundary, with some shift due to bulk leader transport number changes. These discontinuities are suspected to be caused by CO_3^{2-} migrating in an enforced or zone manner. This is supported by the fact that no discrete zone or zone length increase was observed near AA zones when 5 μg CO_3^{2-} was injected in the L3–T2 electrolyte system. Thus CO_3^{2-} may act as a pseudo-leader in these systems and cause the lengthy analysis times observed at high Cu content.

Most probably all twenty common protein amino acids cannot be successfully separated by ITP using these types of electrolytes. The seven amino acids tested here are among those that bind copper most strongly. Less dramatic mobility shifts are anticipated for other amino acids. However, electrolyte systems suggested here offer a new method of altering ITP separations of free amino acids. In addition, such systems could be useful for obtaining improved separations of related compounds such as peptides and proteins.

REFERENCES

1 F. M. Everaerts, J. L. Beckers and Th. P. E. M. Verheggen, *Isotachophoresis—Theory, Instrumentation and Applications*, Elsevier, Amsterdam, 1976, pp. 311–322.
2 T. Hirokawa, T. Gojo and Y. Kiso, *J. Chromatogr.*, 369 (1986) 59.
3 D. Kaniansky and F. M. Everaerts, *J. Chromatogr.*, 148 (1978) 441.
4 P. Gebauer, P. Boček, M. Deml and J. Janák, *J. Chromatogr.*, 199 (1980) 81.
5 F. S. Stover and J. H. Wagenknecht, *Anal. Chim. Acta*, 135 (1982) 347.
6 F. M. Everaerts, J. L. Beckers and Th. P. E. H. Verheggen, *Isotachophoresis—Theory, Instrumentation and Applications*, Elsevier, Amsterdam, 1976, p. 319.
7 D. Kaniansky, V. Madajová, J. Marak, E. Šimuničová, I. Zelenský and V. Zelenská, *J. Chromatogr.*, 390 (1987) 51.
8 C. J. Holloway, *J. Chromatogr.*, 390 (1987) 97.
9 F. S. Stover and B. L. Haymore, unpublished data.
10 J. M. Broge and D. L. Leussing, *Anal. Chem.*, 58 (1986) 2237.
11 P. Gozel, E. Gassmann, H. Michelsen and R. N. Zare, *Anal. Chem.*, 59 (1987) 44.
12 H. Sigel and R. B. Martin, *Chem. Rev.*, 82 (1982) 385.
13 D. Kaniansky, V. Madajová, I. Zelenský and S. Stankoviansky, *J. Chromatogr.*, 194 (1980) 11.
14 R. J. Motekaitis and A. E. Martell, *Can. J. Chem.*, 60 (1982) 2403.
15 R. M. Smith and A. E. Martell, *Critical Stability Constant*, Vol. 1, Plenum Press, New York, 1974, pp. 1–61.

Journal of Chromatography, 470 (1989) 139–153
Elsevier Science Publishers B.V., Amsterdam — Printed in The Netherlands

CHROM. 21 219

ON-COLUMN RADIOMETRIC DETECTOR FOR CAPILLARY ISOTACHOPHORESIS AND ITS USE IN THE ANALYSIS OF ^{14}C-LABELLED CONSTITUENTS

D. KANIANSKY*

Institute of Chemistry, Faculty of Science, Komenský University, Mlynská dolina CH-2, 842 15 Bratislava (Czechoslovakia)

J. MARÁK

Institute of Radioecology and Applied Nuclear Techniques, Chrapčiakova 1, 052 80 Spišská Nová Ves (Czechoslovakia)

P. RAJEC and A. ŠVEC

Institute of Chemistry, Faculty of Science, Komenský University, Mlynská dolina CH-2, 842 15 Bratislava (Czechoslovakia)

and

M. KOVAĽ, M. LÚČKA and G. SABANOŠ

Institute of Radioecology and Applied Nuclear Techniques, Chrapčiakova 1, 052 80 Spišská Nová Ves (Czechoslovakia)

SUMMARY

A radiometric detector suitable for capillary isotachophoresis (ITP) is described. This detector, based on solid scintillation counting, consists of three subunits, *viz.*, an on-column detection module, measurement electronics and a microcomputer system. A key part of the detector, a small volume detection cell, has a sensing part made of a plastic scintillator. Counting efficiencies of 10–15% were typical for these cells of effective volumes of 70 or 210 nl (0.3 mm I.D.) for ^{14}C-labelled constituents in a coincidence mode of measurement. By using the cell of effective volume of 210 nl, *e.g.*, a detection limit of *ca.* 16 Bq was achieved for [U-^{14}C]acetate under typical ITP working conditions. It is shown by practical examples (cytidine 5′-tri- and diphosphates) that the detector can be very useful in the purity control of ^{14}C-labelled chemicals by ITP. A practical utility of the detector in monitoring a biotransformation of ^{14}C-labelled Cytostasane (a cytostatic drug) by ITP indicates its potential, *e.g.*, in pharmaceutical research. From the ITP analysis of an [U-^{14}C]protein hydrolysate it can be deduced that the radiometric detector in conjunction with suitable spacing constituents is convenient also for analytical work with complex mixtures of radiolabelled constituents.

INTRODUCTION

The separating abilities associated with an inherent concentrating power as well as typical submicroanalytical features make capillary isotachophoresis (ITP) an

0021-9673/89/$03.50

attractive alternative in the analysis of radioactive and/or radiolabelled ionogenic compounds. To exploit these analytical potentials of ITP, off-line techniques were proposed by Arlinger[1–4]. This approach to radiometric detection was shown to be useful also in analytical applications characterized by complex sample matrices[5–7].

However, when a wider analytical use is considered these off-line combinations are less convenient for the following reasons: (i) increased labour requirements; (ii) a time delay between the separation and detection; (iii) a possible loss of resolution during the isolation step; (iv) uncertainties in the recoveries of the analytes, *e.g.*, when they are isolated from the trapping strips[1–7]; (v) risk of contamination due to extensive handling of radioactive material. These disadvantages stimulated feasibility studies devoted to the developments of on-column radiometric detection in ITP[8–10]. Despite sceptism (see, *e.g.*, refs. 3 and 4), it was clearly shown that this detection mode is applicable in ITP for a wide range of radionuclides. For example, with the exception of ^{3}H (very weak β emitter), it is suitable to the detection of β radiation emitted from nuclides currently employed in biosciences[8–10].

The aim of this work is to describe an on-column radiometric detector for ITP developed recently in our laboratory. As is illustrated practically, based on solid scintillation counting, this detector is very convenient for the analysis of ^{14}C-labelled constituents present in various matrices.

EXPERIMENTAL

Instrumentation

A CS isotachophoretic analyser (ÚRVJT, Spišská Nová Ves, Czechoslovakia) was used. It was assembled in the column-coupling configuration of the separation unit[11,12] by using modules as delivered by the supplier. An on-column radiometric detection module developed in this work was assembled into the analytical stage of the separation unit (see Figs. 1 and 2). The measurement electronics of the detector comprised commercially available subunits for the radioactivity measurement (JANA, ÚRVJT), see Fig. 2. Data acquisition from the radiometric detector was performed with a PMD 85 microcomputer (Tesla, Bratislava, Czechoslovakia). This microcomputer system served also for post-analysis treatment of data and for printing of the results (see below).

For preparative ITP experiments a discontinuous fractionation technique[12,13] was employed in the column-coupling configuration of the separation unit[14].

Chemicals

Chemicals used for the preparation of the leading and terminating electrolytes were obtained from Sigma (St. Louis, MO, U.S.A.), Serva (Heidelberg, F.R.G.), Reanal (Budapest, Hungary) and Lachema (Brno, Czechoslovakia). They were purified by conventional methods[15]. Water supplied by a two-stage laboratory demineralization unit (Rodem-1; OPP, Tišnov, Czechloslovakia) and further purified on a mixed-bed ion exchanger (Amberlite MB-1; BDH, Poole, U.K.) was used for the preparation of the solutions. Hydroxyethylcellulose 4000 (Serva) was used as an anticonvective additive to the leading electrolytes. Its stock solutions were purified on a mixed-bed ion exchanger (Amberlite MB-1).

Carbon-14-labelled chemicals were obtained from the Institute for Research,

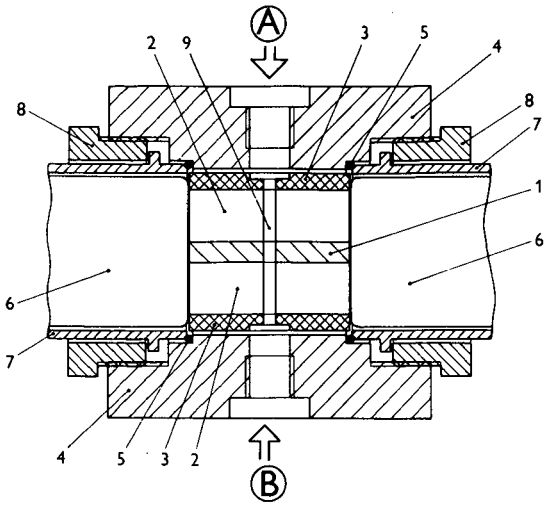

Fig. 1. On-column part of the radiometric detector. 1 = Sensing layer made of plastic scintillator; 2 = transparent plastic material compatible with the scintillator; 3 = black layer made of plastic material preventing stray light effects from the side of the column (A) and from the side of the counter-electrode compartment (B); 4 = duralumin housing of the on-column module; 5 = O-rings for light-tight connections of the photomultipliers (6) to the detection cell; 7 = metal housing for the photomultipliers; 8 = screws fixing photomultipliers; 9 = capillary channel in the detection cell.

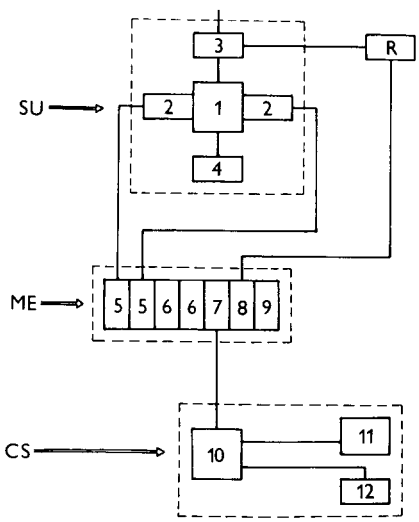

Fig. 2. Block diagram of the on-column radiometric detector for ITP. SU = On-column part of the detector (see Fig. 1); ME = measurement electronics; CS = microcomputer system; R = line recorders; 1 = duralumin housing for the detection cell; 2 = photomultipliers; 3 = conductivity detector; 4 = refilling block with the counter-electrode compartment for the analytical column; 5 = power supplies for photomultipliers; 6 = amplifiers; 7 = coincidence modul; 8 = ratemeter; 9 = system power supply; 10 = microcomputer; 11 = monitor; 12 = printer.

Production and Applications of Radioisotopes (Prague, Czechoslovakia). Reaction mixtures from a biotransformation study of ^{14}C-labelled 5-bis(2-chloroethyl)amino-1-methylbenzimidazolyl-2-butanoic acid (Cytostazane) were obtained from Dr. V. Ščasnár (Institute of Pharmacology, Biomedical Centre of Slovak Academy of Science, Bratislava, Czechoslovakia).

RESULTS AND DISCUSSION

Description of the detector

The detector developed in this work consists of three subunits, *viz.*, (1) on-column detection module, (2) measurement electronics, (3) microcomputer system (see Figs. 1 and 2). In its design we paid special attention to the detection module since it is a key subunit when the overall analytical performance of the detector is considered. Fig. 1 shows that it consists of a light-tight assembly made of metal (4) in which an exchangeable detection cell (1–3) is placed between a pair of photomultipliers (6). The sensing part of the detection cell (1) is made of a plastic scintillator (SPB 31; Tesla, Přemyšlení, Czechoslovakia). A capillary channel in the cell (9) has a diameter identical to that of the I.D. of the analytical column (0.3 mm). In spite of the fact that very different values for the average range of ^{14}C β radiation in aqueous solutions can be found in the literature (see, *e.g.*, refs. 16 and 17), such a diameter of the capillary channel in the sensing part is rather large to achieve an high counting efficiency in the radioactivity measurement (see below). However, we preferred compatibility of the on-column module with current ITP columns on the account of lower counting efficiency.

To achieve an high resolving power of the detector it is desirable to use a very thin scintillating layer in the detection cell ($\approx$ 0.1 mm). While such a thickness of the sensing part is technologically feasible, from a theoretical treatment of our type of detector it can be concluded that the thickness should not be less than 1 mm as otherwise a considerable decrease in the precision of the radioactivity measurement is unavoidable[10]. This means that our type of detection cell to some extent compromises the resolving power of the detector relative to that achieved by the separation process. To keep the precision of the radioactivity measurement at an optimum, we used cells having a thickness of the sensing layer of 3 mm (effective cell volume 210 nl) while problems due to the decreased resolving power were solved by using (when required) discrete spacing constituents (see below).

A block diagram of the detector is given in Fig. 2. In the design of the measuring subunit (ME in Fig. 2) we preferred a coincidence mode of the radioactivity measurement to minimize detector noise. This subunit is also provided with a ratemeter module and thus enables recording of an analogue signal from the detector by a line recorder. This possibility is convenient for a quick test of the detector in troubleshooting. The signal acquired by the computer system, however, is more convenient for the evaluation of the ITP analysis. The computer is coupled to a coincidence module of the measuring subunit provided with a circuit converting the registered counts into TTL pulses. The low capacity of the computer memory restricts the abilities of the system in real time processing of the acquired data. Therefore, during an experiment only the data acquisition is possible, while data handling has to be performed subsequently.

An algorithm describing the data acquisition is available elsewhere[10]. The minimum counting time (fixed by the hardware) was 1 s. Software, written in Assembly language, enables in post-analysis mode the following operations with the acquired data:

(1) graphical plotting of the data on the system display
(2) selection of the counting time in the interval 1–60 s
(3) selection of a start time for display of the data
(4) selection of a scale on the axis of the registered counts for a given time interval
(5) calculation of the sum of the registered counts for a chosen time interval in absolute or relative mode
(6) printing of a hardcopy of the display

Some performance characteristics of the detector

The counting efficiencies of the detection cells developed in this work were evaluated with [U-^{14}C]acetate. A commercially available preparation used for this purpose was purified in our laboratory by preparative ITP (see Experimental). This purification step was necessary in order to avoid systematic errors due to the presence of other ^{14}C-labelled constituent(s) in the preparation. ITP was performed in operational system 1 (Table I). The nett number of counts as registered on passage of the acetate zone through the detection cell (divided by the mean residence time of the labelled ions in the cell) was related to the nett number of counts obtained for the same amount of purified acetate and for the same time interval by liquid scintillation counting (LSC). When an 100% counting efficiency is assumed for the measurements by LSC the counting efficiencies for our detection cells were in the range 10–15%. Such values are considerable lower in comparison to those reported for ^{14}C-labelled compounds in packed cells designed for liquid chromatography (see, *e.g.*, refs. 17–19).

TABLE I

OPERATIONAL SYSTEMS

His = Histidine; MES = morpholinoethanesulphonic acid; Glu = glutamic acid; HEC = hydroxyethylcellulose; BALA = β-alanine; CAPR = caproic acid; Tris = tris(hydroxymethyl)aminomethane; Gly = glycine; HOAc = acetic acid.

Parameter	*System No.*			
	1	*2*	*3*	*4*
Solvent	Water	Water–methanol	Water	Water
Proportion	–	80:20	–	–
Leading ion	Cl^-	Cl^-	Cl^-	Cl^-
Concentration (m*M*)	10	10	10	10
Counter ion	His	BALA	Tris	MES
pH_L	6.0	3.85	8.0	6.1
Additive to the leading electrolyte	HEC	HEC	HEC	HEC
Concentration (%, w/v)	0.2	0.2	0.2	0.2
Terminating ion	MES (Glu)	CAPR	Gly	HOAc
Concentration (m*M*)	5	5	5	5

A less favourable ratio of the diameter of the capillary channel in the detection cell to the average range of ^{14}C β radiation in aqueous solutions (see above) is the main but probably not the only explanation for these differences (see, *e.g.*, ref. 20). On the other hand, packed detection cells have some serious disadvantages for use in ITP:

(i) packed cells having effective volumes of several tens of nl are difficult to manufacture,

(ii) less favourable surface/volume ratio, typical for the packed cells, can lead to problems due to adsorption phenomena[19],

(iii) particulate material is also less favourable when a suppression of the electroosmotic flow is desirable,

(iv) interactions of the separands with the particulate material may have undesirable influences on their effective mobilities during the detection,

(v) assembly of a packed cell into the ITP separation compartment increases its hydrodynamic resistance, thus making a rapid refilling of the compartment between experiments with viscous solutions of the leading electrolytes practically impossible.

These facts suggest that, despite its inherently lower counting efficiency for ^{14}C-radiolabelled constituents, our capillary type of detection cell has some favourable features from the point of view of ITP. In addition, a positive impact of the concentrating power of ITP on the precision of the radioactivity measurement (see below) makes it applicable also for typical trace analysis problems.

By using a general equation for the precision of the radioactivity measurement in flowing systems (see, *e.g.*, refs. 20 and 21), for our type of on-column detector in the ITP steady-state we obtained[10]

$$\delta_x = \frac{v_{iso}}{SOl_d\bar{c}_{x,x}l_x} + \frac{v_{iso}R_{c,o}(l_d + l_x)}{S^2O^2l_d^2\bar{c}_{x,x}^2l_x^2} + \frac{R_{c,o}(l_d + l_x)^2}{t_0S^2O^2l_d^2\bar{c}_{x,x}^2l_x^2} \quad (1)$$

where δ_x is the relative standard deviation of the measurement, v_{iso} is the steady-state migration velocity, $R_{c,o}$ is the counting rate for the background measurement (determined in the time interval t_0), l_d is the thickness of the scintillating layer in the detection cell in the direction along the capillary tube having the cross-section O, $\bar{c}_{x,x}$ is the concentration of the constituent X in its zone or in the interzonal boundary layer (when its amount is not sufficient to create its own zone) while l_x is the length of the zone X or the thickness of the interzonal boundary layer, respectively, and S is the sensitivity of the detection which includes both the decay constant of the radionuclide and the counting efficiency of the detector.

From eqn. 1 it is clear that the precision of the radioactivity measurement by the detector is related to the factors describing the ITP working conditions (v_{iso}, $\bar{c}_{x,x}$, l_x) as well as to those which characterize the detector and the radionuclide employed (l_d, S, O, $R_{c,o}$, t_0). Since the steady-state data in ITP can be calculated[22,23], eqn. 1 is useful to estimate their importance in the on-column radiometric detection. Thus, when the precision in the radioactivity measurement at the steady-state concentration of the analyte is compared to that corresponding to its concentration in the sample (under otherwise identical conditions), it is possible to quantify the rôle of the concentration adaptation of the analyte on the precision of the radioactivity measurement. The plots in Fig. 3, calculated for a concentration range of more than four decades, show that in some instances (low concentrations of the analytes in the samples) this adaptation

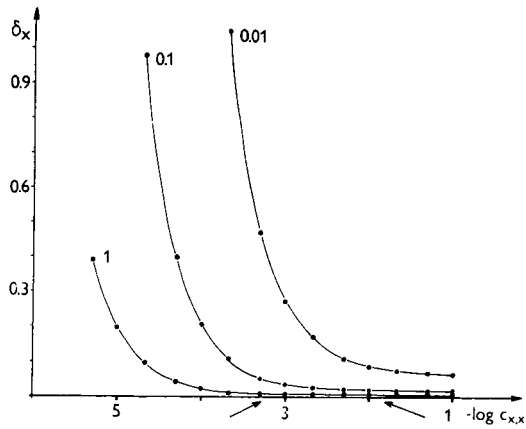

Fig. 3. Calculated dependence of the relative standard deviation of the radioactivity measurement (δ_x) on the concentration of the ^{14}C-labelled constituent present in the zone migrating isotachophoretically. Plots for relative abundances 0.01, 0.1 and 1 of the labelled form in the zone were obtained for the same injected amount of the constituent (21.2 nmol) migrating through the on-column detector at v_{iso} = 0.5 mm/s. The total concentration of the constituent was the variable and the length of its zone was calculated with respect to the constant injected amount. For the rest of the parameters the following values were used in the calculations (for the meaning of the symbols see the text); l_d = 3 mm; t_0 = 500 s; $R_{c,o}$ = 4.5 counts/s; O = 0.071 mm^2. A counting efficiency of 10% and a specific activity of 2.31 kBq/nmol (at 100% isotopic abundance) were used for the calculation of S. The arrows indicate the range of steady-state concentrations of the analytes in their zones under typical working conditions in ITP.

process is of key importance in the on-column radiometric detection in ITP. These plots also show that, in general, an high concentration of the leading ion is desirable when this detection is employed. This is true, especially, for analytes accompanied in the samples by their unlabelled analogues (dilution of the labelled form). However, the solubilities of the separands under the chosen ITP conditions as well as thermal effects determine the highest concentration of the leading ion in practical analysis.

The isotachopherograms in Fig. 4 were obtained from the on-column radiometric detector for [U-^{14}C]acetate at various concentrations of the leading anion. Since the rest of the parameters influencing the precision of the radiometric measurement (see eqn. 1) were kept constant, the practical importance of the concentrating power of the ITP separation process in the on-column detection is clearly illustrated. Here, the experiment corresponding to the isotachopherogram B can be taken as a reference since the volume of the acetate zone was similar to the injection volume, *i.e.*, neither dilution nor concentration occurred in this instance. On the other hand, in experiment A (Fig. 4), acetate was diluted during the separation to half of its sample concentration, while in C it was concentrated *ca.* 5 times. As expected from eqn. 1, lower precisions were typical for experiments with lower concentrations of the leading anion (longer zones of the analyte) for the same injected amount. However, a further increase in its concentration (D in Fig. 4) did not improve the precision as in C the acetate zone was shorter than the thickness of the sensing part of the detection cell.

An experimental estimation of the detection limit was carried out with the purified [U-^{14}C]acetate (see above) in system 1 (Table I). The measurements were

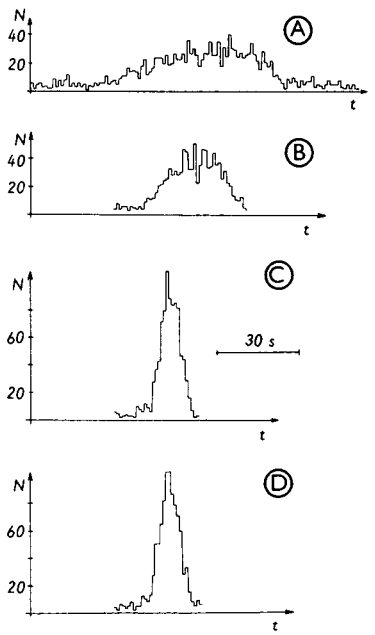

Fig. 4. Isotachopherograms from the analysis of [U-^{14}C]acetate at various steady-state concentrations. The compositions of the operational systems were as for system 1 (Table I) except that the concentrations of the leading anions were: 1 (A), 2 (B), 10 (C) and 20 m*M* (D). The driving currents during the detection were 2.5, 5.0, 25 and 50 μA for A, B, C and D, respectively. Volumes of 1 μl [U-^{14}C]acetate (purified as described in the text) were injected. *N*, *t* = increasing number of counts and time, respectively.

carried out with the detection cell having a thickness of 3 mm of the scintillating sensing layer. This cell was chosen for this work because from a theoretical treatment of the detection limit in the on-column radiometric detection[10] it is apparent that such a thickness of the sensing layer is an optimum when a compromise between a low detection limit and an high resolving power has to be achieved. The value of the signal-to-noise ratio of 2 (corresponding to $\delta_x = 0.5$) was taken as the detection limit and in our particular case it was *ca.* 7 pmol (16 Bq). This experimentally obtained value was in a reasonable agreement with the one predicted with the aid of eqn. 1 (9 pmol, 21 Bq).

The sensing part of the detection cell employed is *ca.* 30 times longer relative to a reasonable estimate of the thickness of the interzonal boundary layer[24]. This is an obvious disadvantage of the cell from the point of view of the overall resolving power of the detection. As already mentioned, the use of suitable spacing constituents can alleviate this disadvantage. With respect to an high selectivity of detection, the choice of suitable spacing constituents is less restrictive than, for example, in UV photometric detection.

From eqn. 1 it can easily be deduced that an high precision in the radioactivity measurement requires a low migration velocity. Such a requirement is associated with a decreased sharpness of the zone boundaries (see, *e.g.*, refs. 22 and 24) and, therefore, it is hardly acceptable for high resolution detectors. On the other hand, from previous

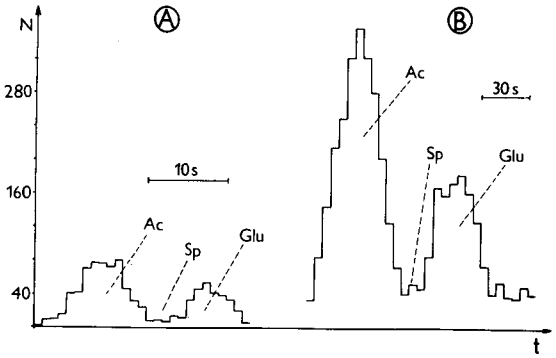

Fig. 5. Influence of the migration velocity on the number of registered counts. Volumes of 1 μl of the sample (prepared by mixing commercially obtained preparations of [U-^{14}C]acetate (Ac) and [U-^{14}C]glutamate (Glu) in the ratio 1:1) were injected in both A and B together with 1.5 nmol of β-bromopropionate (Sp). The driving currents during the separations were identical except during the detection they were 50 (A) and 10 μA (B).

discussion it is apparent that for on-column radiometric detection this is to a certain extent a reasonable way to increase the precision in the radioactivity measurement. This possibility is illustrated by the isotachopherograms given in Fig. 5. In these experiments the same amounts of a sample containing [U-^{14}C]acetate, [U-^{14}C]-glutamate and β-bromopropionate (spacing constituent) were separated under identical working conditions, except that the driving currents during the detection were 50 μA in A and 10 μA in B. To illustrate the difference in the registered counts the isotachopherograms were plotted at "chart speeds" having the same ratio as the driving currents during the detection.

ITP analysis of ^{14}C-labelled nucleotides

At present, the application of radiolabelled compounds is widespread, especially in various branches of bioscience. Of these compounds the ones labelled with ^{14}C are mostly used. Therefore, in spite of the fact that the detector described above is suitable also for the detection of other β emitters, in this work we paid attention to its use in the analysis of ionogenic compounds carrying this label.

^{14}C-labelled nucleotides represent an important group of compounds employed in biochemical and biological research. For obvious reasons, purity control of the preparatives employed for these purposes is essential, especially when impurities or naturally occurring compounds disturb the reaction(s) under investigation. The isotachopherograms given in Fig. 6 were obtained from the analysis of commercially available cytidine 5'-triphosphate (CTP) labelled with ^{14}C (ref. 25). A freshly delivered preparation (37 MBq/ml) was used in this instance. The actual content of the labelled CTP was 91.2% as determined by high-performance liquid chromatography (HPLC) in the laboratory of the supplier. From the ITP analysis it was apparent that besides CDP and CMP (cytidine 5'-di- and monophosphates, respectively) it contained also other ^{14}C-labelled impurities of which the one marked with u (Fig. 6) represented 13.8% of the registered counts. When we assumed that only the labelled constituents migrating between the leading and terminating anions were present in the sample, the

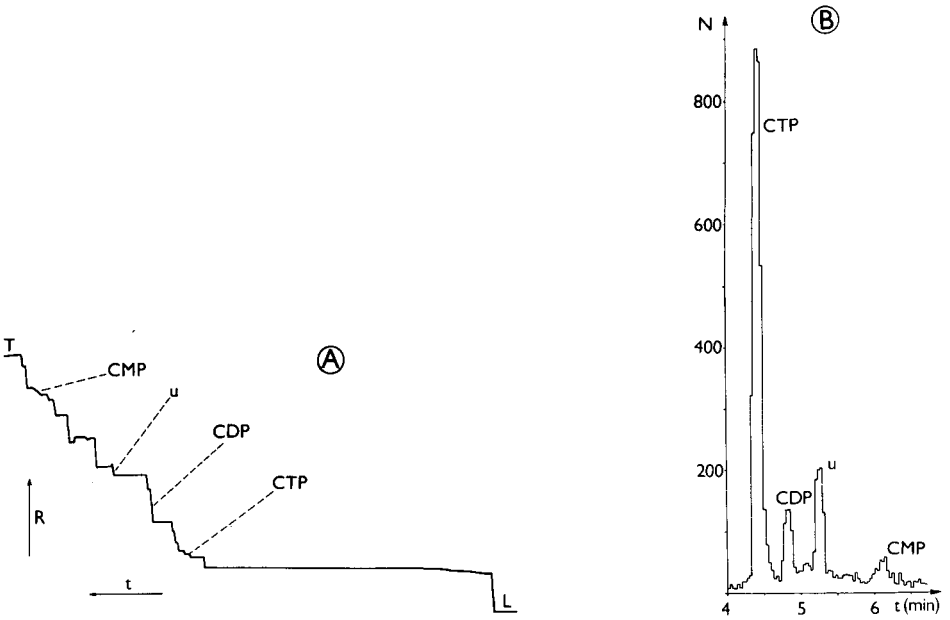

Fig. 6. Isotachopherograms from the analysis of [U-^{14}C]CTP. The separation was carried out in system 2 (Table I) and 1 μl of CTP was injected together with a mixture of spacing constituents, a (Table II). Records from the conductivity (A) and radiometric (B) detectors were registered at 45 μA. The driving current in the preseparation column was 200 μA. N, R, t = increasing number of counts, resistance and time, respectively.

actual content of CTP (expressed via relative distribution of the registered counts) was 63.9%. This value indicates a large discrepancy between ITP and HPLC. The difference was large also when CDP and CMP present in the sample were ascribed to the decomposition of CTP since its production (78.3% of the registered counts). A reasonable agreement between HPLC (91.2%) and ITP (92.0%) was obtained only when the constituent was considered as originating from CTP, *e.g.*, via a radiolytic degradation or as unresolved from it by HPLC.

In the analysis of ^{14}C-labelled CDP stored for a longer time (immediately after the expiration time), several labelled constituents were detected under similar conditions to those employed in the analysis of CTP (see Fig. 7). Of these only CDP and CMP were identified by spiking the sample with the unlabelled nucleotides. To save the preparative for further experimental work, we employed preparative ITP to isolate the labelled CDP. The isolation was carried out in the operational system 2 (Table I) by using the column-coupling configuration of the instrument adapted for the preparative work (see Experimental). An isotachopherogram from the radiometric detector shown in Fig. 7B was obtained in the analytical control of the preparative experiment. In this instance a small aliquot of the isolated fraction was taken for the analysis. This experiment performed with a delay of 20 h after the isolation also shows a degree of hydrolytic conversion of CDP kept in the trapped solution (pH $\approx$ 4.0). Nevertheless, these experiments clearly indicate an high purification efficiency of the preparative ITP in this instance. We feel that this approach to the purification of

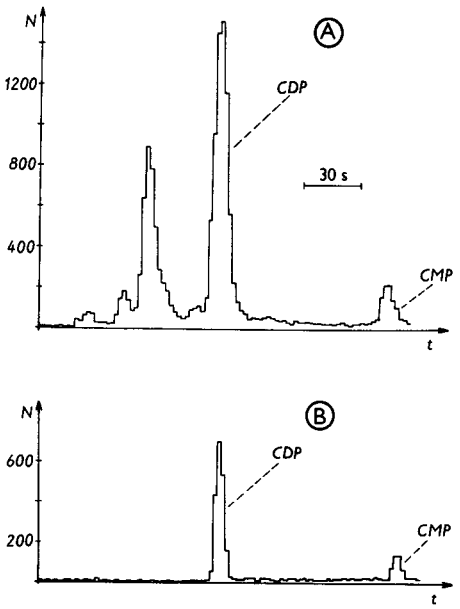

Fig. 7. Purification of [U-^{14}C]CDP by preparative capillary ITP. The working conditions were as in Fig. 6. In A, 5 μl of the CDP preparative were injected and in B the injection volume was 2 μl of the same preparation purified as described in the text.

radiolabelled ionogenic compounds is of general applicability, especially for less stable compounds currently employed in biological and biochemical research. Its advantages are obvious: (i) pure and well defined material can be prepared immediately before the experiment; (ii) the capillary type of separation unit enables purification in a reasonable time (*ca.* 25 min in our instance); (iii) in some instances, hundreds of μg of target compounds can be obtained in one experiment; (iv) with the exception of the columns, the same instrumentation can be used for both the preparative and analytical experiments.

ITP profiling of biotransformation products of ^{14}C-labelled cytostasane

Analysis of radiolabelled transformation products is a current task, *e.g.*, pharmacological evaluation of drugs. Since the biotransformation products are often ionogenic in nature, ITP is a method of choice in this research area. In this work we briefly investigated its capabilities in the analysis of samples obtained from a biotransformation study of ^{14}C-labelled cytostasane. Previous work with this drug in which HPLC was employed to monitor the course of biotransformation did not give satisfactory results in spite of the fact that at least one product was detected[26]. Since no more preliminary data were available we performed cationic and anionic ITP profiling of the labelled products present in the incubation mixture.

ITP profiles as obtained by the radiometric detector in the operational systems 3 and 4 (Table I) are given in Fig. 8. The cationic profiles were obtained in a system in which the effective mobility of H^+ is very low (for an estimation see ref. 27). Only

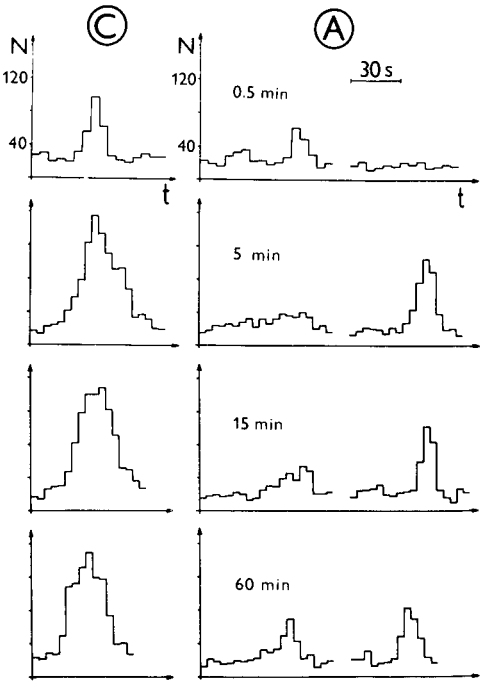

Fig. 8. Cationic (C) and anionic (A) ITP profiles of radiolabelled biotransformation products of ^{14}C-labelled Cytostasane. The ^{14}C-labelled drug was incubated with hepatocytes ($4 \cdot 10^6$ cells/ml) in Krebs-Henseleit buffer solution at pH 7.4 (the hepatocytes were obtained by a collagenase perfusion of rat liver). Volumes of 1 ml of the incubation mixtures taken at 0.5, 5, 15 and 60 min were centrifued (3000 rpm) and the supernatants were stored at −25°C until the ITP measurements. Volumes of 10 μl of the supernatants were taken for ITP. The driving current during the detection in the cationic profiling was 20 μA and in the anionic profiling was 40 μA. The zone of the carbonate spacing the radiolabelled constituents in the anionic profiling (*ca.* 120 s) was omitted from the isotachopherograms. For other details see the text.

under such extreme conditions could we achieve the cationic migration of the labelled constituent(s). From the response of the detector, the presence of only one constituent (migrating with an effective mobility similar to that of H^+) is visible. This, however, cannot be accepted as conclusive since the number of radiolabelled cationically migrating constituents must be determined in experiments in which the degree of chemical homogeneity of this zone is investigated, *e.g.*, the use of suitable spacing constituents, preparative experiments followed by analysis under various working conditions, etc.

The anionic profiles were evaluated in the operational systems 1–3 (Table I). Radiolabelled constituents migrated only at $pH_L = 8.0$ (system 3). Under these conditions two zones were detected by the radiometric detector (Fig. 8). The sum of the registered counts for these zones for a given incubation time was very close to half of the registered counts in the corresponding cationic profiles. At the same time, the migration velocity in the cationic system was approximately half of the value in the anionic system. When we consider the influence of the migration velocity on the number of registered counts (see Fig. 5 and accompanying explanation), it is seen that

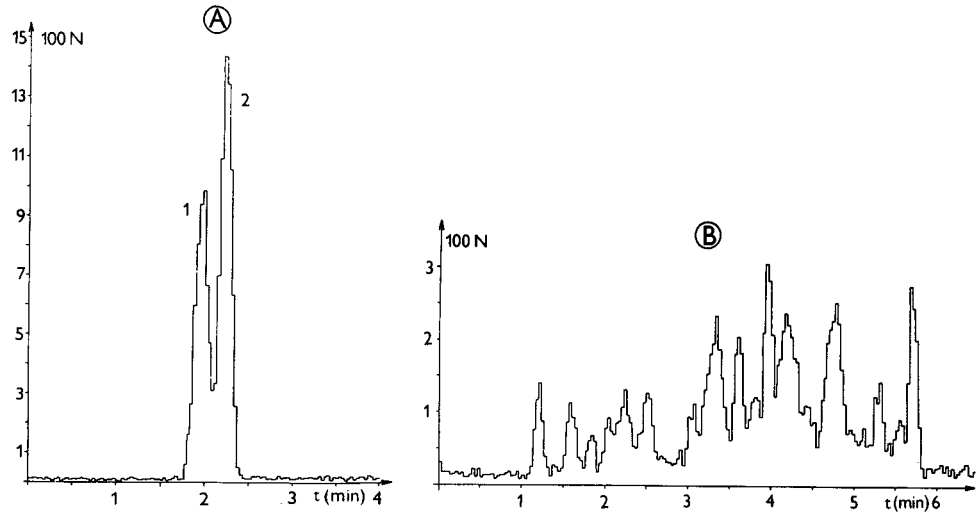

Fig. 9. Isotachopherograms from the analyses of an [U-^{14}C]protein hydrolysate. Volumes of 50 μl of the sample isolated as described in the text were injected without (A) and with (B) the spacing constituents, b (Table II). These volumes corresponded to 2.5 μl of the original sample having a specific activity of 40 MBq/ml. The driving currents were 250 and 50 μA in the preseparation and analytical columns, respectively.

the same amounts of the radiolabelled analytes were extracted in both profiling systems. This result suggests that in the cationic system there are two unresolved radiolabelled constituents formed by the biotransformation process. In addition, from their migration behaviours we can deduce that they have typical zwitterionic properties.

These preliminary experiments imply that ITP with the on-column radiometric detector may be a very useful analytical tool in biotransformation studies, *e.g.*, in combination with other separation and identification methods.

Detection of ^{14}C-labelled constituents present in a protein hydrolysate

ITP is a method suitable for the analysis of complex mixtures of ionogenic compounds. In this respect the column-coupling configuration of the separation unit[11,12] has many practical advantages. To illustrate these possibilities in the analysis of complex mixtures of radioactive or radiolabelled ionogenic constituents we carried out experiments with an [U-^{14}C]protein hydrolysate.

In the direct analysis of the hydrolysate (ref. 25, p. 33) we observed a trailing zone along the terminator (operational system 1). As this zone might be misinterpreted as a memory effect of the detection cell, we employed in these experiments a fraction trapped by preparative ITP (see Experimental). This fraction included the constituents migrating in the mobility interval determined by the leading and terminating ions of the operational system 1 (Table I).

In the analysis of the fraction two zones were resolved by the radiometric detector (Fig. 9A). To confirm their purities the fraction was analyzed under identical conditions with a mixture of spacers (b, Table II). An isotachopherogram obtained

TABLE II

COMPOSITIONS OF THE MIXTURES OF SPACING CONSTITUENTS

Mixture	*Constituents*[a]
a	Formate, trichloroacetate, lactate, succinate, N-acetylleucine, glutarate, glutamate, monomethyl succinate, acetate, monoethyl succinate, mono *n*-propyl succinate, propionate, butyrate, monomethyl adipate
b	Tartronate, malonate, citrate, succinate, glutarate, adipate, N-acetylglutamate, glycolate, acetate, dichloroacetate, trichloroacetate, β-bromopropionate, butyrate, aspartate, valerate, N-hydroxyethyliminodiacetate, glutamate, enantate, glucuronate, α-aminoadipate, α-aminopimelate, pantothenate

[a] The orders of the constituents agree with their migration orders at pH_L = 3.85 (a) and 6.0 (b).

from such an analysis (Fig. 9B) clearly shows that this fraction of the protein hydrolysate which should ideally contain only amino acids migrating anionically at pH 6.0 with effective mobilities higher than that of MES (aspartic and glutamic) was a complex mixture of radiolabelled constituents. Some of these constituents migrated between the spacers and some of them were spread along their zones. Reasons for the presence of such a number of radiolabelled constituents in the analyzed fraction were not investigated in this work. However, it can be explained via autoradiolytic and biochemical processes as well as via the presence of some peptidic fragments. Nevertheless, the isotachopherograms from the analysis of this sample clearly indicate that the on-column radiometric detector in conjunction with the column-coupling configuration of the separation unit is a promising analytical alternative also for complex mixtures of radiolabelled ionogenic compounds.

CONCLUSIONS

From this work it is clear that the described on-column radiometric detector is a very convenient solution to the detection of ^{14}C-labelled constituents under typical ITP working conditions. Its inherently lower counting efficiency for this radionuclide (in comparison to the packed detection cells used in liquid chromatography) is at least compensated by the concentrating power of the ITP separation process. In the detection of ^{14}C we can expect a further improvement of the counting efficiency by decreasing the diameter of the capillary channel in the detection cell. With the exception of ^{3}H (undetectable), however, the detector provides considerable higher counting efficiencies for other currently employed β radiation emitting nuclides (^{32}P, ^{35}S, ^{99m}Tc, etc.).

Problems associated with the lower resolving power of the detector (when compared to current high resolution detectors in ITP) can be solved via the use of spacing constituents. However, in this approach the resolution of some constituents with very close physico-chemical properties can be tedious. In this respect, a further improvement of the counting efficiency of the detection in the suggested way will automatically provide a possibility to increase the resolution of the detection via a decrease in the thickness of the sensing part of the detection cell without sacrificing the precision in the radioactivity measurement.

In this work we found preparative ITP to be a very suitable method for purification of radiolabelled chemicals. It is obvious that its use can be extended to isolations of the radiolabelled constituents from reaction mixtures, *e.g.*, in experiments aimed at the identification of radiolabelled products.

REFERENCES

1 L. Arlinger, *J. Chromatogr.*, 119 (1976) 9.
2 L. Arlinger, in Z. Deyl (Editor), *Electrophoresis, A Survey of Techniques and Applications*, Part A, Elsevier, Amsterdam, Oxford, New York, 1979, p. 373.
3 *LKB Application Note 300*, LKB, Bromma, 1977.
4 L. Arlinger, in B. J. Radola and D. Graesslin (Editors), *Electrofocusing and Isotachophoresis*, W. de Gruyter, Berlin, New York, 1977, p. 505.
5 G. Eriksson, *Thesis*, University of Lund, Lund, 1983.
6 G. Eriksson and U. Stenram, in C. J. Holloway (Editor), *Analytical and Preparative Isotachophoresis*, W. de Gruyter, Berlin, New York, 1984, p. 135.
7 G. Eriksson, A. Malström, B. Särnstrand, G. Jonsson and R. Pero, in C. J. Holloway (Editor), *Analytical and Preparative Isotachophoresis*, W. de Gruyter, Berlin, New York, 1984, p. 153.
8 D. Kaniansky, P. Rajec, A. Švec, P. Havaši and F. Macášek, *J. Chromatogr.*, 258 (1983) 238.
9 D. Kaniansky, P. Rajec, P. Havaši, A. Švec and F. Macášek, *J. Radioanal. Nucl. Chem., Lett.*, 104 (1986) 157.
10 D. Kaniansky, P. Rajec, A. Švec, J. Marák, M. Koval, M. Lúčka, Š. Franko and G. Sabanoš, *J. Radioanal. Nucl. Chem., Articles*, 129 (1989) 305.
11 F. M. Everaerts, Th. P. E. M. Verheggen and F. E. P. Mikkers, *J. Chromatogr.*, 169 (1979) 21.
12 D. Kaniansky, *Thesis*, Komenský University, Bratislava, 1981.
13 D. Kaniansky, V. Zelenská and I. Zelenský, *J. Chromatogr.*, 256 (1983) 126.
14 D. Kaniansky, V. Madajová, M. Hutta and I. Žilková, *J. Chromatogr.*, 286 (1984) 395.
15 D. D. Perrin, W. L. F. Armarego and D. R. Perrin, *Purification of Laboratory Chemicals*, Pergamon, Oxford, 2nd ed., 1980.
16 K. Diem and C. Lentner (Editors), *Wissenschaftliche Tabellen*, CIBA, Basle, 7th ed., 1968, p. 286.
17 L. N. Mackey, P. A. Rodriguez and F. P. Schroeder, *J. Chromatogr.*, 208 (1981) 1.
18 *HPLC Radioactivity Monitor LB 506*, LB 042-1-1185-2000, Laboratorium Prof. Dr. Berthold, Wildbad, 1987.
19 *The Radioactivity Monitor for Sophisticated HPLC*, 1208-965-04, LKB Wallac, Turku, 1986.
20 P. Markl, in J. F. K. Huber (Editor), *Instrumentation for High-Performance Liquid Chromatography*, Elsevier, Amsterdam, Oxford, New York, 1978, p. 151.
21 G. B. Sieswerda, H. Poppe and J. F. K. Huber, *Anal. Chim. Acta*, 78 (1975) 343.
22 F. M. Everaerts, J. L. Beckers and Th. P. E. M. Verheggen, *Isotachophoresis: Theory, Instrumentation and Applications*, Elsevier, Amsterdam, Oxford, New York, 1976.
23 T. Hirokawa, M. Nishino, N. Aoki, Y. Kiso, Y. Sawamoto, T. Yagi and J. I. Akiyama, *J. Chromatogr.*, 271 (1983) D1.
24 J. C. Reijenga, Th. P. E. M. Verheggen and F. M. Everaerts, *J. Chromatogr.*, 328 (1985) 353.
25 *Labelled Compounds*, Institute for Research, Production and Application of Radioisotopes, Prague, 1986.
26 V. Ščasnár, Institute of Pharmacology, Biomedical Centre of Slovak Academy of Science, Bratislava, personal communication.
27 P. Boček, P. Gebauer and M. Deml, *J. Chromatogr.*, 217 (1981) 209.

Journal of Chromatography, 470 (1989) 155–169
Elsevier Science Publishers B.V., Amsterdam — Printed in The Netherlands

CHROM. 21 268

PHOTOMETRIC DETECTION OF METAL CATIONS IN CAPILLARY ISOTACHOPHORESIS BASED ON COMPLEX EQUILIBRIA[a]

I. ZELENSKÝ

Department of Analytical Chemistry, Faculty of Science, Komenský University, Mlynská Dolina CH-2, CS 842 15 Bratislava (Czechosovakia)

D. KANIANSKY* and P. HAVAŠI

Institute of Chemistry, Faculty of Science, Komenský Univerity, Mlynská Dolina CH-2, CS 842 15 Bratislava (Czechoslovakia)

and

Th. P. E. M. VERHEGGEN and F. M. EVERAERTS

Laboratory of Instrumental Analysis, Eindhoven University of Technology, P.O. Box 513, 5600 MB Eindhoven (The Netherlands)

SUMMARY

The possibilities of photometric detection of metal cations based on the formation of kinetically labile, light-absorbing complexes (chelates) during isotachophoretic (ITP) separation were studied. Xylenol orange was used as a chelating co-counter ionic constituent in the cationic mode of ITP. The metal cations formed, under the working conditions employed, light-absorbing chelates with this chelating agent and could be detected with high selectivity at 580 nm when their cationic migration was preserved.

Bleeding of the analyte zones caused by xylenol orange and probably also by chelating impurities present in its precursors were the most serious sources of systematic errors, especially at the parts per 10^9 concentration level. At such concentrations, adsorption of the metal cations in the separation compartment also appeared important. Means of minimizing these losses of the analytes were studied. Under optimized ITP working conditions Mn^{2+} and Cd^{2+} had detection limits of *ca.* 10^{-8} mol/l for a 30-μl sample volume. These values represent almost a three orders of magnitude improvement relative to current high-resolution universal detectors. Consequently, the metals could be reliably determined at concentrations lower than $5 \cdot 10^{-8}$ mol/l.

INTRODUCTION

Complex equilibria are currently employed to optimize selectively the separation conditions in the analysis of metal cations by capillary isotachophoresis (ITP). Various

[a] This paper is dedicated to the memory of Professor Samo Stankoviansky on the occasion of his 80th birthday.

0021-9673/89/$03.50

complexing agents, mostly in the cationic mode of analysis, have been studied in this respect and a key role of these equilibria in the ITP analysis of some important groups of metals is apparent (see, *e.g.*, refs. 1–18). However, the overall selectivity of the analysis may be low as universal, conductivity and potential gradient detectors are almost exclusively used. Indirect photometric detection has been proposed for these analytes[19,20] but has similar disadvantages. In addition, these detection alternatives may not be sensitive enough when trace determinations are required. In spite of the fact that these disadvantages can be reduced by using a suitable sample preparation procedure before the ITP analysis[9,17], developments aimed at improving the detection capability of ITP for metals are desirable.

In the determination of metals, their conversion into visible light-absorbing complexes (usually chelates) is the basis of the physico-chemical principles of various titration[21–24] and spectrophotometric[24–27] methods. Many of the chelating agents used for these purposes are ionic and their complexes with the metal cations are kinetically labile. In this work we performed an introductory study devoted to the use of these reactions in the photometric detection of metal cations in ITP. The detection approach is based on the following idea.

A chelating agent migrating anionically in the cationic mode of ITP and partially forming kinetically labile, light-absorbing chelates with the metal cations of analytical interest is added to the leading electrolyte. The working conditions (pH of the leading electrolyte and the concentration of the chelating agent) are chosen in such a way that the cationic migration of the analytes is preserved. In the choice of the chelating agent it is also important that the light absorption spectra of its free ionic forms prevailing under the ITP working conditions differ sufficiently from those of the metal chelates. Then, on-column photometric detection carried out at a wavelength from that part of the absorption spectra of the chelates where the light absorption by the free chelating agent is negligible provides the desired analytical information. Thus, the metal ions are detected via their light-absorbing chelates formed during the migration. It is apparent that in this instance the detection signal is proportional to the concentration of the metal ions present in the chelates and hence this is a direct mode of photometric detection.

Some of the chelating agents suitable for this detection aproach are probably also applicable for work in the anionic mode (see *e.g.*, refs. 14–18). Altough in this way we could expect a higher sensitivity of detection (complete conversion of the metal cations into chelates), small differences in the effective mobilities of the chelates and/or their decomposition (bleeding) during the separation[15,16] can considerably restrict its practical utility.

In this paper we present the results of feasibility study in which xylenol orange was used for the photometric detection of some metals (Mn^{2+}, Cd^{2+}, Zn^{2+} and Pb^{2+}) in the cationic mode of the ITP.

EXPERIMENTAL

Instrumentation

A CS Isotachophoretic Analyzer (VVZ PJT, Spišská Nová Ves, Czechoslovakia) was used in the column-coupling configuration of the separation unit. The analytical column of the analyser was provided with a laboratory-made on-column photometric

detector. The detection cell was placed *ca.* 2 cm upstream of the conductivity sensor. An LQ 1411 light-emitting diode (Tesla, Rožnov, Czechoslovakia) was employed as the monochromatic light source of the detector as its emission maximum at 580 nm agreed well with the light absorption maxima of the metal chelates. A KPX 81 phototransistor (Tesla) served as the photosensing element of the detector[28].

A Specord UV–VIS spectrophotometer (Carl Zeiss, Jena, G.D.R.) was used in the measurement of the absorption spectra of the chelating agents and the corresponding chelates in the preliminary choice of the agents for the ITP experiments.

Chemicals

The chemicals used for the preparation of the leading and terminating electrolytes were obtained from Serva (Heidelberg, F.R.G.), Sigma (St. Louis, MO, U.S.A.) and Lachema (Brno, Czechoslovakia). Some were purified by conventional methods. Hydroxyethylcellulose 4000 (Serva), after purification on an Amberlite MB-1 mixed-bed ion exchanger (BDH, Poole, U.K.), was used as an additive to the leading electrolyte.

3,3′-Bis[N,N-di(carboxymethyl)aminomethyl]-*o*-cresolsulphonphthalein (xylenol orange), 3,3′-bis[N-(carboxymethyl)aminomethyl]thymolsulphonphthalein (glycine thymol blue), 5,5′-nitrilodibarbituric acid (murexide) and 2-hydroxy-1-(1-hydroxynaphthyl-2-azo)-6-nitronaphthalene-4-sulphonic acid (Eriochrome Black T) were obtained in indicator-grade purities from Lachema and Merck (Darmstadt, F.R.G.). Their Na^+ and NH_4^+ salts were converted before the use into the free acids on a column packed with Dowex 50W-X8 (H^+) cation exchanger (Serva). Of these chelating agents only xylenol orange was stored as a 10^{-2} mol/l stock solution.

Stock solutions of metal cations (10^{-2} mol/l) were prepared from their analytical-reagent grade salts obtained from Lachema and Merck.

Water delivered by a Rodem-1 two-stage demineralization unit (OPP, Tišnov, Czechoslovakia) was further purified by circulation through laboratory-made polytetrafluoroethylene (PTFE) cartridges packed with a mixed-bed ion exchanger (Amberlite MB-1; BDH). The solutions were prepared from freshly recirculated water.

Sample and solution handling

To avoid problems due to contamination of the solutions with heavy metals and/or to minimize the losses of the analytes, the following precautions were taken: (i) The solutions (leading and terminating electrolytes, sample solutions containing the metal cations at concentrations of 10^{-4} mol/l and less) were stored in polyethylene or quartz vessels cleaned as recommended in the literature (see, *e.g.*, refs. 29 and 30). (ii) In the work on the concentration level of the analytes at 10^{-5} mol/l and less, only the samples prepared immediatey before a series of the experiments were used. (iii) The samples were transferred into the injection valve of the analyser with polyethylene disposable syringes. The syringes were cleaned before use by storing them for several days in 1 mol/l nitric acid. They were washed with demineralized water immediately before use. (iv) Those parts of the injection valve of the analyser which came into contact with the solutions were made of PTFE. In addition, we employed a terminating compartment made of PTFE and any contact of the terminating electrolyte solution present in this compartment with the laboratory environment was avoided.

RESULTS AND DISCUSSION

Choice of the chelating agent

As is clear from the previous description of the detection principle, the choice of the chelating agent had to follow requirements important for both the separation of metal cations and their detection. Obviously, general requirements concerning the constituents used for the preparation of the leading electrolyte solutions in ITP also had to be considered[1]. In summary, the chelating agent suitable for our detection purposes should fulfil the following criteria: kinetic lability of the complexes formed during the migration; desired separating effect or no disturbances to the separation when other constituent(s) is (are) responsible for the resolution of the separands; its use must not introduce a systematic bias into the quantitation due to zone bleeding[15,31,32]; different light absorption spectra of the chelate and the free chelating agent; high molar absorptivities of the metal chelates at the detection wavelength; chemical stability; and availability in a sufficient degree of purity.

As our experiments were intended to study the detection of metals we did not evaluate in detail the separating capabilities of the chelating agents used in the investigation. Obviously, their influence on the ITP separations of metal cations cannot be neglected (also at low concentrations of the agents) when the corresponding values of the stability constants are taken into consideration (refs. 21, 33 and references cited therein).

Among the group of chelating agents potentially applicable for our detection purposes, we preferred metallochromic indicators as their complexes are usually kinetically labile[21,22]. Our preliminary choice was based on measurements of the absorption spectra in a wide pH range. In this way we obtained relevant data for the indicators, *i.e.*, their pH working range and optimum detection wavelength for ITP. The chemical purities of the indicators used in further investigations were evaluated via their ITP anionic profiles. In general, the profiles showed low chemical purities of the available preparations (see, *e.g.*, Fig. 1). The use of simple purification procedures as recommended[21] did not lead to improvements in this respect. Therefore, we had to take into account that mixtures of chelating agents (probably with different chelating properties) rather than individual agents were employed in our experiments.

The low chemical stabilities of some indicators (murexide, Eriochrome Black T) further restricted our choice. This undesirable property of the indicators led us to evaluate regularly the actual content of the chelating agent(s) present in the leading electrolyte. Ba^{2+} served for this purpose and the amplitude of the signal of the photometric detector for its zone was taken as a measure of the concentration of the indicator present in the leading electrolyte.

Of the metallochromic indicators studied we chose xylenol orange for a detailed investigation because, with the exception of its lower chemical purity, it best met the remainder of the above criteria. Its light absorption maximum was at 445 nm (under experimental conditions close to those employed in ITP) whereas the maxima for the metal chelates ranged from 570 to 580 nm. In addition, at the detection wavelength (580 nm) the contribution of the free chelating agent to the light absorption was negligible.

The composition of the leading electrolyte is given in Table I. Here, both the concentration of xylenol orange and pH_L were chosen to illustrate the analytical possibilities of the detection method and problems encountered in its use.

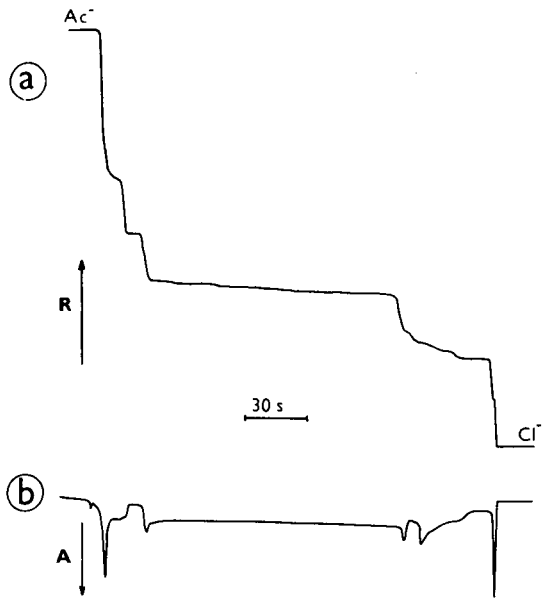

Fig. 1. Anionic profile of xylenol orange at $pH_L = 3.5$. 10 m*M* HCl buffered to $pH_L = 3.5$ with β-alanine was used as the leading electrolyte [HEC at 0.1% (w/v) concentration served as the additive]. 5 m*M* acetic acid was used as the terminating electrolyte. A 30-μl volume of the leading electrolyte solution used for the separation of metals (Table I) containing 1.5 m*M* xylenol orange was injected. The isotachopherograms from (a) conductivity and (b) photometric detectors were recorded at a 45-μA driving current. *R*, *A* = increasing resistance and light absorption at 580 nm, respectively.

TABLE I
OPERATIONAL SYSTEM

Parameter	*Electrolyte*	
	Leading	*Terminating*
Solvent	H_2O	H_2O
Cation	NH_4^+	H^+
Concentration (m*M*)	20	1
Counter ion	OAc^- [a]	NO_3^-
Co-counter ion	XO[a]	–
Concentration (m*M*)	0.4	–
pH	5.0	*ca.* 3.0
Additive	HEC[a]	–
Concentration (%, w/v)	0.1	–

[a] OAc = Acetate; XO = xylenol orange; HEC = hydroxyethylcellulose.

Migration behaviour of the metal cations and their photometric detection with xylenol orange

The isotachopherograms in Fig. 2 were obtained from the analysis of a model mixture containing Mn^{2+}, Zn^{2+}, Cd^{2+} and Pb^{2+} at 10^{-4} mol/l concentrations. It can be seen that for the cations that form light-absorbing chelates with xylenol orange the expected responses were obtained. It is also apparent that their migration order followed the stabilities of the chelates ($Mn^{2+} < Cd^{2+} < Zn^{2+} < Pb^{2+}$). Pb^{2+} formed to a great extent $PbHL^{3-}$ species (HL represents the singly protonated ionic form of the chelating agent) with xylenol orange at pH values close to our pH_L (ref. 27, p. 292) and was retarded into the terminating zone. As the decomposition of the Pb chelate in this zone was not sufficient to achieve a higher effective mobility of Pb relative to that of the H^+ ion (owing to a lower pH and a lower steady-state concentration of the free chelating agent), the Pb injected was completey lost during the separation. Such behaviour of the metal cations must be considered when the complex equilibria are involved in the ITP separation[31,32]. In this particular instance we investigated the possibility of eliminating these losses of Pb by the use of a competitive metal cation. Cu^{2+} was tested for this purpose, with positive results. Unfortunately, the concentration of Cu^{2+} that had to be added to the sample was critical. A concentration of Cu^{2+} below a very narrow optimum concentration range only partly prevented the

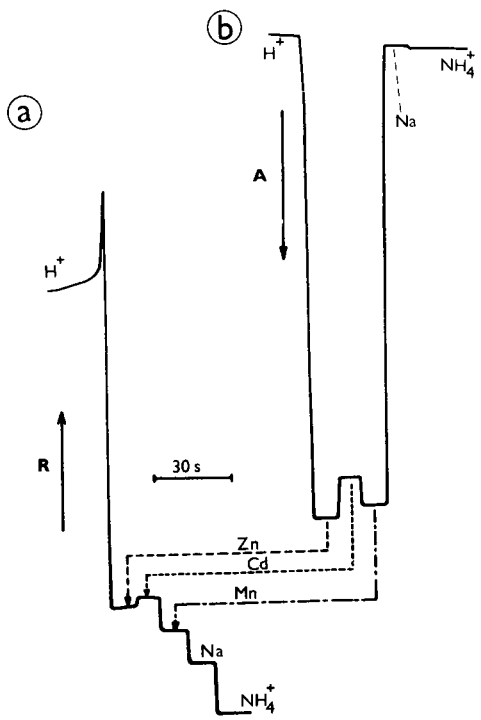

Fig. 2. ITP separation of Mn^{2+}, Cd^{2+} Zn^{2+} and Pb^{2+} with xylenol orange used as a chelating co-counter ion. A 30-μl volume of the injected sample contained the metal cations at 10^{-4} mol/l concentrations. The isotachopherograms from (a) conductivity and (b) photometric detectors were recorded at a 100-μA driving current. Composition of the operational system as in Table I and symbols as in Fig. 1.

losses of Pb. On the other hand, at a higher Cu^{2+} concentration the detection of Pb^{2+} was disturbed by a strongly light-absorbing copper chelate. As such a solution was impractical for use in the detection of very low concentrations of the metals it was not studied further.

Organic bases, cationically migrating amino acids, tetraalkylammonium cations and alkali metal cations were considered as spacing constituents. Here, unexpected migration behaviours of the metal cations were observed. The isotachopherogram in Fig. 3 serves as an illustration of this behaviour. It can be seen that Tris (having a lower effective mobility than Zn and Cd) not only spaces the Mn zone but also acts as a carrier for the injected Zn and Cd. Moreover, these metal constituents, spread along the rear part of the Tris zone, were mutually separated by a sharp boundary. The corresponding response from the conductivity detector also indicates that part of the Tris zone occupied by the metals and suggests a higher resistance. However, when the measuring electrodes were cleaned electrochemically[1] this enhanced response disappeared. Hence it can be ascribed to a higher sensitivity of the coated measuring electrodes to the multiple charged ions[1,34]. Further, the observed migration behaviours of Zn and Cd can again be explained in terms of the bleeding of the zones of metals into the Tris zone. At the same time, competition of the metal ions for the ligand explains their resolution in this zone. These results also suggest that in the ITP analysis

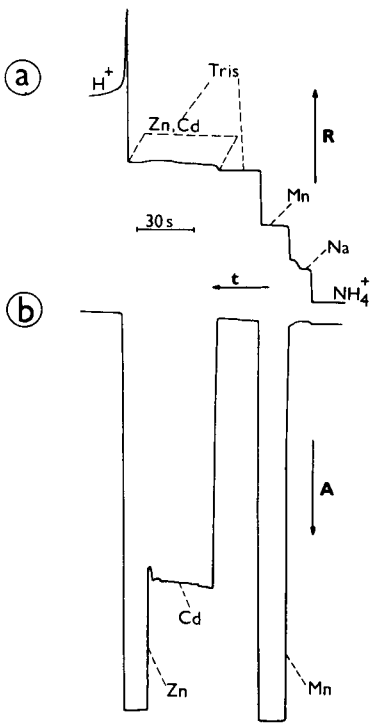

Fig. 3. Carrying and spacing effects of Tris in the separation of metal cations. A 30-μl volume of the injected sample contained Tris ($5 \cdot 10^{-4}$ mol/l), Mn^{2+} (10^{-4} mol/l), Cd^{2+} (10^{-4} mol/l), Pb^{2+} (10^{-4} mol/l) and Zn^{2+} ($5 \cdot 10^{-5}$ mol/l). ITP working conditions and symbols as in Fig. 2. The length of the Tris zone increased by *ca.* 5% in comparison with the run without metal cations.

of metals present in samples containing non-complexing cationically migrating constituents the choice of the complexing agent must consider this behaviour of the metal ions also in instances when their bleeding into the terminating zone does not occur[31,32].

We further investigated in detail the migration behaviours of Cd and Zn in multi-component mixtures of non-complexing cations. In these experiments the concentrations of Zn^{2+} and Cd^{2+} in the samples were varied while the concentrations of the non-complexing cations were kept constant. Isotachopherograms from such experiments for Zn are shown in Fig. 4. The isotachopherograms show that Zn was retarded by xylenol orange into the rear part of the BALA zone (the chelate was decomposed at the front of the terminating zone) when its concentration in the sample was 10^{-5} mol/l (Fig. 4b). At a 5-fold higher concentration Zn was spread along the zones of BALA and EACA and along the rear part of the Tris zone (Fig. 4c) whereas at a $1.5 \cdot 10^{-4}$ mol/l concentration it was present along all of these zones and also, partially, in its own zone characterized by the same effective mobility as in Fig. 2. These isotachopherograms suggest that in each of the zones of non-complexing constituents the degree of complexation of Zn^{2+} was different and decreased stepwise in the direction of the terminating zone. This is an expected agreement with a decrease in the pH of the zones and with a decrease in the concentration of the chelating co-counter ion. It is also apparent that each of the zones of non-complexing constituents (migrating behind the zone of the metal) had, therefore, a certain carrying capacity for Zn under given working conditions. This carrying capacity will be zero for the zone in which the chelate is decomposed to such an extent that the effective mobility of the

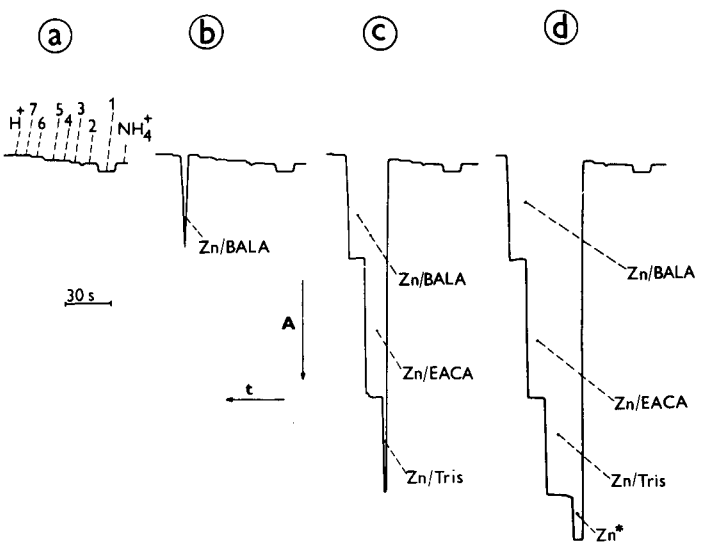

Fig. 4. Migration behaviour of Zn present in a multi-component mixture of non-complexing cationic constituents. A blank solution (No. I; Table II) (see the isotachopherogram) (a) was spiked with Zn at (b) 10^{-5} mol/l, (c) $5 \cdot 10^{-5}$ mol/l and (d) $15 \cdot 10^{-5}$ mol/l concentrations. 1 = Ba^{2+}; 2 = Na^{+}; 3 = TMA^{+}; 4 = Li^{+}; 5 = Tris; 6 = EACA; 7 = BALA. Zn/BALA, Zn/EACA, Zn/Tris and Zn* indicate Zn present in the zones of BALA, EACA, Tris and in its own zone, respectively. The isotachopherograms were recorded at a 100-μA driving current. Composition of the operational system as in Table I and symbols as in Fig. 1.

metal is higher than that of the constituent forming this zone. The terminating constituent acts in this way for Zn. On the other hand, when the areas of the signals obtained for different concentrations of Zn are compared, some loss of this cation is clear. Bleeding of Zn into the terminating zone is a possible explanation. The losses of the metal were much lower than for Pb. They could be detected only with difficulty with the aid of the photometric detector because Zn^{2+} was present as an impurity in

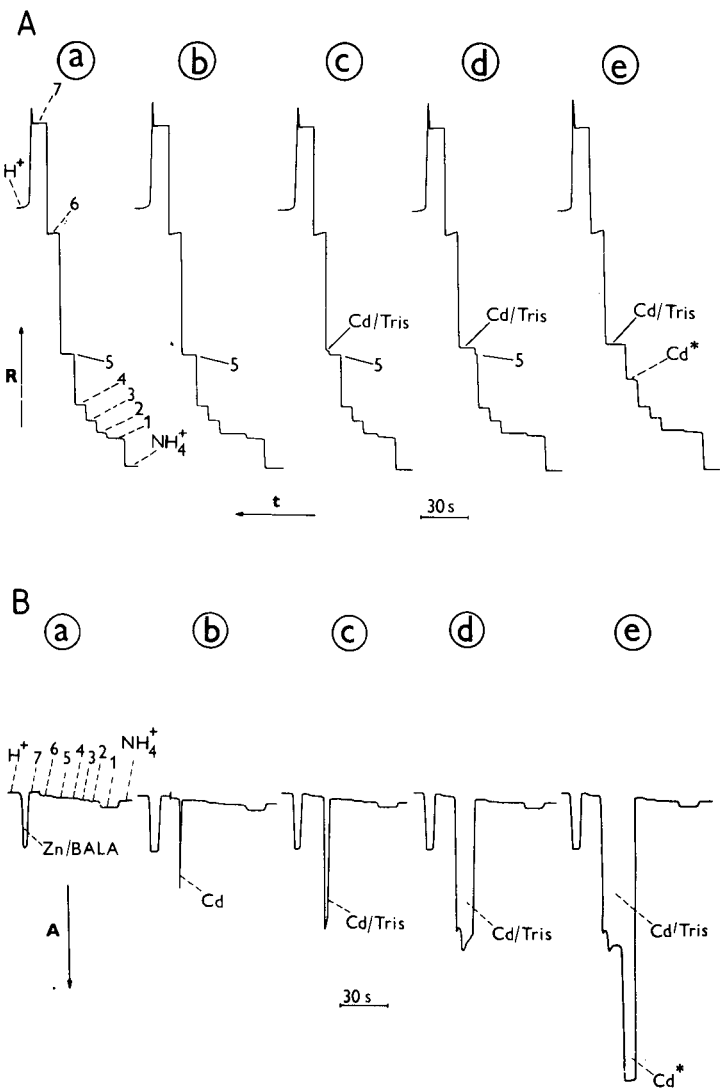

Fig. 5. Migration behaviour of Cd present in a multi-component mixture of non-complexing cationic constituents. The composition of the blank solution (a) was the same as in Fig. 4 except Zn^{2+} was added at $2.5 \cdot 10^{-6}$ mol/l concentration. Cd^{2+} was present in the injected samples at 10^{-6}, $5 \cdot 10^{-6}$, $2 \cdot 10^{-5}$ and $8 \cdot 10^{-5}$ mol/in runs b, c, d and e, respectively. Isotachopherograms from (A) photometric and (B) conductivity detectors. Other details as in Fig. 4.

the chemicals used for the preparation of the leading electrolytes. Consequently, the losses of the injected Zn^{2+} could not be distinguished from the fluctuations of the signal due to the varying amount of the impurity present in the separation compartment.

Cd^{2+} forms with xylenol orange a chelate with a lower stability constant than those of Pb^{2+} and Zn^{2+}. Therefore, its decomposition was detected at the front of the EACA zone (Fig. 5). It can be seen that either BALA or EACA can be used to space the migrating positions of Zn and Cd. In terms of the previous discussion, this is due to the fact that both amino acids act as carriers for Zn and the fronts of their zones decompose the Cd chelate.

When our detection approach was employed for the concentrations of metals below 10^{-6} mol/l their losses were typical. The isotachopherograms in Fig. 6 show such a situation. At this concentration level of the analytes we found that Ba^{2+} and Li^{+} had a positive effect in eliminating these losses. In this respect comparisons of the isotachopherograms b, d and e in Fig. 6 are illustrative. The cations were originally added to the samples as a spacer (Li^{+}) and as an internal standard (Ba^{2+}) for the evaluation of the concentration of the chelating agent. Nevertheless, these results suggest that bleeding of the analytes may not be the only cause of their losses. In spite of the fact that in this particular instance there is no experimentally based evidence, it seems appropriate to expect that adsorption phenomena in the separation compartment can also be important at such sample concentrations. Then, competition of Ba^{2+} and, partially, also Li^{+} with the analytes for the adsorption sites can provide an explanation of the positive effects of these cations.

When the isotachopherograms in Fig. 6b and c are compared it can be seen that an increase in the concentration of Zn^{2+} in the sample (the Zn stock solution was

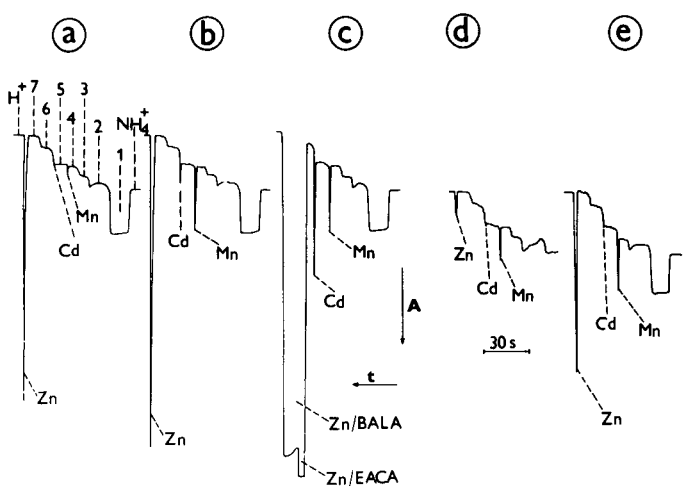

Fig. 6. Influence of Ba^{2+} and Li^{+} on the detectability of Mn^{2+} and Cd^{2+} at low ppb concentrations. The isotachopherograms from the photometric detector were obtained for 30-μl volumes of samples of the following compositions: (a) blank solution No. I (Table II); (b) same as (a) but with Cd^{2+}, Mn^{2+} and Zn^{2+} added at $2 \cdot 10^{-7}$ mol/l; (c) same as (b) but the concentration of Zn was $8 \cdot 10^{-6}$ mol/l; (d) and (e) sample compositions as in (b) but the blank solution without Ba^{2+} and Li^{+}, respectively, were used. Other details as in Fig. 4.

proved to be free of Cd) led to a higher signal for a $2 \cdot 10^{-7}$ mol/l concentration of Cd^{2+}. This result implies that in the run shown in Fig. 6b part of the Cd was present along the EACA zone (and to a smaller extent also in the BALA zone) and/or adsorbed in the separation compartment. Then, on increasing the concentration of Zn^{2+} in the sample (Fig. 6c) it was displaced into its migration position. This displacement effect of Zn can be ascribed either to its preferential trapping on the adsorption sites or to its higher complexing ability, leading (via competition with Cd^{2+} for the ligand) to a higher effective mobility of Cd in the zones of non-complexing constituents.

From the previous discussion it is apparent that at the concentrations of the metal cations detectable by the conductivity detector, the bleeding of their zones [either to the terminating zone or to the zone(s) of non-complexing cation(s)] is potentially the most serious source of the analytical errors. At parts per 10^9 (ppb) concentrations the losses cannot be explained only in this way. Adsorption of the metal cations in the separation compartment (hardly detectable by the conductivity detector) could provide a reasonable explanation in our particular case. However, uncertainty concerning the chelating properties of the impurities present in the precursors of xylenol orange used in these experiments (see Fig. 1) means that such an interpretation must be also treated with caution. This discussion implies that a further study with xylenol orange of a higher purity could be helpful in clarifying these results.

Detection limits and quantitative analysis

The above results clearly show that our approach to the photometric detection of metal cations provides considerably lower detection limits than current alternatives. However, to exploit its potential in trace ITP analysis it is necessary to minimize system errors due to the losses of the analytes during the ITP separation. In spite of the fact that origin of these losses is not yet exactly known, the experiments performed at concentrations of the analytes below 10^{-6} mol/l suggest that one way to solve this problem is to add suitable cationic constituents, such as Ba^{2+}, to the sample and to compensate for the losses of the analytes associated with the use of non-complexing spacing (carrying) constituents by adding the corresponding amounts of the metal cations to the sample.

In determining the detection limits for Mn^{2+} and Cd^{2+} we followed this solution, obtaining the values from fluctuations of the heights of the Mn and Cd peaks in the blank runs (for the composition of the blank sample, see the legend to Fig. 7 and Table II). The fluctuations expressed via the standard deviations of the peak heights corresponding to *ca.* $5 \cdot 10^{-9}$ mol/l of these cations. For a signal-to-noise ratio of 2 this gives detection limits of *ca.* 10^{-8} mol/l under the experimental conditions (30-μl sample volume, operational system as described in Table I and detection at 580 nm). For both metals this is an improvement of approximately three orders of magnitude compared with the detection limits given by a conductivity detector. The isotachopherograms at $2.5 \cdot 10^{-8}$ and $5 \cdot 10^{-8}$ mol/l Cd^{2+} and Mn^{2+} (Fig. 7b and c, respectively) illustrate their detectabilities at concentrations close to the detection limits. At this concentration level the relative standard deviations of the peak heights were in the range 10–35% (higher values being obtained for the lower concentrations).

For Zn^{2+} the detection limit was lower than those for Mn^{2+} and Cd^{2+}. However, problems caused by relatively high concentrations of this cation in the chemicals used for the preparation of the leading electrolyte solutions (also after their purification) made this value unreliable.

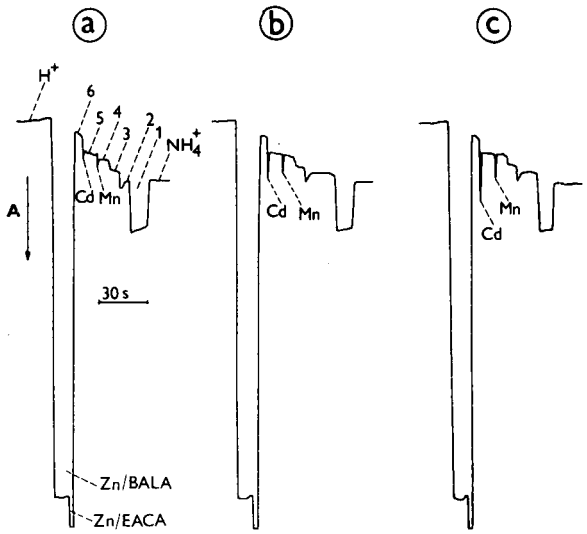

Fig. 7. Isotachopherograms from the analyses of Mn^{2+} and Cd^{2+} at concentrations close to the detection limits. (a) Obtained with blank solution No. II (Table II) and serves as a reference; (b) blank solution was spiked with $2.5 \cdot 10^{-8}$ mol/l of Mn^{2+} (1.4 ppb) and Cd^{2+} (2.8 ppb); (c) as (b) but with double the amounts spiked.

TABLE II
COMPOSITIONS OF THE BLANK SOLUTIONS

Component[a]	*Blank solution*[b]		
	I	*II*	*III*
Ba^{2+}	10^{-4}	10^{-4}	–
Na^{+}	10^{-4}	10^{-4}	$2 \cdot 10^{-4}$
TMA^{+}	10^{-4}	10^{-4}	–
Li^{+}	10^{-4}	10^{-4}	$2 \cdot 10^{-4}$
Tris	10^{-4}	10^{-4}	$2 \cdot 10^{-4}$
EACA	10^{-4}	10^{-4}	–
BALA	10^{-4}	10^{-4}	$2 \cdot 10^{-3}$
Mg^{2+}	–	–	$2 \cdot 10^{-4}$
Ca^{2+}	–	–	$2 \cdot 10^{-4}$
Mn^{2+}	–	$2 \cdot 10^{-8}$	$4 \cdot 10^{-8}$
Cd^{2+}	–	$7 \cdot 10^{-8}$	$3 \cdot 10^{-7}$
Zn^{2+}	–	$8 \cdot 10^{-6}$	$13 \cdot 10^{-7}$
HNO_3	$5 \cdot 10^{-4}$	$5 \cdot 10^{-4}$	10^{-3}

[a] TMA^{+} = Tetramethylammonium; Tris = tris(hydroxymethyl)aminomethane; EACA = ε-aminocaproic acid; BALA = β-alanine.

[b] Constituent concentrations are given in mol/l.

The calibration lines for Mn^{2+} and Cd^{2+} were evaluated from their peak heights in the concentration range $5 \cdot 10^{-8}$–$50 \cdot 10^{-8}$ mol/l (see Table III). It must be stressed that the slopes of the calibration lines obtained in this way depended on the spacing (carrying) constituents employed. This is obvious when it is considered that the quantified metal cations migrated in the interzonal boundaries. Here, both the pH at which the chelates were formed and the steady-state concentrations of the chelating agent, and hence the degree of chelate formation, were partially determined by the spacing constituent used.

From the migration behaviours of the metal cations (Figs. 4 and 5) it can be seen that determinations based on the peak height (peak area) measurement are *a priori* restricted to a certain concentration range of the analyte for a given composition of the leading electrolyte. An increase in the concentration of the chelating agent in the leading electrolyte solution is effective in increasing this range only to a limited extent as the effective mobility of the metal is also influenced in this way. Hence an undesirable change in its migration position can result when the concentration of the chelating agent is higher than a certain critical value. Therefore, once a leading electrolyte of an optimum composition is employed at a certain concentration of the analyte, only the area corresponding to the signal from the photometric detector on the isotachopherogram provides analytical information relevant to the quantitation (the analyte is spread along the zone of the front spacing constituent). We found that in this instance also the length of the zone of the spacer occupied by the metal as detected by the photometric and/or the conductivity detectors (see Fig. 3) is proportional to the concentration of the analyte. Obviously, here it is desirable that the analyte is preferably present only in one spacing (carrying) zone. A detailed investigation of these alternatives in the quantitation is in progress.

Practical applicability of the proposed detection method

The photometric detection of metal cations is intended mainly for their ITP trace analysis. In this respect, we carried out preliminary experiments with tap water samples. The isotachopherograms in Fig. 8 were obtained in these experiments. Here, the sample was mixed with the blank solution before the analysis. The roles of the cations present in this solution were explained in the previous discussion. In this particular instance we used Mg^{2+} and Ca^{2+} instead of Ba^{2+} to avoid analytical disturbances due to the precipitation of sulphate.

TABLE III

REGRESSION EQUATIONS AND CORRELATION COEFFICIENTS FOR Mn^{2+} AND Cd^{2+} IN THE $5 \cdot 10^{-8}$–$50 \cdot 10^{-8}$ mol/l CONCENTRATION RANGE

The metal cations were injected in 30-μl sample volumes and they were present in blank solution No. II (Table II).

Cation	*Regression equation*[a]	*Correlation coefficient*	*Number of data points*
Mn^{2+}	$y_H = 4.66 + 1.64 \cdot 10^8 x$	0.9961	34
Cd^{2+}	$y_H = 4.39 + 1.47 \cdot 10^8 x$	0.9950	34

[a] y_H = peak height (mm); x = concentration (mol/l).

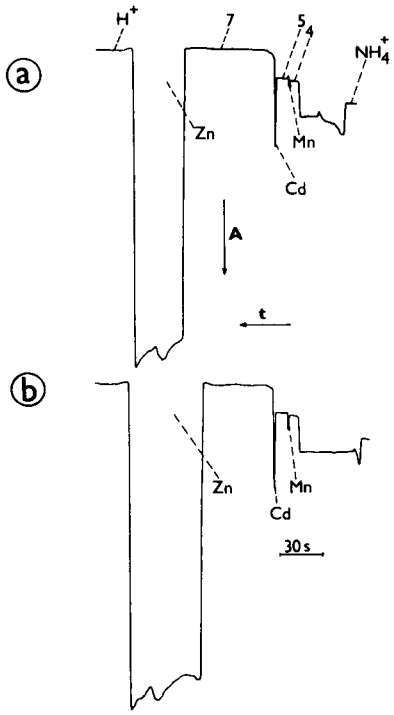

Fig. 8. Detection of Mn^{2+}, Cd^{2+} and Zn^{2+} in a tap water sample. (b) A 30-μl volume of the sample mixed with blank solution No. III (Table II) was injected; a) the same volume of the blank solution mixed (1:1) with demineralized water was injected. Other details and symbols as in Fig. 4.

When the isotachopherogram from the photometric detector obtained for tap water (Fig. 8b) is compared with that from the blank run (Fig. 8a), it is clear that the sample contained Zn^{2+}, Mn^{2+} and Cd^{2+} at detectable concentrations. By adding Zn^{2+} to the sample of tap water and to the corresponding blank solution we confirmed experimentally that the difference between the peaks of Cd^{2+} was due to the presence of this metal in the sample and it could not be ascribed to the displacement effect of Zn (see Fig. 6 and the accompanying discussion). These results also show that the loss of Cd^{2+} along the BALA zone was negligible under our experimental conditions (compare the isotachopherograms in Fig. 6b and c).

Although our results for the analyses of the tap water samples were reproducible and, in comparison with the above model experiments, no other disturbing phenomena (*e.g.*, due to the sample matrix) were observed, further experimental work is essential before this promising detection method can be considered for routine use. In this respect, at least comparative studies with analytical methods currently used in the trace analysis of metals are required in order to evaluate its accuracy.

CONCLUSIONS

This work has shown that the photometric detection of metal cations via their kinetically labile, light-absorbing chelates formed during the migration is

a promising detection alternative for the trace determination of this important group of analytes. To exploit its potential fully in the analysis of practical samples, it is necessary to investigate a wider range of chelating agents.

However, problems inherent in the ITP separation itself as studied here for xylenol orange will require further investigation. In this respect, the availability of chelating agents of considerably higher purities relative to those produced, *e.g.*, for complexometric titrations seems very important for a better understanding of the problems associated with losses of the analytes at low ppb concentrations.

REFERENCES

1 F. M. Everaerts, J. L. Beckers and Th. P. E. M. Vereggen, *Isotachophoresis—Theory, Instrumentatiom and Applications*, Elsevier, Amsterdam, Oxford, New York, 1976.
2 Y. Kiso and T. Hirokawa, *Chem. Lett.*, (1980) 745.
3 I. Nukatsuka, M. Taga and H. Yoshida, *J. Chromatogr.*, 205 (1981) 95.
4 I. Nukatsuka, M. Taga and H. Yoshida, *Bull. Chem. Soc. Jpn.*, 54 (1981) 2629.
5 T. Hirokawa, T. Matsuki, H. Takemi and Y. Kiso, *J. Chromatogr.*, 280 (1983) 233.
6 H. Yoshida and Y. Hirama, *J. Chromatogr.*, 298 (1984) 243.
7 I. Matejovič and J. Polonský, *J. Chromatogr.*, 390 (1987) 155.
8 I. Valášková, I. Zelenský, V. Zelenská, A. Komarnicki and D. Kaniansky, *Collect. Czech. Chem. Commun.*, 53 (1988) 515.
9 F. M. Everaerts, Th. P. E. M. Verheggen, J. C. Reijenga, G. V. A. Aben, P. Gebauer and P. Boček, *J. Chromatogr.*, 320 (1985) 263.
10 J. Vacík and I. Muselasová, *J. Chromatogr.*, 320 (1985) 199.
11 M. Tazaki, M. Takagi and K. Ueno, *Chem. Lett.*, (1982) 639.
12 F. Stover, *J. Chromatogr.*, 298 (1984) 203.
13 A. A. G. Lemmens, F. M. Everaerts, J. W. Venema and H. D. Jonker, *J. Chromatogr.*, 439 (1988) 423.
14 H. Yoshida, I. Nukatsuka and S. Hikine, *Bunseki Kagaku*, 28 (1979) 382.
15 P. Gebauer, P. Boček, M. Deml and J. Janák, *J. Chromatogr.*, 199 (1980) 81.
16 K. Fukushi and K. Hiiro, *Anal. Sci.*, 1 (1985) 345.
17 Y. Hirama and H. Yoshida, *Nippon Kagaku Kaishi*, (1986) 943.
18 I. Zelenský, E. Šimuničová, V. Zelenská, D. Kaniansky, P. Havaši and P. Chaláni, *J. Chromatogr.*, 325 (1985) 161.
19 L. Arlinger and H. Lundin, *Protides Biol. Fluids, Proc. Colloq.*, 21 (1973) 667.
20 *LKB Application Note*, No. 107, LKB, Bromma, 1974.
21 R. Přibil, *Komplexometrie*, SNTL, Prague, 1977.
22 R. Přibil, *Applied Complexometry*, Pergamon Press, Oxford, 1982.
23 B. Buděšinský, in H. A. Flaschka and A. J. Barnard, Jr. (Editors), *Chelates in Analytical Chemistry*, Vol. 1, Marcel Dekker, New York, 1967, p. 15.
24 E. Bishop (Editor), *Indicators*, Pergamon Press, Oxford, 1972.
25 J. Fries and H. Getroot, *Organic Reagents for Trace Analysis*, E. Merck, Darmstadt, 1977.
26 Z. Marczenko, *Separation and Spectrophotometric Determination of Elements*, Ellis Horwood, Chichester, 2nd ed., 1986.
27 Z. Holzbecher, L. Diviš, M. Král, L. Šucha and F. Vláčil, *Organická Činidla v Anorganické Analýze*, SNTL, Prague, 1975.
28 P. Havaši and D. Kaniansky, *J. Chromatogr.*, 325 (1985) 137.
29 R. Sturgeon and S. S. Berman, *CRC Crit. Rev. Anal. Chem.*, 18 (1987) 209.
30 A. Mizuike, *Enrichment Techniques for Inorganic Trace Analysis*, Springer, Berlin, Heidelberg, New York, 1983.
31 P. Gebauer and P. Boček, *Folia Fac. Sci. Nat. Univ. Purkynianae Brun., Chem.*, 20 (1985) 37.
32 P. Gebauer and P. Boček, *J. Chromatogr.*, 242 (1982) 245.
33 S. Kotrlý and L. Šucha, *Handbook of Chemical Equilibria in Analytical Chemistry*, Wiley, Chichester, 1985.
34 F. M. Everaerts and P. J. Rommers, *J. Chromatogr.*, 91 (1974) 809.

Journal of Chromatography, 470 (1989) 171–183
Elsevier Science Publishers B.V., Amsterdam — Printed in The Netherlands

CHROM. 21 220

COMPLEMENTARY INFORMATION FROM ISOTACHOPHORESIS AND HIGH-PERFORMANCE LIQUID CHROMATOGRAPHY IN PEPTIDE ANALYSIS

P. S. L. JANSSEN*, J. W. VAN NISPEN, M. J. M. VAN ZEELAND and P. A. T. A. MELGERS
AKZO Pharma Division, Organon International B.V., Analytical and Bio-Organic Chemistry R&D Laboratories, P.O. Box 20, 5340 BH Oss (The Netherlands)

SUMMARY

Reversed-phase high-performance liquid chromatography is a valuable analytical technique to support the synthesis, isolation and purification of peptides, as is illustrated by some critical separations. In addition to this technique, capillary isotachophoresis can give useful information on the purity determination of peptides and on the presence of ionic compounds of a non-peptidic nature. With regard to the latter aspect, isotachophoresis proved to be a suitable technique as a check on the effective removal of salts after preparative high-performance liquid chromatography.

INTRODUCTION

Adequate analytical support for complicated multi-step synthetic, isolation and purification procedures is of utmost importance in current peptide chemistry. Moreover, the end-product, *i.e.*, the purified peptide preparation, should meet high quality requirements. A wide range of analytical techniques are now available to support peptide synthesis. Among these, reversed-phase high-performance liquid chromatography (RP-HPLC), mainly performed on alkyl-bonded silica supports, has found wide application[1]. In addition, capillary isotachophoresis (ITP) has also been successfully applied to the analysis of peptide preparations[2–11].

This paper describes applications of both ITP and HPLC and the complementary nature of the information obtained is demonstrated.

EXPERIMENTAL

HPLC

All experiments were performed on an HP 1090 M liquid chromatograph (Hewlett-Packard, Palo Alto, CA, U.S.A.) provided with a ternary solvent delivery system, an auto-injector and autosampler and a diode-array detector. The apparatus was equipped with a computer workstation and printer/plotter facilities.

As supporting material a reversed-phase octadecylsilica (Supelcosil LC-18DB, 3-μm particles) column (150 × 4.6 mm I.D.) (Supelco, Bellefonte, PA, U.S.A.) was

0021-9673/89/$03.50

used. A guard column (20 × 4.6 mm I.D.) filled with the same material preceded the analytical column.

Details of the chromatographic conditions applied in the various separations are given in Table I. Prior to use the mobile phases were filtered and degassed with helium. Peptide samples were dissolved in the initial mobile phase and 100 μl of this solution, corresponding to 10–20 μg of peptide material, were injected. Detection was at 210 nm. The retention times (RT) and the peak areas (%) were recorded.

Uvasol-quality acetonitrile (Merck) and ultra-pure Milli-Q water (Millipore, Bedford, MA, U.S.A.) were used. Type HA filters (0.45 μm, Millipore) were used for the filtration of the aqueous mobile phases and Type FM filters (0.5 μm) for those containing acetonitrile.

ITP

All experiments were performed with a home-made apparatus constructed according to Everaerts *et al.*[12]. The polytetrafluoroethylene separation capillary was 320 mm long × 0.2 mm I.D. Resistance detection and UV detection (254 nm) were applied. A constant electric driving current was obtained from a Wallis (Worthing, U.K.) VCS 303/1 power supply (0–30 kV; 0–100 μA). Isotachopherograms were recorded using a Model BD 9-725 dual-channel recorder (Kipp & Zonen, Delft, The Netherlands).

Details of the isotachophoretic procedure were described previously[11]. For the electrolyte systems applied, see Table II.

Peptide characteristics

Human, porcine and bovine insulin were obtained from Diosynth (Oss, The Netherlands). All other peptide preparations were synthesized by the peptide chemistry group of Organon (Oss, The Netherlands); several of them had purposely

TABLE I

CHROMATOGRAPHIC CONDITIONS

All separations were performed at a flow-rate of 1.0 ml/min and a temperature of 45°C.

System	*Mobile phase*	*Elution profile*			
		Time (min)	*A (%)*	*B (%)*	*C (%)*
1	(A) 0.5 *M* NaH_2PO_4 + 0.05 *M* SOS[a] and H_3PO_4 to pH 2.1	0	30	30	40
	(B) Water	3	30	30	40
	(C) Acetonitrile–water (60:40)	10	30	25	45
		20	30	25	40
2	(A) 0.5 *M* Na_2SO_4 + 0.3 *M* NaH_2PO_4 and $HClO_4$ to pH 2.5	0	20	30	50
	(B) Water	3	20	30	50
	(C) Acetonitrile–water (60:40)	30	20	22.5	57.5
3	(A) 0.5 *M* NaH_2PO_4 and H_3PO_4 to pH 2.1	0	20	70	10
	(B) Water	3	20	70	10
	(C) Acetonitrile–water (60:40)	40	20	40	40

[a] Sodium octanesulfonate.

TABLE II

ELECTROLYTE SYSTEMS

System	*Analytes*	*Leading electrolyte*[a]			*Terminating electrolyte*[a]
		Leading ion	*Counter ion*	*pH*	
1	Neutral and basic peptides	Na^+	Acetate	4.50	β-Alanine–CH_3COOH to pH 5.00
2[b]	Acidic peptides/anions	Cl^-	Histidine	5.60	MES[c]–Tris to pH 5.60
3	Halides	NO_3^-	Cadmium	5.60	Tartaric acid–NaOH to pH 5.60
4	Cations	K^+	Acetate	4.80	β-Alanine–CH_3COOH to pH 4.80
5	Ammonium	H^+	Chloride	2.00	Sodium citrate–HCl to pH 7.50

[a] Concentrations 0.01 mol/l, except for cadmium nitrate (0.004 mol/l).
[b] Additive to the leading electrolyte: 0.2% hydroxypropylmethylcellulose.
[c] Morpholinoethanesulphonic acid.

not been purified before use. For the primary structures of the peptides, see Table III.

Insulin. Insulin is the well known polypeptide hormone concerned with the regulation of the carbohydrate metabolism. It contains 51 amino acid residues arranged in two covalently linked chains (A and B). Minor differences in primary structure are found between the bovine, porcine and human insulins. At room temperature and especially in acid solution insulin undergoes deamidation, principally at the A-21 asparagine residue, which is converted into the corresponding aspartic acid residue. For a reliable and rapid discrimination between the three insulins a clear mutual separation is necessary between six closely related polypeptides, *viz.*, bovine, porcine and human insulin and their respective monodesamido (MDA) derivatives.

ACTH. The adrenocorticotropic hormone ACTH contains 39 amino acid residues and has as its principal activity the stimulation of the adrenal cortex to produce and release steroid hormones. The N-terminal part ACTH-(1–24) possesses full biological activity. Fragments of ACTH-(1–24) and their analogues have been the subject of many biological and pharmacological investigations.

Org 2766. Structure–activity studies of peptides derived from ACTH with regard to avoidance behaviour in rats resulted in the development of the modified ACTH fragment Org 2766. During the synthesis of this peptide in solution the histidine residue can racemize, *i.e.*, L-histidine may be partially converted into D-histidine. A rapid and accurate determination of possible racemization is essential in this aspect. For further quality control, racemization studies of the other amino acid residues are also important.

β-Endorphin. β-Endorphin, the C-terminal 31-peptide of β-lipotropin, was originally isolated from pituitaries of several species. It was shown to have a high affinity for opiate-binding sites in the brain and to induce many behavioural effects.

In order to support metabolism studies of the candidate antipsychotic drug β-endorphin-(6–17) (Org 5878), we aimed at the separation of the parent compound and its possible metabolites. Especially the separation of β-endorphin-(6–17) from the -(7–17), -(8–17) and -(9–17) fragments was essential in this respect.

Vasopressin. The pituitary nonapeptide 8-arginine vasopressin (AVP) is long known for its influence on blood pressure and diuresis. Later it was found that AVP is also involved in behavioural processes. It has been shown that the complete

TABLE III

PEPTIDE SEQUENCES

Peptide	*Sequence*
Insulin (porcine)	H-Gly-Ile-Val-Glu-Gln-Cys-Cys-Thr-Ser-Ile-Cys-Ser-Leu-Tyr-Gln-Leu-Glu-Asn-Tyr-Cys-Asn-OH (A-chain) H-Phe-Val-Asn-Gln-His-Leu-Cys-Gly-Ser-His-Leu-Val-Glu-Ala-Leu-Tyr-Leu-Val-Cys-Gly-Glu-Arg-Gly-Phe-Phe-Tyr-Thr-Pro-Lys-Ala-OH (B-chain)
ACTH-(1–24)	H-Ser-Tyr-Ser-Met-Glu-His-Phe-Arg-Trp-Gly-Lys-Pro-Val-Gly-Lys-Lys-Arg-Arg-Pro-Val-Lys-Val-Tyr-Pro-OH
β-Endorphin (human)	H-Tyr-Gly-Gly-Phe-Met-Thr-Ser-Glu-Lys-Ser-Gln-Thr-Pro-Leu-Val-Thr-Leu-Phe-Lys-Asn-Ala-Ile-Ile-Lys-Asn-Ala-Tyr-Lys-Lys-Gly-Glu-OH
AVP	H-Cys-Tyr-Phe-Gln-Asn-Cys-Pro-Arg-Gly-NH_2
CCK-8S	H-Asp-Tyr(SO_3H)-Met-Gly-Trp-Met-Asp-Phe-NH_2
Org 2766	H-Met(O_2)-Glu-His-Phe-D-Lys-Phe-OH

Species	A-8	A-10	B-30
Bovine	Ala	Val	Ala
Porcine	Thr	Ile	Ala
Human	Thr	Ile	Thr

nonapeptide structure is essential for full endocrine activity while the central activity of the 9-desglycinamide fragment [AVP-(1–8) or DGAVP] remains nearly intact.

CCK. Cholecystokinin (CCK) was originally isolated from the gastrointestinal tract and found to be involved in digestive functions and feeding behaviour. Later, high concentrations, especially of a sulphated octapeptide sequence (CCK-8S), were demonstrated to be present in several brain regions.

RESULTS AND DISCUSSION

HPLC

Over a 10-year period we have performed many critical RP-HPLC peptide separations[13–15]. Some recent characteristic examples are given here.

β-Endorphin-(6–17) family. The application of ion-pair HPLC proved to be necessary in the development of an adequate mobile phase system for the separation of β-endorphin-(6–17) and fourteen fragment peptides in a 100-min run[14]. If the chromatographic parameters pH, type and concentration of the ion-pairing agent, buffer concentration and temperature are chosen well, β-endorphin-(6–17) and its N-terminally shortened fragments -(7–17), -(8–17) and -(9–17) are baseline separated in a 20-min gradient run (see Fig. 1).

Insulin. At an earlier stage we reported on the separation of bovine, porcine and human insulin and their respective MDA derivatives in a 60-min run[13]. By application of a mobile phase containing sodium sulphate and sodium dihydrogenphosphate acidified to pH 2.5 with perchloric acid, a clear separation between the six components is obtained within 30 min, as can be seen in Fig. 2. By comparison with a reference insulin preparation, three-fold information is obtained in one run: identification of species of origin, purity determination and biological potency determination. With regards to the last aspect, insulin formulations are still tested for their potency in a bioassay[16,17]. However, applying adequate reference insulin preparations of known

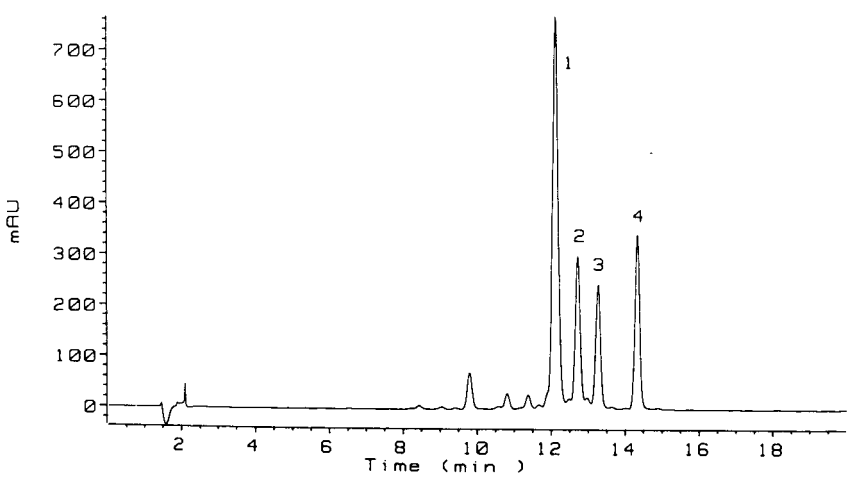

Fig. 1. HPLC separation of β-endorphin-(6–17) and its N-terminally shortened fragments. For the chromatographic conditions, see system I, Table I. 1 = β-Endorphin-(6–17); 2 = -(7–17); 3 = -(8–17); 4 = -(9–17). mAU = milli absorbance units.

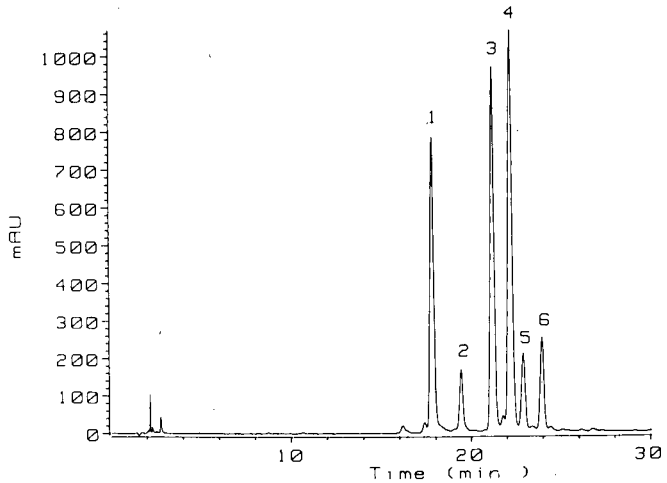

Fig. 2. HPLC separation of insulins. For the chromatographic conditions, see system 2, Table I. 1 = Bovine insulin; 2 = bovine MDA insulin; 3 = human insulin; 4 = porcine insulin; 5 = human MDA insulin; 6 = porcine MDA insulin.

potency in combination with a well validated assay procedure, HPLC seems an attractive alternative to the time-consuming, expensive and less reproducible bioassays.

ACTH fragment analogue (Org 2766). In continuation of an earlier study in which we reported on the HPLC separation of Org 2766 and its D-histidine analogue[13], we developed a procedure in which Org 2766 and its six single D- or L-amino acid substituted diastereoisomeric peptides are separated in one run (see Fig. 3).

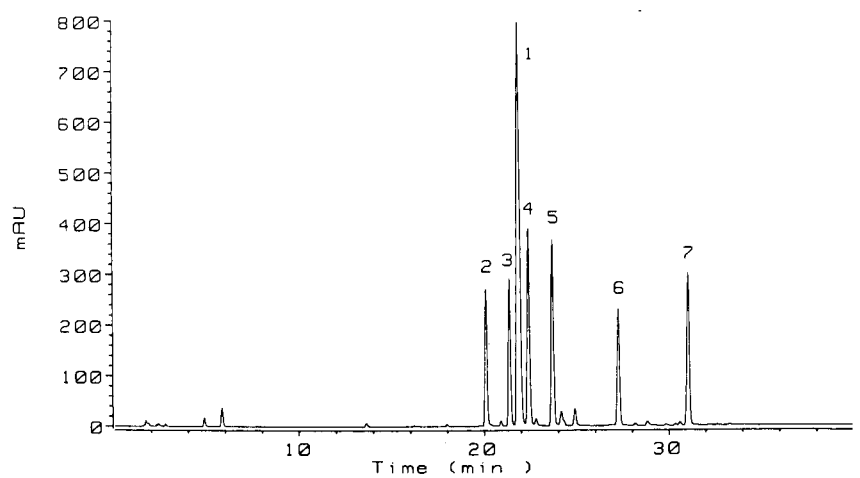

Fig. 3. HPLC separation of Org 2766 and its six diastereoisomers. For the chromatographic conditions, see system 3, Table I. 1 = Org 2766; 2 = D-Glu analogue; 3 = D-His analogue; 4 = D-Met(O_2) analogue; 5 = C-terminal D-Phe analogue; 6 = 4-D-Phe analogue; 7 = L-Lys analogue.

ITP

The application of ITP in peptide analysis is two-fold, *viz.*, purity determination of the native peptides and determination of ionic compounds of non-peptidic nature possibly present in the preparations.

ITP of the peptides. As an indication of the high resolving power of ITP in peptide analysis, we present here some characteristic examples of the separation of closely related components.

Fig. 4 shows the separation of β_h-endorphin from the (2–31) sequence in which only the N-terminal tyrosine residue is lacking. Although this separation is critical, it is reproducible and the considerable difference in UV response between the two peptides is an extra help in the interpretation of the isotachopherogram. Fig. 5 shows the separation of five closely related basic ACTH fragments. We found a good correspondence between the effective mobilities and the calculated isoelectric point (p*I*) values[18] of these peptides. The same holds for ACTH-(1–24) and its -(1–10) and -(11–24) fragments and for AVP and the desglycinamide fragment DGAVP (see Figs. 6 and 7, respectively). The isotachopherogram of the sulphated and non-sulphated forms of an analogue of the octapeptide CCK-8 is shown in Fig. 8.

Anions and cations in peptides. During the synthesis and purification of peptides, a wide variety of ionic compounds are applied. The ITP determination of these non-peptidic substances in peptide preparations proves to be an important additional purity check.

For reference purposes a mixture of ten anions, which are frequently applied

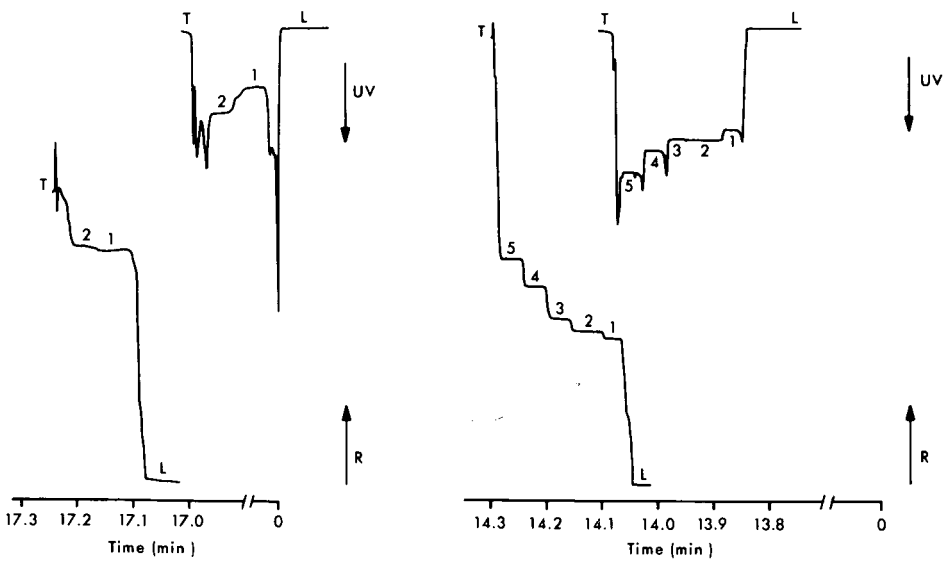

Fig. 4. ITP separation of β-endorphin from β-endorphin-(2–31). Electrolyte system 1, Table II. 1 = β-endophin-(2–31); 2 = -(1–31). *R* = Resistance.

Fig. 5. ITP separation of closely related ACTH fragments. Electrolyte system 1, Table II. 1 = ACTH-(1–18), p*I* 11.5; 2 = -(1–17), p*I* 10.9; 3 = -(1–16)NH_2, p*I* 10.9; 4 = -(1–16), p*I* 10.4; 5 = -(1–13)NH_2, p*I* 10.3.

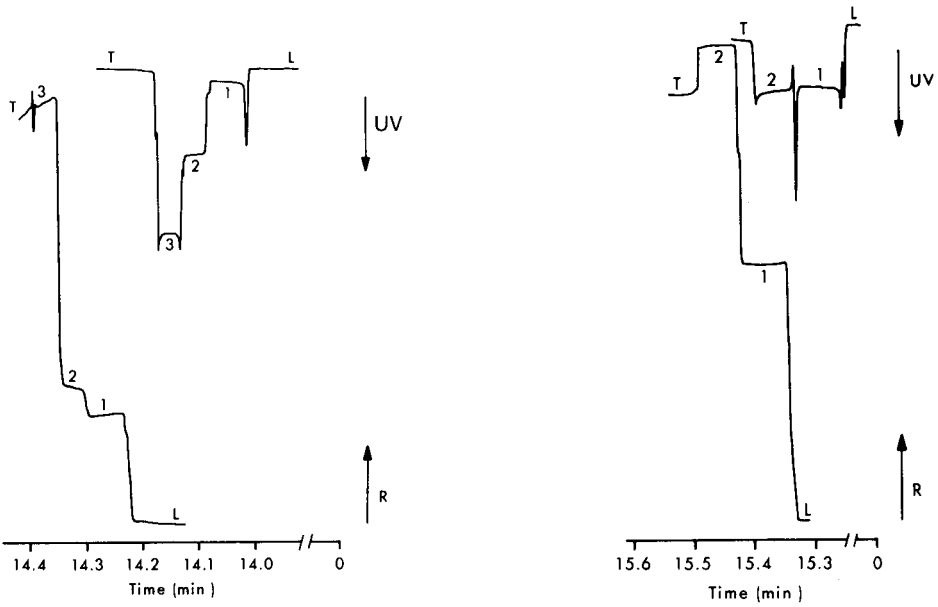

Fig. 6. ITP separation of ACTH-(1–24) and fragments. Electrolyte system 1, Table II. 1 = ACTH-(11–24), p*I* 11.7; 2 = -(1–24), p*I* 11.0; 3 = -(1–10), p*I* 7.6.

Fig. 7. ITP separation of AVP and DGAVP. Electrolyte system 1, Table II. 1 = AVP, p*I* 9.3; 2 = DGAVP, p*I* 8.3.

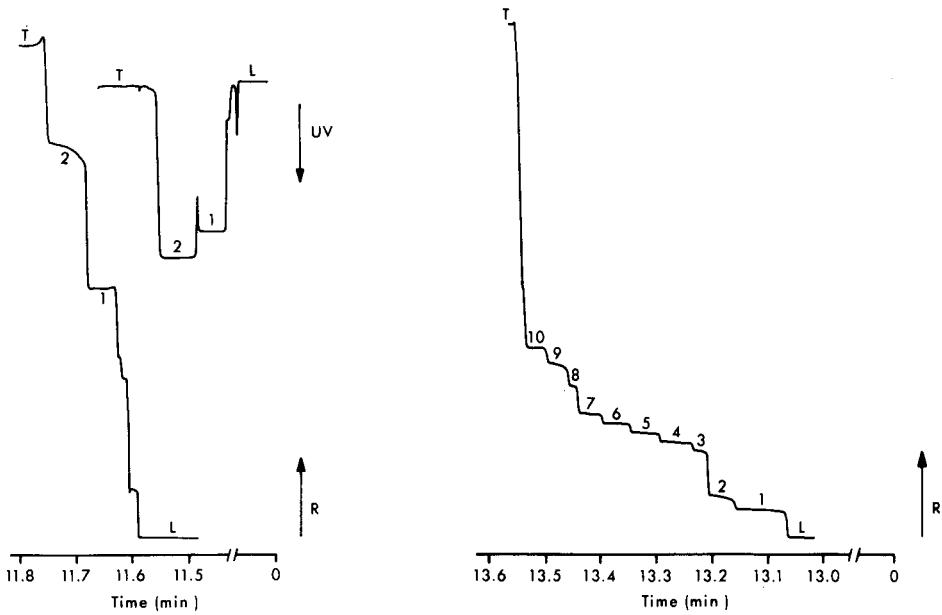

Fig. 8. ITP separation of a sulphated and a non-sulphated analogue of CCK-8. Electrolyte system 2, Table II. 1 = Sulphated analogue; 2 = non-sulphated analogue.

Fig. 9. ITP separation of the anion reference mixture. Electrolyte system 2, Table II. 1 = Sulphate; 2 = formate; 3 = methanesulphonate; 4 = trifluoromethanesulphonate; 5 = trifluoroacetate; 6 = monochloroacetate; 7 = acetate; 8 = phosphate; 9 = *p*-toluenesulphonate; 10 = 1-hydroxybenzotriazole.

during peptide synthesis and isolation, is used. The separation of this mixture is shown in Fig. 9.

As most of our peptide preparations are converted into their acetate salts, which have good stability and are a suitable form for biological testing, we paid special attention to the determination of acetic acid in peptide preparations[11].

An illustration of the additional information that ITP can give is the simultaneous determination of acetic acid and trifluoroacetic acid (TFA). TFA is frequently applied as a deprotecting agent in peptide synthesis and is also used as a volatile modifier in preparative HPLC[19]. One should ensure that in the final product the TFA has been removed completely, *e.g.*, by repeated lyophilization and/or by treatment of the preparation with an anion-exchange resin in which TFA is exchanged for acetic acid. A characteristic example of the combined use of HPLC and ITP is shown in Fig. 10. Preparative HPLC purification of a peptide was performed with TFA as modifier in the mobile phase. The bulk of TFA was removed by evaporation and finally an anion-exchange treatment (Dowex 2-X8 in the acetate form) was performed to convert the TFA salt into the acetate form. However, an ITP check on this product indicated that a considerable amount of residual TFA was present (ratio of acetate to TFA = 1:0.12). Three successive ion-exchange treatments were necessary to remove the TFA completely.

The same phenomenon as for TFA was also found for phosphate, which is also widely used as a mobile phase additive to improve chromatographic performance[20]. As with TFA, three successive ion-exchange treatments were required to remove the phosphate completely.

For the determination of halides we applied system 3 in Table II, which was adapted from Boček *et al.*[21] as reported previously[11].

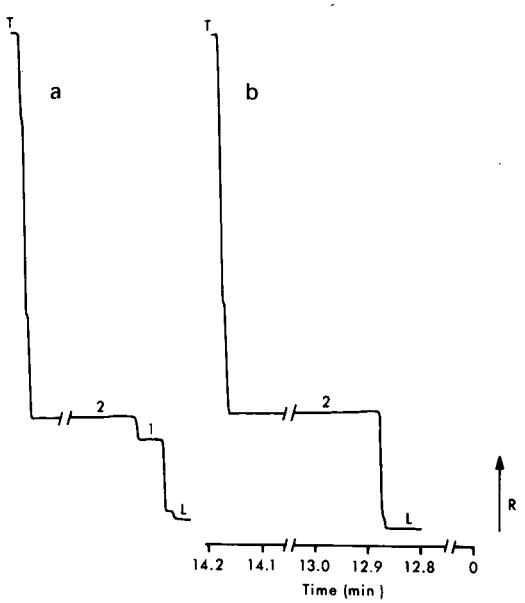

Fig. 10. Check by ITP on TFA removal after preparative HPLC; (a) after one ion-exchange treatment; (b) after three ion-exchange treatments. Electrolyte system 2, Table II. 1 = Trifluoroacetate; 2 = acetate.

Like anionic compounds, cations are also frequently used in peptide synthesis and purification. As with the anions, we used a cation reference mixture, the separation of which is given in Fig. 11.

Alkylamine buffers such as triethylamine (TEA) or tetramethylammonium (TMA) phosphate are often added to the mobile phase to reduce the non-specific interaction of the compounds with the unreacted silanol groups of the material[22,23]. In preparative HPLC these buffer components have to be removed in the final preparation. ITP proved to be a suitable technique for checking the desalting procedure applied.

Non-volatile buffers such as TMA phosphate can be removed by (repeated) ion-exchange procedures. As an alternative desalting procedure for the micrograms to milligrams range, Böhlen *et al.*[24] proposed the use of an octadecylsilica HPLC column. The salt-containing peptide preparation is loaded on a C_{18} column and elution of the salt ions is performed with an aqueous mobile phase, whereas the peptide in question is retained on the hydrophobic support. Elution of the peptide is achieved with an organic solvent-containing mobile phase (methanol, *n*-propanol). The effectiveness of the desalting procedure is monitored by on-line conductivity measurement.

We applied this procedure in the desalting of several peptides of different nature, in which we monitored not only the UV but also the conductivity signal. As expected, not only the salt fractions but also the peptide itself, in a sense being an amphoteric electrolyte, gave an increase in conductivity. Hence the possible co-elution of peptide and residual salt could not be deduced from the HPLC conductivity signal. A careful check of the HPLC-desalted fractions with the sensitive ITP technique indicated that up to 4% of residual TMA salt was present, although the HPLC conductivity

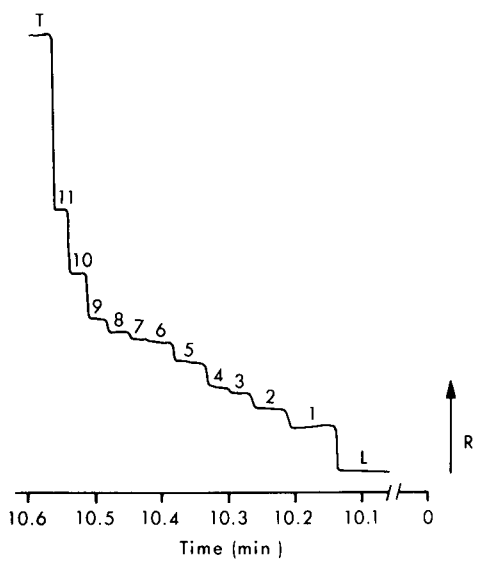

Fig. 11. ITP separation of the cation reference mixture. Electrolyte system 4, Table II. 1 = Hydrazine; 2 = sodium; 3 = trimethylamine; 4 = tetramethylammonium; 5 = pyridine; 6 = piperidine; 7 = 4-dimethylaminopyridine; 8 = N-ethylmorpholine; 9 = N,N-diisopropylethylamine; 10 = triethylamine; 11 = dicyclohexylamine.

monitoring has led us to believe that we had removed all of the salt present[15]. A more efficient desalting procedure proved to be ultrafiltration. Applying a filter with a cut-off range of 500 daltons (Amicon UM 05), complete removal of TMA from a DGAVP preparation was obtained[11].

In the application of the check by ITP on the effective salt removal in peptide preparations, care should be taken to avoid misinterpretation due to the co-migration of the salt ion and the peptide under investigation. This is illustrated by the basic peptide ACTH-(1–24), which was purified by preparative HPLC using a mobile phase containing the volatile salt TEA formate. To control the effectiveness of the TEA removal by lyophilization, we performed ITP in the normally applied cation system at pH 4.8 (see Table II, system 4). However, owing to co-migration of the peptide and TEA, only one zone was monitored in an ACTH-(1–24)–TEA reference mixture. Lowering the pH of the system to 4.5 had no effect. However, increasing the pH to 5.1 resulted in the clear separation of the two components (see Fig. 12).

Ammonium-containing buffers have also been proposed as a separation-improving medium in preparative HPLC[25]. Ammonium acetate is generally considered to be volatile, so in theory it can be removed fairly easily by lyophilization of the pooled HPLC fractions. Two control this procedure by ITP, the "general" cation system cannot be applied owing to the high effective mobility of the ammonium ion. For this reason we developed an electrolyte system in which ammonium can be determined adequately[11].

Application of this system to three ammonium acetate-containing peptides of basic, neutral and acidic nature indicated that the degree of salt removal depends strongly on the nature of the peptide. With the basic peptide two lyophilization steps were necessary to remove the salt to a level of less than 1%; the neutral peptide required an additional step to attain this 1% level and finally the acidic peptide contained up to 9% ammonium even after three lyophilization steps (see Table IV).

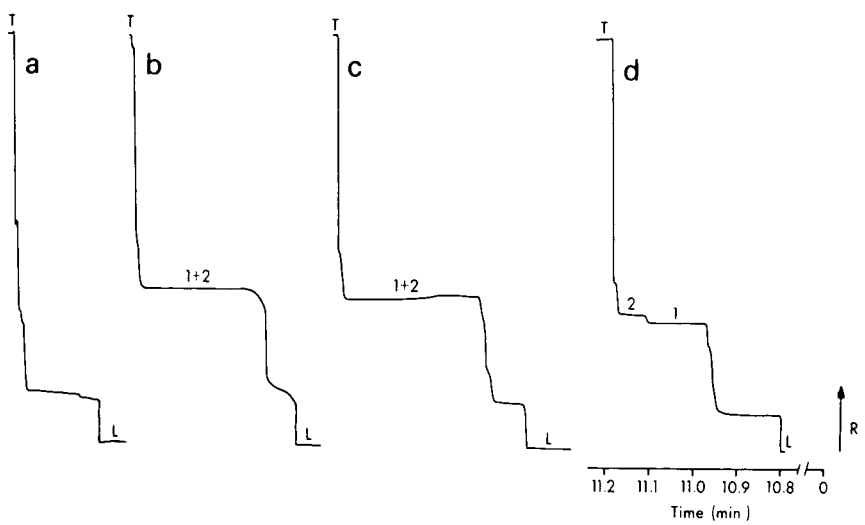

Fig. 12. Influence of pH on the separation of ACTH-(1–24) and TEA. Electrolyte system 4, Table II. (a) Blank; pH set at (b) 4.5, (c) 4.8, (d) 5.1. 1 = TEA; 2 = ACTH-(1–24).

TABLE IV

RESIDUAL AMMONIUM IN PEPTIDES AFTER ONE, TWO AND THREE LYOPHILIZATION STEPS

Peptide nature	*Ammonium (wt.-%)*		
	Step 1	*Step 2*	*Step 3*
Basic	14	0.9	
Neutral	42	21	1
Acidic	49	28	9

CONCLUSION

Owing to its versatility in performance and its high separation power, HPLC is an established technique in peptide chemistry. In the analytical mode HPLC can give information on both chemical and optical purity. Moreover, HPLC can be used to determine the species of origin of a preparation (*e.g.*, insulin) and in the determination of the biological potency of a peptide.

Characteristic general features of carrier-free capillary ITP are a high resolution capacity, high sensitivity (nanogram range), simultaneous determination of various anions or cations, easy performance, short analysis time, small amount of sample preparation needed (0.1–1 mg), low running costs and the absence of undesirable analyte–carrier interactions.

The ITP technique complements the HPLC method regarding the analysis of peptides. For a check on the purity of the peptide itself ITP is a valuable alternative. In this respect it is important to bear in mind that the ITP approach to purity determination is based on a different physico-chemical parameter, *viz.*, electrophoretic mobility, than that used in RP-HPLC analysis, in which the peptide hydrophobicity is the main separation mechanism. Moreover, ITP may give a general indication of the p*I* value of a peptide under investigation.

Complementary to this information, ITP is a reliable and sensitive technique for determining quantitatively non-peptidic ionic compounds in preparations (intermediates and end-products). A wide variety of anions and cations used in peptide synthesis and the purification of a peptide are easily monitored. The use of ITP as a check on the effective removal of unwanted mobile phase components introduced by preparative HPLC employed for peptide purification is especially illustrative.

In our opinion, the ITP technique is a most valuable addition to the current methods of analysis in the peptide field.

ACKNOWLEDGEMENTS

We are grateful to Professor F. M. Everaerts and Th. P. E. M. Verheggen for the apparatus schemes and stimulating discussions. We also thank Dr. H. Berkeley for critical reading of the manuscript.

REFERENCES

1 W. S. Hancock (Editor), *Handbook of HPLC for the Separation of Amino Acids, Peptides and Proteins*, Vols. I and II, CRC Press, Boca Raton, FL, 1984.
2 A. Kopwillem, U. Moberg, G. Westin-Sjödahl, R. Lundin and H. Sievertsson, *Anal. Biochem.*, 67 (1975) 166.
3 C. J. Holloway and V. Pingoud, *Electrophoresis*, 2 (1981) 127.
4 R. Jannasch, *Pharmazie*, 38 (1983) 379.
5 P. Stehle and P. Fürst, *J. Chromatogr.*, 346 (1985) 271.
6 P. Hermann, R. Jannasch and M. Lebl, *J. Chromatogr.*, 351 (1986) 283.
7 M. A. Firestone, J.-P. Michaud, R. H. Carter and W. Thormann, *J. Chromatogr.*, 407 (1987) 363.
8 V. Kašička and Z. Prusík, *J. Chromatogr.*, 470 (1989) 209.
9 J. W. van Nispen, P. S. L. Janssen, B. C. Goverde, J. C. M. Scherders, F. van Dinther and J. A. J. Hannink, *Int. J. Pept. Protein Res.*, 17 (1981) 256.
10 J. W. van Nispen, P. S. L. Janssen, B. C. Goverde and H. M. Greven, in K. Brunfeldt (Editor), *Peptides 1980, Proceedings of the 16th European Peptide Symposium, Denmark, August 31–September 6, 1980*, Scriptor, Copenhagen, 1981, p. 731.
11 P. S. L. Janssen and J. W. van Nispen, *J. Chromatogr.*, 287 (1984) 166.
12 F. M. Everaerts, J. L. Beckers and Th. P. E. M. Verheggen, *Isotachophoresis—Theory, Instrumentation and Applications (Journal of Chromatography Library*, Vol. 6), Elsevier, Amsterdam, 1976.
13 P. S. L. Janssen, J. W. van Nispen, R. L. A. E. Hamelinck, P. A. T. A. Melgers and B. C. Goverde, *J. Chromatogr. Sci.*, 22 (1984) 234.
14 P. S. L. Janssen, J. W. van Nispen, P. A. T. A. Melgers and R. L. A. E. Hamelinck, *Chromatographia*, 21 (1986) 461.
15 J. W. van Nispen and P. S. L. Janssen, in W. S. Hancock (Editor), *Handbook of HPLC for the Separation of Amino Acids, Peptides and Proteins*, Vol. II, CRC Press, Boca Raton, FL, 1984, p. 229.
16 *British Pharmacopoeia 1980, Addendum 1986*, H.M. Stationary Office, London, 1986, p. 414.
17 *European Pharmacopoeia*, Maisonneuve, Sainte Ruffine, 2nd ed., 1984, Method of Analysis V.2.2.3.
18 J. D. Rodwell, *Anal. Biochem.*, 119 (1982) 440.
19 H. P. J. Bennett, C. A. Browne and S. Soloman, *J. Liq. Chromatogr.*, 3 (1980) 1353.
20 C. A. Bishop, in W. S. Hancock (Editor), *Handbook of HPLC for the Separation of Amino Acids, Peptides and Proteins*, Vol. I, CRC Press, Boca Raton, FL, 1984, p. 153.
21 P. Boček, I. Miedziak, M. Deml and J. Janák, *J. Chromatogr.*, 137 (1977) 83.
22 J. E. Rivier, *J. Liq. Chromatogr.*, 1 (1978) 83.
23 M. E. F. Biemond, W. A. Sipman and J. Olivié, *J. Liq. Chromatogr.*, 2 (1979) 1407.
24 P. Böhlen, F. Castillo, N. Ling and R. Guillemin, *Int. J. Pept.. Protein Res.*, 16 (1980) 306.
25 R. Burgus and J. Rivier, in A. Loffet (Editor), *Peptides 1976, Proceedings of the 14th European Peptide Symposium*, Editions de l'Université de Bruxelles, Brussels, 1976, p. 85.

Journal of Chromatography, 470 (1989) 185–190
Elsevier Science Publishers B.V., Amsterdam — Printed in The Netherlands

CHROM. 21 269

INVESTIGATIONS ON THE INTERFERON-INDUCED 2′–5′ OLIGOADENYLATE SYSTEM USING ANALYTICAL CAPILLARY ISOTACHOPHORESIS

GERNOT BRUCHELT*
Children's Hospital, Department of Hematology, University of Tuebingen, Ruemelinstrasse 23, D-7400 Tuebingen, (F.R.G.)
MANFRED BUEDENBENDER
Children's Hospital, Department of Surgery, University of Tuebingen, Tuebingen (F.R.G.)
and
JÖRN TREUMER and DIETRICH NIETHAMMER
Children's Hospital, Department of Hematology, University of Tuebingen, Tuebingen (F.R.G.)
and
KARLHEINZ SCHMIDT
Children's Hospital, Department of Surgery, University of Tuebingen, Tuebingen (F.R.G.)

SUMMARY

The activity of the interferon inducible enzyme 2′–5′ oligoadenylate synthetase (2–5A synthetase, E.C. 2.7.7) which converts ATP into a series of 2′–5′ oligoadenylates was measured using analytical capillary isotachophoresis. The turnover rate of ATP during the reaction was monitored by determination of its concentration at the beginning and the end of the 2–5A synthetase reaction. The enzyme was analysed in extracts of peripheral blood mononuclear cells either pretreated or not with interferon.

INTRODUCTION

Interferons are (glyco)proteins with antiviral, antiproliferative and immunoregulatory effects[1]. After interaction with cell surface receptors, the interferons cause several metabolic changes in the cells including the activation of the 2–5A system[2]: an enzyme, the 2–5A synthetase, is produced *de novo*, converting ATP into a series of 2′–5′ oligoadenylates:

$$n\ \mathrm{ATP} \rightarrow \mathrm{ppp5'A2'(p5'A)}_{n-1} + (n-1)\mathrm{PP} \qquad (n = 2\text{–}14)$$

These oligoadenylates activate an endoribonuclease (RNaseL) which splits mRNA, finally resulting in inhibition of protein synthesis. The determination of 2–5A synthetase in mononuclear blood cells has been used clinically as a response parameter during therapy with interferon[3]. Most methods described in the literature use assays with radioactively labelled compounds. Here we describe a non-radioactive test system using analytical capillary isotachophoresis.

0021-9673/89/$03.50

EXPERIMENTAL

Preparation of cell lysates

Peripheral blood mononuclear cells (PBMNCs) were isolated using lymphoprep gradient centrifugation. The cells were cultivated at 37°C for 18 h either in the absence or presence of interferon-beta (Fiblaferon; Bioferon, Laupheim, F.R.G.); 1000 U/ml cell suspension ($2 \cdot 10^6$ cells/ml). Cell lysis was carried out using a buffer solution containing 0.5% Nonidet-P 40.

2–5A synthetase assay

A 20–50 μl volume of cell lysates ($2 \cdot 10^6$ cells per 100 μl) was incubated with Poly(IC)-agarose beads (Pharmacia, Freiburg, F.R.G.) for isolation of the 2–5A synthetase. Thereafter, the beads were added to 25 μl incubation buffer containing ATP (5 m*M*) and creatine phosphate (10 m*M*)/creatine phosphokinase as an ATP-regenerating system. The incubation was carried out at 30°C for up to 20 h. Aliquots of the reaction mixture were withdrawn for isotachophoretic analysis at the beginning and the end of the incubation period (diluted 1:10 in water). A more detailed description of the incubation conditions is given in ref. 4.

Isotachophoresis

The isotachophoretic analysis was carried out on an LKB Tachophor 2127 equipped with an UV (254 nm) and conductivity detector. Current during signal registration: 75 μA. Analyses were carried out at 15°C. Leading electrolyte: 0.01 *M* HCl–β-alanine, pH 3.65 + 0.3% (w/v) methylcellulose. Terminating electrolyte: 0.01 *M* caproic acid. Usually, 6.7-μl samples from the reaction mixtures were injected diluted (usually 1:10) into the Tachophor. Chart speed during detection: 10 cm/min. Capillary: 23 cm × 0.5 mm I.D.

Conversion of ATP into ADP

ATP-containing samples (1–5 mmol/l) were incubated with a solution of glucose (10 m*M*) and hexokinase (10 U/ml) for 1 h at 37°C. Under these conditions, ATP is quantitatively converted into ADP. Isotachophoresis was carried out after dilution of samples (1:10).

RESULTS AND DISCUSSION

Isotachopherogram of ATP in the incubation mixture

In contrast to ADP, AMP and the 2′–5′-oligoadenylates, ATP did not yield a sharp rectangular signal when dissolved in the incubation mixture for the 2–5A synthetase reaction. The reason is not clear; using phosphate-buffered saline, neither the presence nor absence of Mg^{2+} and Ca^{2+} nor of EDTA influence this ATP signal. Rectangular ATP signals were observed only in aqueous solution (Fig. 1a). Therefore, it was advantageous to convert the reaction mixture into ADP for a more accurate determination of the ATP concentration at the beginning and the end of the 2–5A synthetase reaction. This was done using the glucose–hexokinase reaction. Under these conditions, evaluation was possible even at small ATP-turnover rates during the 2–5A synthetase reaction (Fig. 1b). Fig. 2 shows the calibration graph for

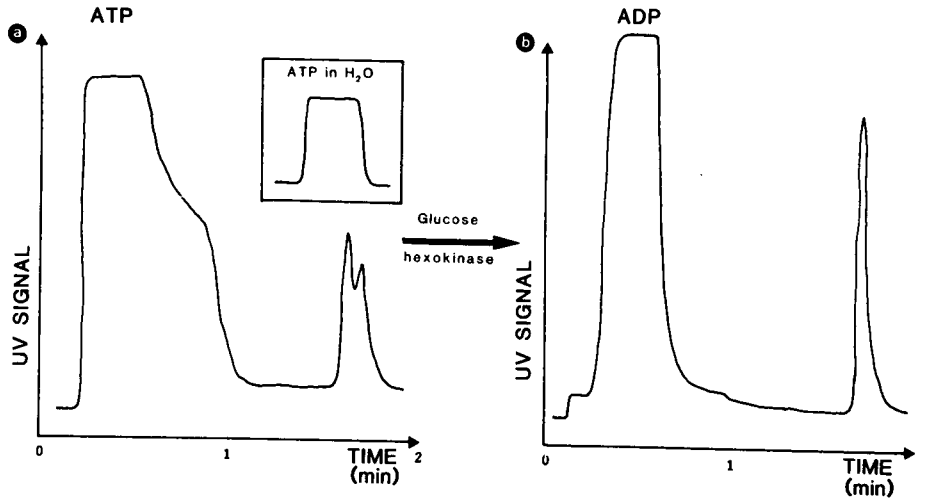

Fig. 1. Isotachopherograms of (a) ATP dissolved in 2–5A synthetase buffer and (b) the same ATP solution in 2–5A synthetase buffer after incubation with glucose–hexokinase.

ATP obtained by measuring the zone lengths of ADP after the glucose–hexokinase reaction.

Changes of the ATP concentration during the 2–5A synthetase reaction

For determination of the 2–5A synthetase activity, the decrease in ATP concentration during the incubation period (up to 20 h) was measured. Because of this long incubation time it was necessary to measure potential non-specific ATP decomposition: Fig. 3a,b shows that non-specific destruction does not occur, probably because of the high efficacy of the ATP-regenerating system, creatine phosphate–creatine phosphokinase, in the incubation mixture. The conversion of ATP into 2'–5' oligoadenylates in the presence of 2–5A synthetase is shown in Fig. 3c. In the example

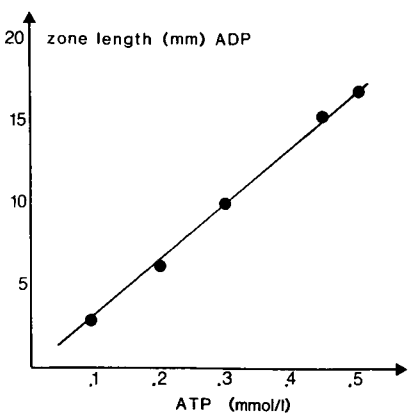

Fig. 2. Calibration graph for different amounts of ATP (1–5 mmol/l) after conversion into ADP using the glucose–hexokinase reaction (samples diluted 1:10 prior to isotachophoresis).

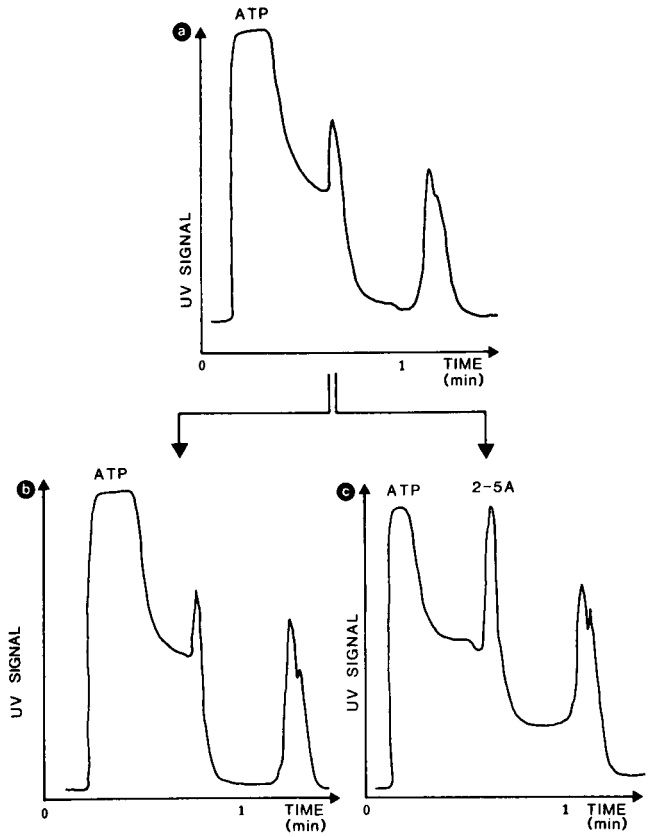

Fig. 3. Isotachopherograms of the 2–5A synthetase reaction. (a) At the start of the reaction; (b) after incubation for 20 h without 2–5A synthetase (lysis buffer instead of cell lysates was used); (c) after incubation for 20 h, in the presence of 2–5A synthetase lysate of $1 \cdot 10^6$ cells incubated with Poly(IC)-agarose beads.

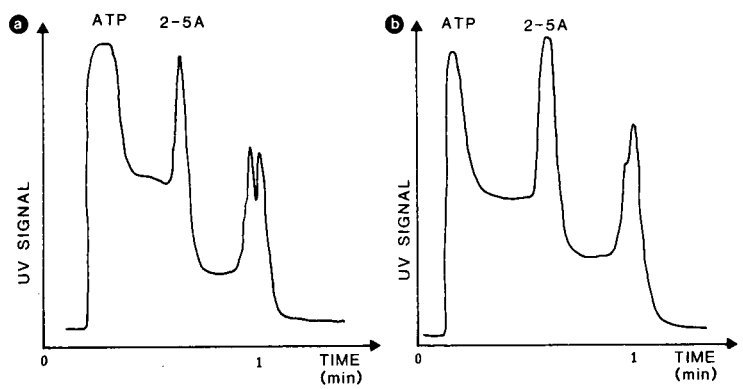

Fig. 4. Isotachopherograms after incubation for 20 h using Poly(IC)-agarose beads loaded with extracts of $5 \cdot 10^5$ PBMNC, (a) not pretreated with interferon, (b) treated with interferon-beta (1000 U/ml cell suspension, incubation time 18 h at 37°C).

given the turnover of ATP during a 20-h incubation period caused by 2–5A synthetase present in the lysate of $1 \cdot 10^6$ PBMNC, is depicted: 50.7% of the amount of ATP present at the beginning of the reaction were transformed to 2'–5' oligoadenylates; therefore, the activity of this cell lysate can be given as the consumption of 3.15 nmol ATP per hour per 10^6 cells.

Influence of pretreatment of PBMNC with interferon on the 2–5A synthetase activity

Fig. 4 shows the ATP signal after incubation for 20 h using 2–5A synthetase isolated from 20-μl lysates of PBMNCs compared with the signal obtained from 20-μl lysates of PBMNCs that were pretreated with 1000 U interferon-beta for 18 h. Simultaneously with the decline of the ATP signal, the signals of oligoadenylates increase. The ATP turnover rate using the extracts from cells pretreated with interferon was 8.75 nmol ATP per hour per 10^6 cells, and that in lysates of PBMNCs not pretreated with interferon was 4.46 nmol ATP per hour per 10^6 cells; *i.e.*, treatment with interferon led to a 1.96-fold increase in 2–5A synthetase activity.

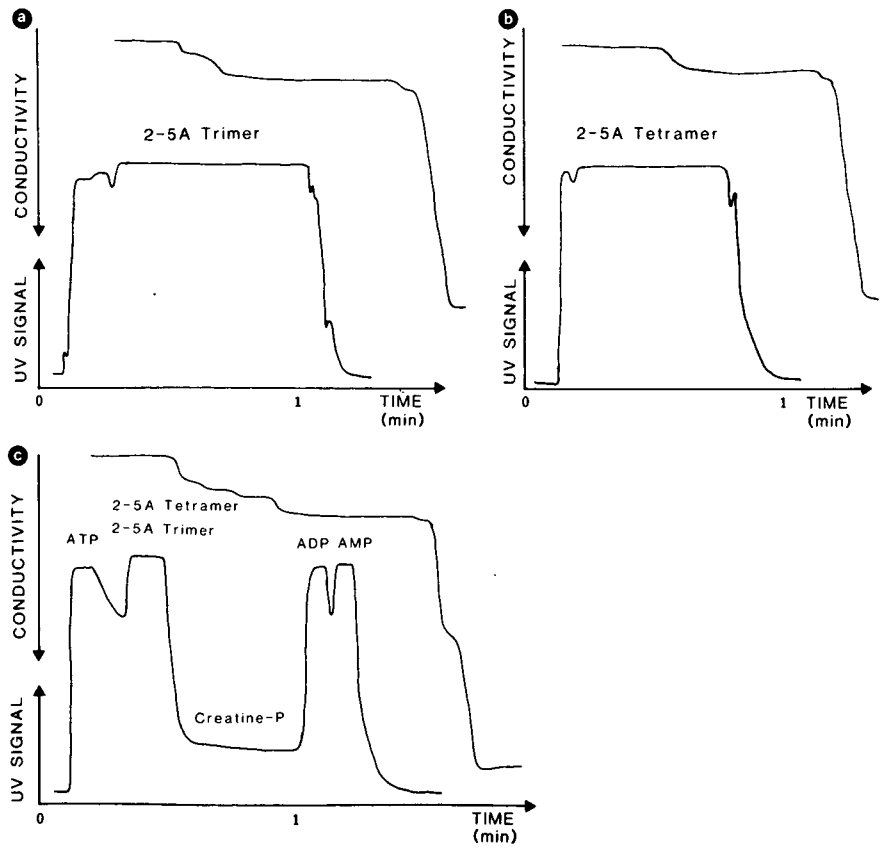

Fig. 5. Isotachopherograms of commercially available 2'–5' oligoadenylates. (a) 2–5A trimer (pppA2'p5'A2'p5'A), 2.3 mmol/l; (b) 2–5A tetramer (pppA2'p5'A2'p5'A2'p5'A), 2.3 mmol/l; (c) tachogram of a mixture consisting of ATP (0.4 mmol/l), ADP (0.4 mmol/l), AMP (0.4 mmol/l), 2–5A trimer (0.17 mmol/l), 2–5A tetramer (0.17 mmol/l) and creatine phosphate (1.0 mmol/l); sample volume 6.7 μl.

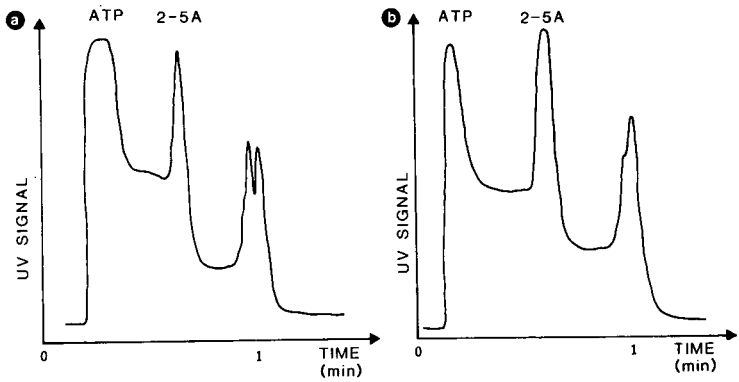

Fig. 6. Characterization of the isotachopherogram of the 2–5A synthetase reaction. (a) After incubation for 20 h; (b) after addition of 2–5A trimer [1 μl 2–5A trimer (50 nmol) + 9 μl reaction mixture].

Isotachophoretic characterization of 2′–5′ oligoadenylates

Fig. 5a shows the isotachopherogram of pppA2′p5′A2′p5′A (2–5A trimer), Fig. 5b that of the 2–5A tetramer (pppA2′p5′A2′p5′A2′p5′A). Both commercially available compounds contain impurities. The net mobilities of the trimeric and tetrameric forms representing the major fraction of oligoadenylates formed during the 2–5A synthetase reaction are very similar, therefore they cannot be separated from each other by isotachophoresis using the system described here. This is demonstrated in Fig. 5c: in a synthetic mixture of ATP, ADP, AMP, creatine phosphate, 2–5A trimer and 2–5A tetramer only the two oligoadenylates were not separated. Separation was also not possible in the presence of spacer molecules (Ampholine carrier ampholytes, LKB; pH 3.5–10; data not shown). However, for the estimation of the activity of 2–5A synthetase, this fact is not relevant because it is more advantageous to determine the decrease in ATP instead of the heterogeneous population of 2–5 oligoadenylates that is formed during the 2–5A synthetase reaction. Although a series of different oligoadenylates are formed, preferentially the trimeric and the tetrameric forms, only one additional peak appears in the isotachophoregram. Evidence that this second peak consists of 2–5 oligoadenylates formed during the 2–5A synthetase reaction was obtained by substitution of 2–5A as shown in Fig. 6: after addition of 2–5A trimer to the 2–5A synthetase reaction mixture after incubation for 20 h, no additional peak appeared, but the zone length of the second peak increased.

In conclusion, analytical capillary isotachophoresis can be successfully used for determination of 2–5A synthetase activity, especially when small numbers of samples are to be analysed. The determination of nucleotides is highly reproducible, therefore also very small turnover rates of enzymatic reactions can be measured accurately. This is especially advantageous in the case of the 2–5A synthetase reaction because it is difficult to perform the assay under ATP-saturated conditions[4].

REFERENCES

1 S. Pestka, J. A. Langer, K. C. Zoon and Ch. E. Samuel, *Annu. Rev. Biochem.*, 56 (1987) 727–777.
2 M. I. Johnston and P. F. Torrence, in R. M. Friedmann (Editor), *Interferon*, Vol. 3, Elsevier, Amsterdam, New York, Oxford, 1984, Ch. 7.
3 J. A. Merritt, D. M. Meltzer, L. A. Ball and E. C. Borden, *Prog. Clin. Biol. Res.*, 202 (1985) 423–430.
4 G. Bruchelt, J. Beck, K. Schilbach-Stückle, E. Koscielniak, J. Treuner and D. Niethammer, *J. Clin. Chem. Clin. Biochem.*, 25 (1987) 879–888.

Journal of Chromatography, 470 (1989) 191–199
Elsevier Science Publishers B.V., Amsterdam — Printed in The Netherlands

CHROM. 21 221

APPLICATION OF CAPILLARY ISOTACHOPHORESIS TO THE ANALYSIS OF GLUTATHIONE CONJUGATES

D. TSIKAS and G. BRUNNER*

Division of Gastroenterology and Hepatology, Medizinische Hochschule Hannover, Podbielskistrasse 380, D-3000 Hannover 51 (F.R.G.)

SUMMARY

An analytical capillary isotachophoretic method has been applied for the quantitative assay of reduced glutathione (GSH) conjugates produced by the cytosolic enzyme GSH S-transferase. The donor molecule GSH in reduced and oxidized (GSSG) forms and the GSH conjugates of at least two electrophilic acceptors can be assayed in a single analysis. This technique also permits the quantitative assay of further metabolites of GSH conjugates including mercapturic acids. The total analysis time was of the order of 30 min. The sensitivity of the method is sufficient for the accurate detection of 0.15 nmol GSH conjugate of 1-chloro-2,4-dinitobenzene and *p*-nitrobenzyl chloride, 0.2 nmol GSH conjugate of 1,2-epoxy-3-(*p*-nitrophenoxy)-propane and 0.15 nmol GSH. The present method is simple, accurate and does not require radioactively labelled compounds or separate analytical procedures.

INTRODUCTION

Reduced glutathione (GSH) S-transferases (GST) (E.C. 2.5.1.18) are a key phase II enzyme system, initiating the detoxification of potentially alkylating physiological and exogenous agents including drug metabolites[1–4]. These enzymes catalyze the conjugation of GSH with a variety of electophilic toxic compounds to GSH conjugates. The latter are further metabolized in the mercapturic acid pathway to the corresponding mercapturic acids, which are excreted in bile and urine.

Several analytical methods have been developed for the quantitation of GSH conjugates, including radioimmunoassay[5], ion-exchange high-performance liquid chromatography (HPLC)[6,7] and reversed-phase HPLC (RP-HPLC) with UV and fluorescence detection[8,9]. The ion-exchange HPLC method with precolumn derivatization with *o*-phthaldialdehyde, recently described by our group[7], is suitable for the detection of all GSH conjugates and GSH. However, this method does not allow the determination of mercapturic acids. By using the RP-HPLC method with UV detection, GSH conjugates and mercapturic acids can be sensitively detected but not GSH and oxidized glutathione (GSSG)[8]. Furthermore, the chromatographic methods require particularly large sample volumes and elaborate sample preparation. An optimum method for the investigation of metabolic studies would allow simultaneous measurement of all these major compounds of the mercapturic acid pathway.

0021-9673/89/$03.50

Capillary isotachophoresis has proved useful for the quantitation of a wide range of ionogenic organic compounds and inorganic ions. Recently, this technique has been reported to allow the simultaneous analysis of GSH in reduced and oxidized forms[10]. Since all GSH conjugates involve GSH in their molecules, they could theoretically also be determined by capillary isotachophoresis. Holloway and Battersby[11] have recently reported that this technique can also be applied to the determination of GSH conjugates. Parallel and independent of this group, we investigated the applicability of analytical capillary isotachophoresis to the analysis of GSH conjugates and mercapturic acids. Capillary isotachophresis offers three major advantages: (a) a rapid analysis without extraction steps; (b) detection of GSH conjugates of which the original substrates do not show UV absorbance, fluorescence or radioactivity and (c) simultaneous detection of GSH, GSH conjugates and mercapturic acids.

This paper demonstrates the applicability of the analytical capillary isotachophoretic technique to the analysis of GSH conjugates. This technique has been applied[10] for the study of GSH conjugation reactions catalyzed by cytosolic glutathione S-transferase (GST). Furthermore, it has been extended to the determination of mercapturic acids.

EXPERIMENTAL

Chemicals and reagents

GSH, GSSG, N-acetylcysteine, 1,2-epoxy-3-(*p*-nitrophenoxy)propane (EPNP) and the GSH conjugate of *p*-nitrobenzyl chloride (PNBC) were obtained from Sigma (München, F.R.G.), phenylglycidether (PGE) from Fluka (Neu-Ulm, F.R.G.), styrene oxide (SE) from Janssen (Nettetal, F.R.G.) and hydroxypropylmethylcellulose (HPMC) from Ega-Chemie (Steinheim, F.R.G.). These chemicals were of the highest quality available. All other chemicals were from Merck (Frankfurt/Main, F.R.G.).

Exogenous conjugates (except for PNBC-SG) and mercapturic acids were prepared non-enzymatically from the corresponding substrates and GSH or N-acetylcysteine in an ethanolic solution of sodium hydroxide at 25°C. Buffer solutions of these substances were used as standards for calibration of zone lengths.

Cytosol containing large amounts of GST was prepared from liver homogenates of rats by a standard centrifugation technique (200 000-*g* fraction) using 0.1 *M* Tris–HCl, pH 7.4, containing 1 m*M* ethylenediaminetetraacetic acid (EDTA) and 1.15 g% KCl for homogenization of the fresh liver (20%, w/v). Protein concentrations were determined by the method of Bradford[12].

Apparatus

The isotachophoretic analyses were performed on the LKB 2127 Tachophor (Bromma, Sweden) fitted with a poly(tetrafluoroethylene) capillary (23 cm × 0.5 mm I.D. and 40 cm × 0.5 mm I.D.). All analyses were carried out at ambient temperature. The zones were detected by UV (254 nm) and conductivity detection.

Methods

Two electrolyte systems were employed. System A: the leading electrolyte system was 5 m*M* HCl, corrected to pH 7.0 by the addition of Tris, and containing 0.25 g%

HPMC. The terminating electrolyte was 10 m*M* phenol, adjusted to pH 10.0 by the addition of freshly prepared and filtered barium hydroxide solution. System B: the leading electrolyte was 10 m*M* HCl, corrected to pH 3.3 by the addition of β-alanine, and containing 0.25 g% HPMC. The terminating electrolyte was 10 m*M* hexanoic acid. System B was previously employed by our group in the assay of glucuronides derived from phenolic compounds[13]. Separations were carried out at an initial constant current of 50 μA, which was reduced to 25 μA when the voltage reached 10 (system A) or 8 kV (system B). The terminator passed the detectors at a potential of around 10 (system A) and 8.4 kV (system B) at 25 μA. The injection volume was 1–5 μl. The total analysis time was in the order of 30 min.

GSH conjugation reactions were carried out in 0.1 *M* Tris–HCl or 0.1 *M* potassium phosphate buffer, each of pH 6.5, containing GSH at a concentration of 2.5–5 m*M*. The acceptor concentration was varied in the range of 0.5–5 m*M*. Because of the low water solubility of the acceptors, their solutions were prepared in ethanol. The final ethanol concentration in the assay mixture was less than 5% (v/v). The total protein concentration in the assay mixture ranged from 0.1 to 1.0 mg/ml. The enzymatic reaction was stopped by rapid mixing with ice-cold methanol (1:1, v/v). As references for the isotachophoretic analysis of the GSH conjugation reactions, photometric and HPLC techniques were employed[1,14].

The width of an UV-absorbing zone was measured at half its height and was converted into units of time according to the set chart speed. The width of a non-UV-absorbing zone was estimated at half the height of the lower absorbing neighbouring peaks, which can either be sample zones or a peak due to an impurity.

RESULTS AND DISCUSSION

Fig. 1 shows isotachopherograms of an incubation mixture at an early and later stage of the enzymatic GSH conjugation of SE, respectively. GSSG and SE-SG appear as slight UV-absorbing zones, while GSH gives a non-UV-absorbing zone. GSSG shown in Fig. 1 is derived from GSH by autooxidation during incubation. Fig. 1 demonstrates that GSH conjugates, the cosubstrate GSH and the non-conjugating GSSG can be determined in a single analysis. Since all electrophilic substrates used in this study are neutral molecules, they cannot be detected by this method. The order of migration of the organic anions involved in this study from high to low mobility was GSSG, GSH, mercapturic acid and GSH conjugate by using both electrolyte systems.

The calibration graphs obtained by injection of the reference substances were linear for the range 1–25 nmol. Fig. 2 shows an example for GSSG, GSH and SE-SG. The slopes of the calibration plots for GSH, GSSG, some GSH conjugates and the mercapturic acid of 1-chloro-2,4-dinitrobenzene (CDNB) by using both electrolyte systems are given in Table I. As can be seen from this Table, the zone widths of all substances measured by using system A were longer than those obtained by using system B. These differences may result from the different pH values of the leading electrolytes used in the two systems.

Fig. 3a–d show isotachopherograms obtained by using system A from separate incubations of CDNB, PNBC, EPNP and PGE with GSH and rat liver cytosolic GST. Fig. 4a and b show isotachopherograms from a separation of a mixture of PNBC-SG and PGE-SG obtained by using systems A and B respectively. Complete separation

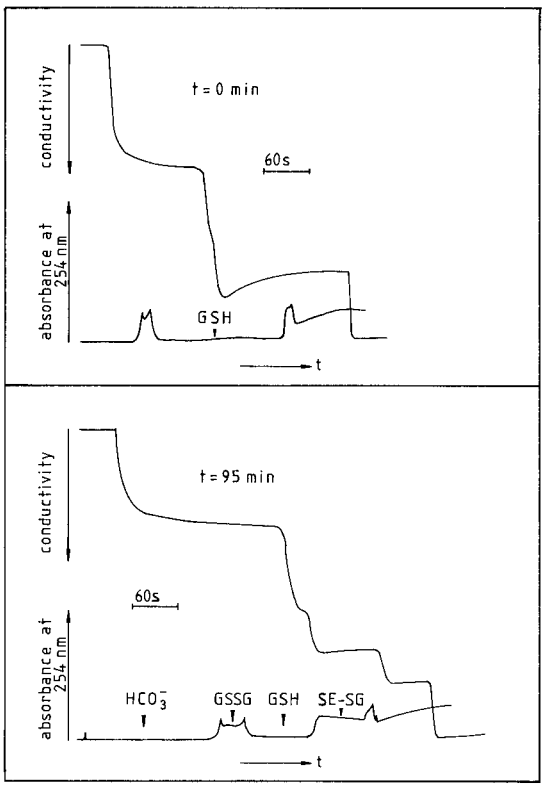

Fig. 1. Isotachopherograms from an incubation of SE (4.4 m*M*) with GSH (5 m*M*) and cytosolic GST (0.3 mg/ml) at $t = 0$ min and 95 min. System A, 23-cm capillary.

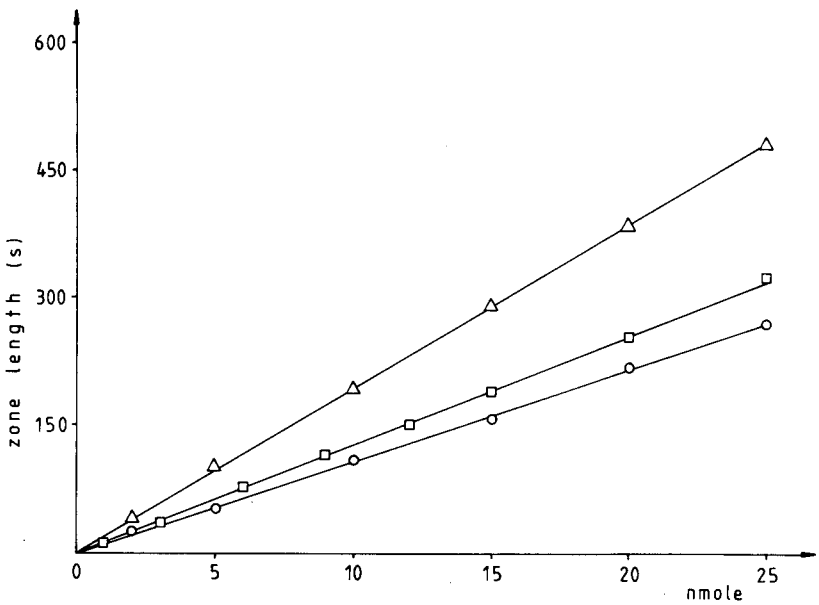

Fig. 2. Calibation graphs for GSH ( ), GSSG (△) and SE-SG (□). System A, 23-cm capillary.

TABLE I

ZONE LENGTHS FOR A SERIES OF SUBSTANCES OBTAINED IN THE TWO ELECTROLYTE SYSTEMS

Substance injected	*Slope of plot (s/nmol)*	
	System A	*System B*
GSH	10.4	7.0
GSSG	18.9	12.1
SE-SG	12.5	–
PGE-SG	13.2	7.7
PNBC-SG	12.8	8.1
EPNP-SG	12.1	7.2
CDNB-SG	11.8	–
CDNB-mercapturic acid	12.0	–

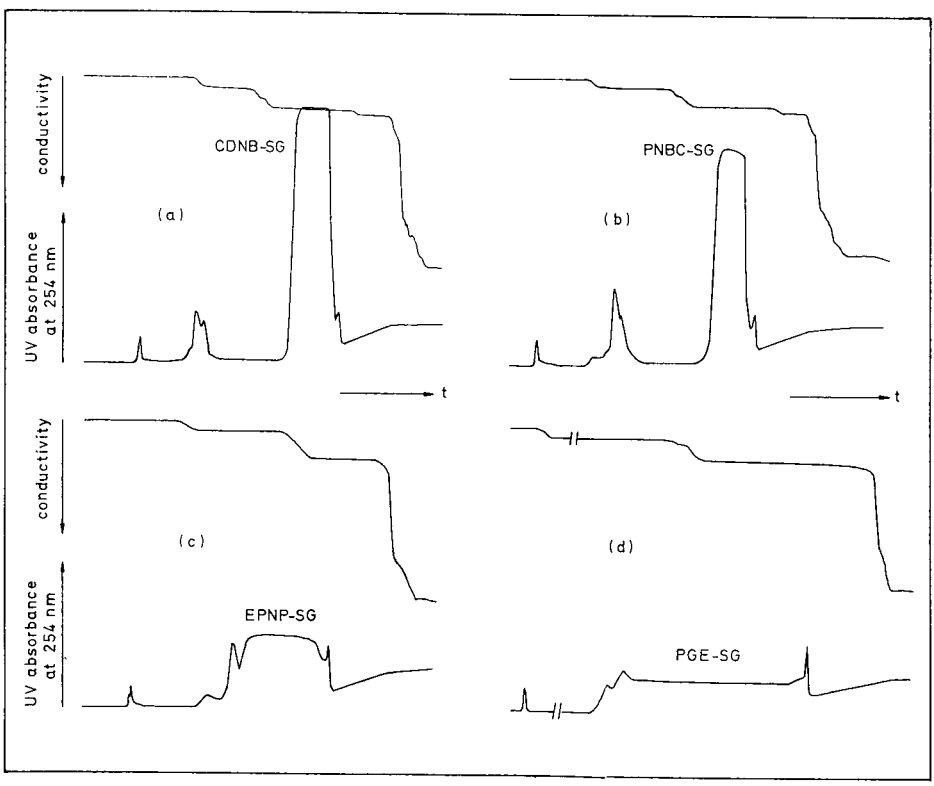

Fig. 3. Isotachopherograms from separate GSH conjugation of (a) CDNB, (b) PNBC, (c) EPNP and (d) PGE in the presence of rat liver cytosolic GST; system A, 23-cm capillary.

was achieved with both systems. Fig. 5a and b show isotachophoretic separations of a mixture of PNBC-SG, PGE-SG and EPNP-SG carried out by using the two electrolyte systems. With both systems a separation of this ternary mixture of GSH conjugates was achieved. The peaks of the GSH conjugates appeared in the same order of migration in both systems (Figs. 4 and 5). Although the GSH conjugates investigated have similar chemical structures, mixtures of at least two conjugates can be clearly separated by using this analytical capillary isotachophoretic method. It was shown that GSH and GSSG in mixtures of GSH conjugates do not disturb the separation of the conjugates. While higher resolution of the GSH conjugates was achieved by using system B, the use of system A led to a more sensitive determination. Differences in resolution between systems A and B as well as between our data and those of Holloway and Battersby[11] may be explained by disturbances from the terminator zone caused by OH^- in our unbuffered terminating electrolyte (high pH).

Generally, GSH conjugates are metabolized to mercapturic acids and excreted in urine or bile after further metabolism in the kidney. Therefore, it was of interest to investigate whether capillary isotachophoresis also allows the determination of mercapturic acids, which are GSH derivatives. Fig. 6 shows an isotachopherogram obtained after complete reaction of 1 m*M* CDNB with a ten-fold molar excess of

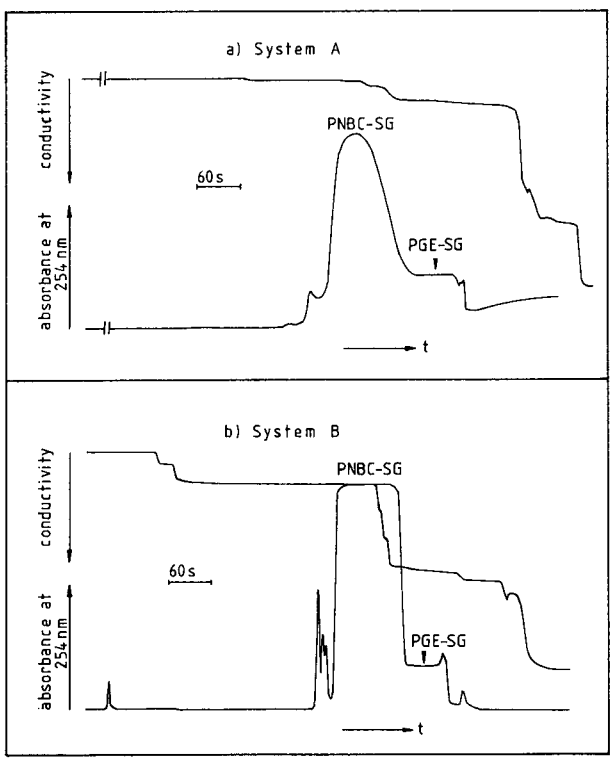

Fig. 4. Isotachopherograms from the separation of a mixture of PNBC-SG and PGE-SG obtained in the electrolyte systems A (a) and B (b).

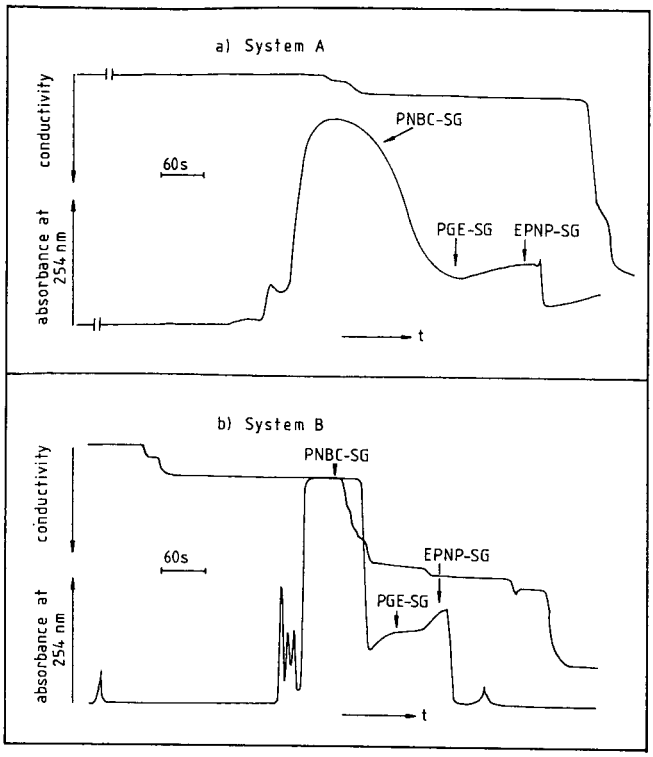

Fig. 5. Isotachopherograms from the separation of a mixture containing PNBC-SG, PGE-SG and EPNP-SG obtained by using the electrolyte systems A (a) and B (b).

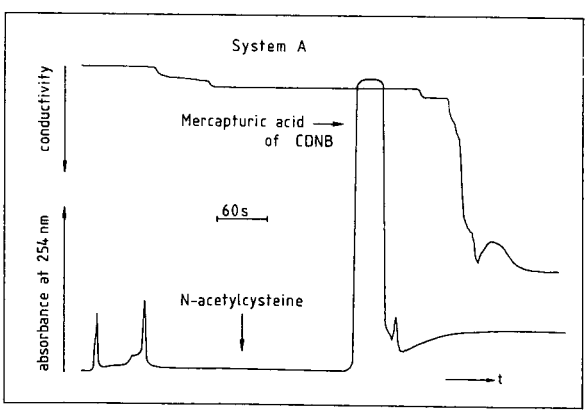

Fig. 6. Isotachopherogram from an incubation of 1 m*M* CDNB with 10 m*M* N-acetylcysteine in alkaline solution after complete reaction.

N-acetylcysteine in alkaline aqueous solution. The mercapturic acid of CDNB appears in the isotachopherogram as a strongly UV-absorbing peak. An addition of GSH, GSSG and CDNB-SG to this mixture resulted in a complete separation of the mercapturic acid from these substances.

The method presented has been applied to the study of reactions for which GSH is a substrate. In Fig. 7 the kinetic profile derived from the isotachophoretic analysis of the enzymatic GSH conjugation of SE at different pH values of the incubation mixture is given. For simplicity, concentration–time courses only of the SE-SG are shown. The decrease in GSH concentration was nearly proportional to the increase of SE-SG. Throughout the incubations the amount of GSSG formed from GSH by autooxidation was negligible (<5%). The higher the pH the higher is the enzymatic and non-enzymatic (not shown) GSH conjugation rate of SE. At pH 9.2 the enzymatic and non-enzymatic reaction rates are equal. This results from the high reactivity of SE and the strong nucleophilicity of the SH group of GSH at high pH values (pK_a SH = 9.2). The pH optimum for the enzymatic GSH conjugation of exogenous and endogenous epoxides was found to be 8.2–8.5[14]. The application of this isotachophoretic method to the determination of GSH stability in various complex media was previously described[14].

The reproducibility and accuracy of the method were checked by repeated isotachophoretic analysis of standard solutions of GSH and EPNP-SG with both electrolyte systems. The specific zone lengths (s/nmol) for GSH obtained from analyses on different days were (mean ± S.D.) 10.38 ± 1.12 for system A (n = 8) and 6.62 ± 0.48 for system B (n = 6). The specific zone lengths (s/nmol) for EPNP-SG determined by injections on different days were found to be (mean ± S.D.) 11.96 ± 0.384 for system A (n = 4) and 7.36 ± 0.45 for system B (n = 4). The standard deviations for GSH and EPNP-SG determined within the same day were of the order of ±0.2.

The sensitivity of the method was sufficient for the accurate detection of 0.1 nmol GSSG, 0.15 nmol GSH, CDNB-SG and PNBC-SG respectively and 0.2 nmol EPNP-SG, when the electrolyte system A was used. The sensitivity could be drastically increased if fluorescence detectors were used. Furthermore, since isotachophoretic

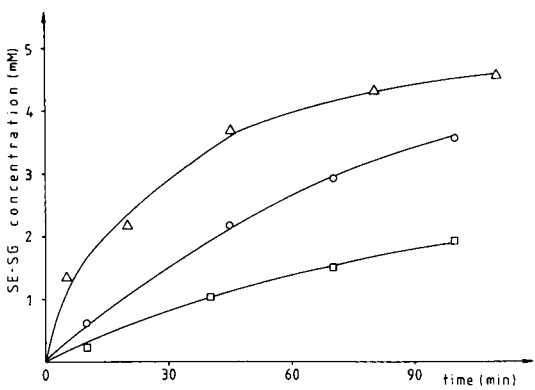

Fig. 7. Kinetic profile derived from the enzymatic GSH conjugation of SE at pH 7.4 (□), 8.5 (○) and 9.2 (△).

analysis of glucuronidation, sulphation and GSH conjugation reactions is possible with the same electrolyte system (system B), we have now started to investigate the applicability of this analytical technique to the simultaneous detection of glucuronides, sulphates and GSH conjugates.

CONCLUSION

The present capillary isotachophoretic method allows a rapid, sensitive and simultaneous determination of at least two GSH conjugates, GSH and GSSG without the need for radioactively labelled compounds or separate analytical procedures. This method also permits the simultaneous determination of GSH conjugates and the corresponding mercapturic acids. The major advantage of this analytical method is its general applicability to the study of reactions involving GSH as substrate.

ACKNOWLEDGEMENTS

The work described constitutes part of the doctoral thesis of D. Tsikas, and was carried out with financial support from the Bundesministerium für Forschung und Technologie (BMFT). The authors thank Miss A. Hofrichter for excellent technical assistance.

REFERENCES

1 W. H. Habig, M. J. Pabst and W. B. Jakoby, *J. Biol. Chem.*, 249 (1974) 7130.
2 E. Boyland and L. F. Chasseaud, *Adv. Enzymol.*, 32 (1969) 172.
3 J. R. Mitchell, D. J. Jollow, W. Z. Potter, D. C. Davis, J. R. Gillette and B. B. Brodie, *J. Pharmacol. Exp. Ther.*, 187 (1973) 185.
4 *IARC Monographs on the Evaluation of Carcinogenic Risk of Chemicals to Man*, 11 (1976) 115.
5 T. Watabe, T. Sawahata and J. Horie, *Biochem. Biophys. Res. Commun.*, 87 (1979) 469.
6 B. Jernström, J. R. Babson, P. Moldéus, A. Holmgren and D. J. Reed, *Carcinogenesis*, 3 (1982) 861.
7 D. Tsikas and G. Brunner, *Chromatographia*, in press.
8 D. Tsikas and G. Brunner, *Fresenius' Z. Anal. Chem.*, in press.
9 R. T. Dobrowsky, G. O'Sullivan, L. M. Ballas, L. N. Fleisher and N. C. Olson, *J. Liq. Chromatogr.*, 10 (1987) 137.
10 C. J. Holloway and R. V. Battersby, in C. J. Holloway (Editor), *Analytical and Preparative Isotachophoresis*, Walter de Gruyter, Berlin, New York, 1984, p. 193.
11 C. J. Holloway and R. V. Battersby, *Electrophoresis*, 7 (1986) 304.
12 M. M. Bradford, *J. Biochem. (Tokyo)*, 72 (1976) 248.
13 C. J. Holloway, S. Husmann-Holloway and G. Brunner, *Electrophoresis*, 2 (1981) 25.
14 D. Tsikas, *Ph.D. Thesis*, University of Hannover, Hannover, 1987.

Journal of Chromatography, 470 (1989) 201–208
Elsevier Science Publishers B.V., Amsterdam — Printed in The Netherlands

CHROM. 21 270

SPACER PERFORMANCE IN THE CATIONIC ISOTACHOPHORESIS OF PROTEINS

FREDERICK S. STOVER
Central Research Laboratories, Monsanto Co., 800 N. Lindbergh Blvd., St. Louis, MO 63167 (U.S.A.)

SUMMARY

Performance of narrow range ampholytes and a discrete spacer mixture is evaluated for improved protein separations by cationic isotachophoresis. A spacer mixture containing 22 cations is developed and relative step heights of components are presented. Different ampholytes and the discrete spacer give unique results for test mixtures of model proteins. While no spacer mixture can be universally recommended, discrete spacers offer the possibility of optimizing separations based on component selection. An example of optimizing a separation of five model proteins is presented.

INTRODUCTION

In a previous paper[1], the potential for cationic isotachophoresis (ITP) separations of proteins in potassium acetate–acetic acid electrolytes was demonstrated. Cationic ITP of proteins is characterized by wide applicability, low μg/ml detection limits and good quantitative linearity. In addition, complete resolution of proteins is seen if relative step height differences (mobility differences) are greater than *ca.* 10%. One difficulty with the method is the visualization of protein resolution from UV signals. While wide range ampholytes are effective for spacing cationic protein mixtures, use of these spacers results in sample/spacer mixing, reduced sensitivity and broadened zone profiles.

Advantages of discrete spacers for protein ITP in anionic systems have been discussed, both for serum[2] and model protein[3] separations. This work investigates the use of narrow range ampholytes and discrete spacer mixtures for improved resolution in cationic protein ITP. A mixture of 22 cations is used for discrete spacing and advantages *vs.* ampholytes are seen. Spacer performance is seen to be mixture-dependent, but optimized separations can be obtained using the flexibility inherent in discrete spacing.

EXPERIMENTAL

Proteins, amino acids, 2-amino-2-methyl-1,3-propanediol (ammediol), galactosamine, tris(hydroxymethyl)aminomethane (Tris) and lyophillized human serum were obtained from Sigma (St. Louis, MO, U.S.A.). Triethanolamine, potassium

0021-9673/89/$03.50

acetate and glacial acetic acid were obtained from Fisher Scientific (Pittsburgh, PA, U.S.A.). Other amines or salts were obtained from either Aldrich (Milwaukee, WI, U.S.A.) or Eastman Kodak (Rochester, NY, U.S.A.).

The 22-ion discrete spacer mixture was prepared by diluting appropriate amounts of the compounds or salts to a final concentration of *ca.* 50 μg/ml of each cation in water. Ampholyte solutions (1%) were prepared by diluting 5 μl LKB Ampholines® (Bromma, Sweden) with 200 μl water. The leading electrolyte was 10 m*M* potassium acetate adjusted to pH 4.5 with 10% acetic acid, and the terminating electrolyte was 10 m*M* acetic acid. Distilled, de-ionized water was used for all spacer and electrolyte dilutions. Model protein mixtures were prepared by diluting weighed amounts in the leading electrolyte. Human serum was reconstituted by diluting 20 mg lyophillized powder with 200 μl water.

Cationic ITP was run on an LKB 2127 Tachophor isotachophoresis instrument using a 200 mm × 0.8 mm PTFE capillary and an LKB 2127-140 conductivity–UV detector. UV detection was performed at 280 nm. Separation currents were 250 μA for 10 min and detection currents were 50 μA. UV and conductivity signals were recorded on a Kipp and Zonen (Delft, The Netherlands) BD-41 strip chart recorder at a chart speed of 1.2 cm/min.

RESULTS AND DISCUSSION

Narrow range ampholytes and discrete spacers were evaluated for their performance in cationic ITP. For discrete cationic spacing, a mixture of 22 alkylammonium ions and amino acids or derivatives thereof was tested. Discrete spacer components and their relative step heights (rsh) are listed in Table I. Numerous compounds tested as spacers were not included in the final mix. Several components failed to

TABLE I

PERCENT RELATIVE STEP HEIGHTS OF SPACER CATIONS AND PROTEINS IN pH 4.5 POTASSIUM ACETATE–ACETIC ACID ELECTROLYTE

	rsh(%)		*rsh(%)*
Tetraethylammonium	42	Dodecylamine	72
Ammediol	47	Dodecyltrimethylammonium	74
Triethanolamine	50	Tributylamine	76
Tris	52	Carbonic anhydrase (CAN)	85
Lysozyme (LYS)	52	Trypsinogen (TRP)	85
Cytochrome *c* (CYC)	53	ε-Aminocaproic acid	87
Lysine	56	8-Aminocaprylic acid	88
Creatinine	57	Tetrabutylammonium	90
Myoglobin (MYO)	57	γ-Aminobutyric acid	94
Histidine	59	Cetyltrimethylammonium	95
Tripropylamine	62	Conalbumin (CAL)	95
Galactose amine	63	Tetrapentylammonium	98
Tetrapropylammonium	67	β-Lactoglobulin B (BLB)	103
Glycylhistidine	68	β-Lactoglobulin A (BLA)	105
Arginine	70	β-Alanine	124
Ribonuclease A (RNA)	71	Ovalbumin (OVA)	150

migrate in the pH 4.5 electrolyte (glycine, glycylglycylglycine, tricine, N-acetylhistidine, betaine). Other cations had high mobilities, which made them inappropriate for spacing proteins (Li^+, ethylenediamine, choline, pyridine, 4-methylmorpholine). Finally, UV absorbance at 280 nm ruled out other potential spacers (diphenylguanidine, 4-hydroxypyridine, adenine).

The final 22-spacer mixture contains components at rsh 42–124%. Spacer mobilities are distributed across this range, but several gaps occur at rsh 76–87 and 98–124%. Relative step heights were determined from injections of single spacer cations, and no attempt was made to assess their separability.

A comparison of mobility distributions for the different spacer solutions tested is shown in Fig. 1. Conductivity traces are given for the electrolyte blank, four ampholyte solutions (pH 3.5–10, 3.5–5, 5–8 and 7–9) and the discrete spacer mixture. As expected, pH 3.5–5 ampholyte contains predominantly low-mobility species while pH 7–9 contains predominantly high-mobility species. The discrete spacer mixture shows a mobility distribution similar to pH 7–9 ampholytes, but with more distinct zones observed on the conductivity trace.

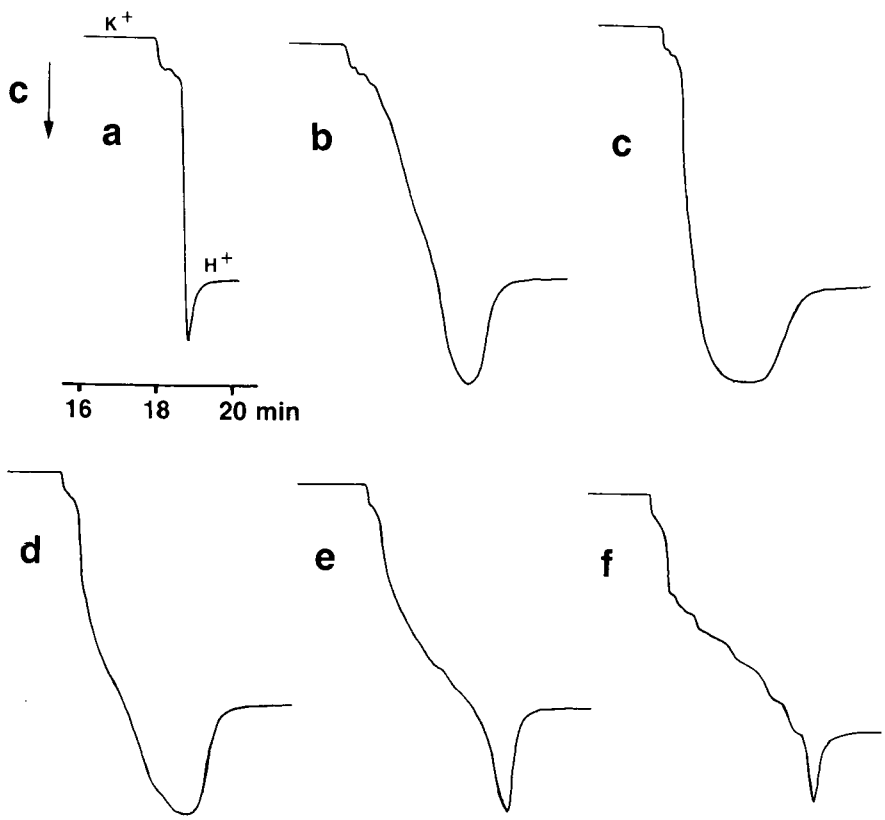

Fig. 1. Isotachopherograms for (a) electrolyte blank and injections of 0.5 μl 1% ampholytes pH, 3.5–10 (b), 3.5–5 (c), 5–8 (d), 7–9 (e) and 5 μl (f) discrete spacer mixture. K^+ = leader, H^+ = terminator. C axis is decreasing conductivity.

TABLE II

SPACER DISTRIBUTION (%) IN DIFFERENT STEP HEIGHT RANGES

rsh(%)	*Ampholyte pH range*				
	3.5–10	*3.5–5*	*5–8*	*7–9*	*Discrete*
<50	17	3	3	9	16
50–100	25	9	26	53	65
>100	58	88	71	38	19

Close inspection of mobility distributions reveals that all ampholytes tested have low mobility components, even pH 7–9 ampholytes. Table II lists the percent of total spacer zones at different rsh values. Narrow range ampholytes have components in all mobility ranges. The polymeric nature of these materials means that low effective mobilities are possible even though all ionized groups are positively charged.

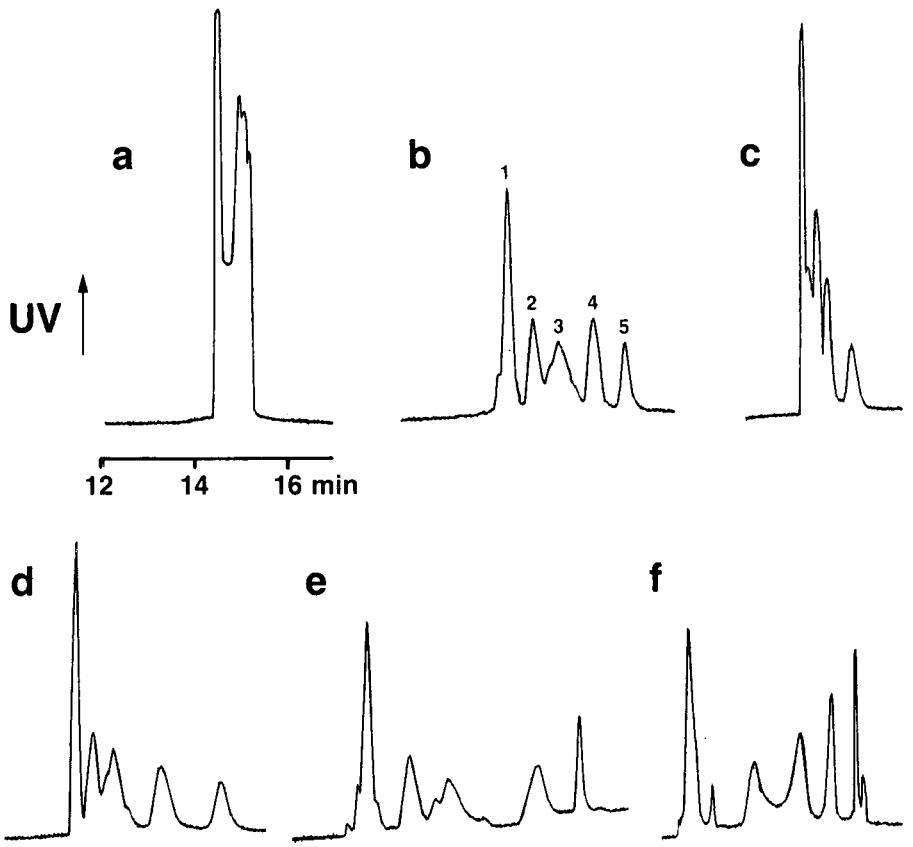

Fig. 2. Isotachopherograms for a mixture of 1 mg/ml LYS (1), 2.2 mg/ml RNA (2), 1.0 mg/ml TRP (3), 1.0 mg/ml BLA (4) and 1.3 mg/ml OVA (5). Spacers injected were (a) none, (b) 2 μl pH 3.5–10, (c) 2 μl pH 3.5–5, (d) 2 μl pH 5–8, (e) 2 μl pH 7–9 and (f) 10 μl discrete spacers. Volume protein mixture injected is (a) 4 μl, and (b)–(e) 2 μl. UV axis is increasing absorbance at 280 nm.

To test the performance of the different spacer solutions, a mixture of model proteins with disparate mobilities at pH 4.5 was separated. Fig. 2 shows the UV traces obtained from injections of a mixture of LYS, RNA, TRP, BLA and OVA. Good resolution of these five proteins is obtained with all spacers except pH 3.5–5 ampholytes. This narrow range spacer has insufficient high mobility components to space proteins other than OVA. Wide range ampholytes also give good spacing, but with considerable dilution and broadening of the peaks. pH 5–8 ampholytes give less broadening of LYS, but small impurity peaks seen with other spacers are unresolved.

Best resolution of this mixture is obtained with pH 7–9 ampholytes or discrete spacers. With pH 7–9 ampholytes, three impurity peaks near LYS and two near TRP are resolved. Little broadening is seen for well resolved OVA. Discrete spacers also give good resolution of the five proteins, with BLA and OVA showing less broadening than with ampholytes. However, RNA and TRP show distinct mixing. The apparently resolved impurity trailing OVA in Fig. 2f is a spacer impurity.

Fig. 2 reveals several important points regarding the use of these spacers for cationic ITP. Narrow range pH 7–9 ampholytes contain sufficient low mobility components to yield high overall resolution. Since the p*I* range of proteins separated is 4.8–11, this narrow range ampholyte can space proteins with p*I* values much less than the pH range indicated for isoelectric focusing. Similar observations of the utility of narrow range ampholytes at pH values different from the indicated p*I* range were made for anionic spacing[4]. Secondly, sharp peaks can be obtained with a discrete spacer mixture *vs.* ampholytes. Such separations may be useful for obtaining the desired resolution of a single component or for maximizing sensitivities to specific proteins.

The effect of increasing the volume of discrete spacers on the above model protein separation is shown in Fig. 3. A minimum of 10 μl spacers gives good resolution of the five proteins. A 20-μl volume allows separation of some impurity peaks near LYS, but both LYS and TRP show extreme broadening at this spacer loading.

Unspaced cationic ITP showed sensitivities in the 50 ng range for model proteins[1]. Higher resolution separations with wide range ampholyte spacing gave decreased UV sensitivities due to spacer/sample mixing. Fig. 4 shows separations of the above model protein mixture at different loadings to assess sensitivity with discrete

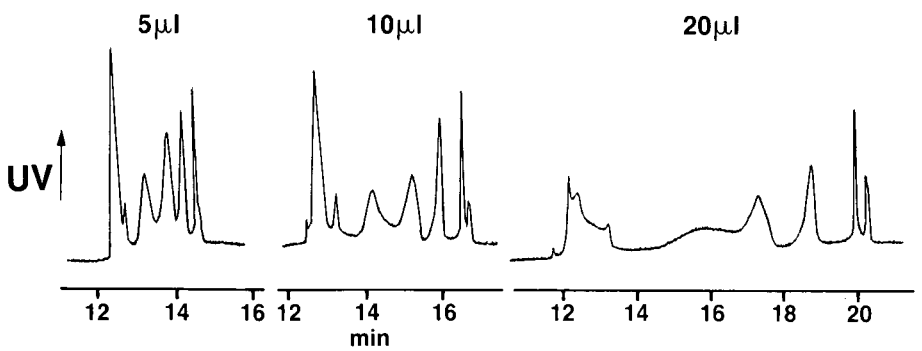

Fig. 3. Isotachopherograms for 2 μl protein mixture from Fig. 2. Volume discrete spacers added is noted in the figure. UV axis same as in Fig. 2.

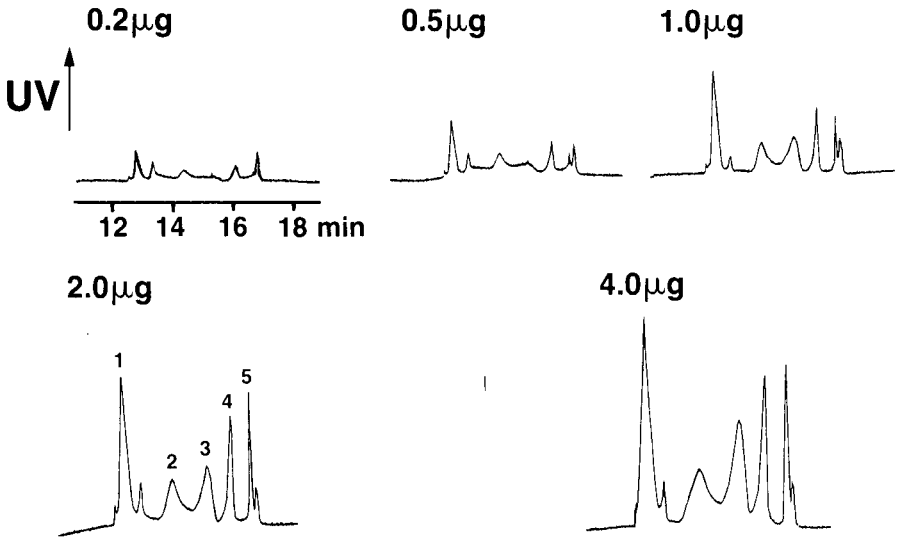

Fig. 4. Isotachopherograms for protein mixture from Fig. 2 with 10 μl discrete spacers. Approximate μg of each protein injected is noted in the figure. UV axis same as Fig. 2.

spacers. Estimated detection limits are 100–500 ng for individual proteins. Approximate quantitative linearity is observed on the basis of peak area over the concentration range studied. Some decrease in resolution is seen with increasing sample load. For example, injection of $\leqslant 2$ μl of the protein mixture is necessary to obtain baseline resolution of BLA and TRP.

To determine if the relative performance of the different spacers depends on sample composition, a second mixture of MYO, CYC, CAN, CAL and BLB was studied. Fig. 5 shows the separations obtained without spacers, with pH 3.5–10 and

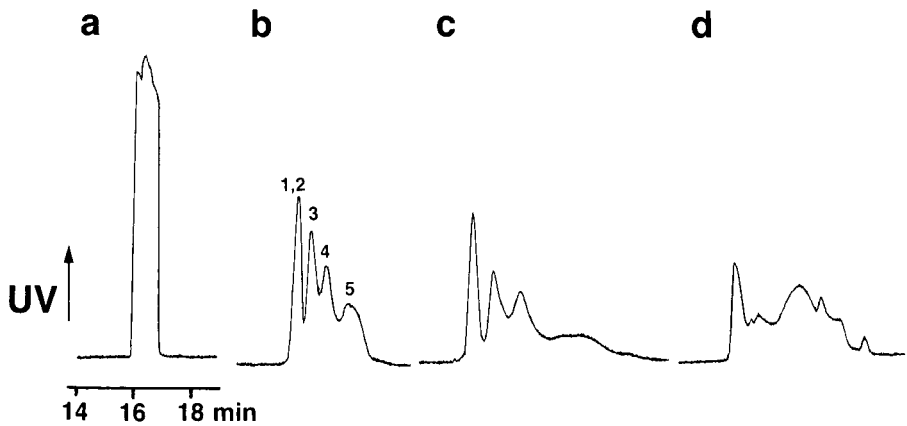

Fig. 5. Isotachopherograms for a mixture of 1.0 mg/ml MYO (1), 1.2 mg/ml CYC (2), 1.3 mg/ml CAN (3), 1.9 mg/ml CAL (4) and 1.1 mg/ml BLB (5). Spacers injected were (a) none, (b) 2 μl pH 3.5–10, (c) 2 μl pH 7–9 and (d) 10 μl discrete spacers. Volume protein mixture injected is (a) 4 μl, and (b)–(d) 2 μl. UV axis same as Fig. 2.

7–9 ampholytes and with discrete spacers. Poorer spacing performance is seen than in the previous mixture, with MYO and CYC unresolved with any spacer used. Differences also are noted concerning the relative performance of the spacers. pH 7–9 ampholytes give considerable dilution of BLB, rendering it less useful than pH 3.5–10 ampholytes. Poorer performance of discrete spacers also is seen, despite the resolution of an impurity between CAL and BLB. Thus, relative spacer performance is mixture-specific, and no spacer can be generally recommended.

Cationic ITP was tested on reconstituted serum and the results are shown in Fig. 6. Unspaced serum gives essentially a single zone with little UV resolution. Wide range ampholytes yield only two, poorly defined peaks that are considerably diluted. The discrete spacers separate four distinct peaks, with the trailing zone being particularly sharp. No attempt was made to identify the resolved peaks.

Fig. 6d shows a separation of reconstituted serum with a larger amount of spacer applied. The broad leading peak seen in Fig. 6c is not detected, but several sharp leading peaks are seen. These peaks have heights and relative positions that are not particularly reproducible, suggesting a non-steady-state situation. Preliminary serum separations shown in Fig. 6 compare poorly with similar anionic separations. However, the potential for cationic serum separations is seen, and specific components may benefit from cationic *vs.* anionic analysis.

It is apparent that for complex mixtures of proteins, separate runs with different spacer solutions are desirable to assess ultimate separability. Kenndler and Reich[5] used cluster analysis to indicate the best 2 or 3 electrolyte systems for testing anionic ITP separations of organic and inorganic acids. A similar analysis of different discrete spacer mixtures and ampholytes with a variety of protein mixtures could yield a small, optimum set to test protein separability.

One advantage of discrete spacers is the ability to fine-tune spacer compositions to achieve desired separations. Judicious selection of spacer components can yield better performance, as shown in Fig. 7 for an optimized separation of LYS, RNA, TRP, BLA, and OVA. Despite preliminary knowledge of spacer mobilities (Table I), such an optimization is largely a trial-and-error operation. For instance, determina-

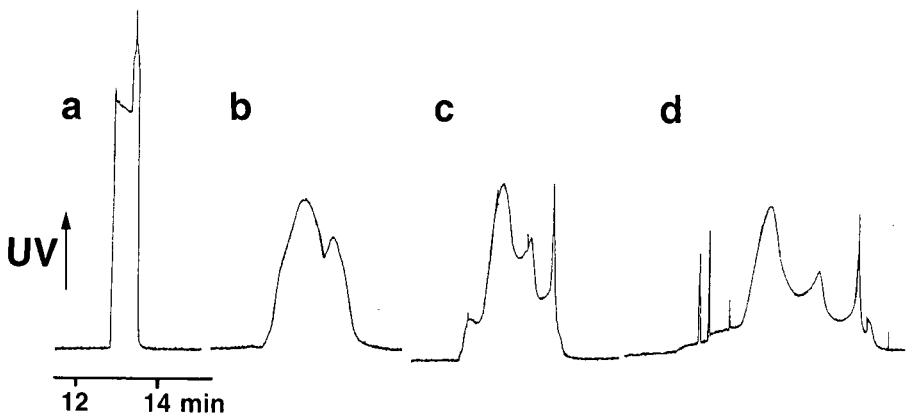

Fig. 6. UV isotachopherograms of 1 μl reconstituted human serum diluted 1:1 with leading electrolyte. Spacers injected are (a) none, (b) 2 μl pH 3.5–10, (c) 10 μl and (d) 20 μl discrete spacers. UV axis same as Fig. 2.

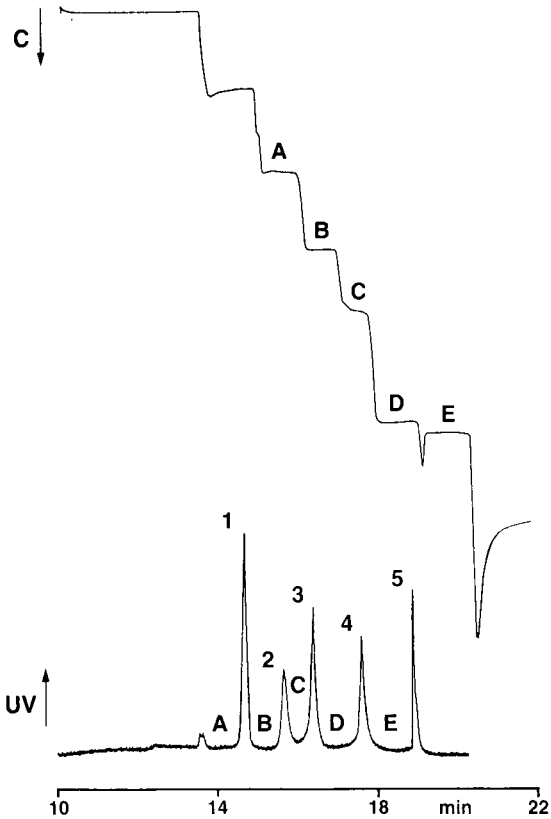

Fig. 7. Isotachopherograms for 2 μl of protein mixture from Fig. 2 with optimized, discrete spacing. Spacers are 2 μg each (A) tetraethylammonium, (B) tripropylammonium, (C) tributylammonium, (D) tetrapentylammonium and (E) γ-aminobutyric acid. C axis of upper trace is decreasing conductivity and UV axis is increasing absorbance at 280 nm. Time offset in conductivity and UV signals is due to physical separation of detectors in the capillary.

tion of single cationic mobilities gave no indication that BLA is enforced by γ-aminobutyric acid or that OVA is enforced by β-alanine. To date, no spacers can be recommended for separating the following proteins with pH 4.5 potassium acetate–acetic acid electrolytes: LYS, MYO and CYC; TRP and CAN; and BLB and BLA.

REFERENCES

1 F. S. Stover, *J. Chromatogr.*, 445 (1988) 417.
2 T. Yagi, K. Kojima, M. Yagi and Y. Kajita, in H. Hirai (Editor) *Electrophoresis '83*, Walter DeGruyter, Berlin, 1984, p. 503.
3 S. Husmann-Holloway and E. Borriss, *Fresenius Z. Anal. Chem.*, 311 (1982) 465.
4 F. M. Everaerts, J. Beckers and Th. P. E. M. Verheggen, *Isotachophoresis–Theory, Instrumentation and Applications*, Elsevier, Amsterdam, 1976, p. 326.
5 E. Kenndler and G. Reich, *Anal. Chem.*, 60 (1988) 120.

Journal of Chromatography, 470 (1989) 209–221
Elsevier Science Publishers B.V., Amsterdam — Printed in The Netherlands

CHROM. 21 222

ISOTACHOPHORETIC ANALYSIS OF PEPTIDES

SELECTION OF ELECTROLYTE SYSTEMS AND DETERMINATION OF PURITY

VÁCLAV KAŠIČKA and ZDENĚK PRUSÍK*
Institute of Organic Chemistry and Biochemistry, Czechoslovak Academy of Sciences, Flemingovo nám. 2, 166 10 Prague 6 (Czechoslovakia)

SUMMARY

Capillary isotachophoresis (ITP) was applied to the qualitative and quantitative analysis of both natural and synthetic oligo- and polypeptides. Based on the mathematical model of acid–base equilibria for a general ampholyte, a procedure and a computer program for the calculation of the pH dependence of the effective and specific charge and effective mobility of peptides with known amino acid sequence were developed which allow the selection of electrolyte systems for peptide isotachophoretic analysis to be rationalized.

Basic peptides (bovine pancreatic trypsin inhibitor, bull seminal isoinhibitors of trypsin, arginine vasopressin and adamantylamide–alanylisoglutamine) were analysed with a cationic ITP system at acidic pH. Neutral and acidic peptides (insulin, proinsulin, bull seminal isoinhibitors of trypsin, cow colostrum isoinhibitors of trypsin) were analysed with an anionic ITP system, mostly at alkaline pH.

Peptide purity (electrophoretic homogeneity) was determined from the ITP degree of purity defined by a peptide itself and the zone length ratio of its admixtures. Enrichment of peptide in the sample during the purification procedure was measured by its zone length relative to unit mass of the amount of sample analysed.

INTRODUCTION

In the chemistry of peptides, capillary isotachophoresis (CITP) is most frequently used as a method to control the purity of both natural and synthetic peptide preparations. Utilization of CITP for this purpose was introduced by Kopwillem *et al.*[1,2] in the analysis of the fragments of human growth hormone. Following this work, CITP has been used for the analysis of many other naturally occurring and/or synthetically prepared biologically active peptides, *e.g.*, hormones [oxytocin, vasopressin, adrenocorticotropic hormone (ACTH)[3] and insulin[4,5], drugs[6,7], nutritional additives[8,9] and others[10–18]. CITP was used not only as a method to control the purity of the final peptide preparation but also for monitoring the peptide purity after individual steps in a purification procedure, thus providing information on the

0021-9673/89/$03.50

efficiency of the preparative separation method used. In addition, CITP has also been used for the determination of low-molecular-weight ionic admixtures in peptide preparations[19,20].

The aim of this work was to apply CITP to the determination of the purity of several peptide preparations either isolated from a natural material or synthesized, *e.g.*, enzyme inhibitors, hormones, protein fragments and immunomodulators. In order to rationalize the selection of the conditions for ITP analyses of peptides, a procedure and a computer program for the calculation of the pH dependence of the effective and specific charges of peptides was developed and rules for the selection of the pH of the leading electrolyte were established.

THEORETICAL

For the rational selection of conditions for peptide ITP analysis, it is advantageous to know the dependence of their effective or specific charge on pH. Therefore, we have developed a procedure and a computer program that make it possible to calculate the pH dependence of the effective and specific charges of any peptide the amino acid sequence of which is known. The procedure is based on a mathematical model of the acid–base equilibria of a general ampholyte.

Let X(M) and X(N) be ionic forms of peptide X with a maximum charge M and a minimum charge N. The magnitude of the charge is considered in elementary units, including the sign, *i.e.*, maximum and minimum are meant in the mathematical sense. If $K(J)$ is the apparent dissociation constant of the equilibria between the components with charge $(J+1)$ and J, then

$$\mathrm{X}(J+1) \rightleftharpoons \mathrm{X}(J) + \mathrm{H}^+ \tag{1}$$

$$K(J) = c_{\mathrm{X}(J)} \cdot H / c_{\mathrm{X}(J+1)} \tag{2}$$

where $c_{\mathrm{X}(J)}$ and $c_{\mathrm{X}(J+1)}$ are the equilibrium concentrations of the corresponding ionic forms of peptide X and H is the equilibrium concentration of hydrogen ions. Further, the molar fraction, $D_{\mathrm{X}(J)}$, of the component X(J) is introduced, referred to the total concentration c_{X} of peptide X:

$$D_{\mathrm{X}(J)} = c_{\mathrm{X}(J)} / c_{\mathrm{X}} \tag{3}$$

This formulation[21] permits the derivation of the following relationship for the molar fraction $D_{\mathrm{X}(J)}$:

$$D_{\mathrm{X}(J)} = \frac{\left[\prod_{l=0}^{J-1} K(l)/H^{|J|}\right]^{-1} \cdot (J>0) + \left[\prod_{l=J}^{-1} K(l)/H^{|J|}\right] \cdot (J<0)}{1 + \sum_{i=N}^{-1} \prod_{l=i}^{-1} K(l)/H^{|i|} + \sum_{i=1}^{M} \left[\prod_{l=0}^{i-1} K(l)/H^{|i|}\right]^{-1}} \tag{4}$$

$J \in \langle N, M \rangle$, $J \neq 0$

where $K(l)$ are dissociation constants of the acid–base equilibria between the components $X(l+1)$ and $X(l)$, and i and l are auxiliary variables.

The effective charge, z_X, of compound X at a given pH is then given by the equation

$$z_X = \sum_{J=N}^{M} J \cdot D_{X(J)} \tag{5}$$

where $D_{X(J)}$ is given by eqn. 4 in which $H = 10^{-pH}$. From the effective charge, z_X, the specific charge, $z_{X,s}$, may be calculated, *i.e.*, the charge referred to unit relative molecular mass, M_X, of the peptide X:

$$z_{X,s} = z_X/M_X \tag{6}$$

In addition to the effective or specific charge, we can also calculate the effective mobilities, m_X, of peptide X as a function of pH, if known or estimated values of the actual mobilities, $m_{X(J)}$, of individual ionic forms $X(J)$ are available:

$$m_X = \sum_{J=N}^{M} \text{sign}(J) \cdot m_{X(J)} \cdot D_{X(J)} \tag{7}$$

where $D_{X(J)}$ is given by eqn. 4 in which $H = 10^{-pH}$.

From the obtained dependences of effective mobility, effective charge and specific charge on pH, important conclusions can be inferred for the selection of conditions for the ITP separation of peptides and proteins. For the ITP separation the only pH that is suitable is that at which the effective mobilities are sufficiently high, *i.e.*, if their absolute values are approximately higher than $1 \cdot 10^{-9}$–$2 \cdot 10^{-9}$ $m^2\ V^{-1}\ s^{-1}$ (ref. 22), having the same sign, *i.e.*, moving in the same direction (either cationic or anionic), and the differences in their mobilities, Δm, are sufficient for their separation, *i.e.*, $\Delta m \approx 1 \cdot 10^{-9}$ $m^2\ V^{-1}\ s^{-1}$ (ref. 23).

If only the dependence of specific charge on pH is known, then a pH for separation is selected such that the absolute value of the specific charge of the peptide to be separated is greater than $2 \cdot 10^{-4}$–$5 \cdot 10^{-4}$ e (ref. 24).

From the course of the calculated dependence of effective and/or specific charge on pH, the regions of minimum and maximum charge, the regions important for influencing the charge and the isoionic (isoelectric) point can be determined.

Fig. 1 shows the calculated pH dependence of the effective charge of pig insulin. Based on its amino acid sequence[25], the ionogenic groups and the values of the minimum and maximum charge of fully ionized forms of insulin ($N = -10$, $M = +6$) were determined. The average values from the pK ranges of amino acid residues in polypeptide chains[26] were used as values of the dissociation constants of ionogenic groups present in insulin. This leads to a certain inaccuracy because the pK values of individual ionogenic groups can be different not only in different peptides but also in the molecule of the same peptide, as a consequence of the electrostatic and configurational effects of their environment. This inaccuracy and the fact that we consider only the charges formed by dissociation or association of hydrogen ions and

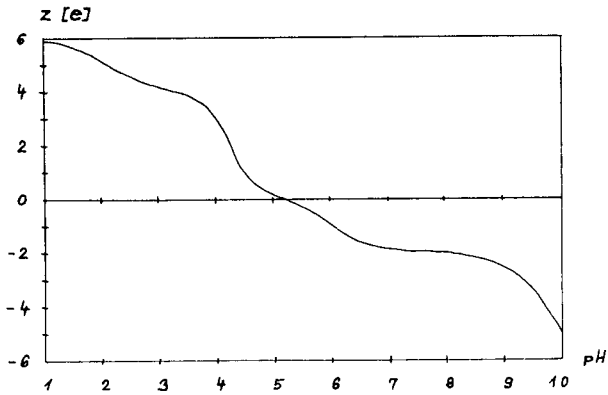

Fig. 1. Calculated pH dependence of effective charge z of insulin (for more details, see text).

not the charges formed by interaction of the peptide with other ions present in solution accounts for the difference between the calculated isoelectric (isoionic) point (5.2) and the experimentally determined values 5.3–6.15[27].

From the course of the pH dependence of the specific charge, z_s, of insulin (see Fig. 2), the pH region of sufficient charge density, *i.e.*, $z_s > 2 \cdot 10^{-4}$–$5 \cdot 10^{-4}\,e$ can be determined. Comparison of the specific charges of insulin and glycine in Fig. 2 allows the ability of glycine to serve as a terminating ion to be judged. Glycine can be considered as a candidate for a terminating ion in the region where its specific charge is lower than that of insulin but greater than the minimum specific charge required for sufficient electrophoretic mobility.

In spite of the inaccuracy of the model, the calculation affords useful information; the calculated isoionic point and the dependences of both the effective and specific charges of insulin of pH were important characteristics that were taken into account in the selection of conditions for its ITP analysis (see Experimental).

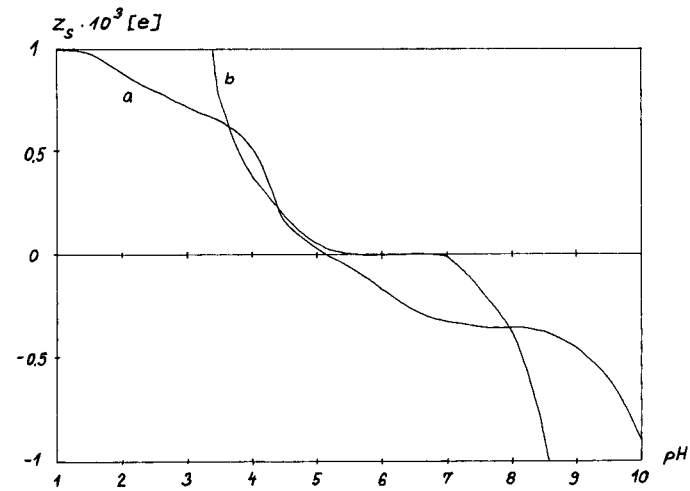

Fig. 2. Calculated pH dependence of specific charge (z_s) of (a) insulin and (b) glycine.

The inaccuracy (given by the inaccuracy of the chosen pK values) and the complexity of the calculation increase with increasing number of ionogenic groups in the molecule. Therefore, the calculation could afford more reliable data for oligopeptides than for polypeptides and proteins. With polypeptides and proteins it is more advantageous to use the electrophoretic titration curves[28], which, however, cannot be obtained for small peptides (up to 20–30 amino acids) as a consequence of the difficulties with their fixation and staining in the gel. Hence both methods, *i.e.*, based on theoretical calculation and experimental titration curves, are complementary, covering a wide range of relative molecular masses of peptides and proteins.

The separation conditions and the pH of the leading electrolyte must be selected not only according to the effective or specific charge of the peptides to be separated, but also with respect to their solubility, stability and biological activity. For the correct choice of the pH of leading electrolyte, the following rules should be adopted: let pH_1 be the pH range compatible with the ITP separation principle (*ca.* 2–11); let pH_2 be the pH range of sufficient solubility of the given peptides (at least about 1 mmol/l); let pH_3, be the pH range in which the given peptides are chemically stable; let pH_4 be the pH range in which the biological activity of the given peptides is preserved; let pH_5 be the pH range in which the given peptides possess sufficient effective mobility or sufficient specific charge of the same sign, *i.e.*, $|m_{ef}| > 1 \cdot 10^{-9}$ m^2 V^{-1} s^{-1} or $|z_s| > 2 \cdot 10^{-4}$–$5 \cdot 10^{-4}$ e; and let pH_6 be the pH range in which the relative differences in the effective mobilities of the peptides (Δm_{ef}) are sufficient for their separation ($\Delta m_{ef} \geqslant$ 2–3%). Then, the pH range suitable for the ITP separation of these peptides pH (ITP, PEP) is given by the multiplication in the algebraic sense of classes (logical product) of the above ranges:

$$\text{pH (ITP, PEP)} = \bigcap_{i=1}^{6} (\text{pH}_i) \tag{8}$$

If the conservation of biological activity for a given ITP peptide separation is not required (*e.g.*, for amino acid and sequence analyses even denaturated polypeptides suffice), then the pH_4 interval is not included in the logical product[8].

EXPERIMENTAL

Chemicals

All chemicals were of analytical-reagent grade. Sodium hydroxide, potassium hydroxide, acetic acid and glycine were obtained from Lachema (Brno, Czechoslovakia), N-2-hydroxyethylpiperazine-N′-2-ethanesulphonic acid (HEPES), tris-(hydroxymethylaminomethane) (Tris) from Serva (Heidelberg, F.R.G.), β-alanine (BALA) from Koch-Light (Colnbrook, U.K.), histidine (His) from Pierce (Rockford, IL, U.S.A.), poly(vinyl) alcohol (PVA) (Mowiol) from Hoechst (Frankfurt, F.R.G.) and barium hydroxide from Merck (Darmstadt, F.R.G.).

Bovine pancreatic trypsin inhibitor (BPTI) (Trasylol) was purchased from Bayer (Leverkusen, F.R.G.), pig proinsulin from Novo (Bagsvaerd, Denmark) and insulin and adiuretin ([8-D-Arg]deaminovasopressin) from Léčiva Pharmaceuticals (Prague, Czechoslovakia).

The other samples were obtained from laboratories where they were isolated

from natural material or synthesized. Bull seminal isoinhibitors of trypsin BUSI II[29], BUSI IIb[30], BUSI IA, IB1, IB2[31], cow colostral isoinhibitors of trypsin CTI A, B, C[32] and bovine basic pancreatic inhibitor of trypsin BPTI[33] were obtained from Dr. D. Čechová and Dr. V. Jonáková (Institute of Molecular Genetics, Czechoslovak Academy of Sciences, Prague, Czechoslovakia). Tryptic and cyanogen bromide fragments of human haemopexin[34,35] were obtained from Dr. B. Meloun and Dr. L. Morávek and muramine dipeptide (Mur–Ala–Gln)[36] from Dr. J. Ježek (Institute of Organic Chemistry and Biochemistry, Czechoslovak Academy of Sciences, Prague, Czechoslovakia). Adamantylamide-L-alanyl-D-isoglutamine[37] was provided by Dr. M. Flégl (Pharmacological Institute, Czechoslovak Academy of Sciences, Prague, Czechoslovakia).

Apparatus

All ITP analyses were performed in an apparatus of our own construction[38]. It is an all-PTFE capillary-type ITP analyser equipped with two universal potential gradient detectors and a specific UV photometric detector operated at 254 nm. The separation capillary (23 cm × 0.45 mm I.D. × 0.7 mm O.D.) is placed in a thermostated bath filled with Savant EC 123 electrophoresis coolant. Its temperature is controlled over the range 7–25°C by Peltier thermocouples. Samples were introduced by means of a dosing valve (constant volume 2 μl) or with a Hamilton microsyringe (0.5–10.0 μl).

RESULTS AND DISCUSSION

CITP was used for both qualitative and quantitative analysis of selected oligo- and polypeptides. CITP was utilized not only for determination of purity (electrophoretic homogeneity) of peptides both isolated from natural material and synthesized, but also for the analysis of complex polypeptide mixtures of protein fragments resulting from enzymatic and chemical protein cleavage. Further, CITP was applied to monitoring the efficiency of peptide purification procedures.

A survey of peptides analysed in the cationic mode is shown in Table I and in the anionic mode in Table II; qualitative and quantitative characteristics of the peptides are also given. As a qualitative index the relative step height (*RSH*)[39] of the analysed peptide was used, defined by

$$RSH = [(h_P - h_L)/(h_T - h_L)] \cdot 100 \tag{9}$$

where h_L, h_P and h_T are the step heights (voltage of the potential gradient detector) of the leading electrolyte, peptide sample and terminating electrolyte, respectively.

As a quantitative index of the purity (electrophoretic homogeneity) of peptides, the so-called ITP degree of purity was adopted[3]. Let l_S represent the total zone length of all zones having absorption at a given wavelength of the UV detector on an isotachophoregram for the analysis of peptide sample S, and l_A the length of the zone of peptide A, representing the main component of the sample S (see Fig. 3). Then the ITP degree of purity of peptide A, p_A, is given by the ratio of the lengths l_A and l_S:

$$p_A = (l_A/l_S) \cdot 100 \tag{10}$$

TABLE I

SURVEY OF PEPTIDES ANALYSED IN THE CATIONIC ITP MODE

ES No. = electrolyte system number; *RSH* = relative step height; *p* = ITP degree of purity (*RSH* and *p* are average values of two experiments). HOAc = acetic acid.

ES No.	*Leading electrolyte*				*Terminating electrolyte*				*Sample*	*RSH (%)*	*p (%)*
	L:	*leading ion constituent (mol/l)*		*pH*	*T:*	*terminating ion constituent (mol/l)*		*pH*			
	C:	*counter ion constituent (mol/l)*			*P:*	*pH-adjusting constituent (mol/l)*					
	A:	*additive (%, w/v)*									
1	L:	NaOH	0.01	4.8	T:	BALA	0.01	4.5	Bovine pancreatic trypsin		
	C:	HOAc			P:	HOAc			inhibitor (BPTI)	33.3	73.9
	A:	PVA	0.02						Bull seminal trypsin inhibitors:		
									BUSI II	42.9	72.7
									BUSI IIb	31.4	69.4
2	L:	NaOH	0.01	5.0	T:	BALA	0.01	4.7	Adiuretin ([8-D-Arg]deamino-		
	C:	HOAc			P:	HOAc			vasopressin)	81.7	90.4
3	L:	KOH	0.005	5.0	T:	BALA		5.0	Adamantylamide–L-alanyl-D-		
	C:	HOAc			P:	HOAc			isoglutamine	82.5	88.2

TABLE II

SURVEY OF PEPTIDES ANALYSED IN THE ANIONIC ITP MODE

ES No. = electrolyte system number; *RSH* = relative step height; *p* = ITP degree of purity (*RSH* and *p* are average values of two experiments).

ES No.	*Leading electrolyte*				*Terminating electrolyte*				*Sample*	*RSH (%)*	*p (%)*
	L:	*leading ion constituent (mol/l)*		*pH*	*T:*	*terminating ion constituent (mol/l)*		*pH*			
	C:	*counter ion constituent (mol/l)*			*P:*	*pH-adjusting constituent (mol/l)*					
	A:	*additive (%, w/v)*									
4	L:	HCl	0.005	6.1	T:	HEPES	0.01	8.1	Muramine dipeptide		
	C:	His	0.01		P:	$Ba(OH)_2$			(Mur–Ala–Gln)	32.8	88.0
	A:	PVA	0.2								
5	L:	HCl	0.01	6.1	T:	HEPES	0.01	8.1	Tryptic fragments of human		
	C:	His	0.02		P:	$Ba(OH)_2$			haemopexin	–	–
6	L:	HCl	0.005	8.1	T:	Gly	0.01	10.5	Bull seminal trypsin inhibitors:		
	C:	Tris	0.01		P:	$Ba(OH)_2$			BUSI IA	12.3	76.4
	A:	PVA	0.02						BUSI IB1	12.3	61.3
									BUSI IB2	12.2	83.0
									Cow colostral trypsin inhibitors:		
									CTI A	33.3	34.9
									CTI B	44.1	51.1
									CTI C	54.7	46.8
									Pig insulin	33.3	79.5
									CNBr fragments of human		
									haemopexin	–	–
7	L:	HCl	0.005	8.1	T:	Gly	0.01	10.2	Pig insulin	15.2	69.2
	C:	Tris	0.01		P:	$Ba(OH)_2$			Pig proinsulin	50.0	87.3
	A:	2-propanol 10% (v/v)									

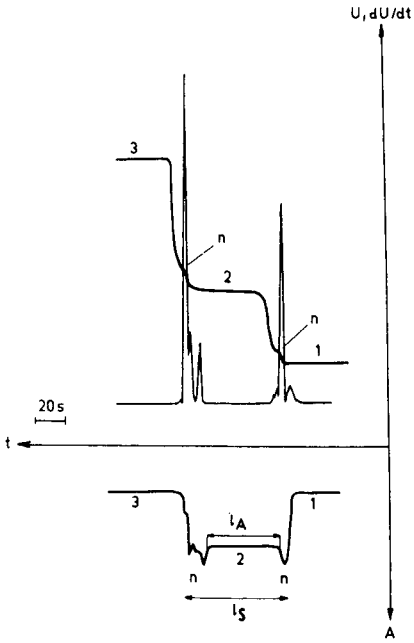

Fig. 3. Determination of ITP degree of purity of bull seminal trypsin isoinhibitor (BUSI II). l_A = Zone length of pure BUSI II; l_S = total length of UV-positive zones. 1 = Na^+; 2 = BUSI II; 3 = BALA; n = unidentified sample admixtures. A = Absorbance at 254 nm; U = voltage of PG detector; t = time; dU/dt = differentiation of PG detector signal. Analysis in ES No. 1 (see Table I); 9 μg of BUSI II in 2 μl of leading electrolyte were applied.

However, the zone lengths of possible impurities from the electrolyte system must not be included in the total length l_S. The lengths of these impurity zones can be determined during the blank run of the ITP analysis without the application of a sample. The degree of purity defined in this manner can be approximately identified with the molar fraction of the given peptide in the analysed mixture. This approximation is the more precise the closer are the charges and the effective mobilities of the components present and the higher is the proportion of the main component in the sample. This requirement is fulfilled to a considerable extent with peptide preparations purified to a relatively high degree. The error caused by this approximation is in the range of units of percent and in some instances [with equal values of the charge, close effective mobilities (deviations up to several percent) and at a relatively low mobility of the counter ion of the leading electrolyte] it can be almost negligible[40,41].

The degree of purity or the ratio of concentrations of individual components can therefore be approximately determined even without standards of individual compounds, merely on the basis of the ratio of zone lengths. This is an advantage of ITP over high-performance liquid chromatography, because in chromatographic analysis with photometric detection at one constant wavelength (254 or 280 nm) the concentration ratios of individual components cannot be determined without a knowledge of their molar absorption coefficients.

Some examples of peptide ITP analyses are given. Fig. 4 shows the ITP analysis

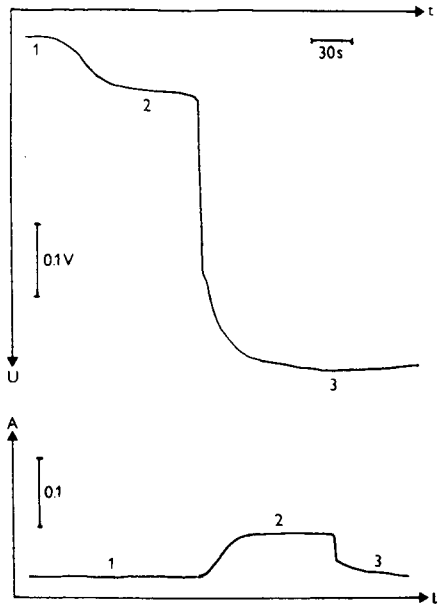

Fig. 4. ITP analysis of pig insulin. 1 = Carbonates; 2 = pig insulin; 3 = glycine. A = Absorbance (at 254 nm); U = voltage of PG detector; t = time. Analysis in ES No. 6 (see Table II); 10.2 μg of pig insulin in 3 μl of leading electrolyte were applied. Separation current, 50 μA; detection current, 20 μA; time of analysis, 30 min.

of pig insulin, the conditions of which and the pH of the leading electrolyte (pH_L) were selected according to the following parameters described and calculated under Theoretical:

(1) Isoelectric (isoionic) point pI: 5.2–6.15 $\Rightarrow$ pI − 1.5 > pH_L > pI + 1.5, *i.e.*, 3.7 > pH_L > 7.65.

(2) Specific charge z_s: $|z_s| > 2 \cdot 10^{-4}\ e \Rightarrow 4.5 > pH_L > 6.2$ (see Fig. 2).

(3) Effective charge z: weakly dependent on pH in the range 6.5–8.5 (see Fig. 1).

(4) Solubility: bad solubility near pI $\Rightarrow$ pH_L should not be in the range pI ± 1, *i.e.*, 4.2 > pH_L > 7.15.

(5) Chemical stability and biological activity: trans-sulphidation can occur under higher alkaline conditions, pH $\Rightarrow$ pH_L < 8.5.

Based on these data, electrolyte system ES 6 (see Table II) was chosen for the ITP analysis of insulin. A relatively high degree of purity of the given preparation was confirmed (see Table II).

One of immunologically most dangerous admixtures in insulin preparations is proinsulin, the prohormone form of insulin. A very good separation of these two polypeptides (see Fig. 5) was achieved in a mixed-solvent ITP electrolyte system (ES 7 in Table II) using water–2-propanol (90:10, v/v) as the solvent of the leading electrolyte.

Determination of peptide purity is important not only with regard to the final products. Using CITP as a control technique for purity determination after different steps in a purification procedure, we can obtain important information about the

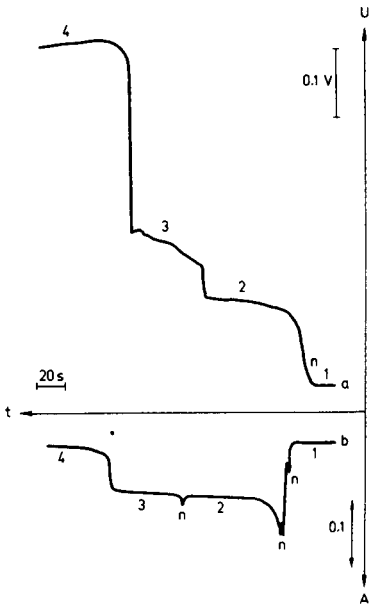

Fig. 5. ITP separation of pig insulin and pig proinsulin. 1 = Carbonates; 2 = insulin; 3 = proinsulin; 4 = glycine; n = unidentified sample components. (a) Signal of PG detector; (b) signal of photometric detector. A = Absorbance at 254 nm; U = voltage of PG detector; t = time. Analysis in ES No. 7 (see Table II); sample, 8.8 μg of lyophilized pig insulin and 8.5 μg of lyophilized pig proinsulin in 5 μl of leading electrolyte were applied. Separation current, 30 μA; detection current, 20 μA; time of analysis, 20 min.

efficiency of different purification methods, from which the suitability of applied methods can be judged.

Using CITP, the efficiency of the purification procedure for the preparation of pure basic bovine pancreatic trypsin inhibitor (BPTI) was monitored. Fig. 6a shows the ITP analysis of the crude BPTI product which was obtained by magnesium sulphate precipitation[33] from the waste solution after trypsin isolation. In this record the zone of BPTI forms a relatively small part of the total length of UV-positive zones, whereas in Fig. 6b, which shows the ITP analysis of BPTI after ion-exchange chromatography on CM-Sephadex, the zone of BPTI already prevails. The ITP degree of purity was further increased after rechromatography on CM-Sephadex. The determined degrees of purity of different BPTI preparations (including a commercial one) are given in Table III.

The degree of enrichment of BPTI was also monitored by another quantitative parameter, the relative zone length, *i.e.*, the zone length relative to unit mass of the applied amount of sample:

$$p_{A,m} = l_A/m_S \tag{11}$$

The calculated values of $p_{A,m}$ are given in Table III. These values are useful especially for monitoring the first steps in a purification procedure, because in their values content of non-ionogenic admixtures and salts is also reflected. In the analysis shown

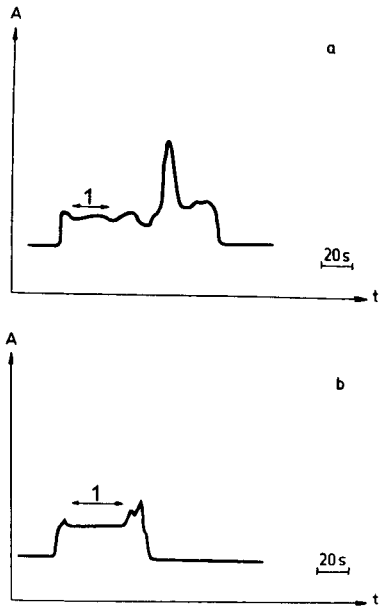

Fig. 6. ITP analysis of bovine pancreatic trypsin inhibitor (BPTI) in ES No. 1 (see Table I) (a) 200 μg of crude BPTI product (precipitated by $MgSO_4$); (b) 6 μg of BPTI purified by ion-exchange chromatography. A = Absorbance at 254 nm; t = time. 1 = BPTI zone.

in Fig. 6a this relative zone length is 0.05 mm/μg (the amount of sample applied was 200 μg) and in Fig. 6b the relative zone length is 2.3 mm/μg (the amount of sample applied was 6 μg). The ratio of these relative zone lengths gives the degree of enrichment after the purification step. In the given example this means that sample analysed in Fig. 6b contains 46 times more BPTI per unit mass than that analysed in Fig. 6a. This high degree of enrichment (in comparison with only a 2.2 times higher ITP degree of purity derived from the UV zone-length ratio) is caused by the high salt content in the crude BPTI product.

TABLE III

ITP DEGREE OF PURITY OF DIFFERENT PREPARATIONS OF BOVINE PANCREATIC TRYPSIN INHIBITOR (BPTI)

p = Degree of purity defined on the basis of zone-length ratio (see eqn. 10); p_m = degree of purity defined on the basis of zone length relative to unit mass (see eqn. 11); IEC = ion-exchange chromatography.

BPTI preparation	*Degree of purity*	
	p (%)	*p_m (mm/μg)*
Crude	20.3	0.05
Purified by IEC	43.1	2.3
Repurified by IEC	73.2	4.1
Commercial (Trasylol)	50.0	3.0

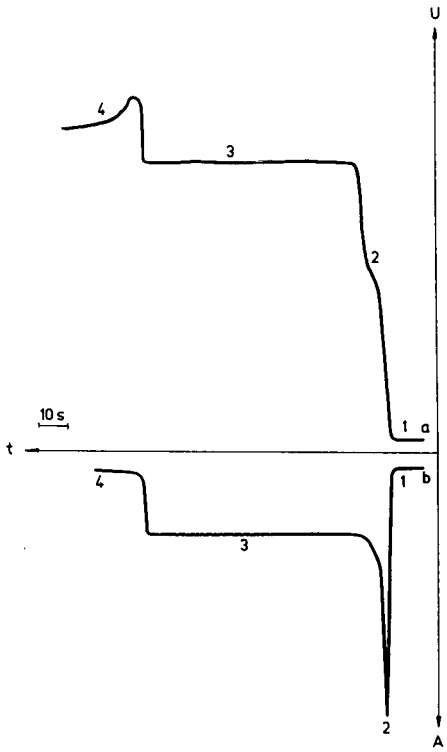

Fig. 7. ITP analysis of adiuretin, synthetic ([8-D-Arg]deaminovasopressin), in the cationic mode, in ES No. 2 (see Table I). 2 μl of an aqueous solution of 8 μg of adiuretin were applied. Current during separation, 50 μA; during detection, 35 μA. (a) Signal of PG detector; (b) signal of UV detector. A = Absorbance at 254 nm; U = voltage of PG detector; t = time. 1 = Na^+; 2 = unidentified sample component; 3 = adiuretin; 4 = BALA.

The zone lengths were measured manually and in some instances, *e.g.*, in Fig. 6, only approximately from the UV record of the ITP analysis as only a contactless UV detector affords a reproducible signal in ITP analyses of polypeptides and proteins. The potential gradient (PG) detector does not provide completely reliable and reproducible data owing to protein adsorption on the electrodes of the detector and to electrode polarization. For this reason, the PG detector signal is of minor importance in polypeptide ITP analysis and its differentiation was not used.

Determination of peptide purity is important especially with peptides used as drugs and in biological tests, where admixtures may cause unwanted additional side effects. An example of the ITP analysis of adiuretin ([8-D-Arg]deaminovasopressin), which is used as a drug against diabetes insipidus, is shown in Fig. 7. A relatively high degree of purity was confirmed (see Table I).

CONCLUSION

CITP has been demonstrated to be a fast, high-performance, sensitive method of peptide microanalysis on the nanomole and subnanomole scale, giving both qualitative and quantitative information on peptide purity.

ACKNOWLEDGEMENT

We thank to Mrs. V. Lišková for skilful technical assistance.

REFERENCES

1 A. Kopwillem, F. Chillemi, A. B. Bosisio-Righetti and P. G. Righetti, *Protides Biol. Fluids, Proc. Colloq.*, 21 (1974) 657.
2 A. Kopwillem, *LKB Application Note No. 110*, LKB, Bromma, Sweden, 1974.
3 *LKB Isotachophoresis News IN 2*, LKB, Bromma, Sweden, 1977.
4 A. J. P. Martin and F. Hampson, in P. G. Righetti (Editor), *Progress in Isoelectric Focusing and Isotachophoresis*, North-Holland, Amsterdam, 1975, p. 327.
5 A. Baldesten, in D. Brandenburg, A. Wollmer (Editors), *Proceedings of the 2nd International Insulin Symposium*, Walter de Gruyter, Berlin, 1980, p. 207.
6 R. Jannasch, *Pharmazie*, 38 (1983) 379.
7 R. Jannasch, *Pharmazie*, 40 (1985) 398.
8 P. Stehle, B. Kühne, P. Pfaender and P. Fürst, *J. Chromatogr.*, 249 (1982) 408.
9 P. Stehle, P. Pfaender and P. Fürst, *J. Chromatogr.*, 294 (1984) 507.
10 A. Kopwillem, U. Moberg, G. Westin-Sjödahl, R. Lundin and H. Sievertsson, *Anal. Biochem.*, 67 (1975) 166.
11 H. Miyazaki and K. Katoh, *J. Chromatogr.*, 119 (1976) 369.
12 F. M. Everaerts, M. Geurts, F. E. P. Mikkers and T. P. E. M. Verheggen, *J. Chromatogr.*, 119 (1976) 129.
13 L. Pradayrol, J. A. Chayvialle, M. Carlquist and V. Mutt, *Biochem. Biophys Res. Commun.*, 85 (1978) 701.
14 K. Friedel and C. J. Holloway, *Electrophoresis*, 2 (1981) 116.
15 P. Stehle and P. Fürst, *J. Chromatogr.*, 346 (1985) 271.
16 P. Stehle, H.-P. Bahsitta and P. Fürst, *J. Chromatogr.*, 370 (1986) 131.
17 P. Hermann, R. Jannasch and M. Lebl, *J. Chromatogr.*, 351 (1986) 283.
18 M. A. Firestone, J.-P. Michaud, R. H. Carter and W. Thormann, *J. Chromatogr.*, 407 (1987) 363.
19 J. W. van Nispen, P. S. L. Janssen, B. C. Goverde, J. C. M. Scherders, F. van Dinther and J. A. J. Hannink, *Int. J. Pept. Protein Res.*, 17 (1981) 256.
20 P. S. L. Janssen and J. W. van Nispen, *J. Chromatogr.*, 287 (1984) 166.
21 J. Vacık, in Z. Deyl (Editor), *Electrophoresis, Part A: Techniques*, Elsevier, Amsterdam, 1979, p. 1.
22 L. Křivánková, F. Foret, P. Gebauer and P. Boček, *J. Chromatogr.*, 390 (1987) 3.
23 T. Hirokawa, T. Gojo and Y. Kiso, *J. Chromatogr.*, 390 (1987) 201.
24 B. A. Cunningham and D. L. Roerig, *U.S. Pat.*, 4 305 798 (1981).
25 M. O. Dayhoff, R. V. Eck, M. A. Chang and M. R. Sochard, *Atlas of Protein Sequence and Structure*, National Biomedical Research Foundation, Silver Spring, MD, 1965.
26 Z. Prusík, in Z. Deyl (Editor), *Electrophoresis, Part B: Applications*, Elsevier, Amsterdam, 1983, p. 81.
27 B. S. Welinder, *Acta Chem. Scand.*, 25 (1971) 3737.
28 P. G. Righetti, R. Krishnamoorthy, E. Gianazza and D. Labie, *J. Chromatogr.*, 166 (1978) 455.
29 D. Čechová, V. Jonáková, E. Sedláková and O. Mach, *Hoppe-Seyler's Z. Physiol. Chem.*, 360 (1979) 1753.
30 P. Štrop, D. Čechová and K. Wüthrich, *J. Mol. Biol.*, 166 (1983) 669.
31 D. Čechová, V. Jonáková, M. Havranová, E. Sedláková and O. Mach, *Hoppe-Seyler's Z. Physiol. Chem.*, 360 (1979) 1759.
32 V. Jonáková, D. Čechová and O. Mach, *Collect. Czech. Chem. Commun.*, 46 (1981) 807.
33 V. Jonáková, unpublished results.
34 B. Meloun, unpublished results.
35 V. Frantíková, J. Borvák, I. Kluh and L. Morávek, *FEBS Lett.*, 178 (1984) 213.
36 J. Ježek, *Thesis*, Institute of Organic Chemistry and Biochemistry, Czechoslovak Academy of Sciences, Prague, 1981.
37 M. Flégl, unpublished results.
38 Z. Prusík, J. Štěpánek, K. Ženíšek, J. Weisgerber and V. Kašička, unpublished results.
39 F. M. Everaerts, J. L. Beckers, T. P. E. M. Verheggen, *Isotachophoresis —Theory, Instrumentation and Applications*, Elsevier, Amsterdam, 1976.
40 M. Svoboda, *Thesis*, Faculty of Science, Charles University, Prague, 1982.
41 E. Šimuničová and D. Kanianský, *J. Chromatogr.*, 390 (1987) 121.

Journal of Chromatography, 470 (1989) 223–233
Elsevier Science Publishers B.V., Amsterdam — Printed in The Netherlands

CHROM. 21 271

ISOTACHOPHORETIC DETERMINATION OF SHORT-CHAIN FATTY ACIDS IN DRINKING WATER AFTER SOLID-PHASE EXTRACTION WITH A CARBONACEOUS SORBENT

M. HUTTA and E. ŠIMUNIČOVÁ

Department of Analytical Chemistry, Faculty of Science, Komenský University, Mlynská Dolina CH-2, 842 15 Bratislava (Czechoslovakia)

D. KANIANSKY*

Institute of Chemistry, Faculty of Science, Komenský University, Mlynská Dolina CH-2, 842 15 Bratislava (Czechoslovakia)

and

J. TKAČOVA and J. BRTKO

Research Institute for Water Treatment, nábr. arm. gen. L. Svobodu 5, 812 49 Bratislava (Czechoslovakia)

SUMMARY

A macroporous carbon sorbent, packed into disposable columns (Separcol-Carb), was investigated for the off-line preconcentration of short-chain fatty acids from drinking water in conjunction with their determination by capillary isotachophoresis (ITP). Of the acids investigated (C_1–C_9), butyric acid and higher homologues could be enriched into a high degree from samples of drinking water. Their detection limits from the ITP conductivity detector were in the low parts per 10^9 range when an amount equivalent to 8 ml of the sample was taken for analysis. The lowest homologues (C_1–C_3) were not adsorbed sufficiently to achieve their reasonable enrichment by the sorbent under the working conditions employed (acidification of the sample to pH 2.0). Acetone and diethyl ether were employed for the elution of the adsorbed analytes. The latter was more convenient in the analysis of practical samples as it co-eluted a considerably smaller number of the adsorbed anionic constituents. Octadecyl-bonded silica, evaluated in parallel, was found to be of only very limited utility for the same purpose.

INTRODUCTION

The presence of fatty acids (FAs) in sources of drinking water can be associated with human activities (*e.g.*, leaks from industrial and agricultural wastes) and also with biological processes and/or degradation of organic material naturally occurring in water (see, *e.g.*, ref. 1). As this group of ionogenic compounds need to be determined in water in general (waste, surface, precipitation, drinking water), considerable efforts have been devoted to the development of suitable analytical methods.

Gas–liquid chromatography (GLC), after conversion of FAs into suitable

0021-9673/89/$03.50

derivatives or without a derivatization step, plays a dominant rôle in this area[2–8]. In reversed-phase high-performance liquid chromatography (RP-HPLC), FAs are only seldom determined as the free acids[9] and their derivatization to improve both the separability and detection limits is commonly used[2,4,10–13]. When either GLC or RP-HPLC is used for the determination of FAs in water, a sample preparation step (trace enrichment, sample clean-up) is usually included in the analytical procedure. The same often applies also in ion chromatography, in spite of the fact that this method was shown to be very useful in the direct determination of short-chain (C_1–C_3) FAs in relatively clean samples (rain water)[14].

Capillary isotachophoresis (ITP), having an inherent analytical specificity for ionogenic compounds, is an alternative separation method suitable for the determination of FAs[15–22]. Its use is very convenient when the acids need to be determined in complex non-ionic matrices[20] or when their concentrations in the sample are comparable to those of other anionic macro constituents[17–19]. A column-coupling configuration of the separation unit[23] was advantageous in the ITP determination of some short-chain FAs present in high salinity waters associated with oil-bearing formations[21,22]. In the ITP work quoted no sample praparation steps were necessary (excluding filtration, sample dilution, etc.).

We have studied the use of ITP in the determination of C_1–C_9 FAs in water samples taken from (potential) sources of drinking water[24]. When the separation was carried out in a water–methanol operational system[20] (see also Table I) and the ITP analyser was assembled in the column-coupling mode, we could detect *ca.* 10^{-6} mol/l concentrations of FAs (*i.e.*, 50–160 ppb for the C_1–C_9 homologues) present in a 150-μl volume of directly injected sample. A further increase in the injection volume to achieve detection limits of low ppb concentrations was not convenient as a considerable higher load capacity of the separation compartment[25] became essential. In addition, long analysis times and/or problems associated with impurities present in the electrolyte system are obvious disadvantages of such an approach[26,27]. To solve this problem, the use of one of the sample preparation procedures elaborated for GLC and RP-HPLC (see, *e.g.*, refs. 3–9) appeared to be an alternative solution for our purposes. When these procedures were evaluated and/or preliminarily tested for use in combination with ITP, we found them to be less suitable (low recoveries of some acids, long sample preparation time, low clean-up efficiency).

Solid-phase extraction (SPE) is one of the preferred sample preparation techniques, especially in HPLC (for reviews see, *e.g.*, refs. 28–33). Carbon, porous polymers, ion exchangers and metal-loaded chelating resins are suitable alternatives for medium- and high-polarity compounds[28,29]. Of these, carbon sorbents were found to be advantageous in the trace analysis of various groups of ionogenic compounds[34–37]. Although data from a detailed investigation of the adsorption properties of graphitized carbon black by Laganà *et al.*[38] suggested a good potential of carbon sorbents for the trace enrichment of organic acids, no attention was paid to their use for sample preparation in FA analysis.

In this work we evaluated a macroporous carbonaceous sorbent[39,40] for the trace enrichment of C_1–C_9 FAs from aqueous solutions and its capabilities for sample preparation in the determination of these compounds in drinking water by ITP. Measurements of the retention characteristics of FAs on octadecyl-bonded silica (Si-C_{18}) showed[24] that this sorbent could be useful for the clean-up of samples

containing butyric acid and higher FA homologous. Therefore, we also evaluated this possibility, which could be useful in combining clean-up of the sample on a disposable Si-C_{18} column with the inherent concentrating power of ITP (a high injection volume of the sample free from inorganic macro constituents).

EXPERIMENTAL

Instrumentation

A CS Isotachophoretic Analyser (VVZ PJT, Spišská Nová Ves, Czechoslovakia) was assembled with the column-coupling configuration of the separation unit[23,41] using module provided by the manufacturer. The samples were injected with the aid of a 30-μl sampling valve. The lengths of the zones from the conductivity detector were measured electronically[42].

A laboratory-made vacuum manifold capable of simultaneously handling ten disposable columns (see below) was used in SPE experiments.

A Model 915 B total organic carbon analyser (Beckman, Irvine, CA, U.S.A.) was used for the measurements of total organic carbon present in water samples taken for the determination of FAs.

Chemicals and purification

Histidine was obtained from Reanal (Budapest, Hungary) and morpholinoethanesulphonic acid (MES) and hydroxyethylcellulose 4000 (HEC) from Serva (Heidelberg, F.R.G.). Histidine and MES were purified by repeated precipitation (dissolution in water, purified as described below, and precipitation with doubly distilled ethanol and acetone). A 1% (w/v) aqueous stock solution of HEC was purified on a mixed-bed ion exchanger (Amberlite MB-1; BDH, Poole, U.K.).

Water delivered by a RODEM-1 two-stage demineralization unit (OPP, Tišnov, Czechoslovakia) was further purified by circulation through laboratory-made polytetrafluoroethylene (PTFE) cartridges packed with Amberlite MB-1 mixed-bed ion exchanger and only freshly recirculated water was employed for the preparation of the solutions and for the SPE experiments.

Doubly glass-distilled methanol and acetone of analytical-reagent grade were employed throughout. Diethyl ether was purified from ionogenic impurities on an activated alumina column[43] and its ionic purity was checked by ITP analysis of its aqueous extract.

FAs obtained from Lachema (Brno, Czechoslovakia), Loba-Chemie (Vienna, Austria), Reachim (Moscow, U.S.S.R.) and Fluka (Buchs, Switzerland) were used without further purification. The other chemicals were purchased from the above manufacturers in analytical-reagent grade purity and were used as received.

Disposable SPE minicolumns packed with octadecyl-bonded silica (Si-C_{18}L, 250 mg sorbent bed) and macroporous carbon (Carb, 250 mg sorbent bed) were obtained from the Centre of Chemical Research (Slovak Academy of Sciences, Bratislava, Czechoslovakia). The Si-C_{18}L columns were washed with 5-ml volumes of acetone, methanol and water before use. The Carb columns were cleaned successively with 5 ml of dimethylformamide, 5 ml of acetone, 5 ml of diethyl ether, 5 ml of methanol and 10 ml of water. The columns were used repeatedly and before their re-use the sorbent beds were washed (activated) in the same way. The activation solvent was removed by percolating 5 ml of water through the sorbent bed.

Sample preparation

Procedure A. The sample volume (100, 250 or 500 ml) was acidified to pH 2.0 with sulphuric acid then percolated through the column at 10 ml/min. The sorbent bed was washed with 5 ml of water and the adsorbed compounds were eluted with 4 ml of acetone. The eluate was mixed with 700 μl of aqueous histidine ($5 \cdot 10^{-3}$ mol/l). Acetone was evaporated by a flow of nitrogen at ambient temperature to a final sample volume of 1 ml. A 30-μl volume of this sample solution was analysed by ITP.

Procedure B. The sorption and washing steps were the same as in *Procedure A.* Water present in the voids of the column bed was sucked out and the elution was carried out with two 2-ml volumes of diethyl ether. The eluate was mixed with 500 μl of aqueous sodium hydroxide (10^{-2} mol/l). The organic phase was evaporated under a stream of nitrogen and the aqueous phase was diluted with water and methanol to 1 ml so that the final concentration of the latter solvent in the sample was 25% (v/v).

RESULTS AND DISCUSSION

ITP analysis of fatty acids

The composition of the operational system used in the ITP analyses throughout this work is given in Table I. In this instance, the concentration of the leading ion was lower than that suggested previously[20] in order to decrease the detection limits of the analytes.

Relative differences in the effective mobilities of FAs in the steady state are clear from the isotachopherogram in Fig. 1. Here, a model mixture with a composition similar to that of drinking water was spiked with C_1–C_9 normal saturated FAs. With the exception of the C_1 and C_4 compounds the concentration of the acids present in the mixture were identical with the maximum values in the measurements of the calibration lines (Table II).

From the numerical values of the parameters of the regression equation characterizing the slopes of the calibration lines, it can be seen that these experimentally based values did not follow exactly the tendency that could be expected from the simulated data[44]. We found that these deviations could be ascribed to lower

TABLE I

OPERATIONAL SYSTEM EMPLOYED IN THE ITP ANALYSIS OF FATTY ACIDS

Parameter	*Electrolyte*	
	Leading	*Terminating*
Solvent	H_2O–CH_3OH	H_2O–CH_3OH
Proportions (v/v)	80:20	70:30
Anion	Cl^-	MES
Concentration (m*M*)	5	2.5
pH[a]	6.0	6.0
Additive	HEC	–
Concentration (%, w/v)	0.1	–

[a] Methanol was added to the aqueous solutions containing the required constituents at appropriate concentrations and pH values as measured for aqueous solutions are given.

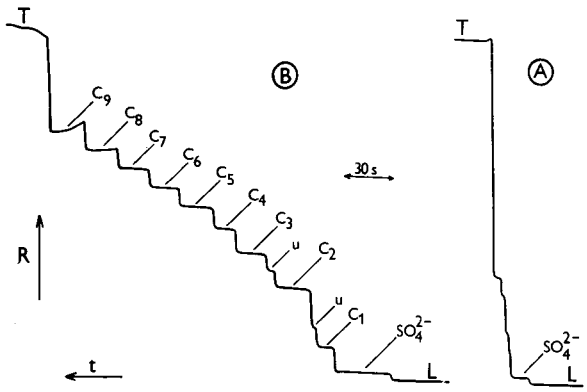

Fig. 1. Isotachopherograms from the analysis of short-chain fatty acids (C_1–C_9) present in a model mixture with a composition of inorganic constituents similar to that of drinking water. The records from the conductivity detector in the analytical column are only given. A = Blank run (no sample injection); B = model mixture spiked with fatty acids (C_1 at $4 \cdot 10^{-5}$ mol/l, C_4 at $6 \cdot 10^{-5}$ mol/l and the other acids at $8 \cdot 10^{-5}$ mol/l). The driving currents were 100 and 15 μA in the preseparation and analytical columns, respectively. L = Leading anion; T = terminating anion; u = unidentified impurities present in the operational system. *R*, *t* = increasing resistance and time, respectively.

actual contents of the acids in the preparations used (titrimetric analysis of some of the preparations). However, as the same preparations were used throughout and our measurements were relative rather than absolute (breakthrough curves, recovery data), no systematic errors were involved in this way.

The reproducibilities of the ITP analyses of the acids present in the samples at $3 \cdot 10^{-5}$–$8 \cdot 10^{-5}$ mol/l concentrations were typically in the range 1.5–3%.

Measurements of breakthrough curves

The breakthrough characteristics of the analytes on the sorbents used gave data relevant to their applicabilities for sample preparation. These characteristics were

TABLE II

REGRESSION EQUATIONS AND CORRELATION COEFFICIENTS FOR C_1–C_9 FATTY ACIDS IN THE $8 \cdot 10^{-6}$–$80 \cdot 10^{-6}$ mol/l CONCENTRATION RANGE

No. of data points = 10.

Acid	*Regression equation*[a]	*Correlation coefficient*
C_1	$y = 2.36 + 0.1868x$	0.9993
C_2	$y = 1.82 + 0.2458x$	0.9996
C_3	$y = 0.61 + 0.2152x$	0.9999
C_4	$y = 0.57 + 0.2172x$	0.9998
C_5	$y = 0.67 + 0.2179x$	0.9998
C_6	$y = 0.96 + 0.2194x$	0.9999
C_7	$y = 0.52 + 0.2393x$	0.9997
C_8	$y = 0.41 + 0.2314x$	0.9997
C_9	$y = 0.09 + 0.2446x$	0.9996

[a] x = concentration (10^{-6} mol/l); y = zone length (s).

measured for the sorbents packed in disposable columns and treated before the use as described under Experimental.

The Si-C_{18}L sorbent was studied for two modes of the sorption process, *viz.*, ion suppresion (by decreasing the pH of the sample solution to *ca.* 3.0) and ion exchange [by modifying the surface of the sorbent by strongly retained cetyltrimethylammonium cation ($CTMA^+$) before the sample application]. In both modes the sample solutions percolating through the beds were collected into 1–2-ml fractions. The fractions were analysed by ITP and the breakthrough curves given in Fig. 2 were reconstructed from the results of the analyses. These curves clearly show that in both instances the sorbent provides only a very limited utility from the point of view of sample preparation.

Analogous data for the Carb sorbent (Fig. 3) indicate considerable higher breakthrough volumes, especially for the C_4–C_9 homologues. For obvious reasons only this sorbent, having a surface area of 1600 m^2/g (refs. 39 and 40), was studied in detail for sample preparation in the ITP determination of FAs in drinking water.

Recoveries of fatty acids on the Carb sorbent

In experiments with model samples spiked with FAs at concentrations of 10^{-6} mol/l or less, we found that the adsorption by the Carb columns was quantitative for the C_4–C_9 homologues and a very high enrichment factor (>250) was easily achieved for these constituents. On the other hand, propionic acid could be quantitatively adsorbed only from *ca.* 10-ml sample volumes and acetic and formic acids were not adsorbed with reasonable recoveries even from smaller sample volumes. From the practical point of view it is important that inorganic macro and micro constituents which are present in drinking water (Cl^-, SO_4^{2-}, NO_2^-, NO_3^-, F^- and PO_4^{3-}) are not retained by this sorbent. Hence it provides a very effective clean-up of the adsorbed

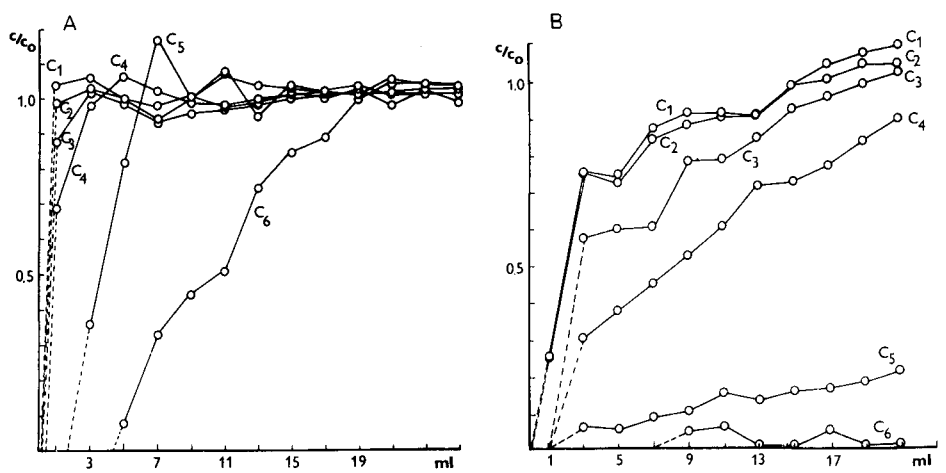

Fig. 2. Breakthrough curves of C_1–C_6 fatty acids on octadecyl-bonded silica. (A) Sample acidified to pH 3.0 with H_2SO_4 percolated through the column; (B) sample applied to the column with surface modified by $CTMA^+$ (35 ml of 10^{-3} mol/l aqueous $CTMA^+$ Br^- was percolated through the column before the application of the sample). In both instances tap water spiked with fatty acids at $5 \cdot 10^{-5}$ mol/l were percolated through the columns at 1 ml/min. c_0, c = Initial and post-column concentrations of the acids, respectively.

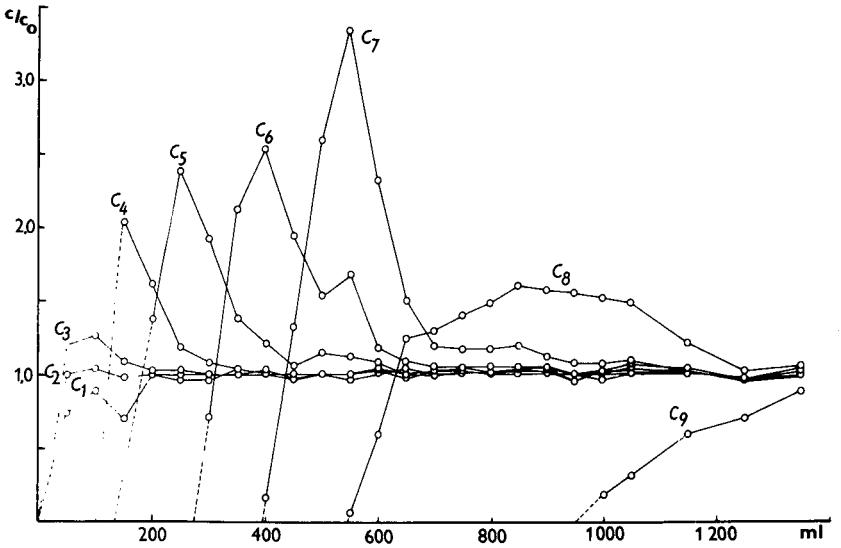

Fig. 3. Breakthrough curves of C_1–C_9 fatty acids on a macroporous carbon sorbent (Separcol-Carb). The same sample as in Fig. 2 was percolated through the sorbent bed at 10 ml/min. Fractions of 50 ml collected from the column were evaluated by ITP (the first 50-ml portion was collected in 10-ml fractions).

FAs. In the model experiments acetone was used as a suitable eluting solvent for FAs (see *Procedure A* in Experimental).

Drinking water contains organic compounds of various polarities in trace concentrations[45] and these compounds can be evaluated as total organic carbon (TOC). When we consider that carbonaceous sorbents are not very selective in the adsorption step (see, *e.g.*, refs. 38 and 45), many of these compounds can be expected to be trapped by the Carb column. From the point of view of the ITP determination of FAs various groups of organic acids (*e.g.*, subgroups of humic and fulvic acids[1,45]) need to be considered as potential interferents introduced in this way. As it is almost impossible to prepare model samples of the corresponding compositions, we employed samples of drinking water with relatively high TOC values (17–19 mg/l) to investigate problems of this kind and to optimize the elution conditions for the FAs. The isotachopherograms in Fig. 4 were taken from the analysis of such a sample of drinking water. Volumes of 500 ml of the same sample treated by the sample preparation procedures as described under Experimental were used. It is apparent that *Procedure B* (Fig. 4B) provided a less complex anionic profile. Consequently, in the analysis of samples spiked with FAs (see Fig. 5) it gave a lower bias of the quantitations due to the enriched matrix constituents.

The recovery experiments summarized in Table III were carried out within a period of 2 months with nine samples of drinking water taken from the same sampling site (TOC = 19 mg/l). For obvious reasons, in these experiments we employed sample preparation *Procedure B*. The samples and those spiked at various concentrations with FAs (see Table III) were processed identically. The spiking concentrations were chosen so that the total amounts of the individual FAs were constant.

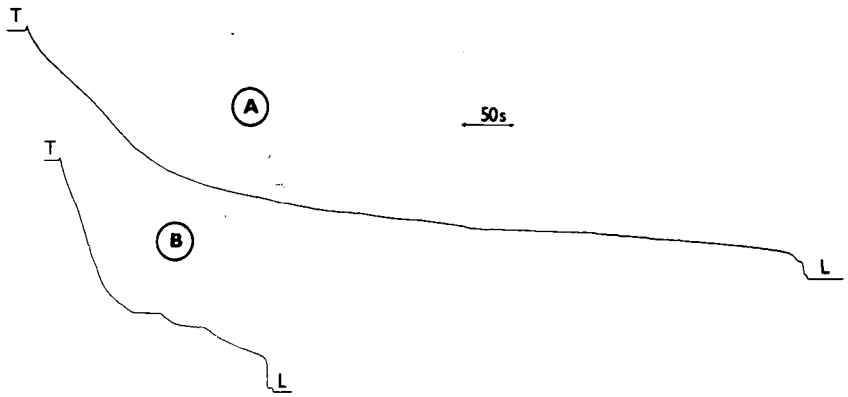

Fig. 4. Comparison of (A) acetone and (B) diethyl ether in the desorption of organic anionic constituents from the Carb sorbent. In both instances 500-ml volumes of the same sample taken from a potential source of drinking water (TOC = 19 mg/l) were adsorbed in an identical manner (for further details see the text). For the impurities introduced from the operational system, see Fig. 1A. ITP working conditions as in Fig. 1.

With the exception of 500-ml sample volumes, the reproducibilities of the recoveries for the same sample repeatedly processed on the same column were 2–3 times higher than the long-term reproducibility data. However, the evaluation of a set of data obtained over a long period of time gives a better measure of the overall reproducibility of the proposed sample preparation procedure because it includes random errors in the sample manipulation steps, dispersion in the sorption properties of the columns and errors due to variability of the matrix. In these long-term recovery data systematic errors due to changes in the compositions of the calibration mixtures (gradual decreases in the concentrations of some FAs) were avoided by relating the concentrations of the recovered acids to those in the reference sample from which the samples of drinking water were spiked.

In general, the lower mean values and higher relative standard deviations of the recoveries for 500-ml sample volumes can be ascribed to the displacement effects of preferentially adsorbed organic constituents from drinking water. This problem can be

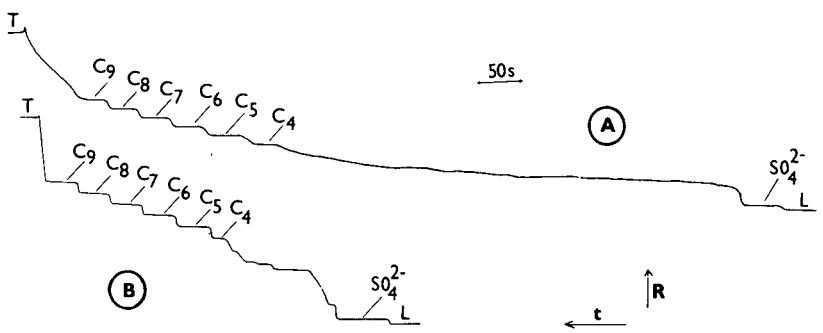

Fig. 5. Isotachopherograms from the analysis of drinking water spiked with fatty acids at $1.6 \cdot 10^{-7}$ mol/l with different sample preparation procedures. (A) Elution with acetone; (B) elution with diethyl ether. The same samples and procedures as in Fig. 4 were used. ITP working conditions as in Fig. 1.

TABLE III

RECOVERIES OF C_4–C_9 FATTY ACIDS FROM DRINKING WATER ON THE SEPARCOL-CARB COLUMN

Relative standard deviations of the recoveries for 100-, 250- and 500-ml sample volumes were calculated from the analyses of 14, 9 and 13 samples, respectively. The analyses were carried out within a period of 2 months. The concentrations of FA in the samples were $8 \cdot 10^{-7}$, $3.2 \cdot 10^{-7}$ and $1.6 \cdot 10^{-7}$ mol/l for sample volumes of 100, 250 and 500 ml, respectively.

Acid	*Sample volume*[a]					
	100 ml		*250 ml*		*500 ml*	
	$\bar{x}$ (%)	s_r (%)	$\bar{x}$ (%)	s_r (%)	$\bar{x}$ (%)	s_r (%)
C_4	96.6	16.7	100.7	7.8	100.2	21.5
C_5	92.0	10.5	95.8	5.5	97.3	16.1
C_6	93.4	10.8	94.0	7.2	90.3	22.5
C_7	95.7	11.3	100.3	8.4	87.6	20.9
C_8	88.7	13.7	93.8	5.3	76.6	26.7
C_9	86.9	12.3	101.3	10.8	79.5	28.0

[a] $\bar{x}$ = mean recovery; s_r = relative standard deviation.

solved by packing a larger amount of the sorbent in the column when a further decrease in the detection limits is to be achieved via the use of higher sample volumes. Such a solution, however, is not necessary in our particular case when it is realized that only 3% of the final sample volume was taken for one ITP run. Therefore, when desirable a larger injection volume can provide a more convenient means of decreasing the detection limits. Here, it is important that the Carb sorbent is very effective in removing inorganic anionic macro constituents (Cl^-, SO_4^{2-} and NO_3^-) from the sample, thus minimizing the requirements concerning the load capacity of the separation compartment. In this work 250-ml volumes of the samples of drinking water were taken for analysis. After the sample preparation step the enriched acids were present in a 1-ml volume, 30 μl of which were analysed by ITP. Under these conditions we could detect with confidence *ca.* $5 \cdot 10^{-8}$ mol/l concentrations of the analytes (*i.e.*, 4.5–8.0 parts per 10^9, ppb, for the C_4–C_9 homologues). A 10-fold decrease in this value appears feasible by simply increasing the injection volume to 300 μl.

Typical isotachopherograms for the determination of FAs in a practical sample of drinking water are shown in Fig. 6. In this instance, the sample and that spiked with FA at $3.2 \cdot 10^{-7}$ mol/l were preconcentrated 250-fold before the ITP analyses. The recoveries of the acids in this particular instance were in the range 90–100% and the reproducibilities of the recoveries were in the range 6–9% (three parallel analyses).

CONCLUSIONS

Solid-phase extraction on a macroporous carbon sorbent (Separcol-Carb) has been shown to be effective in decreasing the detection limit in the ITP determination of some short-chain FAs in drinking water to the low ppb level even when the acids are

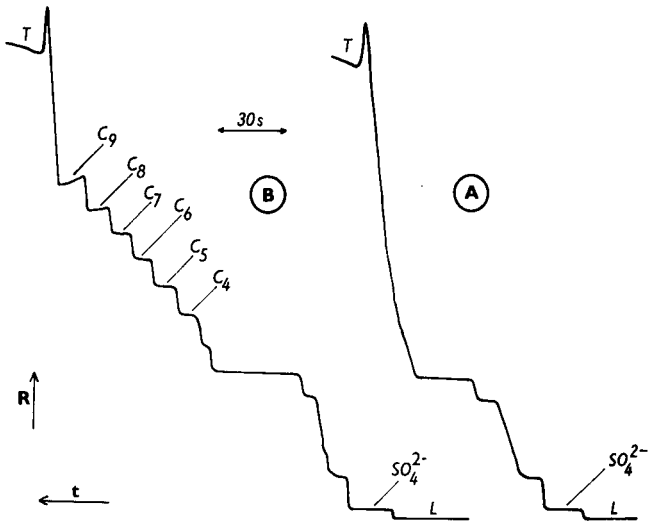

Fig. 6. Determination of C_4–C_9 fatty acids in drinking water of TOC 19 mg/l. The sample was taken from the same site as shown in Figs. 4 and 5 with a 2-month delay. Volumes of 250 ml of (A) the sample and (B) the sample spiked with fatty acids at $3.2 \cdot 10^{-7}$ mol/l were pretreated by the sample preparation *Procedure B* (see Experimental). The zones of the acids were six times longer than the values calculated as the detection limits. ITP working conditions as in Fig. 1.

present in complex organic matrices. This sorbent was found to be of only limited utility in adsorbing the C_1–C_3 homologues and thus it did not provide a sample preparation procedure applicable to the complete group of investigated acids. However, analogous disadvantages are common also to other sample preparation procedures currently in use in the determination of FAs with prior separation methods.

In spite of the fact that the Carb sorbent (like other types of carbonaceous sorbents) is inherently less selective and it adsorbs both apolar and polar organic compounds, its use for sample preparation in the ITP determination of FAs is convenient when a high analytical specificity of ITP to the ionogenic compounds is considered. From the practical point of view, by using this sorbent we could achieve simple and rapid sample preparation (*ca.* 30 min by simultaneously handling ten samples) with good recoveries of the adsorbed acids. It is also important that this procedure can be easily adapted for field work and can be used for simple sample storage (we found that the acids adsorbed on the column bed and stored for 1 week at 4°C in a capped tube gave recoveries that agreed well with a control experiment).

REFERENCES

1 G. G. Choudhry, in O. Hutzinger (Editor), *The Handbook of Environmental Chemistry*, Vol. 1, Part C, Springer, Berlin, Heidelberg, New York, Tokyo, 1984, p. 1.
2 D. R. Knapp, *Handbook of Analytical Derivatization Reactions*, Wiley, New York, 1979.
3 J. J. Richard, C. D. Chriswell and J. S. Fritz, *J. Chromatogr.*, 199 (1980) 143.
4 M. J. Barcelona, H. M. Liljestrand and J. J. Morgan, *Anal. Chem.*, 52 (1980) 321.
5 K. Kawamura and I. R. Kaplan, *Anal. Chem.*, 56 (1984) 1616.

6 V. Janda, F. Pehal and J. Hrivňák, *J. High Resolut. Chromatogr. Chromatogr. Commun.*, 7 (1984) 540.
7 J. J. Richard and G. A. Junk, *Anal. Chem.*, 56 (1984) 1625.
8 I. Borkovcová, *Fyzikálně Chemické Metody Stanovení Organických Sloučenin v Přírodninách*, Ústřední Ústav Geologický, Prague, 1986, p. 99.
9 D. L. Manning and M. P. Maskarinec, *J. Liq. Chromatogr.*, 6 (1983) 705.
10 J. F. Lawrence and R. W. Frei, *Chemical Derivatization in Liquid Chromatogrphy*, Elsevier, Amsterdam, Oxford, New York, 1976.
11 R. L. Patience and J. D. Thomas, *J. Chromatogr.*, 234 (1982) 225.
12 R. Schuster and W. Haecker, *Automated Sample Preparation System, Application Note*, Hewlett-Packard, Waldbronn, 1987.
13 H. Tsuchiya, T. Hayashi, H. Naruse and N. Takagi, *J. Chromatogr.*, 234 (1982) 121.
14 D. Brocco and R. Tappa, *J. Chromatogr.*, 367 (1986) 240.
15 J. L. Beckers, F. M. Everaerts and W. J. M. Houtermans, *J. Chromatogr.*, 76 (1973) 277.
16 F. M. Everaerts, J. L. Beckers and Th. P. E. M. Verheggen, *Isotachophoresis—Theory, Instrumentation and Applications*, Elsevier, Amsterdam, Oxford, New York, 1976.
17 P. Boček, S. Pavelka, K. Grigelová, M. Deml and J. Janák, *J. Chromatogr.*, 154 (1978) 356.
18 *Application Note*, No. 2, VVZ PJT, Spišská Nová Ves, 1984.
19 A. Kopwillem and K. Eriksson, *LKB Application Note No. 111*, LKB, Bromma, 1974.
20 M. Koval, D. Kaniansky, M. Hutta and R. Lacko, *J. Chromatogr.*, 325 (1985) 151.
21 T. Barth, *Anal. Chem.*, 59 (1987) 2232.
22 T. Barth, *Chemometrics Intell. Lab. Syst.*, 2 (1984) 155.
23 F. M. Everaerts, Th. P. E. M. Verheggen and F. E. P. Mikkers, *J. Chromatogr.*, 169 (1979) 21.
24 J. Tkáčová, D. Kaniansky, M. Hutta and V. Zelenská, *Research Report No. R99-531-138-02*, Research Institute for Water Treatment, Bratislava, 1987.
25 F. E. P. Mikkers, F. M. Everaerts and J. A. F. Peek, *J. Chromatogr.*, 168 (1979) 293.
26 V. Dolník, *Thesis*, Institute of Analytical Chemistry, Czechoslovak Academy of Sciences, Brno, 1987.
27 V. Dolník, M. Deml and P. Boček, *J. Chromatogr.*, 320 (1985) 89.
28 R. W. Frei, *Swiss Chem.*, 6 (1984) 55.
29 M. W. F. Nielen, *Thesis*, Free University, Amsterdam, 1987.
30 B. Tippins, *Int. Lab.*, 17, April (1987) 28.
31 C. E. Goewie, *Thesis*, Free University, Amsterdam, 1983.
32 *Applications Bibliography*, Analytichem International, Harbor city, CA, 1986.
33 *Baker-10 SPE, Application Guide*, Vols. 1 and 2, J. T. Baker, Phillipsburg, NJ, 1984.
34 C. E. Werkhoven-Goewie, U. A. Th. Brinkman and R. W. Frei, *Anal. Chem.*, 53 (1981) 2072.
35 C. Borra, A. Di Corcia, M. Marchetti and R. Samperi, *Anal. Chem.*, 58 (1986) 2048.
36 A. Di Corcia, M. Marchetti and R. Samperi, *J. Chromatogr.*, 405 (1987) 357.
37 F. Andreolini, C. Borra, F. Caccamo, A. Di Corcia and R. Samperi, *Anal. Chem.*, 59 (1987) 1720.
38 A. Laganà, G. Goretti, B. M. Petronio and M. Rotatori, *J. Chromatogr.*, 219 (1981) 263.
39 O. Chiantore, I. Novák and D. Berek, *Anal. Chem.*, 60 (1988) 638.
40 *Separcol Preseparation Minicolumns*, Institute of Polymers, Centre of Chemical Research, Slovak Academy of Science, Bratislava, 1988.
41 D. Kaniansky, *Thesis*, Komenský University, Bratislava, 1983.
42 I. Zelenský, E. Šimuničová, V. Zelenská, D. Kaniansky, P. Havaši and P. Chaláni, *J. Chromatogr.*, 325 (1985) 161.
43 D. D. Perrin, W. L. F. Armarego and D. R. Perrin, *Purification of Laboratry Chemicals*, Pergamon Press, Oxford, 2nd ed., 1980, p. 259.
44 T. Hirokawa, M. Nishino, N. Aoki, Y. Kiso, Y. Sawamoto, T. Yagi and J. I. Akiyama, *J. Chromatogr.*, 271 (1983) D 1.
45 P. Pitter, *Hydrochemie*, SNTL, Prague, 1981.

Journal of Chromatography, 470 (1989) 235–240
Elsevier Science Publishers B.V., Amsterdam — Printed in The Netherlands

CHROM. 21 272

STUDY OF ALKALINE HYDROLYSIS OF THE INSECTICIDE ALPHAMETHRINE BY ISOTACHOPHORETIC DETERMINATION OF DECOMPOSITION PRODUCTS

VÁCLAV DOMBEK*
Institute of Industrial Landscape Ecology, Czechoslovak Academy of Sciences, Chittussiho 10, 710 00 Ostrava 2 (Czechoslovakia)
and
ZDENĚK STRÁNSKÝ
Department of Analytical and Organic Chemistry, Faculty of Natural Sciences, Palacký University, Leninova 8, 771 46 Olomouc (Czechoslovakia)

SUMMARY

Alkaline hydrolysis of the pyrethroid insecticide alphamethrine has been studied. After hydrolytic cleavage at various temperatures and pH values, the degradation products, phenoxybenzoic acid and the dichloro derivative of chrysanthemic acid, were identified and determined by means of capillary isotachophoresis . Rate constants, activation energies and the reaction enthalpy and entropy were calculated.

INTRODUCTION

Alphamethrine (I) belongs to the group of pyrethroid insecticides which have recently been widely applied. It is essentially an isomeric form of a substance called cypermethrine.

Studies of the determination of pyrethroid insecticides and their residues have

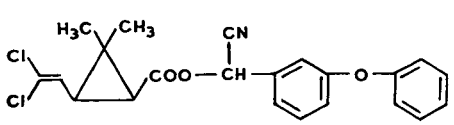

I Alphamethrine

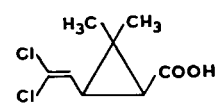

III Dichlorochrysanthemic acid

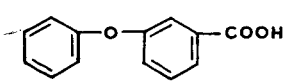

II m-Phenoxybenzoic acid

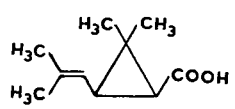

IV Chrysanthemic acid

0021-9673/89/$03.50

concentrated especially on separation methods. A number of gas chromatographic methods especially with electron-capture detection[1–8] and several liquid chromatography procedures, especially high-performance liquid chromatography (HPLC)[3,5,7,9–11], have been published for the determination of the content of cypermethrine and its isomers in various materials.

Insecticides from the pyrethroid group undergo a variety of decomposition reactions, *eg.*, photodegradation, hydrolysis and metabolic transformations[11–16]. In the case of alphamethrine, alkaline hydrolysis results in the degradation products II and III which, due to their chemical structure, permit employment of analytical capillary isotachophoresis for the determination.

Capillary isotachophoresis has so far been little used for the analysis of pesticide formulations. However, recently several studies employing this technique have appeared[17,18].

In the present work we have focused on the investigation of the hydrolytic degradation of alphamethrine using isotachophoresis.

EXPERIMENTAL

Pure compounds I–IV were prepared for the isotachophoretic determination of hydrolysis degradation products.

The compound alphamethrine, (*R,S*)-cyano(3-phenoxyphenyl)methyl (*R,S*)-*cis*-3-(2,2-dichlorovinyl)-2,2-dimethylcyclopropanecarboxylate, was isolated from a formulation Vaztak 10 EC (Shell) and repurified by a multiple crystallization from hexane and acetone.

m-Phenoxybenzoic acid was prepared at the Palacký University Olomouc, while compounds III and IV were synthesized at the Institute of Organic Chemistry of the Polish Academy of Sciences (Warsaw, Poland). The purity of the compounds prepared was monitored by elemental analysis.

Calibration solutions of the compounds II–IV at the concentrations $1 \cdot 10^{-5}$–$1.5 \cdot 10^{-3}$ mol l^{-1} were prepared by dissolution in deionized water under mild alkalization.

Solutions of Kolthoff–Vleeschhouwer buffer were used to maintain pH values during hydrolysis: Na_2CO_3 and $Na_2B_4O_7$ (ionic strength $I = 0.15$) for pH 10; Na_2HPO_4 and NaOH ($I = 0.158$ *M* and 0.193 for pH 11 and 12, respectively).

Analytical isotachophoresis

Isotachophoretic determinations were performed on an instrument for capillary isotachophoresis in a two-capillary array ZKI 01 (ÚRVJT Spišská Nová Ves, Czechoslovakia). The driving current in the pre-separation capillary (150 mm × 0.8 mm I.D.) was 250 μA while a current of 30 μA was used in the analytical capillary (150 mm × 0.3 mm I.D.). Separated zones were detected by a conductivity detector the signal of which was recorded on a two-line recorder. The sampling was performed by a microsyringe (Hamilton), volume 5 μl.

The operational systems used are given in Table I.

Alkaline hydrolysis

Alkaline hydrolysis of alphamethrine was carried out in sealed ampoules (10 ml) in an atmosphere of argon. Always, 2.5 ml of buffering solution were added to 2.5 ml of

TABLE I

OPERATIONAL SYSTEMS USED

MES = Morpholinoethanesulphonic acid; PVA = poly(vinyl alcohol).

System	*Leading ion, c (mol l^{-1})*	*Counter ion*	*pH*	*Additive*	*Terminating electrolyte, concentration (M)*
A	Cl^- 10^{-2}	ε-Aminocaproic acid	4.30	0.05% PVA	MES $5 \cdot 10^{-3}$
B	Cl^- 10^{-2}	Creatine	4.80	0.05% PVA	MES $5 \cdot 10^{-3}$
C	Cl^- 10^{-2}	Histidine	6.00	0.05% PVA	MES $5 \cdot 10^{-3}$

alphamethrine solution ($2 \cdot 10^{-2}$ mol l^{-1} in ethanol). After removal of air by a flow of argon, the ampoules were sealed and thermostatted at 30, 35, 40, 45 and 50°C. At intervals of 10 min to 28 h and after cooling, the contents were made up to 50 ml with deionized water in a volumetric flask. A 5 μl volume of this sample was injected into the isotachophoretic analyzer. The concentrations of the degradation products formed upon hydrolysis were found from calibration graphs.

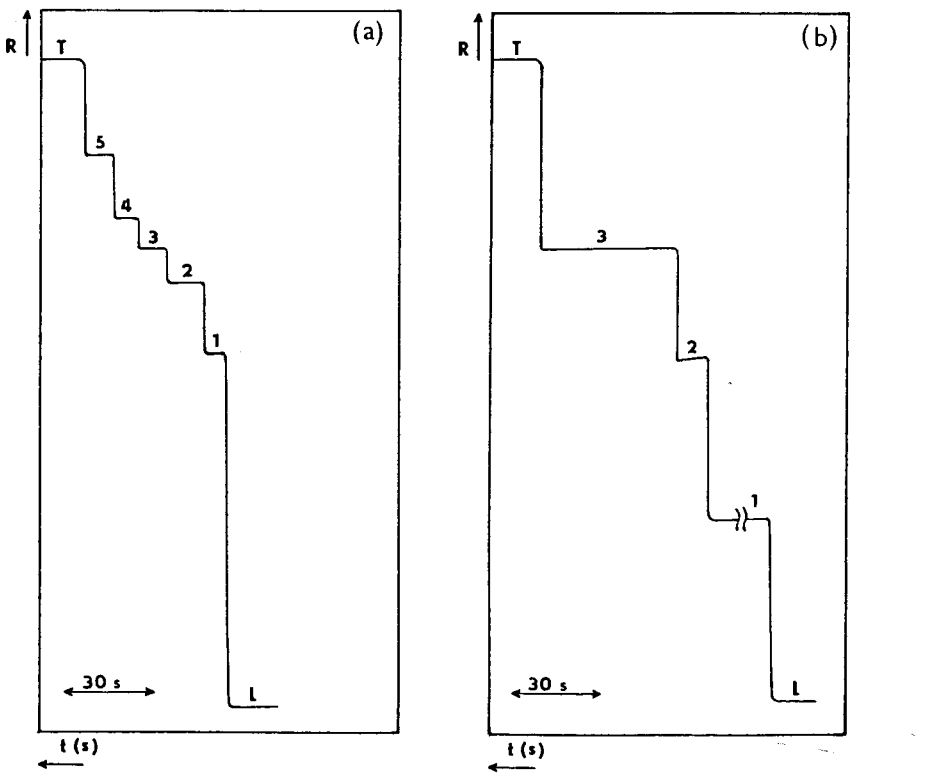

Fig. 1. Separation of degradation products: (a) system B, injection of 5 μl of mixture; 1 = II, 2 = III-*trans*, 3 = III-*cis*, 4 = IV-*trans*, 5 = IV-*cis*; (b) system B, injection of 5 μl of hydrolysate; 1 = PO_4^{3-}, 2 = II, 3 = III-*cis*. L = Cl^-; T = MES; *t* = time; *R* = resistance.

TABLE II
RELATIVE STEP HEIGHTS

Compound	*Heights relative to trichloroacetic acid*		
	System A	*System B*	*System C*
II	1.66	1.69	1.44
III-*cis*	2.08	2.00	1.50
III-*trans*	1.90	1.84	1.50
IV-*cis*	2.36	2.33	1.58
IV-*trans*	2.12	2.05	1.52

RESULTS AND DISCUSSION

Three electrolyte systems (Table I) were tested to choose a suitable separation system for the isotachophoretic determination of compounds II–IV. In systems A–C the separation of all three compounds takes place. In systems A and B, even *cis* and *trans* isomers of compounds III and IV (Fig. 1) are fairly well separated. Separation in systems leading electrolytes of lower pH values ($pH_L = 3.60$) could not be performed due to the low mobilities of the compounds. For single electrolytes the relative zone heights were calculated, relative to trichloroacetic acid (step height 1.00, Table II).

From the isotachophoretically determined concentrations of compounds II and III in hydrolysates, the time dependences were constructed and the recovery upon hydrolysis after 28 h was calculated (Table III). The relative standard deviations of recovery ranged from 1.3 to 2.6% for *cis*-dichlorochrysanthemic acid (III-*cis*) and from 1.7 to 4.0% for *m*-phenoxybenzoic acid (II), respectively (mean of four parallel determinations).

The course of hydrolysis satisfies a first-order kinetic equation from which the values of the rate constants (Table IV) were obtained and their dependence on the reciprocal of the temperature was plotted (Fig. 2). The Arrhenius equation

$$\Delta H = E_A + RT \tag{1}$$

TABLE III
RECOVERY UPON HYDROLYSIS FOR 28 H

Temperature (°C)	*Mean recovery (%)*					
	pH 10		*pH 11*		*pH 12*	
	II	*III-cis*	*II*	*III-cis*	*II*	*III-cis*
30	2.9	13.2	4.5	18.1	7.8	39.2
35	4.3	19.0	4.8	25.3	10.1	45.0
40	5.7	27.3	6.6	32.0	12.8	52.1
45	7.7	35.0	8.8	40.0	18.1	68.4
50	10.0	45.2	12.0	49.3	19.3	93.0

TABLE IV

RATE CONSTANTS, k (AT TEMPERATURE T = 50°C), ARRHENIUS EQUATION, ACTIVATION ENTHALPY AND ENTROPY

The k values are given as the means of four parallel determinations; CI = Confidence interval expressed as twice the estimated standard deviation.

pH	$k \pm CI$ *(l/mol · s)*	*Arrhenius equation*	ΔS *(J/mol · K)*	ΔH *(kJ/mol)*
10	$(7.60 \pm 0.12) \cdot 10^{-5}$	$\ln k = 6.00 - 5.00 \cdot 10^3\ T^{-1}$	−202.6	43.8
11	$(1.14 \pm 0.02) \cdot 10^{-4}$	$\ln k = 6.60 - 5.10 \cdot 10^3\ T^{-1}$	−197.6	44.7
12	$(2.35 \pm 0.02) \cdot 10^{-4}$	$\ln k = 7.79 - 5.34 \cdot 10^3\ T^{-1}$	−187.7	46.7

was used for calculation of the activation energy, E_A, and activation enthalpy, ΔH, as well as for activation entropy, ΔS

$$\Delta S = R\,(\ln A - \ln \frac{k_B T}{h} - 1) \tag{2}$$

where A, k_B and h are the frequency factor, Boltzmann and Planck constants, respectively. Calculated values are given in Table IV.

Recovery of *m*-phenoxybenzoic acid from hydrolysates ranged from 2.9 to 19.3% (Fig. 1b), was poorly reproducible and could not be employed for the investigation of the degradation process.

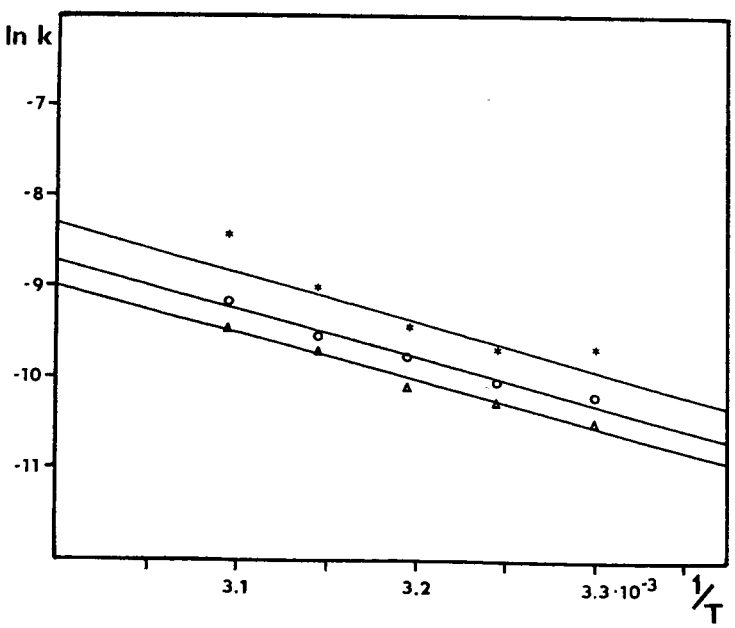

Fig. 2. Graphical expression of the Arrhenius equation. pH 10 (⅓), 11 (@) and 12 (*).

ACKNOWLEDGEMENTS

The authors thank Dr. Roman Balicki (Institute of Organic Chemistry, Polish Academy of Sciences, Warsaw) for providing standards of *cis* and *trans* isomers of chrysanthemic acids as well of their dichloro derivatives.

REFERENCES

1 R. A. Chapman and H. S. Simmons, *J. Assoc. Off. Anal. Chem.*, 60 (1977) 977.
2 R. A. Chapman and C. R. Harris, *J. Chromatogr.*, 166 (1978) 513.
3 P. G. Baker and P. Bottomley, *Analyst (London)*, 107 (1982) 206.
4 A. E. M. Marei, L. O. Ruzo and J. E. Casida, *J. Agric. Food Chem.*, 30 (1982) 558.
5 A. Sapiets, H. Swaine and M. J. Tandy, in G. Zweig (Editor), *Analytical Methods for Pesticides and Plant Growth Regulators*, Vol. XIII, Academic Press, New York, 1984.
6 V. Kocourek and L. Havlíková, *Sborník ÚVTIZ-Potrav. vědy*, 3 (1985) 247.
7 N. Mikami, *J. Pestic. Sci.*, 12 (1987) 539.
8 J. F. C. Tyler, *J. Assoc. Off. Anal. Chem.*, 70 (1987) 51.
9 E. Papadopoulou-Mourkidou, Y. Iwata and F. A. Gunther, *J. Agric. Food Chem.*, 29 (1981) 1105.
10 R. A. Chapman, *J. Chromatogr.*, 258 (1983) 175.
11 G. R. Cayley and B. W. Simpson, *J. Chromatogr.*, 356 (1986) 123.
12 L. Rozanski, *Wiad. Chem.*, 39 (1985) 427.
13 N. Takahashi, N. Mikami, T. Matsuda and J. Miyamoto, *J. Pestic. Sci.*, 10 (1985) 643.
14 K. Furuzawa, N. Mikami, H. Yamada and J. Miyamoto, *J. Pestic. Sci.*, 11 (1986) 253.
15 S. Sakata, N. Mikami, T. Matsuda and J. Miyamoto, *J. Pestic. Sci.*, 11 (1986) 71.
16 K. Furuzawa, N. Mikami, H. Yamada and J. Miyamoto, *Nippon Noyaku Gakkashi*, 11 (1986) 253.
17 D. Kanianský, V. Madajová, M. Hutta and I. Žilková, *J. Chromatogr.*, 286 (1984) 395.
18 Z. Stránský, *J. Chromatogr.*, 320 (1985) 219.

Journal of Chromatography, 470 (1989) 241–250
Elsevier Science Publishers B.V., Amsterdam — Printed in The Netherlands

CHROM. 21 223

CAPILLARY ZONE ELECTROPHORESIS OF HISTIDINE-CONTAINING COMPOUNDS

FREDERICK S. STOVER*, BARRY L. HAYMORE and RANDY J. McBEATH
Central Research Laboratories, Monsanto Co., 800 N. Lindbergh Blvd., St. Louis, MO 63167 (U.S.A.)

SUMMARY

Capillary zone electrophoresis has been tested for the separation of angiotensins, cationic heptapeptides and model histidine derivatives. Good separation efficiencies are seen for peptides and model compounds with negative to small positive net charges. For net charge greater than +2, addition of putrescine to pH 6 buffer greatly suppresses ion exchange at anionic sites on fused silica. When operating at pH values where histidine groups are neutral, addition of Zn^{2+} allows separations based on metal, rather than proton, binding. Separation efficiencies and relative migration times are dependent on capillary length when ion-exchange behavior occurs.

INTRODUCTION

Capillary zone electrophoresis (CZE) is a powerful, high-speed separation technique featuring high resolution, flexible operating conditions and on-line detection[1,2]. The method has proved particularly valuable for separating proteins[3–6] and amino acids [7–9]. Relatively little work has been done on peptide separations by CZE. Firestone *et al.*[10] used a commercial isotachophoresis (ITP) analyzer with a 0.5 mm I.D. PTFE capillary to determine Phe–His purity. Use of CZE–mass spectroscopy for the identification of Phe–Phe, Trp–Phe, leucine enkephalin and vasotocin has been reported[11]. Labeled peptides from tryptic digests of chicken egg white have been separated[12], but not identified.

The predominant factor affecting peptide mobility changes over the CZE operating pH range 4–10 is ionization of His moeities. At low pH values, accumulation of positive charge due to protonation of His could lead to interactions with fixed, negative charges on capillary walls, resulting in decreased efficiencies. Previous studies[4] have discussed difficulties in obtaining high efficiency CZE separations of positively charged proteins due to surface interactions. It is not clear how serious this problem is for small peptide separations.

This study reports CZE separations of various His containing compounds: model His derivatives, blocked His–Gly copeptides and human form angiotensins. The net positive charge necessary for significant peak broadening due to surface interactions is assessed, and improvements in efficiencies of cationic peptide separations are explored through use of metal or organic cation additives. Investigations

0021-9673/89/$03.50

are performed using a modified, commercial ITP instrument and a liquid chromatography UV–VIS detector.

EXPERIMENTAL

Apparatus

LKB 2127 Tachophor (Bromma, Sweden) power supply and analyzer units were used to supply high voltage to the CZE buffer reservoirs. The ITP capillary and detector were replaced with two 50-cm 1.5 mm × 0.8 mm I.D. PTFE capillaries. These wide-bore capillaries were filled with working buffer and provided electrical contact to the 25-ml polypropylene beakers used as CZE reservoirs. The terminating reservoir of the Tachophor was fitted with a membrane to prevent drainage to the CZE reservoir. Reservoirs in the Tachophor analyzer unit were filled with deionized water. A schematic diagram of the connections for CZE are shown in Fig. 1. One potential advantage of this arrangement with buffer filled electrical contacts is isolation of the electrolysis products from the CZE reservoirs.

Untreated 75 μm I.D. fused-silica capillaries (Scientific Glass Engineering, Austin, TX, U.S.A.) were used for electrophoresis. Active capillary lengths (anode-to-detector) were 40 or 70 cm with total lengths (anode-to-cathode) of 70 and 100 cm, respectively. Capillaries were mounted through a 1-mm, straight-bore, preparative flow cell cassette of an ISCO V4 UV–VIS detector (Lincoln, NE, U.S.A.), as shown in Fig. 2. A 1-cm section of the outer polymer coating on the capillary at the location of the detector window was removed with a razor blade prior to mounting.

Chemicals

Buffer solutions used for electrophoresis are shown in Table I. CHES, MES and Tricine were obtained from Sigma (St. Louis, MO, U.S.A.). Potassium phosphate

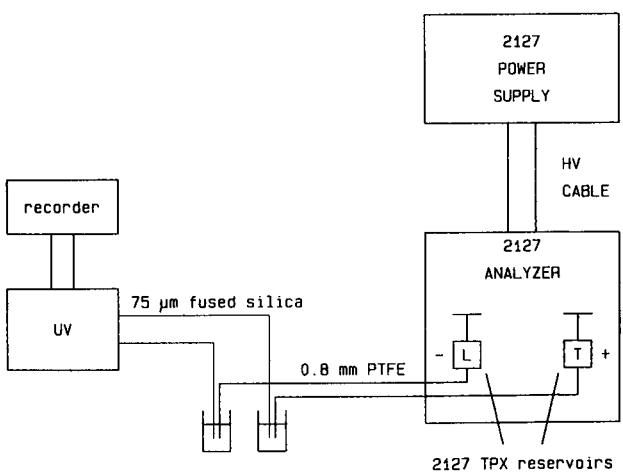

Fig. 1. Schematic diagram of connections from LKB 2127 Tachophor to external buffer compartments and ISCO V4 for CZE.

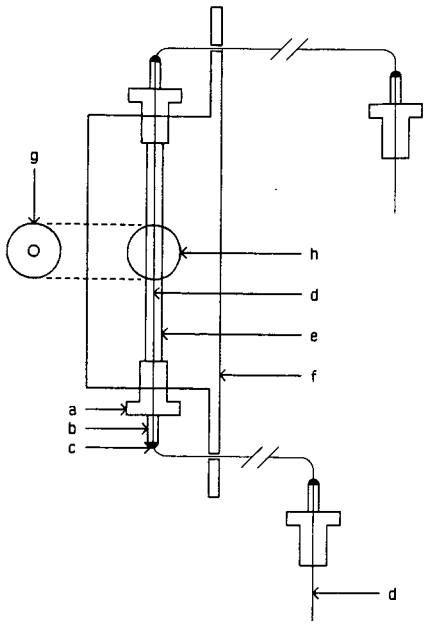

Fig. 2. Detail of connection of fused-silica capillary to ISCO V4 1 mm, preparative flow cell cassette. Side view of cassette. (a) Omnifit 1/4 in. × 28 fitting, (b) 1.5 × 0.3 mm PTFE tubing, (c) epoxy seal, (d) fused-silica capillary, (e) 1-mm flow path, (f) cassette, (g) 0.8-mm incident aperture, (h) flow cell window.

monobasic, potassium hydroxide and potassium chloride were obtained from Fisher Scientific (Pittsburgh, PA, U.S.A.). Zinc perchlorate hexahydrate was obtained from Johnson Matthey (Seabrook, NH, U.S.A.). Buffers were prepared at the molarities listed in Table I, and the pH was adjusted with 1 *M* KOH.

His-containing compounds tested are listed in Table II. All compounds were obtained from Sigma, except for the 4-His, 3,5-diHis and 2,4,6-triHis heptapeptides.

TABLE I

COMPOSITION OF BUFFER SYSTEMS AND RESULTING CURRENTS IN THE 40 cm AND 70 cm × 75 μm CAPILLARIES

pH	*Buffer system*	*μA at 15 kV*	
		40 cm	*70 cm*
6	20 m*M* N-morpholinoethanesulfonic acid (MES) 10 m*M* KCl	17	–
7	10 m*M* KH_2PO_4	14	9.7
7.5	20 m*M* N-tris(hydroxy methyl)methyl glycine (Tricine) 10 m*M* KCl	13	–
8	20 m*M* Tricine 10 m*M* KCl	17	–
9	20 m*M* N-cyclohexylaminoethanesulfonic acid (CHES) 10 m*M* KCl	15	–

TABLE II

COMPOUNDS STUDIED

Histidine derivatives	
(1)	L-Histidine methyl ester (HME)
(2)	Glycyl-L-histidine (Gly–His)
(3)	L-Histidine (His)
(4)	N-Acetyl-L-histidine (NAH)
Model heptapeptides	
(M)	Hca–Gly–Gly–Gly–His–Gly–Gly–Gly–NH–CH_3 (4-His) (Hca = hydrocinnamyl)
(D)	Hca–Gly–Gly–His–Gly–His–Gly–Gly–NH–CH_3 (3,5-diHis)
(T)	PMH–Gly–His–Gly–His–Gly–His–Gly–NH–CH_3 (2,4,6-triHis) (PMH = p-methoxy hydrocinnamyl)
Angiotensins	
(I)	Asp–Arg–Val–Tyr–Ile–His–Pro–Phe–His–Leu
(II)	Asp–Arg–Val–Tyr–Ile–His–Pro–Phe
(III)	Arg–Val–Tyr–Ile–His–Pro–Phe

These peptides were synthesized by standard solid-phase techniques on an automated peptide synthesizer (Biosearch Model 9500, San Rafael, CA, U.S.A.). All His were double coupled using Boc-tosyl His. The resin used was a standard polystyrene 1% cross-linked with divinylbenzene. The peptides were cleaved from the resin using neat methylamine at 4°C (8 p.s.i.g.) for 12 h. Methylamine was removed under vacuum and residual amine neutralized with acetic acid, all at 4°C. The crude mixture was dissolved in water and separated from the spent resin. Purification to homogeneity was accomplished by preparative reversed-phase chromatography using Vydac C_{18} alumina (The Separations Group, Hesperia, CA, U.S.A.) eluted with a linear acetonitrile–water gradient containing 1% trifluoroacetic acid.

Procedures

UV detection was performed at 220 nm, 0.01 a.u.f.s. for all runs. The LKB power supply was operated at a separation voltage of 15 kV in a constant current mode. Sampling was performed by electromigration at 5kV for 5 s from samples diluted in the appropriate buffer. Electropherograms were recorded on a Kipp and Zonen BD-41 strip chart recorder at 1 cm/min chart speed, or were processed using a data acquisition system described previously[13].

pK_a titrations

Concentration-based pK_a values for the synthetic heptapeptides were determined by potentiometric titration in 0.5 *M* $NaClO_4$. A Metrohm 636 Autotitrator (Herisau, Switzerland) was used with a Metrohm Model 6-0210-100 combination pH electrode. The reference filling solution was 3 *M* NaCl–0.5 *M* $NaClO_4$. The titrant 10 m*M* NaOH–0.5 *M* $NaClO_4$ was standardized *vs.* dried potassium acid phthalate from the National Bureau of Standards (Gaithersburg, MD, U.S.A.). Electrode calibration in pH was performed by titrating 10 ml of 2 m*M* $HClO_4$–0.5 *M* $NaClO_4$. Peptides

were diluted to 1 m*M* in 0.5 *M* $NaClO_4$ and, if needed, excess $HClO_4$ added. All titrations were performed in duplicate and the data analyzed using Motekaitis and Martell's PKAS program[14].

RESULTS

Model compounds

Fig. 3 shows separations obtained for the four model compounds listed in Table I. These compounds were selected to give one anionic species (NAH,4), one cationic species (HME,1) and two nominally neutral species (His,3 and Gly–His,2) in the pH range covered. Good separations are seen with each buffer. Numbers of theoretical plates, *N*, are highest for anionic NAH, 170 000 at pH 9, and are lowest for cationic HME, 11 000 at pH 6. Broader peaks for His are due to a comigrating impurity, which can be seen at pH 7. Peak broadening for the cationic model compounds is measurable; however, reasonable efficiencies for all compounds are seen across this pH range.

Of interest is the reversal of migration order for His and Gly–His between pH 7 and 8. These migration orders are consistent with calculated charges on the molecules at different pH values (see Discussion, Table III).

Cationic heptapeptides

Heptapeptides containing a glycine backbone with one (M), two (D) or three (T) His, as given in Table I, were run at pH 6 – 9. The peptides are blocked at both N- and C-termini, so that only charges on the His govern the total peptide charge.

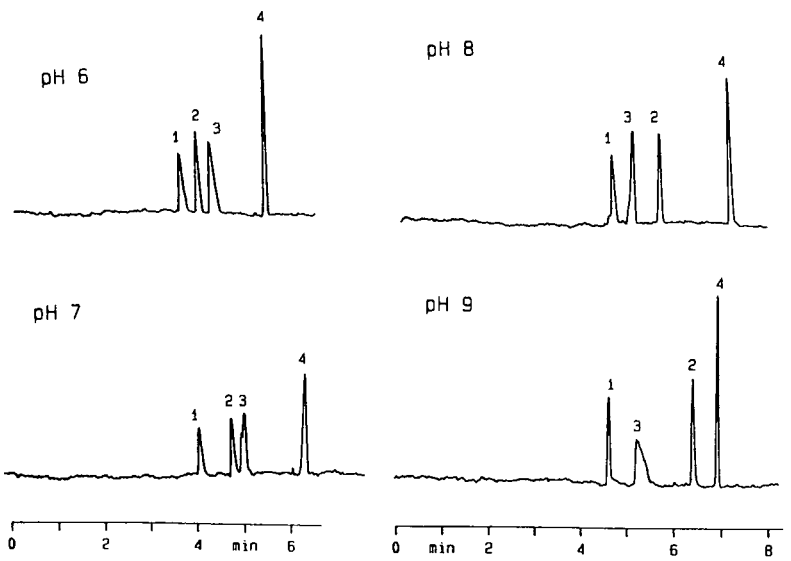

Fig. 3. Separation of small model compounds *vs.* pH. 1 = HME, 2 = Gly–His, 3 = His, 4 = NAH. 0.4 mg/ml each compound; 40-cm capillary; 15 kV.

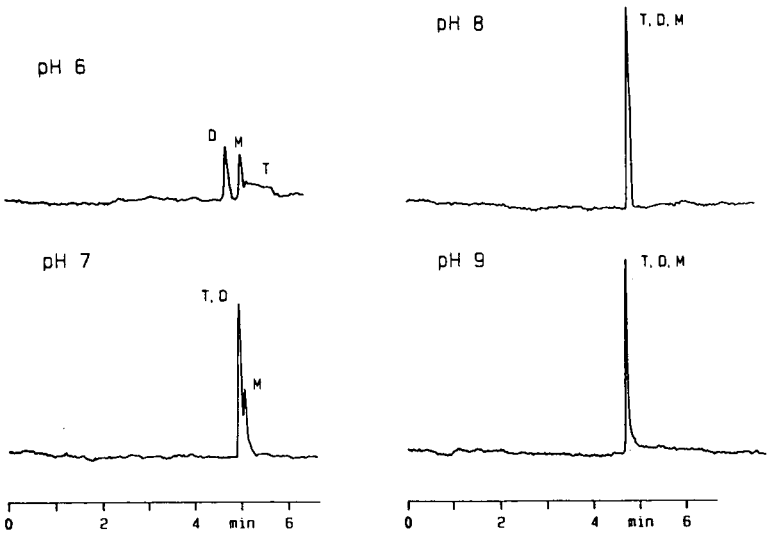

Fig. 4. Separation of cationic heptapeptides *vs.* pH. M = 4-His, D = 3,5-diHis, T = 2,4,6-triHis. 0.5 mg/ml each peptide; 40-cm capillary; 15 kV.

Blocking of the C-terminus also allows relatively high positive charges at neutral-to-basic pH's.

Electropherograms of these peptides are shown in Fig. 4. Separation of the mono- (M) and di-His (D) peptides at pH 6 gives N values of 26 000 and 15 000 and a resolution of 2.8. However, the highly cationic tri-His migrates after mono-His and shows extreme peak broadening. At higher pH values these peptides comigrate as histidines become deprotonated and all net charges approach zero.

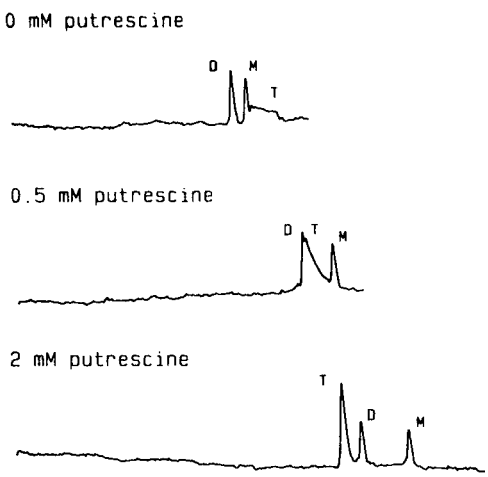

Fig. 5. Separation of cationic heptapeptides in pH 6 buffer with varying amounts of putrescine added. Same conditions as Fig. 4.

Band broadening in CZE will result from any process that is not homogeneously distributed in a radial direction (*e.g.* surface interactions, thermal gradients, laminar flow). While most discussions of adsorptive broadening have focused on proteins, poor efficiencies also have been observed for di- and tri-valent metals[15]. Adsorption of cationic species in CZE can be viewed as simple ion exchange with buffer cations at negative sites on the capillary wall. Ion exchange could be minimized by using buffer cations with strong affinities for surface exchange sites. Lauer and McManigill[4] suggested that polyvalent organic cations can sharpen CZE protein peaks.

Fig. 5 gives the results of adding putrescine to pH 6 buffer to minimize ion exchange of the tri-His peptide. Putrescine (2 m*M*) gives an improved separation of the three His-containing peptides. The peptides now migrate in order of His content with plate numbers of 19 000–62 000. Analysis times are increased only marginally by ζ-potential changes and reductions in electroosmotic flow.

Use of a metal containing buffer also was tested for obtaining improved separation of the peptides. As described above, excessively high charges can occur when protonation of His alone is used to affect a separation. Differential affinities for metals, rather than protons, could be another basis for separation. Fig. 6 shows separations obtained in pH 7.5 tricine buffer with and without added Zn^{2+}. pH 7.5 was chosen so that His protonation would be minimized and Zn–His interactions maximized. Also, operation at a pH substantially less than the buffer pK_a minimizes $Zn(tricine)_2$ formation and possible Zn deactivation.

Improved separation is seen with the Zn-containing buffer. However, the peptides do not migrate in order of expected Zn affinity (tri > di > mono). The tri-His peptide displays a long migration time and relatively low efficiency (N = 7000). Large positive charges are possible for complexes of Zn^{2+}, tricine (HB) and tri-His peptide (H_3T), namely ZnT^{2+}, $ZnHT^{3+}$ and $Zn(B)HT^{2+}$. Thus, late migrating tri-His can be explained by ion exchange of the Zn complexes.

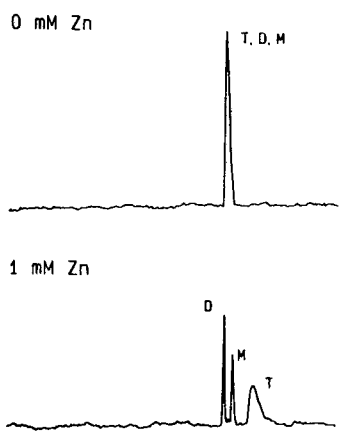

Fig. 6. Separation of cationic heptapeptides in pH 7.5 buffer with and without addition of 1 m*M* Zn $(ClO_4)_2$. Same conditions as Fig. 4.

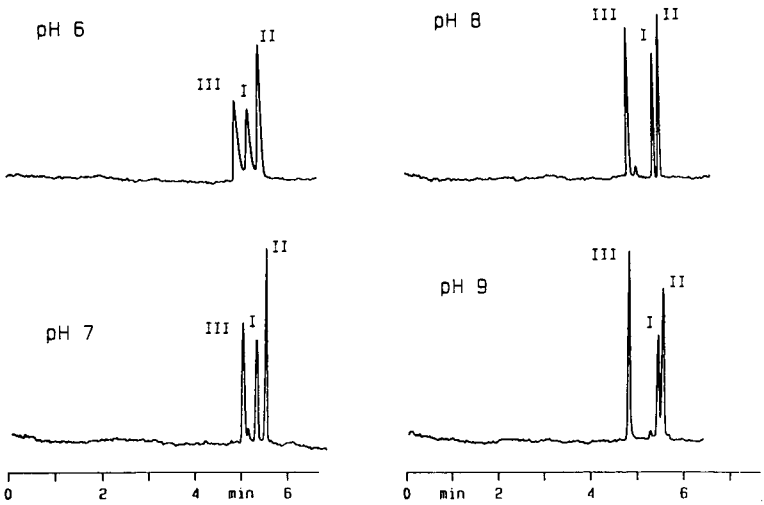

Fig. 7. Separation of human form angiotensins I, II and III *vs.* pH. 0.5 mg/ml each peptide; 40-cm capillary; 15 kV.

Angiotensins

To test CZE for the separation of biologically important cationic peptides, angiotensins I, II and III were run at pH 6–9. Fig. 7 shows that excellent separations are obtained, with the best efficiencies and resolutions occuring at pH 8. *N* values are 64 000 for III, 180 000 for I and 192 000 for II. Resolutions are 3.4 for III/I and 2.5 for I/II. Lower efficiencies are seen as positive charge on the angiotensins increase; however, peak broadening does not rule out the high-resolution separation of these compounds as cations.

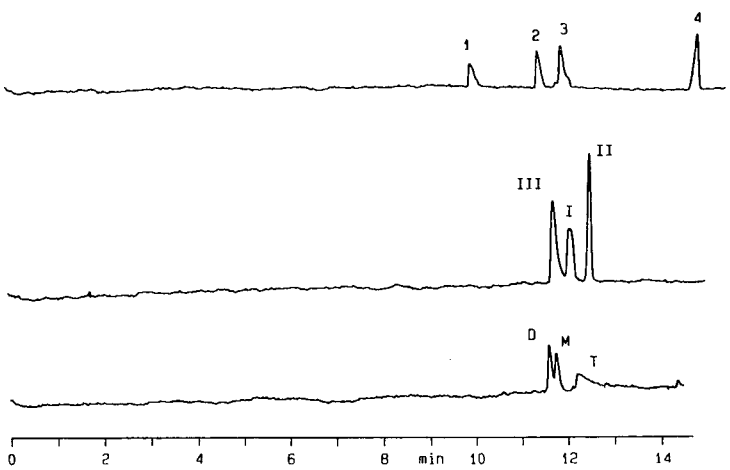

Fig. 8. Separation of His containing compounds in 70-cm long capillary, pH 7 buffer. Top: model compounds, middle: angiotensins, bottom: synthetic peptides. Concentrations same as in Figs. 3, 4 and 7; 15 kV.

The 70-cm capillary separations

Separations are shown in Fig. 8 for each class of compounds using a 70 cm × 75 μm capillary and pH 7 buffer. The longer capillary was used to test for thermal broadening in the previous 40-cm separations. Efficiencies increased by a factor of 2.3 for HME and 3.5 for Gly–His and NAH, indicating that the thermal effect of reducing the current from 14 μA to 9.7 μA on going to the longer capillary is significant.

For cationic peptides, a striking difference in the total separation pattern is seen. All three peptides can be separated at pH 7 in the long capillary, but with tri-His migrating last. Also, N for the tri-His peptide is only 6000 at 70 cm while N = 18 000 for the combined di/tri peak at 40 cm. Finally, the migration time of angiotensin III is longer for the 70-cm capillary relative to I and II, with essentially no increase in plate number.

These results indicate that ion-exchange retardation of highly charged, cationic compounds is dependent on capillary length. Increased capillary length leads to lower efficiencies for ion-exchanging cations, in contrast to diffusion limited separations where N is independent of length[2].

DISCUSSION

While the results presented here show lower separation efficiencies for cations than for neutrals and anions, acceptable peak shapes were obtained for all compounds except tri-His at pH 6. To assess the positive charge necessary for severe peak

TABLE III

CONCENTRATION-BASED pK_a VALUES AND CALCULATED CHARGE *VS.* pH FOR COMPOUNDS STUDIED

pK_a		*Calculated net charge*			
		pH 6	*pH 7*	*pH 8*	*pH 9*
Histidine derivatives[a]					
HME	7.2, 5.3	+1.1	+0.6	+0.1	0.0
Gly–His	8.1, 6.7, 2.5	+0.8	+0.3	−0.4	−0.9
His	9.1, 6.0, 1.7	+0.5	+0.1	−0.1	−0.4
NAH	7.0, 2[b]	−0.1	−0.5	−0.9	−1.0
Heptapeptides[c]					
tri-His	7.3, 6.7, 6.2	+2.4	+1.1	+0.2	0.0
di-His	7.1, 6.3	+1.6	+0.7	+0.1	0.0
mono-His	6.8	+0.9	+0.4	+0.1	0.0
Angiotensins[d]					
III His =	6.7	+1.9			
I His =	7.1, 6.3	+1.6			
II His =	6.7	+0.9			

[a] Ref. 18, I = 0.1 or 0.16 M.
[b] Estimated.
[c] This work, I = 0.5 M.
[d] Estimated, see text.

degradation due to surface ion exchange, net charges for each compound were calculated using cumulative Henderson–Hasselbach relations[16]. Heptapeptide pK_a values were determined as described in the Experimental section, while literature values were used for His derivatives. For angiotensins, N-termini, Tyr and Arg side chains were assumed to be fully protonated and C-termini and Asp side chains were assumed to be fully deprotonated at pH 6. His residues were given values corresponding to those for the mono- and di-His heptapeptides. Charges at pH > 6 were not calculated for the angiotensins due to uncertainties in N-terminus and interior Tyr pK_a values.

Table III gives the calculated charge-pH data for the compounds tested. Inspection of the Table reveals that a net charge of $> +2$ is necessary for the severe ion-exchange retardation seen with tri-His in a 40-cm capillary. Good correlations are seen between charge and migration orders within compound classes. Accurate determination of migration times and electroosmotic flow *vs.* pH should enable CZE to be used for pK_a determinations, similar to procedures developed for ITP[17].

Results presented here indicate that CZE in 40-cm capillaries is capable of high efficiency separations of peptides and model compounds if charges are $< +2$. Use of ion-exchange supressors such as putrescine extends the range of CZE to more positively charged compounds. Alternatively, metal binding at higher pH's can be used to improve separations of His-rich peptides. Separation of the 3,4-, 3,5-, 3,6- and 2,6-positional isomers of the di-His heptapeptide was attempted using Zn^{2+} buffers. pH 7.5 buffer containing 1 m*M* Zn^{2+} is slightly effective in splitting out one isomer, but higher metal concentrations give excessive ion-exchange broadening. Tailoring the pH/metal content of CZE buffers and use of ion-exchange suppressors or deactivated capillaries could yield high-resolution separations of peptides based on both His content and spacing. Also, mobility modifications observed here with Zn^{2+} complexation suggest the potential for chiral separations of underivatized enantiomers using simple UV detection.

REFERENCES

1 J. W. Jorgenson and K. De Arman Lukacs, *J. Chromatogr.*, 218 (1981) 209.
2 A. S. Cohen, A. Paulus and B. L. Karger, *Chromatographia*, 24 (1987) 15.
3 Y. Walbroehl and J. W. Jorgenson, *J. Chromatogr.*, 315 (1984) 135.
4 H. H. Lauer and D. McManigill, *Anal. Chem.*, 58 (1986) 166.
5 A. S. Cohen and B. L. Karger, *J. Chromatogr.*, 397 (1987) 409.
6 S. J. Hjertén, K. Elenbring, F. Kilár, L.-L. Liao, A. J. C. Chen, C. J. Siebert and M.-D. Zhu, *J. Chromatogr.*, 403 (1987) 47.
7 P. Gozel, E. Gassmann, H. Michelsen and R. N. Zare, *Anal. Chem.*, 59 (1987) 44.
8 K. Otsuka, S. Terabe and T. Ando, *J. Chromatogr.*, 332 (1985) 219.
9 R. A. Wallingford and A. G. Ewing, *Anal. Chem.*, 59 (1987) 1762.
10 M. A. Firestone, J.-P. Michaud, R. H. Carter and W. Thormann, *J. Chromatogr.*, 407 (1987) 363.
11 R. D. Smith, J. Olivares, N. T. Nguyen and H. R. Udseth, *Anal. Chem.*, 60 (1988) 436.
12 J. S. Green and J. W. Jorgenson, *J. Chromatogr.*, 352 (1986) 337.
13 F. S. Stover, K. L. Deppermann and W. A. Grote, *J. Chromatogr.*, 269 (1983) 198.
14 R. J. Motekaitis and A. E. Martell, *Can. J. Chem.*, 60 (1982) 168.
15 T. Tsuda, K. Nomura and G. Nakagawa, *J. Chromatogr.*, 264 (1983) 385.
16 B. Skoog and A. Wichman, *Trends Anal. Chem.*, 5 (1986) 82.
17 T. Hirokawa, M. Nishino and Y. Kiso, *J. Chromatogr.*, 252 (1982) 49.
18 R. M. Smith and A. E. Martell, *Critical Stability Constants*, Vol. 1, Plenum Press, New York, 1974. pp. 61, 80, 305; Vol. 2, p. 159.

Journal of Chromatography, 470 (1989) 251–260
Elsevier Science Publishers B.V., Amsterdam — Printed in The Netherlands

CHROM. 21 273

HIGH-VOLTAGE CAPILLARY ZONE ELECTROPHORESIS OF RED BLOOD CELLS

AN ZHU*,[a] and YI CHEN
Institute of Chemistry, Academia Sinica, 100080 Beijing (China)

SUMMARY

The high-voltage wide-bore capillary zone electrophoresis of red blood cells was investigated. The reproducibility of the retention time (electrophoretic mobility) is excellent and the differentiation among various species is good. The peaks in the electropherogram describe the distribution of the size and/or surface charge of the cells and are therefore broad. The relationship between the peak height and the number of cells injected is good, with linear correlation coefficients better than 0.98. Details of the preparation of cell suspensions and support electrolytes are given, which is essential for obtaining reproducible results. The inner surface of FEP capillary tubing is degraded by the application of high voltage and a pause is necessary between successive experiments if good and reproducible peak shapes are to be obtained. The length of the pause increases with the number of experiments made, and finally the tubing becomes useless. Inspection of the inner surface by X-ray photoelectron spectroscopy showed the breakdown of CHF bonds, but the actual mechanism is not known.

INTRODUCTION

Since 1979[1,2], capillary zone electrophoresis (CZE) developed rapidly. With a capillary of 1 m or less long, both small and large molecules can be separated with efficiency of 10^4–*ca.* 10^6 theoretical plates. Whereas high-performance liquid chromatography (HPLC) suffers from a decrease in efficiency when dealing with large molecules, CZE features a high and increasing efficiency because the larger the molecules are the smaller is the diffusion coefficient. In previous work mainly small ions were studied. A few papers were devoted to protein separations[3]. It was found that in the separation of charged biomolecules by CZE, care had to be taken to avoid adsorption on the inner wall of the tubing, otherwise no peak is observed. Recently, CZE of proteins was accomplished with an efficiency of *ca.* $8 \cdot 10^5$ theoretical plates[3].

An attempt was made in our laboratory to explore the advantages of the CZE of cells or suspensions, which are several orders of magnitude larger than proteins or other biomacromolecules if a single cell or particle is counted as a molecule. Human,

[a] Present address: Department of Chemical Engineering, Yale Univerity, New Haven, CT 06520-2159, U.S.A.

chicken, porcine and rabbit red blood cells (RBC) were electrophoresed and the mobilities of the RBC and their distribution thus determined were comparable to previously reported data. The high-voltage CZE of cells has advantages such as outstanding reproducibility, rapidity, simultaneous measurement of a swarm of cells and hence good statistical significance, automatic recording and relatively simple apparatus. The operating conditions were found to be critical and were systematically studied. The inner surface of the FEP (fluorinated ethylene–propylene copolymer) tubing was degraded during electrophoresis, leading to a steadily increasing relaxation time between two successive experiments until the tubing surface became permanently damaged.

EXPERIMENTAL

Chemicals

N-2-Hydroxyethylpiperazine-N′-2-ethanesulphonic acid (HEPES), morpholino-ethane sulphonic acid (MES) and other organic electrolytes were donations from Dojindo Laboratories (Kumamoto, Japan) and the FEP capillary was donated by Dr. Shigeru Terabe (Department of Industrial Chemistry, Kyoto University, Kyoto, Japan). Hydroxypropylmethylcellulose (HPMC) II was purchased from Sigma (St. Louis, MO, U.S.A.) and Tris, glucose (chemically pure) and the inorganic salts (analytical-reagent grade) were purchased from Beijing Chemical Works (Beijing, China). Triply distilled water was prepared in this laboratory.

Electrolytes

As a medium for RBC, the support electrolyte must be isotonic and of the same density as the blood. The electrolytes used in this study are listed in Table I. The use of glucose instead of sucrose will be discussed elsewhere.

Apparatus

The Model RHR 40 PN high-voltage power supply (0–40 kV, 0–3 mA) was purchased from Spellman (Plainview, NY, U.S.A.) and the UV Model 238 detector was from LKB (Bromma, Sweden), in which a filter of 206 nm was mounted. The sensitivity range was set at 0.005 a.u.f.s. The laboratory-made CZE apparatus is shown

TABLE I
COMPOSITIONS OF THE SUPPORT ELECTROLYTES

Code	*Ingredients*[a,b]	*pH adjuster*
H1	0.012 *M* HEPES, 5.14% G	Tris
H2	0.012 *M* HEPES, 4.70% S, 2.50% G	Tris
M	0.0055 *M* MES, 5.30% S, 2.50% G	Tris
P1	$2.2 \cdot 10^{-4}$ *M* KH_2PO_4, $4.0 \cdot 10^{-4}$ *M*, KCl $1.14 \cdot 10^{-4}$ *M* $MgCl_2$, 5.30% S, 2.50% G	Na_2HPO_4
P2	$4.4 \cdot 10^{-4}$ *M* KH_2PO_4, $8.0 \cdot 10^{-4}$ *M*, KCl $2.3 \cdot 10^{-4}$ *M* $MgCl_2$, 7.60% S, 1.00% G	Na_2HPO_4

[a] The pH and the percentage of the additive (HPMC) are specified in the text.
[b] S = Sucrose; G = glucose.

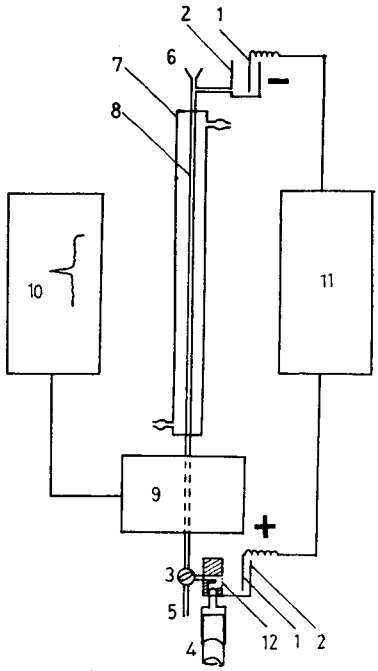

Fig. 1. Schematic diagram of the CZE apparatus. 1 = Pt electrode; 2 = electrolyte reservoir; 3 = three-way valve; 4 = 20-ml plastic syringe; 5 = drain; 6 = injection port; 7 = water cooling jacket; 8 = FEP capillary; 9 = UV detector; 10 = recorder; 11 = high-voltage power supply; 12 = semipermeable membrane.

schematically in Fig. 1; an FEP tube (8) of 0.45 mm I.D. was fitted vertically. The electrolyte solution in the capillary was cooled by a water-jacket (7), with a few exceptions when air cooling was used as specified in the text. A semipermeable membrane (12) at the outlet of the tubing formed a seal to prevent the solution from flowing by gravity. A small hole was drilled at the top of the UV detector housing as the inlet passage for the FEP tubing, which protruded out from the front panel and the part of it in the housing served as the flow cell. The upper and lower electrolyte reservoirs (2) were LKB injection block 2127-007 and membrane block 2127-008, respectively. The three-way valve (3) was a built-in part of the latter. The lower electrode was grounded.

Filling the tubing with electrolyte

Valve 3 (fig. 1) was turned so that the electrolyte solution in the upper reservoir was sucked into the capillary by drawing the plunger of the 20-ml plastic syringe (4). The valve was then turned to connect the capillary and the lower reservoir and 30 s later the sample was injected with a microlitre syringe. The high-voltage power supply was turned on to start the electrophoresis.

Renewal of electrolyte

After the electrophoresis had ended, valve 3 (Fig. 1) was turned to drain the liquid in the capillary and the inside of it was washed successively three times with

distilled water and twice with the electrolyte before it was refilled. If the electric current differs considerably from the normal value while the voltage remains the same, the electrolyte in the reservoir must be renewed. One filling of the reservoir sufficed for four CZE experiments provided that the organic electrolyte was used. If the electrolyte is to be replaced with another the whole flow system should be washed carefully with distilled water.

Preparation of cell suspensions

Fresh arterial blood from chicken and pig, venous blood from rabbit and human blood from the finger tip were taken and the anticoagulant trisodium citrate was added. They were washed four times with 100 volumes of phosphate-buffered physiological saline (PBS) and then diluted to 40 times the original volume (*ca.* 10^5 cells mm^{-3}) in the support electrolyte; they were then ready for the CZE experiment. If lysis happened to occur, the suspension was centrifuged at 2500 rpm for a few minutes and the settled cells were diluted as above.

Fixation of cells

CZE of fixed RBC was also studied. The blood with anticoagulant was allowed to settle and the cells were washed four times with 20 volumes of PBS and then mixed with 8 volumes of 3% (v/v) formalin in PBS. The mixture was kept at 4–6°C with occasional tapping for 4 h, then 2 volumes of cooled 37% (w/v) formalin were added and thorougly mixed and the mixture was kept consecutively at 4–6°C and room temperature each for 24 h with occasional tapping. The fixed cells were washed 4–5 times with 0.9% (w/v) saline and diluted with 9 volumes of the saline and stored in a refrigerator.

If glutaraldehyde was used instead of formalin, the blood with anticoagulant was first washed five times with 10–20 volumes of 0.9% saline, the cells and 1% (v/v) glutaraldehyde in saline were first separately cooled to 4°C and 10 volumes of the 1% glutaraldehyde were added to the cells slowly while tapping. The reaction was allowed to proceed for 30–45 min and the fixed cells were washed five times with physiological saline, diluted with 9 volumes of water and then stored in a refrigerator.

RESULTS AND DISCUSSION

Addition of HPMC

Previous work met with difficulties when proteins were electrophoresed in a capillary because proteins were adsorbed on the inner wall of the tubing no matter what material was selected for the tubing. The problem was solved by increasing the pH of the electrolyte to more than 8.25[3] so that both the protein molecules and the wall of the tubing were negatively charged. This approach does not seem to be widely applicable. At the beginning of this work the adsorption of the cells was also of concern and bovine serum albumin was tried as an additive to the electrolyte to alleviate the adsorption. Reasonable peaks could be observed but the reproducibility was poor. HPMC, an additive for suppressing unwanted electroosmotic flow, was unexpectedly found to be excellent in obtaining good CZE peaks. It is the linear agglomeration of the RBC rather than adsorption which spoils the CZE of erythrocytes. HPMC presumably acted as a surface-treating agent which broke down the linear agglomerates.

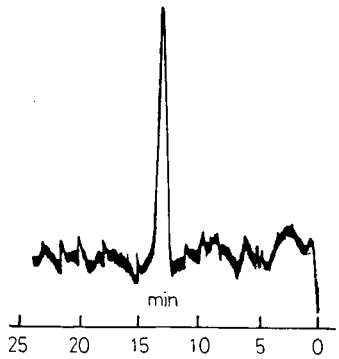

Fig. 2. Electropherogram of human RBC. Electrolyte: H1 containing 0.10% (w/v) HPMC, pH 7.18. $V = 20$ kV; $I = 120$ μA; $T = 19$°C. Q (injection volume) = 1 μl.

Without HPMC, there were many spikes superimposed on the peak of RBC which stemmed from the agglomerates of irregular size and charge. The RBC peak also tailed slightly.

Effect of inner diameter of the tubing

No peak could be observed with tubing of I.D. $\leqslant 0.3$ mm and good results were obtained with I.D. = 0.45 mm. Tubing of 0.5 and 0.6 mm I.D. gave similar results, but the current was high, the baseline became too noisy and spurious peaks frequently emerged. Hence tubing of 0.45 mm I.D. was employed in this study through-out. The total length was 85 cm and the distance from the injection block to the detector was 60 cm.

The CZE of RBC

A typical electrophorogram of the RBC of a healthy man is shown in Fig. 2. The distribution of electrophoretic mobility can be directly seen from the curve and the most probable mobility can easily be calculated from the retention time. As

$$V = V_E + V_{os} \tag{1}$$

where V, V_E and V_{os} are the velocities of the apparent migration of the cells, the electrophoretic migration due simply to the electric field and the electroosmotic flow, respectively, the effective electrophoretic mobility, m ($cm^2\ s^{-1}\ V^{-1}$), of RBC is obtained as

$$m = \frac{(L/t_R) - V_{os})}{E} \tag{2}$$

where L is the length of the tubing from the injection point to the detector (cm), t_R the retention time (s) and E the electric field strength ($V\ cm^{-1}$). The sedimentation of the cells in the vertical tubing is negligible (*ca.* 1 cm h^{-1}) and is not included in eqn. 1 because the electrolyte was so prepared that its density was nearly identical with that of the RBC. By injecting pyridine into the lower end of the capillary, V_{os} was

TABLE II
RETENTION TIMES OF VARIOUS RBC ELECTROPHORESED INDIVIDUALLY AND MIXED WITH OTHERS

RBC	*CZE conditions*	*Retention time (min)*	
		Individual	*Mixed*
(a) Chicken, formalin fixed	Electrolyte M1 + 0.010% HPMC, pH 7.33; V = 15 kV; I = 110 μA; T = 17°C (air cooled)	28.3	28.3 (a + b)
(b) Porcine, glutaraldehyde fixed		32.8	32.5 (a + b)
(c) Rabbit	Electrolyte H1 + 0.10% HPMC, pH 7.18; V = 20 kV; I = 120 μA; T = 18°C	26.6	26.9 (c + d)
(d) Human		14.0	14.1 (c + d)

measured[4] to be 25 cm in 36.5 min, *i.e.*, 0.0114 cm s^{-1}. From the retention time of 13.9 min of the peak in Fig. 2, m is calculated to be $-3.55 \cdot 10^{-4}$ cm^2 s^{-1} V^{-1}. This agrees with the result of $-4.3 \cdot 10^{-4}$ cm^2 s^{-1} V^{-1} (refs. 5 and 6) if the difference in the viscosity and the isotonic additive of the electrolytes used are taken into consideration[7]. The base width of the peak measured with the laser Doppler technique, $0.65 \cdot 10^{-4}$ cm^2 s^{-1} V^{-1} (ref. 8), is twice that in Fig. 2, and the latter is close to the value resulting from microscopic cell electrophoresis[5]. This serves to illustrate the high efficiency of the CZE technique.

When human and rabbit RBC and a mixture of them were electrophoresed successively, no distortion of the peak or shift of the peak maxima was observed in the electropherogram of the mixture, which indicates the absence of interaction between the RBC of the two species. Similar results were obtained for the formalin-fixed chicken RBC and glutaraldehyde-fixed porcine RBC. The retention times are listed in Table II. The differentiation of RBC from different sources or the cells of patients from those of normal persons might therefore be possible.

The number of cells in a single injection was *ca.* $1 \cdot 10^5$, hence the peak shape was a good approximation to the distribution of the mobilities, which could be obtained in less than 30 min, while the microscopic cells electrophoresis measured the cell one after another. Even modern computerized apparatus such as the Parmoquant II (G.D.R.) took more than 1 h to measure 100 cells, which was less than sufficient for describing the distribution of the mobilities.

Reproducibility of the determination of mobilities

The retention times (mobilities) of various cells under different conditions are compared in Table III. The coefficients of variation were always below 2.0%, and injections with different concentrations (Table III, No. 4) or different sample volumes (Table III, No. 1) did not impair the reproducibility. With such a high precision, minor changes in surface charge (and hence mobility) due to disease could then be detected with ease. The reproducibility of microscopic cell electrophoresis was bad and it would consume too much time if a host of cells (say, more than 500) are measured in order to give results with sufficient statistical significance.

TABLE III
REPRODUCIBILITY OF THE RETENTION TIME OF VARIOUS RBC
Injection volume 1 μl unless stated otherwise.

RBC	*Electrolyte and CZE conditions*	*Retention time (min)*	*n*	*Coefficient of variation (C.V.) (%)*
(a) Chicken, formalin	P2 + 0.008% HPMC, pH 7.40; V = 15 kV; I= 140 μA; T $\approx$ 20°C (air)	23.9	5	1.8
(b) Chicken, formalin fixed[a]	P1 + 0.020% HPMC, pH 7.40; V = 15 kV; I = 110 μA; T $\approx$ 16°C (air)	27.5	5	1.6
(c) Chicken, formalin fixed	M1 + 0.010% HPMC, pH 7.33; V = 15 kV; I = 110 μA; T $\approx$ 16°C (air)	28.2	4	0.3
(d) Chicken	M1 + 0.010% HPMC, pH 7.33; V= 15 kV; I = 130 μA; T = 20°C	23.5	5	1.2
(e) Human[b]	H1 + 0.10% HPMC, pH 7.40; V = 20 kV; I = 150 μA; T = 18°C	15.1	5	0.5

[a] Different concentrations, $1.1 \cdot 10^5$, $0.64 \cdot 10^5$, $0.89 \cdot 10^5$ and $0.5 \cdot 10^5$ cells μl^{-1}, were injected.
[b] Different volumes, 0.2, 0.5,1.0, 1.5 and 2.0 μl of the RBC, were injected.

Another example is the retention times of the RBC of healthy male and female persons, as shown in Table IV. The coefficient of variation of the six measured mobilities was 1.32%, which was no worse than measuring the RBC from a single person.

Linearity

The peak height varied linearly with the sample size as in chromatographic analysis. Table V shows the linearity at different pH values and with different ranges of

TABLE IV
RETENTION TIMES OF THE RBC OF HEALTHY INDIVIDUALS
Electrolyte H1 + 0.10% HPMC, pH 7.18; V = 20 kV; I = 120 μA; T = 19°C.

No.	*Age*	*Sex*	*Retention time (min)*
1	20	Male	14.0
2	28	Female	13.6
3	23	Male	13.7
4	30	Male	13.6
5	21	Female	13.8
6	27	Male	14.1
			13.8
Mean			(C.V. 1.32%)

TABLE V
EQUATIONS OF REGRESSION LINES UNDER DIFFERENT CONDITIONS

Experiment	*CZE conditions*	*Regression line*[a]
A	Electrolyte H1 + 0.10% HPMC, pH 7.40; V = 20 kV; I = 150 μA; T = 18°C; injection volumes, 0.5, 1, 2, 3 and 4 μl	$H = 2.91Q + 2.19$ ($r = 0.9835$)
B	Electrolyte H1 + 0.10% HPMC, pH 7.18; V = 20 kV; I = 120 μA; T = 19°C; injected volumes, 0.2, 1.0, 1.5 and 2 μl	$H = 9.06Q + 0.93$ ($r = 0.9903$)

[a] H = peak height (cm); Q = injection volume (μl); r = correlation coefficient.

sample size. The good linearity might be the basis of quantitative analysis or a means of cell counting. At pH 7.40 (Table V, A) the current passed was considerably higher than at pH 7.18, which might be responsible for the regression line deviating from the origin. However, it is not clear why the slope of the regression line at pH 7.40 was less than one third of that of the line at pH 7.18.

The pause between two experiments

When a piece of FEP tubing had been subjected to a high electric field strength a number of times, the CZE results became irreproducible. The initial performance could be restored if a pause from a few minutes up to 1 h was allowed before the next experiment was started. It seems that the inner surface of the tubing was subjected to certain physical/chemical changes which necessitated a relaxation period. Careful study showed that the necessary minimum pause for reproducible results depended on the history of the tubing, as outlined in Table VI.

It can be seen from Table VI that the necessary pause time increased steadily with the number of experiments made, which led to the conclusion that an irreversible breakdown process was taking place. When the tubing had been used more than 200–250 times, it was no longer useful. The upper end (high voltage end) of this useless tubing was cut off and the inner wall surface was examined by X-ray photoelectron spectroscopy (XPS). Fig. 3 shows that the peak of binding energy 285.9 eV (C_{1s} electrons) almost disappeared (curve b) which implies that the CHF^9 structure was broken under a high electric field strength. What really happens is not clear. A field strength below 300 V cm^{-1} as in this study is unlikely to be able to cleave the chemical bonds, but an uneven distribution of the electric field might be a cause. If a gas bubble is formed in the vicinity of the tubing wall, the high field strength across the bubble would induce a spark discharge that is sufficient to destroy the linkages among the various atoms on the surface of the wall. It should be pointed out that the so-called

TABLE VI
RELATIONSHIP BETWEEN THE NECESSARY PAUSE TIME AND THE HISTORY OF THE CAPILLARY TUBING

Number of CZE experiments already made	0–10	10–50	50–100	>100
Minimum pause time needed (min)	10	15	30	>40

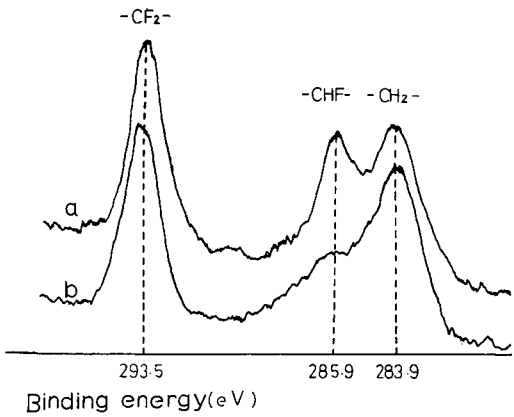

Fig. 3. XPS spectrum of inner surface of FEP tubing. (a) New tubing; (b) used tubing (electrophoresed more than 200 times).

useless tubing behaved well if small molecules were electrophoresed. This again serves to demonstrate the difficulty in electrophoresing proteins, which are abundant in the cell membrane.

Washing of cells

The RBC must be carefully and thoroughly washed so that correct peak shapes and accurate and reproducible results are obtained. Experiments showed the PBS was the most suitable washing solution, and 4–6 washings gave the best results. Washing less than three times led to much longer retention times, and after washing more than six times lysis was liable to occur.

Storage of RBC suspension

Conventionally the RBC were dispersed in 50 volumes of physiological saline and kept at 4°C. However, the peak of the RBC was difficult to observe when the

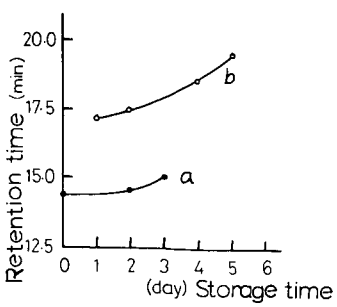

Fig. 4. Effect of storage time on the retention time of human RBC. (a) Electrolyte, H1 + 0.10% (w/v) HPMC, pH 7.40; V = 20 kV; I = 150 μA; T = 20°C. (b) Electrolyte, H2 + 0.10% (w/v) HPMC, pH 7.30; V = 20 kV; I = 110 μA; T = 17°C.

storage time exceeded 2 days. The electrolyte for CZE containing HPMC was found to be a satisfactory medium for the storage of RBC and good electrophoretic peaks resulted after storage for 7 days. However, the retention time of RBC increased with storage time, although slowly, as shown in Fig. 4. Large errors in the retention times could result of RBC are stored for more than 3 days, whereas the peak shape improves considerably.

REFERENCES

1 F. E. P. Mikkers, F. M. Everaerts and Th. P. E. M. Verheggen, *J. Chromatogr.*, 169 (1979) 11.
2 J. W. Jorgenson and K. D. Lukacs, *Anal. Chem.*, 53 (1981) 1298.
3 H. H. Lauer and D. McManigill, *Anal. Chem.*, 58 (1986) 166.
4 T. Tsuda, K. Nomura and G. Nakagawa, *J. Chromatogr.*, 264 (1983) 385.
5 D. H. Heard and G. V. F. Seaman, *J. Gen. Physiol.*, 43 (1960) 635.
6 E. E. Uzgiris and J. H. Kaplan, *J. Colloid Interface Sci.*, 55 (1976) 148.
7 S. Levine, M. Levine, K. A. Sharp and D. E. Brooks, *Biophys. J.*, 42 (1983) 127.
8 E. E. Uzgiris, J. H. Kaplan, T. J. Cunningham, S. H. Lockwood and D. Steiner, in N. Catsimpoolas (Editor), *Electrophoresis '78*, Elsevier, Amsterdam 1978, pp. 427–440.
9 C. R. Ginnard and W. M. Riggs, *Anal. Chem.*, 44 (1972) 1310.

6th Symposium on Isotachophoresis and Capillary Zone Electrophoresis, Vienna, September 21–23, 1988

END OF SYMPOSIUM PAPERS

Journal of Chromatography, 470 (1989) 263–275
Elsevier Science Publishers B.V., Amsterdam — Printed in The Netherlands

CHROM. 21 224

PHASE-HETEROGENEOUS ZONES IN CAPILLARY ISOTACHOPHORESIS OF LOW-SOLUBILITY BASES

VLADIMÍR JOKL*, BORIS VÍTKOVIČ and MIROSLAV POLÁŠEK
Analytical Chemistry Department, Faculty of Pharmacy, Charles University, Heyrovského 1203, CS-501 65 Hradec Králové (Czechoslovakia)
(Received October 7th, 1988)

SUMMARY

The effective mobility of a low-mobility base is regulated by a coupled protolytic and precipitation equilibrium. Assuming that the latter is rapid enough, a procedure for calculating parameters of the isotachophoretic phase-heterogeneous zone of a base in the steady state is suggested. The effect of the leading ion concentration on the effective mobilities as well as the correctness of migration, separability and stability of zones in slightly alkaline electrolyte systems are considered theoretically and experimentally verified for a group of basic drugs. The relationships ascertained serve as a basis for satisfactory separation of compounds of very similar basicities and ionic mobilities but having different solubilities. This is demonstrated by the analyses of two model binary mixtures involving amitriptyline and nortriptyline or moxastine and embramine. Practical analyses, though partly limited by the fact that the heterogeneous zones are analytically not quite stable (a minute zone "bleeding" occurs) and therefore the detection limit is adversely affected, are possible.

INTRODUCTION

In the course of experiments concerning the isotachophoretic determination of ionization constants and ionic mobilities of weak monoacidic bases, we have observed that some bases behave anomalously. This applied namely to bases involving an aliphatic amino group in a side chain attached to a cyclic structure ($pK_{a,B} \approx 9$) under the conditions of isotachophoresis (ITP) with slightly alkaline leading electrolytes ($pH_L \approx 8$). The visual evaluation of the recorded steps showed that they are regular, thus indicating correct ITP migration, but the steps were unexpectedly high which implied that the effective mobilities are lower than would follow from the basicities of these compounds and the acidity conditions in the zones. Moreover, the effective mobility values were apparently affected by the concentration of the leading ion to an extent which distinctly exceeded the effect of ionic strength. Some pairs of bases having very similar ionization constants and ionic mobilities exhibited remarkable differences in effective mobilities. This effect was clearly not caused by a specific interaction with the counter ion (the results were practically the same when using borate, diethylbarbiturate or phosphate buffers as leading electrolytes), but it seemed to correlate to some extent with the solubility of the free base in water.

0021-9673/89/$03.50

Generally, the condition of solubility of all forms of a substance is considered necessary for ITP analysis. Assuming that there exists a sufficiently rapid heterogeneous precipitation equilibrium between the dissolved and undissolved fraction of the free base in its suspension, it may be possible to accept an hypothesis of regular ITP migration of such a heterogeneous zone. (The existence of "micellar" zones was described earlier[1].) According to the acidity conditions in the zone, the adapted "concentration"[a] is distributed as the free undissolved and dissolved base and its protonated form:

$$\bar{c}_B = [B]_s + [B]_l + [HB^+]_l$$

In this paper we have attempted to verify the above hypothesis. If the correct ITP migration of the heterogeneous zones and their stability were confirmed, it would be possible to use for the separation of bases, beside the commonly employed factors (differences in ionic mobilities, ionization constants, interactions with the counter ion and solvation), also the differences in the solubilities of the free bases.

THEORETICAL

When neglecting the effect of the ionic strength (in ITP it usually does not exceed 10 mmol l^{-1}) on the protolytic equilibrium, the molar fraction of the protonated form of a monoacidic fairly soluble base, x_{HB}, is affected only by the pH and does not depend on the concentration

$$x_{HB} = [H^+]/([H^+] + K_{a,B}) \qquad (1)$$

see curve 1 in Fig. 1.

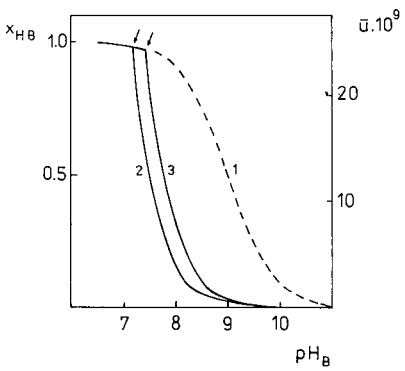

Fig. 1. Molar fraction of the protonated form, x_{HB}, and effective mobility, $\bar{u}$, of bases ($pK_{a,B} = 9.0$; $u_{HB} = 25 \cdot 10^{-9}$ m^2 V^{-1} s^{-1}) as a function of the base zone acidity, pH_B. 1, Readily soluble base; 2,3, for explanation see the text.

[a] The term "concentration" here means the overall analytical concentration of all forms of a base including the undissolved fraction.

The overall solubility, S (mol l^{-1}), of a monoacidic sparingly soluble base depends on the pH of the solution according to the relationship[2]

$$S = S_0(1 + [H^+]/K_{a,B}) \tag{2}$$

where S_0 is the solubility of the free (non-protonated) base; the physical value of S is limited only by the solubility of the salt of the base. In eqn. 2 the term $S_0[H^+]/K_{a,B}$ represents the concentration of the protonated form HB^+ and hence its molar fraction depends on the pH and S_0 as well as on its "concentration", $\bar{c}_B$ (see curves 2 and 3 in Fig. 1)

$$x_{HB} = [HB^+]/\bar{c}_B = S_0[H^+]/K_{a,B}\bar{c}_B \tag{3}$$

where $\bar{c}_B$ is the adapted "concentration" in the ITP zone.

The effective mobilities, $\bar{u}_B$, of a monoacidic base are directly proportional to the molar fraction of the protonated form HB^+

$$\bar{u}_B = u_{HB}x_{HB} \tag{4}$$

(u_{HB} is the ionic mobility of the base) and their values can be obtained by combining eqns. 1 and 4 or 3 and 4 for fairly or sparingly soluble bases respectively. Therefore the corresponding plots of $\bar{u}_B$ *vs.* pH are shaped in an analogous manner (Fig. 1).

In plots 2 and 3 characteristic breaks appear (indicated by arrows). At pH values lower than correspond to these breaks the overall solubility of the base, S, is higher than the adapted "concentration", $\bar{c}_B$, and the base behaves as a well soluble one; its effective mobility is regulated only by the zone acidity. On the contrary, at higher pH the adapted "concentration" is higher than the solubility, S, and the effective mobility of the base is determined by the pH as well as by the solubility of the free base, S_0, and its adapted "concentration", $\bar{c}_B$. Thanks to selected model parameters, the curves 2 and 3 in Fig. 1 have a double meaning:

(a) For a pair of equally strong and mobile bases in borate operational systems with the concentration of the leading ion K^+, c_L = 10 mmol l^{-1}, curve 2 is valid for a base having a solubility of S_0 = 0.1 mmol l^{-1} and curve 3 for a base with S_0 = 0.2 mmol l^{-1}. The course of the curves indicates possible separability based on the differences in S_0.

(b) For a base having solubility S_0 = 0.1 mmol l^{-1}, curve 2 is valid in borate operational systems with c_L = 10 mmol l^{-1} (according to the regulatory function $\bar{c}_B$ = 6.2 mmol l^{-1}); in the same diluted systems with c_L = 5 mmol l^{-1} ($\bar{c}_B$ = 3.1 mmol l^{-1}), curve 3 is valid. In this instance the course of the mobility curves shows the differences in effective mobility at the same pH_L caused by the change of $\bar{c}_B$ adapted to different c_L.

However, under real conditions of ITP with a particular counter ion system, the practically important pH interval in the zone of base is substantially narrower than that depicted in Fig. 1; it is hardly wider than one pH unit (*cf.*, Fig. 6).

On the basis of the above assumptions, the algorithm for the calculation of the zone parameters of a low-solubility monoacidic base in the steady state by the RFQ method[3] was modified. The necessary input data are: the ionic mobilities of H^+, u_H,

leading ion, u_L, counter ion, u_R, and the base, u_{HB}; ionization constants of the counter ion, $K_{a,R}$, and the base, $K_{a,B}$; concentration of the leading ion, c_L, and counter ion in the leading zone, $c_{R,L}$; solubility of the free base, S_0. The algorithm neglects the concentrations of H^+ and OH^- in the summing expressions and it involves the following steps of the iteration procedure:

calculation of

pH_L: $\quad [H^+]_L = K_{a,R}(c_{R,L} - c_L)/c_L$

adapted concentration according to the regulatory function:

$$\bar{c}_B = c_L u_{HB}(u_{HB} + u_R)^{-1}(u_L + u_R)u_L^{-1}$$

solubility of the base:

$$S = S_0(1 + [H^+]_B/K_{a,B})$$

decision whether $S \geqslant \bar{c}_B$:

(a) If the answer is "yes" then the effective mobility of the base is:

$$\bar{u}_B = u_{HB}[H^+]_B([H^+]_B + K_{a,B})^{-1} \tag{5}$$

(b) If $S < \bar{c}_B$ then:

$$\bar{u}_B = u_{HB}S_0[H^+]_B/K_{a,B}\bar{c}_B \tag{6}$$

The next steps, *i.e.*, the calculation of the effective mobility of the counter ion in the zones of the leading ion and the base, concentration of the counter ion in the zone of base and finally the evaluation of the RFQ function are the same as in the original procedure[3]. In the first iteration cycle the pH_L is substituted for pH_B and thereafter the pH_B is successively approximated to minimize the RFQ function until the correct value of pH_B and other parameters of the zone of base in the steady state are attained. An appropriate program was written in BASIC for a microcomputer. The program was used for computing simulated effective mobilities presented in the following parts of this paper.

A space diagram (Fig. 2) illustrates the dependence of the effective mobilities of bases having the ionic mobility, $u_{HB} = 30$[a] on the base strength and solubility for ITP performed in the operational system E (see Table I). Bases with parameters located in the plane ABC behave as readily soluble ones. Otherwise the mobilities decrease with decreasing strength and solubility of the base. The existence of the zone of base is theoretically limited by the mobility of the terminating ion (indicated by the arrow). Diagrams for bases having ionic mobility values higher or lower than 30 are correspondingly shifted up or down along the vertical axis but their shape is analogous to that shown in Fig. 2.

[a] All mobilities are expressed in $10^9 \cdot m^2\ V^{-1}\ s^{-1}$ in this paper.

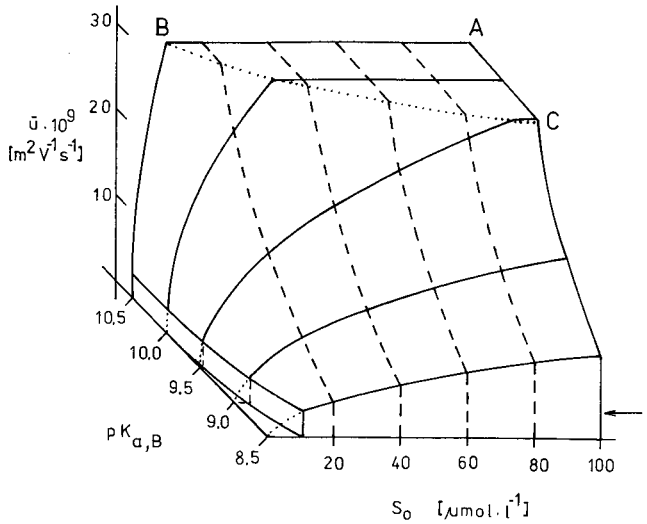

Fig. 2. Space diagram of the dependence of the effective mobility $\bar{u}$, of low-solubility bases with ionic mobility $u_{HB} = 30 \cdot 10^{-9}$ m^2 V^{-1} s^{-1} on their strength, p$K_{a,B}$, and solubility, S_0, in operational system E.

TABLE I

OPERATIONAL ELECTROLYTE SYSTEMS

MES = 2-Morpholinoethane sulphonic acid; EACA = 6-aminohexanoic acid.

System	*Leading electrolyte, L*			*Terminating electrolyte, c (mmol l^{-1})*
	Cation, c_L (mmol l^{-1})	*Counter ion, c_R (mmol l^{-1})*	*pH (exptl.)*	
A, ref. 8	K^+, 10	Acetate, 20	4.74	Acetic acid, 20
B	K^+, 10	Borate, 110	8.17	L-Histidine, 10
C	K^+, 10	Borate, 60	8.43	L-Histidine, 10
D	K^+, 10	MES, 15	6.43	EACA, 10
E	As in B but diluted 1:1 (c_L = 5)		8.13	L-Histidine, 10
F, ref. 5	K^+, 5	2-Pyridine carboxylate, 10	5.35	Formic acid, 10
G	As system E; L = Na^+		8.12	L-Histidine, 10

EXPERIMENTAL

Apparatus

The ITP experiments were carried out with the use of a CS isotachophoretic analyser (URVJT, Spišská Nová Ves, Czechoslovakia) equipped with a non-thermostatted PTFE capillary column (200 mm × 0.3 mm), a conductivity detector and a 30-μl sampling valve.

Materials

Tricyclic antidepressants: amitriptyline hydrochloride (AT); nortriptyline hydrochloride (NT) (partially N-demethylated AT). Antihistamines: moxastine hydrochloride (MX); embramine hydrochloride (EM) (brominated MX). Local anaesthetics: tetracaine hydrochloride (TC) (a basic ester); heptacaine hydrochloride (HC) (a basic carbamate). The above basic drugs, obtained from the State Institute for Drug Control, Prague, were of pharmacopoeial purity. Aqueous stock solutions containing 1 mmol l^{-1} of a drug were appropriately diluted before the ITP separation. All other chemicals were of the highest attainable purity.

The effective mobilities of bases were determined with the use of tetraethylammonium (u = 33.8, ref. 4) as the reference ion, according to

$$\bar{u} \cdot 10^9 = 60.9/(h_{rel} + 0.8) \quad m^2\ V^{-1}\ s^{-1}$$

where h_{rel} is the relative step height of a base[5].

The simulated steady state parameters were computed by using an IQ 151 microcomputer (ZPA, Nový Bor, Czechoslovakia). The earlier published mobility and ionization constants (except for the bases studied) used in the simulations were: u_H = 362.5; u_{Na} = 51.9; u_K = 76.1 (all ref. 5); borate, u = 33.0 (ref. 6), pK_a = 9.14; MES, u = 28.0, pK_a = 6.10; L-histidine, u = 29.6, pK_a = 6.04; EACA, u = 28.8, pK_a = 4.37 (all ref. 7).

RESULTS AND DISCUSSION

Some parameters of the basic drugs studied are presented in Table II.

The pK_a values in Table II indicate that in slightly acidic operational systems A or F (Table I) all the bases are fully ionized and hence the effective mobilities determined are their ionic mobilities; $\bar{u}_B = u_{HB}$.

TABLE II

PHYSICAL-CHEMICAL CONSTANTS OF THE COMPOUNDS STUDIED

Unless stated otherwise our results obtained by turbidimetry according to ref. 2.

Compound	*Molar mass of base (g/mol)*	*p$K_{a,B}$*	*$S_0 \cdot 10^4$ (mol l^{-1})*
Amitriptyline, AT	277.3	9.4[a]	0.46
Nortriptyline, NT	263.4	9.7[b]	1.7
Moxastine, MX	269.3	9.5	4.6
Embramine, EM	348.2	9.3	0.57
Tetracaine, TC	264.3	8.2[c]	12
Heptacaine, HC	362.5	7.6[d]	0.55[e]

[a] Ref. 2.
[b] Ref. 9.
[c] Ref. 10.
[d] Ref. 11.
[e] Ref. 12.

Effect of the leading ion concentration on the effective mobilities

In this series of experiments the operational systems A to D (Table I) were used and the leading electrolytes were diluted to adjust the leading ion concentration to c_L = 4, 6, 8, 10 m*M*. The systems B–D were selected according to the strength and the solubility of the bases: system B for NT, AT, MX and EM; C for TC; D for HC. The working conditions of ITP were adjusted to suit the individual electrolyte dilutions (see Table III). These conditions were found empirically for system B with regard to the increase in voltage and then were kept constant also for systems A, C and D. At very low mobilities (in concentrated leading electrolytes) a mixed zone of the base and the terminator was sometimes formed thus making the evaluation of the base step height impossible; in such cases the base was used directly as the terminating electrolyte (10 m*M*).

The results are presented in Fig. 3. All the compounds exhibit an increase in effective mobility in system A at the lowest dilution, c_L = 4 m*M*, which is probably connected with the decreased ionic strength. Since one can assume an analogous effect when working with systems B–D, the observed individual mobility values were substituted for ionic mobilities, u_{HB}, in the simulation calculations.

The effective mobilities of compounds NT and MX in system B differ negligibly from the results obtained in system A. NT and MX are fairly strong and relatively soluble bases (Table II). Their solubility, *S*, at pH_B (*ca.* 7.9) is much higher than is the adapted concentration in the zone, $\bar{c}_B$ (*cf.*, NT in Fig. 4), and therefore they behave as readily soluble bases.

Compounds AT and EM are in fact as strong bases as NT and MX but they are by one order less soluble. In system B they form zones of pH_B 7.6 to 7.8 and under such conditions their solubility is lower than the adapted "concentration", $\bar{c}_B$, in the whole concentration range studied (Fig. 4). The effective mobilities strongly depend on the concentration of the leading ion. The experimental values exhibit a distinctly parallel course with respect to the simulated function. The positive shift might be caused by an inaccurate value of S_0 or by its temperature dependence in the non-thermostatted apparatus; as follows from eqn. 6, the calculation of the effective mobility is influenced by the value of S_0. The compound HC is a poorly soluble and relatively weak base and therefore it was analysed in system D. Also in this instance the solubility at pH_B (5.8 to 6.0) is lower than the adapted "concentration" and the ITP behaviour of HC is similar to that of AT and EM.

TABLE III

WORKING CONDITIONS OF ITP IN DILUTED SYSTEMS

t' = Time of current switching; t_L = approximate time elapsed before the passage of the first zone boundary through the detector.

c_L (m*M*)	*Separation current* (μ*A*)	t' (*min*)	*Detection current* (μ*A*)	t_L (*min*)
4	10	30	7.5	33
6	15	30	10	35
8	25	20	15	27
10	30	20	20	26

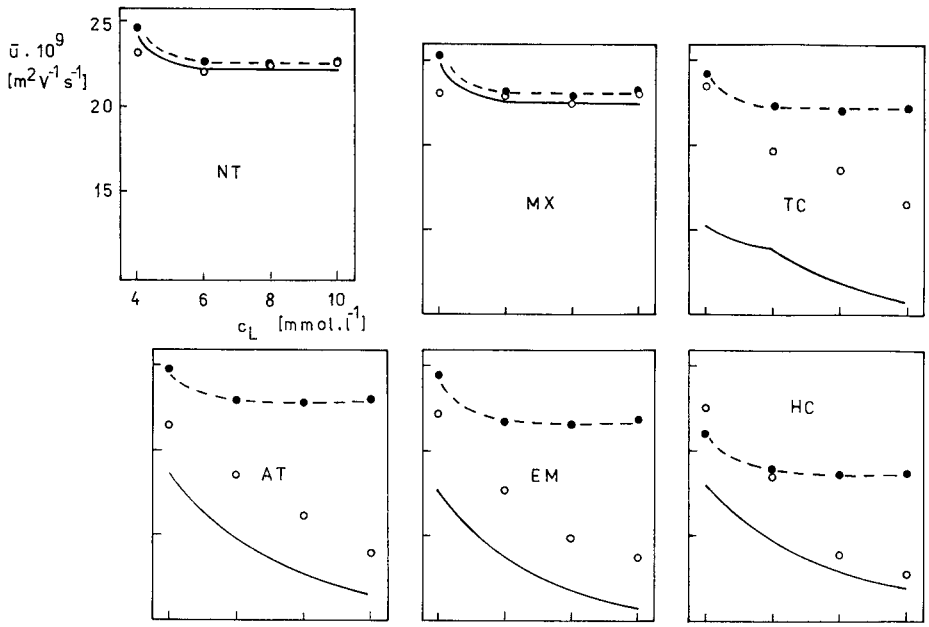

Fig. 3. Dependence of effective mobilities, $\bar{u}$, of bases (see Table II) on the concentration of the leading ion, c_L. Experimental data: ⅛, in system A; @, in systems B (for NT, AT, MX, EM), C (for TC) and D (for HC); solid line, simulated $\bar{u}$ *vs.* c_L function.

Compound TC, thanks to its basicity and solubility, exhibits a characteristic break in the simulated function $\bar{u}_B$ *vs.* c_L in system C; this is caused by the relationship between the solubility and adapted "concentration" (*cf.*, Fig. 4): at $c_L = 4$ mM, $S > \bar{c}_B$; at $c_L = 8$ or 10 mM, $S < \bar{c}_B$. The experimental effective mobility values roughly follow this trend.

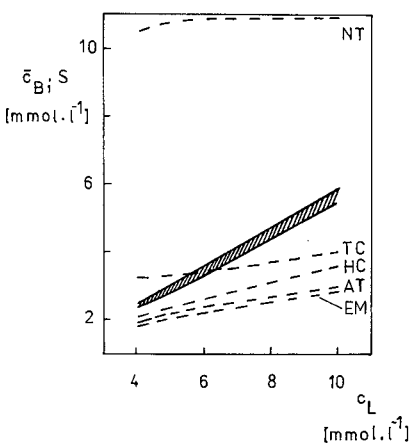

Fig. 4. Dependence of calculated adapted "concentrations", $\bar{c}_B$, of bases and their solubilities, S, in their own zones (in systems B–D) on the concentration of the leading ion, c_L. ———, $\bar{c}_B$ (very similar values); – – –, S.

TABLE IV

CALCULATED PARAMETERS: pH, SOLUBILITY AND MOBILITY IN THE BASE AND TERMINATOR ZONES

Compound	*System*	pH_T	$S_{B,T}$ *(mM)*	$\bar{u}_{T,T}$	$\bar{u}_{B,T}$	pH_B[a]	$\bar{u}_{T,B}$[a]	$\bar{u}_{B,B}$[a]
AT	B	6.97	12.4	3.1	22.8	7.60	0.8	11.5
EM	B	6.97	12.2	3.1	21.6	7.58	0.8	10.7
TC	C	7.11	17.0	2.3	20.7	7.86	0.4	10.8
HC	D	5.06	19.1	4.8	18.6	5.79	1.1	12.0

[a] Values calculated for c_L = 10 m*M*.

Correctness of the ITP migration

The efficiency of the self-sharpening effect at the leading ion, K^+–base zone boundary lies outside this discussion. For evaluating the situation at the base–terminator boundary it is first necessary to consider the solubility of bases in the terminator zone; the pH_T is practically independent of c_L. (The bases NT and MX which are soluble in their own zones were not considered.)

The solubilities of the bases in the terminator, $S_{B,T}$, are more than twice the values of their adapted "concentrations", $\bar{c}_B$ (*cf.*, Fig. 4); hence the relation 5 holds for the calculation of $\bar{u}_{B,T}$. By comparing the calculated mobilities, in all cases considered the following inequalities are valid[13]:

$$\bar{u}_{B,T} > \bar{u}_{T,T} \quad \text{and} \quad \bar{u}_{T,B} < \bar{u}_{B,B}$$

Therefore the base–terminator boundary exhibits a self-sharpening effect in both directions and the migration of the individual bases is correct.

In the set of compounds studied we have concentrated on the separation of the pair AT–NT and MX–EM. These are chemically closely related substances; their separation would be of practical importance for pharmacokinetic studies, purity control, etc. Considering the sensitivity requirements, time consumption and the determined effective mobilities, the operational system E (Table I) was chosen: the separation current of 30 μA was decreased to 10 μA after 500 s; the terminating histidine can be replaced by β-picoline which has similar parameters.

To substantiate theoretically the separability of the above pairs of bases in the system E, the effective mobilities of bases in their own and neighbouring zones were compared[13]. The mobilities of NT and MX were calculated according to eqn. 5 and those of AT and EM according to eqn. 6. For the zones of bases the following inequalities hold:

zone NT (pH_B 7.91), $\bar{u}_{AT,NT}$ (11.1) < $\bar{u}_{NT,NT}$ (22.7)
zone AT (pH_B 7.75), $\bar{u}_{NT,AT}$ (22.8) > $\bar{u}_{AT,AT}$ (16.4)
zone MX (pH_B 7.91), $\bar{u}_{EM,MX}$ (10.6) < $\bar{u}_{MX,MX}$ (23.0)
zone EM (pH_B 7.73), $\bar{u}_{MX,EM}$ (23.1) > $\bar{u}_{EM,EM}$ (15.5)

It is clear that the self-sharpening effect of the boundaries is established in both directions for these pairs of bases and that the migration is again correct. (The

differences in the effective mobilities are distinct and the above trend is valid in the whole range of c_L investigated, *i.e.*, also for other dilutions of the system B.)

Stability of zones and the zone existence diagram

Calibration graphs for some of the bases were examined as the criterion of the zone stability. Fig. 5 depicts the calibration graphs for drugs in the concentration range 20–100 μM for ITP in both slightly acidic (A or F) and alkaline (E) operational systems. (The leading electrolyte of system A was diluted 1:1, c_L = 5 mM, for this purpose.)

The corresponding linear regression equations and the correlation coefficients, k_r, are summarized in Table V. The results obtained in system E indicate that the zones of the more soluble bases (NT, MX) are quite stable; the intercept is negligibly small. The calibration graphs for sparingly soluble bases (AT, EM) are also perfectly rectilinear but the intercept has a negative value. This means that during the migration of the zone in the capillary from the injector valve to the detector a constant amount of the base is lost. This loss is independent of the amount injected and hence it represents the systematic error of the ITP determination. Under the given experimental conditions, the loss amounts to 0.2 nmol of AT or 0.4 nmol of EM. The effect of the separation current (25, 20, 10 μA) (and consequently the analysis time) was also examined but no significant dependence was observed. That is why it can be concluded[14] that the loss is a certain form of zone bleeding and not tailing. Some kind of sorption of the free base in the capillary must be assumed since in successive blank experiments (injections of the terminating electrolyte instead of the sample) the ITP records revealed successively decreasing amounts of the base residue which may interfere with further analyses. For that reason the analytical procedure was modified

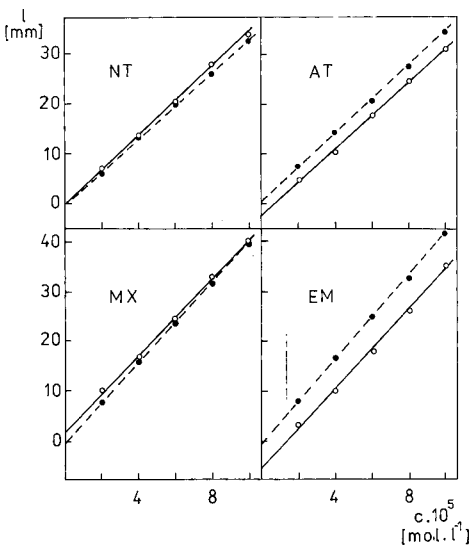

Fig. 5. Calibration graphs, l (step lengths, mm) *vs.* c (concentration of base, 10^{-5} mol l^{-1}). Full dots and dashed lines, points and regression lines in systems F (for AT, NT) and A, 1:1 (for MX, EM); empty dots and solid lines, the same in system E.

TABLE V

LINEAR REGRESSION EQUATIONS OF CALIBRATION GRAPHS

Compound	*System*	*l (mm)* =	k_r
NT	F	$3.33\ c \cdot 10^5 - 0.5$	0.9999
AT		$3.34\ c \cdot 10^5 + 0.7$	0.9999
NT	E	$3.39\ c \cdot 10^5 + 0.2$	0.9993
AT		$3.30\ c \cdot 10^5 - 2.2$	0.9991
MX	A(1:1)	$4.02\ c \cdot 10^5 - 0.5$	0.9999
EM		$4.17\ c \cdot 10^5 - 0.4$	0.9999
MX	E	$3.83\ c \cdot 10^5 + 1.8$	0.9997
EM		$3.98\ c \cdot 10^5 - 5.4$	0.9987

in such a way that after each separation the capillary was rinsed with a small volume (*ca.* 0.5 ml) of 0.1 *M* acetic acid and thereafter it was filled with fresh leading electrolyte. In this case the ITP record of a subsequent blank experiment was regular. The above procedure was employed in all analyses performed with alkaline operational systems. Finally it can be concluded that the migration of the heterogeneous zones of sparingly soluble bases is correct but the zones are not absolutely stable. In principle, quantitative analyses are possible but the detection limits are influenced negatively.

The possibilities of the ITP migration of low-solubility bases in system E are shown in the zone existence diagram[13], Fig. 6. The point T corresponds to the terminating histidine. The area of the diagram is limited on the right hand side by the line AB of strong soluble bases ($\bar{u}_B = u_{HB}$) with ionic mobility, $u_{HB} \geqslant \bar{u}_T$ (segment TA indicates possible inversion of mobilities of weak soluble bases fulfilling the limiting condition $\bar{u}_{B,T} = \bar{u}_{T,T}$). As it is necessary to consider three variable parameters of the bases (u_{HB}, $pK_{a,B}$, S_0), the vertical lines of the internal system of coordinates (that normally mark the $pK_{a,B}$) are individual for parametrically introduced values of S_0.

Separations

System E was used for a model separation of pairs of drugs under the following working regime: the separation current of 30 μA was switched to 10 μA after 500 s; the time of passage of the first boundary through the detector, t_L, was 20–21 min. The recorder chart speed was increased from 0.05 to 0.5 mm s^{-1} just after the passage of the zone of impurities.

In acidic operational systems, NT and AT have the same mobility and their separation is impossible. Fig. 7a illustrates their successful separation accomplished in system E. The detection limit of NT in the mixture is about 20 pmol and this value approaches the real limit of the ITP method; for the reasons discussed above, the detection limit of AT is an order higher and amounts to 300 pmol.

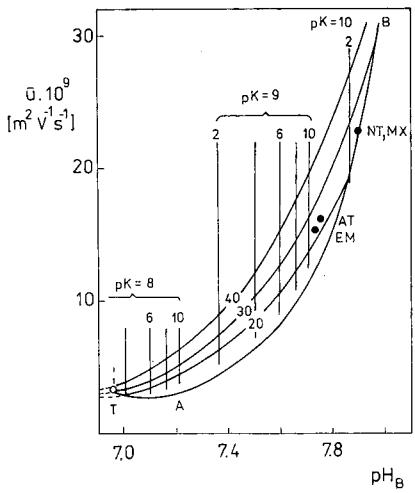

Fig. 6. The zone existence diagram in system E. The numbers 20, 30, 40 refer to the ionic mobilities of the bases, u_{HB} (10^{-9} m^2 V^{-1} s^{-1}); 2, 6, 10 are the solubilities of the bases, S_0 (10^{-5} mol l^{-1}). For a more detailed explanation see the text.

MX and EM exhibit slightly different mobilities in acidic systems but the selectivity, $(\bar{u}_{MX} - \bar{u}_{EM})/\bar{u}_{EM} = 0.05$, is poor; in system A both bases form a transient mixed zone (Fig. 7b) though the injected quantity is small (0.5 nmol of either base). On the other hand, their separation in system E (Fig. 7c) is perfect (practical selectivity *ca.*

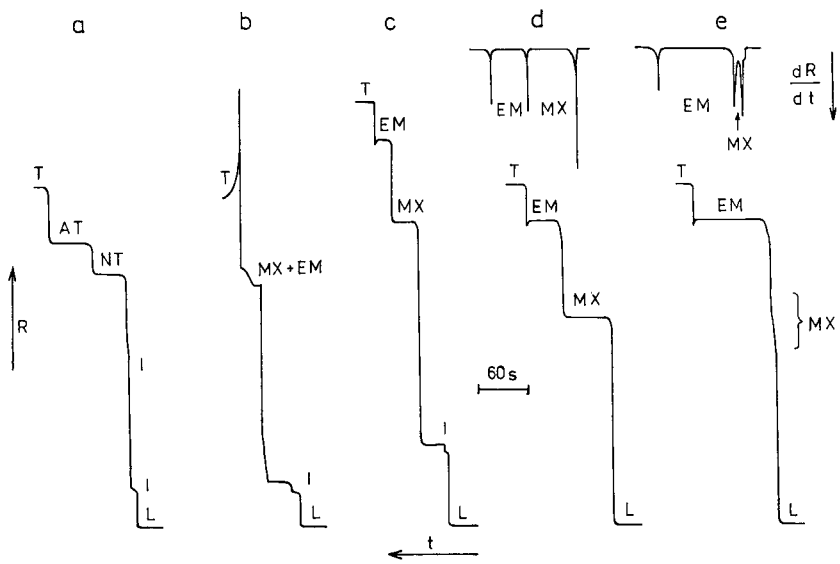

Fig. 7. Analyses of mixtures. Detection current: 10 μA. Chart speed: 0.5 mm s^{-1}. I = Impurities in the operational system. (a) 2.4 nmol AT + 1.5 nmol NT, system E; (b) 0.5 nmol MX + 0.5 nmol EM, system A; (c) 0.9 nmol MX + 0.9 nmol EM, system E; (d) 1.5 nmol MX + 1.5 nmol EM, system G; (e) 30 pmol MX + 3 nmol EM, system G.

0.2). The interfering effect of impurities (Na^+ and other metal ions which cannot easily be removed from the electrolyte system) can be overcome by modifying system E, by using Na^+ as the leading ion (system G), without any negative effect on the separation efficiency (see Fig. 7d). The detection limits are 20 pmol of MX (Fig. 7e) and 400 pmol of EM in a mixture.

All the separations described apply to pure aqueous solutions and the presence of a matrix in real samples might worsen their parameters. Practical applications to drug analysis will be published elsewhere.

REFERENCES

1 Z. Chmela, J. Čižmárik and Z. Stránský, *Collect. Czech. Chem. Commun.*, 51 (1986) 993.
2 A. L. Green, *J. Pharm. Pharmacol.*, 19 (1967) 10.
3 F. M. Everaerts, J. L. Beckers and Th. P. E. M. Verheggen, *Isotachophoresis: Theory, Instrumentation and Applications*, Elsevier, Amsterdam, 1976.
4 R. A. Robinson and R. H. Stokes, *Electrolyte Solutions*, Butterworths, London, 1959.
5 V. Jokl, J. Pospíchalová and M. Polášek, *Electrophoresis*, 7 (1986) 433.
6 B. M. Muchow, *Electrophoresis*, 6 (1985) 471.
7 T. Hirokawa, M. Nishino, N. Aoki and Y. Kiso, *J. Chromatogr.*, 271 (1981) D 1.
8 P. Boček, P. Gebauer and M. Deml, *J. Chromatogr.*, 219 (1981) 21.
9 R. J. Flanagan and I. Jane, *J. Chromatogr.*, 323 (1985) 173.
10 A. Sekera, *Ann. Pharm. Fr.*, 16 (1958) 525.
11 J. Čižmárik, A. Borovanský and P. Švec, *Pharmazie*, 33 (1978) 297.
12 M. Pešák, F. Kopecký, J. Čižmárik and A. Borovanský, *Pharmazie*, 35 (1980) 150.
13 P. Gebauer and P. Boček, *J. Chromatogr.*, 267 (1983) 49.
14 P. Gebauer and P. Boček, *J. Chromatogr.*, 299 (1984) 321.

Journal of Chromatography, 470 (1989) 277–287
Elsevier Science Publishers B.V., Amsterdam — Printed in The Netherlands

CHROM. 21 382

DETERMINATION OF THE SPECIFIC ZONE RESISTANCE AND CALCULATION OF THE RESPONSE FACTOR IN ISOTACHOPHORESIS

J. L. BECKERS and F. M. EVERAERTS*
Laboratory of Instrumental Analysis, Eindhoven Uinversity of Technology, P.O. Box 513, 5600 MB Eindhoven (The Netherlands)
(First received December 18th, 1988, revised manuscript received January 19th, 1989)

SUMMARY

If the electric current density applied in isotachophoresis (ITP) experiments is not too high, a linear relationship between the step heights (using an a.c. detector) and the specific zone resistance at 25°C (SZR_{25}) is obtained. In this way the SZR_{25} of a substance in ITP experiments can be obtained using two standard substances for which the SZR_{25} values can be calculated using the mathematical model for the steady state in ITP. From the step heights of these two standards a linear relationship between step height and SZR_{25} can be set up and from this relationship and the step height of an ionic species its SZR_{25} can be calculated. From the SZR_{25} values all qualitative parameters such as the absolute mobility of the substances can be calculated. Hence no corrections for the differences in the temperature of the different zones have to be made. The absolute mobilities obtained show good agreement with literature values. If the absolute mobility and pK value of a substance are known, the response factor, RF, can be calculated; this is useful for quantitative determinations, in which case calibration graphs are not necessary. RF values were calculated and determined experimentally for several leading electrolyte systems. An average accuracy of about 3% can be obtained in practice.

INTRODUCTION

In a related paper, Gladdines *et al.*[1] proposed the concept of the dimensionless response factor (RF), defined as:

$$RF = t_i I/|z| FQ \quad (1)$$

with t_i is the zone length (s), I the applied electric current (A), $|z|$ the valence of the ionic species (in equiv./mol), F the Faraday constant (C/equiv.) and Q the amount of the sample ionic species (mol).

The RF value is a universal constant useful for quantitative determinations in isotachophoresis (ITP), independent of the apparatus used (*e.g.*, diameter of the cap-

illary tube and detector) and electric current applied[a]. The RF value was used for the analysis of intravenous injection solutions for 26 drugs and an accuracy of 2–3% was obtained.

This concept of the RF is especially interesting because it can easily be calculated with a steady-state model for ITP if the absolute mobility[b] and pK value of the sample substances are known. From the measured step heights in ITP, the absolute mobilities and pK values of substances can be calculated with the concept of the isoconductor[2]. This means that from a single experiment (if the pK value is known) or from two experiments in two different leading electrolyte systems (if the mobility and pK are unknown), from the step heights the absolute mobility and/or pK value of an unknown sample substance can be calculated and hence, calculating the RF, the amount of sample can be obtained from the measured zone lengths. This powerful technique is based on the fact that in ITP the separation mechanism is well defined and the step height contains all qualitative and the zone length all quantitative information.

Using the concept of the isoconductor, the zone resistances must be obtained from the measured step heights. These step heights (zone resistances), however, depend on the type of apparatus (*e.g.*, type of detector and diameter of the capillary tube) and applied electric current (*e.g.*, temperature and condition of the measuring electrodes). Some workers therefore use R_E values[3], PU values[4] and relative step heights[5] to standardize the step heights. Although, *e.g.*, R_E and PU values can be used satisfactorily with potentiometric detectors, they are not suitable with a.c. detectors, although these parameters can be calculated from a.c. data. Gas *et al.*[6] presented a method for the measurement of mobilities by regulating the electric current applied in such a way that the thermal power at the detection site is constant and a constant temperature is created, so that corrections for the differences in temperature are superfluous.

In this paper we present a method for determining the specific zone resistance (SZR) at 25°C from two standard step heights. Using the concept of the isoconductor, absolute mobilities can be calculated. Further, it is shown how the RF can be calculated if the mobility and pK values of sample substances are known, and theoretical RF values are compared with those obtained experimentally.

THEORETICAL

If in ITP experiments the steady state is reached, all sample ionic species migrate with equal velocity and a well defined concentration in consecutive zones. For an ionic species i this means that

$$Q_i = l_i A c_i \tag{2}$$

where Q_i is the amount of sample, l_i the zone length (m), A the surface area of the

---

[a] This is true only for not too large differences in the electric current, otherwise too large differences in zone temperatures can cause large differences in temperature-dependent parameters such as the mobilities and pK values.

[b] By absolute mobility, always the ionic mobility at infinite dilution is meant.

capillary tube (m^2) and c_i the total concentration in the zone (mol/m^3). The time t_i (s) needed to pass the detector will be

$$t_i = l_i / v_i \tag{3}$$

where v_i is the ITP velocity (m/s). Because

$$v_i = m_i E_i \tag{4}$$

where m_i is the effective mobility of the substance (m^2/Vs) and E_i the electric field strength in the zone (V/m), eqn. 3 can be written as

$$t_i = Q_i / A c_i m_i E_i \tag{5}$$

Using the equation

$$E_i = I \rho_i / A \tag{6}$$

where I is the electric current (A) and ρ_i the specific zone resistance (Ω m), eqn. 5 can be written as

$$t_i = Q_i / c_i m_i I \rho_i \tag{7}$$

or

$$t_i I / Q_i = 1 / c_i m_i \rho_i \tag{8}$$

In fact this is the RF (C/mol) and it represents the slope of a calibration graph of the product $t_i I$ (sA) *versus* the amount of the sample, Q_i.
Although for strong electrolytes the definition of Gladdines *et al.*[1] (eqn. 1) is applicable, it is preferable to use the RF in C/mol in order to avoid working with an "average charge z" for multi-valent weak electrolytes. With a steady-state model for ITP, all zone parameters, including c_i, m_i and ρ_i can be calculated, from which the RF value can be obtained.

It must be noted that the formulation of the universal quantitative parameter RF has already been used implicitly and calculated for 287 anionic species by Hirokawa *et al.*[3] using the parameter t (ref. 3, Table IV), which is the time-based zone length (s) for 10-nmol samples at a driving current of 100 μA. Hence the RF value (C/mol) will be $t \cdot 10^4$.

APPARATUS

In order to obtain quantitative data, isotachophoretic equipment developed and built by Everaerts *et al.*[5] was used. The separation compartments consisted of capillary tubes of both 0.4 and 0.2 mm I.D. The d.c. current was taken from a modified Brandenburg (Thornton Heath, U.K.) high-voltage power supply. The

zones were detected with a laboratory-made high-performance a.c. conductivity detector.

For the qualitative data, isotachophoretic equipment as described elsewhere[7] was used. In this equipment a casted separation and detection unit is used, through which optimum heat transfer leads to minimum temperature differences between the consecutive zones.

EXPERIMENTAL

In order to calculate the mobilities of ionic species using the concept of the isoconductor[2], the zone resistances must be obtained from the measured step heights. These step heights (zone resistances), however, depend on the type of apparatus (*e.g.*, type of detector and diameter of the capillary tube) and applied electric current (*e.g.*, temperature and condition of the measuring electrodes). First we checked the expected linear relationship between the measured step heights and SZR using the a.c. detector, by measuring the step heights for several dilute solutions of potassium chloride, the SZR of which are precisely known at 25°C, without applying an electric current. The relationship obtained is shown in Fig. 1 for an ITP apparatus with a capillary tube of 0.4 mm I.D. On applying different electric currents, heat will be produced so that all measurements on standard solutions of potassium chloride, even with a thermostated apparatus, will be made at different temperatures, resulting in lower step heights. Corrections for these temperatures are difficult as they are not known exactly.

However, the relationship set up between the measured step heights (for a specific electric current) and the SZR of the potassium chloride solutions at 25°C (SZR_{25}) can be used to determine the SZR_{25} of other substances. Because all ionic species show very similar temperature dependences of their mobilities, it can be assumed that ionic species with a SZR (step height) equal to that of a specific potassium chloride solution will have identical temperatures during the measurement and will have an identical SZR_{25}.

In Fig. 1 the relationships between step heights and SZR_{25} values for different

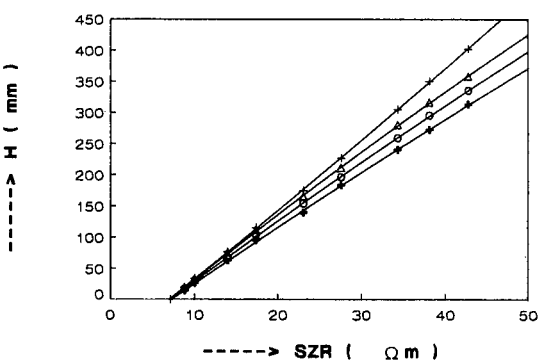

Fig. 1. Relationships between measured step heights (H) and the specific zone resistance (SZR) at 25°C of different KCl solutions for applied electric currents of (+) 0, (△) 40, (○) 80 and (+) 120 μA. I.D. of capillary tube, 0.4 mm.

potassium chloride solutions are given for several electric currents, which can be used to determine the SZR_{25} of components from ITP measurements. Over a wide range of SZR_{25} values a linear relationship is obtained, although for very dilute solutions of potassium chloride too low step heights were obtained, possibly owing to a high heat production, resulting in higher temperatures.

In Table I the calculated SZR_{25} values of potassium chloride solutions and the measured step heights (for capillary tubes of both 0.4 and 0.2 mm I.D.) are given for the different electric currents. The SZR_{25} values were calculated using the Debye–Huckel–Onsager relationship[8]:

$$\Lambda = \Lambda^\circ - (a + b\,\Lambda^\circ)\sqrt{c} \tag{9}$$

for water at 25°C, $a = 60.20\ \Omega^{-1}\ \mathrm{cm}^2\ \mathrm{mol}^{-1}\ (\mathrm{mol\ dm}^{-3})^{-0.5}$ and $b = 0.229\ (\mathrm{mol\ dm}^{-3})^{-0.5}$. For KCl $\Lambda^\circ = 149.86\ \Omega^{-1}\ \mathrm{cm}^2\ \mathrm{mol}^{-1}$.

Determination of SZR_{25} in Ω m

From the above, it can be concluded that for not too high electric currents and ionic species of not too low mobility, a linear relationship between the step heights and SZR_{25} can be expected (of course, the diameter of the capillary tube and the cooling capacity of the detector system also play an important part). Hence the SZR_{25} of a substance can be obtained using two standard substances for which the SZR_{25} values can be calculated (based on the mathematical model for the steady state in ITP). From the step heights of these two standard substances, the linear relationship between step height and SZR_{25} can be set up and from this relationship and the step height of an ionic species its SZR_{25} can be calculated. The SZR_{25} values obtained are used as experimental parameters for the calculation of the absolute mobil-

TABLE I

MEASURED STEP HEIGHTS AND CALCULATED SZR_{25} VALUES FOR POTASSIUM CHLORIDE SOLUTIONS FOR SEVERAL APPLIED ELECTRIC CURRENTS AND CAPILLARY TUBES OF 0.4 AND 0.2 mm I.D.

KCl concentration (mol/l)	*SZR_{25} (Ω m)*	*Step height (mm)*					
		I.D. 0.4 mm				*I.D. 0.2 mm*	
		0 μA	*40 μA*	*80 μA*	*120 μA*	*0 μA*	*20 μA*
0.0100	7.122	0	−0.5	−1.9	−4.0	0	−0.2
0.0080	8.840	19.6	18.9	17.0	14.1	3.8	3.5
0.0070	10.064	33.5	32.3	30.0	26.5	6.7	6.2
0.0050	13.970	76.7	73.6	67.0	62.5	15.9	14.7
0.0040	17.375	115.0	110.8	103.5	95.5	24.5	23.0
0.0030	23.039	174.5	165.0	153.3	139.0	39.5	36.8
0.0025	27.561	227.0	211.0	196.0	183.0	51.5	48.0
0.0020	34.333	305.0	280.0	259.0	240.0	70.8	66.0
0.0018	38.091	350.0	316.0	295.0	272.0	82.5	77.0
0.0016	42.785	402.0	358.0	335.0	313.0	96.8	91.8
0.0014	48.820	473.0	415.0	390.0	360.0	116.5	110.0

ities of sample ionic species and these can be used to calculate the RF values. As standard substances both the leading ions, terminating or other ionic species can be used. For substances of very low mobility standards can be chosen with mobilities close to that of the sample component. In our calculations, corrections for the concentration dependence of the mobilities and for activities were made.

To check the accuracy of this method for the determination of the SZR_{25} values and the calculation of absolute mobilities, we measured the step heights of some anions using several leading electrolytes. In Table II the pK values and absolute mobilities of the leading, counter and standard ionic species used in the calculations are given. In Table III the absolute mobilities calculated from the experimentally obtained step heights are given. All leading electrolyte solutions were prepared by adding the counter ionic species to 0.01M hydrochloric acid until the pH_L was reached. The counter ionic species for the solutions were histidine ($pH_L = 6.08$), creatinine ($pH_L = 4.75$) and β-alanine ($pH_L = 4.40$, 3.73 and 3.71). All values given in Table III were measured twice; the differences between the duplicates were less than 1%. The differences between the absolute mobilities obtained from different electrolyte systems are often larger, especially with low pH_L values. In such a case the accuracy of both the pH_L and the pK values is very important. As an example, the absolute mobility of phenylacetic acid was calculated with a pK value of 4.41 (ref. 3) and 4.28 (ref. 9); the mobilities with the pK value of 4.28 were significantly better.

As standards the leading ion chloride and acetate were always used and the electric current was 15 μA, except for the system at $pH_L = 3.71$, where the standards were chloride and propionate and the electric current was 10 μA. This was done because in the systems at low pH the SZR are relatively high (about 50 Ωm) compared

TABLE II

pK VALUES AND ABSOLUTE MOBILITIES FOR LEADING, COUNTER AND STANDARD IONIC SPECIES USED IN THE CALCULATIONS

Ionic species	*Mobility* (10^{-5} $cm^2/V \cdot s$)	*pK*
Acetate	42.4	4.756
p-Aminobenzoate	31.6	4.853
β-Alanine	36.7	3.552
Chlorate	67.0	−2.7
Chloride	79.1	−2.0
Creatinine	37.2	4.828
2,4-Dihydroxybenzoate	32.0	3.395
Formate	56.6	3.75
Histidine	29.6	6.04
Imidazole	52.0	7.15
Lithium	40.1	14
Nitrate	74.0	−2
Potassium	76.2	14
Propionate	37.1	3.75
Sodium	51.9	14
Tetramethylammonium	44.3	>7
Tetraethylammonium	32.7	>7

TABLE III

CALCULATED ABSOLUTE MOBILITIES FROM SZR_{25} VALUES, OBTAINED FROM MEASURED STEP HEIGHTS IN ELECTROLYTE SYSTEMS AT DIFFERENT pH VALUES

The electric current applied was 15 μA, except for the system at pH_L = 3.71, where it was 10 μA. For further explanation, see text.

Ionic species	*pK*	*Absolute mobility (10^{-5} cm²/V·s)*				
		Lit.[3,10]	*Experimentally determined*			
			6.08	*4.75*	*4.40*	*3.73*	*3.71*
Chloric acid	−2.7	67.0	66.9	66.0	66.5	67.7	66.0
Chloroacetic acid	2.87	43.7	40.4	40.1	40.3	42.1	40.9
2,4-Dihydroxybenzoic acid	3.40	32.0	30.9	30.2	30.9	32.6	32.1
Glutamic acid	4.38	28.9	28.3	28.5	29.0	29.8	29.5
Glycolic acid	3.89	42.4	42.4	41.6	42.4	43.9	43.7
Glyoxilic acid	3.34	39.6	–[a]	39.2	39.9	40.8	40.7
Hydrofluoric acid	3.17	57.4	57.0	56.8	57.2	57.8	57.5
Hydroxyphenylacetic acid	3.17	26.9	30.5	29.2	28.9	29.6	28.2
o-Aminobenzoic acid	4.94	31.6	32.8	32.2	–	31.7	31.3
o-Methoxybenzoic acid	4.09	28.3	30.3	29.3	30.3	31.0	30.5
Nitric acid	−1.37	74.1	74.3	75.1	74.1	75.3	74.0
Phenylacetic acid	4.41	31.7	30.9	30.5	32.6	34.2	–
	4.28	–	30.8	30.0	30.6	30.9	30.5
Phenylglyoxilic acid	–[b]	–	33.4	32.0	32.1	33.8	32.5
Propionic acid	4.87	37.1	37.1	37.5	38.1	36.9	37.1
Sulphosalycilic acid	–[b]	–	54.5	53.7	55.1	55.6	54.6
Trimethylacetic acid	5.04	31.8	30.9	31.7	31.9	31.5	32.1

[a] Sloping step height.
[b] Considered to be fully ionized.

TABLE IV

CALCULATED AND EXPERIMENTALLY DETERMINED RF VALUES

For all experimental values the number of measuring points (*N*), regression coefficient and *RF* values are given. For further explanation, see text.

pH	*Ionic species*	*Ref.*	*N*	*Regression coefficient*	*RF (10^5C/mol)*			*Deviation (%)*
					Calc.	*Ref.3*	*Exptl.*	
6	Acetate	11	3	0.9997	1.622	1.622	1.670	+3.0
7	Acetate	11	3	1.0000	2.163	2.161	2.191	+1.3
7	Formate	11	3	0.9993	1.848	1.848	1.883	+1.9
6	Acetate	11	20	0.9997	1.622	1.622	1.675	+3.3
6	Formate	11	20	0.9996	1.447	1.448	1.424	−1.6
6	2,4-Dihydroxybenzoate		5	0.9998	1.856	1.853	1.924	+3.7
6	*p*-Aminobenzoate		3	0.9984	1.868	1.865	1.785	−4.4
4.5	TMA		13	0.9977	1.938	–	1.840	−5.1
4.5	TEA		13	0.9994	2.350	–	2.264	−3.7
4.5	Sodium		13	0.9998	1.781	–	1.744	−2.1
4.5	Barium		8	0.9998	3.263	–	3.24	−0.7
4.5	Imidazole		8	0.9993	1.809	–	1.753	−3.1
4.5	Lithium		8	0.9997	2.055	–	2.00	−2.7

with those of the other systems. A comparison with the literature values[3,10] showed good agreement.

Calculated and determined RF values

In order to check the applicability of the RF values, we compared calculated and experimentally obtained RF values. In Table IV the calculated RF value (with eqn. 8), the value of $t \cdot 10^4$ (ref. 3) and experimental values are given for a number of ionic species. The deviation is calculated as follows:

$$\text{Deviation (\%)} = (RF_{exp} - RF_{calc}) / RF_{calc} \cdot 100\% \qquad (10)$$

For all calibration graphs the number of data points (N) and the regression coefficients are given. The calculated values and the values of $t \cdot 10^4$ are nearly equal although small differences arise owing to differences in the corrections to pK values and absolute mobilities in the calculations. The experimental data from ref. 11 measured with a thermometric detector also fit well.

Although the impact of the use of RF values is large, the differences between the experimentally determined and calculated RF values are fairly high (average deviation 3%), although the differences of -5.1% (TMA) and -3.7% (TEA) are possibly due to inaccurate absolute mobilities and that of -4.4% (p-aminobenzoic acid) may be due to the impurity of this substance.

The practical value of the RF data will depend strongly on both the accuracy of the measurement of the electric current and the accuracy of the preparation of the sample solutions. For example, for the measurement of the RF value of Li^+ we prepared a stock solution using lithium nitrate. The RF value agrees well with the calculated value. In the first instance, however, we prepared twice a stock solution from undried lithium chloride. The experimentally obtained RF values were 1.66 and

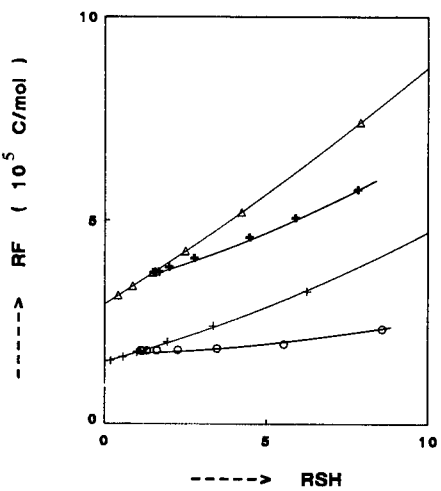

Fig. 2. Relationship between calculated RF values and RSH for (+) strong monovalent, (△) strong divalent, (○) weak monovalent and (✦) weak divalent cationic species. Leading electrolyte, 0.01 M KOH at pH 5, adjusted by adding acetic acid.

1.65, respectively. After drying the lithium chloride an RF value of 1.91 was obtained, showing the importance of sample preparation.

Of course, theoretical RF values cannot be used when complex formation occurs or other factors that affect the effective mobility of the sample ionic species arise, if appropriate corrections are not made in the computer program.

For a further comparison, the theoretical relationship between calculated RF values and calculated RSH values (relative step heights calculated using the standard

TABLE V

CALCULATED RSH AND RF VALUES FOR STRONG AND WEAK MONOVALENT AND DIVALENT CATIONS USING A LEADING ELECTROLYTE OF 0.01 *M* POTASSIUM HYDROXIDE AND ACETIC ACID AT A pH OF 5

For further explanation, see text.

Valency	*Absolute mobility* (10^{-5} $cm^2/V \cdot s$)	*pK*	*Calculated RF value* (10^5 *C/mol*)	*RSH*
1	70	14	1.549	0.1875
	60	14	1.641	0.574
	50	14	1.787	1.121
	40	14	2.012	1.951
	30	14	2.4035	3.360
	20	14	3.251	6.254
2	70	14	3.139	0.428
	60	14	3.370	0.876
	50	14	3.706	1.519
	40	14	4.236	2.511
	30	14	5.190	4.239
	20	14	7.388	7.912
1	50	9	1.787	1.121
	50	8	1.787	1.123
	50	7	1.788	1.143
	50	6.5	1.789	1.189
	50	6	1.791	1.318
	50	5.5	1.797	1.627
	50	5	1.811	2.272
	50	4.5	1.849	3.476
	50	4	1.954	5.544
	50	3.5	2.330	8.584
	50	3	6.044	10.110
2	50	9	3.706	1.519
	50	8	3.706	1.520
	50	7	3.711	1.537
	50	6.5	3.722	1.576
	50	6	3.754	1.691
	50	5.5	3.843	2.008
	50	5	4.065	2.781
	50	4.5	4.582	4.480
	50	4	5.747	7.839
	50	3.5	8.371	12.843

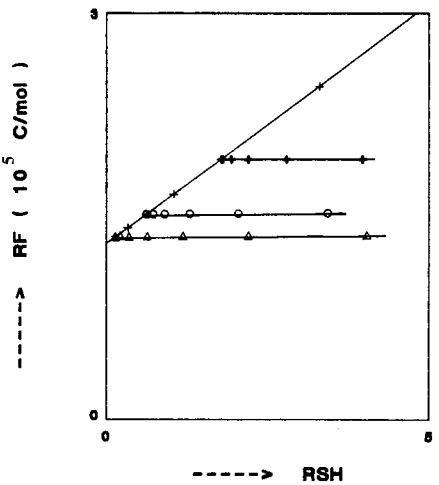

Fig. 3. Relationship between calculated RF values and RSH for (+) strong monovalent and weak monovalent anionic species with absolute mobilities of (△) $70 \cdot 10^{-5}$, (○) $50 \cdot 10^{-5}$ and (✚) $30 \cdot 10^{-5}$ $cm^2/V \cdot s$.

step height of sodium) are given in Fig. 2 for a leading electrolyte of 0.01 *M* potassium hydroxide at a pH_L of 5 adjusted by adding acetic acid. The relationships are given for strong and weak monovalent and divalent ions. The absolute mobilities for the weak cations are taken as $50 \cdot 10^{-5}$ $cm^2/V \cdot s$. All the calculated data are given in Table V.

From Fig. 2, it can be seen that the RF values for the strong divalent ions are about twice those for the monovalent ions. For weak cations the RF values are lower than those for strong cations with the same RSH, as their total concentration is higher in their zones. In Fig. 3 the relationships between RF values and RSH are

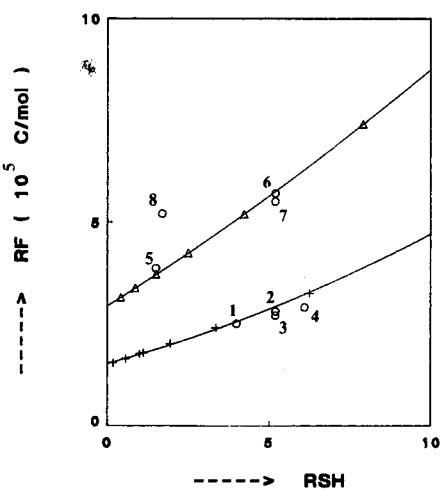

Fig. 4. Relationship between calculated RF values and RSH for strong (+) monovalent and (△) divalent cationic species. The experimentally obtained values from ref. 1 (○) of some cationic species are included and fit the calculated values. For further explanation, see text.

given for strong monovalent negative ions and weak monovalent ionic species for a leading electrolyte consisting of 0.01 *M* hydrochloric acid at a pH_L of 6 adjusted by adding histidine.

In Fig. 4 the relationships between the calculated RF values and the calculated RSH values are given for strong monovalent and divalent ions (identical with Fig. 2), but some values from Gladdines *et al.*[1] have been added (recalculated to C/mol). It can easily be seen that the values for neostigmine methylsulphate (1), imipramine hydrochloride (2), procaine hydrochloride (3) and tetracaine hydrochloride (4) fit the relationship for monovalent ions, whereas suxamethioninechloride (5), isoprenaline sulphate (6) and atropine sulphate (7) belong to the divalent ions. Gallamine triethiodide (8) must be a trivalent cation, as would be expected from its molecular structure.

CONCLUSION

It can be concluded that the determination of SZR_{25} values using two standards in ITP experiments and the calculation of absolute mobilities from these SZR_{25} values lead to satisfactory results. If the absolute mobility and p*K* values of an ionic species are known, the RF values useful for quantitative determinations in ITP can be calculated.

The differences between experimentally determined and calculated RF values are about 3%. Too low experimental RF values can be caused if stock solutions are prepared with impure and undried substances; the theoretical RF values are then more reliable. Too high experimental RF values mean that the effective mobility of the ionic species is lower than as expected owing, *e.g.*, to complex formation. It is advisable always to consider the experimentally obtained RSH values as a check on these effects.

REFERENCES

1 M. M. Gladdines, J. C. Reijenga, R. G. Trieling, M. J. S. van Thiel and F. M. Everaerts, *J. Chromatogr.*, 000 (1989) 000.
2 J. L. Beckers, *J. Chromatogr.*, 320 (1985) 147.
3 T. Hirokawa, M. Nishino, N. Aoki, Y. Kiso, Y. Sawamoto, T. Yagi and J.-I. Akiyama, *J. Chromatogr.*, 271 (1983) D1–D106.
4 H. Miyazaki and K. Katoh, *J. Chromatogr.*, 119 (1976) 369.
5 F. M. Everaerts, J. L. Beckers and Th. P. E. M. Verheggen, *Isotachophoresis, Theory, Instrumentation and Applications*, Elsevier, Amsterdam, 1976.
6 B. Gaš, J. Zuska and J. Vacík, *J. Chromatogr.*, 470 (1989) 69.
7 Th. P. E. M. Verheggen, J. L. Beckers and F. M. Everaerts, *J. Chromatogr.*, 452 (1988) 615.
8 P. W. Atkins, *Physical Chemistry*, Oxford University Press, Osford, 1981.
9 R. C. Weast (Editor), *Handbook of Chemistry and Physics*, CRC Press, Boca Raton, FL, 63rd ed., 1982–183, p. D171.
10 *Landolt-Bornstein, Zahlenwerte und Funktionen*, 6 Aufl. Bd. II, Teil 7, Springer, Berlin, 1960.
11 J. Beckers, *Thesis*, University of Technology, Eindhoven, 1973.

Journal of Chromatography, 470 (1989) 289–297
Elsevier Science Publishers B.V., Amsterdam — Printed in The Netherlands

CHROM. 21 383

DIFFERENTIATION OF Al^{3+} AND Al SPECIES IN ENVIRONMENTAL SAMPLES BY ISOTACHOPHORESIS

SUSANNE SCHMID*, W. KÖRDEL, H. KLÖPPEL and W. KLEIN
Fraunhofer-Institut für Umweltchemie und Ökotoxikologie, D-5948 Schmallenberg (F.R.G.)
(First received December 22nd, 1988; revised manuscript received January 24th, 1989)

SUMMARY

An isotachophoretic method for the determination of free $[Al(H_2O)_6]^{3+}$ ions in different aluminium salt solutions was developed. The electrolyte system consists of 0.01 *M* sodium acetate (leading system) and 0.01 *M* tris(hydroxymethyl)aminomethane (terminating system). Separation was effected with a precapillary tube (diameter 0.05 cm) followed by a main capillary tube of length 20 cm and of smaller cross-section. The detection limit for $[Al(H_2O)_6]^{3+}$ ions was 0.05 mg/l. The method was applied to the determination of free Al^{3+} ions $\{[Al(H_2O)_6]^{3+}\}$ in soil leachates and aqueous soil extracts.

INTRODUCTION

The increasing acidification of soils by deposition of acid rain in the forest ecosystem results in leaching and washing out of nutrient elements in the soil and also causes the release and mobilization of phytotoxic metals in soil[1]. In this process the release of bioavailable aluminium is of special importance. Especially the free Al^{3+} species $\{[Al(H_2O)_6]^{3+}\}$ is responsible for the high phytotoxic effect of aluminium in acidic soils[2–4]. The release of aluminium depends on the buffer system of the soil, the exchange buffer range (pH 4.2–5.0) and the aluminium buffer range (pH 3.8–4.2)[5].

In soil solutions or pore solutions, elements such as Pb, Cd, Cu, Ca, Mn and Al exist in both free and complex forms. The kind of linkage has a decisive influence on the bioavailability of these ions and therefore also on their phytotoxicity. The different species of aluminium are of great importance for its phytotoxic potential, as shown by studies on hydroponics.

The microbial decomposition of the organic materials in soils results in soluble organic acids such as fulvic acids and humic acids or further hydrophilic degradation products (salicylic acid, phenols, carbon acids). As $[Al(H_2O)_6]^{3+}$ ions can be bound by these organic acids, the activity and mobility of Al^{3+} ions depends strongly on the content and composition of the organic substances in the soil solution. The amount of organically bound aluminium decreases with increasing soil depth, whereas that of inorganically bound aluminium increases.

Previous studies on the characteristics of organically bound aluminium did not

0021-9673/89/$03.50

describe the actual kind of linkage of aluminium to organic molecules in soil solutions. In addition, there has been a need to develop an appropriate method for the determination of free Al^{3+} ions $\{[Al(H_2O)_6]^{3+}\}$ in soil solutions. The conventional methods differentiate between kinetically unstable aluminium and total aluminium[6] or inorganic mononuclear and organically bound aluminium[7] as well as mononuclear and polynuclear aluminium species[8]. A disadvantage of these methods is that the real distribution of aluminium species in soil solutions cannot be established, as the addition of buffer or other reagents modifies the original character on analysis.

This paper reports a feasible method for determining environmentally relevant concentrations of free $[Al(H_2O)_6]^{3+}$ ions in soil solutions.

EXPERIMENTAL

Lysimeters

The release of aluminium into soil leachate was investigated using lysimeters with a surface area of 1 m^2. Six lysimeters with different depths were installed on the ground in the Institute to observe the vertical gradients of aluminium: two lysimeters L (LI/F, LII/F), depth 25 cm, surface humus; two lysimeters L (LIII/F, LIV/F), depth 40 cm, surface humus with A/B horizons; and two lysimeters L (LV/F, LVI/F), depth 70 cm, surface humus with 50 cm A/B horizons. The lysimeters contained undisturbed soil monoliths from Hunau, a hill in the Rothaargebirge. In spring 1987, one of each group of lysimeters was treated with the equivalent to 3 t/ha of calciumcarbonate/magnesium carbonate–lime to study the effect of liming. In December 1987 the second lysimeter, which was protected against natural rainfall, was watered with 5-fold concentrated artificial precipitation to simulate stress in soils under strong acidic conditions. The amount of artificial precipitation was identical with the original precipitation at this site.

Apparatus

The total content of aluminium in the leachates was determined with a Perkin-Elmer 3030 graphite furnace atomic absorption spectrometer with Zeeman-effect background correction in pyrolytic graphite-coated graphite tubes and an argon/argon–methane atmosphere. Each sample was acidified and measured three times for statistical assessments.

The content of free Al^{3+} ions $\{[Al(H_2O)_6]^{3+}\}$ was determined by isotachophoresis (ITP) using an LKB 2127 Tachophor equipped with a high-voltage power supply (0.1–30 kV, 10–500 μA), an integrated conductivity detector and a UV detector. For the detection of $[Al(H_2O)_6]^{3+}$ ions only the linear and differential conductivities were registered (GILA 2000 Laumann recorder). Additionally, a precapillary tube (6 cm × 2 mm I.D.) from ITABA (Sweden) was installed to separate irrelevant ions and to increase the sensitivity. The main capillary tube (20 cm × 0.3 mm I.D.) served to separate free Al^{3+} ions from other mononuclear and polynuclear aluminium species. The samples were injected with various microsyringes.

Reagents

All solutions were prepared using analytical-reagent grade chemicals.

Aluminium standard solutions. 1 g/l $AlCl_3$–tritisol (Merck) ≡ 1 g/l Al^{3+}; 13.89 g/l

$Al(NO_3)_3 \cdot 9\ H_2O \equiv 1$ g/l Al^{3+}; 12.35 g/l $Al_2(SO_4)_3 \cdot 18\ H_2O \equiv 1$ g/l Al^{3+}; 17.57 g/l $KAl(SO_4)_2 \cdot 12\ H_2O \equiv 1$ g/l Al^{3+}.

Solution of sodium citrate. 1.56 g/l sodium citrate $\cdot$ 2 $H_2O \equiv 1$ g/l citrate.

Buffer solutions for the ITP method. 1.36 g/l sodiumacetate $\cdot$ 3 H_2O; 1.21 g/l tris(hydroxymethyl)aminomethane (Tris).

Procedure

The aluminium standard solutions were diluted so as to contain 1 mg/Al^{3+}. The compositions of the two buffer systems are shown in Table I.

Mixtures of aluminium chloride and sodium citrate were prepared by adding various amounts of a solution of sodium citrate (10 or 100 mg/l citrate) to a standard solution of $0.37 \cdot 10^{-3}$ mol/l (1 mg/l) Al^{3+} to obtain Al^{3+}: citrate molar ratios between 0 and 1.5. The pH of these solutions was 4.67 $\pm$ 0.2.

The soil solutions were analysed as soon as possible after collection. The samples were filtered through a 0.45-μm membrane filter (Millipore). The injection volumes, V, of the soil solutions depended on the concentration of Al^{3+} ($V \leqslant 50\ \mu$l).

RESULTS AND DISCUSSION

Isotachophoresis is based on carrier-free electrophoretic methods inducing migration of ionic species in an electric field. With two different electrolyte systems (leading and terminating electrolyte), ITP represents a discontinuous electrophoretic system. All ions that have the same velocity in the electric field but are mobile between the leading and the terminating electrolyte are separated and determined.

Various electrolyte systems were tested to find an appropriate system for separating the free Al^{3+} ions in solutions from other cations. An electrolyte system consisting of 0.01 M sodium acetate (leading electrolyte) and 0.01 M Tris (terminating electrolyte) proved to be most suitable, as the mobility of free Al^{3+} ions lay between those of the leading cation Na^+ and the terminating cation Tris.

An aluminium solution of 1 mg/l was acidified to pH 2.0. The equilibrium

$$Al^{3+} + H_2O \rightleftharpoons Al(OH)^{2+} + H^+ \qquad (1)$$

TABLE I

COMPOSITION OF AQUEOUS ELECTROLYTE SYSTEM FOR SEPARATING Al^{3+} IONS IN SOIL SOLUTIONS

Parameter	*Leading electrolyte*	*Terminating electrolyte*
Cation	Na^+	Tris
Concentration	0.01 M	0.01 M
pH	3.6	3.3
Additions	1% HPMC	1% HPMC
Counterion	Acetate	Acetate
Temperature	Room temperature	Room temperature
Current	30 μA	30 μA

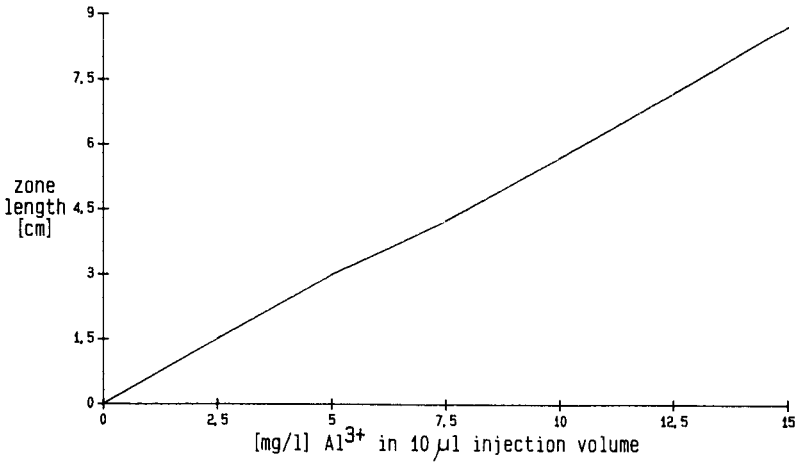

Fig. 1. Calibration graph for $[Al(H_2O)_6]^{3+}$.

was shifted in favour of the initial products. Under these conditions, aluminium occurs predominantly as free Al^{3+} ion. In the range 0.1–2.0 mg/l Al^{3+} we obtained a linear calibration graph (Fig. 1). The detection limit for Al^{3+} ions was 0.05 mg/l. The kinetics of the aluminium hydrolysis reaction depends on the ratio of Al to OH and it may take from 1 h to several months to reach equilibrium[9–11]. After the preparation of an aluminium solution and adjusting the pH with sodium hydroxide immediate measurement of the solutions resulted in higher concentrations of $[Al(H_2O)_6]^{3+}$ than in measurements performed 1 day later. To obtain equilibrium, the solution was given a reaction time of 1 week before measurement.

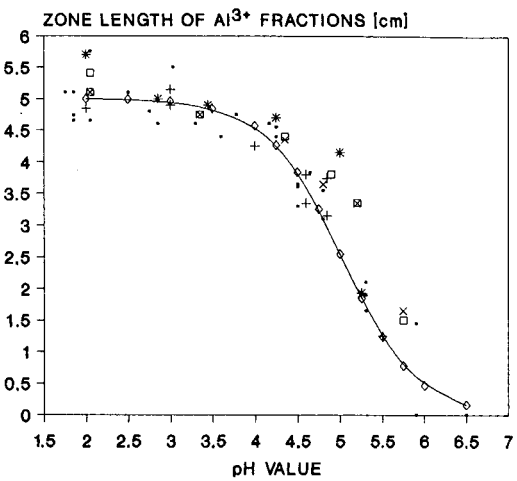

Fig. 2. Determination of $[Al(H_2O)_6]^{3+}$ in different Al salt solutions as a function of the pH of the samples. Volume injected: 10–50 µl. • = $AlCl_3$; + = $Al_2(SO_4)_3$; ✳ = $KAl(SO_4)_2$; □ = $Al(NO_3)_3$; × = $Al(NO_3)_3$; ◇—◇ = theoretical Al.

To establish the effect of various anionic and cationic complexes, different aluminium salt solutions [$AlCl_3$, $Al(NO_3)_3$, $Al_2(SO_4)_3$, $KAl(SO_4)_2$] were acidified to pH 1.7. Identical calibration graphs were obtained for all solutions, indicating that no measurable interferences of non-complexed cations and anions are to be expected in the determination of free Al^{3+} ions.

If only free Al^{3+} ions are detected by the described method, it should be possible to determine the pK_s value of the first hydrolysis equilibrium (see eqn. 1). For each of the aluminium salt solutions with various pH values, identical pH dependence curves were obtained. A comparison with the calculated pH curve (see Fig. 2) showed no differences between the curves. From the pH curves a pK_s value of 5.05 $\pm$ 0.15 was calculated, which is comparable to literature values, ranging from 4.60 to 5.69[9,11,12].

Another verification of the method is the determination of the formation constant of a weak Al complex. As a tridentate ligand citrate was selected, which forms different metal–ligand complexes:

$$2\ Al^{3+} + 3\ Cit^{3-} \rightleftharpoons (Al\text{–}Cit)^0 + [Al(Cit)_2]^{3-}$$

For this experiment a mixture of aluminium chloride and sodium citrate was prepared and 10 μl of the different solutions were injected. The results of these measurements are shown in Fig. 3. From the inflection point on the curve the formation constant, pK, was calculated as $pK(Al\text{–}Cit)^0 = -7.87 \pm 0.32$ (literature values -7.37[12] and -7.87 ± 0.32[13]).

As the aim of this study was to develop a method for the determination of free Al^{3+} ions in environmental solutions, various soil solutions were tested using the above method. In soil solutions with a high content of dissolved organic carbon, the zone length of free Al^{3+} ions between pH 6 and 7.5 does not decrease as far as zero.

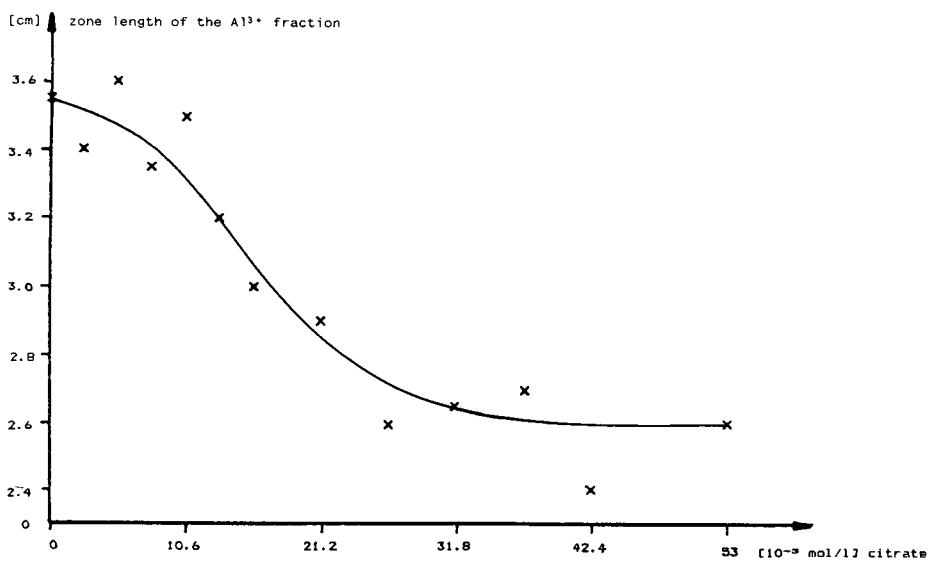

Fig. 3. Determination of "free Al^{3+} ions", $[Al(H_2O)_6]^{3+}$, in an aluminium–citrate mixture. pH of the mixture: 4.67 $\pm$ 0.2. Al concentration: $0.37 \cdot 10^{-3}$ mol/l. Volume injected: 10 μl of the mixture.

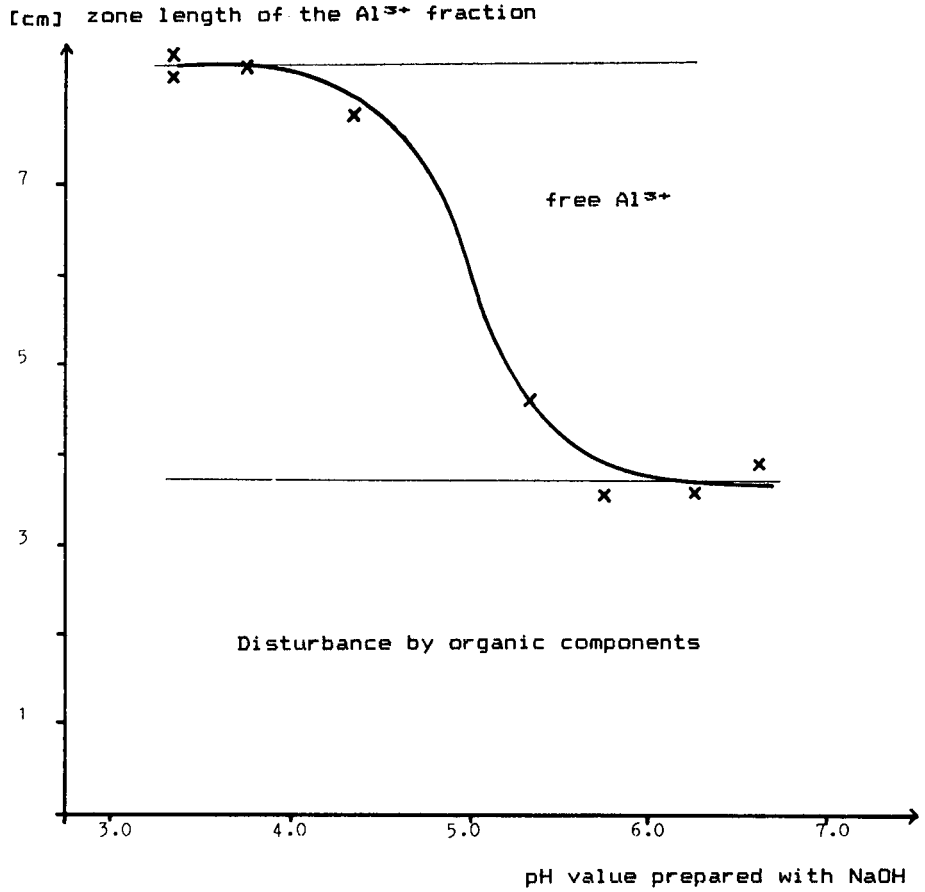

Fig. 4. Analysis of a soil extract of a surface soil and the pH dependence of the $[Al(H_2O)_6]^{3+}$ signal. Volume injected: 10 μl. The pH values on the abscissa relate to the sample solutions.

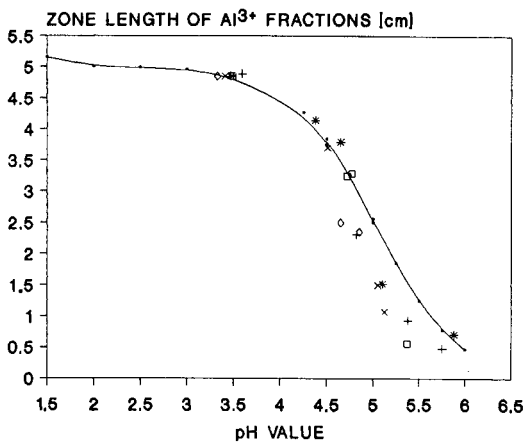

Fig. 5. Determination of $[Al(H_2O)_6]^{3+}$ in soil solutions of lysimeters [LI/F (25 cm), LIII/F (40 cm), LV/F (70 cm), LI/A (100 cm)] by variation of the pH of the samples and comparison with a pure $AlCl_3$ solution. Volume injected dependent on the pH: 10–50 μl. •—• = $AlCl_3$; + = LI/F, 10.8.87; ✳ = LIII/F, 10.8.87; □ = LV/F, 10.8.87; × = LI/A, 11.8.87; ◇ = LIII/F, 2.3.87. Extrapolation to pH 3.5.

Several organic substances seem to have mobilities in the electric field which are comparable to that of free Al^{3+} ions and therefore a complete separation is impossible. As the concentration of free Al^{3+} ions between pH 6 and 7.5 is zero according to the first equilibrium of hydrolysis (eqn. 1), the value can easily be corrected, however, by subtracting the zone length of the signal at neutral pH from the zone length of the signal at the original pH value. This is demonstrated by the shape of the pH dependence curve for a soil extract (Fig. 4) representing the results obtained on checking this method in the presence of low-molecular-weight organic complexes occurring in original soil solutions.

The theoretical curve for $Al^{3+}/Al(OH)^{2+}$ is compared with the pH dependence curves of some soil solutions with lysimeters by standardization and extrapolation to pH 3.5 (Fig. 5). This correction was not carried out in Fig. 4, representing the original state. All measurements in Fig. 5 show the same shape as inferred from eqn. 1. In

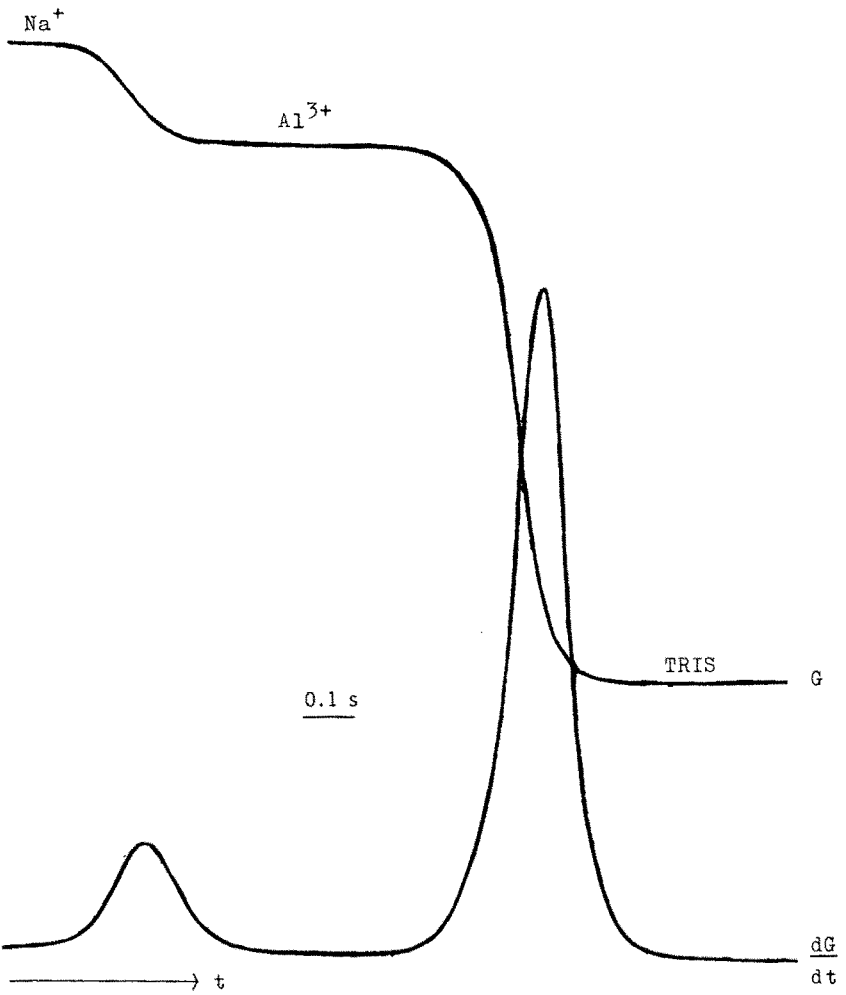

Fig. 6. Isotachopherogram of a soil extract (pH 4.23). Volume injected: 10 μl, t = Time; G = response of the conductivity detector; dG/dt = time derivative of the conductivity detector response.

TABLE II

COMPARISON OF THE RESULTS OF THE DETERMINATION OF $[Al(H_2O)_6]^{3+}$ AND TOTAL Al UNDER DIFFERENT CONDITIONS

Sampling date, November 20–23, 1987; AAS = atomic absorption spectrometry; concentration of Al in mg/l. Various types of treatment of the lysimeters: (a) untreated variant; (b) liming in spring 87; (c) 5-fold concentrated rain.

Lysimeters	*AAS (total Al)*			*ITP (free Al^{3+})*		
	Not treated	*Liming*	*Acid rain*	*Not treated*	*Liming*	*Acid rain*
LI, 25 cm		1.22			0.50	
LII, 25 cm	0.86		3.29	0.56		2.94
LIII, 40 cm		4.89			2.73	
LIV, 40 cm	1.01		2.54	0.67		1.40
LV, 70 cm		1.15			0.89	
LVI, 70 cm	0.91		1.53	0.72		1.36

addition, this comparison shows that no other substances interfere with the signal of free Al^{3+} ions (Fig. 6).

The reproducibility depends on the composition of the samples and varies between 1% and 10%, depending on the impurities and aluminium concentration.

In Table II the total content of aluminium (determined by atomic absorption

TABLE III

COMPARISON OF THE RESULTS OF THE DETERMINATION OF Al IN SOIL SOLUTIONS OF LYSIMETERS OBTAINED BY AAS, ITP AND CLASSICAL METHODS

Various types of treatment of the lysimeters: (a) liming in spring 87 (sampling date, 25.1.88–2.2.88); (b) untreated variant (sampling date, 25.9.87–13.10.87); (c) 5-fold concentrated rain (sampling date, 25.1.88–2.2.88). Photometric methods: OXIN = 8-hydroxyquinoline method; CV = catechol violet S method. DOC = dissolved organic carbon.

Lysimeters	*Free Al^{3+} (mg/l)*	*Al(OXIN) (mg/l)*	*Al(CV) (mg/l)*	*Total Al (mg/l)*	*DOC (mg/l)*	*pH*
LI, 25 cm, (a)	0.08	0.47	0.83	0.96	25.40	4.45
LII, 25 cm, (b)	0.04	0.61	0.83	0.82	12.90	4.49
LII, 25 cm, (c)	4.07	4.74	4.90	5.80	5.90	4.18
LIII, 40 cm, (a)	3.36	3.72	3.76	4.15	3.70	4.49
LIV, 40 cm, (b)	0.48	0.46		0.64	2.00	4.64
LIV, 40 cm, (c)	2.83	3.44	4.63	4.88	0.80	4.45
LV, 70 cm, (a)	0.72	1.54	1.23	1.72	2.00	4.67
LVI, 70 cm, (b)	0.18	0.36	0.28	0.63	2.60	4.75
LVI, 70 cm, (c)	1.57	1.73	2.15	2.15	1.50	4.62
LII/A, 70 cm (control)	0.36	0.72	0.81	0.89	0.20	4.82

spectrometry) and the concentration of "free Al^{3+} ions" (determined by isotachophoresis) are compared for the fertilization and acidification experiments. Over the investigation period of 1 year, fertilization with lime did not reduce the concentration of total aluminium. The high content of dissolved organic carbon in the soil solutions of the 25-cm deep lysimeters immobilized all "free Al^{3+} ions" that had been released from soil (Table III). After watering with "acid rain", however, the content of aluminium in the soil solutions immediatedly increased considerably. The content of "free Al^{3+} ions" increased between 2- and 5-fold, which is illustrated by the values obtained for LII/F (25 cm), LIV/F (40 cm) and LVI/F (70 cm).

CONCLUSION

The results show that ITP is suitable for detecting the species "$[Al(H_2O)_6]^{3+}$" in soil solutions at environmentally relevant concentrations $\{>0.05$ mg/l $[Al(H_2O)_6]^{3+}\}$. The aluminium complexes and further cations and anions did not influence the determination of $[Al(H_2O)_6]^{3+}$ in soil solutions. In contrast to the photometric methods of complexing aluminium mentioned in the Introduction, which change the original soil solutions by displacing the systems with buffer solutions of different pH values (see Table III), the advantage of the ITP method is that the original condition of the solution is maintained and the actual situation in soil solutions is registered.

ACKNOWLEDGEMENTS

The investigations were supported by the Ministerium für Umwelt, Raumordnung und Landwirtschaft des Landes Nordrhein-Westfalen (grant No. FP 04). The authors thank Mr. U. Henrichs and Mrs. M. Decker for technical assistance.

REFERENCES

1 B. Ulrich, *Forstwiss. Centralbl.*, 100 (1981) 228–236.
2 B. Ulrich, *Mitt. LÖLF Sonderheft*, Lölf, Recklinghausen, 1982, pp. 9–25.
3 A. Hüttermann, *Ber. Forschungszentrums Waldökosysteme/Waldsterben*, 4 (1984) 249–263 (Publisher: Universität Göttingen, D-3400 Göttingen, F.R.G.).
4 B. Ulrich, *Göttinger Bodenkdl. Ber.*, 68 (1981) 72–89.
5 B. Ulrich, *Z. Pflanzenernähr. Bodenk.*, 144 (1981) 289–305.
6 B. R. James, C. J. Clark and S. J. Riha, *Soil Sci. Soc. Am. J.*, 47 (1983) 893–897.
7 C. T. Driscoll, *Int. J. Environ. Anal. Chem.*, 16 (1984) 267–283.
8 B. D. La Zerte, *Can. J. Fish. Aquat. Sci.*, 41 (1984) 766–776.
9 J. D. Hem and C. E. Roberson, *Water Supply Pap. Geol. Surv. G.B.*, No. 1827-A (1967).
10 R. W. Smith, *Adv. Chem. Ser.*, 106 (1971) 250–279.
11 M. Havas and J. F. Jaworski, *Aluminium in the Canadian Environment* (*Adv. Chem. Ser.*, Publication No. NRCC 24759 of the Environmental Secretariat, Ottawa, Canada), 1986, p. 51–79.
12 J. O. Ares, *Dissertation*, Göttingen, 1985.
13 G. E. Jackson, *S. Afr. J. Chem.*, 35 (1982) 87–92.

Journal of Chromatography, 470 (1989) 299–308
Elsevier Science Publishers B.V., Amsterdam — Printed in The Netherlands

CHROM. 21 384

INDIRECT PHOTOMETRIC DETECTION IN CAPILLARY ZONE ELECTROPHORESIS

F. FORET[a], S. FANALI and L. OSSICINI
Istituto di Cromatographia CNR, Area della Ricerca di Roma, P.O. Box 10, 00016 Monterotondo Scalo, Rome (Italy)
and
P. BOČEK*
Institute of Analytical Chemistry, Czechoslovak Academy of Sciences, Leninova 82, 611 42 Brno (Czechoslovakia)
(First received January 9th, 1989; revised manuscript received January 23rd, 1989)

SUMMARY

An indirect photometric detection method is described which is based on the use of an absorbing co-ion as the principal component of the background electrolyte. The zones of non-absorbing ionic species are revealed by changes in light absorption due to charge displacement of the absorbing co-ion. Theoretical considerations are given for selecting a suitable absorbing co-ion to achieve a high sensitivity of detection.

The role of electromigration dispersion is illustrated by experiments and the effects of the differences in the effective mobilities of sample ions and that of the absorbing co-ion are discussed. The highest sensitivity can be achieved for sample ions having an effective mobility close to the mobility of the absorbing co-ion. In such a case, the concentration of the sample component in its migrating zone can be high while electromigration dispersion is still negligible. The useful dynamic range of the detection is then limited by the linearity and noise of the detector, the former parameter being given mostly by the shape of the on-column detection cell. The best sensitivities can be obtained in low-concentration background electrolytes containing a co-ion with high absorption at a given detection wavelength.

It is shown that indirect photometric detection can be useful for detecting substances that have no optical absorption in the UV and/or visible region, provided that the composition of the background electrolyte is selected correctly.

INTRODUCTION

Sensitive and reliable universal detection of all migrating zones in capillary zone electrophoresis (CZE) is of key importance for the utilization of this technique in practice.

[a] Permanent address: Institute of Analytical Chemistry, Czechoslovak Academy of Sciences, Leninova 82, 611 42 Brno, Czechoslovakia.

0021-9673/89/$03.50

In capillary isotachophoresis[1], potential gradient and conductivity detectors are currently used for this purpose. In CZE[2], the use of potential gradient[3] and conductivity[4–6] detectors is limited to ionic species that have an effective mobility that is substantially different to that of the background electrolyte co-ion. When this difference decreases, the detector signal also decreases and it can often be masked by the noise generated by electrochemical reactions on the sensing electrodes of the detector cell[4]. Therefore, selective optical detectors are currently used here in either the absorbance[7] or the fluorescence mode[8]. Promising results were reported also with electrochemical[9] and mass spectrometric[10] detection. The possibility of using a selective optical detection system as a universal detector is offered by the utilization of the indirect photometric mode. Indirect photometric detection has already been well adopted in ion chromatography[11,12] and, by monitoring the counter ion, it has also been used as a universal detector in isotachophoresis[13].

In CZE, indirect fluorescence detection has been used to monitor the migration of zones of some amino acids[14], nucleotides, iodate, hydrogencarbonate and lysozyme[15]. The reported detection limits are impressive, mainly owing to the high intensity of the excitation laser beam and small inner diameter (15 μm) of the separation capillary used. In this paper we propose a method for the universal indirect detection of zones in CZE based on absorption photometric monitoring of a suitable absorbing co-ion which is the principal component of the background electrolyte.

THEORETICAL

The excellent separation properties of CZE are due mainly to the low dispersive performance of the equipment. In the optimum limiting case, the dispersion of the migrating zones is determined only by diffusion, initial sample pulse width and Joule heat[16,17]. In practice, however, dispersion due to sorption phenomena[17–19] and electromigration dispersion[4,20] contributes significantly to the dispersion of migrating zones. The latter type of dispersion is closely related to the detection. It always occurs during the migration of sample ions which possess effective mobilities different to that of the background electrolyte co-ion; the higher the concentration of the sample component in its zone, the more pronounced is the electromigration dispersion. The electromigration dispersion is different for different ions, and the method of suppressing it is to keep the solute concentrations in their zones sufficiently lower than the concentration of the background electrolyte (BGE).

Obviously, the supprssion of electromigration dispersion by lowering the concentration of the solutes in their zones places greater demands on the detection sensitivity and limits the useful concentration range of detection in CZE. Generally, electromigration dispersion is considered to be negligible when the concentration of the solute ions is two orders of magnitude lower than that of the BGE co-ion[4,18].

The absorbance detectors currently used in CZE exhibit a noise level of *ca.* $1 \cdot 10^{-4}$ absorbance units (A.U.) and their useful dynamic concentration range covers roughly three orders of magitude, as the upper limit of linearity is *ca.* 0.1 A.U. This upper limit is given mainly by the shape of the on-column detector cell, which is exclusively of circular cross-section in present practice. Here the Lambert–Beer law does not hold true in the form derived for a cell with plane parallel windows.

The situation is shown schematically in Fig. 1. The light beams delimited by the

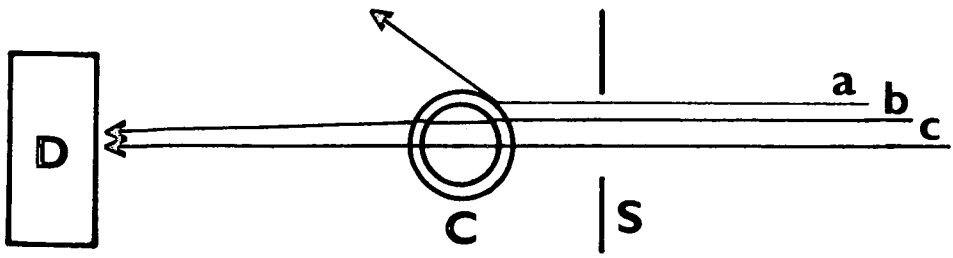

Fig. 1. On-column absorbance detection in capillaries. For details, see text.

slit S strike the capillary C at different positions. The part of the radiation denoted by a is refracted by the wall of the capillary and is lost. The beams b and c pass through the solution inside the capillary and serve for the detection. Their path lengths are, however, different. Hence, for each beam i a special equation can be written in the form

$$I_i = I_{0i} \cdot 10^{-\varepsilon c d_i} \tag{1}$$

where I_i is the intensity of the ith beam, ε is the molar absorption coefficient of a sample of concentration c and d_i is the optical path length of the ith beam. To obtain explicitly the mean intensity of the radiation detected by the detector D, integration is necessary and the resulting absorbance is not a linear function of the concentration c. A more detailed numerical treatment of this problem can be found in the literature[21]. However, for low values of the exponent $\varepsilon c d_i$, eqn. 1 can be expanded into a series and, by neglecting higher terms, it can be derived that for the intensity I detected by the detector

$$I = I_0 (1 - 2.3\, \varepsilon c \bar{d}) \tag{2}$$

where $\bar{d}$ is the mean optical path length in the capillary ($\bar{d} \approx 0.6$ I.D.). Eqn. 2 can be used in practice to describe the attenuation of the light beams up to *ca.* 0.1 A.U. At higher absorbance, the detected and registered peaks are already significantly distorted owing to the non-linearity of the detector.

When considering a capillary of I.D. 100 μm filled with a solution of a solute having $\varepsilon = 10\,000$ l mol^{-1} cm^{-1}, the corresponding admissible maximum concentration is about 10^{-3} M. It is interesting that according to eqn. 2, the detector to be used in capillary techniques does not need to be equipped with a logarithmic converter.

Returning to the mutual relationship between the detection linearity and electromigration dispersion, it follows that if indirect photometry is to be used for detection in CZE, and if simultaneously the concentrations of solutes in the zones should be 100 times lower than that of the BGE co-ion, then the useful dynamic decrease in the BGE absorbance due to the migration of a zone (useful signal) would be only 0.001 A.U. When using a photometer with a noise level of 0.0001 A.U. the resulting signal-to-noise ratio is only 10, which is too low for practical use. Hence, another means of suppressing electromigration dispersion must be found which is based on the selection of a co-ion with a mobility close to those of sample components.

In such a case, the electromigration broadening of zones during the migration is negligible even if the concentrations of solutes reach the concentration of the BGE co-ion. It should be stressed here that this method of suppression of the electromigration dispersion is of key importance as it is advantageous both for detection (direct or indirect) and for achieving high separation efficiencies (number of theoretical plates). Concerning the selection of the counter ion of the BGE, species of low mobility should be selected to ensure a low conductivity of the BGE and hence prevent excessive Joule heating during the analysis.

Another practical hint concerns the sample injection. It is convenient to inject a low-concentration sample which is not mixed with the BGE[4]. In this instance the concentration effect applies across the stationary boundary and the narrow sample pulse obtained facilitates an increase in both the sensitivity of detection and the separation power. Of course, the Joule heat limits the injection of low-concentration (low-conductivity) samples by possible overheating at the point of injection.

EXPERIMENTAL

Equipment

The experiments were carried out in fused-silica capillaries of 130 μm I.D. kindly supplied by Dr. Doupovec (Physical Institute, Slovak Academy of Sciences, Bratislava, Czechoslovakia) and of 100 μm I.D. deactivated fused-silica capillaries (Chrompac International, Middelburg, The Netherlands). One end of the capillary was connected to the electrode vessel via a block of Perspex, equipped with a Hamilton valve, enabling the capillary to be rinsed and filled after each analysis with the help of a syringe. The other end of the capillary served for sample introduction and was held in a mechanical moving arm for easy movement of the capillary orifice from the electrode vessel to the raised sample vial for hydrodynamic injection and back for the analysis. A laboratory-made power supply delivering up to 14 kV and 100 μA was used to drive the separation.

The zones separated in a 130 μm I.D. fused-silica capillary that was 46 cm long (42 cm to the detection cell) were detected by a single-beam UV detector from a Tachophor 2127 ITP analyser (LKB, Bromma, Sweden) with the aid of a previously described fibre-optic on-line detection cell[5].

In some experiments a Varian 2550 variable-wavelength detector was used. In this instance the original flow cell was replaced by a holder made of hard black PVC, which held the 100 μm I.D., 40 cm long (30 cm to the detector) capillary tightly in the optical path of the detector.

Chemicals and electrolytes

All chemicals were of analytical-reagent grade, supplied by Fluka (Buchs, Switzerland). Distilled water was deionized on a mixed-bed ion exchanger.

Two types of background electrolytes were used. The first contained 0.02 *M* benzoic acid as the UV-absorbing anion and was titrated with histidine to pH 6.2; 0.1% Triton X-100 was added to this BGE to suppress the electroosmotic flow. The second BGE contained a lower concentration of the anion with a higher UV absorbance and consisted of 0.007 *M* sorbic acid titrated with histidine to pH 6.2. The elimination of electroosmosis by the addition of Triton X-100 failed in this instance

and, therefore, no additive was used. In both instances the concentration of the BGE was selected so that its absorbance was the limit of the detector linearity.

All values of mobilities were taken from published isotachophoretic data[22].

RESULTS AND DISCUSSION

The ranges of linear response of the detectors used were determined by filling the capillary with standard solutions of benzoic acid. The plot of signal *vs.* concentration of benzoic acid for the LKB detector is shown in Fig. 2. It can be seen that undistorted peaks can be recorded for a detector signal up to 250 mV. The noise level was *ca.* 2 mV. Similar plots were obtained with the Varian 2550 detector. This double-beam detector is equipped with a logarithmic converter and the response was linear up to 0.08 A.U. The noise level was lower than 0.0001 A.U., which is an order of magnitude better performance than that of the single-beam LKB detector.

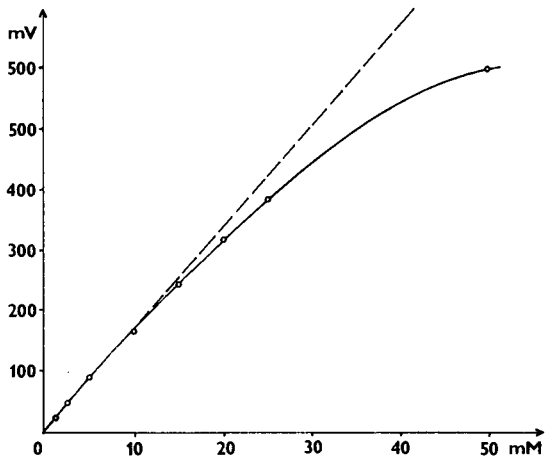

Fig. 2. Detector response *vs.* concentration of benzoic acid inside the 130 μm I.D. capillary.

In Fig. 3 the separation of fourteen model anions in BGE I with both indirect and direct photometric detection is shown. The model sample composition covers a wide mobility range from chloride ($u = 79.08 \cdot 10^{-5}$ cm^{2}V^{-1}s^{-1}) to glucuronate ($\bar{u} = 25.4 \cdot 10^{-5}$ cm^{2}V^{-1}s^{-1}). The effective mobility of the UV-absorbing BGE co-ion (benzoate) is $32 \cdot 10^{-5}$ cm^{2}V^{-1}s^{-1} at this pH.

The electroosmotic flow was suppressed by the presence of 0.1% Triton X-100 in the BGE I and its magnitude was determined from the migration times of individual zones. The resulting electroosmotic mobility was low, being *ca.* $1 \cdot 10^{-4}$ cm^{2}V^{-1}s^{-1} in the cathodic direction.

As expected, highly mobile anions provide broad peaks with a diffuse front and sharp rear boundary and a low detector response. As the mobility of migrating anions decreases, the detector response increases and the peaks become narrower.

The best signal is obtained for the zone of hydroxyisobutyrate (HIBA), which

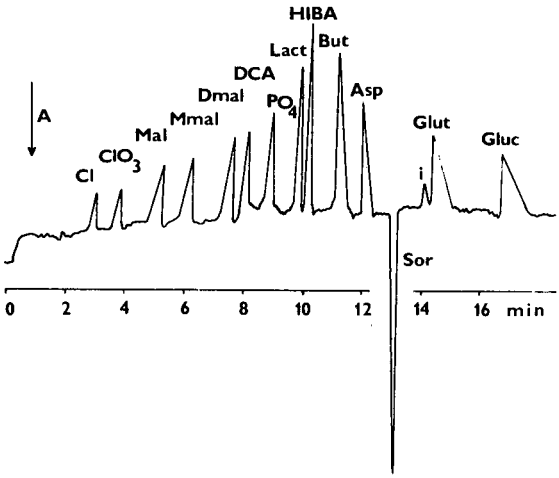

Fig. 3. CZE separation of anions in 130 μm I.D. capillary with indirect photometric detection with a modified LKB Tachophor detector operating at 254 nm. BGE I: 0.02 *M* benzoic acid–histidine at pH 6.2 + 0.1% Triton X-100. Driving current: 35 μA at 13 kV. Abbreviations: Mal = malonate; Mmal = methylmalonate; Dmal = dimethylmalonate; DCA = dichloroacetate; Lact = lactate; HIBA = hydroxyisobutyrate; But = butyrate; Asp = aspartate; Sor = sorbate; i = impurity; Glut = glutamate; Gluc = glucuronate.

has roughly the same effective mobility as benzoate. The slow ions form zones with a sharp front and diffuse rear boundary. Owing to the longer time of migration these zones are broader than the zones of fast ions.

As the noise of the LKB detector was *ca.* 0.001 A.U., a further increase in the sensitivity can be expected with the detector having lower noise. This is demonstrated by Fig. 4, where the separation of thirteen non-UV-absorbing ions was performed in a 100 μm I.D. capillary with the Varian 2550 spectrophotometric detector. Although a 3-fold lower concentration of the sample in comparison with previous experiments

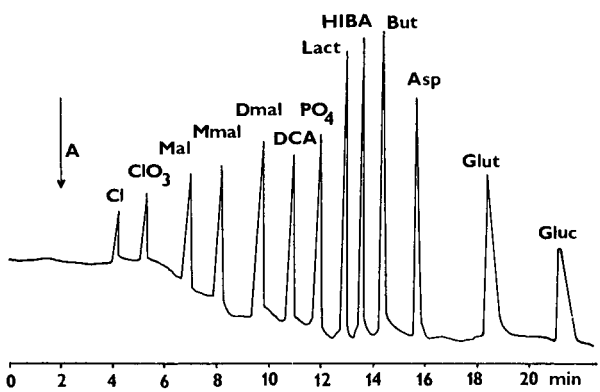

Fig. 4. CZE separation with indirect photometric detection using a Varian 2550 double-beam spectrometric detector operating at 254 nm. The 100 μm I.D. capillary was filled with BGE I. Driving current: 20 μA at 10 kV. For details, see text.

was injected here, a better signal-to-noise ratio was still obtained. On the other hand, a new problem arose here with the baseline drift, which was found to fluctuate with the BGE absorption owing to Joule heating during the analysis. For this reason the use of thinner capillaries seems to be advantageous, where theoretically also better separation efficiencies should be obtained[17,23].

Concerning the separation efficiency, it seems to be of interest to illustrate how it is limited by electromigration dispersion. In Fig. 5, the number of theoretical plates is plotted *vs* the difference between the mobility of the BGE co-ion and that of a sample species. Obviously, the number of theoretical plates reaches its maximum for ionic species having effective mobilities close to that of the co-ion. For greater differences in mobilities the separation efficiency decreases strongly.

Apparently, the use of BGE I provides satisfactory results, however, some conditions should be mentioned. The use of a relatively high concentration of BGE enables the electroosmosis to be reduced substantially by the simple addition of Triton X-100. On the other hand, the low absorbance of benzoate is the reason why the sensitivity of indirect detection is low in comparison with that of the direct detection of highly absorbing substances. This can result in peak masking even by trace UV-absorbing components in the sample. Such a situation is demonstrated in Fig. 6, where the original model mixture was enriched with *o*-aminobenzoate (OAB) and picrate at concentrations of $2 \cdot 10^{-4}$ *M*. Obviously the concentrations of both species added were three times lower than those of other sample components. It can be seen that the aspartate peak is partly overlaped by OAB and seems to be much sharper, and

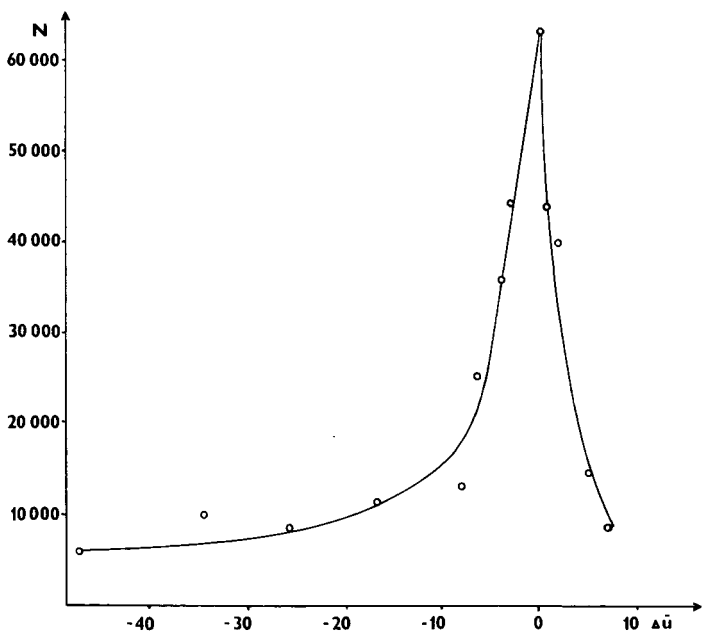

Fig. 5. Effect of electromigration dispersion on the separation efficiency. *N* is the number of theoretical plates, Δu is the difference $\bar{u}_c - \bar{u}_i$ (10^{-5}cm^{2}V^{-1}s^{-1}), where i and c are sample ionic species and co-ion, respectively.

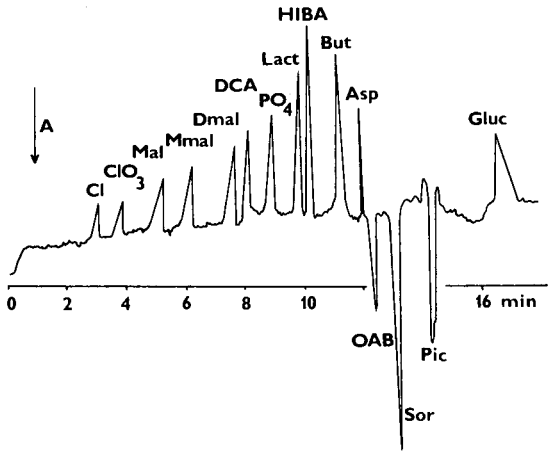

Fig. 6. Indirect photometric detection with peak masking by strongly absorbing trace components in the sample. The concentrations of *o*-aminobenzoate (OAB) and picrate (Pic) were $2 \cdot 10^{-4}$ *M*. The concentrations of other components were $6 \cdot 10^{-4}$ *M*. Other conditions as in Fig. 3.

the peak corresponding to glutamate disappeared completely owing to migration of picrate in the same zone.

The sensitivity of detection can be greatly increased by using a low-concentration but highly absorbing co-ion in BGE, namely, BGE II containing $7 \cdot 10^{-4}$ *M* sorbic acid. This solution has a low ionic strength and with the given instrumental arrangement strong cathodic electroosmotic flow was observed. The use of additives, *e.g.*, Triton X-100 did not suppress electroosmosis significantly. Therefore, no additives were used in further experiments and cathodic electroosmosis was utilizd to drive sample components through the detection cell. The separation of the model mixture of anions, driven cathodically by electroosmosis, is shown in Fig. 7.

The first detected positive peaks belong to potassium and lithium originating

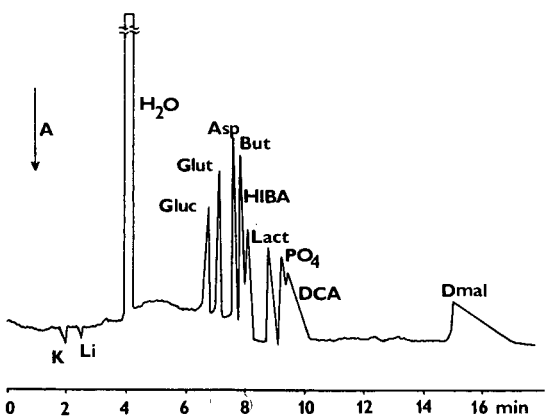

Fig. 7. CZE separation of anions with indirect photometry in low-concentration BGE II consisting of $7 \cdot 10^{-4}$ *M* sorbic acid–histidine at pH 6.2 with no additives. Driving current: 2 μA at 13 kV. LKB detector. For details, see text.

from the potassium phosphate and lithium lactate used for the sample preparation. The large rectangular peak of water transported by electroosmotic flow corresponds to the volume of sample injected and can be used as an electroosmotic marker.
The value of electroosmotic mobility, *i.e.*, the term $\varepsilon\zeta/\eta$, where ε, ζ and η are the permitivity of the BGE, the zeta potential and viscosity of the BGE, respectively, in the Helmholtz–Smoluchovski equation was found to be *ca.* $60 \cdot 10^{-5}$ $cm^2V^{-1}s^{-1}$. Obviously, the first peaks of anionic sample components correspond to low-mobility anions, whereas the highly mobile anions with electrophoretic velocities comparable to or higher than the electroosmotic velocity are not detected at all.

After the start of the analysis the sample ions migrate across the concentration boundary between the BGE and sample solution. As the sample concentration is low here ($2 \cdot 10^{-5}$ *M* of each ionic species), the migrating species are first concentrated across the above-mentioned boundary into a narrow sample zone in which their concentrations are adjusted to the values fulfilling the Kohlrausch regulation function[24]. Hence a sharp starting sample zone is created which aids positively the detection of sample components. During the following migration (superposition of electroosmosis and electrophoresis), however, zones containing ions with effective mobilities different from that of the sorbate ion are broadened by electromigration dispersion. The sharpest zones with the best detector response again provide anions with a mobility close to that of the BGE co-ion (sorbate).

The detection sensitivity in this system is roughly 50 times better than that in the previous instance and the detection limit even with a single-beam detector approaches 0.5 pmol injected.

Finally, we should mention an important practical aspect of the utilization of electroosmotic flow for driving the sample species along the separation path. The magnitude of the electroosmotic flow is strongly dependent on the history of the capillary used. This is demonstrated in Fig. 8, which shows the separation of a sample

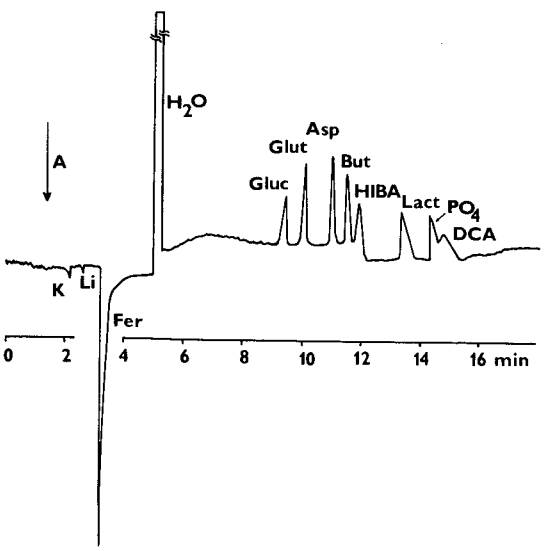

Fig. 8. Variation of migration times due to changes in electroosmotic flow caused by the sorption of the sample component. Fer = Ferroin. Other conditions as in Fig. 7.

to which 10^{-6} *M* ferroin was added. The sorption of ferroin on the capillary wall manifests itself not only by the tailing of the ferroin peak but also by a substantial decrease in the electroosmotic flow, which led to longer migration times and loss of the dimethylmalonate zone.

ACKNOWLEDGEMENTS

Our thanks are due to Mr. V. Monaco and Mr. R. Di Nino for the construction of the capillary holder for the Varian detector.

REFERENCES

1 P. Boček, M. Deml, P. Gebauer and V.Dolník, *Analytical Isotachophoresis (Electrophoresis Library)*, Verlag Chemie, Weinheim, 1988.
2 J. W. Jorgenson and K. D. Lukacs, *Anal. Chem.*, 53 (1981) 1298.
3 P. Gebauer, M. Deml, P. Boček and J. Janák, *J. Chromatogr.*, 267 (1983) 455.
4 F. E. P. Mikkers, F. M. Everaerts and Th. P. E. M. Verheggen, *J. Chromatogr.*, 169 (1979) 11.
5 F. Foret, M. Deml, V. Kahle and P. Boček, *Electrophoresis*, 7 (1986) 430.
6 X. Huang, M. J. Gordon and R. N. Zare, *J. Chromatogr.*, 425 (1988) 385.
7 Y. Walbroehl and J. W. Jorgenson, *Chromatographia*, 315 (1984) 135.
8 J. S. Green and J. W. Jorgenson, *J. Chromatogr.*, 352 (1986) 337.
9 R. A. Wallingford and A. G. Ewing, *Anal. Chem.*, 59 (1987) 1762.
10 J. A. Olivares, N. T. Nguyen, C. R. Yonker and R. D. Smith, *Anal. Chem.*, 59 (1987) 1230.
11 H. Small and T. E. Miller, Jr., *Anal. Chem.*, 54 (1982) 462.
12 M. Janeček and K. Šlais, *J. Chromatogr.*, 471 (1989) 303.
13 L. Arlinger and H. Lundin, *Protides Biol. Fluids, Proc. Colloq.*, 21 (1973) 667.
14 W. G. Kuhr and E. S. Yeung, *Anal. Chem.*, 60 (1988) 1832.
15 W. G. Kuhr and E. S. Yeung, *Anal. Chem.*, 60 (1988) 2642.
16 H. H. Lauer and D. McManigil, *Trends Anal. Chem.*, 1 (1986) 11.
17 F. Foret, M. Deml and P. Boček, *J. Chromatogr.*, 452 (1988) 601.
18 J. W. Jorgenson and K. D. Lukacs, *Science*, 222 (1983) 266.
19 H. H. Lauer and D. McManigil, *Anal. Chem.*, 58 (1986) 166.
20 F. E. P. Mikkers, F. M. Everaerts and Th. P. E. M. Verheggen, *J. Chromatogr.*, 169 (1979) 1.
21 S. Hjertén, *Chromatogr. Rev.*, 9 (1967) 122.
22 T. Hirokawa, M. Nishino, N. Aoki, Y. Kiso, Y. Sawamoto, T. Yagi and J.-I. Akiyama, *J. Chromatogr.*, 271 (1983) D1.
23 K. D. Lukacs and J. W. Jorgenson, *J. High Resolut. Chromatogr. Chromatogr. Commun.*, 8 (1985) 407.
24 F. Foret and P. Boček, *Adv. Electrophoresis*, in press.

Journal of Chromatography, 470 (1989) 309–312
Elsevier Science Publishers B.V., Amsterdam — Printed in The Netherlands

CHROM. 21 381

Note

Dynamic programming of pH — a new option in analytical capillary electrophoresis

P. BOČEK*, M. DEML, J. POSPÍCHAL and J. SUDOR

Institute of Analytical Chemistry, Czechoslovak Academy of Sciences, Leninova 82, CS-611 42 Brno (Czechoslovakia)

(First received January 9th, 1989; revised manuscript received January 16th, 1989)

It is common in dynamic separation methods, *e.g.*, chromatography, that the analytical and/or separation possibilities are improved by the application of a suitable gradient. In gas chromatography, temperature gradients have been successfully used for a long time[1]; in liquid chromatography, gradient elution[2] has been improved progressively in the last decade. In both instances, the gradients used are dynamically programmed during the analysis itself by instrumental means according to the requirements of the user.

The use of gradients is also of great interest in electrophoretic techniques. In electrophoretic ion focusing[3] and isoelectric focusing[4], a pH gradient is used to focus the sample substances into narrow bands at defined positions in the separation column. In these techniques, it is essential to create a sufficiently stable (constant steepness) and stationary (not moving along the migration path) pH gradient along the separation column, serving subsequently for the separation and focusing of the sample substances. These stationary gradients may be mobilized in order to move through a fixed-point detection site by either hydrodynamic flow or substitution of the counter-ionic system (so that the stability of the gradient is lost)[5,6].

Recently, a paper[7] was published describing the gradient elution method in capillary zone electrophoresis (micellar electrokinetic capillary chromatography), in which a stepwise solvent programme with increasing 2-propanol content in the background electrolyte was used.

To our knowledge, so far no attempt has been made to perform capillary electrophoresis in a mobile pH gradient which is dynamically programmed. The aim of this paper is to illustrate this possibility by preliminary experiments. It involves a description of simple instrumentation that enables one to generate dynamic changes of pH in the separation capillary, thus forming a moving pH profile along the separation path. An example of the effect of a dynamic pH gradient on the migration behaviour of substances is given.

EXPERIMENTAL

The experiments were performed using equipment similar to that described elsewhere[8]; and shown schematically in Fig. 1. The separation capillary was placed

0021-9673/89/$03.50

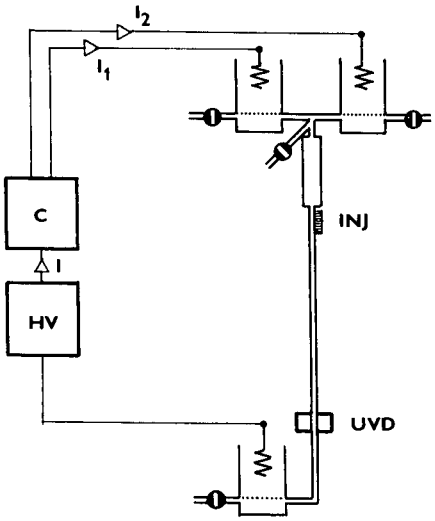

Fig. 1. Schematic diagram of the apparatus used. C = Electric current ratio controller; HV = high-voltage power supply; INJ = injection site; UVD = UV absorption detector.

between two electrode blocks. The starting electrode block consisted of two electrode chambers, one of them containing the primary (or background) electrolyte (0.01 *M* KCl) and the other one the modifying electrolyte (0.01 *M* HCl). The other electrode block contained 0.01 *M* KCl. The two electrode chambers in the starting electrode block were connected to the high-voltage power supply via an electric current ratio controller.

For the construction of the instrument, a CS Isotachophoretic Analyzer (Institute of Radioecology and Applied Nuclear Techniques, Spišská Nová Ves, Czechoslovakia) was modified in such a way that only one separation capillary was placed between the sampling valve and the UV absorption detector (254 nm). The modified electrode chamber was connected to the starting electrode block by a narrow-bore PTFE capillary; the mixing point was at the upper end of the sampling valve.

In all experiments, 0.01 *M* KCl served as the primary electrolyte. For its preparation, freshly boiled distilled water was used; the pH of the solution was adjusted to 4.25 by addition of HCl. The modifying electrolyte was 0.01 *M* HCl.

To prevent disturbances caused by the penetration of the electrode reaction products from the electrode chambers into the separation capillary, two precautions were taken. To suppress the penetration of OH^- ions into the capillary from the cathodic electrode chamber, this chamber was filled with 0.01 *M* HCl. In the anodic electrode chamber filled with 0.01 *M* KCl (see Fig. 1), an electrode made of silver was used to prevent H^+ production.

All chemicals used were obtained from Lachema (Brno, Czechoslovakia). The sample (0.1 μl of 0.005 *M* pyridine + 0.005 *M* *p*-bromoaniline, pH 4.9) was introduced with a 2-μl syringe (Hamilton, Bonaduz, Switzerland) via the septum up to the point of connection between the sampling valve and the detection capillary.

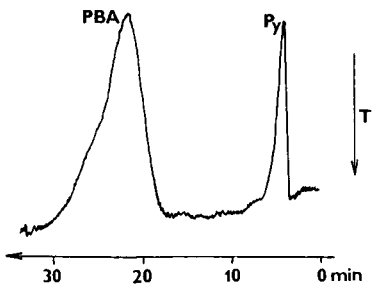

Fig. 2. UV detection record of an analysis in the zone electrophoresis mode. Background electrolyte, 0.01 *M* KCl (pH 4.25); I = 200 μA. Py = pyridine; PBA = *p*-bromoaniline. T = transmittance.

The rate of increase of the pH gradient was controlled electrically by setting up the ratio of the two electric currents, I_1/I_2 (*cf.*, Fig. 1) while keeping the total electric current ($I = I_1 + I_2$) constant (200 μA).

RESULTS

In order to show the possible influence of a dynamic pH gradient in zone electrophoretic analysis, experiments were performed with a model sample containing pyridine and *p*-bromoaniline. Fig. 2 shows the analysis of the sample by classical (isocratic) zone electrophoresis (background electrolyte 0.01 *M* KCl, pH 4.25). It can be seen that the separation of the two substances was effective, but the analysis time was fairly long owing to the relatively slow migration of the *p*-bromoaniline zone, accompanied by considerable broadening of its peak. The pyridine peak was asymmetric owing to electromigrational dispersion caused by the relatively large amount of sample that was necessary to keep the signal-to-noise ratio at a reasonable level.

Fig. 3 shows the result of an analysis of the same mixture at low pH. Electrophoresis was carried out in 0.0167 *M* HCl (pH 1.77), which is the most acidic medium obtainable with 0.01 *M* KCl as the primary electrolyte (when $I_1 = 0$, see Fig. 1). The analysis time for pyridine was three times longer than that in the previous experiment and the peak of *p*-bromoaniline was hardly detected owing to the decrease in its molar absorption coefficient with decrease in pH.

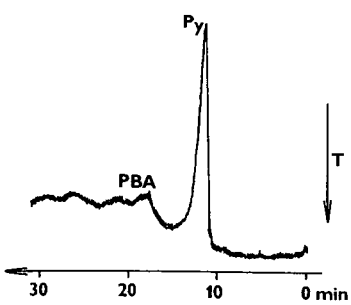

Fig. 3. UV detection record of an analysis in the zone electrophoresis mode. Background electrolyte, 0.0167 *M* HCl (pH 1.77); I = 200 μA. Abbreviations as in Fig. 2.

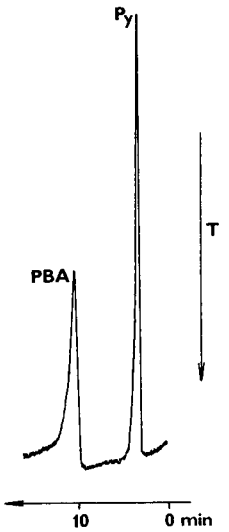

Fig. 4. UV detection record of an analysis with a pH gradient. Primary electrolyte, 0.01 *M* KCl (pH 4.25); modifying electrolyte, 0.01 *M* HCl; I = 200 μA; I_2 was increased and I_1 was decreased at 4 μA/min. Abbreviations as in Fig. 2.

Fig. 4 shows the result of an analysis using a pH gradient. The starting conditions were identical with those in the previous experiment [background (*i.e.*, primary) electrolyte 0.01 *M* KCl, pH 4.25]; the dynamic gradient was then programmed by a stepwise increase in the modifying current (4 μA/min). It can be seen that the analysis time for both substances has decreased and that their peaks have become sharper.

The use of migrating pH gradients in capillary zone electrophoresis seems to be promising and work on this topic is continuing.

REFERENCES

1 W. E. Harris and H. W. Habgood, *Programmed Temperature Gas Chromatography,* Wiley, New York, 1966.
2 P. Jandera and J. Churáček, *Gradient Elution in Column Liquid Chromatography,* Elsevier, Amsterdam, 1985.
3 E. Schumacher, *Helv. Chim. Acta,* 40 (1957) 2322.
4 N. Catsimpoolas (Editor), *Isoelectric Focusing,* Academic Press, New York, San Francisco, London, 1976.
5 Z. Buzás, L. M. Hjelmeland and A. Chrambach, *Electrophoresis,* 4 (1983) 27.
6 S. Hjertén, F. Kilár, L. Liao and M. Zhu, in M. J. Dunn (Editor), *Electrophoresis '86,* VCH, Weinheim, 1986, p. 451.
7 A. T. Balchunas and M. J. Sepaniak, *Anal. Chem.,* 60 (1988) 617.
8 J. Pospíchal, M. Deml, P. Gebauer and P. Boček, *J. Chromatogr.,* 470 (1989) 43.

PUBLICATION SCHEDULE FOR 1989

Journal of Chromatography and Journal of Chromatography, Biomedical Applications

MONTH	J	F	M	A	M	J	J	A	S	O	N	D
Journal of Chromatography	461 462 463/1	463/2 464/1	464/2 465/1 465/2	466 467/1 467/2	468 469 470/1 470/2	471 472/1 472/2 473/1	The publication schedule for further issues will be published later					
Bibliography Section		486/1		486/2		486/3		486/4				
Biomedical Applications	487/1	487/2	488/1 488/2	489/1 489/2	490/1 490/2	491/1	491/2	492 493/1	493/2			

INFORMATION FOR AUTHORS

(Detailed *Instructions to Authors* were published in Vol. 445, pp. 453–456. A free reprint can be obtained by application to the publisher, Elsevier Science Publishers B.V., P.O. Box 330, 1000 AH Amsterdam, The Netherlands.)

Types of Contributions. The following types of papers are published in the *Journal of Chromatography* and the section on *Biomedical Applications:* Regular research papers (Full-length papers), Notes, Review articles and Letters to the Editor. Notes are usually descriptions of short investigations and reflect the same quality of research as Full-length papers, but should preferably not exceed six printed pages. Letters to the Editor can comment on (parts of) previously published articles, or they can report minor technical improvements of previously published procedures; they should preferably not exceed two printed pages. For review articles, see inside front cover under Submission of Papers.

Submission. Every paper must be accompanied by a letter from the senior author, stating that he is submitting the paper for publication in the *Journal of Chromatography*. Please do not send a letter signed by the director of the institute or the professor unless he is one of the authors.

Manuscripts. Manuscripts should be typed in double spacing on consecutively numbered pages of uniform size. The manuscript should be preceded by a sheet of manuscript paper carrying the title of the paper and the name and full postal address of the person to whom the proofs are to be sent. Authors of papers in French or German are requested to supply an English translation of the title of the paper. As a rule, papers should be divided into sections, headed by a caption (*e.g.*, Summary, Introduction, Experimental, Results, Discussion, etc.). All illustrations, photographs, tables, etc., should be on separate sheets.

Introduction. Every paper must have a concise introduction mentioning what has been done before on the topic described, and stating clearly what is new in the paper now submitted.

Summary. Full-length papers and Review articles should have a summary of 50–100 words which clearly and briefly indicates what is new, different and significant. In the case of French or German articles an additional summary in English, headed by an English translation of the title, should also be provided. (Notes and Letters to the Editor are published without a summary.)

Illustrations. The figures should be submitted in a form suitable for reproduction, drawn in Indian ink on drawing or tracing paper. Each illustration should have a legend, all the *legends* being typed (with double spacing) together on a *separate sheet*. If structures are given in the text, the original drawings should be supplied. Coloured illustrations are reproduced at the author's expense, the cost being determined by the number of pages and by the number of colours needed. The written permission of the author and publisher must be obtained for the use of any figure already published. Its source must be indicated in the legend.

References. References should be numbered in the order in which they are cited in the text, and listed in numerical sequence on a separate sheet at the end of the article. Please check a recent issue for the layout of the reference list. Abbreviations for the titles of journals should follow the system used by *Chemical Abstracts*. Articles not yet published should be given as "in press" (journal should be specified), "submitted for publication" (journal should be specified), "in preparation" or "personal communication".

Dispatch. Before sending the manuscript to the Editor please check that the envelope contains three copies of the paper complete with references, legends and figures. One of the sets of figures must be the originals suitable for direct reproduction. Please also ensure that permission to publish has been obtained from your institute.

Proofs. One set of proofs will be sent to the author to be carefully checked for printer's errors. Corrections must be restricted to instances in which the proof is at variance with the manuscript. "Extra corrections" will be inserted at the author's expense.

Reprints. Fifty reprints of Full-length papers, Notes and Letters to the Editor will be supplied free of charge. Additional reprints can be ordered by the authors. An order form containing price quotations will be sent to the authors together with the proofs of their article.

Advertisements. Advertisement rates are available from the publisher on request. The Editors of the journal accept no responsibility for the contents of the advertisements.

Also available in a paperback student edition

Contemporary Practice of Chromatography

by **C.F. Poole** *and* **S.A. Schuette,** *Dept. of Chemistry, Wayne State University, Detroit, MI, USA*

"A tremendous amount of work has gone into the writing of this book, and it may be considered to be one of the few volumes of its kind that could be used both as a text by senior students in the field and by analysts in many industries. All academic, research association and appropriate industrial laboratories should buy at least one copy (preferably more, as borrowers will probably wish to keep it on loan for some time)." (The Analyst)

Written for everyone who uses chromatography as an analytical tool, this book covers all areas of gas, liquid, and thin-layer chromatography; **no other book offers the same scope.** The authors have had considerable experience in teaching graduate-level courses and the material presented here has been tried and tested, having formed the basis for short courses taught to groups of industrial chemists. Emphasis is on the practice of chromatographic methods, including "how to" sections and numerous examples of calculation methods. Extensively illustrated, the book contains numerous tables of all useful constants, materials and formulas frequently used by chromatographers. Valuable features are the chapters on sample preparation for chromatographic analysis, on instrumental methods for sample identification; and the comprehensive literature review.

Contents: 1. Fundamental Relationships of Chromatography. 2. The Column in GC. 3. Instrumental Requirements for GC. 4. The Column in LC. 5. Instrumental Requirements for HPLC. 6. Preparative-Scale Chromatography. 7. Sample Preparation for Chromatographic Analysis. 8. Hyphenated Methods for Identification after Chromatographic Separation. 9. High Performance Thin-Layer Chromatography. Subject Index.

1984. 2nd repr. 1986 x + 708 pages

Hardcover edition:	*Paperback edition:*
US$92.00/Dfl.175.00	US$37.50/Dfl.110.00
ISBN 0-444-42410-5	ISBN 0-444-42506-3

ELSEVIER SCIENCE PUBLISHERS

P.O. Box 211, 1000 AE Amsterdam, The Netherlands
P.O. Box 882, Madison Square Station, New York, NY 10159, USA